

Mutasynthetic Production of Proansamitocin Derivatives

-

Development of Nanoparticle-Antibiotic Conjugates for Selective Drug Release upon Inductive Heating

Von der Naturwissenschaftlichen Fakultät der
Gottfried Wilhelm Leibniz Universität Hannover

zur Erlangung des Grades
Doktorin der Naturwissenschaften (Dr. rer. nat.)

genehmigte Dissertation

von

Friederike Wesemann geb. Schäkel, M. Sc.

2022

Referent: Professor Dr. rer. nat. Andreas Kirschning

Korreferent: Professor Dr. rer. nat. Oliver Plettenburg

Tag der Promotion: 13.04.2022

„Science doesn't always go forwards. It's a bit like doing a Rubik's cube. You sometimes have to make more of a mess with a Rubik's cube before you can get it to go right.” –

Jocelyn Bell Burnell

Abstract

Friederike Wesemann

Mutasynthetic Production of Proansamitocin Derivatives

-

Development of Nanoparticle-Antibiotic Conjugates for Selective Drug Release upon Inductive Heating

Keywords: mutasynthesis, ansamitocin, proansamitocin, superparamagnetic iron oxide nanoparticles, antibiotics, thermosensitive linker

Ansamitocins are anti-proliferative secondary metabolites of *Actinosynnema pretiosum*. They consist of a macrolactam polyketide with AHBA as the starting unit of the biosynthesis. A variety of biological active ansamitocin derivatives have been generated through mutasynthesis using Δ AHBA mutants.

Recently, another mutant of *A. pretiosum* was described, that lacks genes for AHBA synthesis as well as genes for post-polyketide modification. This strain, named AH1, produces proansamitocin derivatives after feeding of various aminobenzoic acids, albeit in lower yields than the single Δ AHBA mutant. Of particular interest were the findings of a macrolactone proansamitocin derivative upon feeding of a hydroxymethylbenzoic acid.

In the first part of this study, the substrate spectrum of strain AH1 was investigated and new proansamitocin derivatives were characterized. Studies were conducted to improve the culture conditions of this strain. This study also aimed at the isolation of large amounts of the macrolactone proansamitocin derivative by a 25 L fermentation using the BIOSTAT[®]CultiBag RM reactor, however without isolation of the desired macrolactone.

In the second part of this work, a new type of a SPION-antibiotic conjugate, connected by a thermosensitive linker, was designed. The use of SPIONs for thermoselective release after inductive heating is a promising tool for new drug delivery systems. A new thermosensitive linker for carboxylic acid release was first developed and tested. This linker showed a facile release of nalidixic acid at 95 °C in <30 min while being stable at 37 °C for several hours. It was then used to link nalidixic acid to MagSilica[®] SPIONs and release upon inductive heating was observed.

Zusammenfassung

Friederike Wesemann

Mutasynthetische Produktion von Proansamitocin Derivaten

-

Entwicklung von Nanopartikel-Antibiotika-Konjugaten zur selektiven Wirkstofffreisetzung bei induktiver Erwärmung.

Schlagwörter: Mutasynthese, Ansamitocin, Proansamitocin, superparamagnetische Eisenoxid-Nanopartikel, Antibiotika, thermosensitive Linker

Ansamitocine sind antiproliferative Sekundärmetaboliten aus *Actinosynnema pretiosum*. Sie bestehen aus einem Polyketid Makrolactam mit AHBA als Starteinheit der Biosynthese. Unter Verwendung von Δ AHBA-Mutanten wurde mithilfe der Mutasynthese bereits eine große Vielfalt biologisch aktiver Ansamitocin-Derivate erzeugt. Kürzlich wurde eine weitere Mutante von *A. pretiosum* beschrieben, der sowohl die Gene für die AHBA-Synthese als auch die Gene für die Post-Polyketid-Modifikation fehlen. Dieser Stamm, AH1 genannt, produziert nach Fütterung mit verschiedenen Aminobenzoesäuren Proansamitocin-Derivate, wenn auch in geringerer Ausbeute als bei der ursprünglichen Δ AHBA-Ausgangsmutante. Besonders interessant waren die Funde eines Makrolacton-Proansamitocin-Derivats nach Fütterung mit einer Hydroxymethylbenzoesäure.

Im ersten Teil dieser Studie wurde das Substratspektrum des Stammes AH1 untersucht und neue Proansamitocin-Derivate charakterisiert. Es wurden Studien zur Verbesserung der Kulturbedingungen für diesen neuen Stamm durchgeführt. Ziel dieser Studie war die Isolierung großer Mengen des Makrolacton-Proansamitocin-Derivats durch eine 25-Liter-Fermentation unter Verwendung des BIOSTAT®CultiBag RM-Reaktors. Jedoch konnte das gewünschte Makrolacton unter diesen Bedingungen nicht isoliert werden.

Im zweiten Teil dieser Arbeit wurde ein neues SPION-Antibiotika-Konjugat synthetisiert, bei dem das Antibiotikum über einen thermosensitiven Linker an das SPION gebunden ist. Die Verwendung von SPIONs zur thermoselektiven Freisetzung nach induktiver Erwärmung ist ein vielversprechendes Werkzeug für neuartige Arzneimittelsysteme. Ein neuer thermosensitiver Linker für die Freisetzung von Carbonsäuren wurde entwickelt und getestet. Dieser Linker zeigte eine schnelle Freisetzung von Nalidixinsäure bei 95 °C in weniger als 30 min, während bei 37 °C über mehrere Stunden keine signifikante Freisetzung beobachtet wurde. Anschließend wurde Nalidixinsäure über diesen Linker mit MagSilica® SPIONs verknüpft, und es wurde eine Freisetzung bei induktiver Erwärmung beobachtet.

Table of Contents

Inspirational Quote	I
Abstract	II
Zusammenfassung.....	III
Table of Contents	IV
1 Abbreviations and Remarks.....	1
1.1 List of Abbreviations.....	1
1.2 Preliminary Remarks.....	5
2 Introduction Part I	6
2.1 Mutasythesis.....	6
2.2 Ansamitocin	7
2.2.1 Bioactivity	8
2.2.2 Biosynthesis.....	10
2.3 Previous Mutasytheses with AHBA Knock Out Mutants.....	11
3 Aim of Study Part I	13
4 Results and Discussion Part I.....	14
4.1 Identification of New Proansamitocin Derivatives	14
4.2 Mutasythesis towards New Proansamitocin Derivatives	16
4.3 Optimization of Proansamitocin (9) Production of Strain AH1.....	21
4.3.1 General Studies on Fermentation of AHBA (7) with Strain AH1.....	21
4.3.2 Additional L-Leucin, L-Valine and <i>iso</i> -Butanol	23
4.3.3 Additional Coconut water, Gibberellic Acid and Fructose	25
4.3.4 Medium Variation	26
4.3.5 Variation of Inoculation Volume and Speed of Rotation.....	27
4.4 Fermentation of Hydroxymethylbenzoic Acid 13 with Strain AH1	29
4.4.1 General Fermentation Studies	29

4.4.2 Large Scale Fermentation.....	31
5 Introduction Part II	34
5.1 Nanoparticles to Combat Antimicrobial Resistance	34
5.1.1 Nanoparticles in Biomedicine	34
5.1.2 Superparamagnetic Iron Oxide Nanoparticles.....	35
5.1.3 Superparamagnetism and its Advantages in Biomedical Context.....	36
5.1.4 Antimicrobial SPIONs.....	38
5.2 Surface Chemistry of Nanoparticles.....	38
5.2.1 Copper Catalyzed Azide-Alkyne 1,3-Dipolar Cycloaddition	39
5.2.2 Thiol-Maleimide MICHAEL Addition	40
5.3 Thermal Controlled Release.....	41
5.3.1 Thermo labile Azo Ligand.....	43
5.3.2 Retro Diels-Alder Reaction	45
5.3.3 Thermo Sensitive Lactamization.....	46
5.3.4 The 2-Py-TPG Thermolabile Protecting Group	47
6 Aim of Study Part II.....	51
7 Results and Discussion Part II	52
7.1 Selection of Antibiotics	52
7.2 2-Py-TPG Design and Synthesis	53
7.3 2-Py-TPG Penicillin G	60
7.3.1 Synthesis.....	60
7.3.2 Release.....	64
7.4 2-Py-TPG Quinolone Antibiotics.....	66
7.4.1 Synthesis.....	66
7.4.2 Release Experiments	74
7.5 PEGylation and Connection to SPION	78
7.5.1 Nanoparticle Conjugate A: Design and Retrosynthesis	78
7.5.2 Nanoparticle Conjugate A: Forward Synthesis	80
7.3.3 Nanoparticle Conjugate B: Design and Retrosynthesis.....	89
7.5.4 Nanoparticle Conjugate B: Forward Synthesis	92

7.5.5 Nanoparticle Conjugate B: Antibiotic Release.....	98
8 Conclusion and Outlook	104
8.1 Conclusion Part I.....	104
8.2 Outlook Part I.....	107
8.3 Conclusion Part II.....	109
8.4 Outlook Part II.....	112
9 Experimentals	115
9.1. Analytical Section	115
9.2 Microbiological Section	120
9.3 General Procedures.....	123
9.4 Experimental Procedures Part I.....	125
9.5 Experimental Procedures Part II.....	137
10 Literature	231
11 NMR Data	241
11.1 NMR Data Part I.....	241
11.2 NMR Data Part II	249
Danksagung.....	314
Lebenslauf und Publikationsliste.....	316

1 Abbreviations and Remarks

1.1 List of Abbreviations

2D	two dimensional
2-Py-TPG	<i>N</i> -2-pyridinyl thermolable protecting group
A	peak area
ACP	acyl carrier proteine
ADE	adenylation domain
AHBA	3-amino-5-hydroxybenzoic acid
AMF	alternating magnetic field
APTES	3-(aminopropyltriethoxysilane)
aq.	aqueous
<i>asm</i>	genes of ansamitocin biosynthesis in <i>Actinosynnema pretiosum</i>
Asm	proteins of ansamitocin biosynthesis in <i>Actinosynnema pretiosum</i>
AT	acyl transferase
BINAP	bis(diphenylphosphino)-binaphthyl
Bn	benzyl
Boc	<i>tert</i> -butylcarbonyl
Bu	butyl
c	concentration (m/V)
cat.	catalytic
CDI	carbonyldiimidazole
CoA	coenzyme A
COSY	correlation spectroscopy
CuAAC	copper-catalyzed azide-alkyne 1,3-dipolar cycloaddition
CW	coconut water
Cy	cyclohexane
d	day; <i>NMR</i> : doublet
Da	dalton
DavePhos	2-dicyclohexylphosphino-2'-(<i>N,N</i> -dimethylamino)-biphenyl
DBU	diazabicycloundecene
DCW	dry cell weight
DH	dehydratase
DHP	dihydropyrane
DIBAL	diisobutylaluminium
DIPA	diisopropylamine
DMAP	4-dimethylaminopyridine

DMF	dimethyl formamide
DMSO	dimethylsulfoxide
DOX	doxorubicin
EDC	1-ethyl-3-(3-dimethylaminopropyl)carbodiimide
EDG	electron donating group
eq.	equivalents
ER	enoyl reductase
ESI	electron spray ionization
Et	ethyl
EWG	electron withdrawing group
FA	formic acid
FITC	fluorescein isothiocyanate
FTIR	fourier-transform infrared spectroscopy
g	gram
GA	gibberellic acid
h	hours
HBTU	hexafluorophosphate benzotriazole tetramethyl uronium
HER2	human epidermal growth factor receptor 2
HMBC	heteronuclear multiple-bond correlation
HPLC	high performance liquid chromatography
HRMS	high resolution mass spectrometry
HSQC	heteronuclear single-bond correlation
Hsp90	Heat shock protein 90
Hz	hertz
<i>i</i>	<i>iso</i>
is	internal standard
<i>J</i>	<i>NMR</i> : scalar coupling constant
K-ECs	KAPOSI's sarcoma associated herpes virus infected enterochromaffin cells
KS	ketosynthase
KR	ketoreductase
L	liter
LDA	lithium diisopropylamine
m	mass, milli; <i>NMR</i> : multiplet
Me	methyl
min	minutes
mmol	millimol
MOM	2-methoxy-ethoxymethyl

MRI	magnetic resonance imaging
Ms	mesyl
MS	mass spectrometry
MTES	maleimideoriorioyletriethoxysilane
μw	microwave irradiation
m/z	<i>MS</i> : mass per charge
NHS	<i>N</i> -hydroxysuccinimide
NMR	nuclear magnetic resonance spectroscopy
NOE	nuclear overhauser effect
NRPS	non-ribosomal peptide synthetase
o2s	over two steps
OD	optical density
p.i.	post inoculation
PKS	polyketide synthase
PEG	polyethylene glycol
PG	protection group
ppm	parts per million
PTSA	<i>para</i> -toluenesulfonic acid
q	<i>NMR</i> : quartet
quant.	quantitative
rDA	retro DIELS-ALDER
R_f	retardation factor
ROS	reactive oxygen species
RP	reverse phase
rpm	revolutions per minute
rt	room temperature
RuPhos	2-dicyclohexylphosphino-2',6'-diisopropoxybiphenyl
s	<i>NMR</i> : singlet
sat.	saturated
SAR	structure-activity relationship
SE	size exclusion
SN	nucleophilic substitution
SPION	superparamagnetic iron oxide nanoparticles
t	tert, <i>NMR</i> : triplet
T3P	propanephosphonic acid anhydride
TBAF	tetrabutylammoniumfluoride
TBAI	tetrabutylammoniumiodide

TBDPS	tertbutyldiphenylsilane
TBS	tertbutyldimethylsilane
<i>t</i> BuXPhos	2-di- <i>tert</i> -butylphosphin-2',4',6'-triisopropylbiphenyl
TES	triethoxysilane
TFA	trifluoroacetic acid
THF	tetrahydrofuran
THP	tetrahydropyrane
Thy	thymin
TIPS	triisopropylsilane
TLC	thin layer chromatography
T_m	melting point
t_R	retention time
UDP	uracil diphosphate
UPLC	ultra performance liquid chromatography
V	volume
Val	valine
w	mass percentage (m/m)
W	watt
wt	wild type
$\Delta_{X,Y}$	double bond between CX and CY
ρ	density
μ	micro

1.2 Preliminary Remarks

The numbering used for the assignment of the hydrogen or carbon atom NMR signals does not comply with the IUPAG rules. The numbering described in the discussion refers to the numbering used in the experimental part. Figures of structures with not clearly defined residue are not numbered.

2 Introduction Part I

2.1 Mutasynthesis

In the last century, natural products have been an important source of small molecule drugs, especially for the development of antibiotics and anticancer drugs.^[1] These secondary metabolites have been optimized by nature during evolution to achieve specific prokaryotic and eukaryotic targets and therefore serve as antibacterial, anticancer and antifungal drugs.^[2] However, only the smallest part of the approved drugs are unmodified natural products. The majority consists of natural product derivatives and synthetic drugs bearing a natural product pharmacophore.^[1]

These modifications are necessary to improve the selectivity, efficacy, safety, human pharmacokinetics and oral bioavailability of the drug.^[3,4] Derivatization is also a rapid means of overcoming drug resistances as was the case with β -lactam antibiotics.^[4] In addition to improving the above properties, analogs of natural products are used in structure-activity relationship (SAR) studies, which are necessary for a better understanding of the drug's target and mode of action.^[5]

Natural product derivatives are usually prepared by total synthesis^[5,6] or semisynthetic derivatization^[4]. Over the last 50 years modern tools of synthetic biology have been developed such as chemobiosynthesis or mutasynthesis that allow modifications of natural products that are difficult to access by the aforementioned methods.^[3,7,8]

In mutasynthesis, a specific enzyme in the biosynthesis of the natural product is genetically switched off in the producing organism, so that the precursor can no longer be produced. However, biosynthesis can be restored by feeding the precursor or its derivatives, the so-called mutasynthons (Figure 1).^[9] The major advantage over precursor-directed synthesis, which is also used, is that in mutasynthesis the competition between the natural starting material and the unnatural chemical derivative can be overcome, leading only to the production of the desired unnatural derivative.

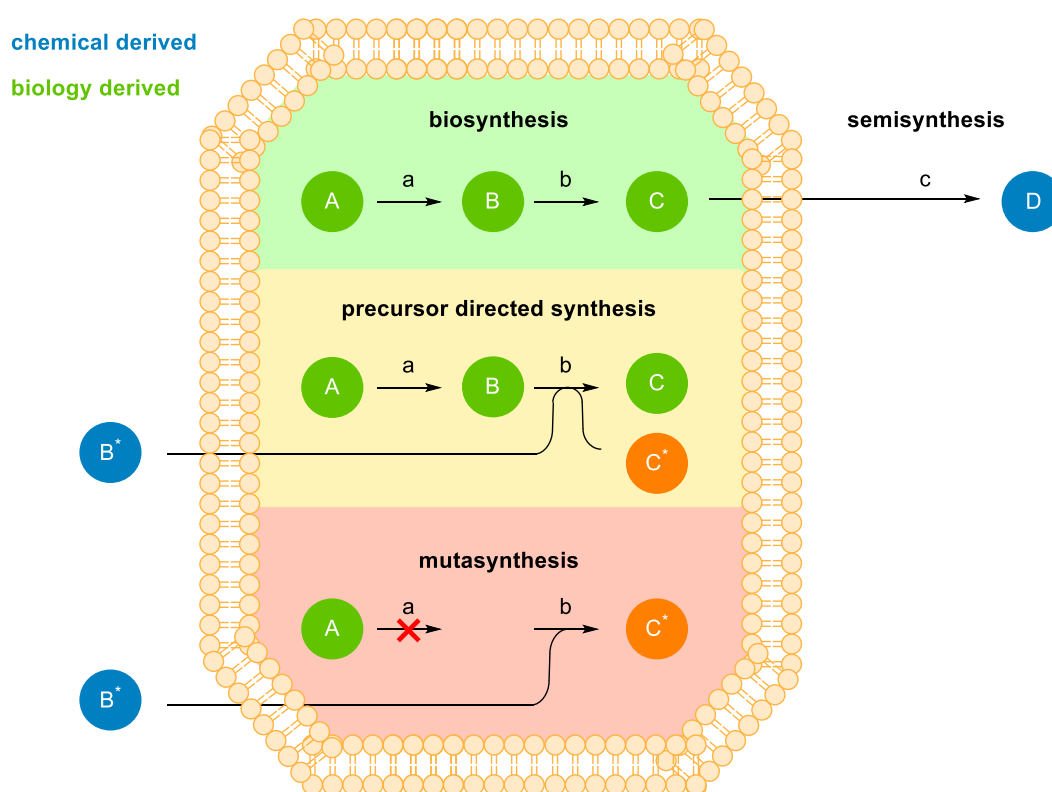


Figure 1: The chemical and biological aspects of semisynthesis, precursor directed synthesis and mutasynthesis. A: starting material, B: intermediate, C: natural product, D: semisynthetic derivative of C. The asterisk exemplifies derivatives.

2.2 Ansamitocin

The three modifications of ansamitocin P-2 (**1**), P-3 (**2**) and P-4 (**3**) were first isolated in 1977 by HIGASHIDE *et al.* from the bacterium *Actinosynnema pretiosum* ssp. *pretiosum*^[10] and belong to the maytansinoids, named after maytansine (**4**). Maytansinoids represent a group of polyketide natural products isolated from plant extracts^[11–13], mosses^[14] and bacteria^[10,15,16] that, with few exceptions, differ only in their C3 ester side chain.^[17] It is likely that maytansinoids from plant isolates are produced by symbiotic endophytes rather than by the plant itself.^[16]

Maytansinoids belong to a family of bioactive macrolactams called ansamycins. This group is characterized by an aromatic moiety branched with a polyketide chain.^[18] Other popular representatives of this group are the antibiotic rifamycin B (**5**) and the heat shock protein 90 (Hsp90) inhibitor geldanamycin (**6**) (Figure 2). The core structure of maytansinoids is the 19-membered macrolactam consisting of a single aromatic ring and a polyketide substitution pattern, that is highly conserved among the isolated members.^[17]

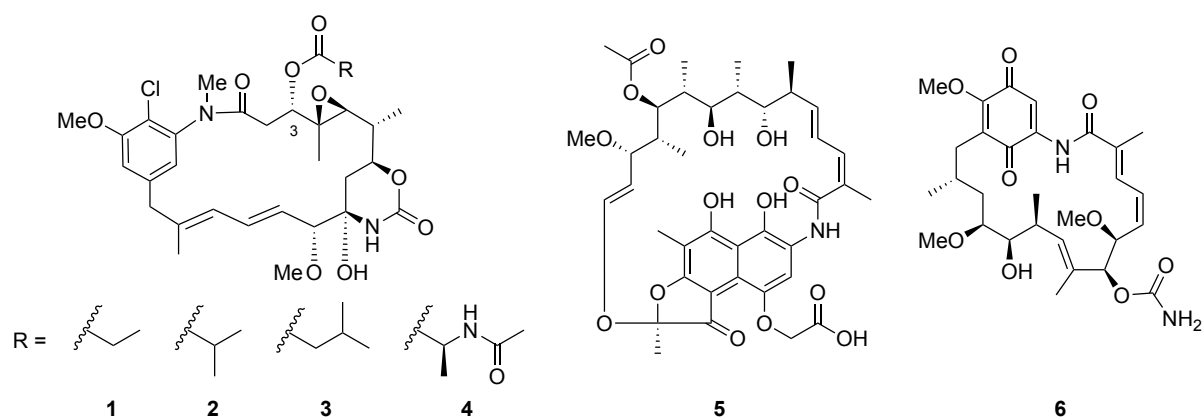


Figure 2: Structure of maytansinoids ansamitocin P-2 (1), P-3 (2), P-4 (3), maytansine (4) and two other members of the ansamycin family rifamycin B (5) and geldanamycin (6).

2.2.1 Bioactivity

Maytansinoids destabilize microtubules by binding on the β -tubuli subunit^[19] and have therefore been studied for cancer treatment since the 1980s. However, phase II trials with unmodified maytansine had to be discontinued because the cytotoxic side effect limited the possible dose range.^[20] The maytansinoid antibody conjugate trastuzumab-DM1 (Figure 3) against human epidermal growth factor receptor 2 (HER2) -positive breast cancer was approved in 2013 for patients with metastatic breast cancer already treated with trastuzumab/taxane.^[21] Our group is currently investigating the use of ansamitocins in conjunction with superparamagnetic iron oxide nanoparticles (SPION) for selective release of ansamitocins in an external oscillating magnetic field. The combination of hyperthermia and release of cytotoxins provides a promising tool for cancer treatment.^[22,23]

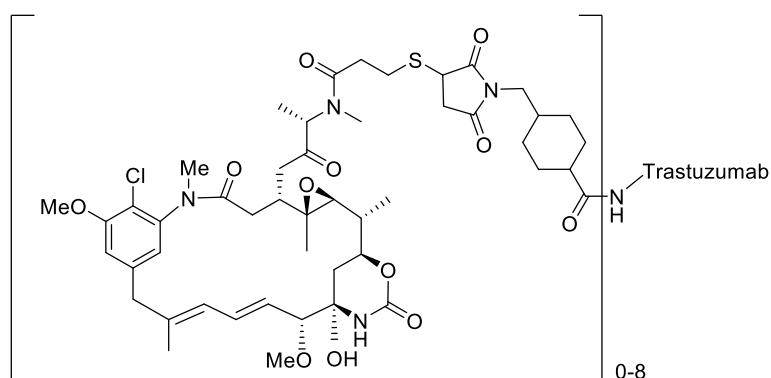


Figure 3: Kadcycla™, a maytansine trastuzumab drug conjugate targeting HER2-positive breast cancer.

Since the 1980's, extensive SAR studies have been performed with maytansinoids to determine the characteristics of the polyketide relevant to bioactivity. Therefore, many

naturally occurring maytansinoids and semisynthetic derivatives have been tested for their inhibition of microtubule synthesis (Figure 4). From naturally occurring maytansinoids lacking the C3 ester, as well as from semisynthetic saponified constructs, it was found that the ester was crucial for bioactivity, while the nature of side chain did not matter.^[24–26] The importance of the carbinolamide for bioactivity was evaluated by a combined biosynthetic, mutasynthetic and semisynthetic approach.^[27] The irrelevance of the substituents on the aromatic moiety was also elucidated with mutasynthetically generated derivatives.^[28,29] Neither the *N*-methyl^[30] nor the epoxide at C4-5^[26] have any effect on tubulin inhibition, and in fact the entire chain from C10 to the arene does not appear to interact with the target, since derivatizations at this position do not alter the bioactivity.^[11–13]

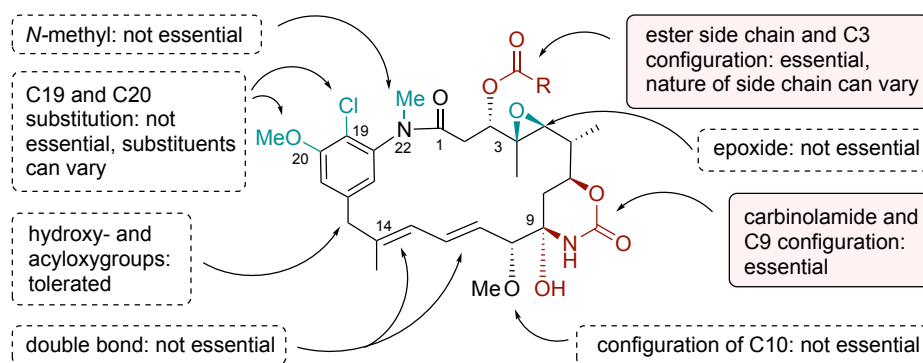


Figure 4: SAR correlations of maytansinoids (modified figure from CASSADY *et al.*^[17]).

For a long time, it was assumed that maytansines would bind to the microtubules on the binding side of the vinca domain, since competitive binding with vinblastine was found.^[31] However, when the first crystal structure of the β -tubulin subunit entrapped with maytansine was published, it became clear that maytansine, together with rhizoxin, occupied a different binding site than vinblastine. The competitive binding is likely due to prevention of formation of the full vinca domain located between α - and β -tubulin from two different α,β -tubulin heterodimers. Since maytansine inhibits the addition of the tubulin subunits, no such dimer can be formed.^[19]

The crystal structure very well shows what the SAR studies have already revealed: Binding occurs via the carbonyl oxygen of the C3 ester interacting with N101 and the carbonyl oxygen of the carbinolamid interacting with N102 and K105. The amid carbonyl of the macrocycle is also involved in the bonding, as is the C9 hydroxy group (Figure 5).^[19] Importance of the latter has been already observed by etherification, but has been attributed to blockage of the carbinolamide.^[25]

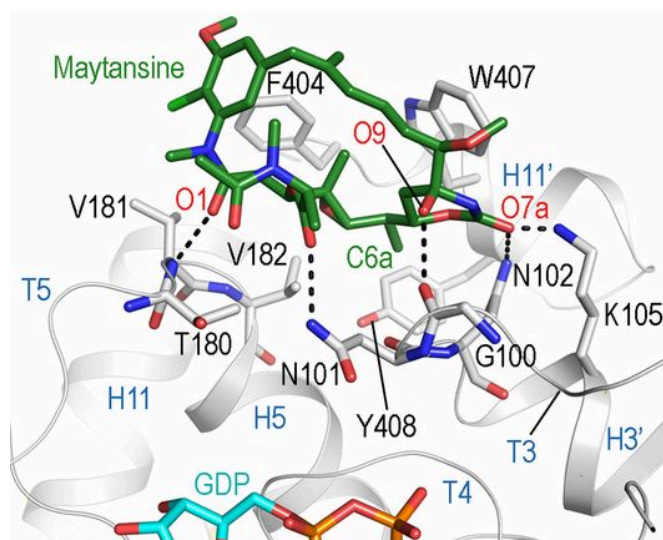


Figure 5: Structures of the tubulin–maytansine and tubulin–PM060184 complexes and pharmacophore model.^[19]

2.2.2 Biosynthesis

Just like the other ansamycins^[32], ansamitocin is biosynthesized by type I polyketide synthase (PKS) with amino hydroxy benzoic acid (AHBA, **7**) as starting unit. AHBA (**7**) is synthesized from UDP-glucose (**8**) via a modified shikimate pathway that incorporates aminodehydroquinone instead of dehydroquinone.^[33,34] AHBA (**7**) is then introduced by a non-ribosomal peptide synthase (NRPS)-like loading module. Its adenylation domain (ADE) transfers AHBA (**7**) to the phosphopantetheinyl side chain of the first acyl carrier protein (ACP), which has also been described for rifamycin B (**5**).^[35,36] Seven modules, encoded on four genes (*asmA-D*), are responsible for elongation of the polyketide chain and introduce malonyl-CoA (module 2, 4 and 7), methylmalonyl-CoA (module 5 and 6) and methoxymalonyl (module 3), which is transferred to the PKS along with its own ACP domain.^[35,37]

The double bond shift of $\Delta_{10,12}$ to $\Delta_{11,13}$ is initiated by a vinylogous *syn*-dehydration from the dehydroxygenase (DH) of module 3.^[38] The complete polyketide chain is finally released from module 7 by the amide synthase *Asm9* with simultaneous macrocyclization, giving rise to the macrocyclic backbone proansamitocin (**9**).^[35] The gene products of *asm12* (halogenation), *asm7* (20-*O*-methylation), *asm21* (carbamylation), *asm19* (acylation), *asm11* (epoxidation) and *asm10* (*N*-methylation) perform the post-PKS modification steps in the order presented to yield the ansamitocins, exemplified here by ansamitocin P-3 (**3**) (Figure 6).

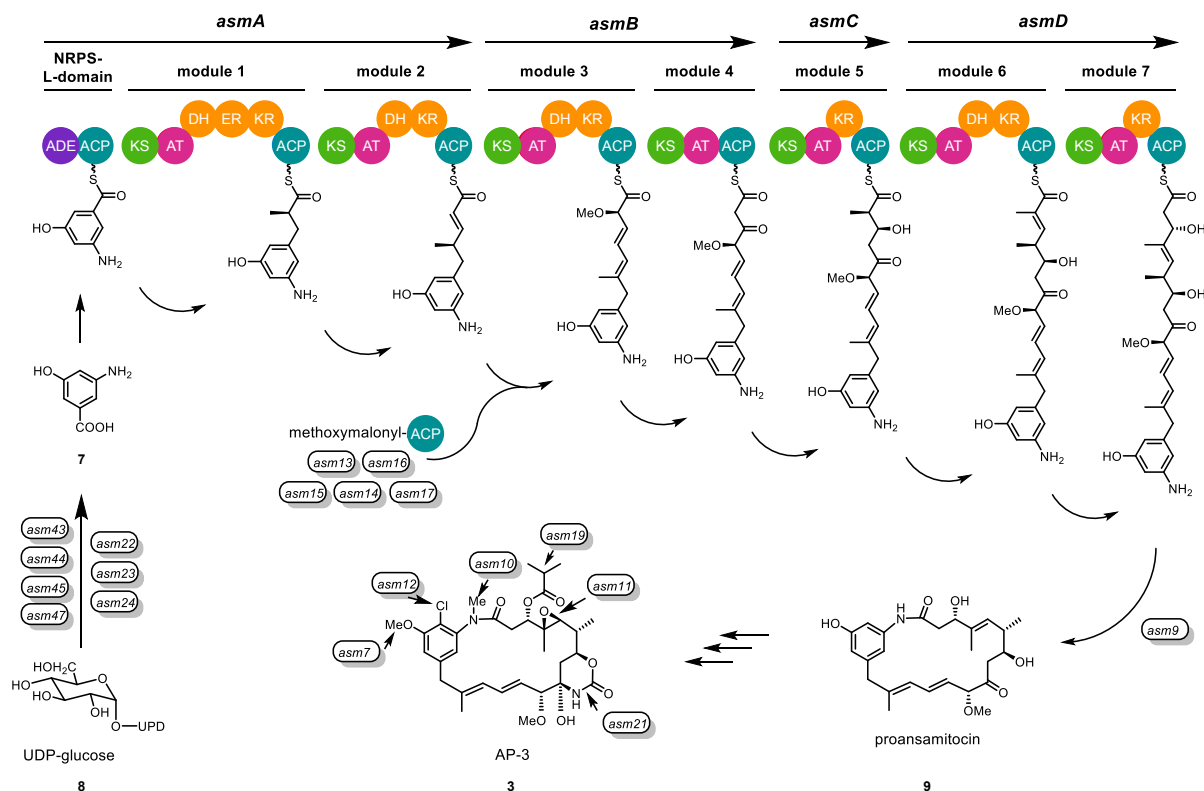


Figure 6: Biosynthesis of ansamitocin.^[35,37,39]

2.3 Previous Mutasyntheses with AHBA Knock Out Mutants

To elucidate the biosynthesis of ansamycins such as ansamitocin, Δ AHBA knock out mutants were generated, which were available for mutasynthesis.^[35,40] A large number of ansamycin derivatives, especially from ansamitocin and geldanamycin (6), were generated by this method, varying in the aromatic ring, quinolone ring or the substituents on the polyketide chain. Some of the geldanamycin derivatives were even more active than the natural geldanamycin.^[28,29,41–43] However, mutasynthesis with rifamycin B (5) resulted only in the isolation of prematurely aborted tetraketides.^[44] For mutasynthesis with ansamitocin, another mutant of *A. pretiosum* was generated that not only lacked the genes for AHBA production, but also could not perform post-PKS modifications due to deletions of genes *asm12* and *asm21*, named AH1. This allows the mutasynthesis of proansamitocin (9) derivatives.^[45]

Particularly remarkable was the result after feeding hydroxymethylbenzoic acid (10) to the Δ AHBA mutant of the geldanamycin producer *Streptomyces hygroscopicus*, which yielded not only the expected macrolactam 11 and derivatives, but also the ring-expanded macrolactone 12 (Scheme 1). Other hydroxymethyl benzoic acids 13–16 also yielded the corresponding macrolactone derivatives after feeding experiments, and with

4 Results and Discussion Part I

4.1 Identification of New Proansamitocin Derivatives

Several known^[27] and new proansamitocin derivatives were isolated from the fermentation of Δ AHBA, Δ *asm12/21* *A. pretiosum* strain AH1 with natural AHBA (7).^[45] One of the structures found in the fermentation of strain AH1 from previous studies was elucidated. NOE experiments with irradiation on protons on carbon 12, 13 and the 14-methyl group revealed an unprecedented *Z*-configuration of the C₁₃-C₁₄ double bond of proansamitocin resulting in $\Delta_{13,14}$ -*Z*-proansamitocin **28**. The $\Delta_{11,12}$ -*Z*-proansamitocin **29** has also been reported previously^[45], but the origin for the unnatural *Z*-configurations can only be speculated (Figure 8).

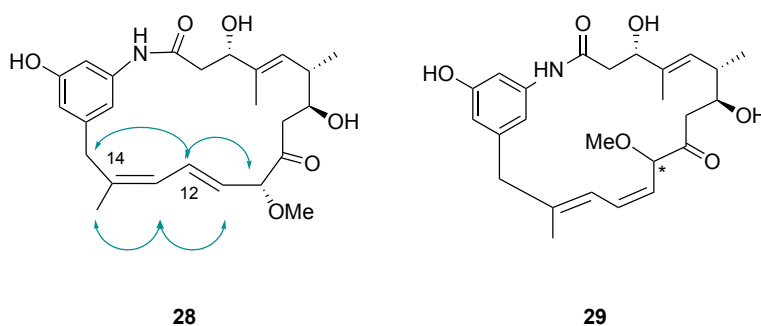


Figure 8: $\Delta_{13,14}$ -*Z*-proansamitocin **28**, a structure elucidated from isolates of previous studies. Blue arrows indicate the NOE interactions compared to already described $\Delta_{11,12}$ -*Z*-proansamitocin **29**.

Previous biosynthetic studies have shown that the shift of the double bond from the natural position $\Delta_{10,12}$ to $\Delta_{11,13}$ in ansamitocin takes place at module 3 of the PKS. The shift is thought to be initiated by vinylogous *syn*-dehydration from the DH domain between the hydroxy group at C3 and the proton at C6. An additional hydrogen bond between the catalytic H194 to the methoxy group at C10 would facilitate the α,β -*syn*-dehydration (Figure 9, case A).

The formation of the *E*-double bond, as found in **29**, would only be possible if the vinylogous dehydrogenation occurs in an *anti*-manner. This could be initiated if proton H194 coordinates the carbonyl moiety instead of the methoxy group (Figure 9, case B). Applying this concept to the *Z*-configuration of the $\Delta_{11,13}$ -double bond as in proansamitocin **28**, the stereochemistry of C6 would either have to be inverted or the aminobenzyl group would have to change its orientation in the active side of the pocket. The latter could be stabilized by other aromatic amino acids (Figure 9, case C and D).

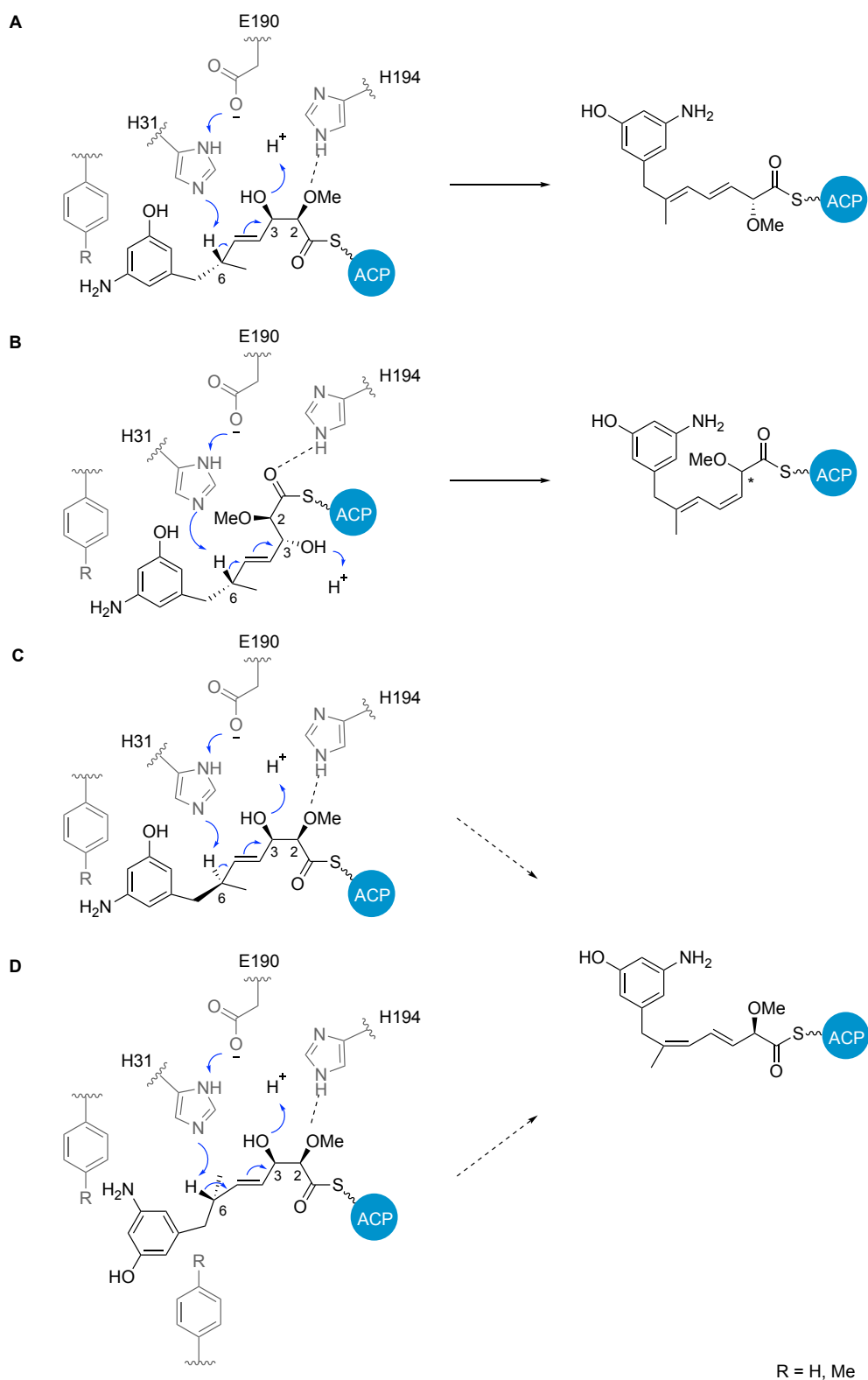
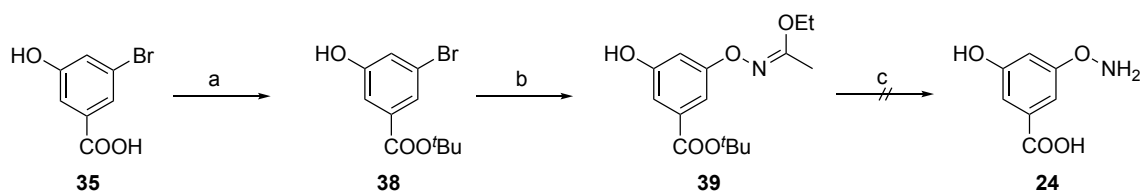
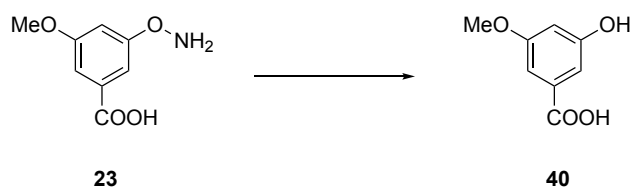


Figure 9: A: Proposed vinylogous *syn*-dehydration mechanism by DH of module 3 for the generation of natural $\Delta_{11,12}$ *E*-double bonds in proansamitocin compared to a possible *anti*-dehydration mechanism (B) to yield *Z*- $\Delta_{11,12}$ proansamitocin **29** C/D: Potential conversion yielding to the *Z*- $\Delta_{13,14}$ -double bond as in derivative **28** with an inverted confirmation at C-14 (C) or different orientation in the active pocket (D).



Scheme 6: Synthesis of hydroxyl-hydroxylamine benzoic acid **24**. a) *t*BuOH, H₂SO₄, MgSO₄, CH₂Cl₂, 48 h, rt, 44%; b) **33**, 5 mol% (PdC₂H₄Cl)₂, *t*Bu-X-Phos, Cs₂CO₃, toluene, 65 °C, 22 h, 50%; c) HCl (6 M in H₂O), 1,4-dioxane, 0 °C – rt, **24** could not be isolated.

All available mutasynthons **23**, **25**, **26** and **30-32** were then fed to 3 x 50 mL culture broth of strain AH1 on day 3, 4 and 5 post inoculation (p.i.). The fermentation broth was extracted on day 10 p.i. and the crude mixture was examined by UPLC-MS analysis.



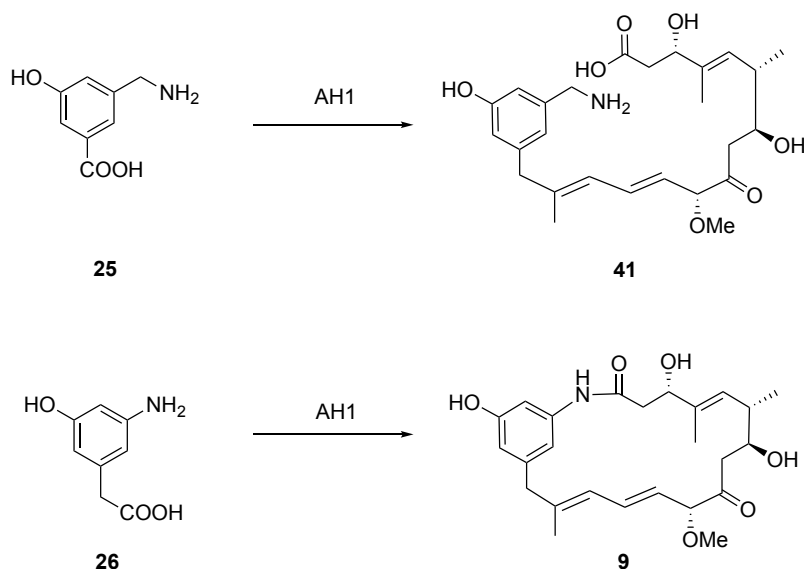
Scheme 7: Reductive cleavage of the aminoxy group of **23**. Corresponding HRMS of **40** was found in UPLC-MS analysis of EtOAc extract from culture broth (3 x 50 mL) of strain AH1 with addition of **23** on day 3-5 p.i.

Fermentation of aminoxybenzoic acid **23** gave only the reductive cleavage product **40** which was detected in HRMS (ESI) *m/z* for C₈H₇O₄ [M-H]⁻ calculated as 167.0344 and found for 167.0340 (Scheme 7). This observation is consistent with the estimate of HERMANE regarding the fermentation of **23** with Δ AHBA *S. hygrosopicus*.^[47] The reductive cleavage could either be enzyme catalyzed or occur spontaneously in the medium at 28 °C.

Next, the fermentation broth of aminomethylbenzoic acid **25** and phenylacetic acid **26** fed AH1 strain were examined. After fermentation with HGF073, no corresponding ansamitocin derivative was found from aminomethylbenzoic acid **25**. The fermentation with phenylacetic acid **26** has not been carried out with *A. prestiosum* mutants before.^[42]

In the extracts of aminomethylbenzoic acid **25** fed bacteria, the corresponding HRMS of the *seco*-proansamitocin derivative **41** was found but, no evidence of a macrolactam ring. This also explains why no ansamitocin derivative was found after fermentation of **25** with Δ AHBA mutant strain HGF073.^[42] In the case of phenylacetic acid **26**, neither proansamitocin derivatives nor the *seco*-proansamitocin was found. Instead, the mass of unaltered phenylacetic acid **26** and small amounts of proansamitocin (**9**) were found (Scheme 8). The

presence of proansamitocin (**9**) in the fermentation broth implies that phenylacetic acid (**26**) was converted to AHBA (**7**) by enzymes from *A. pretiosum*. One mechanism could be the oxidation of the benzyl position in **26** followed by oxidative decarboxylation yielding AHBA-CoA similar to the synthesis of acetyl-CoA from pyruvate.^[45]



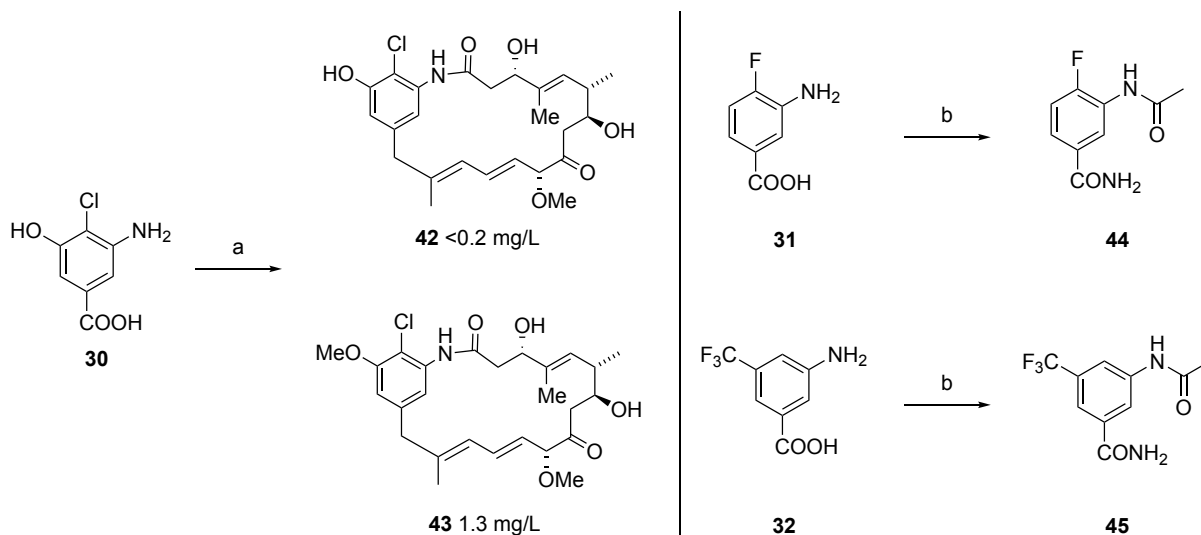
Scheme 8: Fermentation of aminomethylbenzoic acid **25** and phenylacetic acid **26** with strain AH1 to *seco*-proansamitocin derivative **41** and proansamitocin (**9**) respectively. Corresponding HRMS of **41** and **9** were found in UPLC-MS analysis of EtOAc extract from culture broth (3 x 50 mL) of strain AH1 with addition of **25** or **26** on day 3,4 and 5 p.i.

Finally, the fermentation broth of chlorohydroxybenzoic acid **30** contained the corresponding HRMS of chloroproansamitocin **42** and chloromethoxyproansamitocin **43**. To elucidate their final structure and yield, **30** was applied to a larger scale of AH1 culture (24 x 100 mL) batch, and the proansamitocin derivatives were isolated in <0.2 mg/L and 1.3 mg/L yield, respectively (Scheme 9). In contrast to previous mutasynthetic experiments with strain AH1, the methoxylated proansamitocin **43**^[45] was the abundant fermentation product. This is due to the chlorine in position 19, which is required for complete activity of methylating enzyme Asm7.^[39]

Although 4-fluoro derivative **31** in HGF073 gave rise to the corresponding ansamitocin derivatives,^[28] only compound **44** was found in extracts from fermentation with strain AH1 in HRMS, which was derived from a detoxification process of the organism. The absence of the desired product 19-fluoroansamitocin in this work was expected, since the reaction of **31** with HGF073 also led to 20-demethoxy-19-fluoroansamitocin in low yield (1.5 mg/L).^[28] Given

that the strain AH1 provides even lower yields of mutasynthetic derivatives, 19-fluoroproansamitocin could be formed at concentrations below the detection limit.

Similarly, 5-trifluoromethane derivative **32** gave the acylated compound **45**, but this consisted with the results of fermentation of **32** with strain HGF073 (Scheme 9).^[29]



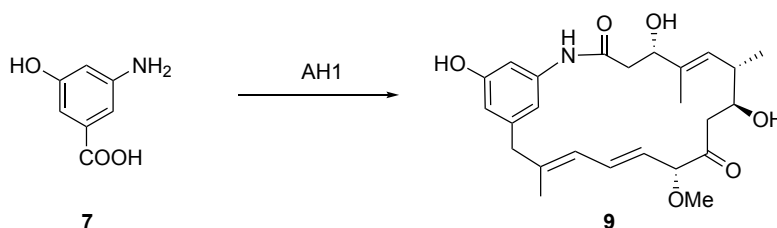
Scheme 9: Fermentation of aminohydroxychlorobenzoic acid **30**, fluorobenzoic acid **31** and trifluoromethanbenzoic acid **32** with strain AH1 to proansamitocin derivatives **42** and **43** the corresponding acylated detoxification products **44** and **45**. a) Chloroproansamitocin **42** and methoxy chloroproansamitocin **43** were isolated from of **41** EtOAc extract from culture broth (24 x 100 mL) of strain AH1 with continuous addition of **30** from day 3-5 p.i.; b) Corresponding HRMS of **44** and **45** were found in UPLC-MS analysis of EtOAc extract from culture broth (3 x 50 mL) of strain AH1 with addition of **31** and **32**, respectively on day 3,4 and 5 p.i.

4.3 Optimization of Proansamitocin (9) Production of Strain AH1

4.3.1 General Studies on Fermentation of AHBA (7) with Strain AH1

Fermentations of AHBA (7) with strain AH1 gave isolated proansamitocin (9) in 13 mg/L yield, which is much lower than the yield of ansamitocin P-3 (2) in HFG073 at 56-100 mg/L or proansamitocin (9) from $\Delta asm12/21$ *A. pretiosum* at 85 mg/L.^[27–29] The yield of proansamitocin (9) after fermentation of AHBA derivatives with strain AH1 decreased even more.^[45] However, several milligrams of macrolactone 21 are required for further semisynthesis towards 27.

Therefore, the fermentation conditions of strain AH1 with the precursor AHBA (7) were optimized to achieve higher yield of proansamitocin (9) (Scheme 10). Quantitative yields were calculated by comparing the integral of the product MS-signal (proansamitocin (9), $m/z[M+Na^+] = 466$) to the integral of the internal standard nimodipine. All experiments were performed in triplets. The calibration is shown in the experimental section.



Scheme 10: Fermentation of AHBA (7) with strain AH1 to proansamitocin (9) for optimization of fermentation conditions.

The K-medium from previous studies on ansamitocin 3 mutasynthesis was chosen as initial medium for optimization and used for the fermentation of HGF073 and $\Delta asm12/21$ *A. pretiosum*. First, the timepoint of highest proansamitocin (9) titers during the fermentation of strain AH1 was investigated. Three independent fermentations were performed, and samples were taken in different intervals (Figure 11, case A). Interestingly, the maximum concentration of proansamitocin (9) was reached 4 days earlier when samples were taken every 12 hours compared with fermentations in which samples were taken every 24 h or 48 h. The production rate of proansamitocin (9) is greatly increased when samples are taken more frequently, but titers also decrease more rapidly, so that only half the maximum concentration is observed on day 10 p.i. When samples were taken every 24 h or 48 h, the highest titers were measured at day 10 p.i., which is consistent with previous results.^[45]

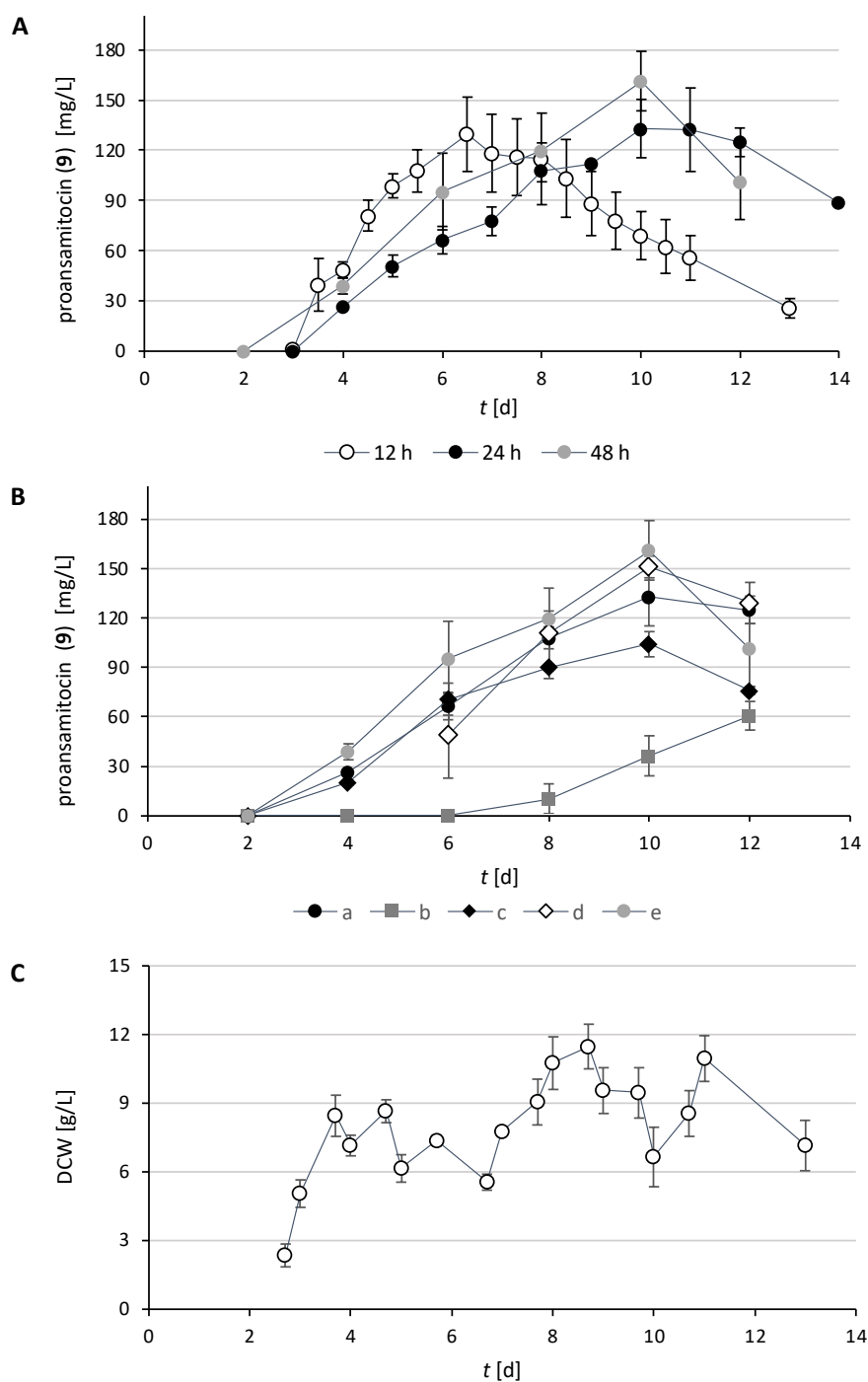


Figure 11: Proansamitocin (**9**) concentration during fermentation of strain AH1 in 50 mL K-medium with addition of 21 μ M AHBA on day 3, 4 and 5 p.i. A: Samples were taken at intervals of 12 h, 24 h and 48 h. B: Five independent experiments (a-e) are compared. C: DCW throughout the fermentation. Shown are the standard deviations from the mean ($n = 3$).

The strong differences in proansamitocin (**9**) production presented in Figure 11, case A could be due to a higher stress level of the cells during sampling. This might trigger the production of secondary metabolite production and thus proansamitocin (**9**).

Figure 11, case B shows the concentration of proansamitocin (**9**) from five independent experiments (a-e) during fermentation of strain AH1 with in K-medium. The graph clearly shows that the concentrations vary greatly from one fermentation to another. Despite these differences in product titers, all fermentations except experiment b give the highest concentrations on day 10 p.i. as shown also in Figure 11, case A. Therefore, for further investigation, samples were taken on day 10 p.i. and compared using K-medium as a control.

Compared to the isolated proansamitocin yields of 13 mg/L, the analytical yields of proansamitocin are on average between 100 mg/L and 150 mg/L and thus about 10-fold higher. This indicates either potential for improvement of the isolation process or a bias in the analytics, e.g., due to the use of the structurally very different compound nimodipine as an internal standard.

In addition, the dry cell weight (DCW), and thus cell growth, was investigated (Figure 11, case C). Since the cells accumulate, it is difficult to get an appropriate sample from a small portion of the fermentation broth. Despite the huge variations between single results, the exponential cell growth until day 3 or 4 p.i. from 2 g/L until over 6 g/L. The cells then reach the stationary phase with 6 - 11 mg/L. Since secondary metabolites are known to be produced in stationary phase^[50], this correlates well with the onset of proansamitocin (**9**) production starting from day 4.

4.3.2 Additional L-Leucin, L-Valine and *iso*-Butanol

HATANO found that the addition of 1 g/L L-leucin (Leu) to the culture medium increased the total production of ansamitocins **1-3** by up to 171% in the wt *A. pretiosum* strain. Equivalent results were observed with additional 1 g/L L-Valin (Val) and 0.1 g/L isobutyl alcohol (*i*BuOH), which increased the production of ansamitocins **1-3** by 121% and 151%, respectively. In addition, the added amino acid controls the ratio of the ansamitocin mixture. Addition of Leu results in higher percentage of ansamitocin P-4 (**3**), whereas the predominant ansamitocin after addition of Val and *i*BuOH is ansamitocin P-3 (**2**).^[51] Previous studies by this group showed that addition of 3 g/L Val further enhanced the production of ansamitocin P-3 (**2**).^[52] Another group was able to quadruple the production of ansamitocin P-3 (**2**) by adding to 0.4% *i*BuOH to the fermentation^[53]. Both Val and *i*BuOH undergo biosynthetic modifications towards isobutyryl-CoA which is loaded as an ester side chain to the alcohol in position C3 of the ansamitocin backbone, which is one reason for higher ansamitocin P-3 (**2**) titers.^[53]

It was hypothesized, that although strain AH1 does not bear enzymes for side-chain esterification, an addition such as Leu, Val or *i*BuOH could enhance the enzyme activity of the *asm* gene cluster, resulting in higher proansamitocin (**9**) titers.^[54] Therefore, fermentation experiments were performed containing 1 g/L or 3 g/L of Leu, Val, combinations thereof, and 0.4% *i*BuOH. To obtain reliable results, the more interesting additives were tested in a second or third independent fermentation.

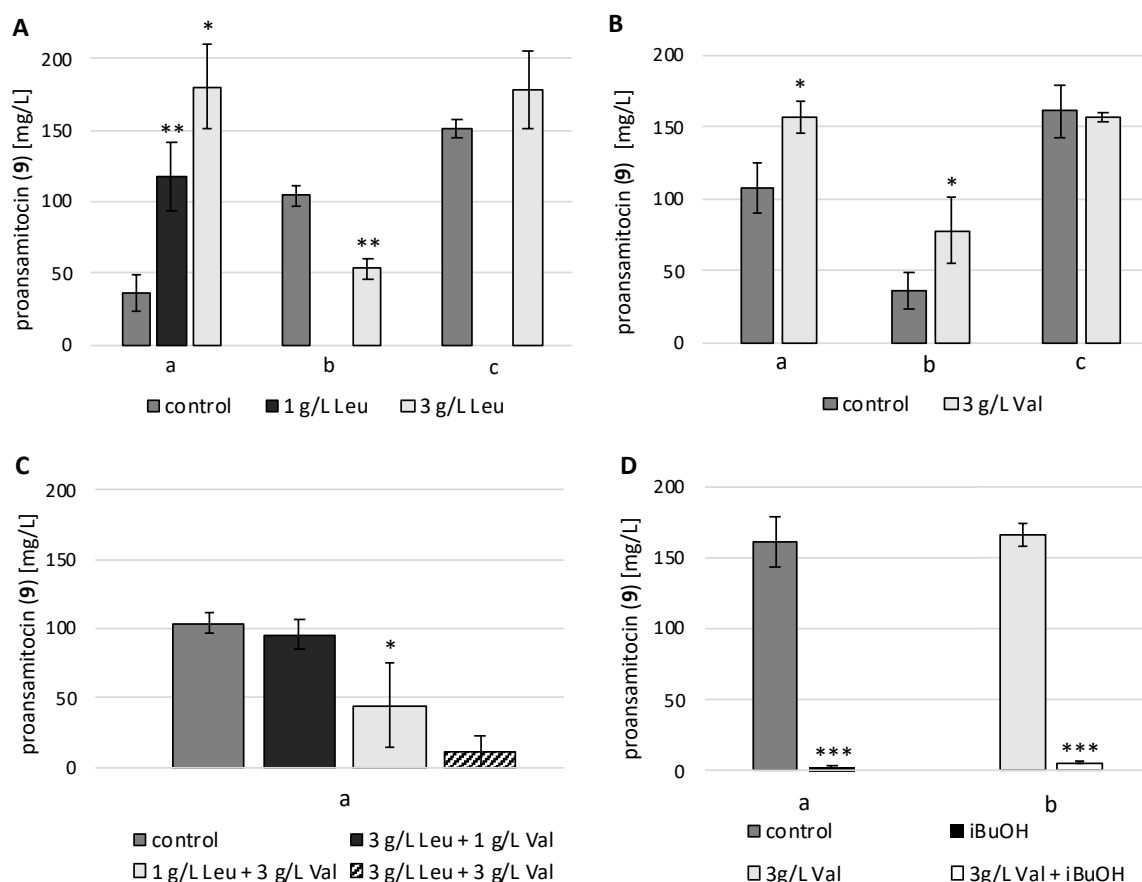


Figure 12: Proansamitocin (**9**) concentrations on day 10 p.i. from strain AH1 in 50 mL K-medium fed with AHBA (**7**), additional amino acids and *i*BuOH. Shown are the standard deviations from the mean ($n = 3$). A: Comparison of 1 g/L and 3 g/L Leu in medium to a control without Leu. Three independent experiments are shown. B: Comparison of 3 g/L Val in medium to a control without Val. Three independent experiments are shown. C: Comparison of different combinations of Leu and Val in medium to a control without amino acids. D: Comparison of additional 0.4% *i*BuOH in medium with and without 3 g/L Val to a control without *i*BuOH. Two independent experiments are shown. * = $P < 0.1$, ** = $P < 0.01$, *** = $P < 0.001$ compared to “control”.

From the results in Figure 12 A and B, it can be seen that neither the addition of Leu nor Val, significantly enhanced the proansamitocin (**9**) concentration. In experiment in Figure 12,

case Aa additional 3 g/L Leu increased the proansamitocin (9) titer more than 4-fold. However, this could not be repeated in the independent experiments Figure 12, case Ab and Ac. The large increase was probably whitewashed by the low titer of the control in this particular experiment. In experiment Figure 12, case Ab, the proansamitocin (9) concentration actually decreased significantly compared with the control, and in Figure 12, case Ac, titers were comparable to those of Aa but not significantly higher than those of the control. Thus, it was postulated that additional Leu did not significantly increase proansamitocin (9) titers.

The addition of Val significantly increased the proansamitocin (9) titer in Figure 12, case Ba and Bb. Only in Figure 12, case Bc was the proansamitocin (9) concentration the same with and without Val.

Combinations of additional Leu and Val show no positive effect. Rather, the increased amino acid concentration appeared to inhibit proansamitocin (9) production (Figure 12, case C). Contrary to the expectations, the addition of 0.4% *i*BuOH almost extinguished the production with and without additional Val (Figure 12, case D). Because Val increased proansamitocin (9) concentration in 2 of 3 cases and no decrease was ever observed, it was decided to use an additional 3 g/L Val in further experiments.

4.3.3 Additional Coconut water, Gibberellic Acid and Fructose

For fermentation with HGF073, 3% v/v additional coconut water (CW) is reported to increase the isolated ansamitocin P3 (2) amount by 2-fold, which is probably caused by the phytohormone gibberellic acid (GA, 10 µg/mL).^[52] Also, pulse feeding of 2.5 g/L fructose on day 3, 4 and 5 of fermentation resulted in a 4-fold increase in ansamitocin P-3 (2) titers in wt *A. pretiosum*.^[55] Herein, all three additives were tested at the reported concentrations for their effect on proansamitocin (9) production in strain AH1. Additives CW and GA were tested with and without 3 g/L Val in K-medium, whereas additional fructose was tested only under conditions together with Val (Figure 13, case A and B).

Unfortunately, CW was found to significantly inhibit the production of proansamitocin (9) in strain AH1 with and without 3 g/L Val. Addition of the pure phytohormone GA resulted in significantly lower concentrations when Val was in the medium. However, even without Val, the titers were not significantly higher compared to the control. In contrast, pulse feeding of 2.5 g/L fructose dramatically increased production 2-fold in the first experiment (Figure 13, case A).

Fermentation with K-medium containing 3 g/L Val was repeated in an independent experiment with and without fructose pulse feeding (Figure 13, case B). Proansamitocin (**9**) titers in this experiment were generally much lower than those in Figure 13, case A. Pulse feeding of fructose did not significantly increase titers.

From this experiment, the positive effect on proansamitocin (**9**) titers during fermentation with CW or GA as additives could not be confirmed for strain AH1. Pulse feeding of fructose significantly increased titers in one of two experiments, although given the wide variation between independent fermentations, the experiments need to be validated by more experiments.

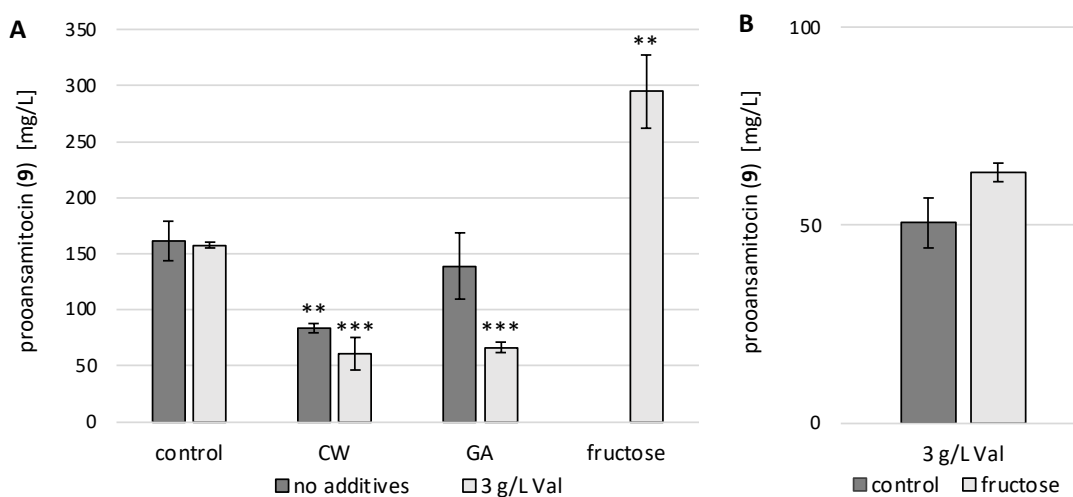


Figure 13: Proansamitocin concentration on day 10 p.i. with strain AH1 in 50 mL A: K-medium and medium with 3 g/L Val compared to media containing 3% (v/v) CW, 10 µg GA and pulse feeding of 2.5 g/L fructose on day 3, 4 and 5 p.i.; B: K-medium containing 3 g/L Val with and without pulse feeding of 2.5 g/L fructose on day 3, 4 and 5 p.i. Shown are the standard deviations from the mean (n = 3). * = P 0.1, ** = P 0.01, *** = P 0.001 compared to “control”.

4.3.4 Medium Variation

In addition to the K-medium used for mutasynthesis in this laboratory, another media for fermentation of wt *A. pretiosum* from the group of ZHONG was tested for fermentation of strain AH1 (Z-medium).^[56]

The differences between K-medium and Z-medium are mainly in the carbon source (dextrin and glycerol, respectively), the additional cottonseed flour in K-medium and addition of 0.4% *i*BuOH in Z-medium.

Three independent experiments were executed and compared with K-medium media containing 3 g/L Val. Z-medium was also tested with different additives described above (Figure 14). The first experiment (Figure 14, a) showed a significant increase of proansamitocin (**9**) in Z-medium to 2-fold. Unfortunately, this result could not be repeated. In a second experiment (Figure 14, b) almost no proansamitocin (**9**) was detected in Z-medium. Proansamitocin (**9**) production could be restored in Z-medium by addition of Val or fructose.

In a third experiment (Figure 14, c), again the lowest proansamitocin (**9**) concentrations were measured in Z-medium. Regarding the large differences between the individual experiments, no clear conclusion can be drawn from this study.

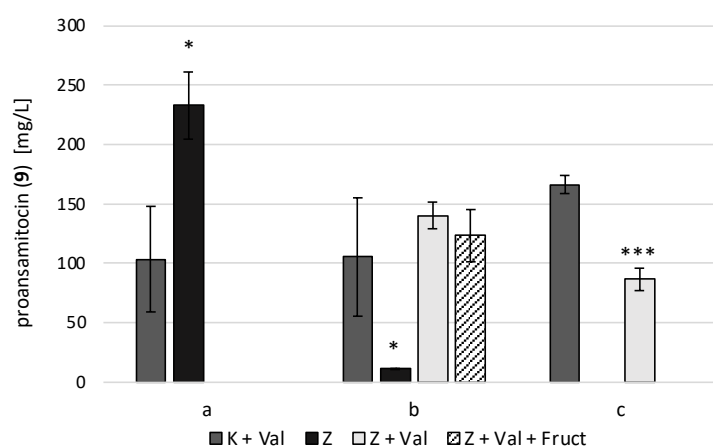


Figure 14: Proansamitocin (**9**) concentration on day 10 p.i. with strain AH1 in 50 mL media. K-medium (K) is compared to Z-medium (Z) containing different additives. Three independent experiments are presented. Shown are the standard deviations from the mean ($n = 3$). * = $P 0.5$, ** = $P 0.01$, *** = $P 0.001$ compared to “K-medium + Val”.

4.3.5 Variation of Inoculation Volume and Speed of Rotation

The inoculation volume from the preculture to the main culture influences the amount of cells during the fermentation process. The aggregation of cells makes it difficult to inoculate the exact same amount of cells to each flask. It was thus hypothesized that this variations of cells in the flask would be related to the high variation in proansamitocin (**9**) production from batch to batch. Therefore, in two independent experiments, different inoculation volumes and thus different cell quantities were tested for their effect on proansamitocin production.

From Figure 15, it is clear that the amount of cells is not significantly related to proansamitocin (**9**) production. In the first experiment (Figure 15, a), it appears that inoculation of 3 mL preculture preferred compared to 1 mL and 2 mL for which no

differences were observed. In a second fermentation (Figure 15, b), inoculation of 2 mL resulted in the highest proansamitocin (**9**) titers. No differences were observed between 3 mL and 4 mL. This result suggests that the amounts of cells used for inoculation does not significantly affect the proansamitocin (**9**) titers and that the optimal inoculation volume is somewhere between 2 mL and 3 mL.

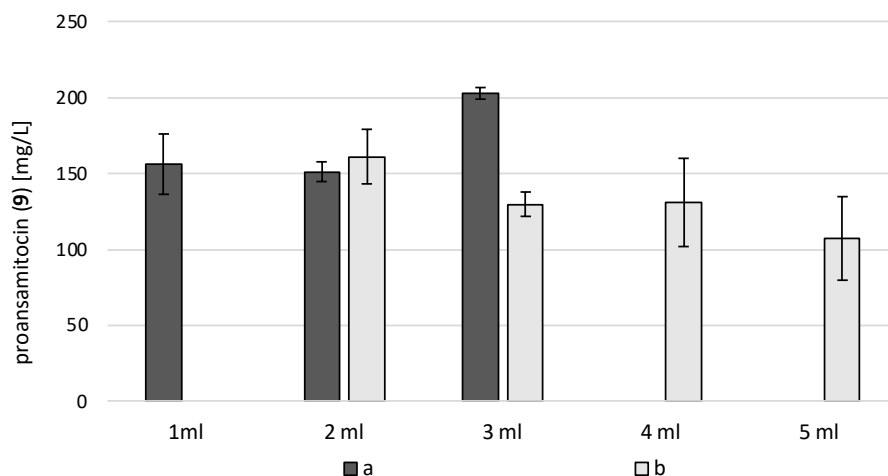


Figure 15: Proansamitocin (**9**) concentration on day 10 p.i. with strain AH1 in 50 mL K-medium and different preculture inoculation volumes. Two independent experiments (a, b) are displayed. Shown are the standard deviations from the mean (n = 3).

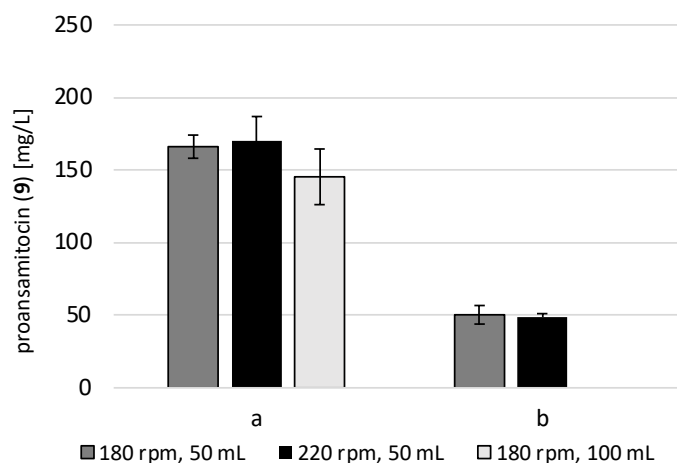


Figure 16: Proansamitocin (**9**) concentration on day 10 p.i. with strain AH1 in K-medium media + 3 g/L L-Val, 50 mL culture volume and 180 rpm are compared to 50 mL at 220 rpm (a, b) and 100 mL at 180 rpm (a). Shown are the standard deviations from the mean (n = 3).

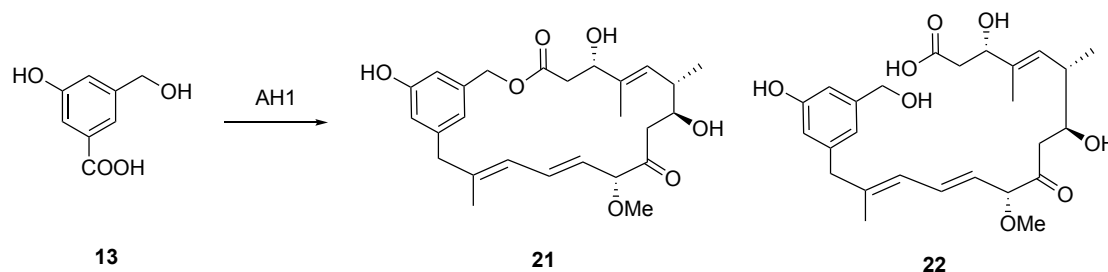
In this group, it was observed that the yield ansamitocin P-3 (**2**) decreased when HGF073 was fermented in larger volumes compared to 50 mL fermentations, which was probably due to a lower partial oxygen pressure (pO_2). The pO_2 strongly depends on the shape of the culture

flask and the rotation speed. The steel springs used in fermentation of *A. pretiosum* mutants already ensure high pO₂ with respect to the flask shape, so the rotation speed was investigated. In the literature, the rotation speeds used in fermentation of *A. pretiosum* vary between 180 rpm and 220 rpm. This group usually applies 180 rpm.^[28,29,45] To test the beforementioned hypothesis, incubation of 50 mL fermentations at 220 rpm (Figure 16, a, b) and 100 mL at 180 rpm (Figure 16, a) were compared with the initial conditions, all in K-medium with 3 g/L Val. No significant differences were observed in a first and second experiment (Figure 16).

4.4 Fermentation of Hydroxymethylbenzoic Acid **13** with Strain AH1

4.4.1 General Fermentation Studies

As discussed in section 1.3, it is known that the fermentation of 3-hydroxy-5-(hydroxymethyl)benzoic acid (**13**) yields macrolactone proansamitocin derivative **21** and the corresponding *seco*-proansamitocin derivative **22** in low yields of 1 mg/L fermentation broth (Scheme 11).^[45] In this study, large amounts of macrolactone **21** were to be obtained for further semisynthetic studies. This should be achieved by a large-scale fermentation using a 50 L BIOSTAT[®]CultiBag RM reactor.



Scheme 11: Ring-expanded macrolactone proansamitocin derivative **21** and its *seco*-proansamitocin acid **22** isolated from fermentation of strain AH1 with 3-hydroxy-5-(hydroxymethyl)benzoic acid (**13**).^[45]

Before starting the large scale fermentation of strain AH1 with hydroxymethylbenzoic acid **13** as substrate in a bioreactor, the production of **21** was studied in 50 mL scale. Different concentrations of benzoic acid **13** were tested, and K-medium + 3 g/L Val was compared to Z-medium (Figure 17). Calibration was performed with hydroxymethylbenzoic acid **13** because macrolactone **21** was not available.

In Figure 17, case A, it is shown that when the usual amount of benzoic acids of 1.13 mmol/L is used as in the previous chapter, the concentration of macrolactone **21** increases up to 3

mg/L until day 4 p.i. The concentration remained constant until day 6 p.i. and then slowly decreased to less than 2 mg/L by day 10 p.i. Significantly higher concentrations were observed with 1.3 times **13** (1.65 mmol/L), reaching over 5 mg/L on day 6 p.i. The titer slowly decreased to 4.5 mg/L on day 8 p.i. On day 10 p.i., the concentration was already less than half that on day 6 p.i. When 1.7 times the amount of **13** (2.13 mmol/L) was added, the concentration of **21** increased to 6.6 mg/L by day 6 p.i., but a dramatic decrease is observed until day 8 p.i.

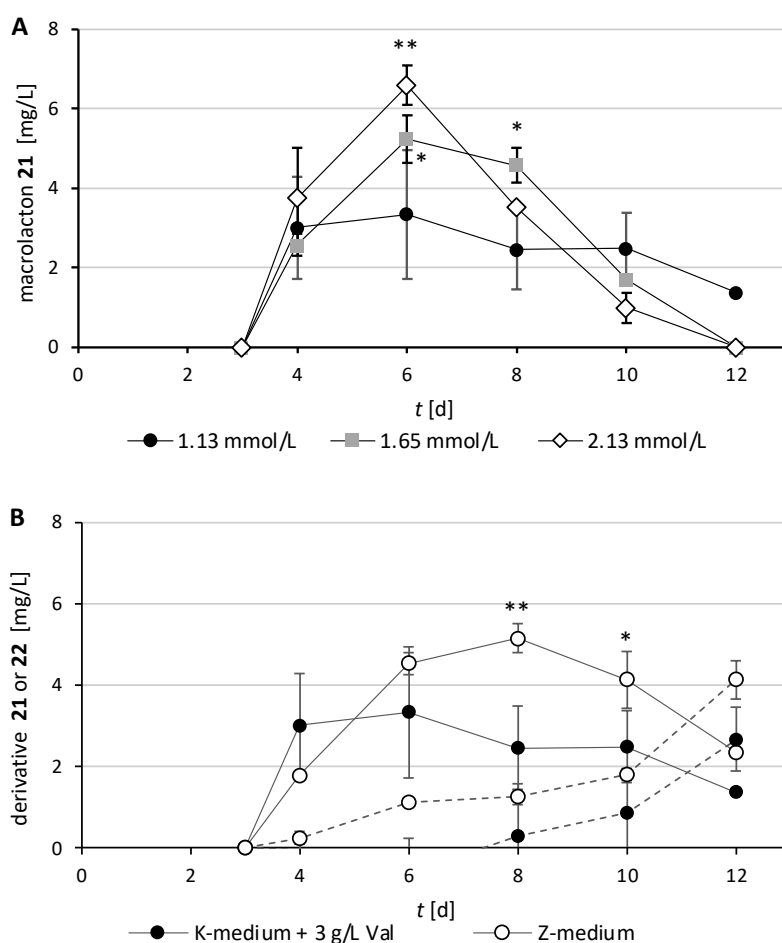


Figure 17: Concentration of macrolactone **21** (A, B) and its *seco*-acid **22** (B, dotted line) during fermentation of hydroxymethylbenzoic acid **13** with strain AH1 in 50 mL medium. A: Addition of different concentrations of **13** in K-medium with 3 g/L Val; B: Comparison of 0.13 mmol/L **13** in K-medium + 3 g/L Val and Z-medium. Shown are the standard deviations from the mean (n = 3). * = P 0.1, ** = P 0.01, *** = P 0.001 compared to “1.13 mmol/L and “K-medium + 3 g/L Val”.

From this experiment it seems that at higher concentrations of hydroxymethylbenzoic acid **13** in the medium correlate with higher concentrations of macrolactone **21**. However, an accelerated degradation of macrolactone **21** titers is observed at the highest concentration of

2.13 mmol/L of hydroxybenzoic acid **13**. Therefore, it was decided to use 1.65 mmol of hydroxymethylbenzoic acid **13** in the large scale fermentation.

When K-medium + 3 g/L Val was compared to Z-medium (Figure 17, case B), the highest titers of **21** were observed in Z-medium at 5.1 mg/L on day 8 p.i. In comparison, the highest titers of **21** in K-medium were observed on day 6 p.i. at 3.3 mg/L. As for the concentrations of the corresponding *seco*-acid derivative **22**, Figure 17, case B clearly shows the correlation between the decrease in macrolactone **21** and the increase of the acid **22** starting from day 8 p.i., suggesting that **22** is generated by hydrolytic ring-opening of **21** rather than by inefficiency of the amid synthase Asm9 during the biosynthetic pathway.

4.4.2 Large Scale Fermentation

In order to obtain a large amount of macrolactone **21**, a 25 L fermentation of hydroxymethylbenzoic acid **13** with strain AH1 was performed. For this purpose, the wave-mixed bioreactor BIOSTAT[®]CultiBag RM with a total bag volume of 50 L was selected. It consists of an inflated, pre-sterilized bag for cell cultivation placed on a rocking platform with integrated heating system (Figure 18).



Figure 18: BIOSTAT[®]CultiBag RM disposable reactor.^[57]

Fermentation was performed in 25 L of Z-medium at 28 °C, and 1.65 mmol/L benzoic acid **13** was added portion wise on day 3, 4 and 5 p.i. The pO₂ was set at 50%, which was controlled by the gas supply and rocking rate. The DCW, optical density at 600 nm (OD₆₀₀), hydroxymethylbenzoic acid **13** concentration and concentration of derivative **21** were monitored every 24 h (Figure 19).

Cell growth was monitored through DCW and OD₆₀₀ (Figure 19, case A). By day 2 p.i., an increase in DCW from 2 mg/L to 8 mg/L was observed, one day earlier than for the 50 mL scale (Figure 11, case C). DCW values vary between 8 mg/L and 10 mg/L, which is comparable to previous results. In the literature, cell concentrations around 12 mg/L are reached in a stirred tank bioreactor fermentation from day 4 p.i.^[55] In contrast, the OD₆₀₀ increases sharply until day 5 p.i. and decreases rapidly until day 8 p.i. The large differences between DCW and OD₆₀₀ can be explained by the growth of *A. pretiosum*. During cell growth, the cells spread out in the medium, leading to higher OD₆₀₀ values before they begin to accumulate into mycelia, resulting in a nearly clear medium with visible mycelia.

The concentration of hydroxymethylbenzoic acid **13** during fermentation is shown in Figure 19, case B and correlates well with the amounts added on day 3, 4 and 5. A significant decrease in concentration, which should correlate with cell uptake, is only observed between day 6 and 7 p.i., when the concentration dropped by 30 mg/L. However, already one day later, about 11 mg/L were found again in the culture, unaltered by the bacteria.

Neither derivative **21** nor **22** could be detected throughout the fermentation with the present analytics. It was initially suspected that this was due low concentrations. Therefore, the fermentation broth was extracted and separated by size exclusion chromatography to concentrate the sample. Nevertheless, no corresponding mass could be detected in the HRM spectrum. Thus, the large-scale fermentation of strain AH1 using the bioreactor BIOSTAT[®]CultiBag RM was unsuccessful.

One reasons could be the large fluctuations between the individual fermentations explained in chapter 3.3. Also, further experiments with the Z-medium in 3.3.4 showed that Z-medium sometimes does not yield any proansamitocin (**9**) at all and thus may not be the optimal medium for fermentation. In the end, the BIOSTAT[®]CultiBag RM may not be the appropriate reactor for fermentation with strain AH1. Wave-mixed bioreactors are particularly known for their low shear stress, which is why they are popular for eucaryotic cell culture or for production of shear-sensitive biomolecules.^[57] Mutasynthetic fermentation of *A. pretiosum* in small 100 mL flasks was always supported with a steel spring to ensure better oxygen supply and mixing. These conditions are associated with high shear stress, which might be necessary for production of secondary metabolites such as ansamitocins.

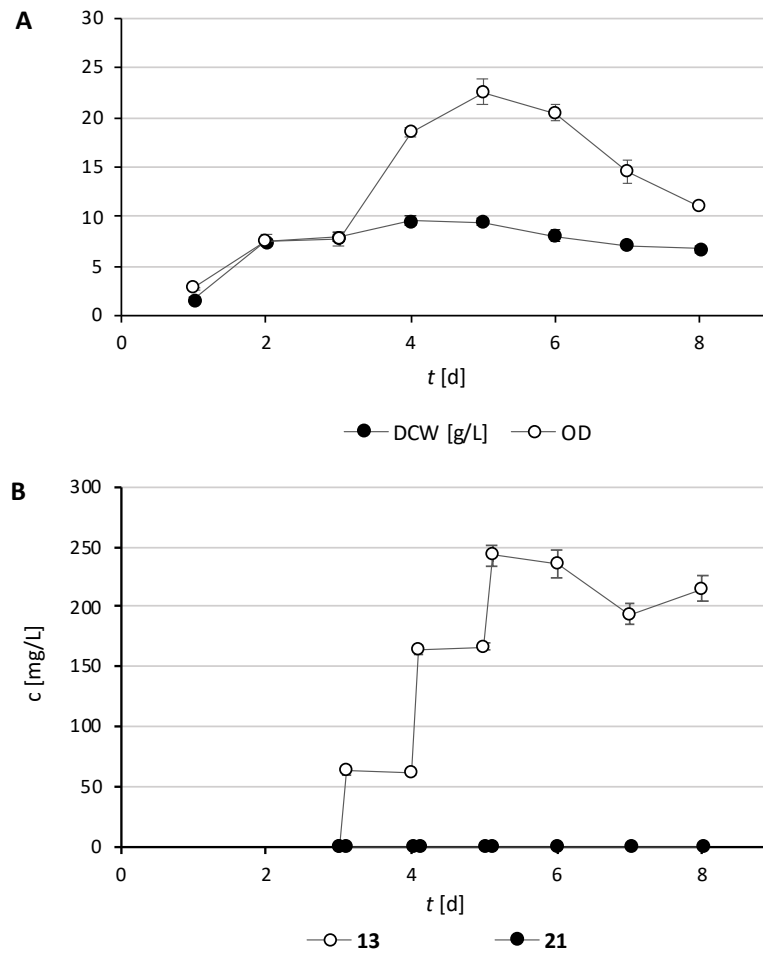


Figure 19: 25 L fermentation of strain AH1 in a 50 L BIOSTAT®CultiBag RM with Z-medium and addition of 1.65 mmol/L benzoic acid **13** addition portion wise on day 3, 4 and 5 p.i. A: DCW and OD; B: Concentration of macrolactone **21** and benzoic acid **13**. Shown are the standard deviations from the mean (n = 3).

5 Introduction Part II

5.1 Nanoparticles to Combat Antimicrobial Resistance

The discovery and development of antibiotics for bacterial infection treatment has rapidly revolutionized medicine in the last century. However, in the last 60 years, bacterial resistance to antibiotics and lack of new antibiotics pose a major threat to the world.^[58] Efforts are being made towards drug discovery from so far under-explored environments using genetics and molecular biology or synthetic strategies to develop new antibiotics.^[58,59] Another promising tool to combat antibiotic resistances is the combination of nanocarriers with antimicrobials. These nanoparticles are able to overcome several drawbacks of antibiotics already approved and under development, such as poor solubility and stability, low bioavailability, difficulty in reaching the site of action, and thus the need for high doses associated with severe side effects and toxicity.^[60-62]

The antibacterial effect of antibiotic nanoparticles can derive from the nanocarrier itself, as in case of nanoparticles made of the antimicrobial polymers such as chitosan^[63], or from metals that inherit antimicrobial activity like silver or SPIONs^[64]. This effect can be enhanced in combination with antimicrobial compounds.^[61] In addition, resistance to antibiotics can be overcome when co-administered with nanoparticles, even if the nanoparticles themselves do not have antibiotic activity.^[65]

5.1.1 Nanoparticles in Biomedicine

Nanoparticles are particles of material with a diameter of 1-100 nm.^[66] For many elements, this reduction in size is accompanied by a variety of properties different from those of the bulk material.^[67] Since the end of the 20th century, nanoparticles have been studied and used for therapeutics^[68], diagnostics^[69,70] and theranostics^[71,72] in medicine.

A biomedical nanoparticle consists of a nanocarrier and active compounds that are either bound on the nanocarriers surface or entrapped inside the nanocarrier. These compounds may be the active ingredient of a drug, dyes or magnetic particles for bioimaging, or targeting structures for targeted delivery, preferably attached to the outer nanoparticle surface.^[73]

Various classes of nanocarriers can be used in biomedicine, such as lipid-based nanocarriers^[74], polymeric nanocarriers^[68,75], inorganic nanocarriers of silica^[76], gold^[77] or iron oxide^[72], and combinations thereof.^[73] Among them, lipid-based nanocarriers are by far the most popular as they are currently used as vehicles for the mRNA vaccines against pandemic respiratory syndrome coronavirus 2.^[78]

5.1.2 Superparamagnetic Iron Oxide Nanoparticles

SPIONs are nanoparticles of maghemite (Fe_2O_3 , $\gamma\text{-Fe}_2\text{O}_3$) or magnetite (Fe_3O_4). Below a size of 20-30 nm they exhibit superparamagnetic properties that are of particular interest in biomedical diagnostics, therapeutics, theragnostic and targeted delivery.^[72,79,80]

Coating of SPIONs is critical for colloidal stability, but also for biocompatibility, bioavailability, and introduction of functional groups for further modifications.^[72,73,81] Surface modification can be conducted either during or after the SPIONs synthesis. They can be of monomeric, polymeric or inorganic origin (Figure 20).

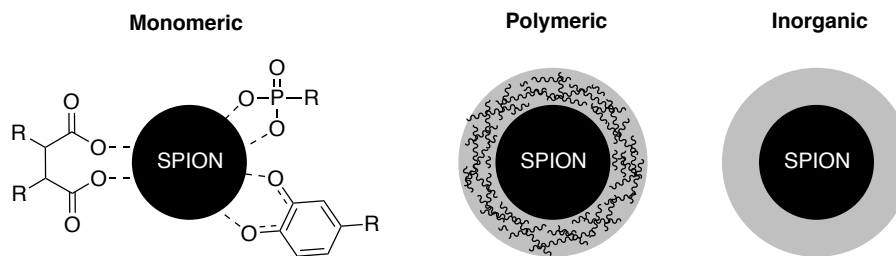


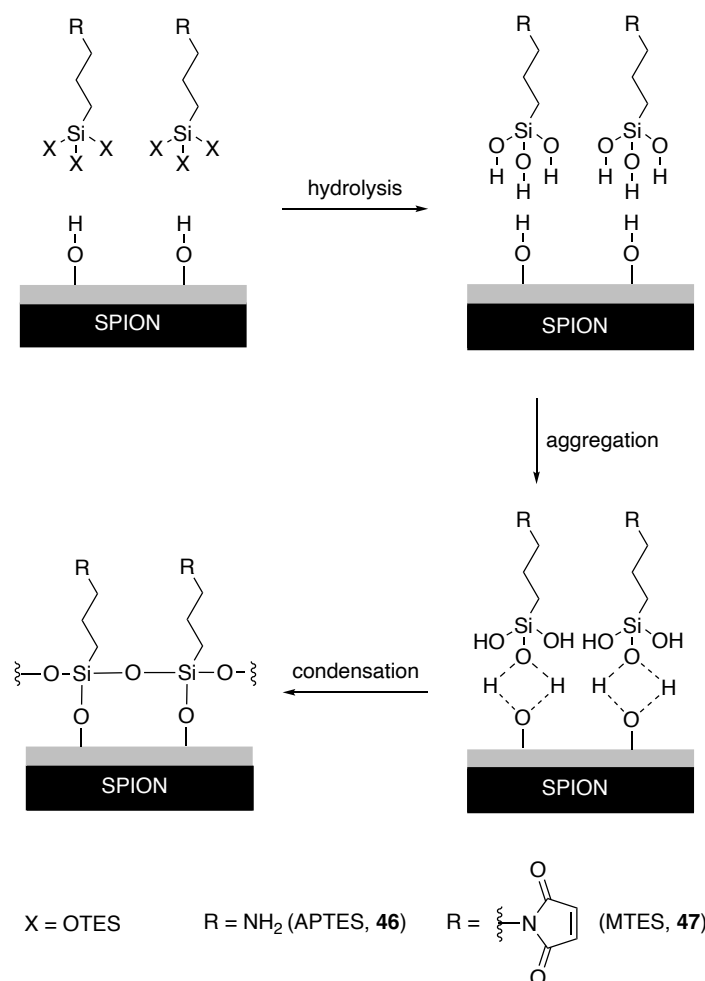
Figure 20: SPIONs with monomeric, polymeric and inorganic coating.

Monomeric coatings use structures such as carboxylates, phosphates, or catechols, which are known to bind the surface of SPIONs. For catechols and phosphates, binding to iron(III)-ions is postulated. The residues can be varied to introduce different surface functionalities or to improve solubility.^[81,82]

Polymers can also be used to stabilize and functionalize the SPION surface. In principle, any biocompatible polymer can be utilized, although in most cases polysaccharides such as modified dextran or alginate are used.^[72,81]

Gold, silver, and other metals have been used as inorganic coatings^[72,81], but the most commonly used coating is silica. Silica not only stabilizes the SPIONs and prevents their aggregation, but also forms silanol groups on the surface, which can further be used for functionalization. Therefore, organosilanes with a leaving group at the silicon, such as ethoxy in triethoxysilanes (TES), are mixed with the silica coated nanoparticles at high temperatures in solvents with a critical amount of water. The leaving groups hydrolyze and adsorb on the silanol surface first through hydrogen bonding and then covalently after condensation at high temperatures. The amount of water during the reaction determines the connectivity between the organosilanes. Instead of silanol coating and subsequent silanization with functionalized organosilanes like aminopropyltriethoxysilane (APTES, **46**) or

maleimidepropyltriethoxysilane (MTES, **47**), the organosilanes can also be used directly to coat the SPIONs (Scheme 12).^[82,83]



Scheme 12: Mechanism for surface functionalization using silanes (modified from^[82,83]).

5.1.3 Superparamagnetism and its Advantages in Biomedical Context

In the bulk material (Fe₂O₃, γ -Fe₂O₃) or magnetite (Fe₃O₄) exhibit ferrimagnetic properties. A decrease in particle size comes along with a decrease of magnetic domains until the particle reaches a single domain state. However, this is associated with an increase of coercivity until a material specific superparamagnetic diameter, for maghemite and magnetite around 20-30 nm, is reached and coercivity drops to zero. The energy barrier to flip the magnetization of these nanoparticles becomes so small that they can spontaneously reverse magnetization from one direction to the other under the influence of temperature. This phenomenon is called superparamagnetism.^[84]

The magnetic moment of superparamagnetic particles has two stable orientations antiparallel to each other and determined by the crystalline anisotropy of the particle. This orientation is called the “easy axis”. When a magnetic field of higher energy than the energy barrier is applied, the domains rotate in the direction of the magnetic field by two mechanisms: the NÉEL and the BROWNIAN rotations.

If the magnetic moment rotates in the particle, while the particle itself remains fixed, NÉEL relaxation (τ_N) takes place, and flipping of the moment between the two “easy axis” releases thermal energy. However, when the entire particle is rotated, the particle undergoes BROWNIAN relaxation (τ_B) and heat is generated by shear stress in the surrounding fluid (Figure 21). BROWNIAN relaxation is favored for larger particles in less viscous fluids, while NÉEL relaxation is favored for smaller nanoparticles in viscous fluids such as tissue. These two effects cause the heating of superparamagnetic particles, like SPIONs, in an alternating magnetic field (AMF).^[80] Noteworthy ultrasmall SPIONs (~ 6 nm) develop no local temperature increase after application of an AMF.^[85]

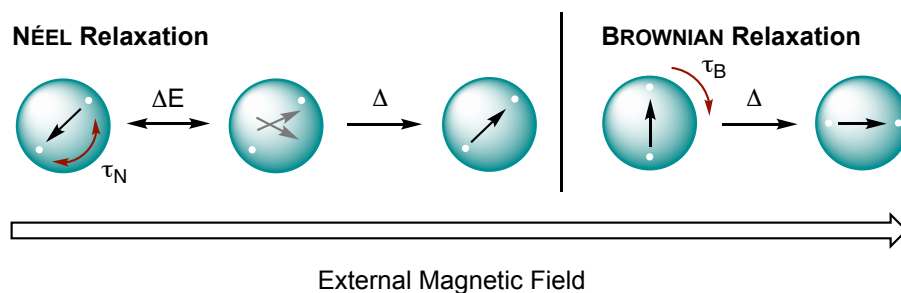


Figure 21: NÉEL relaxation: The magnetic moment aligns with the external magnetic field while the particle remains fixed. BROWNIAN rotation: The magnetic moment remains in the stable orientation with respect to the crystalline structure while the particle rotates (modified from^[81]).

In nanomedicine the characteristic heat induced by an AMF is used and studied in hyperthermia therapy^[80] and controlled drug release through an external stimulus^[79]. In addition, the superparamagnetic properties of SPIONs shorten the relaxation T2 times of the surrounding protons and are thus optimal contrast agents in magnetic resonance imaging (MRI) diagnostics.^[72] Intravenously administered SPIONs can be directed to the pathological site by moving towards a constant magnetic field.^[72,79]

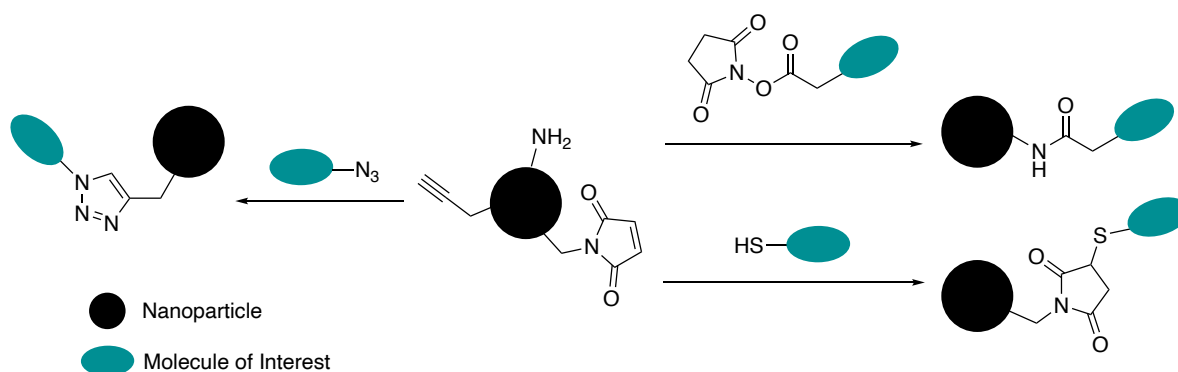
5.1.4 Antimicrobial SPIONs

SPIONs show antimicrobial properties associated with an increase of reactive oxygen species (ROS).^[86] Of particular interest is the ability of SPIONs to penetrate biofilms and kill bacteria. This is highly dependent on the SPIONs coating. While carboxyethylsilanetriol, APTES (46) or alginate coated SPIONs exhibit antibacterial activity, polyethyleneglycol (PEG) coated SPIONs do not result in biofilm inhibition for they are not internalized by the matrix and bacteria. Penetration can be increased by magnetic concentration of the SPIONs.^[87,88] Hyperthermia can also inactivate bacteria. Inhibition and killing of *Pseudomonas aeruginosa* biofilms could be observed within a few minutes with blank and PEG coated SPIONs.^[89,90]

In addition to the inherent antimicrobial activity, antimicrobials can be conjugated to the SPIONs surface to further enhance the activity.^[91–93] Sustained release of gentamicin-coated SPIONs was shown to increase the antibiotic activity by 10-fold.^[92] Bacitracin, a polyketide antibiotic used for wound infections against Gram-positive bacteria, also exhibited activity against Gram-negative *Escherichia coli* when covalently bound to SPIONs.^[93] A similar observation was made for vancomycin, which was also able to interact with Gram-negative bacteria when connected to gold nanoparticles.^[94] These results suggest that some nanoparticles can overcome the lipopolysaccharide barrier and thus antibiotics that inhibit peptidoglycan synthesis can also act against Gram-negative bacteria. Noteworthy, the antimicrobial effect of antibiotics can be enhanced by elevated temperatures^[95], which could be used in combination with AMF induced hyperthermia.^[90]

5.2 Surface Chemistry of Nanoparticles

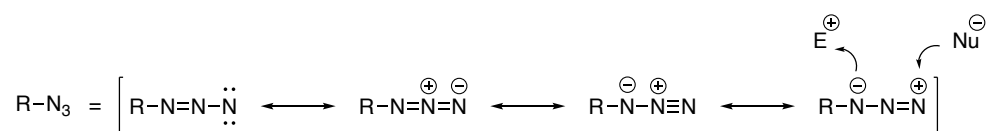
Reactions to conjugate molecules onto the nanoparticle surface must be high-yielding and easy to perform with a variety of starting materials. Furthermore, they should generate almost no byproducts and therefore not require extensive workup. All of these requirements are met by the modular so-called “click” reactions.^[96,97] Some selected “click” reactions used in nanoparticle surface chemistry are shown in Scheme 13, namely the copper-catalyzed azide-alkyne 1,3-dipolar cycloaddition (CuAAC), amide formation between a *N*-hydroxysuccinimide (NHS) activated ester and amine, and the thiol-maleimide MICHAEL addition.



Scheme 13: Selected “click” reactions used in nanoparticle surface chemistry.

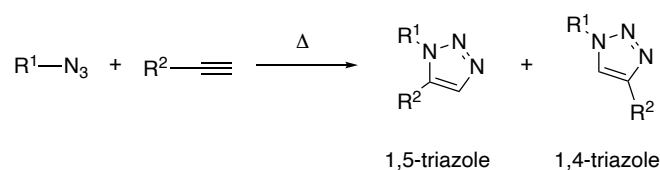
5.2.1 Copper Catalyzed Azide-Alkyne 1,3-Dipolar Cycloaddition

The CuAAC is by far the most commonly used click reaction. Based on the mesomeric structures, the 1,3-dipole character of azides becomes clear. This allows azides to react with both nucleophiles and electrophiles (Scheme 14).^[98]



Scheme 14: Mesomeric structure of organic azides.

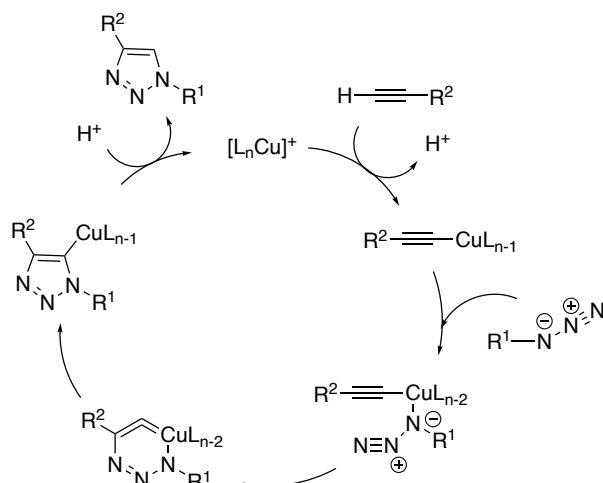
The 1,3-dipolar cycloaddition describes the reaction between an 1,3-dipole and a dipolarophile. The addition undergoes a concerted mechanism and, in case of the addition of azide and alkyne, leads to 1,5-triazoles and 1,4-triazoles depending on the steric and electronic effects of the residue (Scheme 15).^[99]



Scheme 15: 1,3-Dipolar cycloaddition between an azide and alkyne.^[99]

Copper(I) catalysis can accelerate the reaction, allows reactivity at room temperature, and yields only the 1,4-triazole isomer.^[100,101] Usually, the Cu(I) species is generated *in situ* by reduction of Cu(II) salts such as CuSO₄·5 H₂O. In contrast to the concerted mechanism described above, a stepwise mechanism is proposed for the CuAAC. Many studies have been carried out to determine the exact reaction steps. One of the proposed mechanisms is shown in Scheme 16.^[102]

First, the Cu(I) coordinates the alkyne, displacing one of the ligands, which could be the solvent (acetonitrile, water, etc.) or an additional added ligand. A second ligand is then replaced by the azide nitrogen. Subsequently, the distal nitrogen of the azide attacks the C-2 carbon of the acetylide, forming a six membered metallacycle. Ring contraction, followed by proteolysis, leads to the 1,4-triazole and regenerates the copper catalyst.



Scheme 16: Proposed mechanism of CuAAC. L are ligands such as water or acetonitrile.^[102]

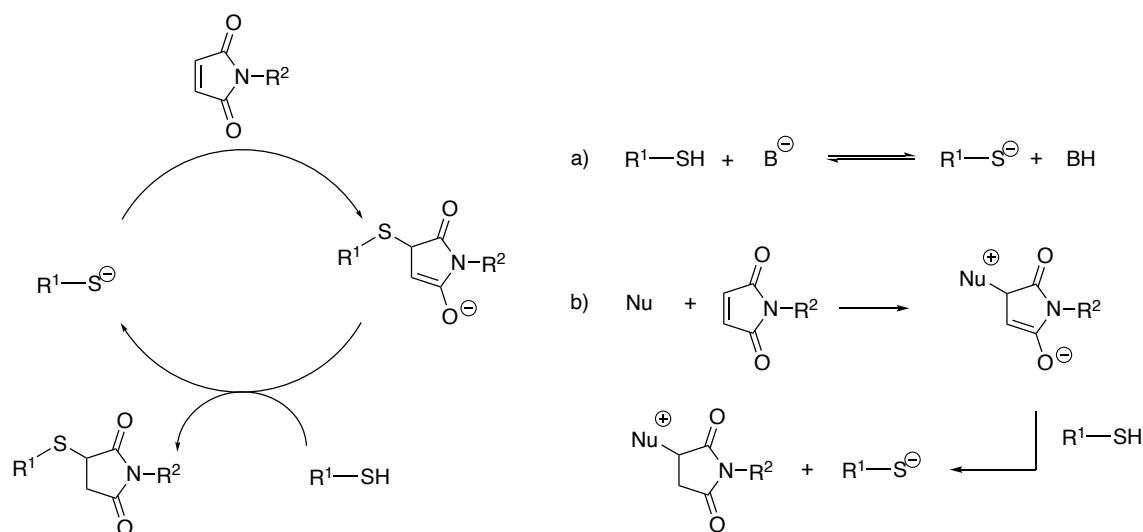
5.2.2 Thiol-Maleimide MICHAEL Addition

The thiol-maleimide MICHAEL addition is another “click” reaction frequently used to conjugate two fragments. It provides a stable thioether bond under mild conditions in a variety of solvents. Reaction times vary from a few minutes to a week, depending on the residue of the thiol. The addition of more equivalents of the thiol or base can reduce the reaction time.^[103]

The mechanism of the thiol-maleimide addition follows a typical MICHAEL addition reaction (Scheme 17). The thiolate adds on the MICHAEL acceptor to form the enolate intermediate. The addition product is formed by protonation of the enolate with another thiol equivalent. The resulting thiolate can then react with a next molecule of maleimide. Formation of the thiolate can occur either *via* an acid-base equilibrium (Scheme 17a) or after an initial attack of a nucleophile on the maleimide, producing small amounts of a nucleophile addition byproduct (Scheme 17b).^[104]

The base-initiated mechanism usually relies on weak bases such as triethylamine (Et₃N). The nucleophile-initiated mechanism typically uses nitrogen- or phosphorous-centered nucleophiles. This results in formation of some amount of nucleophile addition byproducts.

However, since less than 1% of the nucleophile is required to initiate the reaction, the concentration of the byproduct can be neglected.^[104]



Scheme 17: Mechanism of thiol-maleimide MICHAEL addition. a) Thiolate formation from acid-base equilibrium. b) Thiolate formation following nucleophile-initiated pathway.^[104]

5.3 Thermal Controlled Release

In therapeutic application of nanoparticles, the release of the active ingredients can be controlled by different mechanisms. This could be diffusion from a porous scaffold, release by degradation of the nanocarrier, or release from the nanoparticle surface by bond breaking.^[105] The release can occur either by time-dependent diffusion or biodegradation, or can be induced by an internal^[105] or external stimuli^[22,106,107] (Figure 22).

Internal stimuli would be, for example, a physiological change in the target tissue such as a drop in pH during intracellular uptake.^[105] External stimuli such as heat, on the other hand, are induced externally, e.g., by the photothermal effect of gold nanoparticles after light irradiation^[107] or the application of heat to superparamagnetic materials by an AMF.^[22,79,106] Compared to time-dependent release or release by internal stimuli, the external stimulus can be more precise. External stimuli such as an AMF can be induced exclusively in the desired body area. However, because the stimulus is only triggered for a specific period of time, sustained drug release over a longer period of time is compromised.

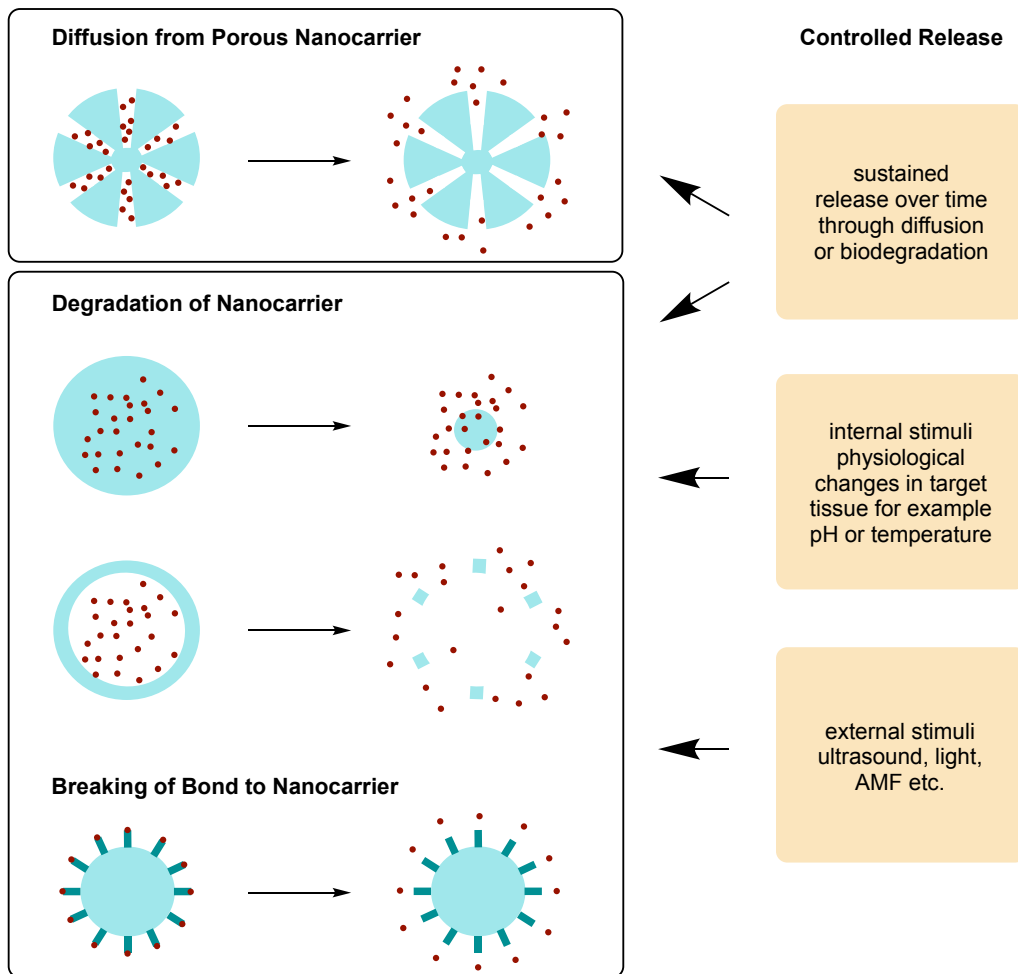


Figure 22: Different mechanisms for the release of active ingredients from nanocarriers (modified from^[73]).

Temperature controlled release is of particular interest for nanoparticles that generate heat after exposure to an external stimulus. When heat is applied to SPIONs by an AMF^[22,79,85,106], typically a magnetic field around 100 – 1000 kHz leads to a gradual increase in the bulk temperature of nanoparticle suspensions. The temperature raises with magnetic field strength and particle diameter^[108] and decays with distance from the SPION core^[85].

This heating properties can be exploited for the controlled release of active substances from a SPION in two ways. One is through the temperature induced shrinkage of polymers, which leads to a burst release of the adsorbed payload^[109], and the other is through the release of covalent bound substances from a thermosensitive linker^[22,85,106,110].

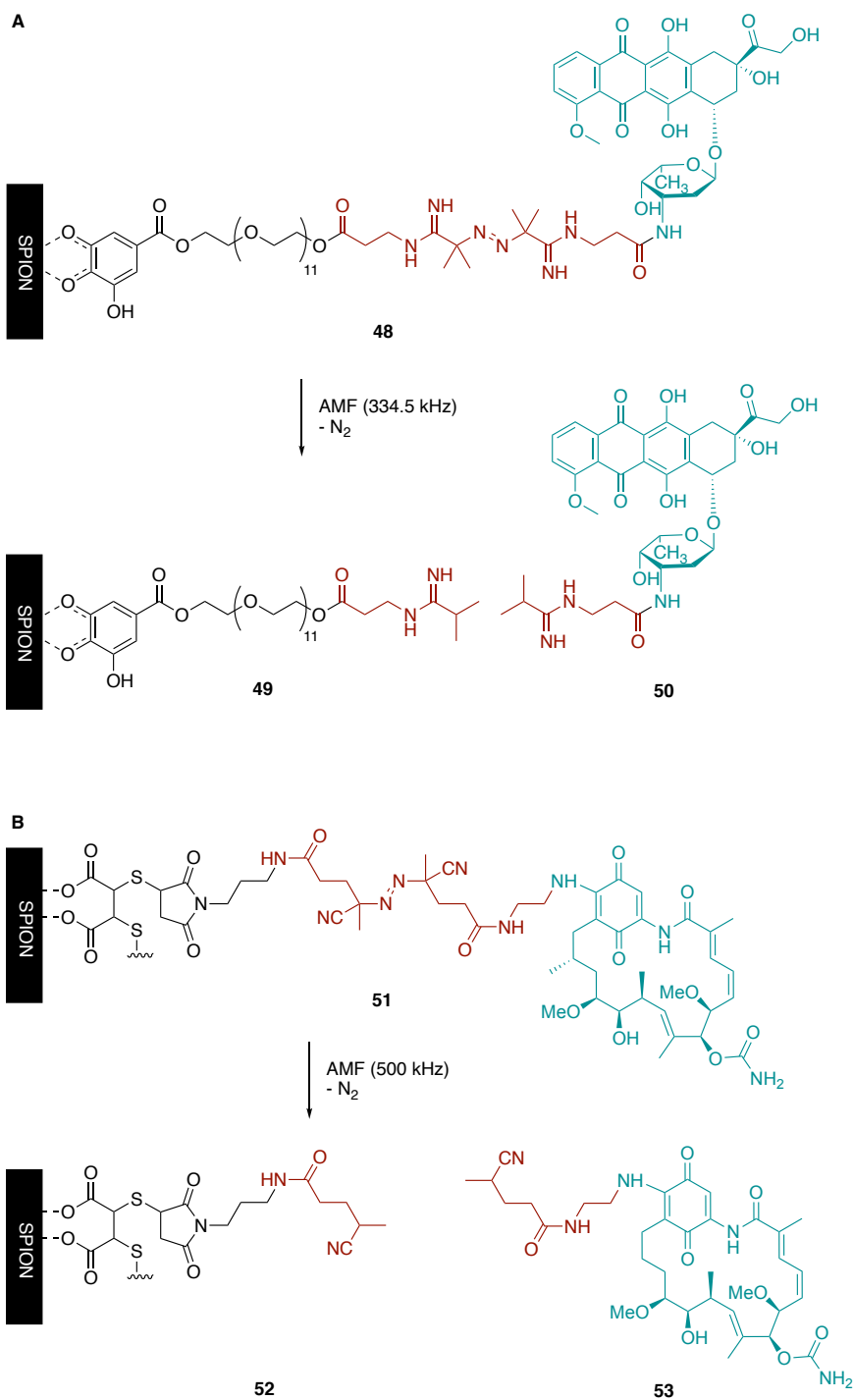
Two thermosensitive linkers are currently used for the controlled release of active substances after AMF exposure of SPIONs: The thermo labile azo ligand^[85,106] and the retro DIELS-

ALDER reaction (rDA)^[22,110]. In addition, lactamization of amino ester linkers has been developed for the release of alcohols at elevated temperatures.^[111]

5.3.1 Thermo labile Azo Ligand

The thermo labile azo ligand was first used to map the temperature decay of SPIONs with distance to the SPION core. Therefore, SPIONs stabilized with gallic acid PEG ester of different lengths, were connected to fluorescein amine *via* an azo linker. The percentage of rhodamine release compared to maximum release after 48 h at 80 °C was used as a temperature probe after application of a magnetic field of a defined strength. A temperature difference between 30 K and 50 K was observed compared to the bulk temperature with a PEG spacer of 500 Da. The azo linker was then used to bind the antitumor drug doxorubicin (DOX) and the toxicity of the SPION@DOX **48** conjugate was tested against KB cells. The application of an AMF did not increase the bulk temperature, but the toxicity was significantly higher after AMF application compared to incubation without AMF, which was attributed to increased DOX **50** release (Scheme 18, case A).^[85]

The thermo labile azo linker was also tested for thermal release of the Hsp90 inhibitor geldanamycin (**6**) from SPIONs. It was envisioned that the combination of hyperthermia and Hsp90 inhibition could enhance antitumor activity. The azide linker design differs from the beforementioned linker. Instead of dimethyl groups in the alpha positions of the azide, one methyl group each is replaced by a cyanide group. Zn-doped SPIONs coated with dimercaptosuccinic acid were used, which are known for their relatively high heat generating ability (Scheme 18, case B). The bulk temperature of the SPION suspension reached 43 °C during AMF application. After 70 min, 100% of geldanamycin **53** was released, whereas only about 7% release was observed during normal heating. The nanoparticles were injected into MDA-MB-231 breast cancer cells xenografted into the right hind legs of mice, and the tumor tissue was to 43 °C by AMF (500 kHz, 37.4 kAm⁻¹) for 30 min. This resulted in inhibition of tumor growth during the next four days. Without geldanamycin **53**, the tumor continued to grow 8 days after treatment, whereas tumors treated with SPION@geldanamycin **51** were eliminated by day 8.^[106]



Scheme 18: Two examples for AMF induced release of drugs using a thermosensitive azo linker. A) release of doxorubicin^[85] and B) geldanamycin^[106]

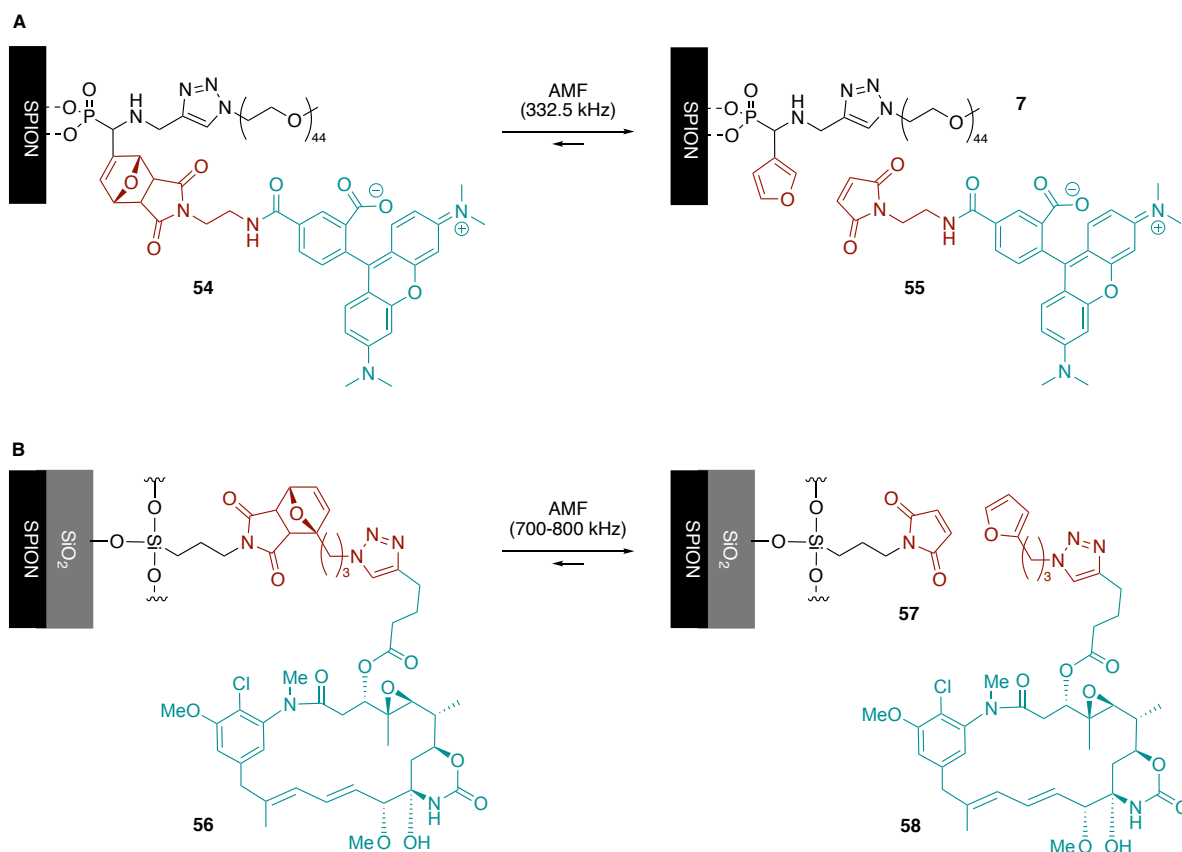
Despite these positive results in the thermal release of drugs from azo linkers, the radical intermediates during decomposition of azo motives could cause problems *in vivo*. An uncontrolled radical reaction with surrounding residues could interfere with the drug release mechanism or cause damage to the biological system.^[79]

5.3.2 Retro Diels-Alder Reaction

The rDA reaction is another temperature-controlled reaction developed as a linker for thermal release of drugs. In particular, the furane-maleimide DIELS-ALDER has been established in this context. This concept was first used to release maleimide grafted rhodamine **55** from a SPION stabilized with PEGylated phosphoric acid. In this case, the PEG was introduced through a CuAAC between the PEG azide and the alkyne grafted SPIONs. In addition to the alkyne, a furan group was attached to the phosphoric acid, which served as an anchor for the [4+2]-cycloaddition and allowed drug loading close to the SPIONs core. The application of an AMF (332.5 kHz, 11.3 kAm^{-1}) to SPION@rhodamine **54** resulted in the release of rhodamine **55** through the rDA without a significant increase of the bulk temperature of $29 \text{ }^\circ\text{C}$ (Scheme 19, case A).^[110]

The same rDA linker was used to release the cytotoxic compound ansamitocin **58** from silica coated, maleimide functionalized SPION@maleimide **57**. Therefore, alkyne modified ansamitocin was prepared by combined mutasynthesis and precursor directed synthesis of the Δ AHBA mutant strain of ansamitocin producer *A. pretiosum*. Feeding of AHBA (**7**) and pen-4-ynoic acid gave the alkyne modified ansamitocin. This was connected to 2-(3-azidopropyl)furan by CuAAC yielding the furan grafted ansamitocin **58**. The [4+2]-cycloaddition between the SPION@maleimide **57** and the ansamitocin **58** was performed at $62 \text{ }^\circ\text{C}$ for 3 d in CH_3CN . After the application of AMF (700 – 800 kHz), an effective release of ansamitocin **58** was observed (Scheme 19, case B), which affected antiproliferation in human hepatocellular carcinoma (Huh-7) cell lines. Significant tumor shrinkage was observed after injection of SPION@ansamitocin **56** into Huh-7 xenografts on the flanks of mice followed by AMF application.^[22]

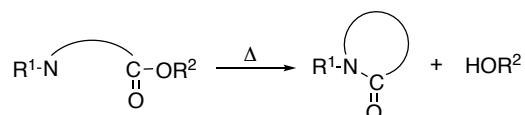
In addition, macrophages such as J77a.1. can take up SPION@ansamitocin **56**. After application of an AMF, these macrophages undergo heat induced apoptosis, releasing ansamitocin **58**, which induces cell killing of neighboring target cells. 3D spheroid co-cultures of SPION@ansamitocin **56** loaded J77a.1. macrophages with KAPOSI's sarcoma associated herpes virus infected enterochromaffin cells (K-ECs) were completely disrupted after AMF application, due to a combination of hyperthermally induced apoptosis and toxin release. These experiments were designed to mimic tumor infiltration by macrophages and demonstrate the efficiency of macrophages as vehicles for SPIONs loaded with toxins by a thermosensitive linker.^[23]



Scheme 19: Two examples for AMF induced release of drugs using a thermosensitive DIELS-ALDER linker. A) release of rhodamine **55**^[110] and B) release of ansamitocin **58**^[22].

5.3.3 Thermo Sensitive Lactamization

Intramolecular cyclization reactions have been exploited as mechanisms for drug delivery. In many cases, intramolecular cyclization aims the rapid release of drugs at physiological temperatures. However, these “self-immolated” degradations processes do not meet the requirements for controlled thermal release.^[112] NANTZ investigated cyclolactamization reactions that release primary alcohols under elevated temperatures and a minimized cyclization rate at 37 °C (Scheme 20).



Scheme 20: Cyclolactamization method for the traceless release of alcohols.^[111]

The group tested a range of different cyclization systems that resulted in cyclolactams and cyclocarbamates with 5 to 7 membered rings with and without *gem*-dimethyl groups. 2-(9-Anthracenyl)ethanol was chosen as test release substrate (Figure 23). The release rate of 2-(9-anthracenyl)ethanol was determined at 55 °C in MeOH. Cyclization rates decreased with

the resulting ring size, (**59a** > **59b** > **59c**), and carbamates were formed more slowly than lactams (**59b** > **60b**). *Gem*-dimethylation also increased the cyclization rate (**61** > **59c**) through the THORPE-INGOLD effect. The release fluorescein isothiocyanate (FITC) covalently bound to a polydimethylsiloxane microchannel by the linker leading to the 6-membered lactam was tested. After heating the microchannel to 60 °C in CH₃CN for 30 min, almost complete release of FITC was observed.^[111]

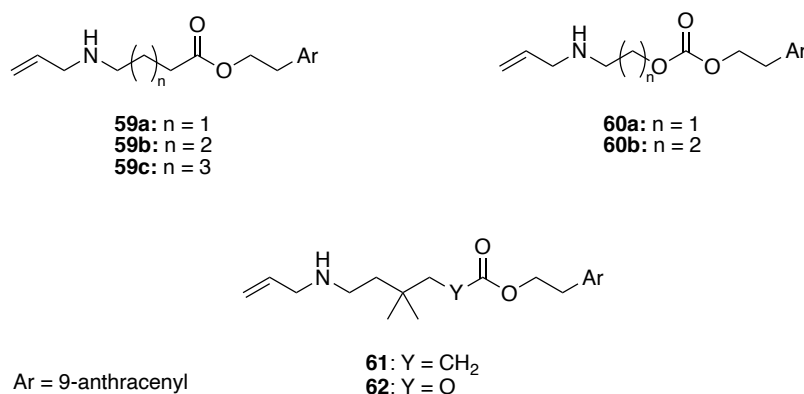


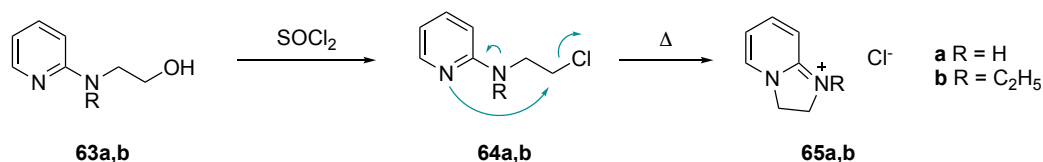
Figure 23: Different linkers synthesized for to evaluate optimal conditions for the temperature induced cyclolactamization for the release of alcohols.^[111]

Compared to the two methods mentioned above, the cyclolactamization method provides a thermal controlled release mechanism of alcohols without alteration of the original compound. The applicability for AMF induced release from SPIONs under physiological conditions is currently investigated.^[113]

5.3.4 The 2-Py-TPG Thermolabile Protecting Group

A method for thermal deprotection of a number of functional groups was described by BEAUCAGE and CHMIELEWSKI.^[114–116]

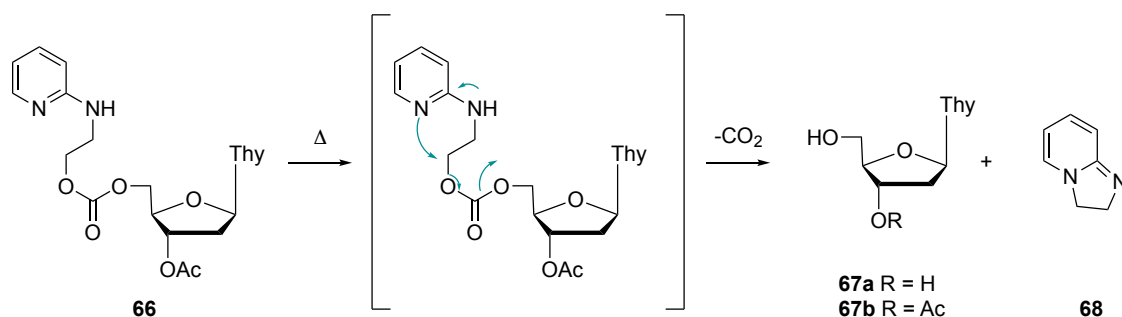
The potential of 2-(pyridinylamino)ethanol species **63a,b** to undergo intramolecular cyclization to the corresponding dihydropyrimidazols **65a,b** after conversion to chlorides **64a,b** at elevated temperatures was already discovered in 1936 by BREMER.^[117] This mechanism occurs by a nucleophilic attack of the pyridine nitrogen of **63a** and **63b** on the electrophilic carbon adjacent to the chlorine, which acts as the leaving group and yields the bicyclic cations **65a,b** (Scheme 21).



Scheme 21: Cyclization of 2-(pyridinylamino)ethanol **63a,b** to the corresponding dihydropyrimidazol **65a,b** upon chlorination followed by exposure to elevated temperatures.

The group of BEAUCAGE began to use this intramolecular cyclization mechanism for the thermoselective deprotection of phosphates in solid-phase oligonucleotide synthesis.^[114]

This method was further developed by CHMIELEWSKI for thermoselective deprotection of the 5'-hydroxyl group of desoxyribonucleosides,^[115] a strategy termed the *N*-2-pyridinyl thermolabile protecting group (2-Py-TPG) (Scheme 22). The release of the alcohol occurs by the same intramolecular cyclization, but with the release of carbon dioxide from the carbonate ester **66** as driving force.



Scheme 22: Application of 2-Py-TPG in the thermoselective deprotection of thymidine **67a**.^[115]

Several experiments have shown that the cyclization rate depends strongly on the nucleophilicity of the pyridine nitrogen. This can be influenced by addition of electron donating (EDG) or electron withdrawing (EWG) groups to the pyridine ring (Figure 24 compounds **66** and **69-70**). The electrophilicity of the target carbon can also be affected by addition of EWG or EDG groups to the α -position of the hydroxyl group (Figure 24 compound **71**).^[115] In addition crystallization studies of several 2-Py-TPG showed that close proximity of nucleophilic nitrogen and electrophilic carbon also increases the cyclization rate, which is favorable for the *N*-benzyl compound **72**. A relationship between the *pK_a* values of the pyridine nitrogen and the cyclization rate was suggested but could not be confirmed.^[116]

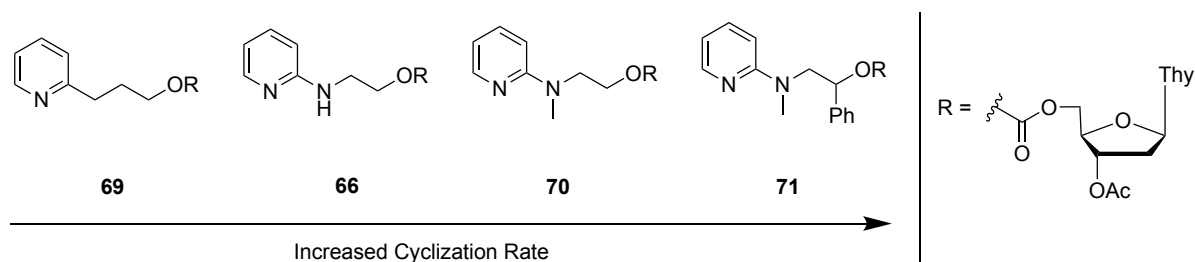


Figure 24: Compounds **66** and **69** – **71** sorted by their cyclodeesterification rate at 90 °C at *pH* 7.^[115]

Despite the faster cyclization rate, the *N*-benzyl derivative **72** was found to also have a higher stability at ambient temperature compared to *N*-methyl derivative **71**.^[118] To further investigate the stability caused by the *N*-benzyl group, fluorine conjugates **73** – **75** were tested for their stability at ambient temperature and at 90 °C (Figure 25).

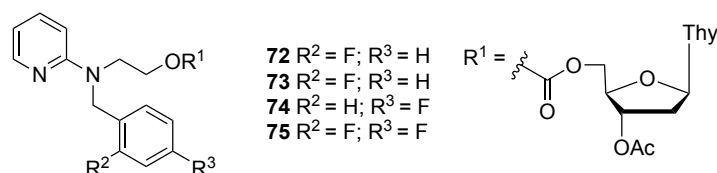
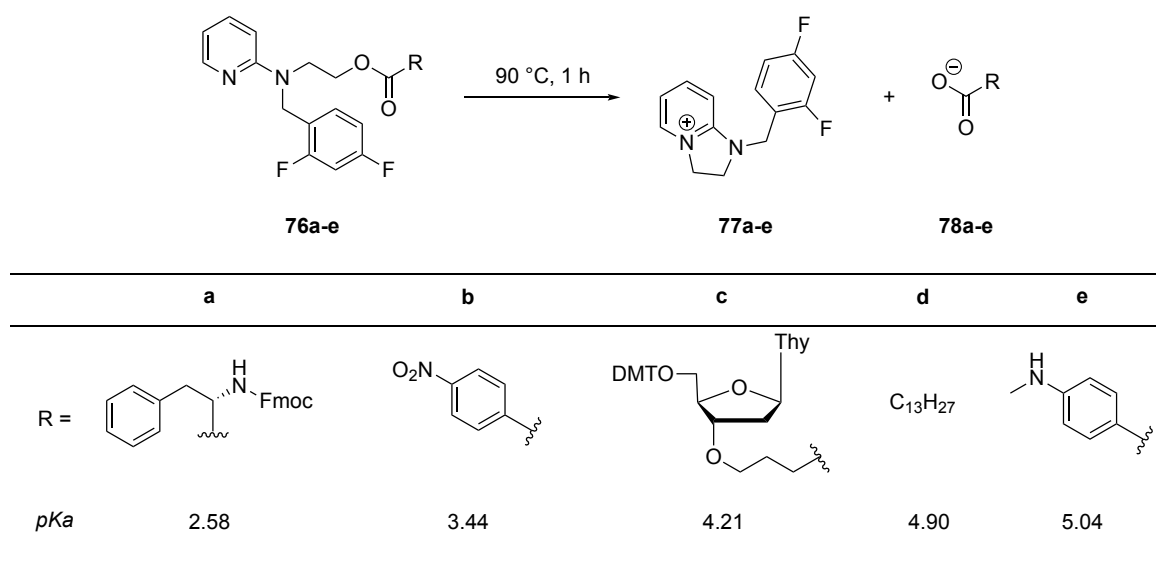


Figure 25: *N*-benzyl derivatives **72** – **75** tested for their stability at ambient temperature.

The fastest cyclization rates were found for **72** and **73** with total release after 8 min at 90 °C and a half-life of 1.8 min. At 20 °C, the half-life of 29 h and 26 h, respectively, was observed. Although difluoro compound **75** had a half-life of 2.7 min at 90 °C, its stability at 20 °C was twice as high at 58 h. Compound **74** was found in the intermediate range.

The increased stability of **75** compared to **72-74** was explained through a 2D NOESY experiment that revealed a strong interaction of the *ortho*-fluorine atom with the protons of the α -carbon. This interaction positions the benzyl ring close to the alkyl chain and could sterically hinder the cyclization reaction at lower temperatures.^[118] Solvent polarity and *pH* also affect cyclization rates. More polar solvents lead to a faster cyclization (CCl₄ < dioxane < MeCN < *t*-BuOH < MeCN:phosphate buffer (3:1 v/v, *pH* 7.0) < EtOH:phosphate buffer (1:1 v/v, *pH* 7.0)). The *pH* dependency is probably due to the decreased nucleophilicity of the partially protonated nitrogen at lower *pH*, which inhibits the cyclization process.

The scope of the 2-Py-TPG has been extended from protection of alcohols and phosphates to carboxylic acids using the *N*-benzyl 2-Py-TPG (Scheme 23).^[119]



Scheme 23: Cyclization of the difluoro-*N*-benzyl 2-Py-TPG groups of **76a-e** to release acids **78a-e** with different *pKa* values.

A strong correlation was found between the *pKa* values of the corresponding acids **78a-e** and the cyclodeesterification rates. This is for the fact that the more stable carboxylic anions are better leaving groups and therefore deprotection rates are faster for acids with low *pKa* values. Phenylalanine **78a** and *para*-nitrobenzoic acid **78b** with *pKa* of 2.58 and 3.44, respectively, were released quantitatively after heating for 1 h at 90 °C. The yields of acids **78c-e** were found much lower under the same conditions, decreasing to 54%, 18% and 14%, respectively, with decreasing *pKa*. It was therefore postulated, that the 2-Py-TPG protecting group is not suitable for acids with *pKa* values above 4.^[119]

6 Aim of Study Part II

In this study the 2-Py-TPG is to be employed as a thermosensitive linker for the traceless release of the carboxyl group of antibiotics from a SPION. So far, there is no report about a linker system that releases carboxyl groups. After selection of appropriate antibiotics, the linker should be designed in such a way, that it is stable at 37 °C and releases the antibiotic at elevated temperatures (Figure 26).

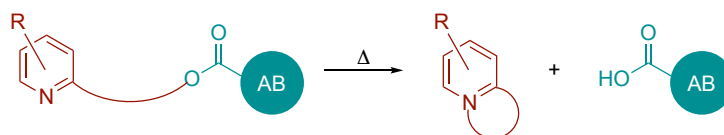


Figure 26: Development of the 2-Py-TPG group as a thermosensitive linker for the traceless release of antibiotics at elevated temperatures.

Once this is achieved, the antibiotic-linker construct should be covalently bond to a SPION. Therefore the silica coated SPION MagSilica[®] was to be used, which has already been established for the release of ansamitocin through rDA after AMF application.^[22,113] Between the MagSilica[®] core and the antibiotic should be a PEG spacer for temperature fine-tuning^[85], increase solubility in water and reduced cytotoxicity. Finally, this SPION@PEG@antibiotic conjugate would have to be tested for its antibiotic release after AMF application (Figure 27).

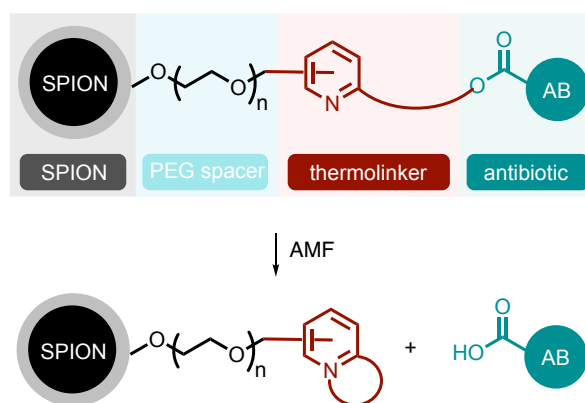


Figure 27: Concept of AMF induced thermal release of an antibiotic from SPION linked *via* 2-Py-TPG.

7 Results and Discussion Part II

7.1 Selection of Antibiotics

In our case, the heat that is generated when the SPIONs are exposed to an oscillating electric field is measured in aqueous solution. However, it can be assumed that the SPIONs themselves reach much higher temperatures, which decrease with distance from the core. Since the antibiotics should be covalently bound to the particles and thus close to the particle core, the antibiotics selected for this conjugate method should be thermally stable.

As described in the introduction, the 2-Py-TPG release mechanism is realized via a SN mechanism. Thus, the reaction kinetics strongly depend on the strength of the leaving group, which in this case is the anion of the acid. This means that leaving group capability of antibiotics depends on the corresponding pK_a values of the acids. An acid with a lower pK_a would be released at lower temperatures than an acid with a higher pK_a .^[119] The antibiotics were therefore selected according to their melting point (above 200 °C) and their pK_a values (Table 1 and 2).

Table 1: Comparison of pK_a values from different heat stable classes of antibiotics and chosen representatives benzylpenicillin (**79**), cephalixin (**80**), nalidixic acid (**81**) and ciprofloxacin (**81**).

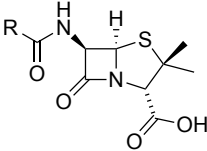
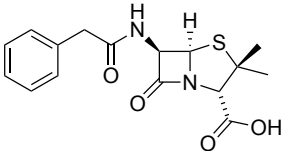
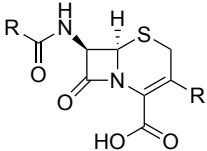
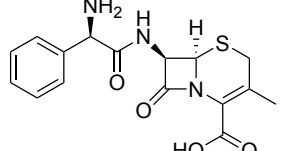
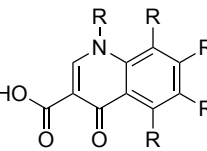
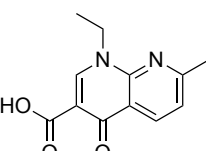
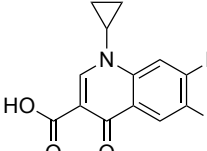
core structure	pK_a	representative antibiotics
 <p>penicillin-type</p>	2.5 – 2.8	 <p>79</p>
 <p>cephalosporin-type</p>	3.0 – 3.5	 <p>80</p>
 <p>quinolone-type</p>	5.5 – 8.0	 <p>81</p>  <p>81</p>

Table 2: Selected antibiotics with $T_m > 200$ °C containing an acid group and sorted by their pK_a values. * = predicted values

entry	structure	name	T_m	pK_a
1	penicillin	benzylpenicillin (79)	214-217 °C	2.74
2	cephalosporin	cephalexin (80)	327 °C	3.36*
3	quinolone	nalidixic acid (81)	229.5 °C	8.6
4	quinolone	ciprofloxacin (82)	255-257 °C	6.1

7.2 2-Py-TPG Design and Synthesis

In the case of the 2-Py-TPG protection of carboxylic acids, four main effects influence the cyclodeesterification kinetics. The first is the nucleophilicity of the pyridine nitrogen. A more electron-rich pyridine would increase the nucleophilicity, while a less electron-rich pyridine would have the opposite effect. Thus, nucleophilicity can be controlled by introducing of EWGs or EDGs into the heteroaromatic compound. Another effect is the electrophilicity of the target carbon. An EWG at this position would increase the cyclization rate.^[115]

The proximity of the pyridine nitrogen to the target carbon also affects the cyclization rate. It is described that this proximity could be adjusted, for example, by introducing a benzyl group on a nitrogen conjugated at the 2-position of the pyridine. Additional fluorine atoms on the *ortho* and *para* positions can stabilize the system at ambient temperature.^[118]

Considering information from the literature, two different sets of linkers were designed; one set for which a slower cyclization rate was estimated that could be used for the release of the penicillin and cephalosporin antibiotics **83** and **84** (Figure 28, case A), and another set with linkers for which a higher cyclization rate was assumed for the selected quinolone antibiotics **85-88** (Figure 28, case B).

The methyl substituents in **86-88** were chosen because it was thought that the THORPE-INGOLD effect could further accelerate the rate of cyclization. This effect is based on the observation that large substituents change the angles of a linear carbohydrate chain in such a way that ring closure is accelerated.^[120] The alcohol **89** without fluorine was to be synthesized to evaluate the importance of the fluorine for room temperature stability postulated in the literature.^[119]

In addition, the synthesis of *N*-methylated compounds **83b-88b** was planned. The methyl group would not only act as an EDG and increase the nucleophilicity of the pyridine nitrogen, but could also serve for subsequent connection to the nanoparticles.

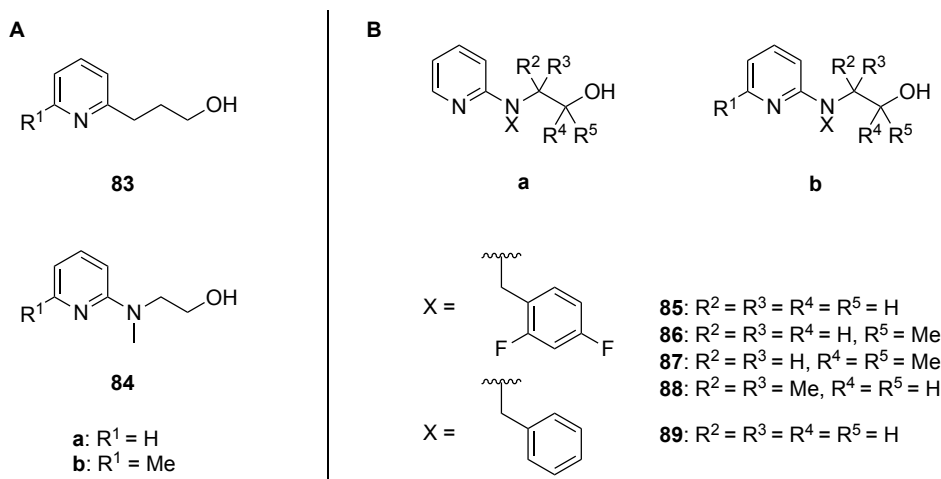
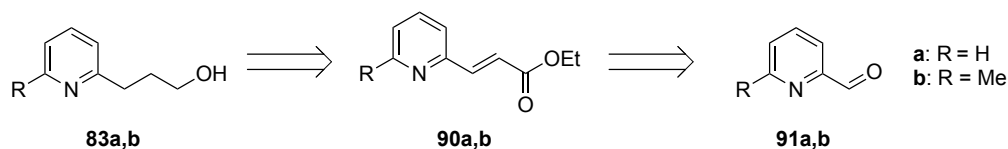


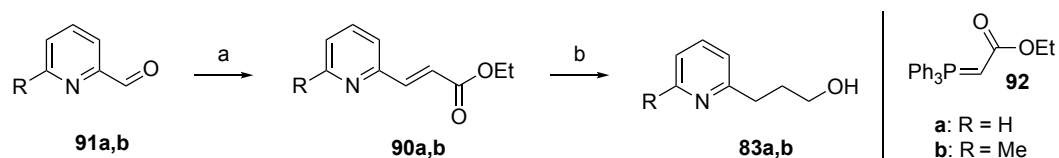
Figure 28: A) Linker with estimated slower cyclization rates for the release of penicillin and cephalosporin antibiotics with low *pK_a* values. B) Linkers envisioned to be synthesized for the release of quinolone antibiotics with *pK_a* values above 4.

Linkers **83a** and **b** should be synthesized from the corresponding esters **90** by hydrogenation of the double bond and subsequent saponification. The esters **90** are easily accessible by WITTIG olefination of aldehydes **91** (Scheme 24). For **83a** this synthesis sequence has already been successfully described.^[121]



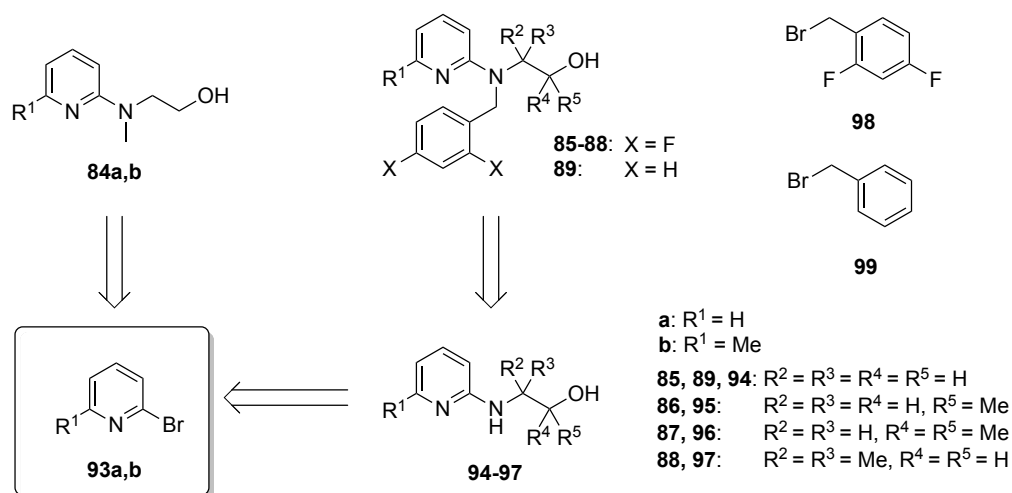
Scheme 24: Retrosynthesis for linker **83**.

As shown in Scheme 25, the synthesis of **83a,b** proceeded smoothly as expected with overall yields of 30% (**83a**) and 68% (**83b**). The low overall yield of **83a** can be explained by problems in purification of the WITTIG product. These were overcome in the synthesis of **83b**. It can therefore be assumed that the yields for **83a** should be similar to that of **83b**. Since the synthesized amount of **83a** was already sufficient, there was no need to repeat the synthesis in order to improve the yields.



Scheme 25: Synthesis of **83a,b**. a) **92**, toluene, 100 °C, 300 W, μw , 15 min, **b** = 92%; b) H_2 , Pd/C, EtOAc, rt, 18 h, **a** = 32% o2s, **b** = 81%; then LiAlH_4 , THF, 0 °C – rt, 30 min, **a** = 91%, **b** = 92%.

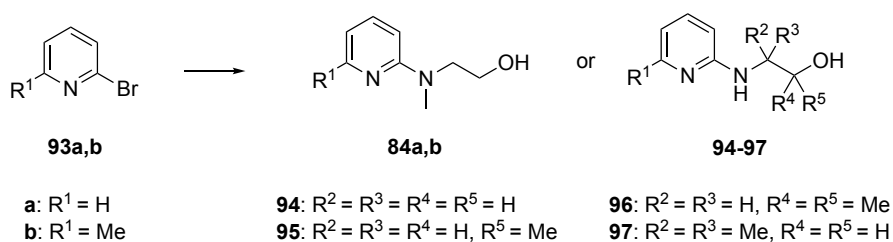
It was planned to synthesize the 2-aminoalkyl linker **84-88** by electrophilic aromatic substitution starting from the common 2-bromopyridine precursor **93a** or **b** together with the corresponding aminoalcohols. In the case of the benzyl derivatives **85-88** and **89**, the benzyl group was introduced by nucleophilic substitution of **94-97** with bromobenzyls **98** and **99** (Scheme 26).



Scheme 26: Retrosynthetic approach towards linker **84-88** and **89**.

Electrophilic aromatic substitution on starting material **93** proceeded in good yields overnight under most conditions. The reaction could also accelerate using microwave conditions (μw , 300 W). The significantly longer reaction time and lower yield of compound **97a,b** are probably due to the increased steric hinderance of the tertiary amino group (Table 3).

Table 3: Synthesis of **84** and **94-97**. a) 4-6 eq. aminoalcohol, 140 °C in oilbath or 160 °C in μ w. * 2-Chloropyridine was used instead of 2-bromopyridine **93a**.

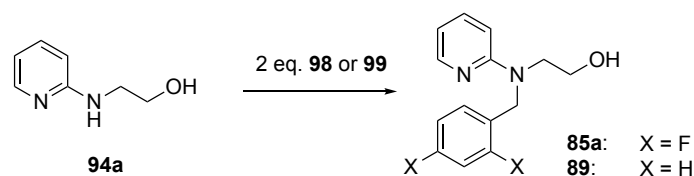


entry	product	aminoalcohol	conditions	reaction time	yield
1	84a *	<i>N</i> -methylethanolamin	μ w	2 h	83%
2	84b		μ w	1 h	99%
3	94a	ethanolamin	140 °C	18 h	82%
4	94b		140 °C	18 h	73%
5	95a	DL-1-amino-2-propanol	μ w	3 h	quant.
6	95b		140 °C	18 h	50%
7	96a	1-amino-2-methylpropan-2-ol	140 °C	1 d	81%
8	96b		140 °C	2 d	94%
9	97a	2-amino-2-methylpropanol	140 °C	3 d	46%
10	97b		140 °C	2d	33%

The subsequent introduction of the benzyl moiety to the secondary amine was first tested using amine **94a** and 2,4-difluoro-benzylbromid (**98**) in THF and with Et₃N as base. The suspension was placed in a microwave tube and stirred at 66 °C and 300 W for 4 h as it was described.^[118] This procedure resulted in a yield of **85a** of 22%. Comparison with the literature was not possible because the yields were not reported.

It was decided to test different conditions to increase the yield. Therefore, traditional heating was employed, which allowed parallel synthesis. Yields were determined by NMR spectroscopy using dimethylsulfone as an internal standard (Table 4).

Table 4 shows the yields of **85a** (based on ¹H-NMR spectroscopy) in THF and MeOH employing various organic and inorganic bases. The difference of 22% in the isolated yield under μ w conditions (entry 1) and 33% in the ¹H-NMR yield after 30 h traditional heating (entry 2) is not so large, that it could not vary from batch to batch. When comparing entries, it is clear that the inorganic bases KOH and K₂CO₃ give lower yields compared to the others. It even appears that when THF is used as a solvent, the addition of base is not necessary (entry 5). The yields decrease further when MeOH is used as a solvent.

Table 4: Nucleophilic substitution of **94a** with benzylbromides **98** and **99** and to **85a** and **89**.

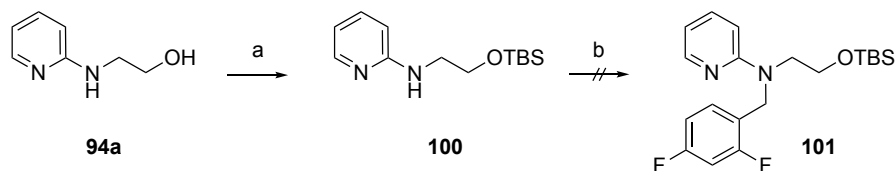
entry	halide	solvent	base	<i>T</i>	<i>t</i> [h]	yield product	yield sm
1			Et ₃ N	66 °C (μw)	4.5 h	22% (isolated)	
2			Et ₃ N	60 °C	30 h	33%	-
3			NaI	60 °C	20 h	33%	-
4		THF	TBAI	60 °C	20 h	33%	-
5			-	60 °C	15 h	20 %	-
6	98		KOH	60 °C	15 h	22 %	-
7			K ₂ CO ₃	60 °C	15 h	22 %	-
8			-	75 °C	36 h	4.2 %	13%
9		MeOH	KOH	75 °C	36 h	15%	38%
10			K ₂ CO ₃	75 °C	36 h	15%	30%
11		Combined aq. phases of 4-9				16%	0.8%
12	99	THF	Et ₃ N	66 °C	15 h	50% (isolated)	

All conditions have in common that the added benzylbromide (2 eq.) was still visible as judged by TLC. This rules out the possibility that competitive bromine elimination could be the reason for low yields. In all cases, the starting material **94a** could not be detected as judged by TLC, whereas it was found again by ¹H-NMR-analysis under conditions with MeOH as solvent (entries 8-10).

Despite the frequent extraction of the aqueous phase (6x with EtOAc), 16% of the product **85a** could still be detected in the concentrated aqueous phase of entries 4-9. This indicates that either a more extensive extraction is required or that EtOAc may not be the appropriate solvent for the extraction of **85a**. With benzylbromide (**99**), the reaction proceeded in higher yields of 50% (entry 12).

It was assumed that the free hydroxyl group might inhibit the reaction to **85a**. This could be prevented by the protection of the alcohol. Therefore, the TBS ether **100** was prepared. Under conditions with THF and Et₃N at 60 °C, no transformation to **101** was observed after 2 days. When DMSO was employed as solvent along with KOH as base, temperatures could be raised

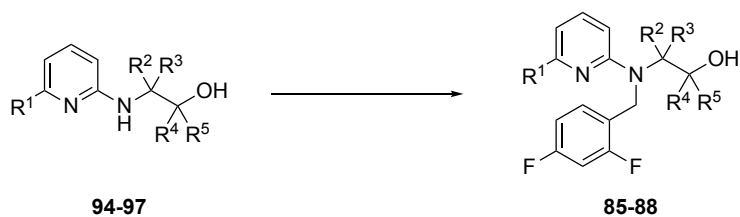
to 110 °C, leading to TBS hydrolysis (Scheme 27). Deprotection could be overcome by using a more stable protecting group such as TIPS. On the other hand, the larger steric hindrance would probably inhibit the substitution reaction to a greater extent than TBS would do.



Scheme 27: a) TBSCl, imidazole, CH₂Cl₂, 5 h, rt, 70%; b) 2 eq. **98**, Et₃N, THF, 2 d, 60 °C no reaction or 2 eq. **98**, KOH, DMSO, 60 °C – 110 °C, deprotection.

Since optimization of the alkylation of amine **94a** to benzylamine **85a** did not lead to higher yields, the other benzylamines **85b-88a,b** were synthesized from amines **94b-97a,b** employing the initial conditions as listed in Table 4, entry 1 (Table 5).

Table 5: Synthesis of **85-88** a) 2 eq. **98**, Et₃N, THF, 66 °C, 300 W, μ w or in oil bath. * Inseparable mixture of product and unidentified compound.



a: R¹ = H **85, 89:** R² = R³ = R⁴ = R⁵ = H **87, 96:** R² = R³ = H, R⁴ = R⁵ = Me
 b: R¹ = Me **86, 95:** R² = R³ = R⁴ = H, R⁵ = Me **88, 97:** R² = R³ = Me, R⁴ = R⁵ = H

entry	product	conditions	reaction time	yield
1	85b	oil bath	24 h	59%
2	86a	μ w	3 h	42%
3	86b	oil bath	18 h	56%
4	87a	oil bath	24 h	40%
5	87b	oil bath	42 h	51%
6	88a	oil bath	48 h	*
7	88b	oil bath	48 h	8%

With the exception of benzylamines **88a** and **b**, all the conversions proceeded in yields of about 40-60%. From Table 4, it can be seen that the yields are always higher in the alkylation of methylpyridine amines **94b**, **95b** and **96b** compared to the pyridine amines **94a**, **95a** and **96a**. This can be explained by the higher electron density of the free amine.

Very low yields were observed for the alkylation of tertiary amines **97a** and **b**, respectively. Methylpyridine benzylamine **88b** was isolated in 8% yield, while **88a** was detected by HRMS and $^1\text{H-NMR}$ spectroscopy but it could not be separated from an unidentified compound. The very low yields are probably due to the higher steric hinderance of the tertiary amines. In both cases, the *O*-alkylated compounds **102a** and **102b** were also isolated in 8% yield each (Figure 29). They can be distinguished from the desired *N*-alkylated alcohols **88a,b** by the carbon shift (δ) of the benzylic carbon in the $^{13}\text{C-NMR}$ spectrum, that is about 45 – 50 ppm for the *N*-alkylation and about 66 ppm for the *O*-alkylation.

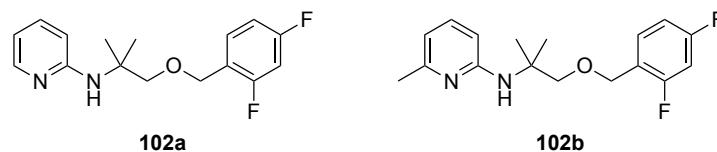


Figure 29: *O*-alkylated side products **52a,b** as side products from synthesis of **88a** and **88b** isolated in 8% yield each.

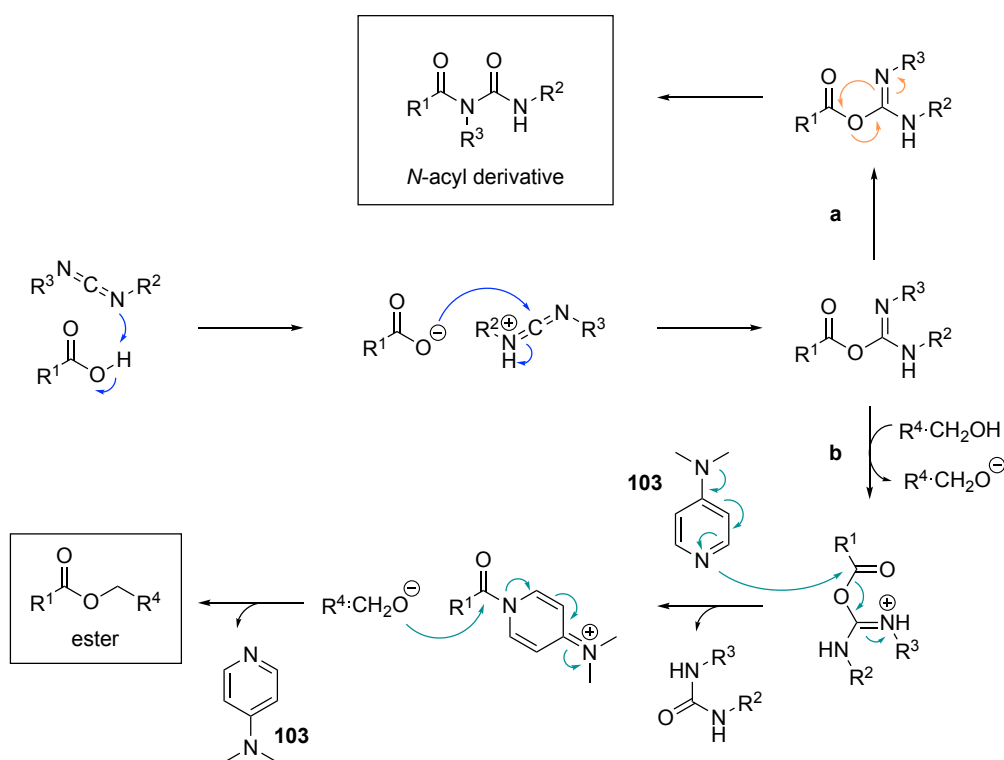
7.3 2-Py-TPG Penicillin G

7.3.1 Synthesis

The successfully synthesized linker element **84a** was to be conjugated to benzylpenicillin (**79**). This was carried out by STEGLICH esterification of benzylpenicillin sodium salt (**104**) and the alcohol **84a**.

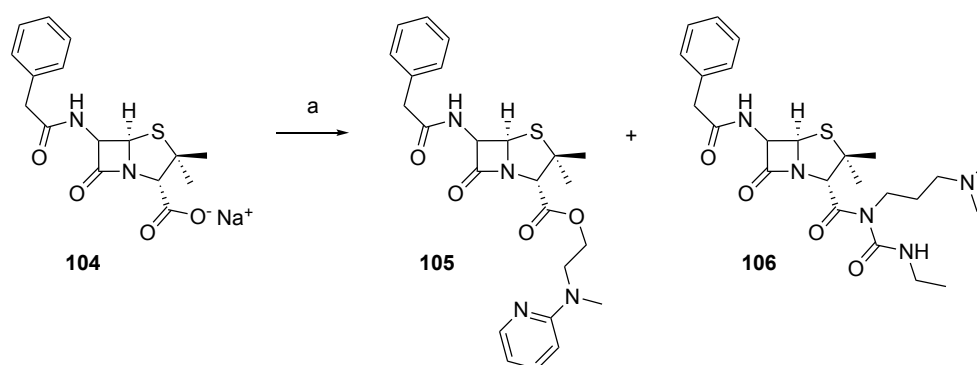
STEGLICH esterification is method for the synthesis of esters from carboxylic acids and alcohols under mild conditions. It involves the use of carbodiimides and catalytic amounts of 4-dimethylaminopyridine (DMAP, **103**).^[122] In the first step of the reaction, the nitrogen of the carbodiimide deprotonates the carboxylic acid. The resulting carboxylate can then attack the electrophilic carbon of the protonated carbodiimide to form an *O*-acyl-intermediate. Depending on the nucleophilicity of the intermediate, under most conditions the *O*-acyl-intermediate would isomerize to the corresponding *N*-acyl-intermediate, also called ureide (Scheme 28, pathway a).^[123,124]

However, if catalytic amounts of DMAP (**103**) are added, the reaction is driven towards the ester synthesis (Scheme 28, pathway b). In this case, DMAP (**103**) is acylated before isomerization to the ureide can occur. The alcoholate can then attack the carbonate of the acylated DMAP forming the ester and releasing the catalyst DMAP (**103**).^[122]



Scheme 28: Mechanism of STEGLICH esterification.

To determine the optimal conditions for esterification, the reaction was first carried out on a small scale and monitored by LCMS in ESI mode. When dicyclohexyl carbodiimide was used as coupling reagent, no conversion of penicillin sodium salt **104** was observed, which could be due to a lack of a proton source. When the hydrochloride of ethyldimethylaminopropyl carbodiimide (EDC) was used instead, benzylpenicillin (**79**) disappeared as judged by TLC after 18 h and the mass for the desired ester product **105** with $m/z[M+H^+] = 469$ detected. Unfortunately, the *N*-acyl derivative of penicillin and EDC **106** with $m/z[M+H^+] = 490$ was also found (Scheme 29).



Scheme 29: Synthesis of 2-Py-TPG penicillin G ester. a) 1.2 eq. **84a**, 2 eq. EDC·HCl, 0.3 eq. DMAP (**103**), on, rt, analytical scale – no isolation.

In order to reduce the amount of the undesired *N*-acyl derivative **106**, a number of conditions were tested. It was decided to optimize the reaction based on the ratio of integrals of $m/z = 469$ and $m/z = 490$ in LCMS. The higher the ratio, the more product **105** is formed compared to the side product **106**.

First, solvents, and temperature were varied. The temperature was lowered because it is known that the *N*-acyl derivative is better formed at higher temperatures.^[123] The solvent also has an effect on the reaction outcome.^[124]

Indeed, it is clear from Table 6 that lower temperatures have a positive effect on the product/side product ratio. While a ratio of 0.6 was obtained at rt, as in entry 1, it increased to 0.87 when the reaction was started ice cold before being warmed to rt (entry 3). When the reaction was kept constantly at 0 °C, the ratio increased to 1.2 (entry 6). The solvent also affected the ratio, because when esterification was conducted in DMSO and DMF only the formation of the byproduct was observed by LCMS, so the ratio could not be calculated (entries 2 and 7). Upon esterification in Et₂O, the ratio changed slightly toward the by product (see entries 3 and 4). A slight improvement of the ratio compared to CH₂Cl₂ was achieved in

THF with a value of 0.98 compared to 0.87 (entries 3 and 4). Pyridine was chosen as the solvent because it exhibits similar catalytic activity compared to DMAP (**103**). It was therefore assumed that pyridine would, compete with isomerization and drive the reaction towards the product **105** due to the large excess. That this is not the case is demonstrated in entry 8, with the smallest ratio of 0.05 found.

Table 6: Variation of the temperature of STEGLICH esterification of penicillin G **104** with 1.2 eq. alcohol **84a**, 2 eq. EDC·HCl, 0.3 eq. DMAP (**103**), on. * only *N*-acyl derivative was found

entry	solvent	<i>T</i>	$A \frac{469}{490}$
1	CH ₂ Cl ₂	rt	0.60
2	DMSO	rt	-*
3	CH ₂ Cl ₂	0 °C - rt	0.87
4	THF	0 °C - rt	0.98
5	Et ₂ O	0 °C - rt	0.67
6	CH ₂ Cl ₂	0 °C	1.2
7	DMF	0 °C	-*
8	pyridine	0 °C	0.05

From these results, it seems like isomerization to **106** is favored in polar solvents such as DMF and DMSO. It is less favored in nonpolar solvents such as CH₂Cl₂ and Et₂O. In contrast to DMF and DMSO, THF provides the least favorable environment for isomerization. This could be due to the stabilization of the *O*-acyl intermediate though hydrogen bonds with the proton at the nitrogen and consequent delocalization of the carbodiimide electron resulting in a less nucleophilic nitrogen (Figure 30). The very low ratio measured when pyridine was used can be explained by the fact that pyridine is not basic enough compared to DMAP (**103**).

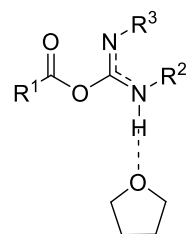


Figure 30: Postulated stabilization of the *O*-acylintermediate by THF.

In a next set of experiments, the equivalents of the catalyst were varied. It was assumed that a higher catalyst concentration would compete isomerization. Indeed, Table 7 shows that this is the case. However, the correlation between increased ratio and the DMAP (**103**) equivalents is

not linear. Tripling the DMAP (**103**) concentration from 0.3 to 0.9 eq. (entries 3,4) resulted in a 1.5-fold increase in the ratio. Addition of 2 equivalents of DMAP (**103**) (6.6-fold increase) led to a 2-fold increase of the ratio (entry 6). Assuming that the ionization of **105** and **106** was in LCMS is the same, even with 5 equivalents of DMAP (**103**), 20% of penicillin sodium salt **3** would end up being converted to the undesired *N*-acyl derivative **106**. Since the addition of more than stoichiometric amounts of catalyst is not desirable, 0.9 equivalents of DMAP (**103**) were chosen for further optimization.

Table 7: Variation of the catalyst eq. in of STEGLICH esterification of penicillin G **104** with 1.2 eq. alcohol **84a**, 2 eq. EDC·HCl, in CH₂Cl₂ at different temperatures on.

entry	<i>T</i>	eq. DMAP (103)	$A \frac{469}{490}$
3	0 °C – rt	0.3	0.87
4	0 °C – rt	0.9	1.27
5	0 °C	0.3	1.20
6	0 °C	2	2.54
7	0 °C	5	4.16

Finally, it was decided to gradually add EDC·HCl to the reaction mixture. The idea was, similarly to increased DMAP (**103**) equivalents, to keep the relative concentration of DMAP (**103**) high compared to EDC·HCl so that the route to the product would always be favored. Table 8 compares successive addition over 30 min is compared to 18 h.

Table 8: Variation of the time of successively addition of 2 eq. EDC·HCl in STEGLICH esterification of penicillin G **104** with 1.2 eq. alcohol **84a**, 0.9 eq. DMAP (**103**) in CH₂Cl₂ on.

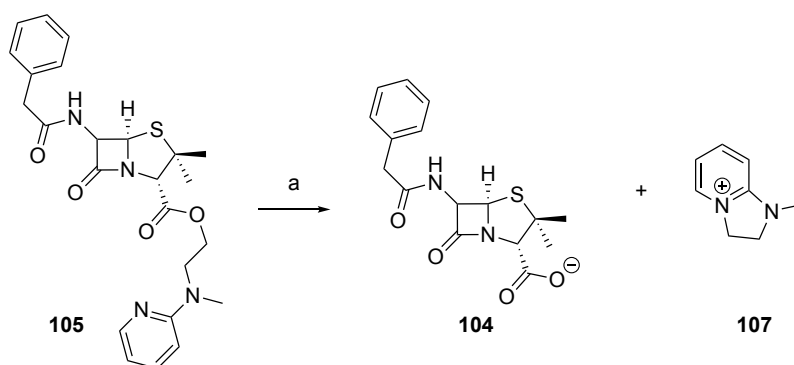
entry	<i>t</i>	<i>T</i>	$A \frac{469}{490}$
1	0.5 h	0 °C	1.7
2	18 h	0 °C	2.4

The ratio is significantly higher when EDC·HCl is added more slowly. Another interesting observation was made when monitoring the reaction of entry 1. Immediately after the addition of EDC·HCl, the product/side product of 9.6 was observed. After only 45 min, it decreased to 2.4, and after 18 h, when no penicillin **104** was present in LCMS, the ratio was 1.7. It was assumed that this ratio could be kept constant if successive addition was extended up to 18 h, but this was not the case (entry 2).

At this point, sufficient material had already been generated to study the release study of 2-Py-TPG penicillin **105**, so further optimization was not required. For future studies, the use of other esterification conditions, such as with the uranium-based coupling reagents COMU[®] (**109**) or HBTU could be tested. These compounds act through uronium salts instead of carbodiimides which would overcome the *N*-acyl formation.

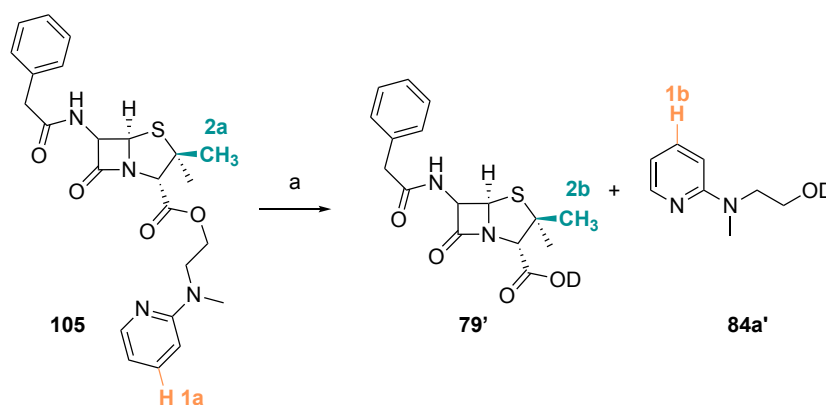
7.3.2 Release

2-Py-TPG penicillin **105** was dissolved in CDCl₃ to perform NMR analysis. When the same sample was measured again after 1 d at 25 °C, a new compound appeared along with the characteristic signals of the penicillin anion **104**. After 14 d at 25 °C, the integrals of the new compound were four times those of **105**. NMR analysis and mass spectrometry revealed that this new product was the 2-Py-TPG salt **35** formed from cyclodeesterification of **105** (Scheme 30).



Scheme 30: Cyclodeesterification of **105**. a) CDCl₃, 25 °C, 14 d, 80% conversion determined by ¹H-NMR spectroscopy.

Encouraged by this result, 37 mg of **105** were dissolved in D₂O:DMSO-d₆ and the cyclodeesterification was monitored by ¹H-NMR spectroscopy at 25 °C (Scheme 31 and Figure 31). Characteristic peaks of the 2-Py-TPG group ($\delta = 7.45$ ppm for **105** and $\delta = 7.86$ ppm for **84a'**) and for penicillin ($\delta = 1.42$ ppm for **105** and $\delta = 1.49$ ppm for **79'**) were selected. After 20 d, 2-Py-TPG penicillin **105** was converted to **84a'** however, the signal intensity for the penicillin **79'** protons did not reach 100%. Instead, one new signal probably belonging to the methyl group of a decomposed penicillin derivative at $\delta = 1.46$ ppm emerged^[125] (Figure 31).



Scheme 31: Cyclodeesterification of **105**, D₂O:DMSO-d₆, 25 °C, 20 d. Protons used for monitoring are highlighted. a) D₂O:DMSO-d₆ = 4:6, 25 °C, 20 d.

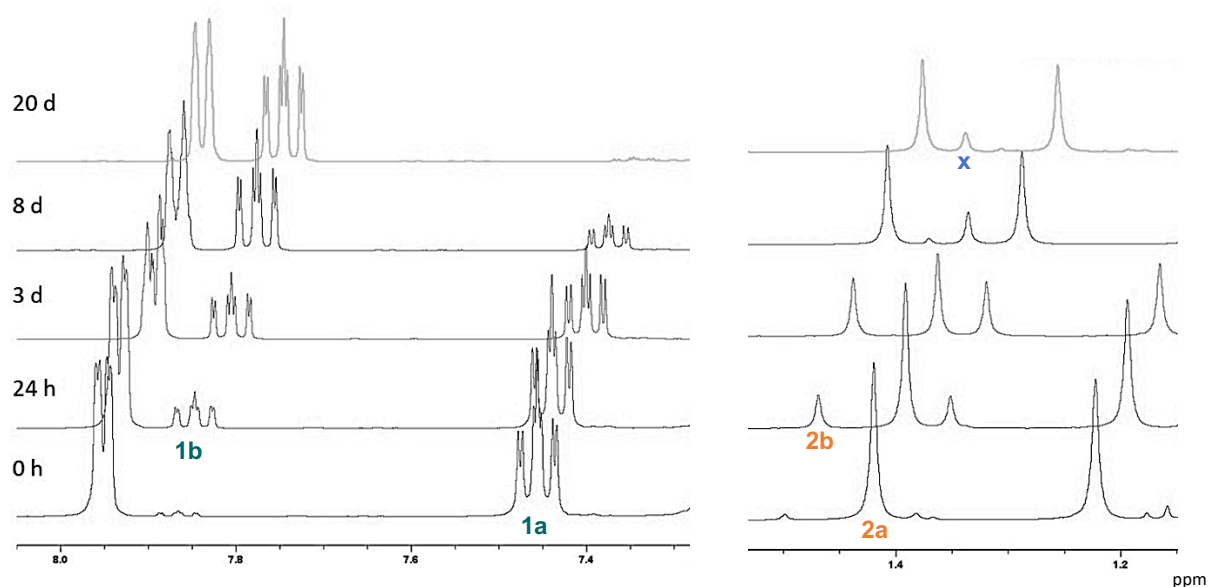


Figure 31: Characteristic protons of **105** (1a and 2a), **79'** (3a) and **84a'** (2b) used for determination of cyclization rate. x: unknown decomposition product.

The plot in Figure 32 shows the change of signal intensity (by integration) of the reaction shown in Scheme 31 over a period 42 days. The cyclodeesterification reaction (filled circles) follows a first order reaction with a half live of $t_{1/2} = 4.4$ d and a reaction rate of $k = 0.162$. These values correlate with the evolution of **84a'** (empty diamonds). As described before, the release of penicillin G **79'** correlates with the cyclodeesterification only up to day 5. Thereafter, it proceeds more slowly and, from day 15, the integrals decrease. This might be due to the linear evolution of an unknown compound (empty circles) that is probably a degradation product of penicillin **79'**. Degradation products of β -lactam antibiotics are well

described in the literature and mainly formed by nucleophilic cleavage of the susceptible β -lactam moiety.^[125]

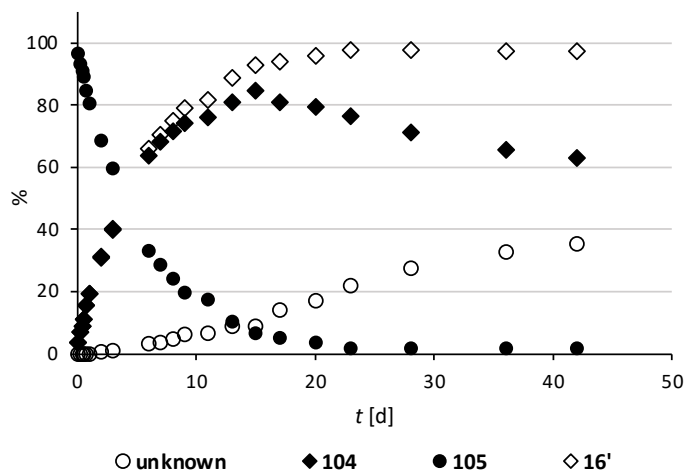


Figure 32: Cyclodeesterification of **105** in $D_2O:DMSO-d_6 = 4:6$ and $25\text{ }^\circ\text{C}$ over 42 days. Percentages are displayed in comparison to decreased integrals of characteristic 2-Py-TPG penicillin **105** peaks.

This release study shows that the designed 2-Py-TPG penicillin **105** is not ideal for use in thermal release of penicillin **104** from a SPION. After only 5 h at $25\text{ }^\circ\text{C}$, 5% of **105** is cyclized, releasing penicillin **79'**. This rate would accelerate at higher temperatures, such as $37\text{ }^\circ\text{C}$ in the human body, making release difficult to control. Synthesis of a 2-Py-TPG conjugate using alcohol **83a** could slow down the cyclization rates at these temperatures because the pyridine nitrogen in **83a** is less nucleophilic than in **84a**. Nevertheless, the penicillin decomposition product in $D_2O:DMSO-d_6$ would also be formed under physiological conditions in the human circulation and, probably more rapidly at higher temperatures during inductive heating of the SPION. All these considerations led to exclusion of β -lactam antibiotics such as cephalexin (**80**) from further studies.

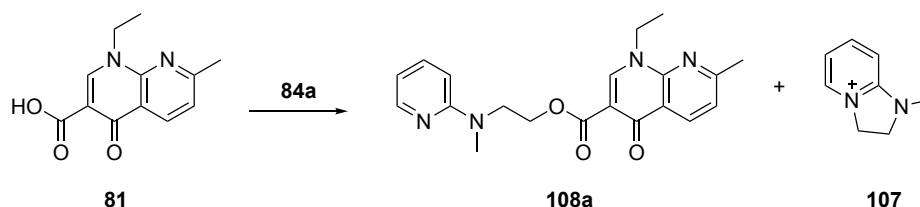
7.4 2-Py-TPG Quinolone Antibiotics

7.4.1 Synthesis

Similar to penicillin **79**, several antibiotic 2-Py-TPG conjugates were to be synthesized and tested for their release kinetics. First, the esterification of nalidixic acid (**81**) was investigated. Therefore 2-Py-TPG derivative **84a** was chosen. Table 9 shows various conditions tested for the esterification of **81**. All reactions were monitored by TLC and LCMS. This is challenging because the appearance of starting materials could either mean that the reaction was not completed or that the chosen conditions lead to cyclodeesterification of the product **108a** back

to the starting materials. For this reason, reactions were generally run for no longer than 24 h at rt.

Table 9: Esterification trials to convert nalidixic acid (**81**) with **84a** to ester **108a**. * Only traces of ester could be isolated after column chromatography although the corresponding $m/z[M+H^+]$ was found in the crude product.



entry	conditions	result
1	SOCl ₂ in CH ₂ Cl ₂ , 1 h, rt, then excess Et ₃ N, 84a , 24 h, rt	no full conversion*
2	(COCl) ₂ , DMF (cat) in CH ₂ Cl ₂ , 2 h, rt, solvent removed then 84a in CH ₂ Cl ₂ and Et ₃ N excess, 18 h, rt	12%
3	(COCl) ₂ , DMF (cat) in CH ₂ Cl ₂ , 2 h, rt, solvent removed then 84a (neat) and Et ₃ N excess, 18 h, rt	traces*
4	(COCl) ₂ , DMF (cat) in CH ₂ Cl ₂ , 48 h, rt, solvent removed then 84a , in CH ₂ Cl ₂ and Et ₃ N excess, 18 h, rt	traces*
5	CDI (113), THF, on, rt, then in 84a , THF, NaH 0°C – rt, on, rt	107
6	CDI (113), Et ₃ N, THF, on, rt, then in 84a , in THF, NaH, 0°C – rt, on, rt	107
7	CDI (113), DBU, THF, on, rt, then in 84a , in THF, NaH, 0°C – rt, on, rt	15%
8	DIAD, PPh ₃ , THF, 18 h, rt	107
9	EDC·HCl, DMAP (103), 84a , CH ₂ Cl ₂ 24 h, rt	no full conversion*
10	HBTU, DBU, 84a , 18 h, THF, rt	traces*
11	COMU [®] (109), DBU, 84a , 18 h, CH ₂ Cl ₂ , rt	34%
12	POCl ₃ , DMAP (103), Et ₃ N, 84a , 22 h, CH ₂ Cl ₂ , rt	no full conversion*
13	T3P, DBU, 84a , THF	107

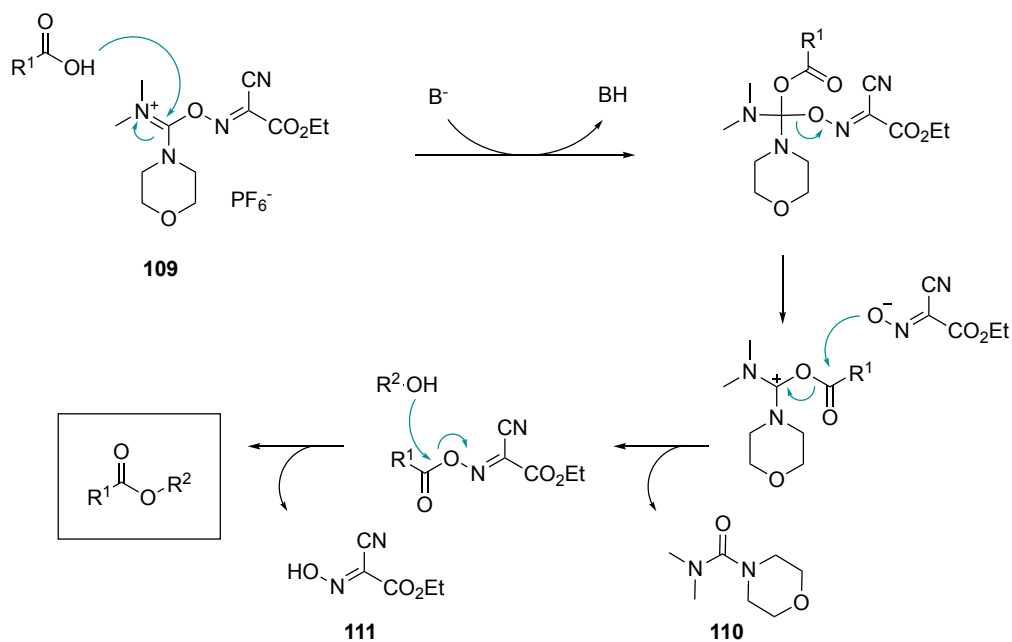
First, attempts were undertaken to convert nalidixic acid (**81**) to the acyl chloride using thionyl and oxalyl chloride, followed by the addition of the alcohol **84a** as described in the literature for the derivatization of nalidixic acid (**81**).^[126,127] However, with thionylchloride, only traces of the product **108a** were to be formed as judged by LCMS, which could not be isolated (entry 1). The reaction conditions with oxalylchloride gave **108a** in 12% yield when

the alcohol was added to the acyl chloride dissolved in CH_2Cl_2 , but not when it was added neat (entries 2,3). The formation of acyl chloride was extended to 48 h at rt, again only trace amounts were obtained (entry 4).

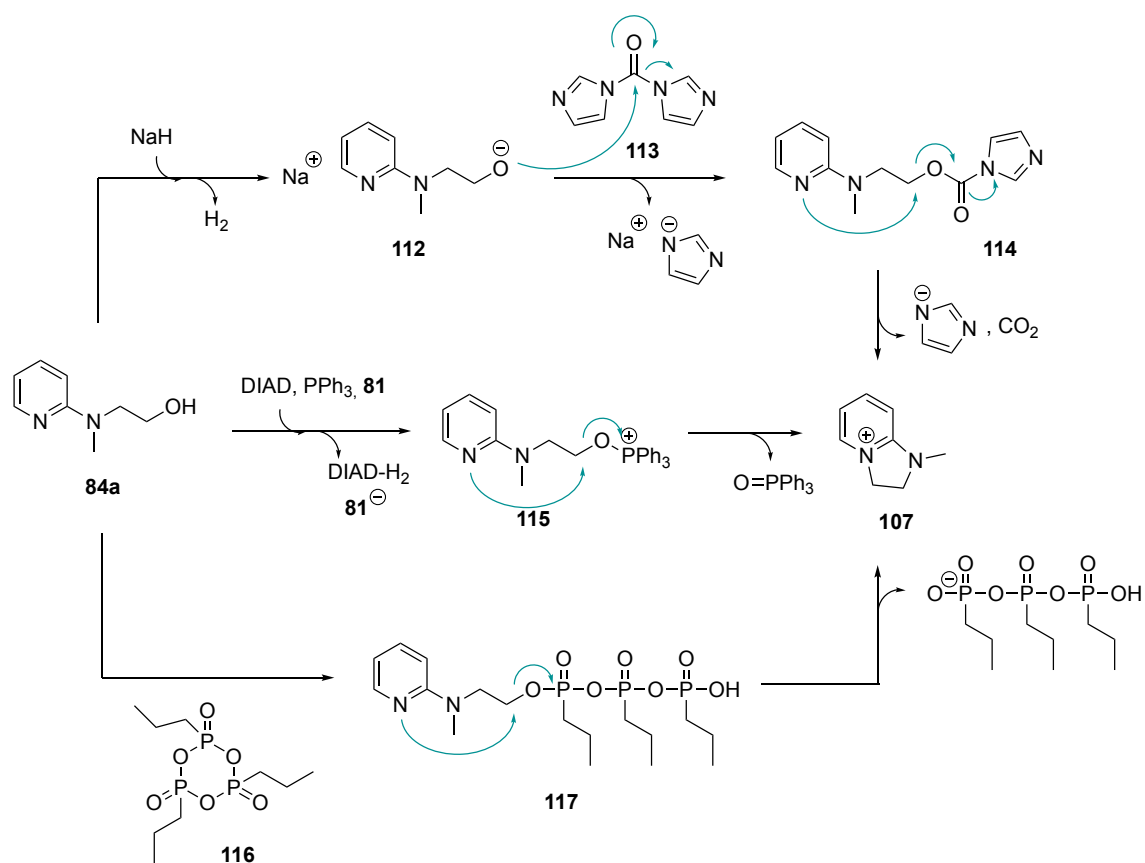
It was then attempted to activate nalidixic acid (**81**) with CDI (**113**) and add it to a solution of alcoholate **112** which was generated using NaH as base (entries 5-7). This reaction gave the ester **108a** in 15% yield only when DBU was used as base in the acylimidazole formation. When no base or Et_3N was used, a bright pink color emerged, indicating the formation of the pyridinium ion **107**, which was also identified by HRMS. Probably neither imidazole nor Et_3N with *pKa* of 6.95 and 10.76, respectively, are strong enough to deprotonate a weak acid such as nalidixic acid (**81**), which would prevent acylimidazole formation. The unreacted CDI (**113**) could then be attacked by the alcoholate **112**, forming carbamate **114** which is subsequently cyclized to **107** with the release of imidazole anion and CO_2 . Similarly, MITSUNOBU conditions lead to cyclized pyridinium ion **107** (entry 8). Again, intramolecular cyclization seems to occur prior to the attack of nalidixic acid (Scheme 33).

The typical coupling conditions using EDC·HCl, DMAP (**103**) or HBTU (entries 9 and 10) also gave only traces of product. Finally, the use of the uronium-based coupling agent COMU[®] (**109**) (entry 11) gave the ester **108a** in 34% yield.^[128] A major problem, however, was the purification. Separation of **37** and the urea product of COMU[®] **110** shown in Scheme 32 was difficult due to their similar *R_f* values. This could be one explanation for the moderate yield.

To overcome the purification problem, coupling with POCl_3 ^[129] was tested. However, similar to EDC·HCl and HBTU coupling, the reaction did not run to completion and only traces of product could be isolated (entry 12). The use of T3P (**116**) with DBU as base should activate nalidixic acid (**81**). However, the appearance of cyclized pyridinium ion **107** together with the bright pink color indicates activation of the alcohol to phosphoester **117** (Scheme 33).



Scheme 32: Postulated reaction mechanism for the esterification with COMU[®] (**109**) as coupling reagent (modified from^[128]).

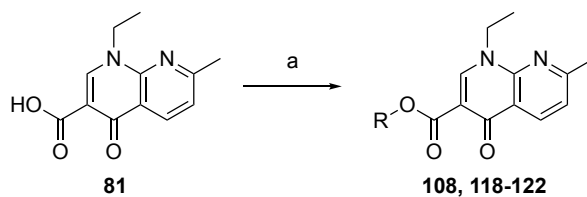


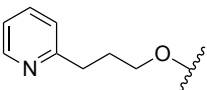
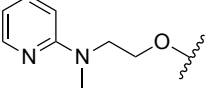
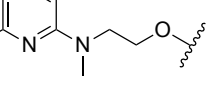
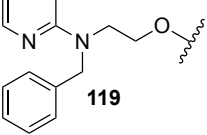
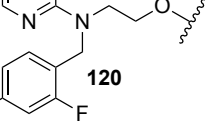
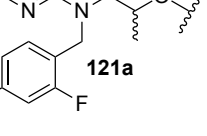
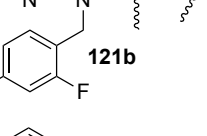
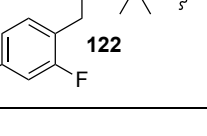
Scheme 33: Reaction pathways and intramolecular cyclization of **84a** to **107**.

Overall, only three conditions resulted in the formation of significant amounts of product **108a**: a) Acyl chloride formation with oxalyl chloride (entry 2) followed by addition of alcohol **84a**, b) activation of nalidixic acid (**81**) with CDI (**113**) and DBU (entry 7) followed by addition of alcoholate **112**, and c) esterification using COMU[®] (**109**) as coupling reagent and DBU as base (entry 11). Each time the alcohol was converted into a leaving group, intramolecular cyclization to the pyridinium ion **107** occurred within the first hour, indicated by the appearance of a bright pink color. Other standard coupling conditions did not lead to any significant formation of the desired product. Despite extensive purification required, the COMU[®] (**109**) conditions were chosen as the standard esterification reaction.

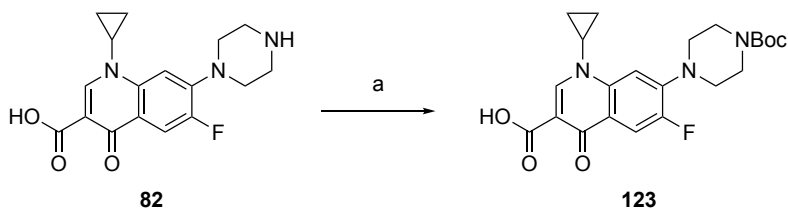
The esterification of nalidixic acid (**81**) was then carried out with a selection of the synthesized alcohols **83-87** (Table 10) using the COMU[®] (**109**) conditions to afford esters **118-62**. The coupling of alcohol **87a** did not give the desired ester **122** even after several days, probably due to steric bulk exerted by the neighboring methyl substituents (entry 8).

Table 10: Synthesis of nalidixic acid esters **118a-72**. a) 1.2 eq. alcohol, 1.5 eq. COMU[®] (**109**), 1.0 eq. DBU, CH₂Cl₂, rt, 18 h.



entry	alcohol	product	yield
1	83a	R=  118	25%
2	84a	R=  108a	36%
3	84b	R=  108b	10%
4	89	R=  119	49%
5	85a	R=  120	3%
6	86a	R=  121a	85%
7	86b	R=  121b	38%
8	87a	R=  122	no conversion

Before esterification with ciprofloxacin (**82**) could be carried out, the secondary amine of the piperazine moiety had to be protected. Therefore, the Boc group was introduced furnishing Boc-ciprofloxacin **123** (Scheme 34).

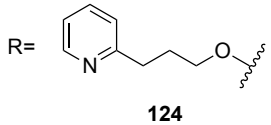
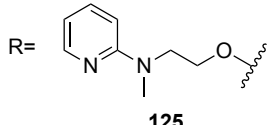
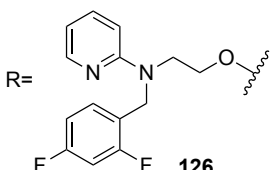
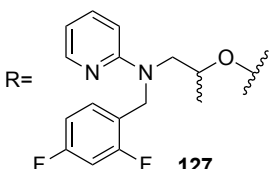


Scheme 34: Preparation of Boc-protected ciprofloxacin (**123**). a) 1.5 eq. di-*tert*-butylcarbonate, NaOH, H₂O:dioxane, rt, 18 h, >99%.

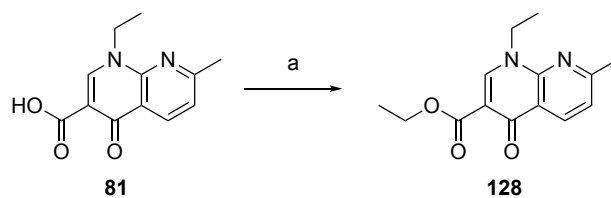
Boc protection proceeded quantitatively after 18 h. The ciprofloxacin **123** could then be used for COMU[®] (**109**) esterification (Table 11). The same conditions were chosen as for the synthesis of the nalidixic esters **118a** - **121**. Immediately after completion of the reaction, TFA was added to the reaction mixture to remove the Boc group. Compared to the nalidixic acid esters **118a** – **121**, the R_f values of the ciprofloxacin esters **124** – **127** are very different in the normal phase, which greatly facilitated the isolation. Nevertheless, the yields are obtained in a moderate range.

Table 11: Synthesis of ciprofloxacin esters **124-127**. a) 1.2 eq. alcohol, 1.5 eq. COMU[®] (**109**), 1.0 eq. DBU, CH₂Cl₂, rt, 18 h then TFA 3 h.

Reaction scheme showing the conversion of ciprofloxacin (**123**) to its ester form (**124-127**) using reagent 'a'.

entry	alcohol	product	yield
1	83a	R=  124	3%
2	84a	R=  125	2%
3	85a	R=  126	30%
4	86a	R=  127	11%

To later compare the cyclodeesterification reaction with ester hydrolysis, nalidixic acid ethyl ester (**128**) was synthesized by the standard esterification procedure in EtOH with H₂SO₄ as catalyst (Scheme 35). This reaction proceeded in only 52% yield, which is consistent with yields for nalidixic acid ethyl ester (**128**) in the literature.^[130]



Scheme 35: Preparation of nalidixic acid ethyl ester (**128**). a) H₂SO₄, EtOH, 90 °C, 4 d, 52%.

7.4.2 Release Experiments

The release of nalidixic acid (**81**) from the conjugates at different temperatures was monitored by LC analysis combined with UV detection. For each ester, the appropriate gradient was determined and calibration of nalidixic acid (**81**) ($\lambda = 256$ nm) was performed.

First, the stability of nalidixic acid (**81**) under the selected conditions had to be confirmed. Thus, approximately 100 ppm of nalidixic acid (**81**) was dissolved in 10% DMSO in H₂O and heated to 95 °C for 3 d. Figure 33 shows that the concentration of nalidixic acid (**81**) did not decrease until day 3. Rather, an increase to 120% was observed, likely due to evaporation of water during heating. Thus, nalidixic acid (**81**) appears to be stable at high temperatures in an aqueous environment, making it an optimal antibiotic for heat-induced release from SPIONS compared with penicillin G (**104**). For subsequent application in the human body, the heat exposure and complete release of the antibiotic should occur in less than one hour, so the increase in concentration after one day should not affect subsequent release studies too much.

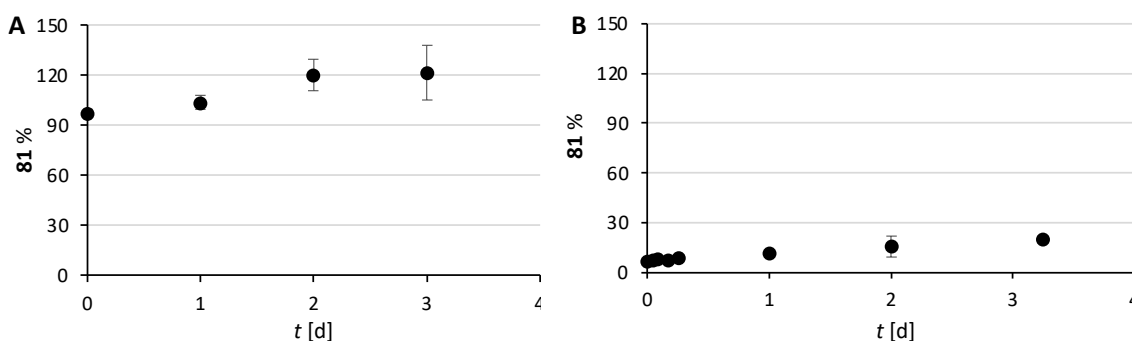


Figure 33: Stability of nalidixic acid (A) and hydrolysis of nalidixic ester **128** (B) in 10% DMSO in H₂O at 95 °C over 3 days. Shown are the standard deviations from the mean (n = 3).

Ethyl ester **128** was used to monitor the ester hydrolysis reaction at 95 °C. For this purpose, ester **128** was dissolved in 10% DMSO in H₂O and heated to 95 °C and the evolution of nalidixic acid (**81**) was measured. Figure 33 shows the nalidixic acid (**81**) as a percentage of the maximum possible release, which was set to 100%. A linear increase from 0% to 30% in the first three days can be seen. This result shows that ester hydrolysis of **128** is relatively slow under aqueous conditions.

Next, the synthesized nalidixic acid esters **108a,b** and **118-121** were tested for the release of nalidixic acid (**81**) at 37 °C and 95 °C (Figure 34). At 37 °C, almost all conjugates tested showed no detectable release of nalidixic acid (**81**) even after 24 h. Only for the esters **108a** and **b**, a release of 2% was observed after 2 h at 37 °C and 14% and 30% after 16 h,

respectively. Another interesting observation was the decrease in the concentration of benzylamine esters **119**, **121a** and **121b** at 37 °C (data not presented), whereas no release of nalidixic acid (**81**) was detected. It was demonstrated that this was due to precipitation of the esters from solution at 37 °C. It was assumed, that incorporation into water soluble nanoparticles would enhance solubility of these esters and thus, precipitation at this temperature was not considered problematic.

At 95 °C, all ester conjugates released nalidixic acid (**81**) much faster than the observed hydrolysis of nalidixic acid ethyl ester (**128**). The fastest release was observed for conjugate **108b** with complete release of acid after only 20 min. The conjugate **108a** and the benzylamines **119** and **120** released nalidixic acid more slowly, with maximum release after approximately 1 h at 95 °C. The differences between the release from methylamines and benzylamines are neglectable (Figure 34). The fact that no release was observed from benzylamine conjugate **119** or difluorobenzyl conjugate **120** at 37 °C, whereas nalidixic acid could be detected from **108a** after a few hours, supports the hypothesis that the benzyl group stabilizes the ester at lower temperatures.^[119]

The release from the secondary esters **121a** and **121b** was significantly slower than from the previously discussed primary esters **108a,b**, **119** and **120**. A release of 100% was observed between 16 h and 24 h (data not presented), and after 3 h only 60% of nalidixic acid (**81**) was released. Here, the 2-methyl group did not have the strong effect on the cyclization rate as found for **108a** and **108b**. The THORPE-INGOLD effect postulated to enhance the cyclization of these secondary esters appears to be neglectable compared with the reduced electrophilicity of the carbon directly next to the ester due to the positive inductive effect of the methyl group. If the tertiary ester from **87a** had been available, the cyclization would probably undergo even slower. To further investigate the THORPE-INGOLD effect, it would have been interesting to observe the release of nalidixic acid (**81**) from the ester of nalidixic acid (**81**) and alcohol **88a** which was not synthesized in this study.

The slowest release of nalidixic acid (**81**) was observed from ester **118** without the amine. As suspected, the pyridine nitrogen of the 2-Py-TPG is less nucleophilic, causing in a slower cyclodeesterification rate.

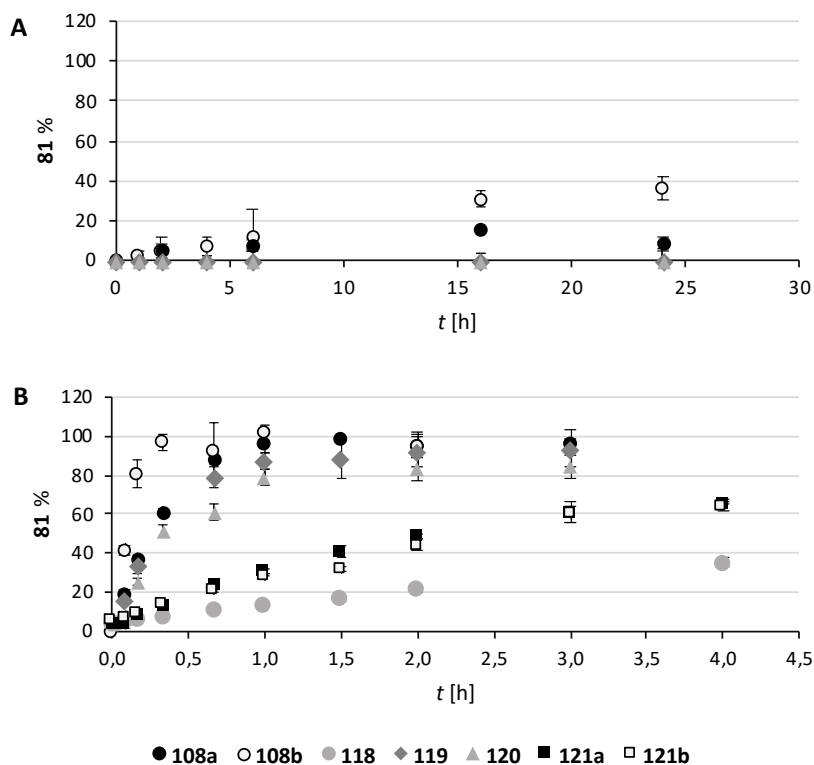


Figure 34: Release of nalidixic acid (**81**) from esters **108a,b** and **118 – 121a,b** through cyclodeesterification at 37 °C (**A**) and 95 °C (**B**) in 10% DMSO in H₂O at 95 °C. Shown are the standard deviations from the mean (n = 3).

The release of ciprofloxacin (**82**) was also monitored (Figure 35). Esters **125** and **127** were selected for comparison to the nalidixic acid esters **108a** and **121a**, respectively. Since the *pKa* of ciprofloxacin (**82**) is lower than of nalidixic acid (**81**) with 6.1 and 8.6, respectively, the cyclization was expected to be faster. The same release conditions were used as for nalidixic acid (**81**) release, and calibration was performed with the hydrochloride of ciprofloxacin (**82**).

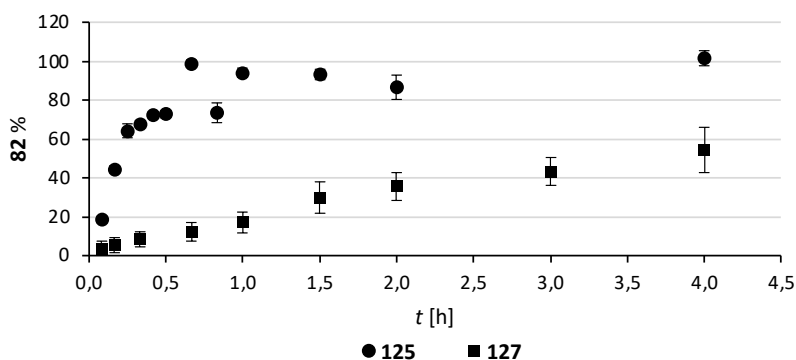


Figure 35: Release of ciprofloxacin (**82**) from esters **125** and **127** through cyclodeesterification at 95 °C in 10% DMSO in H₂O at 95 °C. Shown are the standard deviations from the mean (n = 3).

At 37 °C, no detectable release was observed from either ester during the first 16 h. Ester **127** did not precipitate from the solution as it was observed for nalidixic acid ester **121a** at this temperature. At 95 °C, **125** released ciprofloxacin (**82**) already between 30 and 40 min, which is significantly faster than the corresponding nalidixic ester **108a**. Complete release from conjugate **127** was observed after approximately 12 h at 95 °C. This indicates that the release of the lower *pKa* acid ciprofloxacin (**82**) is indeed faster than nalidixic acid (**81**).

Overall, all quinolone antibiotic esters tested released the antibiotic faster than ester hydrolysis. At 95 °C, the release of the antibiotic during the first hour was observed for esters from alcohols **84a,b**, **89** and **85a**, whereas the release was much slower for the esters from alcohols **83a** and **86a,b**. At 37 °C esters from benzylamine alcohols **84a,b** were sufficiently stable during the first 4 h while all other esters were stable during the entire time of the experiment. The thermal release of ciprofloxacin **82** from the 2-Py-TPG esters was faster than that of nalidixic acid **81**, and the benzylamine esters of ciprofloxacin such as **127** exhibit improved solubility than the corresponding nalidixic acid esters **121a,b**. Therefore, the esters of benzylamine or difluorobenzylamine alcohol **89** and **85a** with ciprofloxacin **82** should be ideal for the nanoparticle conjugate and application in human. However, due to easier accessibility, the first trials for the synthesis of nanoparticle conjugates were conducted using the system of nalidixic acid ester **108a,b**.

7.5 PEGylation and Connection to SPION

7.5.1 Nanoparticle Conjugate A: Design and Retrosynthesis

Having established the appropriate 2-pyridinylalcohol **84a** for the release of quinolone antibiotics, the connection of the construct to the MagSilica[®] SPION was planned. In the following, the 2-pyridinyl alcohols will be referred to as thermolinkers because of their ability to release acids at elevated temperature. A PEG spacer should be placed between the thermolinker-antibiotic conjugate and the SPION. This spacer can not only improve the bioavailability of the SPION, but also be used to fine-tune the thermal release because the length of the PEG spacer correlates with the temperature arriving at the thermolinker from the SPION core^[85]. In a first attempt to synthesize a nanoparticle-antibiotic conjugate consisting of the silica coated SPION MagSilica[®], a PEG spacer, the thermolinker and the antibiotic a three-module approach was chosen to yield the conjugate structure **A**. It consists of the three modules **Ia**, the SPION, the silica functionalization structure **IIa** and the antibiotic conjugate structure **IIIa** (Figure 36).

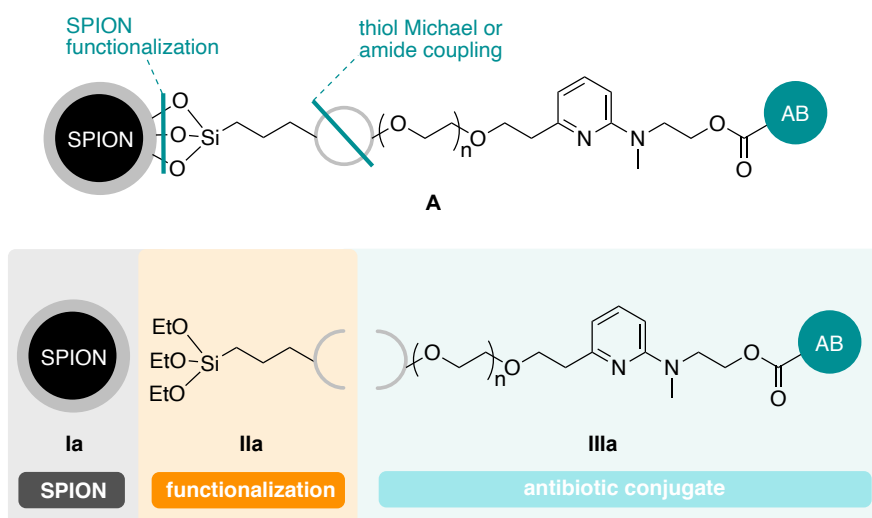


Figure 36: Composition of nanoparticle conjugate structure **A**.

For functionalization of MagSilica[®], APTES (**46**) and the MTES (**47**) were chosen for amino and maleimide functionalization, respectively (Figure 37). The combination of modules **IIa** and **IIIa** was to be realized by amide coupling or thiol MICHAEL addition to maleimide.

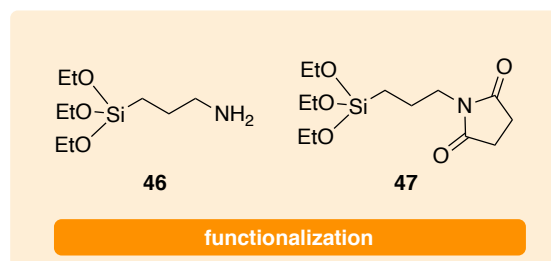
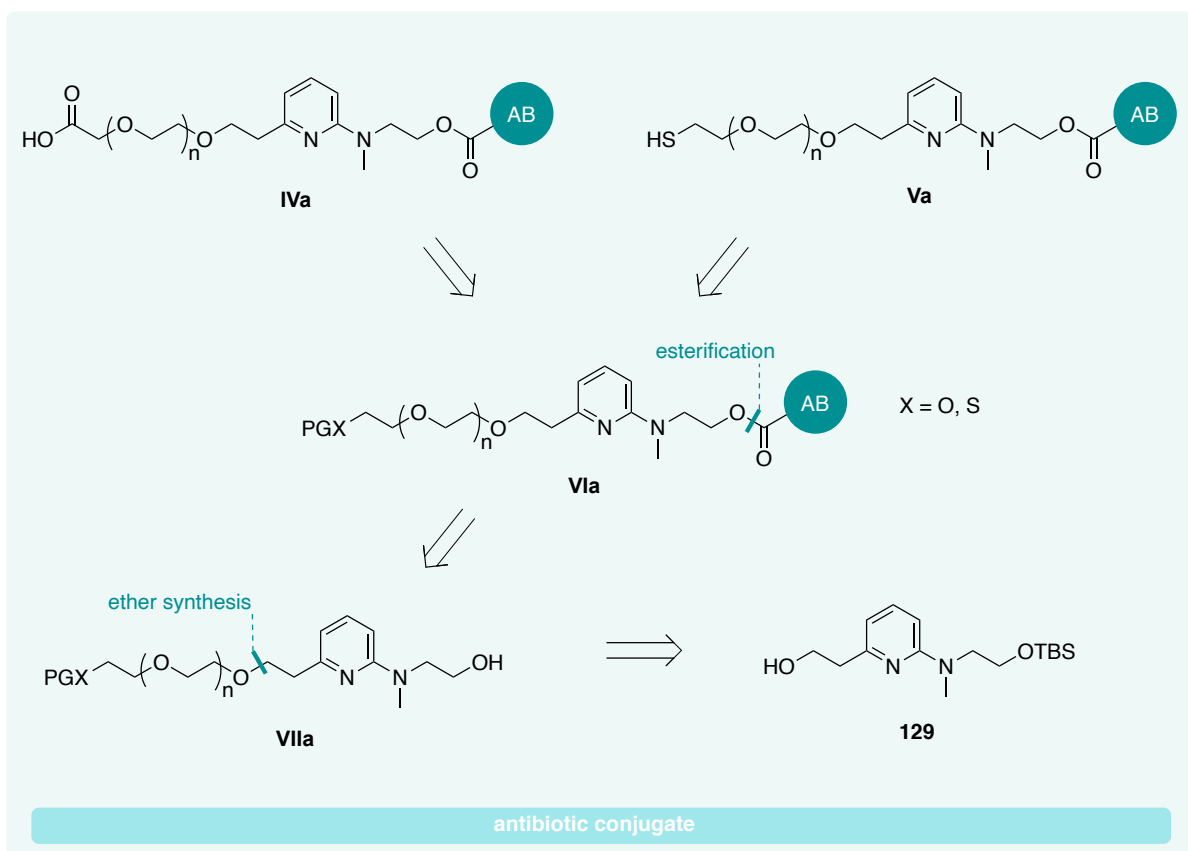


Figure 37: TES ether modules **IIa** for amino functionalization APTES (**46**) and maleimide functionalization MTES (**47**).

Thus, module **IIIa** would have to carry either a terminal carboxylic acid as in **IVa** or a terminal thiol as in **Va** (Scheme 36). The carboxylic acid in conjugate **IVa** should be introduced by late oxidation of a terminal alcohol. Both conjugates **IVa** and **Va** would be synthesized from a similar common precursor **VIa** containing either a protected terminal alcohol or thiol. The antibiotic would be introduced via esterification as in the previous chapter. The PEG spacer of **VIIa** should be introduced by classical ether synthesis of the corresponding PEG with the alcohol **129**.

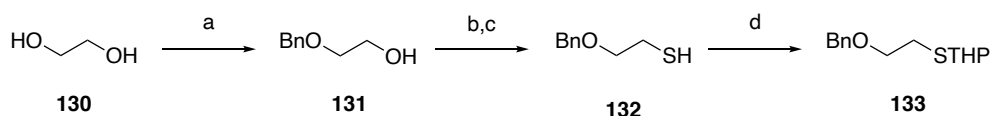


Scheme 36: Retrosynthesis of module **IIIa** for nanoparticle conjugate structure **A** with a terminal acid **IVa** for amid coupling and terminal thiol **Va** for thiol MICHAEL addition.

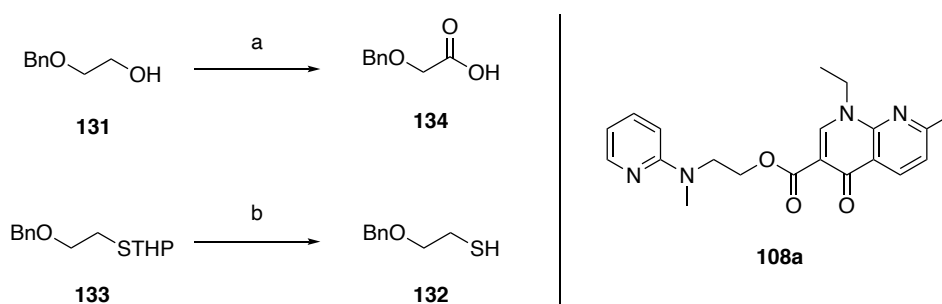
7.5.2 Nanoparticle Conjugate A: Forward Synthesis

It was assumed that the ester group between the thermolinker and the antibiotic in **VIa** is the most sensitive part of the molecular architecture. Therefore, the oxidation of the alcohol to the corresponding acid **IVa** as well as removal of the thiol to **Va** was first tested with more simple substrates. The corresponding test substrates alcohol **131** and thiol **133** were synthesized as benzyl ethers from ethylene glycol (Scheme 37). Nalidixic acid conjugate **108a** was used as a control for ester stability (Scheme 38).

For the oxidation to acid **134**, standard conditions for the direct oxidation were tested first. Oxidation with ruthenium chloride^[131] and TEMPO^[132] afforded the acid, but conjugate **108a** could not be reisolated. However, when the alcohol was oxidized in two steps with DESS-MARTIN periodinane followed by PINNICK oxidation, ester **108a** could be isolated in quantitative yield after basic extraction, while the acid was found after acidic extraction. In the case of deprotection of **133**, the standard conditions with TFA gave **132** and **108a** in quantitative yields.



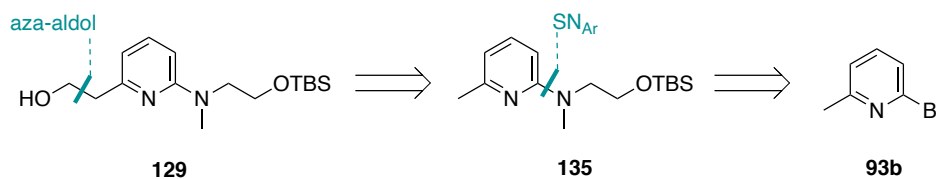
Scheme 37: Synthesis of test substrates alcohol **131** and THP-thiol **132**. a) 0.2 eq. NaH, THF, 0 °C – rt, 1 h then 0.2 eq. BnBr, 66 °C, 12 h, 82% based on BnBr; b) PPh₃, CBr₄, CH₂Cl₂, 0 °C – rt, 18 h, 74%; c) thiourea, EtOH, 80 °C, 3 h then 10% aq. NaOH, 3 h, 19%; d) DHP, MgBr₂, CH₂Cl₂, rt, 2 h, 44%.



Scheme 38: Stability of **108a** during oxidation of **131** and deprotection of **133**. a) DMP, CH₂Cl₂, rt, 1 h then NaClO₂, KH₂PO₄, 2-methyl-2-butene, THF:H₂O = 1:1, rt, 40 min; b) CH₂Cl₂:TFA = 1:1, rt, 2 h, quant.

After ensuring that the final steps prior to joining with the nanoparticle could be carried out without cleavage of the antibiotic, the synthesis of ester **V** was continued (Scheme 39). In a first attempt, alcohol **129** was to be synthesized using *aza*-aldol conditions from

aminomethylpyridine **135**, which was synthesized from 2-bromo-6-methylpyridine (**93b**) as described in the previous chapter.



Scheme 39: Retrosynthesis of common precursor **129** via *aza*-aldol and S_NAr .

The *aza*-aldol conditions for the introduction of an alcohol group into compound **129** were thought to be promising, since they have already been applied to the similar compounds in the literature (Figure 38, alcohols **136** and **137**).^[133]

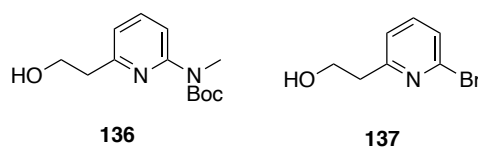
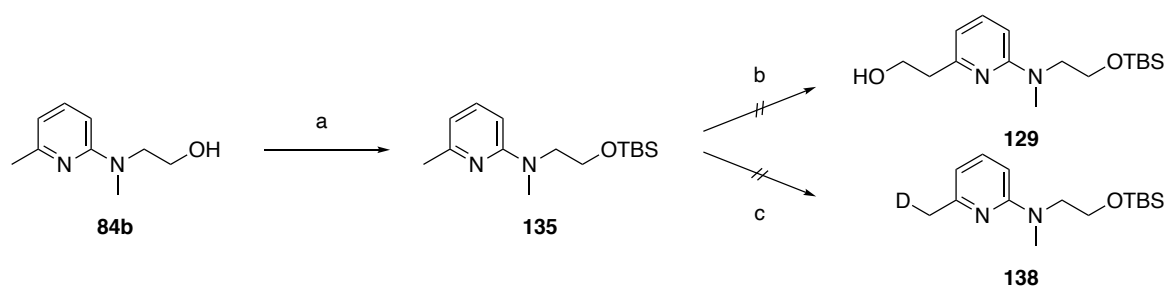


Figure 38: Aminopyridine and bromopyridine alcohols **136** and **137** synthesized through an *aza*-aldol reaction using DMF.^[133]

For the reaction, the benzylic position was deprotonated with lithium diisopropylamine (LDA). DMF was then added to the imine and the resulting tertiary amine was converted to the corresponding aldehyde with methanol and acetic acid. This was then reduced to alcohols **136** and **137** in yields of 44% and 85%, respectively. Unfortunately, the desired alcohol **129** could not be obtained under these conditions (Scheme 40).

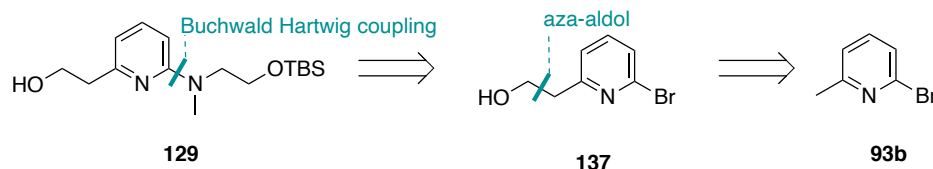


Scheme 40: Attempted synthesis of **129** through an *aza*-aldol reaction. a) TBSCl, imidazole, 48 h, 90%; b) *n*-BuLi, DIPA 0 °C, 1 h then **135** 0 °C, 1 h, then DMF 78 °C, 30 min then MeOH, glacial acetic acid, NaBH₄ -78 °C – rt, 18 h; c) different bases, 0 °C – rt, 1 h – 18 h then MeOD.

It was suspected that the benzylic position was not basic enough for deprotonation due to the electron donating property of the amino substituent of **135** compared to **136** and **137**. Therefore, this step of the reaction was monitored by stopping the deprotonation with

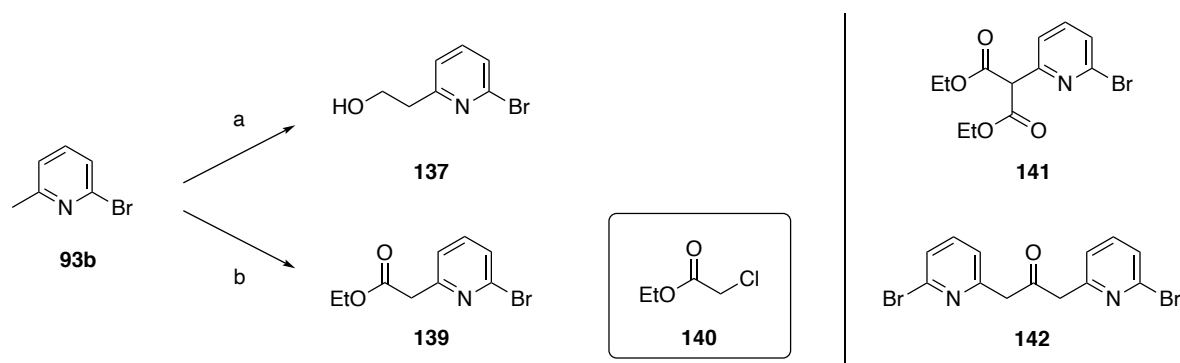
deuterated methanol. None of the conditions tested with various bases at different temperature and time gave the deuterated methylpyridine **138**, confirming this assumption.

The retrosynthesis was then modified. Now the amine in compound **129** was planned to be introduced after the alcohol group through a BUCHWALD-HARTWIG coupling of bromide **137**, which should be synthesized under the *aza*-aldol reaction conditions described above (Scheme 41).



Scheme 41: Retrosynthesis of common precursor **129** via BUCHWALD-HARTWIG coupling and *aza* aldol reaction from **93b**.

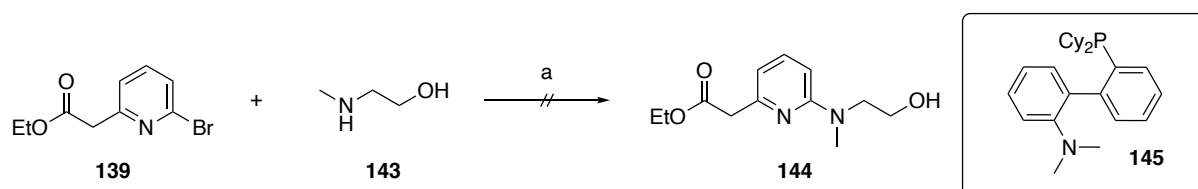
In contrast to the literature, the *aza*-aldol reaction from bromide **93b** to alcohol **137** did not proceed in high yields of 85% as described,^[133] but yields of 18% were obtained. A similar observation was also made by another group that obtained a maximum yield of 31%.^[134] They applied a different approach in which the benzylic position was also deprotonated using LDA, but instead of adding DMF, 0.5 equivalents of ethyl chloroformate (**140**) were added to give the ester **139** in 86% calculated on ethyl chloroformate (**140**). These reaction conditions were successfully applied in 71% yield.



Scheme 42: of **137** and **139** from **93b**.^[134] a) n-BuLi, DIPA 0 °C, 15 min then **93b**, -78 °C, 30 min then DMF, -78 °C, 30 min then MeOH, glacial acetic acid, NaBH₄, -78 °C – rt, 18 h, 18%; b) n-BuLi, DIPA 0 °C, 30 min then **93b**, -78 °C, 30 min, then 0.5 eq. **140**, -78 °C, 30 min, then rt, 1 h, 71% calculated on **140**. Undesired byproducts **141** and **142** are observed with an excess of base, ethylchloroformate **140**, higher temperature or longer reaction time.

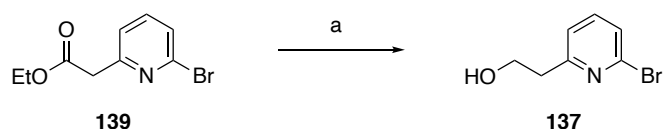
The exact amounts of base and ethyl chloroformate (**140**), as well as temperature, concentration and time are critical in this reaction. An excess of base and ethyl chloroformate (**140**) leads to formation of the undesired diester **141**, which cannot be separated from **139**. This is probably due to the benzylic proton in the ester **139** being more acidic than that of the starting material **93b**. The ketone **142** was observed with longer reaction time at room temperature when the excess of deprotonated methylpyridine was able to attack the ester **139**, releasing ethanol as leaving group (Scheme 42).

The BUCHWALD-HARTWIG coupling was first attempted using the ester **139** together with methylaminoethanol **143** and the mild base Cs_2CO_3 , which was reported to accept esters during coupling.^[135] After 3 h, the starting material had disappeared as judged by TLC, leaving a mixture of various compounds but not the desired product **144** (Scheme 43).



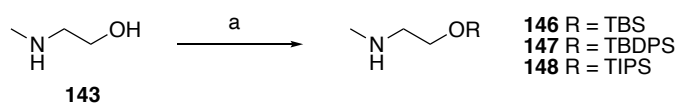
Scheme 43: 5% $\text{Pd}_2(\text{dba})_3$, 6% DavePhos **145**, 1.4 eq. Cs_2CO_3 , 1.2 eq. **143**, toluene, 80 °C, 3 h.

It was then decided to use the free alcohol **137** together with an amino silylether instead.^[136] The reduction of ester **139** was realized with DIBAL-H and gave the alcohol **137** in 99% yield, as described in the literature^[134] (Scheme 44).



Scheme 44: a) 2.2. eq. DIBAL-H, THF, 20 h, rt, 99%.

Three different silyl ethers **146-148** were prepared from methylaminoethanol **143**. It was assumed that their stability and steric hinderance would affect the coupling reaction in different ways (Scheme 45).



Scheme 45: a) 1.1 Eq. silylchloride, 2 eq. imidazole, CH_2Cl_2 , 20 h, 82% **146**, 99.9% **147**, 69% **148**.

The TBS-group of aminoethanol **146** was cleaved under the coupling conditions, so further studies were performed only with TBDPS and TIPS ethers **147** and **148**. The different ligands DavePhos **145**, RuPhos **149** and (\pm)-BINAP **150** (Figure 39), the solvents toluene and THF and weak base Cs_2CO_3 and the stronger base NaOtBu were tested (Table 12).

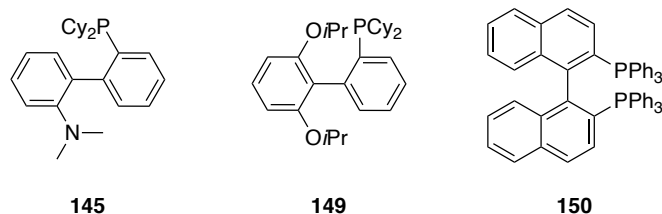
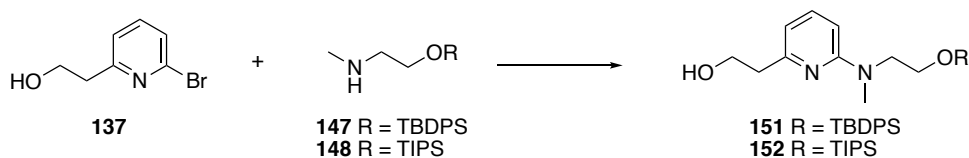


Figure 39: Ligands tested in BUCHWALD-HARTWIG coupling: DavePhos **145**, RuPhos **149** and (\pm)-BINAP **150**.

Table 12: Conditions for the BUCHWALD-HARTWIG coupling between bromide **137** and the amines **147** and **148**. The reactions were conducted at 60 - 80 °C for 20 - 96 h with 2.5 eq. base, 10% $\text{Pd}_2(\text{dba})_3$ and 11% ligand.



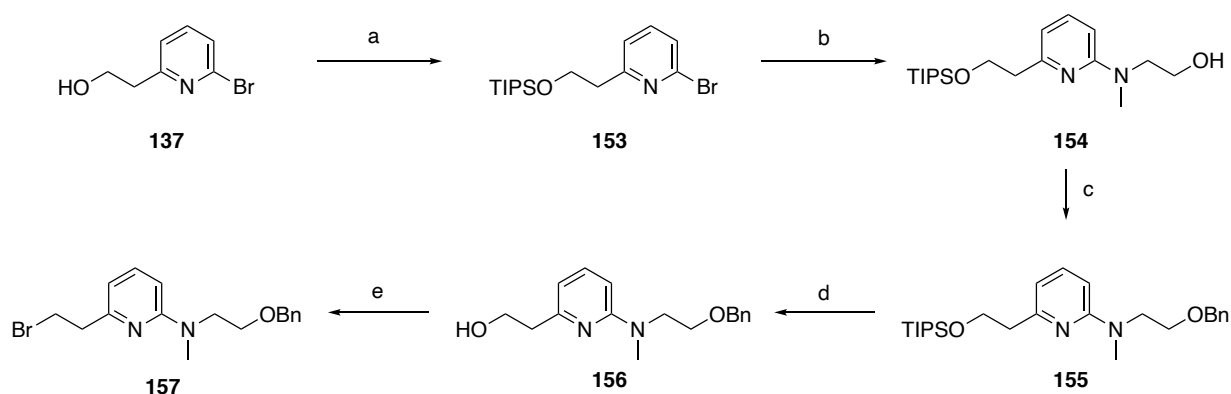
entry	R	base	ligand	solvent	yield
1			145	toluene	14%
2		NaOtBu	149	toluene	27%
3	TBDPS		150	toluene	35%
4			150	toluene	19%
5		Cs_2CO_3	150	THF	9%
6			145	toluene	26%
7		NaOtBu	149	toluene	16%
8	TIPS		150	toluene	34%
9			150	toluene	9%
10		Cs_2CO_3	150	THF	11%

From the results in Table 12 it seems that the silyl group has no significant influence on the coupling yields. Reactions with NaOtBu give higher yields than those with the weaker base Cs_2CO_3 under all tested conditions. DavePhos **145** is the better ligand for the TIPS ether **147** compared to RuPhos **149**, which gives better yields together with the TBDPS ether **148**.

(±)-BINAP **150** gives the highest yields for both silyl groups with 35% for alcohol **151** and 34% for alcohol **152**. No yields above 40% were observed, which was not satisfactory considering the high costs of catalyst and ligand.

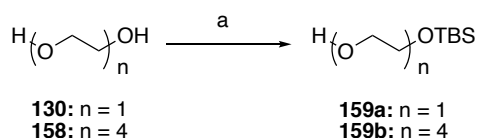
Therefore, it was considered to introduce the silyl ether to the alcohol of **137** instead of the methylaminoethanol **143**. Therefore, the silylation with TIPSCl was chosen because this compound had already been used in the literature for BUCHWALD-HARTWIG coupling.^[133]

Silylation of **137** to **153** proceeded in 99% yield, and the yields of the following coupling reaction to conjugate **154** increased dramatically. The conditions using the (±)-BINAP ligand **150** with NaOtBu as the base in toluene gave 56% yield after only 30 min, while the reaction with Cs₂CO₃ gave 76% after 20 h. Alcohol **154** was then transformed into the benzyl ether **155** in 72% yield. The TIPS group was successfully removed using TBAF to yield alcohol **156** in 89%. The alcohol **156** was then transformed to the bromide **157** using standard conditions with carbon tetrabromide and triphenylphosphine in 86% yield (Scheme 46).



Scheme 46: Silylation of **137** followed by BUCHWALD HARTWIG coupling with aminoethanol **143** to conjugate **154**. a) 1.1 eq. TIPSCl, 2 eq. imidazole, CH₂Cl₂, 20 h, 99%; b) 10% Pd₂(dba)₃, 11% BINAP **150**, 2.5 eq. Cs₂CO₃, 1.2 eq. **143**, toluene, 80 °C, 20 h, 76% or 10% Pd₂(dba)₃, 11% (±)-BINAP **150**, 2.5 eq. NaOtBu, 1.2 eq. **143**, toluene, 80 °C, 30 min, 56%; c) NaH, THF, 0 °C -rt, 1 h, then BnBr, 10% TBAI, 18 h, rt, 72%; d) 2.5 eq. TBAF (1M in THF), THF, 0 °C - rt, 1 h, 89%; e) 1.1 eq. PPh₃, 1.1 eq. CBr₄, CH₂Cl₂, rt, 2 h, 92%.

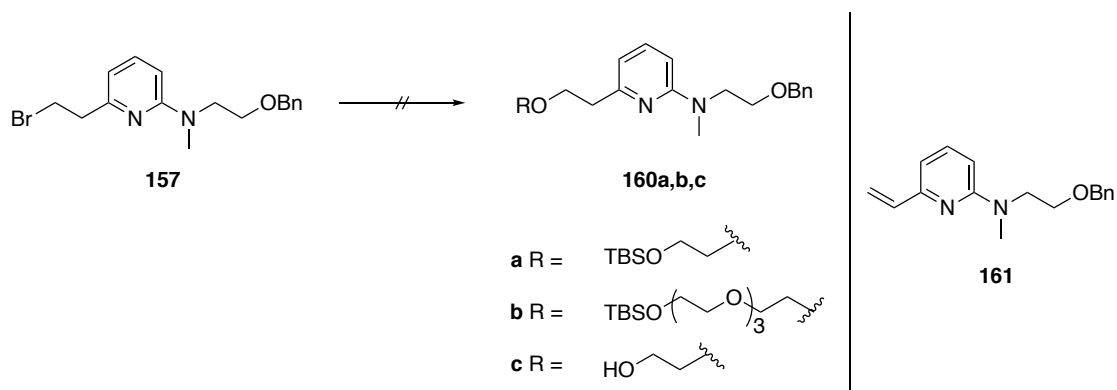
For the subsequent ether synthesis, ethylene glycol (**130**) and tetraethylene glycol (**158**) were transformed into the TBS ethers **159a** and **159b** in 24% and 31%, respectively (Scheme 47). The corresponding alcoholates for ether synthesis were generated *in situ* with NaH at 0 °C for 1 h. Unfortunately, only the elimination product **161** could be isolated under these conditions (Table 13, entry 1, 2 and 4).



Scheme 47: Synthesis of alcohols **159a** and **159b** for ether synthesis with bromide **157**. a) 1.3 eq. TBSCl, 3.7 eq. imidazole, CH₂Cl₂, 0 °C – rt, 18 h, 24% **159a**, 31% **159b**.

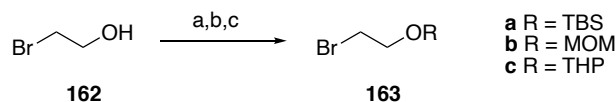
Conditions with catalytic amounts of silver oxide were also tried, since it was assumed that the less basic conditions would prevent elimination (Table 13, entries 3 and 5). Although elimination was prevented at higher temperatures, no conversion was observed either. To test whether steric hinderance by the silyl groups of **159a** and **159b** was responsible for the low reactivity of the alcoholate, 6.0 eq. of ethylene glycol (**130**) were transformed into the alcoholate and reacted with bromide **157** (Table 13, entry 6). As in the other experiments, only alkene **161** could be isolated (Table 13, entry 6).

Table 13: Ether synthesis of bromide **157** with alcohols **159a,b** and **130**. Reactions were conducted with THF as solvent.



entry	alcohol	reagents	temperature	Time	result
1		NaH, TBAI	0 °C - rt	18 h	161
2	1.1 eq. 159a	NaH	0 °C – rt	18 h	sm and 161
3		Ag ₂ O	rt – 80 °C	48 h	no conversion
4	1.1 eq. 159b	NaH	0 °C – 80 °C	18 h	161
5		Ag ₂ O	rt – 80 °C	18 h	no conversion
6	6.0 eq. 130	NaH, TBAI	0 °C – rt – 80 °C	18 h	161

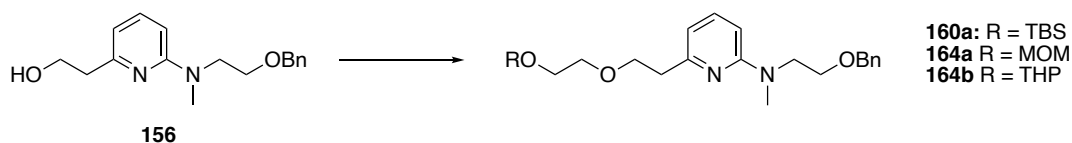
The strategy was then changed to alkylate alcohol **156** with the appropriate haloalkanes **163a-c**. Therefore, bromoethanol (**162**) was transformed into TBS, THP and MOM ethers. The reactions proceeded in considerable yield using standard methods (Scheme 48).



Scheme 48: Protection of bromoethanol (**162**) as different ethers. a) TBSCl, DIPEA, 0 °C – rt, 18 h, quant.; b) dimethoxy ethanol, P₂O₅, 0 °C – rt, 12 h, 60% c) DHP, 0.1 eq. PTSA, rt, 18 h, 84%.

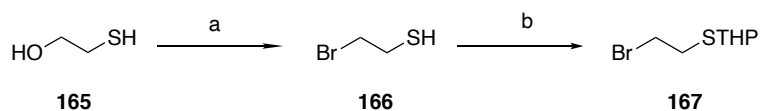
With the alkyl halides in hand, ether synthesis with the alcoholate of **156** was attempted. Different solvents, temperatures and times were tested to find the optimum conditions. The TBS- and MOM- ether alkyl halides **163a** and **163b** showed no conversion (Table 14, entry 1, 3 and 4) or gave only traces of product (Table 14, entry 2). More promising results were obtained with the THP alkyl halide **163c**. However, none of the conditions tested resulted in complete conversion. Maximum yields were observed with NaH as base and TBAI as catalyst after 18 h at rt in THF at about 20% conversion (Table 14, entry 7). These could be increased only slightly to 23% with higher reaction temperatures and longer reaction times (Table 14, entries 8 and 11). Even with the addition of 5 equivalents of alkyl halide, the reaction could not be brought to completion (Table 14, entry 16).

Considering the previous results, it seemed likely that alcoholate formation was incomplete. This was tested by stopping the deprotonation with NaH after 1 h at 0 °C with deuterated methanol. Mass analyses and NMR spectroscopic analysis in DMSO-d₆ showed a complete exchange of the proton for deuterium. Another hypothesis for the incomplete reaction could be steric hinderance induced by the THP group. Since the much smaller MOM alkyl halide **163b** did not yield the desired product, no further optimization was performed.

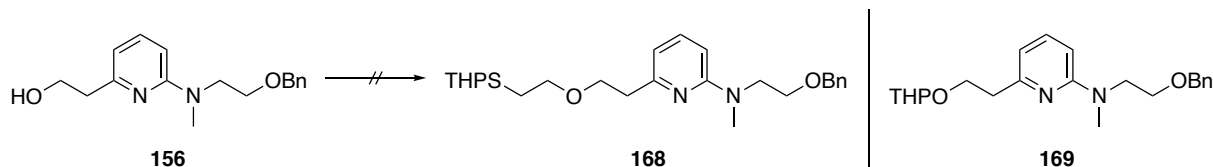
Table 14: Ether synthesis of alcohol **156** with bromides **163a, b, c**.

entry	bromide	solvent	reagents	temperature	Time	result	
1	1.3 eq. 163a	THF	Ag ₂ O	rt – 80 °C	36 h	no conversion	
2			NaH, TBAI	0 °C – 80 °C	36 h	traces of 160a	
3	1.3 eq. 163b	THF	NaH, TBAI	0 °C – rt	18 h	no conversion	
4		DMF	NaH, TBAI	0 °C – rt	18 h	no conversion	
5	1.3 eq. 163c		Ag ₂ O	rt – 80 °C	18 h	no conversion	
6			NaH	0 °C – rt	18 h	15% 164b	
7			THF	NaH, TBAI	0 °C – rt	18 h	20% 164b
8				NaH, TBAI	0 °C – 80 °C	36 h	25% 164b
9				NaH, TBAI	0 °C – 80 °C	4 d	16% 164b
10			DMF	KH	0 °C – rt	18 h	traces of 164b
11				NaH, TBAI	0 °C – 80 °C	36 h	25% 164b
12				NaH, TBAI	0 °C – 100 °C	4 d	20% 164b
13				NaH, TBAI	0 °C – 120 °C	4 d	traces of 164b
14				NaH, TBAI	0 °C – 150 °C	4 d	decomposition
15	acetone	NaH, TBAI	0 °C – rt	18 h	no conversion		
16	5.0 eq. 163c	THF	NaH, TBAI	0 °C – rt	18 h	20% 164b	

Alkylation was also sought with the corresponding thioether **167**. This was synthesized starting from mercaptoethanol **165**, which was halogenated using PBr₃ to obtain bromide **166**. The following ethersynthesis with DHP gave THP ether halide **167** in good yields (Scheme 49). However, subsequent alkylation of **156** did not lead to the desired product, but to the THP ether **168** in 11% yield (Scheme 50).



Scheme 49: a) PBr_3 , $-5\text{ }^\circ\text{C}$ – rt, 3 h, 8%; b) DHP, MgBr_2 , CH_2Cl_2 , rt, 2 h, 88%.



Scheme 50: Alkylation of alcohol **156** with bromide **167**. a) NaH , THF, 0°C –rt, 1 h, then **167**, 10% TBAI, $80\text{ }^\circ\text{C}$, 48 h.

Given the rather low yield of alkylation to introduce PEG to the thermosensitive linker and in view of the upcoming low yielding esterification to introduce the antibiotic, it was decided to consider a more simple approach for nanoparticle assembly.

7.3.3 Nanoparticle Conjugate B: Design and Retrosynthesis

In the previous route, it was planned to perform pegylation of the thermolinker by classical alkylation to obtain module **IIIa**. However, as described above, alkylation of the linker proved to be inefficient. In order to generate large amounts of modified nanoparticle, the simpler conjugate structure **B** was designed (Figure 40).

In this conjugate **B**, the previous module **IIIa** carrying the PEG spacer, thermolinker and antibiotic was divided into three modules **IIIb**, **IVb** and **Vb** respectively. **IIIb** and **IVb** are to be conjugated using the CuAAC^[137,138]. Compared to the previous alkylation reaction, this “click”-reaction can not only be conducted under milder conditions, but also allows the conjugation of the two modules at any point during the assembly of **B**, since they are compatible with almost all functional groups. Moreover, the resulting triazole species proves to be largely biocompatible,^[97] in particular, the ester between thermolinker **IVb** and antibiotic **Vb** is not affected by the conditions. The separation of module **IIIa** also enables a kind of “mix and match” synthesis of PEG spacer **IIIb**, thermolinker **IVb** and antibiotic **Vb**. This greatly simplifies testing of different PEG lengths for optimal physiological conditions or tuning of release temperature, as well as antibiotic screening.

Compared to the previous route to **A**, this conjugate design only considers amino functionalization of the SPION with APTES (**46**) which makes up module **IIb**. For the amide coupling of APTES (**46**) and PEG-spacer **IIIb**, the PEG was designed to have a terminal carboxylic acid on one side. The other side of PEG-spacer **IIIb** must contain either an alkyne or an azide in order to perform the CuAAC with thermolinker **IVb**, which should have the complementary functionality.

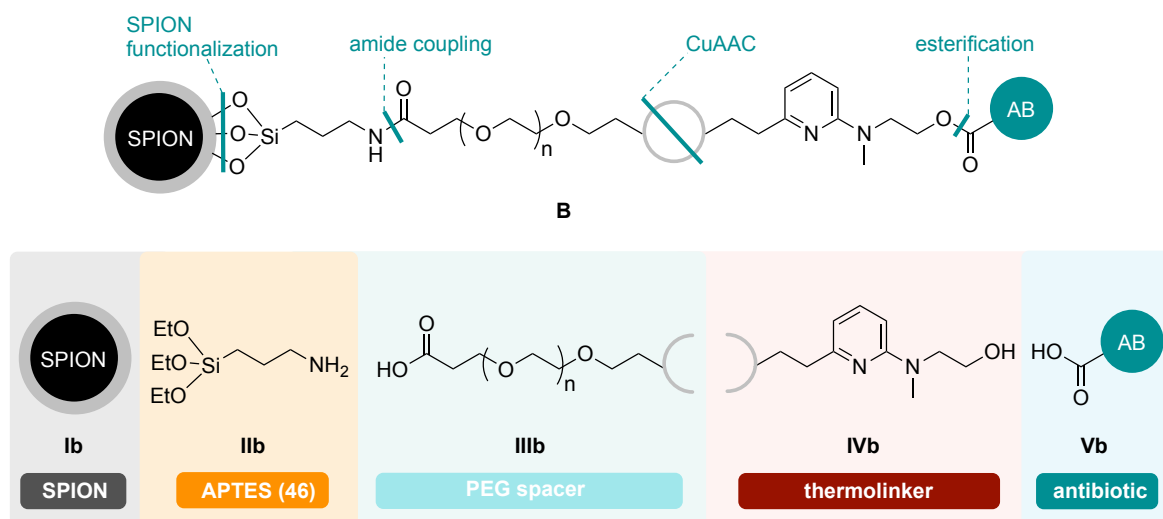
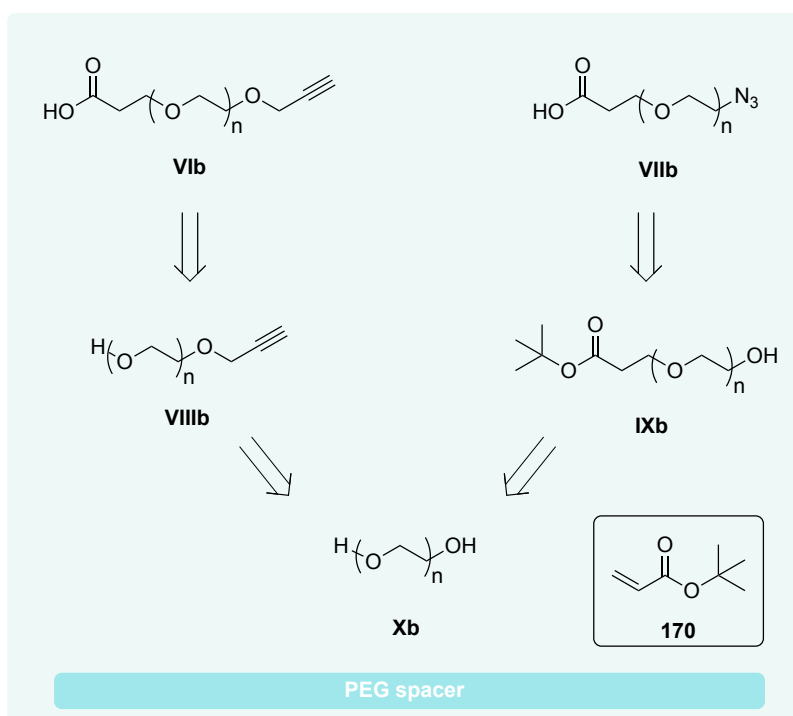


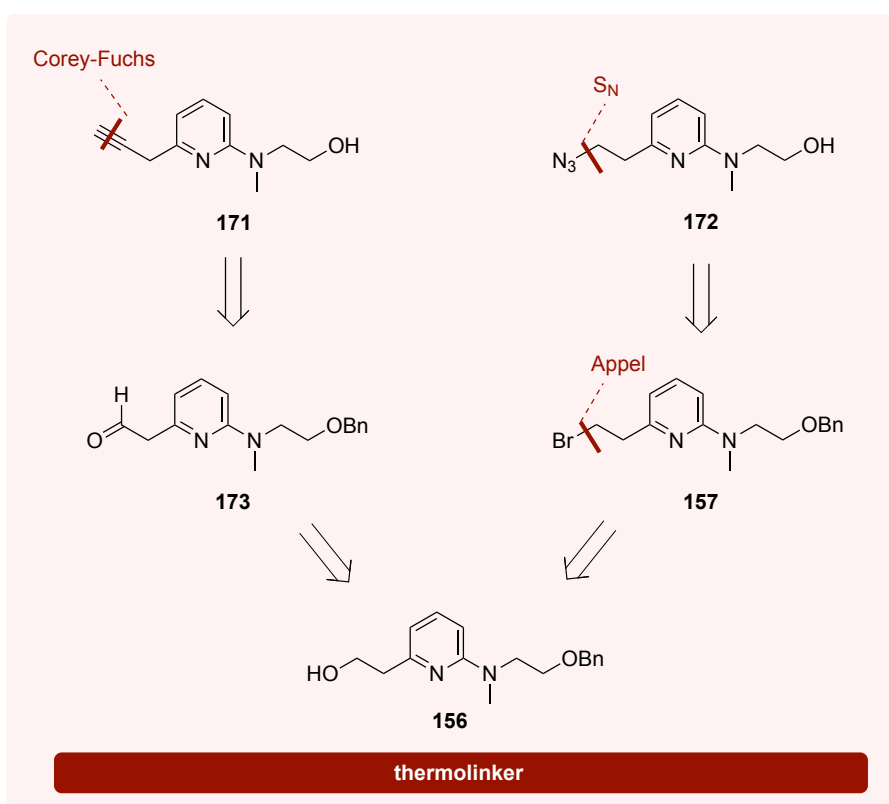
Figure 40: Composition of nanoparticle conjugate structure **B**.

Therefore, the synthesis of PEG-spacers with alkyne **VIb** and azide **VIIb** was planned. The PEG-spacer **VIb** should be synthesized by MICHAEL addition of the alcohol **VIIIb** to *tert*-butyl acrylate (**170**) followed by removal of the *tert*-butyl group with TFA. The alkyne in **VIIIb** is introduced by alkylation of propargyl bromide with PEG **Xb**. The synthesis of the azide **VIIb** follows a similar strategy. The alcohol in **IXb** was planned to be converted into the corresponding mesylate, followed by substitution with NaN_3 . Just as in **VIb** the carboxylic acid should be introduced by MICHAEL addition of PEG **Xb** to *tert*-butyl acrylate (**170**) (Scheme 51).

Similar to the PEG spacer, the thermolinker **IVb** should be synthesized with a terminal alkyne **171** or an azide **172**. The alkyne should be introduced by COREY-FUCHS reaction of aldehyde **173**, which was prepared from the common precursor alcohol **156**. The azide was to be synthesized from bromide **157**, which has already been synthesized in the previous chapter from alcohol **156** (Scheme 52).



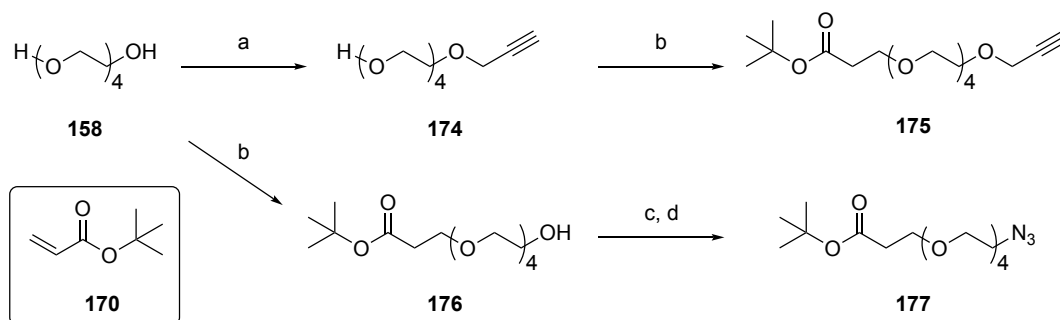
Scheme 51: Retrosynthesis PEG-spacers **VIb** and **VIIb** of module **IIIb** carrying a terminal alkyne or azide for CuAAC.



Scheme 52: Retrosynthesis thermolinkers **171** and **172** for module **IVb** carrying a terminal alkyne or azide for CuAAC.

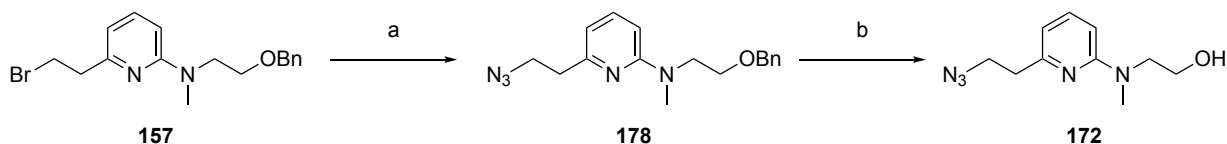
7.5.4 Nanoparticle Conjugate B: Forward Synthesis

The PEG-spacer synthesis **IIIb** was first started with tetraethylene glycol (**158**). Alkylation of the excess of **158** with propargyl bromide gave alkyne **174**. Subsequent MICHAEL addition with *tert*-butyl acrylate (**170**) also proceeded as planned and yielded the *tert*-butoxy PEG-spacer **175**. For the synthesis of **177**, the alcohol **176** was synthesized first. The MICHAEL addition was carried out as before with an excess of **158** and gave **176**. The alcohol **176** was mesylated and exchanged with an azide to give *tert*-butoxy PEG-spacer **177** (Scheme 53).^[139]



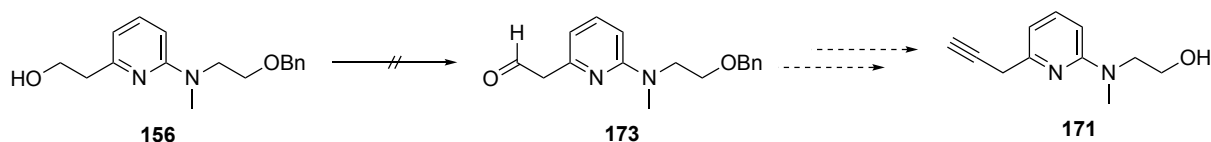
Scheme 53: Synthesis of activated ester **176** as first module **IIIb**. a) NaH, THF, 0 °C -rt, 1 h, then 0.35 eq. BrCH₂CCH, 10% TBAI, rt, 18 h, 89%; b) **170**, 1% NaOMe, THF, rt, 48 h, 79% (**175**), 11% (**176**); c) MsCl, Et₃N, CH₂Cl₂, 0 °C - rt, 16 h, 59%; d) NaN₃, DMF, 50 °C, 48 h, 79%.

In the following, the synthesis of alkyne **171** and azide **172** for module **IVb** was pursued. Starting from bromide **157**, the azide **178** was readily synthesized using the standard procedure with NaN₃. Removal of the benzylic alcohol was first attempted with H₂/Pd, which resulted in only small amounts of free alcohol, probably due to inactivation of Pd caused by the nitrogen. In contrast, when boron trichloride was used, free alcohol **172** was obtained quantitatively within 45 min. However, alcohol **172** did not prove to be stable over the long term, so in further experiments it was stored as benzyl **178** and freshly prepared before the following reaction (Scheme 54).



Scheme 54: Synthesis of azide **172** for module **IVb**. a) NaN₃, DMF, rt, 18 h, 88%; b) 10 eq. BCl₃, CH₂Cl₂, -78 °C, 45 min, quant.

Alkyne **171** was planned to be synthesized *via* COREY-FUCHS reaction starting from aldehyde **173**. Oxidation to the aldehyde was attempted using DESS-MARTIN periodinane. Conditions at -78 °C or -10 °C did not result in any amount of product. Decomposition was observed at 0 °C (Scheme 55). Since azide **172** as thermolinker (module **IVb**) and the corresponding PEG spacer alkyne **175** (module **IIIb**) were already available, further attempts to synthesize **171** were not performed.

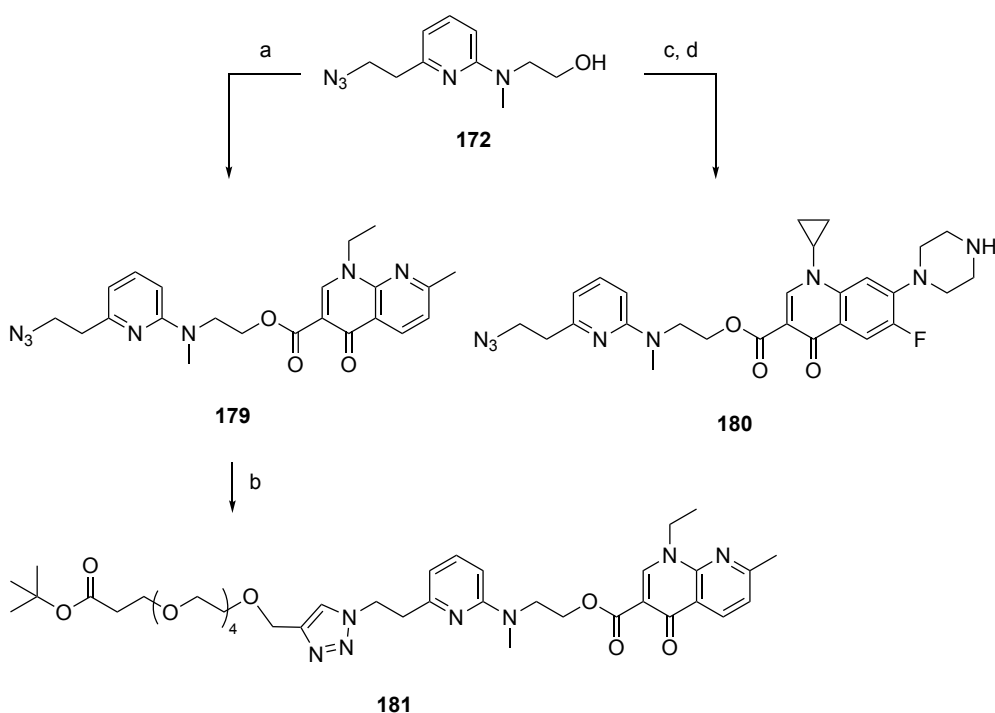


Scheme 55: Attempts to synthesize alkyne **171** for module **IVb**.

Once all the modules for nanoparticle conjugate **B** were in place, assembly was started. As in the previous section, the ester between the thermolinker **IVb** and the antibiotic **Vb** was considered to be the most susceptible part of construct **B**. For that reason, so the stability of the ester was first tested under copper catalysed 1,3-dipolar cycloaddition conditions.

Therefore, alcohol **172** was assembled with nalidixic acid (**81**) under the COMU[®] (**109**) coupling conditions described in section 7.4. The thermolinker-antibiotic conjugate **179** was then connected to the PEG-spacer alkyne **175** using standard conditions with copper sulfate and sodium ascorbate. The reaction gave the desired product in 57% yield, which was considered good enough for the next step. The thermolinker-antibiotic conjugate **180** with ciprofloxacin (**82**) could also be generated from coupling of ciprofloxacin **123** and alcohol **172** followed by Boc removal with TFA in 9% yield over two steps (Scheme 56).

Conjugate **181** was then used to validate the antibiotic release from a more advanced substrate. It was suspected that the longer PEG side chain might interfere with the thermal release. The same release conditions as in section 7.4 were used, and the release of nalidixic acid (**81**) was monitored by UV (Figure 41).



Scheme 56: Conjugation of thermolinker **172** and antibiotics **81** and **82** to **179** and **180**, respectively and evaluation of CuAAC reaction to **181**. a) Nalidixic acid (**81**), COMU[®] (**109**), DBU, CH₂Cl₂, rt, 18 h, 30%; b) **175**, CuSO₄, sodium ascorbate, THF:H₂O = 1:1, rt, 1 h, 57%, c) Boc-ciprofloxacin (**123**), COMU[®] (**109**), DBU, CH₂Cl₂, rt, 18 h; d) CH₂Cl₂, TFA, rt, 1 h, 9% o2s.

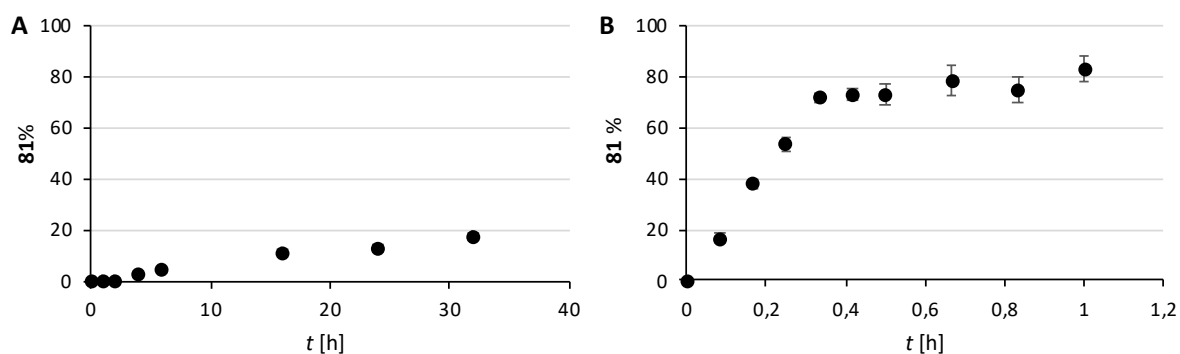
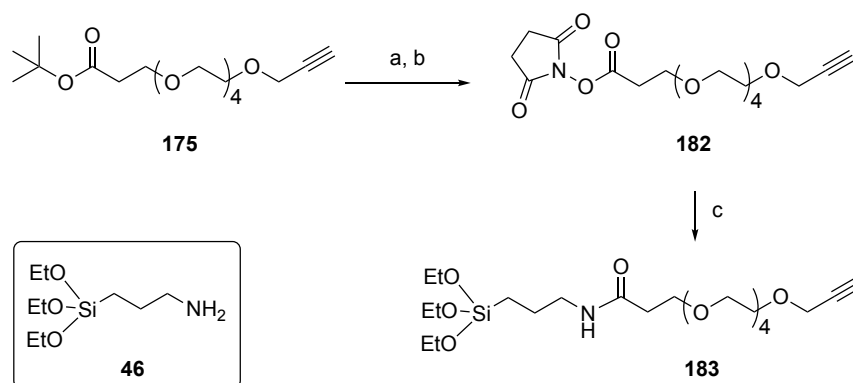


Figure 41: Release of nalidixic acid (**81**) from conjugate **181** at 37 °C (A) and 95 °C (B) in 10% DMSO in H₂O. Shown are the standard deviations from the mean (n = 3).

From the release assay, it is clear that the kinetics of conjugate **181** do not change compared to the test substrates in section 7.4. After one hour at 95 °C, 87% of nalidixic acid (**81**) is released (Figure 41, case B), while at 37 °C no detectible release is observed in the first 3 h and after 24 h less than 20% of nalidixic acid (**81**) is found (Figure 41, case A). Thus, it appears that the side chain does not interfere with the mechanism of cyclodeesterification and

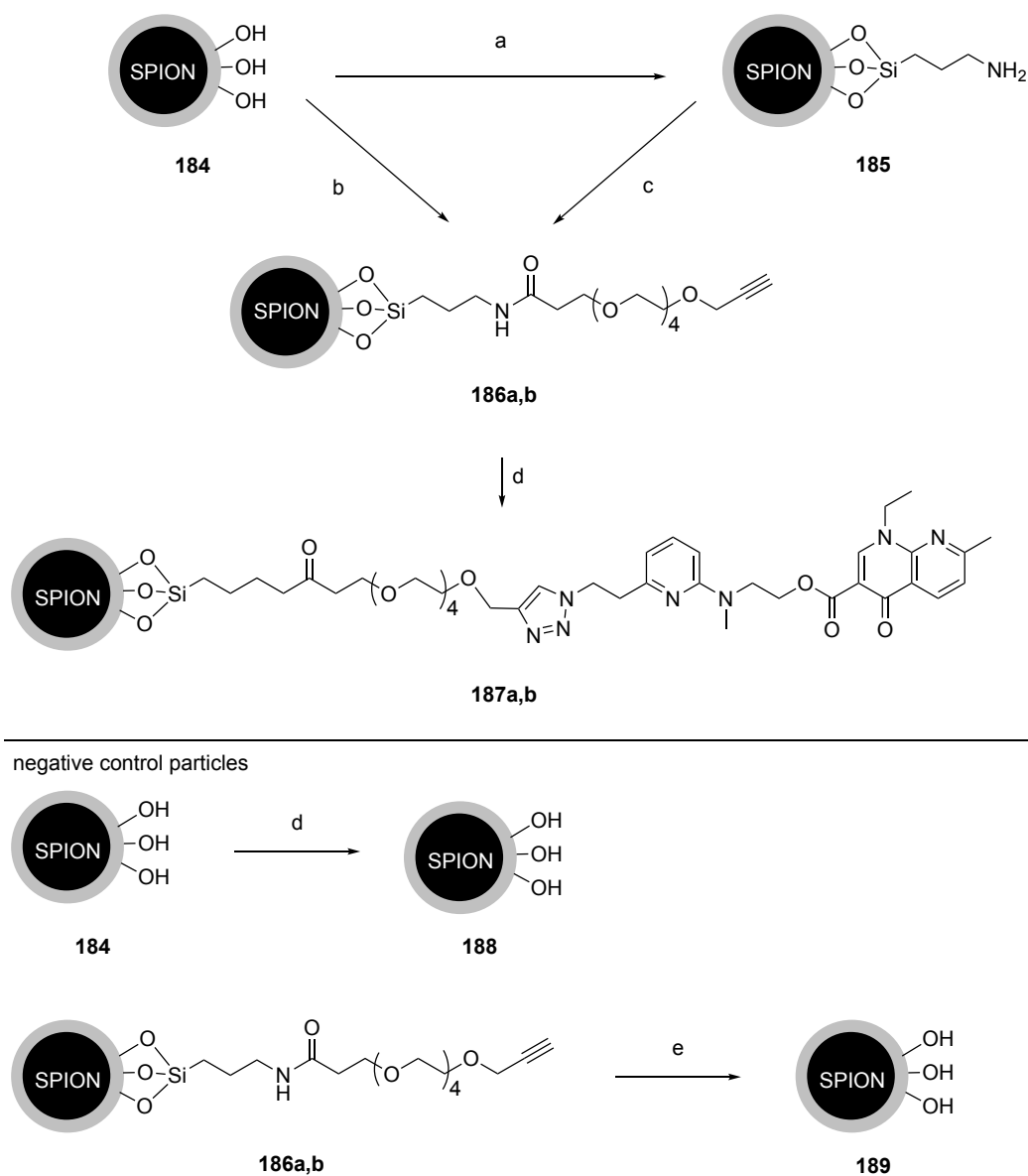
that the rate of the reaction is determined only by the substituents directly linked to the pyridine ring.

Next, the connection of module **IIb** and **IIIb** with APTES (**46**) and alkyne PEG-spacer **175** was tested by amide synthesis. This required saponification of **175** and activation of the carboxylic acid as NHS-ester **182**. The amide synthesis of **182** and APTES (**46**) proceeded in 70% yield after only 1 h at rt (Scheme 57).



Scheme 57: Amide synthesis between APTES (**46**) and PEG spacer **175** for the connection of modules **IIb** and **IIIb**, a) NaOH, MeOH, 40 °C, 1 h; b) NHS, EDC·HCl, CH₂Cl₂, rt, 6 h, 99% o.2.s.; c) **46**, THF, rt, 1 h, 70%.

Finally, the assembly of the first nanoparticle conjugate **B**, **187**, could be started. SPION@nalidixic acid **187** was synthesized *via* two routes. In route a, the MagSilica[®] SPION (**184**) was first functionalized with APTES (**46**) followed introduction of PEG-NHS-ester **182** to yield SPION@alkyne **186a**. In route b, the MagSilica[®] SPION (**184**) was directly functionalized with alkyne **183**, resulting in SPION@alkyne **186b**. Both conjugates **186a,b** were conjugated to the thermolinker, antibiotic conjugate **179** *via* CuAAC as described above. Nanoparticles **188** and **189** were also prepared as negative controls. Nanoparticle **188** was generated using CuAAC conditions together with azide **179** and unmodified MagSilica[®] SPION (**184**). Nanoparticle **189** was generated by mixing the azide **179** with SPION@alkyne **186b** without the copper catalyst. Both controls were chosen to exclude unspecific adhesion of the antibiotic or thermolinker on the surface of the nanoparticle. All nanoparticles were dried *in vacuo* and FTIR spectra were recorded and compared (Scheme 58).



Scheme 58: Assembly of final nanoparticle conjugate **B** as **187a** (three steps) and **187b** (two steps).

a) APTES (**46**), Et₃N, toluene, 65 °C, 72 h; b) **183**, Et₃N, toluene, 65 °C, 72 h; c) **182**, THF, rt, 48 h; d) **179**, CuSO₄, sodium ascorbate, THF:H₂O = 1:1, rt, on; e) **179**, THF:H₂O = 1:1, rt, on.

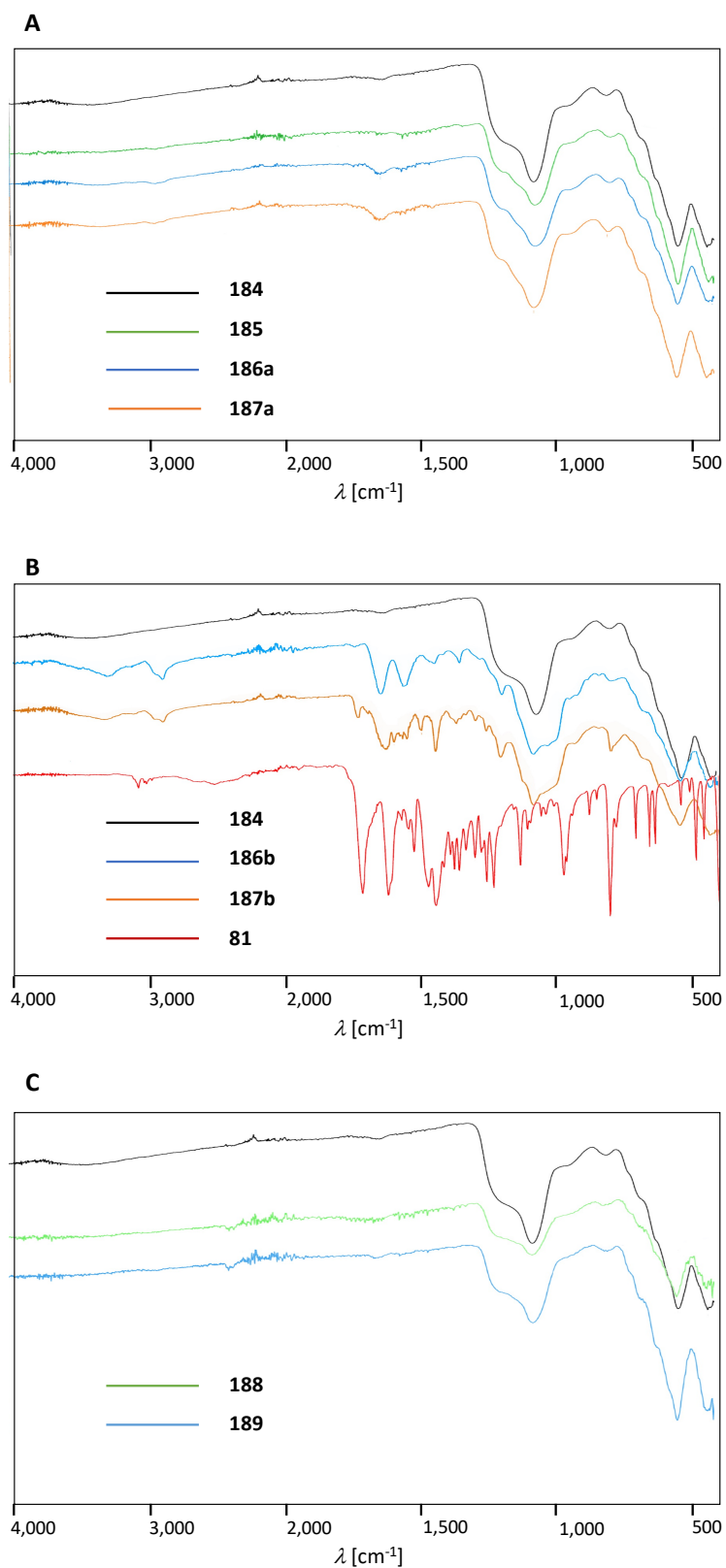


Figure 42: FTIR spectra of nanoparticles of route a (A) **185**, **186a** and **187a**, route b (B) **186b** and **187b** and negative controls **188** and **189** compared to unmodified MagSilica[®] **184** and nalidixic acid (**81**).

The FTIR spectra differ strongly between the two routes a and b towards SPION@alkyne **186a,b** and **187a,b**. The spectra of SPION@APTES **185** does not show any characteristic bands to identify surface modification. Compared to the spectra of MagSilica[®] **184** no differences were observed. After conjugation of SPION@APTES **185** with PEG-spacer **182** to **186a**, a weak band at 1637 can be seen, indicating C=O stretching of the amide and thus pegylation. No difference in the FTIR spectrum is observed after the CuAAC of **186a** with thermolinker **179** (Figure 42, case A). However, when pegylation was performed directly on MagSilica[®] **184** using PEG-spacer **183**, the FTIR of **186b** shows new strong bands at $\lambda = 2864$ (alkane, C-H stretching), 1637 (amide, C=O stretching), 1550 (amide, N-H stretching) cm^{-1} , clearly indicating the presence of PEG though amide bond on the nanoparticle surface. The appearance of characteristic bands of nalidixic acid (**81**) in FTIR of SPION@nalidixic acid **187b**, such as $\lambda = 1720$ (C=O, stretching) and 1440 (C=C, aromatic stretching), suggests that the SPION@nalidixic acid **187b** is the first successfully assembled SPION of conjugate structure **B** (Figure 42, case B).

Negative control particle **188** showed no evidence for surface attachment of thermolinker **179**, indicating that **179** must be bond covalently in SPION **187b**. Interestingly, the FTIR of particle **189** lacks the bands significant for amide-bound PEG found in **186b**. The amide must have been hydrolyzed either during storage or under the reaction conditions.

7.5.5 Nanoparticle Conjugate B: Antibiotic Release

Antibiotic release of from the synthesized nanoparticles was examined next. To see if any antibiotic was released, all synthesized nanoparticles **185 – 187a, b**, negative control particles **188** and **189**, and the original unmodified MagSilica[®] **184** were mixed in water containing 10% DMSO and heated at 95 °C for 18 h. The release was analyzed by LC with MS and UV detection.

Figure 43, case A shows the percentage of nalidixic acid (**81**) released per nanoparticle. It can be seen that, as expected, nalidixic acid (**81**) is only released from nanoparticles **187a,b** and not from **184-186** or the negative control particles **188** and **189**. The release from **187a** is significantly lower at 0.4% than from **187b** at 4.2%, indicating a higher functionalization of **187b**, as already expected from the FTIR intensities. In addition to the mass of nalidixic acid (**81**), three other masses were found in the supernatant of the different nanoparticle construct with $m/z = 138, 627$ and 446 (Figure 43, case B). The masses could be assigned by HRMS and MSMS experiments to different silanols **190-192** caused by hydrolysis from the

nanoparticle surface (Figure 44). Mass m/z $[M+H^+] = 139$ belongs to hydrolysed amine **190**, m/z $[M+Na^+] = 446$ to alkyne **191** and m/z $[M^+] = 627$ to the cyclized thermolinker **192**.

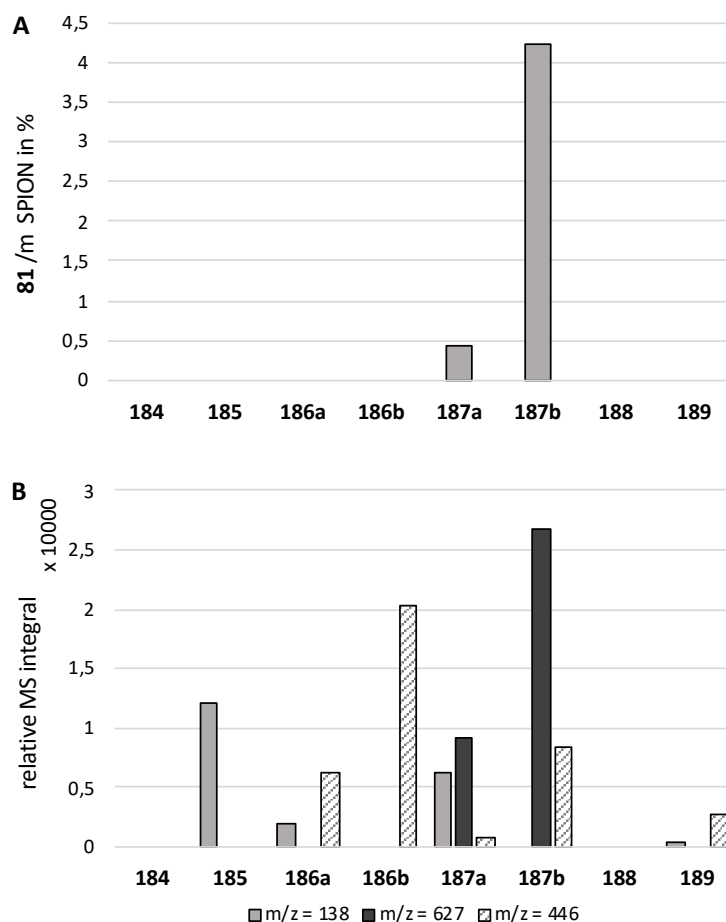


Figure 43: A) Release of nalidixic acid (**81**) from the generated nanoparticles **184** – **189** in % per SPION. B) Relative mass integrals found in addition to nalidixic acid (**81**).

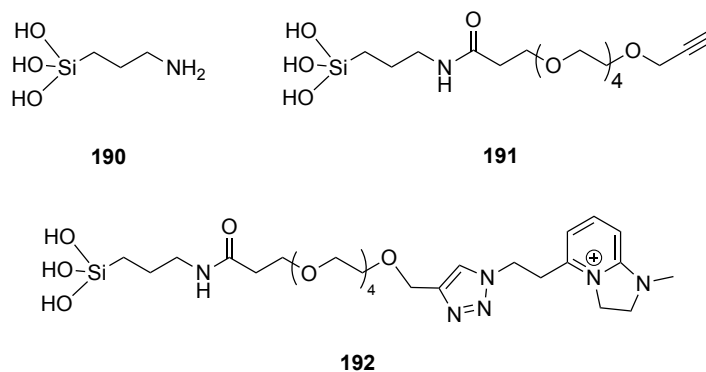


Figure 44: Hydrolyzed silanols **190-192** found after heating of the nanoparticle conjugates in MS.

Silanol hydrolysis is a drawback described for silica coated surfaces under certain conditions.^[83,140] The coating of mesoporous silica SPIONs was found to degrade during AMF induced heating.^[141] Although hydrolysis of the nanoparticle surface was not intended, the mass integrals give an indication of the degree of functionalization of the nanoparticles. From both MagSilica[®] **184** and particle **188**, no compound was found in the supernatant after heating. Aminosilanol **190** is found in the supernatant of SPION@APTES **185** and SPION@alkyne **186a**, indicating incomplete amide coupling of **185** with PEG **175**. In addition, the supernatant of SPION@alkyne **186b** contained PEG-spacer alkyne **191** also found in **186a**, only with a much higher relative mass integral, emphasizing higher alkyne functionalization in route b.

The hydrolyzed cyclization product **192** is formed by cyclodeesterification and release of nalidixic acid (**81**) in the supernatant of nanoparticles **187a** and **b** suspensions. Given that there should be one molecule of **192** for each molecule of nalidixic acid (**81**), it is logical that the integral of **192** is higher in the supernatant of **187b** than **187a**. However, the appearance of **192** raises the question of which reaction occurs first, silanol hydrolysis or cyclodeesterification. The appearance of alkyne **191** in the supernatants of **187a** and **b** indicates incomplete 1,3-dipolar cycloaddition.

Interestingly, the relative integral of aminosilanol **190** in the supernatant of SPION@alkyne **186a** is lower than in **187a**, although in principle the same amount should have released. This shows that the comparison of the relative integrals is only a rough estimate of the actual situation. In addition, the experiments were performed only once, so that no standard deviations could be calculated. Nevertheless, in combination with the FTIR spectra, the data was considered good enough to answer the questions posed.

Another interesting result came from the analysis of supernatant of the negative control particle **189** supernatant. This was generated by mixing SPION@alkyne **186b** with thermolinker **179** in THF:H₂O without the copper catalyst to see if thermolinker **179** would adsorb on the surface without covalent bonding. It can already be seen by FTIR analysis of **189** that the significant bands for C=O and N-H stretching of the amide linking the PEG-spacer have disappeared. Knowing that silanol hydrolysis of the linker can occur, it is only likely that the reaction conditions for 1,3-dipolar cycloaddition can also lead to hydrolysis. This must be taken into account in the following reactions.

In general, hydrolysis of the nanoparticle surface is not desired, as only the antibiotic should be released into the solution. However, in the previous experiments the particles were heated for 24 h, which is much longer than would be the case in human bloodstream. In the following experiments, it was investigated whether hydrolysis already occurs within a short period of time. For this purpose, nanoparticle **187b** was selected and again diluted in water containing 10% DMSO.

First, the release of nalidixic acid (**81**) was monitored at 37 °C and 95 °C (Figure 45, case A and case B, respectively). It is noteworthy that at 37 °C, the initial concentration of nalidixic acid (**81**) in the supernatant was already quite high at 30% of total release. This raises the question whether cyclodeesterification has already occurred under the storage conditions. The concentrations remain at the same level during the first hour, from which the concentration gradually increases to 80% release after 26 h. Thus, it is clear that no significant amount of the antibiotic is released at 37 °C during the first hour, as in all previous experiments without the nanoparticle compound. The release kinetics at 95 °C are also consistent with the experiments from the previous section with complete release of nalidixic acid (**81**) within 1 h.

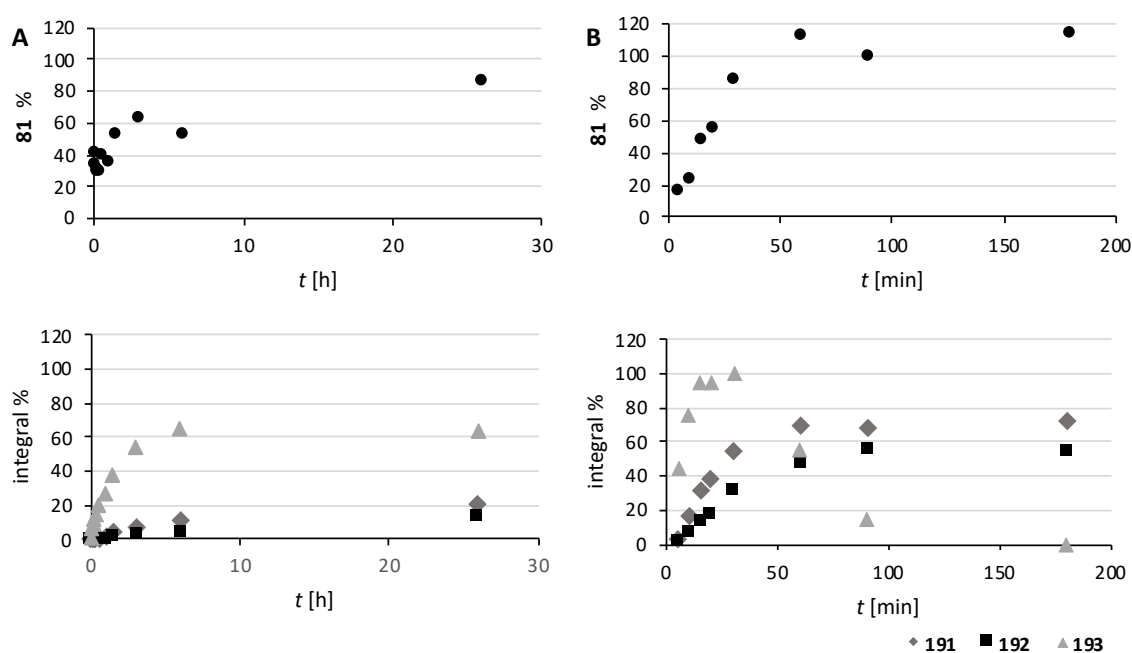


Figure 45: Release of nalidixic acid (**81**) and conjugates **191** – **193** from nanoparticle conjugate **187b** in water with 10% DMSO over time at 37 °C (A) and 95 °C (B) in %. The concentration of nalidixic acid (**81**) and the relative integrals for **191-192** were normalized by the maximal integral after 24 h at 95 °C. The integrals of **193** were normalized by the maximal integral observed during the measurement at 95 °C.

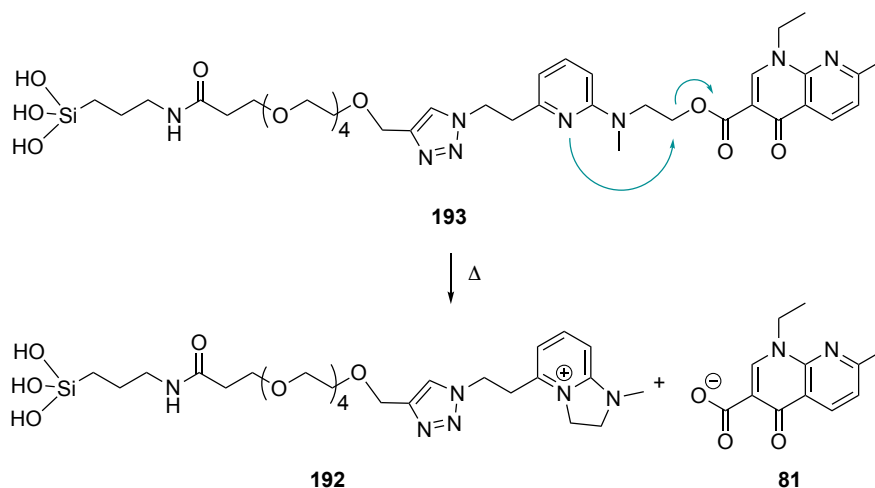
In addition, the occurrence of hydrolysis products **191** and **192** were examined. The observed integrals after heating at 95 °C for 24 h were set to 100%. Similar to the release of nalidixic acid (**81**), hydrolysis products **191** and **192** were not found during the first hour at 37 °C. From then on, their integrals gradually increased to 20% and 13%, respectively, after 26 h. At 95 °C, however, the integral of **191** and **192** increases rapidly during the first hour, reaching 69% after 60 min and 56% after 90 min, respectively.

A new compound with $m/z[M+Na^+] = 881$ was also found in the mass spectra of the supernatant, corresponding to the hydrolyzed conjugate **193** (Scheme 59) without cyclodeesterification, which was also verified by HRMS. The maximum integral found (45 min at 95 °C) was set to 100%. During the study at 37 °C, the mass integral of **193** increased rapidly from 5% after 5 min to 20% after 1 h and reached a concentration of 60% after 6 h. Although, during the first hour, no nalidixic acid (**81**) was released other than the initial high percentage of 30%. At 95 °C, a rapid increase to a maximum integral is observed after only 15 to 30 min. After 60 min, the integral slowly decreases to half of its maximum. This is the time when the nalidixic acid (**81**) concentration reaches its maximum. When after 90 min, only 15% of maximal integral of **193** is observed, the integral of the cyclized product **192** does not increase further.

Considering the strong correlation of the proportions of **192**, **193** and nalidixic acid (**81**), and taking into account that both **192** and (**81**) can arise from **193** as well as from the SPION@nalidixic acid **187b** itself, it appears that hydrolysis of the silanol group from the nanoparticle surface occurs prior to cyclodeesterification. Isolation and calibration of silanol **193** would be necessary to further prove this hypothesis.

Next, the release of nalidixic acid (**81**) and silanols **191-193** were monitored during inductive heating. The same parameters were used as in previous studies with MagSilica® from our group at 12.1 A, 11.2 kW, 1400 V and 335 kHz. A constant bulk temperature of 45 °C was reached after 15 min, and heating was performed for 90 min. As in the previous experiment, an initial concentration of nalidixic acid (**81**) of 10% of maximum release was observed. The concentration increased until 60% after 90 min. Unfortunately, under these conditions, complete release of nalidixic acid (**81**) from SPION@nalidixic acid **187b** cannot be achieved. It was suspected, that the temperature at the SPION surface is 30 – 50 °C higher than the bulk temperature^[85], which would lead to a rapid release of nalidixic acid (**81**) during the first hour, as found in experiments at 95 °C. However, this could not be observed here (Figure 46). It should be noted that the amount of nalidixic acid (**81**) released from silanol **193** is not affected

by the SPIONS's surface temperature, but rather by the bulk temperature of 45 °C. Considering the previous observation, that hydrolysis partially occurs prior to cyclodeesterification, the release of the antibiotic is drastically slowed down.



Scheme 59: Silanol **193** as hydrolysis product from SPION@nalidixic acid **187b** during thermal release and its cyclodeesterification to pyridinium ion **192** and nalidixic acid **81**.

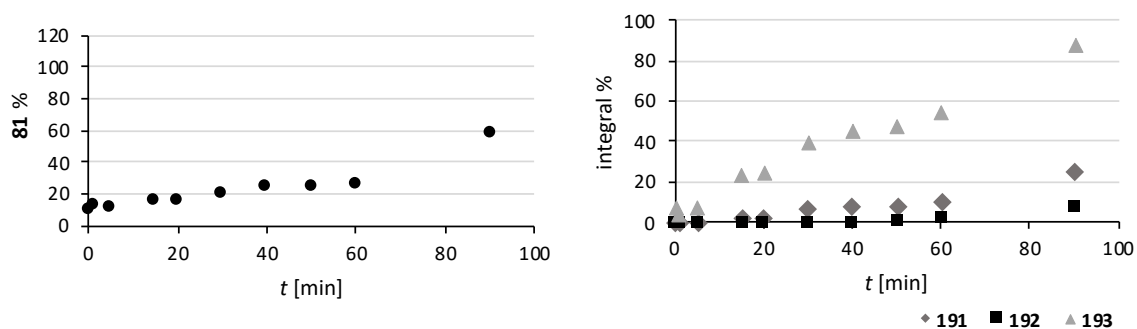


Figure 46: Release of nalidixic acid (**81**) and silanols **191-193** from SPION@nalidixic acid **187b** in water with 10% DMSO over time by inductive heating.

8 Conclusion and Outlook

8.1 Conclusion Part I

In the first part of this work, the Δ AHBA, *asm12/21 A. pretiosum* strain AH1 was used to synthesize new proansamitocin (**9**) derivatives by mutasynthesis. A selection of six mutasynthons was tested: aminooxybenzoic acid **23**, aminomethylbenzoic acid **25**, phenylacetic acid **26**, chloraminobenzoic acid **30**, fluoroaminobenzoic acid **31** and trifluoromethylbenzoic acid **32** (Figure 47).

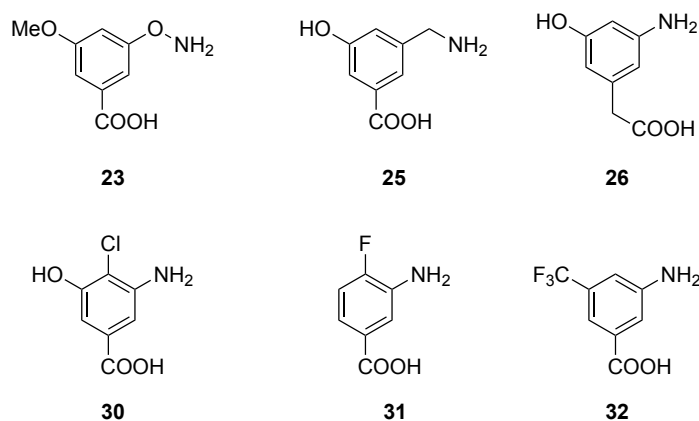
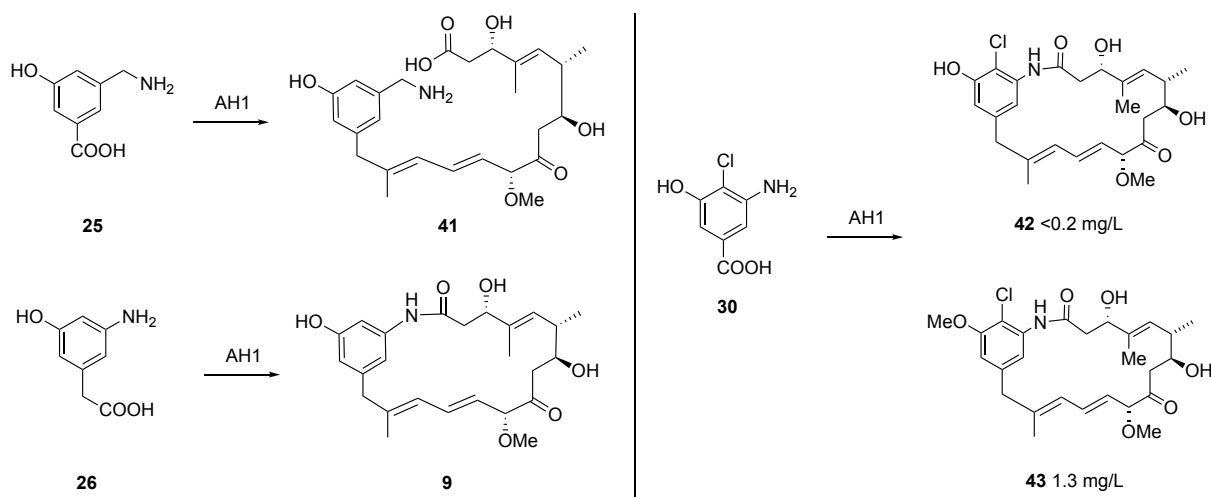


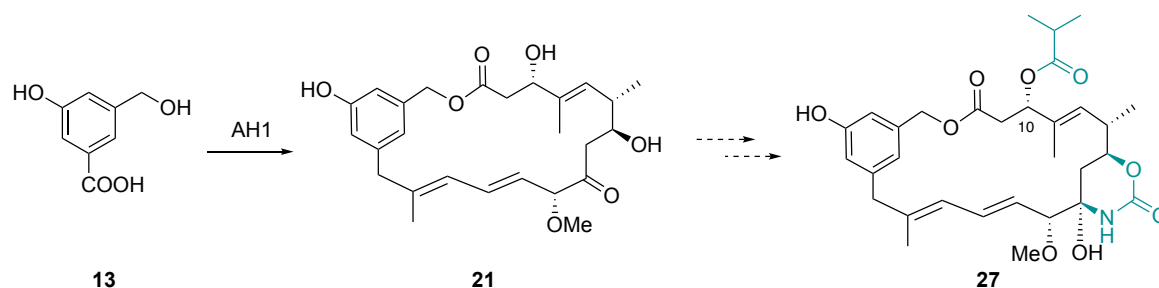
Figure 47: Mutasynthons tested in this study for conversion by Δ AHBA, *asm12/21 A. pretiosum* strain AH1 to proansamitocin derivatives.

Out of the acids used, only **30** was fully converted to the corresponding proansamitocin derivatives **42** and **43** in isolated yields of <0.2 mg/L and 1.3 mg/L, respectively. Fermentation of aminomethylbenzoic acid **25** gave the *seco*-proansamitocin derivative **41** and phenylacetic acid **26** was converted into the original proansamitocin (**9**), probably by decarboxylation of **26** to the natural precursor AHBA (**7**) (Scheme 60). The other three acids resulted in hydrolysis products (found for **25**) and were acylated by the bacterial detoxification system (found for **31** and **32**).

Furthermore, the isolation of the previously reported 20-membered macrolactone **21** from the fermentation of hydroxymethylbenzoic acid **13** with strain AH1^[45] was sought in large quantities. The idea was to semisynthetically introduce functional groups such as the C-10 ester and the carbamoyl moiety, which were reported to be essential for the bioactivity (Scheme 61). Therefore, the fermentation conditions of AHBA, *asm12/21 A. pretiosum* strain AH1 were optimized with the natural AHBA (**7**) precursor.



Scheme 60: *seco*-Proansamitocin derivative **41**, proansamitocin (**9**) and chloroproansamitocins **42** and **43** found in the fermentation broth of Δ AHBA, *asm12/21 A. pretiosum* strain AH1 after mutasythesis with **25**, **26** and **30**. Derivatives **42** and **43** were isolated and the structures were confirmed by NMR spectroscopy.



Scheme 61: Mutasythesis of macrolactone **21** and the planned modifications towards ansamitocin derivative **27**.

A major difficulty in optimizing the fermentation conditions was met by the large batch-to-batch variations of the fermentation (Figure 48). Thus, the most interesting conditions were performed in three independent fermentation batches. Different media and additives were tested for their effect on the production of proansamitocin (**9**). In most cases, the addition of 3 g/L L-Val resulted in significant increased proansamitocin (**9**) titers. Pulse feeding of 2.5 g/L fructose on day 3, 4 and 5 of fermentation also appears to be a promising strategy for increased proansamitocin (**9**) production. Other additives that were described to enhance ansamitocin production before in such as L-Leu^[51], CW, GA^[52], and iBuOH^[53] had no significant effect on the product titers or resulted in decreased yields.

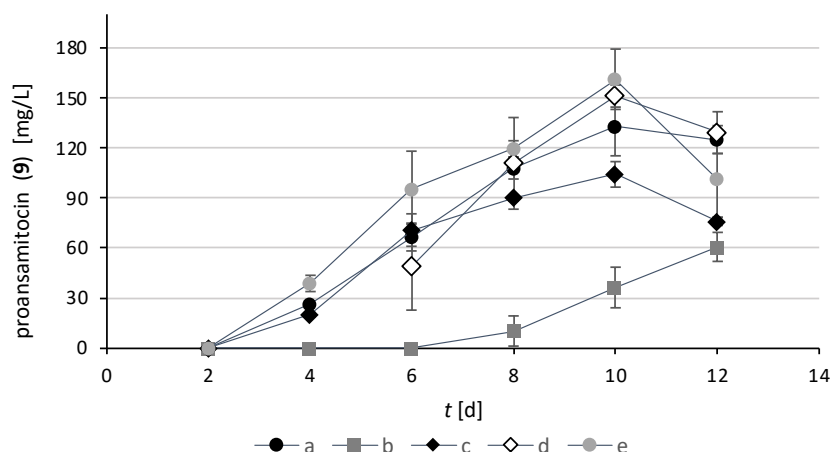


Figure 48: Proansamitocin (**9**) concentrations during fermentation of AHBA (**7**) with Δ AHBA, *asm12/21 A. pretiosum* strain AH1 of five independent experiments. Displayed are the deviations from the mean ($n = 3$).

The concentrations of macrolactone **21** after fermentation of hydroxymethylbenzoic acid **13** to Δ AHBA, *asm12/21 A. pretiosum* strain AH1 were also determined. The highest macrolactone **21** titers of 5.5 mg/L were found in Z-medium after 8 days (Figure 49). A strong correlation between the increase of *seco*-acid **22** and the decrease of macrolactone **21**. This indicates that **22** is probably formed by hydrolytic ring-opening of **21** rather than by inefficiency of the amid synthase *Asm9* during biosynthesis.

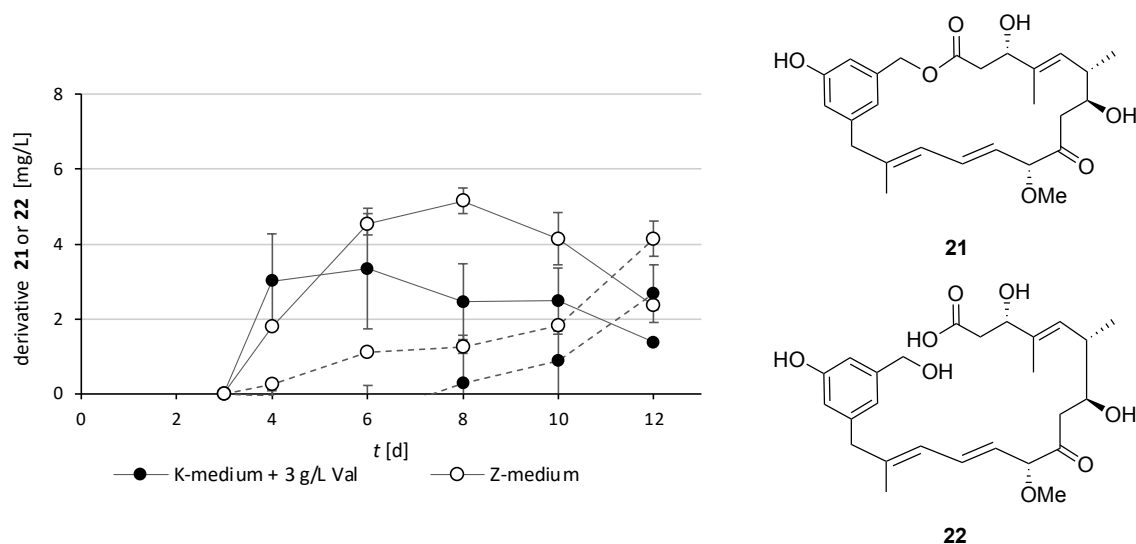


Figure 49: Concentration of macrolactone **21** (A, B) and its *seco*-acid **22** (B, dotted line) during fermentation of hydroxymethylbenzoic acid **13** with strain AH1 in 50 mL medium. A: Addition of different concentrations of **13** in K-medium with 3 g/L Val; B: Comparison of 0.13 mmol/L **13** in K-medium + 3 g/L Val and Z-medium. Shown are the standard deviations from the mean ($n = 3$). * = $P < 0.1$, ** = $P < 0.01$, *** = $P < 0.001$ compared to “1.13 mmol/L and “K-medium + 3 g/L Val”.

The mutasynthesis of macrolactone **21** was also tested in a 25 L scale using the wave-mixed BIOSTAT®CultiBag RM bioreactor with a total bag volume of 50 L. However, neither the macrolactone **21** nor the *seco*-acid **22** were found to be present in the fermentation broth.

8.2 Outlook Part I

The Δ AHBA, *asm12/21 A. pretiosum* strain AH1 is the first strain described so far for the mutasynthetic production of proansamitocin derivatives (**9**). This is a powerful tool, especially for the synthesis of macrolactone **21** from hydroxymethylbenzoic acid **13**, which is not converted into corresponding ansamitocin derivatives by Δ AHBA *A. pretiosum* strain HGF073. However, strain AH1 suffers from low turnover rates to proansamitocin derivatives. The batch-to-batch variation makes medium optimization difficult.

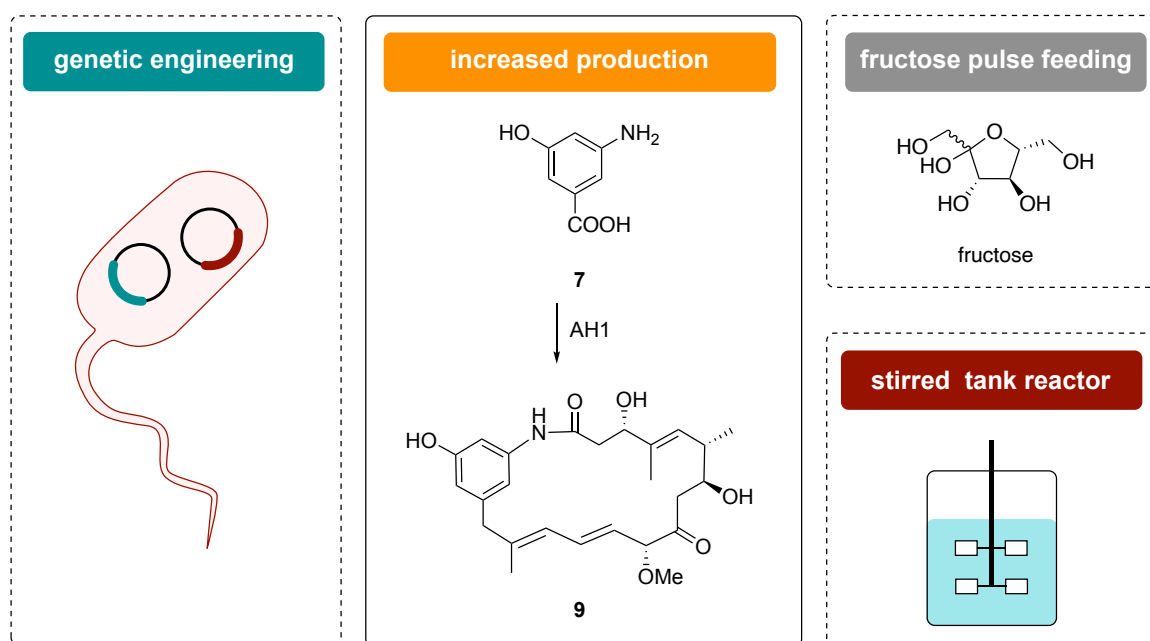
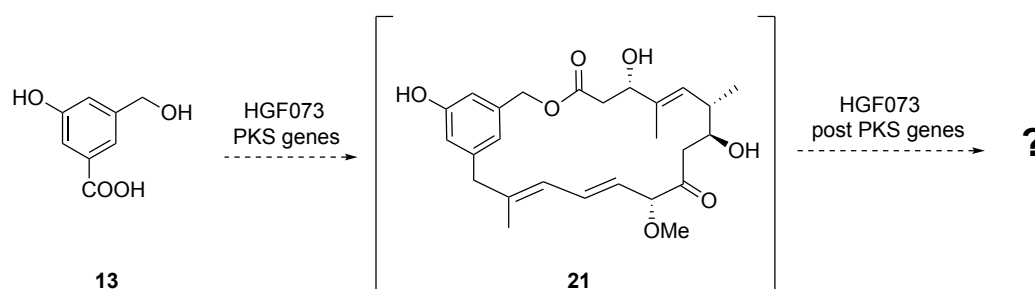


Figure 50: Possibilities to increase proansamitocin production in Δ AHBA, *asm12/21 A. pretiosum* strain AH1.

Pulse feeding of 2.5 g/L fructose on day 3, 4 and 5 of fermentation seems a promising strategy for increased proansamitocin titers but has to be validated by additional experiments. A different strategy to increase the production could be achieved by genetically engineering of the organism. For example, it has been reported that overexpression of the *asm13-17* gene cluster, which is responsible for biosynthesis of methoxymalonyl-CoA, leads to higher yields of ansamitocin in *A. pretiosum* (Figure 50).^[55]

With regards to the large-scale fermentation, the wave-mixed bioreactor may not have been the right choice for fermentation of *A. pretiosum* strains. In this study, flask fermentation was

performed in a chronical flask equipped with a steel spring to assist mixing and oxygen supply. This causes high shear stress to the bacteria, which likely promotes the secondary metabolite production. Wave-mixed bioreactors, on the other hand, are known for their particularly low shear forces, making them ideal reactors for the fermentation of eukaryotic cells and for the production of shear sensitive biomolecules.^[57] These conditions could hinder the proansamitocin (**9**) production of Δ AHBA, *asm12/21* *A. pretiosum* strain AH1. The cultivation of strain AH1 in a classical stirred tank reactor with high oxygen supply and stirring speed should be tested for further large-scale productions of macrolactone **21**.



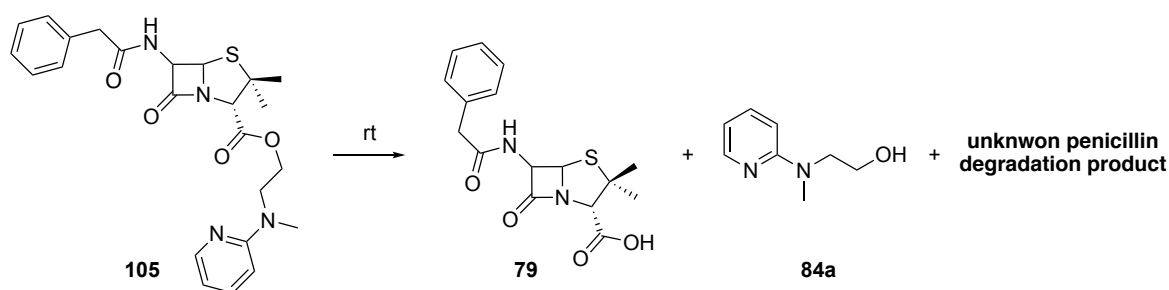
Scheme 62: Fermentation of hydroxymethylbenzoic acid **13** to by Δ AHBA *A. pretiosum* strain HGF073 does not lead to ansamitocin derivatives. The question remains what happens to macrolactone **21** instead.

Finally, it is not clear from this study what happens after fermentation of hydroxymethylbenzoic acid **13** to by Δ AHBA *A. pretiosum* strain HGF073. In view of the production of macrolactone **21** in strain AH1, it seems likely that the macrolactone **21** should also be synthesized in Δ AHBA *A. pretiosum* strain HGF073. The question remains what happens to the lactone thereafter. If the post-PKS enzymes of the *asm* gene cluster simply did not work on the macrolactone **21**, it would be found in the fermentation broth. Thus, there must be a so far unknown conversion of macrolactone **21** caused by the post-PKS enzyme machinery that still has to be elucidated (Scheme 62).

8.3 Conclusion Part II

The 2-Py-TPG group was successfully developed as a thermosensitive linker for the release of carboxylic acid antibiotics through a cyclodeesterification mechanism. Several linkers were synthesized and conjugated to benzylpenicillin (**79**), nalidixic acid (**81**) and ciprofloxacin (**82**), and the thermal release was monitored.

The benzylpenicillin 2-Py-TPG conjugate **105** was found to release benzylpenicillin (**79**) in $D_2O:DMSO-d_6 = 4:6$ at rt over 20 d. However, also an unknown penicillin degradation product was observed to increase with time, likely due to instability of the β -lactam ring^[142] (Scheme 6). Therefore, quinolone antibiotics instead of β -lactam antibiotics were further investigated in this study.



Scheme 63: Release of benzylpenicillin (**79**) from 2-Py-TPG conjugate **105** in $D_2O:DMSO-d_6 = 4:6$ at rt over 20 d.

Nine quinolone 2-Py-TPG conjugates were synthesized from nalidixic acid (**81**) (**108a,b** and **118-121a,b**) and ciprofloxacin (**82**) (**125** and **127**), and the antibiotic release was studied at different temperatures (Figure 51). All the tested conjugates showed negligible antibiotic release during the first hour at 37 °C in $H_2O:DMSO = 10:1$. At 95 °C, the antibiotic release was accelerated to 20 min and 40 min for **108b** and **125**, respectively. For conjugates **108a**, **119** and **120** complete release was observed during the first hour. All other conjugates **118**, **121a,b** and **127** released the antibiotic much more slowly (40%-60% after 4 h). This resulted in the following order with decreasing antibiotic release rate: **108b** > **125** > **108a** = **119** = **120** > **121a** = **121b** > **127** > **118**. Conjugate **108b** was then selected as a thermosensitive linker between a SPION and the antibiotic nalidixic acid (**81**).

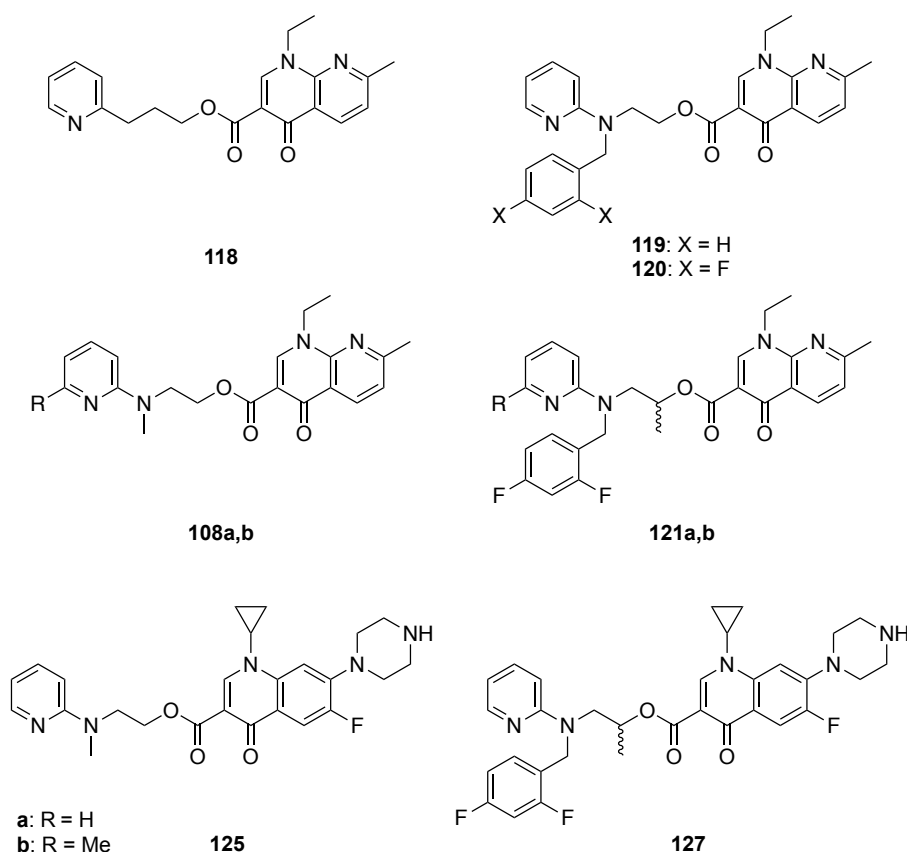
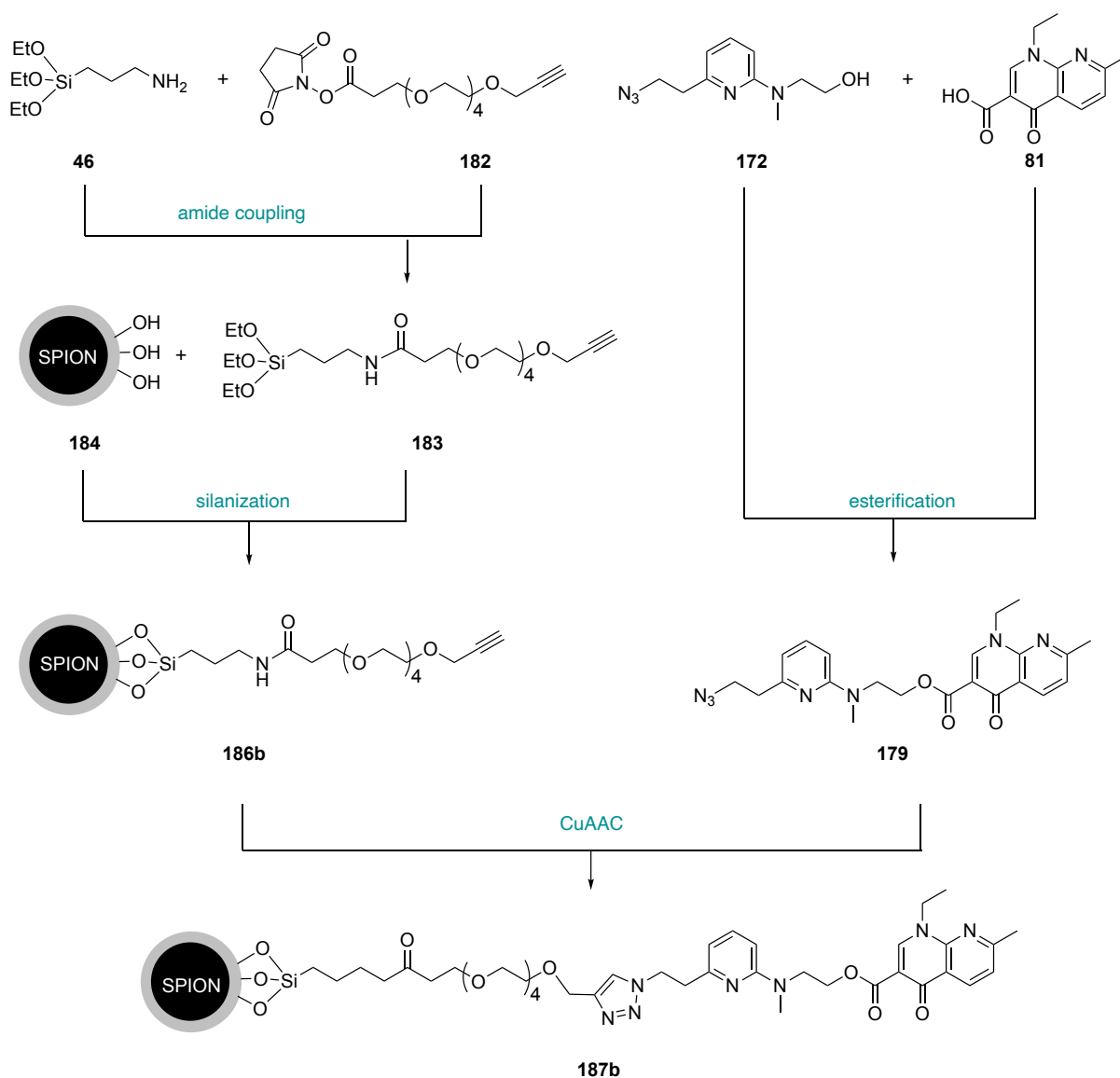


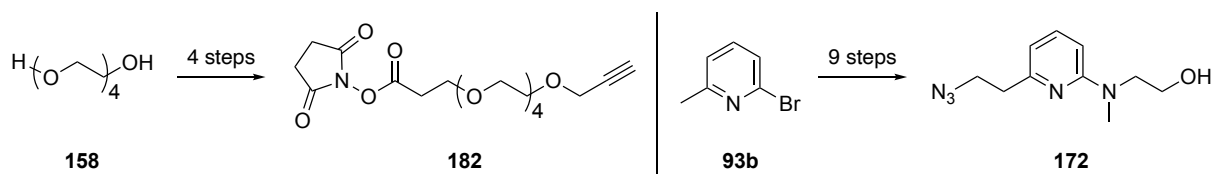
Figure 51: 2-Py-TPG conjugates of nalidixic acid (**81**) and ciprofloxacin (**82**) synthesized in this study and characterized for their ability to release antibiotics.

Having the 2-Py-TPG group validated for its applicability in antibiotic release, the SPION@nalidixic acid **187b** was prepared. SPION@nalidixic acid **187b** was synthesized from MagSilica[®] SPION (**184**), APTES (**46**), PEG-spacer **182**, thermolinker **172** and nalidixic acid (**81**). First APTES (**46**) and PEG-spacer NHS-ester **182** were combined by amide coupling to alkyne **183** and nalidixic acid (**81**) was combined with the thermolinker **171** to ester **179** using COMU[®] as coupling agent. The TES alkyne **183** was then connected to the MagSilica[®] SPION (**184**) by silanization to give SPION@alkyne **186b**. In a final step this was linked to azide **179** via CuAAC (Scheme 64).

PEG-spacer **182** was synthesized from tetraethylene glycol (**158**) in four steps and thermolinker **172** from 4-methyl bromopyridine (**93b**) in nine steps including an *aza*-aldol reaction and BUCHWALD-HARTWIG coupling (Scheme 65).

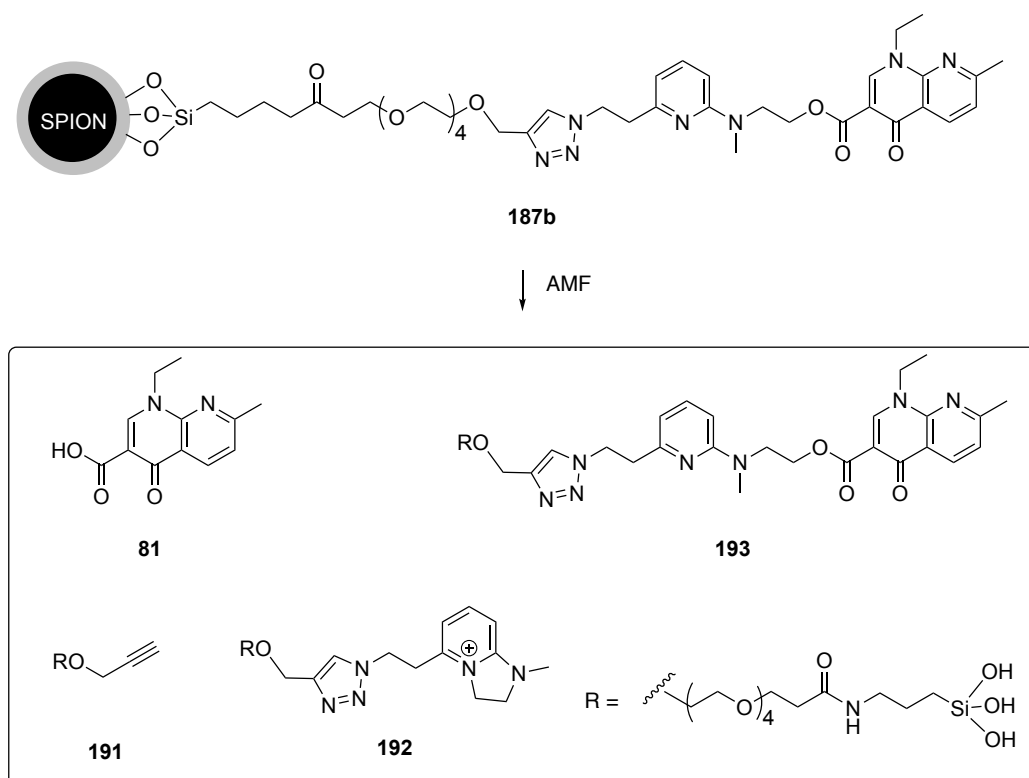


Scheme 64: Synthesis of Spion@nalidixic acid **187b** from MagSilica® SPION (**184**), APTES (**46**), PEG-spacer **182**, thermolinker **172** and nalidixic acid **81**.



Scheme 65: Synthesis of PEG-spacer NHS-ester **182** from tetraethylene glycol (**158**) in 4 steps and synthesis of thermolinker azide **172** from bromide **93b** in 9 steps.

When the SPION@nalidixic acid **187b** were heated to 95 °C in H₂O:DMSO = 10:1, complete release of nalidixic acid (**81**) was observed within 40 min to 60 min of heating. However, silanols **191-193** derived from hydrolysis of the silanol grafted surface were also found. Similar observations were made after inductive heating of SPION@nalidixic acid **187b** (Scheme 66). This silanol hydrolysis hampers the use of SPION@nalidixic acid **187b** for controlled release of antibiotics during inductive heating.

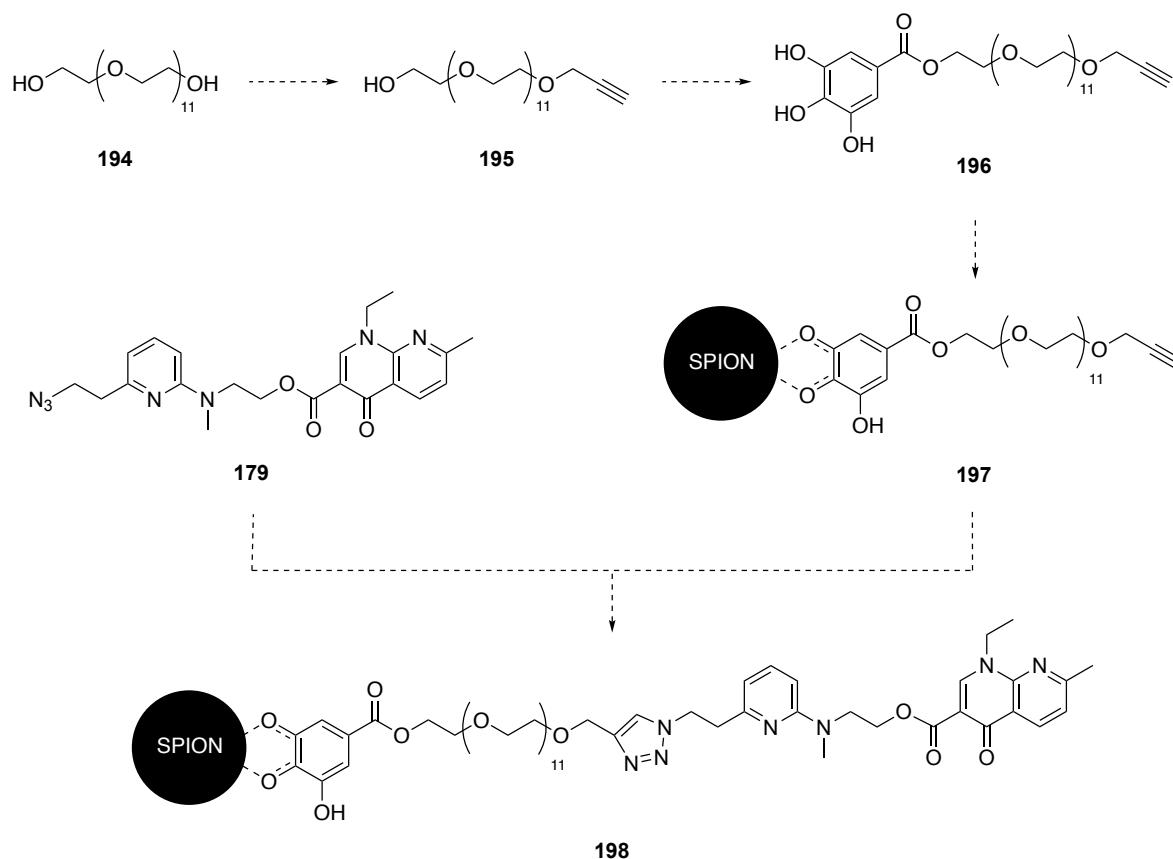


Scheme 66: Release of nalidixic acid (**81**) from SPION@nalidixic acid **187b** after application of a magnetic field and silanols **191-193** from silanol hydrolysis.

8.4 Outlook Part II

The new thermosensitive linker based on the 2-Py-TPG has been proven efficient for the release of antibiotics. However, the connection and the use of the silica coated MagSilica[®] SPIONs **184** is associated with major problems due to the non selective hydrolysis of silanols. Similar problems have already been observed with mesoporous silica coated nanoparticles.^[141] Therefore, for the successful production of SPION@antibiotic, a SPION with a different coating would have to be used. An efficient coating could be the monomeric gallic acid. This coating has been previously described for SPIONs conjugated to the cytostatic drug doxorubicin through a thermosensitive aza-linkage. Moreover, the stability of

this coating was validated by the release of rhodamine dye after application of an AMF. [85] A PEG spacer of $n = 12$ on the gallic acid has been shown to still be close enough to the SPIONs core for optimal heating^[85] while exhibiting optimal solubility in aqueous solution^[143].



Scheme 67: Possible synthesis of SPION@nalidixic acid **198** using gallic acid **196** coated SPION@alkyne **197**.

Starting from dodecaethylene glycol (**194**), alkyne **195** could be synthesized under conditions similar to those described for alkyne **174** in this work. Gallic acid could be introduced by classical ether synthesis to give **196**. The coating of SPIONs with gallic acid is usually achieved by ligand transfer of oleic acid capped SPIONs synthesized by hot colloidal synthesis.^[85,143] In the last step the SPIONs@alkyne **197** the azide **179** can be connected by CuAAC (Scheme 67).

Another future prospect could be the introduction of different antibiotics to the SPION. The ciprofloxacin thermolinker azide **180** synthesized in this study could be introduced to the SPION@alkyne **198** and release of ciprofloxacin (**82**) could be monitored. Although the β -lactam antibiotics such as benzylpenicillin (**79**) were excluded in this study, there is still much room for investigation of other penicillin or cephalosporin antibiotics. However, since

these have a much lower pK_a values compared to the quinolone antibiotics ($pK_a = 5.5-8.0$), 2-Py-TPG thermolinkers with slower release have to be employed. Possible candidates could be esters derived from alcohols **83a,b** and **86a,b**. In addition new thermolinkers could be generated for which a slower release can be estimated, such as esters deriving from alcohols **199a,b** and **200a,b** (Figure 52).

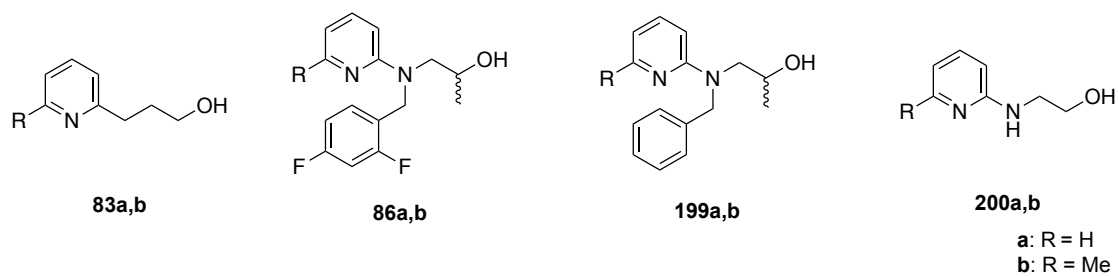


Figure 52: Possible thermolinkers for the release of antibiotics with a $pK_a < 5.5$.

9 Experimentals

9.1. Analytical Section

General remarks

All materials and commercially available reagents were purchased from commercial suppliers and used without further purification unless otherwise stated. Analytical grade solvents were supplied by FISHER CHEMICALS and used as received. Water used in analytical LC-MS and preparative and semi-preparative HPLC was bidistilled and membrane filtered and added 0.1% formic acid (FA) prior to use.

Chromatography

Size exclusion chromatography was performed using Sephadex[®] LH-20 from SIGMA ALDRICH (500 mm x ø 20 mm). Collected fractions were analyzed by LC-MS.

Semi preparative HPLC (< 20 mg) was performed with a MERK HITACHI LaCrome HPLC containing a L-7150 pump, D-7000 interface and a L-7450 diode array detector [$\lambda = 220\text{-}400\text{ nm}$]. Separation was conducted through a RP-C18 (Nucleodur[®], 5 μm) and RP-CN (Nucleodur[®] 100-5, 5 μm) column by MACHEREY NAGEL.

Preparative HPLC (< 400 mg) was performed with a HPLC containing a fraction collector (Varian pro Star, Modell 701) and pumps (Varian preStar, Modell 218) by ALPHACHROM and a variable UV detector (proStar [$\lambda = 248\text{ nm}$]) along with a mass detector (MICROMASS type LCT) by WATERS. Separation was conducted through a RPC18 (Nucleodur[®], 5 μm) and RP-CN (Nucleodur[®] 100-5, 5 μm) column by MACHEREY NAGEL.

Solvent evaporation *in vacuo*

For solutions in EtOAc or MeOH the solvent was removed at 40 °C and 35 °C, respectively, on a conventional rotary evaporator. Solvent mixtures of H₂O and MeOH were removed at ambient temperature and at high vacuum. Solvent mixtures of H₂O and MeCN were removed at ambient temperature either under high vacuum or in a vacuum centrifuge from CHRIST type Alpha RVC connected to a freeze dryer from CHRIST type Alpha 24.

NMR Analysis

^1H -NMR spectra were recorded on Ultrashield-400 and Ascend-400 (400 MHz) and Ultrashield 500 (500 MHz) by BRUKER at ambient temperature. Chemical shifts δ are reported in ppm and relative to the shift of the residual solvents (CHD_2OD $\delta = 3.31$ ppm, C_6HD_5 $\delta = 7.16$ ppm). Coupling constants were reported in Hz. Signals in NMR are described as singlet (s), doublet (d), triplet (t), quartet (q), multiplet (m) or a combination of these, which refers to the spin-spin coupling pattern observed.

^{13}C -NMR spectra were recorded on Ultrashield-400 and Ascend-400 (100 MHz) and Ultrashield 500 (125 MHz) by BRUKER at ambient temperature. Chemical shifts δ are reported in ppm and relative to the shift of the residual solvents (CHD_2OD $\delta = 49.0$ ppm, C_6HD_5 $\delta = 128.0$ ppm).

Two dimensional NMR spectroscopy (COSY, HSQC and HMBC) was used to assist the assignment of signals in ^1H - and ^{13}C -NMR spectra of new compounds.

High Resolution Mass Spectrometry (HRMS)

High resolution mass spectra (HRMS) of chemically synthesized compounds were recorded with a MICROMASS LCT Premier spectrometer in lock spray mode with electrospray ionization (ESI). Ion mass signals (m/z) are reported as values in atomic mass units. Mass spectra were visualized and analyzed with the software MassLynx™ from WATERS.

HRMS and characteristic retention times (t_r [min]) and mass spectra for quantification of mutasynthetic derivatives from fermentation were recorded with a MICROMASS® type Q-ToF Premier™ spectrometer in lock spray mode with Electrospray ionization (ESI) combined with a WATERS ACQUITY UPLC™ system equipped with a WATERS® ACQUITY UPLC® BEH C18 1.7 (SN 01473711315545) column [solvent A: water + 0.1% (v/v) FA, solvent B: MeOH + 0.1% (v/v) FA; flow rate = 0.4 mL/min; gradient (t [min] / solvent B [%]): 0/5, 2.5/95, 6.5/95, 6.6/5, 8/5]. Ion mass signals (m/z) are reported as values in atomic mass units. Mass spectra were visualized and analyzed with the software MassLynx™ from WATERS.

Sample Preparation from Fermentation

Analytical Scale: 250 μL of fermentation broth was diluted with the equal volume of methanol in a 1.5 mL EPPENDORF tube. After mixing, the suspension was centrifuged at 5000 rpm for 5 min in the Centrifuge 5427 R from EPPENDORF. The supernatant was prepared for quantitative analysis.

BIOSTAT[®]CultiBag RM fermentation: 1.0 mL of fermentation broth was put into a 2.0 mL EPPENDORF tube and centrifuged at 5000 rpm for 5 min in the Centrifuge 5427 R from EPPENDORF. The supernatant was extracted with EtOAc (3 x 0.5 mL) and the solvent was removed *in vacuo* in an EPPENDORF Vacufuge[™] at 40 °C for 24 h. The residue was dissolved in 1.0 mL MeOH : H₂O = 1:1 (v/v) and prepared for quantitative analysis of proansamitocin derivative. The aqueous phase was then acidified to pH = 1 with 1 M HCl (0.1 mL), extracted with EtOAc (3 x 0.5 mL) and the solvent was removed *in vacuo* as described above. The residue was dissolved in 1.0 mL MeOH : H₂O = 1:1 (v/v) and prepared for quantitative analysis of hydroxymethylbenzoic acid **13**.

Dry cell weight

In a dried and weighted 1.5 mL EPPENDORF was given 250 μL (analytical scale) 1 mL (> 5 L scale) of fermentation broth. The suspension was centrifuged at 10 000 rpm for 3 min in the Centrifuge 5427 R from EPPENDORF and the supernatant was discarded. The pellet was dried *in vacuo* in an EPPENDORF Vacufuge[™] at 40 °C for 24 h, weighted and the DCW was calculated for the fermentation volume.

Optical Density

A sample from the fermentation broth was mixed well and diluted with a sat. aq. NaCl solution until OD₆₀₀ was between 0.1 and 0.4. OD₆₀₀ was measured with the FoodALYT Photometer by OMNILAB.

Quantification of Proansamitocin (9) and Derivatives

Quantification of proansamitocin (**9**) during fermentation was performed by comparison of peak area (A) of proansamitocin (**9**) ($m/z = 466.2$ [M+Na]⁺) to the internal standard Nimodipin (is₁) ($m/z = 441.1$ [M+Na]⁺) in mass spectra of the UPLC described above for HRMS analysis in positive mode. The prepared sample was diluted with 1:10 MeOH : H₂O = 1:1 (v/v) and

mixed with 300 μL of $\text{MeOH} : \text{H}_2\text{O} = 1:1$ (v/v) containing 1 ppm or 2 ppm is_1 . This was then diluted with $\text{MeOH} : \text{H}_2\text{O} = 1:1$ (v/v) up to 900 μL so that the A of PA in UPLC was between 50 and 210. Integration was performed with MassLynx™ employing ApexTrack Peak Integration using the following parameters:

Peak-to-Peak Baseline Noise	Automatic	Baseline End Threshold	10
Peak Width at 5% Height (Mins)	Automatic	Detect Shoulders	No
Baseline Start Threshold%	0	Response Threshold	Relative Area

Calibration was performed in matrix samples of strain AH1 culture in K-medium without any additives and without AHBA (7) addition. Matrix samples were taken on day 10 p.i. and prepared as described above. 300 μL of 1:10 diluted matrix sample was mixed with 300 μL of $\text{MeOH} : \text{H}_2\text{O} = 1:1$ (v/v) containing 1 ppm or 2 ppm is_1 and 300 μL of $\text{MeOH} : \text{H}_2\text{O} = 1:1$ (v/v) containing different concentrations of proansamitocin (9).

Total concentration of proansamitocin (9) in the fermentation c_{i0} was calculated according formular (1) with x being the analyt, A_x and A_{is} being the peak area of the analyt and internal standard respectively, a being the y-axis intercept of the calibration curve, b being the slope of the calibration curve and d the total dilution. All calculated concentrations < 0 were set to 0. Calibration was performed the day before measurement.

$$c(x) = \frac{A_x}{A_{is}} \cdot \frac{a}{b} \cdot d \quad (1)$$

Quantification 3-hydroxy-5-(hydroxymethyl) Benzoic Acid (13)

Quantification of hydroxymethylbenzoic acid 13 during fermentation was performed by comparison of peak area (A) of hydroxymethylbenzoic acid 13 ($m/z = 167$ [M-H]⁻) to the internal standard 3,5-dihydroxybenzoic acid (is_2) ($m/z = 153$ [M-Na]⁻) in mass spectra of the UPLC as described above in negative mode. The sample was diluted with 1:10 $\text{MeOH} : \text{H}_2\text{O} = 1:1$. 300 μL of the diluted sample was mixed with 600 μL of $\text{MeOH} : \text{H}_2\text{O} = 1:1$ (v/v) containing 16.67 ppm is_2 . Integration was performed as described above for proansamitocin (9) quantification.

Calibration was performed in matrix samples of strain AH1 culture in K-medium without any additives and without AHBA (7) addition. Matrix samples were taken on day 10 p.i. and

prepared as described above. 300 μL of 1:10 diluted matrix sample was mixed with 300 μL of $\text{MeOH} : \text{H}_2\text{O} = 1:1$ (v/v) containing 16.67 ppm is_2 and 300 μL of $\text{MeOH} : \text{H}_2\text{O} = 1:1$ (v/v) containing different concentrations of hydroxymethylbenzoic acid **13**. Total concentration of hydroxymethylbenzoic acid **13** in the fermentation was calculated according formular (1) as described above. Calibration was performed the day before measurement.

Release of Quinolone Antibiotics from Esters

A solution of the ester was prepared in 10% DMSO in distilled H_2O . 200 μL of the solution was placed in a 1.5 mL EPPENDORF[®] tube and heated to the appropriate temperature in an EPPENDORF[®] ThermoStat 5320. On each timepoint three tubes were cooled on ice, 100 μL were diluted with 900 μL distilled H_2O and the samples were kept at 4 $^\circ\text{C}$ until measurement.

Therefore 10 μL sample was injected into a WATERS Alliance HT 2795 separations module combined with a WATERS 2996 photodiode array detector along with a MICROMASS LCT Premier spectrometer in lock spray mode with ESI. Ion mass signals (m/z) are reported as values in atomic mass units. UV and Mass spectra were visualized and analyzed with the software MassLynx[™] from WATERS.

Quantification was performed by integration UV of signals with $\lambda = 256$ nm that for nalidixic acid (**81**) and $\lambda = 277$ nm for quantification of ciprofloxacin (**82**). Calibration was performed one day before measurement. Integration was performed as described above for proansamitocin (**9**) quantification.

For each ester **108a,b**, **118-122**, **125** and **127** the appropriate gradient for separation was determined using a C18: XTERRA[™] MS C18 2.5 μm , 2.1 x 30 mm column with a flow rate of 0.6 mL/min. The gradients are shown in the corresponding experimental procedures.

9.2 Microbiological Section

General remarks

All protocols containing living microorganisms were conducted in the appropriate S1 or S2 facilities. Inoculation, feeding and sampling was executed under a type safe 2020 biological safety cabinet from THERMO SCIENTIFIC. Mutasynthons that were synthesized and provided by former laboratory members were checked for purity by NMR- and HRMS- analyses prior to fermentation.

Bacterial strain

The bacterial strain used in this study, *A. pretiosum* (strain AH19 was provided by ANJA HEUTLING. The mutant strain was generated from *A. pretiosum* $\Delta sm12/21$ and plasmid pHGF9029 through *E. coli* conjugation following the protocol of KIESER *et al.* and is insufficient for AHBA production. The strain was stored at -80°C in 50 % (v/v) cryo media and destroyed with conc. KOH after fermentation.

General Fermentation Protocol

All flasks and cannula/tube-systems of syringe pumps were autoclaved at 121 °C and 2 bar for 15 min in a SYSTEC V-150 prior to fermentation. Medium was prepared in membrane filtered water and autoclaved by the BMWZ service. Heat sensible compounds (coconut water, amino acids and mutasynthon solutions) were filtered through 2 µm filters. Solid cultures were incubated at 30 °C in an Heratherm Incubator from THERMO SCIENTIFIC. Liquid cultures were incubated at 28 °C and 180 rpm in an Innova 44 shaker by NEW BRUNSWICK SCIENTIFIC Co. If not mentioned otherwise, liquid cultures were carried out in ERLLENMEYER flasks (250 mL for 50 mL culture, 500 mL for 100 mL culture) containing a steel spring. One drop of SAG 471-antifoam from GE BAYER SILICONES was added to all liquid media containing flask.

Culture Media

All media were prepared in distilled water.

cryo medium	
20 %	glycerol
10%	sacharose

YMG medium	
4 g/L	D(+)-glucose
10 g/L	malt extract
4 g/L	yeast extract

YMG Agar	
4 g/L	D(+)-glucose
10 g/L	malt extract
4 g/L	yeast extract
2 g/L	Ca ₂ CO ₃
12 g/L	Agar

K-medium	
60 g/L	dextrin
30 g/L	D(+)-maltose · H ₂ O
5.25 g/L	cottonseed flour
5.0 g/L	Ca ₂ CO ₃
4.5 g/L	yeast extract
0.3 g/L	K ₂ HPO ₄
2 mg/L	FeSO ₄ · 7H ₂ O

Z-medium	
2.5 g/L	sucrose
5.0 g/L	D(+)-glucose
10.0 g/L	yeast extract
40.0 g/L	glycerol
0.5 g/L	K ₂ HPO ₄
2 mg/L	FeSO ₄ · 7H ₂ O
0,5 g/L	MgSO ₄
2 g/L	Ca ₂ CO ₃
0.4%	<i>i</i> BuOH

Preculture

Cryo cultures of *A. pretiosum* strain AH1 were plated on yeast/malt/glucose YMG-agar. Plates were incubated 3-5 days until sporulation was clearly visible. 5-8 well sporulating colonies were picked and mixed with 1 mL autoclaved, distilled water. Sterile glass marbles were used to assist mixing. This suspension was then used to inoculate 50 mL of YMG media, hereafter called preculture, in a 250 mL ERLNMEYER flasks containing a steel spring. One drop of SAG 471-antifoam from GE BAYER SILICONES was added to each flask. The preculture was incubated for two days.

Mainculture

Analytical Scale: If not mentioned otherwise 2 mL of preculture was used to inoculate 50 mL of media in a 250 mL ERLLENMEYER flasks containing a steel spring. One drop of SAG 471-antifoam from GE BAYER SILICONES was added to each flask. The cultures were incubated over a period of 12 days. A mutasynthon solution (0.5 mL, 42 mM in H₂O : DMSO = 1:1) was added on days 3, 4 and 5 p.i. Every test fermentation was carried out in three separate flasks along with two positive controls (AHBA (7) addition) and one negative control (addition of H₂O : DMSO = 1:1 solution without mutasynthon).

Preparative Scale: If not mentioned otherwise 4 mL of preculture was used to inoculate 100 mL of media in a 500 mL ERLLENMEYER flasks containing a steel spring. One drop of SAG 471-antifoam from GE BAYER SILICONES was added to each flask. The cultures were incubated over a period of 10 days. The mutasynthon solution (3.0 mL, 21 mM in H₂O : DMSO = 1:1) was added continuously on days 3 to 5 using BS-9000-8 syringe pumps from BRAINTREE SCIENTIFIC connected to TEFZEL-capillaries with luer-lock connection and a flow rate of 83.3 μ L/h.

BIOSTAT[®]CultiBag RM fermentation: 1 L of preculture, 4.65 L of 5 x concentrated Z-medium and 18.35 L sterile water were pumped through a DULCO[®]flex peristaltic pump from PROMINENT[®] into a 50 L Flexsafe[®] RM basic bag placed on a BIOSTAT[®] CultiBag RM 20/50 platform rocker with a BIOSTAT[®]CultiBag RM control tower unit containing two pump modules, a gas inlet and sensor control and an optical detection system for O₂ and pH from SATORIUS STEDIM. The gas outlet filter, port F, was taken out and connected to a waste flask containing aq KOH (3M) to prevent blocking of the filter. The fermentation was conducted at 28 °C, the pO₂ was set to 50% and the pH was not controlled. 250 mL of mutasynthon solution (55 mM in H₂O : DMSO = 1:1) was added on day 3, 4 and 5 p.i. Samples were taken every 24 h and just before and after addition of the mutasynthon solution.

Extraction

If not mentioned otherwise, fermentation broths were extracted with EtOAc (3 x 50 mL per 100 mL culture) 10 days p.i. Phase separation was achieved by centrifugation at 5000 rpm for 10 min in a Sorvall™ LYNX™ 6000 centrifuge from THERMO FISHER SCIENTIFIC. For fermentation over 5 L cells were separated through centrifugation at 5000 rpm for 10 min

prior to extraction with EtOAc. After removal of the cell pellet, phase separation could be achieved without centrifugation. Combined organic phases were concentrated *in vacuo* at 40 °C, washed with a sat., aq. NaCl solution (3 x 50 mL per 50 mL organic fraction), dried over MgSO₄ and filtered. The solvent was removed completely *in vacuo* at 40 °C before analysis or product isolation was carried out.

9.3 General Procedures

General Procedure A

2-Halopyridine (1 eq.) dissolved with aminoethanol (2-6 eq.) in (a) a microwave tube and was irradiated at 300 W and 140 °C for 1-4 h or (b) a sealed tube and stirred at 140 °C for 18 – 24 h. The reaction mixture was separated between CH₂Cl₂ and a sat. aq. Na₂CO₃ solution and extracted with CH₂Cl₂ (3x). The combined organic phases were dried over Na₂SO₄, filtered and the solvent was removed *in vacuo*.

General Procedure B

To a solution of *N*-pyridyl-*N*-benzylaminoethanol (1 eq.) in dry THF (0.5 M) was added benzylbromide (2 eq.) and Et₃N (1 eq.). The reaction was (a) irradiated in a microwave tube (66 °C, 300 W) for 1-6 h or (b) stirred at 66 °C for 18 – 48 h. The reaction mixture was separated between EtOAc and a sat. aq. Na₂CO₃ solution and extracted with EtOAc (3x). The combined organic phases were dried over Na₂SO₄, filtered and the solvent was removed *in vacuo*.

General Procedure C

To a solution of the alcohol (1 eq.) in dry CH₂Cl₂ (0.5 M) and base (2 eq.) was added silyl-chloride or -triflate (1.2 eq if not mentioned otherwise) dropwise. The reaction was stirred at rt until TCL conversion was observed and terminated by addition of a sat. aq. NaHCO₃ solution and was then extracted with EtOAc (3x). The combined organic phases were dried over Na₂SO₄, filtered and the solvent was removed *in vacuo*.

General procedure D

The acid (1.0 eq.) was dissolved in dry CH_2Cl_2 (0.08 M). COMU[®] (1.5 eq.) and DBU (1.0 eq.) were added and the mixture was stirred for 5 min at rt. The alcohol (1.2 eq.) in dry CH_2Cl_2 (0.3 M) was added dropwise and stirring was continued for 18 h at rt.

- a) The reaction was terminated by addition of a sat. aq. Na_2CO_3 solution, extracted with CH_2Cl_2 (3x), washed with a sat. aq. NaCl solution, dried over Na_2SO_4 , filtered and the solvent was removed *in vacuo*.
- b) TFA (5% v/v) was added and the mixture was stirred at rt for 2 h. The reaction was terminated by slow addition of a sat. aq. Na_2CO_3 solution until gas evolution stopped, extracted with CH_2Cl_2 (3x), washed with a sat. aq. NaCl solution, dried over Na_2SO_4 , filtered and the solvent was removed *in vacuo*.

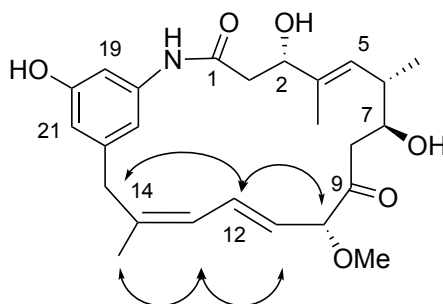
9.4 Experimental Procedures Part I

13,14-Z-Proansamitocin (28)

Fermentation protocol: Preparative Scale, 37 x 100.0 mL

Mutasynthon: 3-Amino-5-hydroxybenzoic acid (7, 804 mg, 4.40 mmol)

Fractions containing $m/z = 400 - 500$ were collected from size exclusion chromatography (Sephadex LH-20, ~ 1.5 mL/min, MeOH) of crude extract and the solvent was removed *in vacuo* at 35 °C resulting in a brown, viscous liquid. The residue was further separated into 6 different fractions by preparative HPLC (RP-C18, MeOH : H₂O = 35% - 80% over 90 min). Fractions collected between 29-35 min were combined and the solvent was removed *in vacuo*. The residue was further purified by semi-preparative HPLC (RP-CN, MeCN : H₂O = 15% - 25% over 60 min). Collection of fractions between 23-25 min gave, amongst other unknown derivatives, 13, 14-Z-proansamitocin.



¹H-NMR (500 MHz, MeOD): δ 7.01 (dd, $J = 1.5, 1.5$ Hz, 1H, 17-H), 6.72 (dd, $J = 15.3, 11.0$ Hz, 1H, 12-H), 6.68 (dd, $J = 2.0, 1.5$ Hz, 1H, 19-H), 6.44 (dd, $J = 2.0, 1.5$ Hz, 1H, 21-H), 6.00 (d, $J = 11.0$ Hz, 1H, 13-H), 5.48 (dd, $J = 15.3, 8.0$ Hz, 1H, 11-H), 5.38 (dd, $J = 9.5, 1.0$ Hz, 1H, 5-H), 4.46 (d, $J = 8.0$ Hz, 1H, 10-H), 4.33 (dd, $J = 8.9, 4.0$ Hz, 1H, 3-H), 3.79 (ddd, $J = 9.5, 8.2, 2.6$ Hz, 1H, 7-H), 3.55 (d, $J = 14.5$ Hz, 1H, 15-H_a), 3.33 (s, 3H, 10-OMe), 3.25 (d, $J = 14.5$ Hz, 1H, 15-H_b), 2.70 (dd, $J = 13.8, 4.0$ Hz, 1H, 2-H_a), 2.61 (dd, $J = 13.8, 8.9$ Hz, 1H, 2-H_b), 2.56 (dd, $J = 15.3, 2.6$ Hz, 1H, 8-H_a), 2.50 (ddq, $J = 9.5, 8.2, 6.8$ Hz, 1H, 6-H), 2.48 (dd, $J = 15.3, 9.5$ Hz, 1H, 8-H_b), 1.79 (s, 3H, 14-Me), 1.66 (d, $J = 1.0$ Hz, 3H, 4-Me), 0.95 (d, $J = 6.8$ Hz, 3H, 6-Me) ppm;

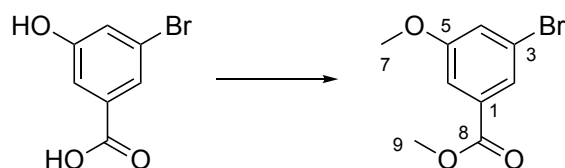
¹³C-NMR (125 MHz, MeOD): δ 210.9 (C-9), 171.1 (C-1), 158.73 (C-20), 141.9 (C-14), 140.4 (C-18), 138.5 (C-4), 134.5 (C-12), 127.2 (C-5), 126.6 (C-13), 125.4 (C-11), 113.2 (C-21), 112.0 (C-17), 105.7 (C-19), 88.8 (C-10), 74.9 (C-7), 73.4 (C-3), 57.2 (10-OMe), 44.9 (C-8), 44.0 (C-2), 40.4 (C-6), 39.4 (C-15), 24.4 (14-Me), 17.8 (6-Me), 15.2 (4-Me) ppm; *

NOE: Arrows indicate interactions

UPLC-MS (grad) $t_R = 2.65$ min;

HRMS (ESI) m/z calcd. for $C_{25}H_{33}NO_6$ $[M+Na]^+$: 466.2206, found 466.2207.

*C-16 could not be identified in the ^{13}C -NMR spectrum.

Methyl-3-bromo-5-hoxybenzoate (36a)

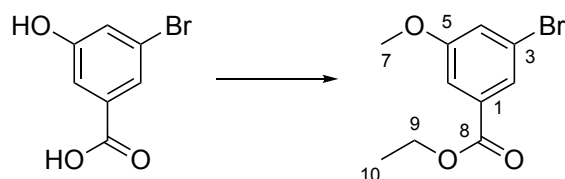
The 3-bromo-5-hydroxybenzoic acid (**35**) (2.0 g, 9.26 mmol, 1.0 eq.) was dissolved in methanol (10 mL). Conc. H₂SO₄ (96%, one drop) was added and the reaction mixture was stirred for 15 – 20 h under refluxing conditions. The solvent was removed *in vacuo* and the residue was separated between a sat. aq. NaCl solution (5 mL) and EtOAc (5 mL). The aq. phase was extracted with EtOAc (2 x 10 mL) and the combined organic phases were dried over MgSO₄, filtered and the solvent was removed *in vacuo*. The crude mixture was dissolved in anhydrous acetone (50 mL). MeI (860 μL, 13.89 mmol, 1.5 eq.), and K₂CO₃ (2.5 g, 18.52 mmol, 2 eq.) were added and the reaction mixture was stirred under refluxing conditions for 18 h. The reaction was terminated by addition of 1 M aq. HCl and the reaction mixture was extracted with EtOAc (3 x 20 mL). The combined organic phases were washed with aq. Na₂S₂O₂ and a sat. aq. NaCl solution (50.0 mL), dried over MgSO₄, filtered and the solvent was removed *in vacuo*. Silica column chromatography (PE:EtOAc = 10:1) gave methyl-3-bromo-5-methoxybenzoate (**36a**, 450 mg, 1.84 mmol, 85% o2s) as a colorless oil.

¹H-NMR (400 MHz, CDCl₃): δ 7.76 (dd, *J* = 1.8, 1.3 H 1H, 2-H), 7.49 (dd, *J* = 2.5, 1.3 H 1H, 4-H), 7.23 (dd, *J* = 2.5, 1.8 H 1H, 6-H), 3.91 (s, 3H, 9-H), 3.84 (s, 3H, 7-H) ppm

¹³C-NMR (100 MHz, CDCl₃): δ 165.8 (C-8), 160.4 (C-5), 132.8 (C-1), 125.0 (C-2, C-3 or C-4), 122.8 (C-2, C-3 or C-4), 122.3 (C-2, C-3 or C-4), 113.6 (C-6), 55.8 (C-7), 52.6 (C-9) ppm

HRMS (EI) *m/z* calcd. for C₉H₉O₃Br [M]⁺: 243.9735; found 243.9732;

R_f (PE:EtOAc = 5:1): 0.4.

Ethyl-3-bromo-5-ethoxybenzoate (36b)

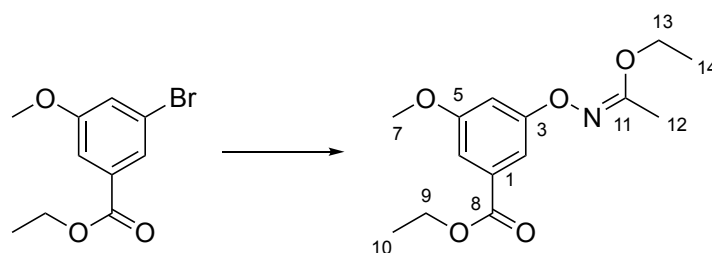
The 3-bromo-5-hydroxybenzoic acid (**35**) (1.0 g, 4.13 mmol, 1.0 eq.) was dissolved in methanol (5 mL). Conc. H₂SO₄ (96%, one drop) was added and the reaction mixture was stirred for 15 – 20 h under refluxing conditions. The solvent was removed *in vacuo* and the residue was separated between a sat. aq. NaCl solution (5 mL) and EtOAc (5 mL). The aq. phase was extracted with EtOAc (2 x 10 mL) and the combined organic phases were dried over MgSO₄, filtered and the solvent was removed *in vacuo*. The crude mixture was dissolved in anhydrous acetone (25 mL). MeI (380 μ L, 6.19 mmol, 1.5 eq.), and K₂CO₃ (1.1 g, 8.26 mmol, 2 eq.) were added and the reaction mixture was stirred under refluxing conditions for 18 h. The reaction was terminated by dropwise addition of 1 M aq. HCl until gas evolution stopped and the reaction mixture was extracted with EtOAc (3 x 10 mL). The combined organic phases were washed with aq. Na₂S₂O₂ and a sat. aq. NaCl solution (20.0 ml), dried over MgSO₄, filtered and the solvent was removed *in vacuo*. Automated flash column chromatography (PE:EtOAc = 20:1 – 1:1) gave ethyl-3-bromo-5-methoxybenzoate (**36b**, 1.23 g, 4.44 mmol, 96% o2s) as a colorless oil.

¹H-NMR (400 MHz, CDCl₃): δ 7.76 (dd, $J = 2.0, 2.0$ Hz, 1H, 2-H), 7.50 (dd, $J = 2.0, 2.0$ Hz, 1H, 4-H), 7.23 (dd, $J = 2.0, 2.0$ Hz, 1H, 6-H), 4.37 (q, $J = 7.0$ Hz, 2H, 9-H), 3.84 (s, 3H, 7-H), 1.39 (t, $J = 7.0$ Hz, 1H, 10-H) ppm;

¹³C-NMR (100 MHz, CDCl₃): δ 165.3 (C-8), 160.3 (C-5), 133.2 (C-1), 124.9 (C-2), 122.7 (C-3), 122.1 (C-6), 113.6 (C-4), 61.5 (C-9), 55.8 (C-7), 14.3 (C-10) ppm;

HRMS (EI) m/z calcd. for C₉H₉O₃Br [M]⁺: 257.9892; found 257.9893;

R_f(PE:EtOAc = 5:1): 0.2.

Ethyl (Z)-3-(((1-ethoxyethylidene)amino)oxy)-5-methoxybenzoate (37b)

The ethyl-3-bromobenzoate (**36b**, 550 mg, 2.12 mmol, 1.0 eq.) was dissolved in degassed toluene (20 mL). (AllylPdCl)₂ (77.0 mg, 0.21 mmol, 0.1 eq.) *t*-BuXPhos (180 mg, 0.42 mmol, 0.2 eq.) dried Cs₂CO₃ (1.0 g, 3.2 mmol, 1.5 eq.) and ethyl-*N*-hydroxyacetimidate (**33**, 330 mg, 3.2 mmol, 1.5 eq.) were added. After stirring for 20 h at 65 °C the reaction mixture was diluted with EtOAc (20 mL) and filtered over Celite[®]. The solvent was removed *in vacuo*. Silica column chromatography (PE:CH₂Cl₂ = 10:1 – 1:1) gave the ethoxyethylidene aminoxybenzoate **37b** (314 mg, 1.12 mmol, 52%) as a colorless solid.

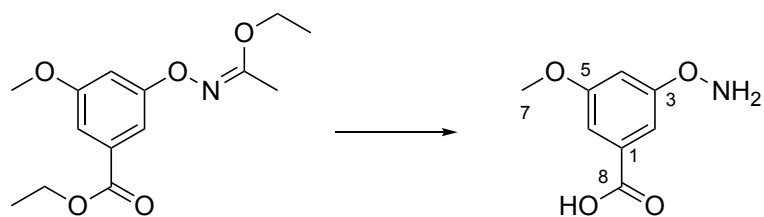
¹H-NMR (400 MHz, CDCl₃): δ 7.39 (dd, *J* = 2.0, 2.0 Hz, 1H, 2-H), 7.18 (dd, *J* = 2.0, 2.0 Hz, 1H, 2-H), 6.94 (dd, *J* = 2.0, 2.0 Hz, 1H, 6-H), 4.36 (q, *J* = 7.0 Hz, 2H, 9-H), 4.20 (q, *J* = 7.0 Hz, 2H, 13-H), 3.84 (s, 3H, 7-H), 2.11 (s, 3H, 12-H), 1.38 (t, *J* = 7.0 Hz, 3H, 10-H), 1.35 (t, *J* = 7.0 Hz, 3H, 14-H) ppm;

¹³C-NMR (100 MHz, CDCl₃): δ 166.5 (C-8 or C-11), 166.1 (C-8 or C-11), 160.8 (C-3 or C-5), 160.6 (C-3 or C-5), 132.3 (C-1), 108.1 (C-2, C-4 or C-6), 107.2 (C-2, C-4 or C-6), 105.1 (C-2, C-4 or C-6), 63.2 (C-9 or C-13), 61.2 (C-9 or C-13), 55.7 (C-7), 14.5 (3C, C-10, C-12, C-14) ppm;

HRMS (ESI) *m/z* calcd. for C₁₄H₂₀O₅N [M+H]⁺: 282.1341; found 282.1342;

R_f(DCM): 0.6;

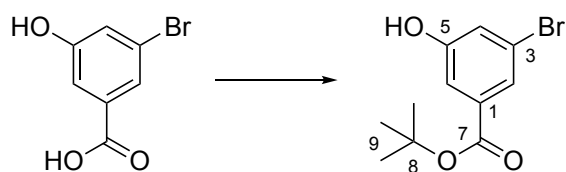
T_m = 42 °C.

3-(Aminoxy)-5-methoxybenzoic acid (23)

The ethoxyethylideneaminoxybenzoate **37b** (52 mg, 0.18 mmol, 1.0 eq.) was dissolved in anhydrous dioxane (0.8 mL) and cooled to 0 °C. A aq. HCl (6 M, 0.2 mL) solution was added dropwise and the reaction mixture was stirred at 0 °C for 15 min and then warmed up to rt. After 2 h the pH of the mixture was adjusted to pH = 12 with LiOH (0.3 M in H₂O:MeOH = 4:3) and the reaction mixture was stirred for 18 h. The reaction mixture was separated between EtOAc (1.0 mL) and H₂O (2.0 mL). The aqueous phase was adjusted to pH = 3 with aq. HCl (2 M) and extracted with EtOAc (3 x 2.0 mL). The combined organic phases were washed with a sat. aq. NaCl solution, dried over MgSO₄, filtered and the solvent was removed *in vacuo*. 3-(Aminoxy)-5-methoxybenzoic acid **23** was obtained as a brown solid (28 mg, 0.15 mmol, 84%).

¹H-NMR (400 MHz, DMSO-*d*₆): δ 12.89 (bs, 1H, *O*-H), 7.26 (s, 1H, 4-H), 7.02 (bs, 2H, *N*-H), 6.98 (s, 1H, 2-H), 6.86 (s, 1H, 6-H), 3.76 (s, 3H, 7-H) ppm.

The analytical data are in accordance with those published in the literature.^[47]

***tert*-Butyl 3-bromo-5-hydroxybenzoate (38)**

Anhydrous MgSO_4 (6.80 g, 55.20 mmol, 12.0 eq.) was mixed with anhydrous CHCl_2 (4.0 mL). H_2SO_4 (0.3 mL, 5.52 mmol, 1.2 eq.) was added and the reaction mixture was stirred vigorously for 15 min. 3-Bromo-5-hydroxybenzoic acid **8** (1.00 g, 4.60 mmol, 1.0 eq.) and anhydrous $t\text{BuOH}$ were added and the flask was stoppered tightly. After stirring for 48 h at rt the reaction was terminated by addition of a sat. aq. NaHCO_3 solution (4.0 mL) and extracted with EtOAc (3 x 3.0 mL). The combined organic phases were washed with a sat. aq. NaCl solution, dried over MgSO_4 , filtered and the solvent was removed *in vacuo*. Silica column chromatography (PE:EtOAc = 1:0 – 6:1) gave *tert*-butyl 3-bromo-5-hydroxybenzoate (**38**) as a colorless solid (560.0 mg, 2.0 mmol, 44%).

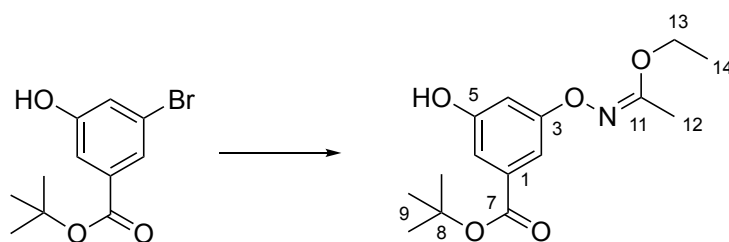
$^1\text{H-NMR}$ (400 MHz, CDCl_3): δ 7.67 (dd, J = 1.6, 1.4 Hz, 1H, 2-H), 7.49 (dd, J = 2.4, 1.4 Hz, 1H, 4-H or 6-H), 7.18 (dd, J = 2.4, 1.6 Hz, 1H, 4-H or 6-H), 5.29 (bs, O-H), 1.56 (s, 9H, 9-H) ppm;

$^{13}\text{C-NMR}$ (100 MHz, CDCl_3): δ 164.9 (C-7), 156.8 (C-5), 134.6 (C-1), 124.8 (C-2 o. C-4), 123.1 (C-2 o. C-4), 122.8 (C-3), 115.5 (C-6), 82.5 (C-8), 28.3 (3C, C-9) ppm;

HRMS (ESI) m/z calcd. for $\text{C}_{11}\text{H}_{12}\text{O}_3\text{Br}$ $[\text{M-H}]^-$: 270.9970; found 270.9969;

R_f (DCM, 5% MeOH, 0.1% acetic acid): 0.8;

T_m = 116 °C.

***tert*-Butyl (*Z*)-3-(((1-ethoxyethylidene)amino)oxy)-5-methoxybenzoate (**39**)**

The corresponding *tert*-butyl-bromobenzoate **38** (250 mg, 0.90 mmol, 1.0 eq.) was dissolved in degassed toluene (10.0 mL). (AllylPdCl)₂ (33.0 mg, 90.0 μmol, 0.1 eq.) *t*-BuXPhos (76.5 mg, 0.18 mmol, 0.1 eq.) dried Cs₂CO₃ (440 mg, 1.35 mmol, 1.5 eq.) and ethyl-*N*-hydroxyacetimidate (232, 2.25 mmol, 1.5 eq.) were added. After stirring for 20 h at 65 °C the reaction mixture was diluted with EtOAc (10 mL) and filtered over Celite[®]. The solvent was removed *in vacuo*. Silica column chromatography (PE:EtOAc = 10:1 – 5:1) gave the ethoxyethylidene aminoxybenzoate **39** (115 mg, 0.38 mmol, 42%) as a colorless solid.

¹H-NMR (400 MHz, CDCl₃): δ 7.30 (dd, *J* = 1.3, 2.0 Hz, 1H, 2 or 6 H), 7.10 (dd, *J* = 1.3, 2.0 Hz, 1H, 2 or 6 H), 6.88 (dd, *J* = 2.0, 2.0 Hz, 1H, 4-H), 4.19 (q, *J* = 7.0 Hz, 2H, 13-H), 2.10 (s, 3H, C-12), 1.58 (s, 9H, 9-H), 1.35 (t, *J* = 7.0 Hz, 3H, 14-H₃) ppm;

¹³C-NMR (100 MHz, CDCl₃): δ 166.1 (C-11), 166.1 (C-7), 160.9 (C-3 or C-5), 157.0 (C-3 or C-5), 133.6 (C-1), 109.5 (C-2 or C-6), 107.6 (C-2 or C-6), 105.7 (C-4), 81.7 (C-8), 63.2 (C-13), 28.3 (C-9), 14.5 (2C, C-12, C-14) ppm;

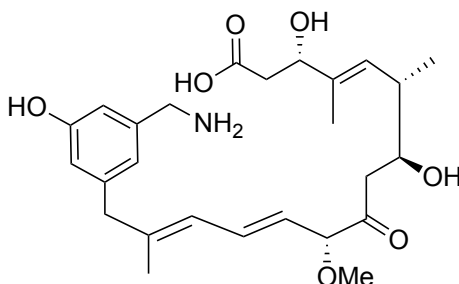
HRMS (ESI) *m/z* calcd. for C₁₅H₂₁NO₅ [M+Na]⁺: 318.1317, found 318.1317;

R_f(PE:tOAc = 5:1): 0.37;

T_m = 110 °C decomposition.

(3S,4E,6S,7S,10R,11E,13E)-15-(3-(Aminomethyl)-5-hydroxyphenyl)-3,7-dihydroxy-10-methoxy-4,6,14-trimethyl-9-oxopentadeca-4,11,13-trienoic acid (41)

Fermentation protocol:	Analytical Scale (3 x 50 mL)
Culture medium:	K-medium containing 3.0 g/L L-Val
Mutasynthon:	3-(Aminomethyl)-5-hydroxybenzoic (25)
Extraction day:	10 days post inoculation



HRMS (ESI) m/z calcd. for $C_{26}H_{37}NO_7$ $[M+Na]^+$: 498.2468, found 498.2467.

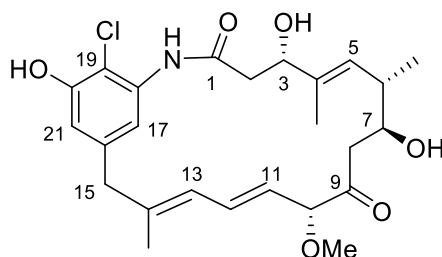
Proansamitocin derivatives from fermentation of chlorhydroxybenzoic acid 30

Fermentation protocol:	Preparative Scale (24 x 100 mL)
Culture medium:	K-medium containing 3.0 g/L L-Val
Mutasynthon:	3-Amino-4-chloro-5-hydroxybenzoic (30 , 677.5 mg, 3.0 mmol)
Extraction day:	10 days post inoculation

After extraction the residue was purified through MPLC (NP, MeOH : CH_2Cl_2 = 0% for 5min, 0% - 20% over 30 min, 20% over 10 min). UV active peaks were combined and the solvent was removed *in vacuo*. The residue was separated into two fractions by preparative HPLC (RP-CN, MeCN : H_2O + 0.1% FA = 10% for 5 min, 10% - 20% over 80 min, 20% - 90% over 15 min).

19-Chloroproansamitocin (42)

Fractions collected between 21-51 min were combined and the solvent was removed *in vacuo*. The residue was further purified by semi-preparative HPLC (RP-18, MeOH : H₂O + 0.1% FA = 10% - 70% over 70 min, 60% - 80% over 30 min). Collection of the fractions between 56-70 min gave **48** in <1 mg yield.



¹H-NMR (600 MHz, MeOD, 330 K): δ 8.56 (bs, 1H, *N*-H), 7.03 (bs, 1H, 21-H), 6.75 (dd, $J = 15.4, 11.0$ Hz, 1H, 12-H), 6.66 (bs, 1H, 17-H), 5.95 (d, $J = 11.1$ Hz, 1H, 13-H), 5.46 (dd, $J = 15.4, 7.8$ Hz, 1H, 11-H), 5.35 (bs, 1H, 5-H), 4.40 (d, $J = 7.8$ Hz, 1H, 10-H), 4.35-4.30 (m, 1H, 3-H), 3.94 (bs, 1H, 7-H), 3.35-3.30 (m, 1H, 15-Ha), 3.33 (s, 3H, 10-OMe), 3.22 (d, $J = 14.2$ Hz, 1H, 15-Hb), 2.78-2.67 (m, 1H, 8-Ha), 2.78-2.67 (m, 1H, 2-Ha), 2.67-2.56 (m, 1H, 2-Hb), 2.46 (dd, $J = 16.4, 7.6$ Hz, 1H, 8-Hb), 2.48-2.40 (m, 1H, 6-H), 1.74 (s, 3H, 14-Me), 1.60 (bs, 3H, 4-Me), 0.93-0.85 (m, 3H, 6-Me) ppm;

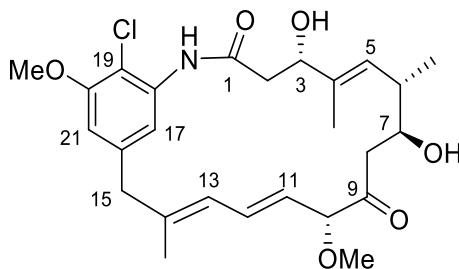
¹³C-NMR (150 MHz, MeOD, 330 K): δ 133.8 (C-12), 129.1 (C-5), 127.7 (C-13), 126.4 (C-11), 89.2 (C-10), 74.2 (C-3), 72.5 (C-7), 57.0 (10-OMe), 46.1 (C-15), 45.2 (C-8), 39.1 (C-6), 16.9 (14-Me), 16.3 (6-Me), 13.3 (4-Me) ppm; Due to low yields not all carbons could be assigned.

UPLC-MS $t_R = 2.48$ min;

HRMS (ESI) m/z calcd. for C₂₅H₃₂NO₆Cl [M+Na]⁺: 500.1816, found 500.1817.

19-Chloro-methoxy-proansamitocin (43)

Fractions collected between 83-95 min were combined and the solvent was removed *in vacuo*. The residue was further purified by semi-preparative HPLC (RP-18, MeOH : H₂O + 0.1% FA = 40% - 90% over 60 min, 100% over 20 min). Collection of the fractions between 25-28 min gave **49** as a white solid (3.0 mg, 0.008 mmol, 0.3%).



¹H-NMR (600 MHz, MeOD, 330 K): δ 8.51 (s, 1H, N-H), 7.19 (s, 1H, 21-H) 6.80 (s, 1H, 17-H), 6.77 (dd, $J = 15.4, 11.0$ Hz, 1H, 12-H), 5.97 (d, $J = 11.0$ Hz, 1H, 13-H), 5.47 (dd, $J = 15.4, 8.1$ Hz, 1H, 11-H), 5.36 (d, $J = 9.0$ Hz, 1H, 5-H), 4.40 (d, $J = 8.1$ Hz, 1H, 10-H), 4.34 (bs, 1H, 3-H), 3.98 – 3.92 (m, 1H, 7-H), 3.89 (s, 3H, 22-OMe), 3.40 (d, $J = 15.5$ Hz, 1H, 15-Ha), 3.36-3.32 (m, 4H, 10-OMe, 15-Hb), 2.75 (dd, $J = 17.0, 4.6$ Hz, 1H, 8-Ha), 2.70 – 2.59 (m, 2H, 2-H), 2.46 (dd, $J = 17.0, 8.9$ Hz, 1H, 8-Hb), 2.51-2.41 (m, 1H, 6-H), 1.77 (s, 3H, 14-Me), 1.60 (s, 3H, 4-Me), 0.90 (d, $J = 6.6$ Hz, 3H, 6-Me) ppm;

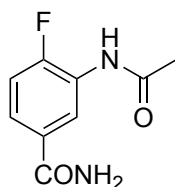
¹³C-NMR (150 MHz, MeOD, 330 K): δ 207.8 (C-9), 156.7 (C-20), 140.7 (C-14), 133.7 (C-12), 128.9 (C-5), 127.7 (C-13), 126.4 (C-11), 89.0 (C-10), 74.2 (C-3), 72.4 (C-7), 56.9 (10-OMe, 20-OMe), 46.3 (C-15), 45.0 (C-8), 39.1 (C-6), 16.8 (14-Me), 16.2 (6-Me), 13.3 (4-Me) ppm; Due to low yields not all carbons could be assigned.

UPLC-MS $t_R = 2.74$ min;

HRMS (ESI) m/z calcd. for C₂₆H₃₄NO₆Cl [M+Na]⁺: 514.1972, found 514.1970.

3-Acetamido-4-fluorobenzamide (44)

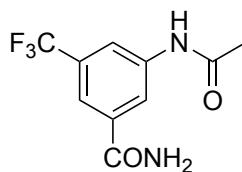
Fermentation protocol:	Analytical Scale, 3 x 50 mL
Culture medium:	K-medium containing 3.0 g/L L-Val
Mutasynthon:	3-Amino-4-fluorobenzoic (31)
Extraction day:	10 days post inoculation



HRMS (ESI) m/z calcd. for $C_9H_{10}N_2O_2F$ $[M+H]^+$: 197.0726, found 197.0725.

3-Acetamido-5-(trifluoromethyl)benzamide (45)

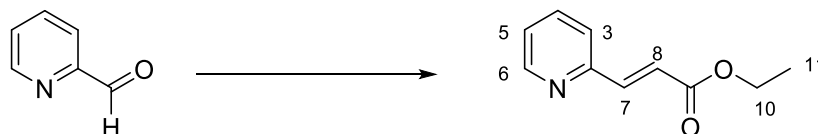
Fermentation protocol:	Analytical Scale, 3 x 50 mL
Culture medium:	K-medium containing 3.0 g/L L-Val
Mutasynthon:	3-Amino-5-trifluoromethylbenzoic (32)
Extraction day:	10 days post inoculation



HRMS (ESI) m/z calcd. for $C_{10}H_9N_2O_2F_3$ $[M+Na]^+$: 269.0514, found 269.0519.

9.5 Experimental Procedures Part II

Ethyl 3-(pyridin-2-yl)acrylate (**90a**)



The aldehyde (500 μ L, 5.28 mmol, 1.0 eq.) and the phosphorene (2.79 g, 7.92 mmol, 1.5 eq.) were dissolved in dry toluene (6.0 mL). The mixture was stirred for 18 h at rt before it was separated between EtOAc (5.0 mL) and a sat. aq. NaCl solution (10 mL). The aq. phase was extracted with EtOAc two more times. The combined organic phases were dried over Na_2SO_4 , filtered and the solvent was removed *in vacuo*. Silica column chromatography (PE:EtOAc = 5:1, 0.1% NEt_3) yielded the *E/Z* ester **90a** (72 mg, 3.9 mmol, 74%) as a bright yellow oil.

E-Alkene

$^1\text{H-NMR}$ (400 MHz, CDCl_3): δ 8.64 (dd, $J = 4.5, 2.0$ Hz, 1H, 6-H), 7.70 (ddd, $J = 7.8, 7.8, 2.0$ Hz, 1H, 4-H), 7.67 (d, $J = 15.6$ Hz, 1H, 7-H), 7.42 (d, $J = 7.8$ Hz, 3-H), 7.26 (d, $J = 7.8, 4.5$ Hz, 5-H), 6.91 (d, $J = 15.6$ Hz, 1H, 8-H), 4.27 (q, $J = 7.1$ Hz, 2H, 10-H), 1.33 (t, $J = 7.1$ Hz, 3H, 11-H) ppm;

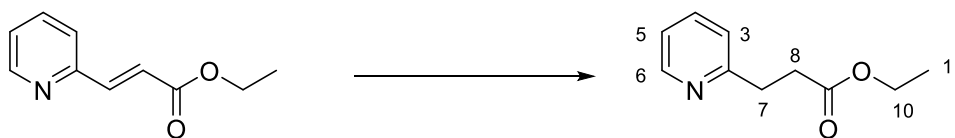
$^{13}\text{C-NMR}$ (100 MHz, CDCl_3): δ 166.8 (C-9), 153.0 (C-2), 150.2, (C-6), 143.6 (C-7), 136.8 (C-4), 124.2 (C-5), 124.0 (C-3), 122.5 (C-8), 60.7 (C-10), 14.3 (C-11) ppm;

Z-Alkene

$^1\text{H-NMR}$ (400 MHz, CDCl_3): δ 8.59 (dd, $J = 4.5, 2.0$ Hz, 1H, 6-H), 7.70 – 7.61 (m, 2H, 3-H, 4-H), 7.19 (dd, $J = 4.5, 1.0$ Hz, 5-H), 6.94 (d, $J = 12.3$ Hz, 5-H), 6.13 (d, $J = 12.3$ Hz, 1H, 8-H), 4.21 (q, $J = 7.1$ Hz, 2H, 10-H), 1.25 (t, $J = 7.1$ Hz, 3H, 11-H) ppm;

$^{13}\text{C-NMR}$ (100 MHz, CDCl_3): δ 166.8 (C-9), 153.7 (C-2), 149.3 (C-6), 139.8 (C-7), 136.1 (C-4), 124.5 (C-3), 123.2 (C-8), 123.1 (C-5), 60.7 (C-10), 14.2 (C-11) ppm;

HRMS (ESI) m/z calcd. for $[\text{M}+\text{H}]^+$: 200.0687; found 200.0688;

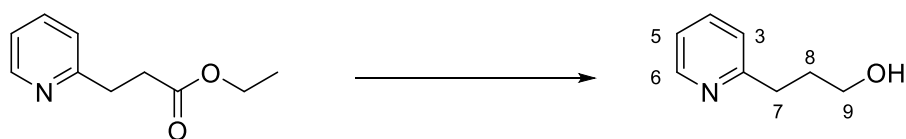
Ethyl 3-(pyridin-2-yl)propanoate (S1a)

The α , β -unsaturated ester was dissolved in EtOAc (13.0 mL) and Pd/C (560 mg, 10 mol%) was added. H₂ was bubbled through the mixture and the reaction was run at rt under H₂ atmosphere for 18 h. The mixture was filtered over Celite[®] and the solvent was removed *in vacuo*. Silica column chromatography (PE:EtOAc = 10:1 – 1:1) gave the title compound (326 mg, 1.6 mmol, 34% o2s) as a colorless liquid.

¹H-NMR (400 MHz, CDCl₃): δ 8.50 (dd, J = 5.3, 1.6 Hz, 1H, 6-H), 7.57 (ddd, J = 8.0, 7.7, 1.6 Hz, 1H, 4-H), 7.16 (d, J = 8.0, 1H, 3-H), 7.09 (dd, J = 7.7, 5.3 Hz, 1H, 5-H), 4.10 (q, J = 7.1, 2H, 10-H), 3.09 (t, J = 7.5 Hz, 2H, 8-H), 2.71 (t, J = 7.5 Hz, 2H, 7-H), 1.20 (t, J = 7.1, 3H, 11-H) ppm;

R_f (PE :EtOAc = 1:1): 0.36.

The analytical data are in accordance with those reported in the literature.^[121]

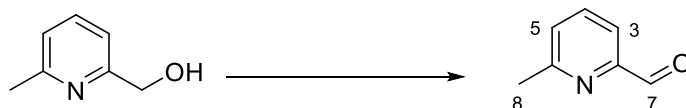
3-(Pyridin-2-yl)propan-1-ol (83a)

The ethyl ester (319 mg, 1.8 mmol, 1.0 eq.) was dissolved in dry THF (4.0 mL). LiAlH₄ (1 M in THF, 2.2 mL, 2.2 mmol, 1.2 eq.) was added dropwise at 0 °C. The reaction was warmed up to rt and stirred for 30 min before it was terminated by addition of EtOAc (5.0 mL). The mixture was poured into a sat. aq. potassium sodium tartrate solution (10 mL) and was vigorously stirred for 18 h before it was extracted with EtOAc (3 x 5 mL). The combined organic phases were washed with brine (5 mL), dried over Na₂SO₄, filtered and the solvent was removed *in vacuo* yielding the desired alcohol **83a** (221 mg, 1.6 mmol, 91%) as a colorless liquid.

¹H-NMR (400 MHz, CDCl₃): δ 8.49 (dd, *J* = 5.3, 1.9 Hz, 1H, 6-H), 7.61 (ddd, *J* = 8.0, 7.8, 1.9 Hz, 1H, 4-H), 7.18 (d, *J* = 8.0, 1H, 3-H), 7.13 (dd, *J* = 7.8, 5.3 Hz, 1H, 5-H), 3.71 (t, *J* = 5.9 Hz, 2H, 9-H), 2.98 (t, *J* = 6.6 Hz, 2H, 7-H), 1.99 (tt, *J* = 6.6, 5.9 Hz, 2H, 8-H) ppm;

R_f(EtOAc): 0.36.

The analytical data are in accordance with those reported in the literature.^[121]

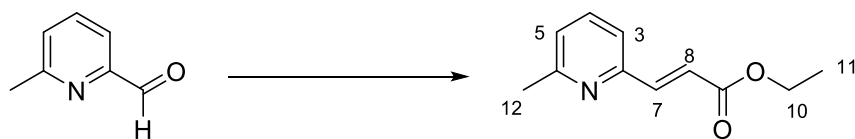
6-Methylpicolinaldehyde (91b)

A solution of 2 M selenious acid (0.1 mL, 0.18 mmol, 0.5 eq.) in water was added to a stirring solution of (6-methylpyridine-2-yl)methanol (47.9 mg, 0.37 mmol, 1.0 eq.) in 1,4-dioxane (1.0 mL). The mixture was heated to 100 °C and left stirring for 6 h. Water (5 mL) and a sat. aq. NaHCO₃ solution (5 mL) was added to the solution and metallic selenium was filtered off. The product was extracted with hot EtOAc (3 x 25 mL) and the combined organic phases were washed with brine (30 mL). After drying over Na₂SO₄ and filtration, the solvent was removed *in vacuo*. The desired aldehyde **91b** was obtained as a yellow oil (36.5 mg, 1.44 mmol, 80%).

¹H-NMR (400 MHz, CDCl₃): δ 10.0 (s, 1H, 7-H), 7.80 – 7.16 (m, 2H, 4-H and 3- or 5-H), 7.40 (dd, *J* = 6.6, 1.9 Hz, 1H, 3- or 5-H), 2.66 (s, 3H, 8-H) ppm;

R_f(EtOAc): 0.67.

The analytical data are in accordance with those reported in the literature.^[144]

Ethyl (E)-3-(6-methylpyridin-2-yl)acrylate (90b)

The aldehyde **91b** (500 mg, 5.28 mmol, 1.0 eq.) and the phosphorene (2.76 g, 7.91 mmol, 1.5 eq.) were dissolved in dry toluene (5.0 mL) in a dry microwave tube. The mixture was stirred for 10 min at 140 °C and 300 W before it was separated between EtOAc (10 mL) and a sat. aq. NaHCO₃ solution (10 mL). The aq. phase was extracted with EtOAc (3 x 10 mL). The combined organic phases were washed with a sat. aq. NaCl solution, dried over Na₂SO₄, filtered and the solvent was removed *in vacuo*. Silica column chromatography (PE:EtOAc = 5:1, 0.1% NEt₃) yielded the *E/Z* ester **90b** (729 mg, 4.86 mmol, 92%) as a bright yellow oil.

E-Alkene

¹H-NMR (400 MHz, CDCl₃): δ 7.65 (d, *J* = 15.5 Hz, 1H, 7-H), 7.57 (t, *J* = 8.0 Hz, 1H, 4-H), 7.22 (d, *J* = 8.0 Hz, 1H, 3-H), 7.11 (d, *J* = 8.0 Hz, 1H, 5-H), 6.89 (d, *J* = 15.5 Hz, 1H, 8-H), 4.25 (q, *J* = 7.2 Hz, 2H, 10-H), 2.56 (s, 1H, 12-H), 1.26 (t, *J* = 7.2 Hz, 3H, 11-H) ppm;

¹³C-NMR (100 MHz, CDCl₃): δ 166.8 (C-9), 158.9 (C-6), 152.3 (C-2), 143.6 (C-7), 136.9 (C-4), 124.0 (C-5), 122.1 (C-8), 121.1 (C-3), 60.6 (C-10), 24.6 (C-12), 14.3 (C-11) ppm;

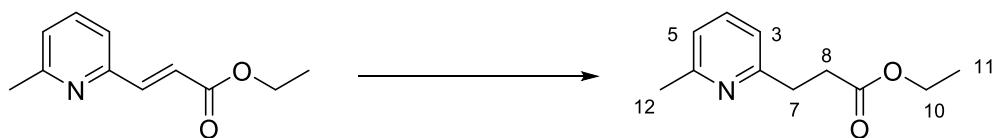
Z-Alkene

¹H-NMR (400 MHz, CDCl₃): δ 7.56 (t, *J* = 8.0 Hz, 1H, 4-H), 7.40 (d, *J* = 8.0 Hz, 1H, 3-H), 7.06 (d, *J* = 8.0 Hz, 1H, 5-H), 6.90 (d, *J* = 12.2 Hz, 1H, 7- or 8-H), 6.10 (d, *J* = 12.2 Hz, 1H, 7- or 8-H), 4.20 (q, *J* = 7.2 Hz, 2H, 10-H), 2.53 (s, 1H, 12-H), 1.32 (t, *J* = 7.2 Hz, 3H, 11-H) ppm;

¹³C-NMR (100 MHz, CDCl₃): δ 167.1 (C-9), 157.9 (C-6), 152.9 (C-2), 139.5 (C-7), 136.3 (C-4), 122.9 (C-8), 122.7 (C-5), 121.5 (C-3), 60.6 (C-10), 24.5 (C-12), 14.2 (C-11) ppm;

HRMS (ESI) *m/z* calcd. for [M+H]⁺: 192.1025; found 192.1027;

R_f(PE:EtOAc = 9:2): 0.29 (*E*-alkene), 0.16 (*Z*-alkene).

Ethyl 3-(6-methylpyridin-2-yl)propanoate (S1b)

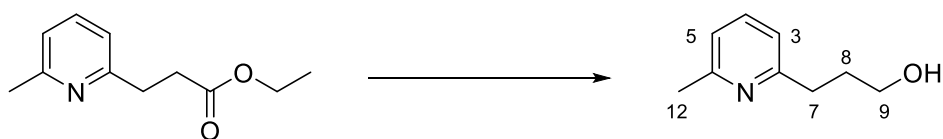
The ester **90b** (23.7 mg, 0.12 mmol, 1.0 eq.) was dissolved in EtOAc (1.0 mL). Pd/C (13 mg, 10 mol%) was added. H₂ was bubbled through the mixture over a period of 1 min and the reaction was run under the H₂ atmosphere for 18 h at rt. The mixture was filtered over Celite[®] and the solvent was removed *in vacuo*. The title compound (19.5 mg, 0.10 mmol, 81%) was obtained as a colorless liquid.

¹H-NMR (400 MHz, CDCl₃): δ 7.31 (t, *J* = 8.0 Hz, 1H, 4-H), 6.81 (t, *J* = 8.0 Hz, 2H, 3-H, 5-H), 4.00 (q, *J* = 7.5 Hz, 2H, 10-H), 2.93 (t, *J* = 7.5 Hz, 8-H), 2.62 (t, *J* = 7.5 Hz, 7-H), 2.35 (s, 3H, 12-H), 1.07 (t, *J* = 7.5 Hz, 11-H) ppm;

¹³C-NMR (100 MHz, CDCl₃): δ 172.6 (C-9), 159.0 (C-2), 157.4 (C-6), 136.2 (C-4), 120.3 (C-5), 119.3 (C-3), 59.8 (C-10), 33.4 (C-8), 32.7 (C-7), 24.0 (C-12), 13.8 (C-11) ppm;

HRMS (ESI) *m/z* calcd. for [M+Na]⁺: 216.1000; found 216.0993;

R_f(PE :EtOAc = 1:1): 0.41.

3-(6-Methylpyridin-2-yl)propan-1-ol (83b)

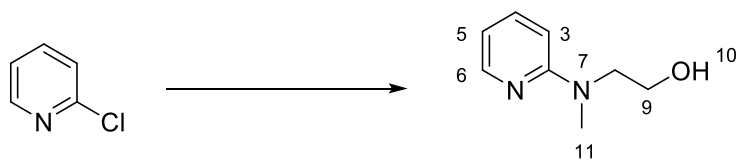
The ethyl ester (484 mg, 2.51 mmol, 1.0 eq.) was dissolved in dry THF (6.5 mL). LiAlH₄ (1 M in THF, 3.0 mL, 3.0 mmol, 1.2 eq.) as added dropwise at 0 °C. The reaction mixture was warmed up to rt and stirred for 30 min before it was terminated by addition of EtOAc (20 mL). The mixture was poured into a sat. aq. potassium sodium tartrate solution (20 mL) and a sat. aq. NaHCO₃ solution (5 mL) and stirred vigorously for 18 h before it was extracted with EtOAc (3 x 10 mL). The combined organic phases were washed with a sat. aq. NaCl solution, dried over Na₂SO₄, filtered and the solvent was evaporated *in vacuo* yielding the product **83b** (347.0 mg, 2.31 mmol, 92%) as a colorless liquid.

¹H-NMR (400 MHz, CDCl₃): δ 7.50 (t, *J* = 7.7 Hz, 1H, 4-H), 6.98 (d, *J* = 7.7 Hz, 2H, 3-H, 5-H), 3.72 (t, *J* = 5.6 Hz, 2H, 9-H), 2.95 (t, *J* = 6.5 Hz, 2H, 7-H), 2.52 (s, 3H, 12-H), 1.96 (tt, *J* = 6.5, 5.6 Hz, 2H, 8-H) ppm;

¹³C-NMR (100 MHz, CDCl₃): δ 160.7 (C-2), 157.4 (C-6), 137.2 (C-4), 120.8 (C-3 or C-5), 120.2 (C-3 or C-5), 62.7 (C-9), 36.0 (C-7), 31.4 (C-8), 24.2 (C-12) ppm;

HRMS (ESI) *m/z* calcd. for [M+Na]⁺: 174.0895; found 174.0895;

R_f(CH₂Cl₂:MeOH = 5:1): 0.32.

2-(Methyl(pyridin-2-yl)amino)ethan-1-ol (84a)

Procedure: A, 300 W, 140 °C

Reactants: 2-Chloropyridine (1.0 g, 8.80 mmol), *N*-methylaminoethanol (2.0 mL, 26.4 mmol)

Reaction time: 2 h

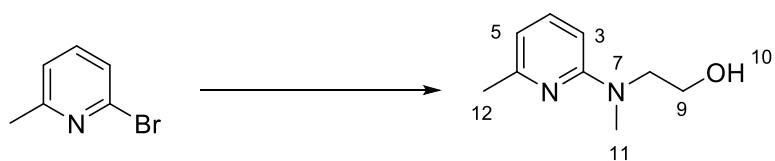
Yield: Silica column chromatography (PE:EtOAc = 1:1 – 0:1) gave **84a** as a colorless oil (950 mg, 7.30 mmol, 83%)

¹H-NMR (400 MHz, CDCl₃): δ 8.04 (dd, *J* = 5.2, 2.0 Hz, 1H, 6-H), 7.46 (ddd, *J* = 8.5, 7.1, 2.0 Hz, 1H, 4-H), 6.56 (ddd, *J* = 7.1, 5.2, 0.8 Hz, 1H, 5-H), 6.52 (dd, *J* = 8.5, 0.8 Hz, 1H, 3-H), 3.84 (t, *J* = 5.3 Hz, 2H, 9-H), 3.70 (q, *J* = 5.3 Hz, 2H, 8-H), 3.05 (s, 3H, 11-H) ppm;

¹³C-NMR (100 MHz, CDCl₃): δ 159.4 (C-2), 147.2 (C-6), 137.9 (C-4), 112.4 (C-5), 106.5 (C-3), 63.2 (C-9), 54.5 (C-8), 38.1 (C-11) ppm;

R_f(PE:EtOAc = 1:1): 0.17.

The analytical data are in accordance with those reported in the literature. ^[145]

2-(Methyl(6-methylpyridin-2-yl)amino)ethan-1-ol (84b)

Procedure: A, 300 W, 140 °C

Reactants: 2-Brom-6-methylpyridine (100.0 μ L, 0.88 mmol), *N*-methylaminoethanol (0.40 mL, 5.28 mmol)

Reaction time: 1 h

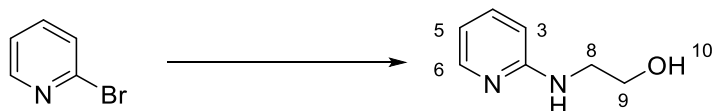
Yield: Silica column chromatography (PE:EtOAc = 5:1 – 0:1) gave **84b** as a colorless oil (146 mg, 0.88 mmol, 99%)

¹H-NMR (400 MHz, CDCl₃): δ 7.37 (dd, J = 8.6, 7.3 Hz, 1H, 4-H), 6.44 (d, J = 7.3 Hz, 1H, 5-H), 6.36 (bs, 1H, *O*-H), 6.34 (d, J = 8.6 Hz, 1H, 3-H), 3.84 (dd, J = 4.5, 4.5 Hz, 2H, 9-H), 3.68 (dd, J = 4.5, 4.5 Hz, 2H, 8-H), 3.04 (s, 3H, 11-H), 2.36 (s, 3H, 12-H) ppm;

¹³C-NMR (100 MHz, CDCl₃): δ 159.4 (C-2), 155.9 (C-6), 138.3 (C-4), 111.8 (C-5), 103.4 (C-3), 63.8 (C-9), 55.0 (C-8), 38.1 (C-11), 24.0 (C-12) ppm;

R_f(PE:EtOAc = 1:1): 0.38;

HRMS (ESI) m/z calcd. for [M+Na]⁺:189.1004; found 189.1005.

2-(Pyridin-2-ylamino)ethan-1-ol (94a)

Procedure: A, 140 °C

Reactants: 2-Bromopyridine (1.00 g, 8.65 mmol), aminoethanol (1.60 mL, 26.5 mmol)

Reaction time: 18 h

Yield: Silica column chromatography (CH₂Cl₂, 2% MeOH) gave **94a** as a colorless solid (1.00 g, 7.24 mmol, 82%)

¹H-NMR (400 MHz, DMSO-d₆): δ 7.92 (dd, *J* = 5.3, 1.3 Hz, 1H, 6-H), 7.33 (ddd, *J* = 8.7, 7.2, 2.1 Hz, 1H, 4-H), 6.46 (d, *J* = 8.7 Hz, 1H, 3-H), 6.45 – 6.40 (m, 2H, 5-H, *N*-H), 4.72 (t, *J* = 5.7 Hz, 1H, *O*-H), 3.50 (q, *J* = 5.7 Hz, 2H, 9-H), 3.29 (q, *J* = 5.7 Hz, 2H, 8-H) ppm;

¹³C-NMR (100 MHz, DMSO-d₆): δ 158.8 (C-2), 147.4 (C-6), 136.5 (C-4), 111.4 (C-3), 108.2 (C-5), 60.2 (C-9), 43.5 (C-8) ppm;

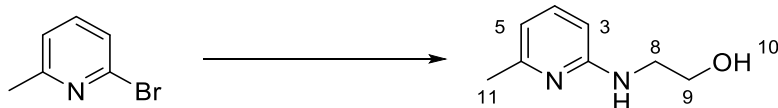
¹H-NMR (400 MHz, CDCl₃): δ 8.02 (dd, *J* = 5.3, 1.7 Hz, 1H, H-6), 7.39 (ddd, *J* = 8.7, 7.2, 1.7 Hz, 1H, H-4), 6.57 (dd, *J* = 7.1, 5.3 Hz, 1H, H-5), 6.44 (d, *J* = 8.7 Hz, 1H, H-3), 4.89 (bs, 1H, H-10), 4.52 (bs, 1H, H-7), 3.80 (dd, *J* = 4.7, 4.7 Hz, 2H, H-9), 3.50 (dd, *J* = 4.7, 4.7 Hz, 2H, H-8) ppm;

¹³C-NMR (100 MHz, CDCl₃): δ 158.9 (C-2), 147.3 (C-6), 137.8 (C-4), 113.3 (C-5), 108.8 (C-3), 63.9 (C-9), 45.7 (C-8) ppm;

HRMS (ESI) *m/z* calcd. for [M+H]⁺: 139.0871; found 139.0870;

R_f(EtOAc, 0.1% Et₃N): 0.23;

T_m: 68-69 °C.

2-(6-Methylpyridin-2-ylamino)ethan-1-ol (94b)

Procedure: A, 140 °C

Reactants: 2-Bromo-6-methylpyridine (300 μ L, 2.72 mmol), aminoethanol (660 μ L, 10.9 mmol)

Reaction time: 18 h

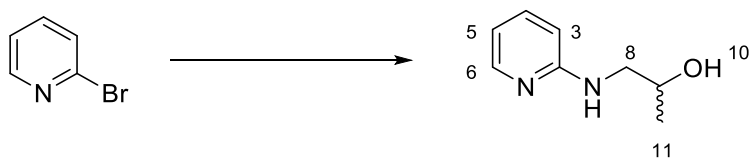
Yield: Silica column chromatography (PE:EtOAc = 4:1 –0:1) gave **94b** as a yellow oil (304 mg, 1.99 mmol, 73%).

¹H-NMR (400 MHz, CDCl₃): δ 7.30 (t, J = 7.2 Hz, 1H, 4-H), 6.45 (d, J = 7.2 Hz, 1H, 3-H), 6.27 (d, J = 7.2 Hz, 1H, 5-H), 5.14 (bs, 1H, O-H), 4.93 (bs, 2H, N-H), 3.47 (dd, J = 9.0, 5.2 Hz, 2H, 9-H), 2.37 (s, 3H, 11-H) ppm;

¹³C-NMR (100 MHz, CDCl₃): δ 158.5 (C-2), 156.0 (C-6), 138.3 (C-4), 112.5 (C-3), 105.4 (C-5), 64.3 (C-9), 46.0 (C-8), 23.9 (C-11) ppm;

HRMS (ESI) m/z calcd. for [M+Na]⁺:175.0847; found 175.0851;

R_f(EtOAc): 0.26.

2-(Pyridin-1-ylamino)propan-2-ol (95a)

Procedure: A, 300 W, 140 °C

Reactants: 2-Bromopyridine (83 mg, 0.53 mmol), 2-aminopropan-1-ol (160 μ L, 2.10 mmol)
3 h

Reaction time: Silica column chromatography (PE:EtOAc = 1:1) gave **95a** as a colorless solid

Yield: (80.4 mg, 0.53 mmol, 99.7 %)

$^1\text{H-NMR}$ (400 MHz, DMSO- d_6): δ 7.91 (dd, J = 5.0, 1.5 Hz, 1H, 6-H), 7.33 (ddd, J = 8.5, 7.5, 2.0 Hz, 1H, 4-H), 6.49 (d, J = 8.5 Hz 1H, 3-H) 6.44 – 6.40 (m, 2H, H-Ar, 5-H, N -H), 4.78 (d, J = 4.8 Hz, 1H, O -H), 3.80-3.71 (m, 1H, 9-H), 3.22 – 3.09 (m, 2H, 8-H), 1.06 (d, J = 6.0 Hz, 3H, 11-H) ppm;

$^{13}\text{C-NMR}$ (100 MHz, DMSO- d_6): δ 158.9 (C2), 147.3 (C-6), 136.5 (C-4), 111.3 (C-3), 108.3 (C-5), 65.3 (C-9), 48.6 (C-8), 21.3 (C-11) ppm;

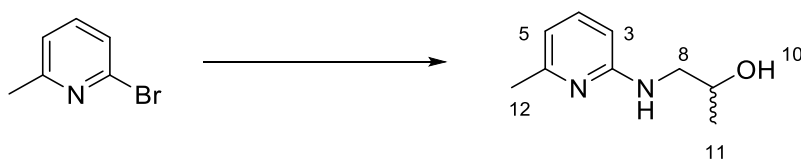
$^1\text{H-NMR}$ (400 MHz, CDCl_3): δ 8.25 (dd, J = 5.6, 1.5 Hz, 1H, H-6), 7.39 (ddd, J = 8.5, 7.5, 1.5 Hz, 1H, 4-H), 6.57 (ddd, J = 7.5, 5.6, 0.8 Hz 1H, 5-H) 6.44 (dd, J = 8.5, 0.8 Hz, 1H, 3-H), 4.78 (s, 1H, O -H), 3.99 (ddq, J = 6.7, 2.1, 6.0 Hz, 1H, 9-H), 3.46 (ddd, J = 14.6, 6.0, 2.1 Hz, 1H, 8- H_a), 3.27 (ddd, J = 14.6, 7.5, 6.0 Hz, 1H, 8- H_b), 1.22 (d, J = 6.0 Hz, 3H, 11-H) ppm;

$^{13}\text{C-NMR}$ (100 MHz, CDCl_3): δ 159.0 (C-2), 147.4 (C-6), 137.7 (C-4), 113.3 (C-3), 108.7 (C-4), 68.4 (C-9), 50.5 (C-8), 21.0 (C-11) ppm;

HRMS (ESI) m/z calcd. for $[\text{M}+\text{H}]^+$:153.1028; found 153.1027;

R_f (PE:EtOAc = 1:1): 0.11;

T_m : 59 °C.

2-(6-Methylpyridin-1-ylamino)propan-2-ol (95b)

Procedure: A, 140 °C

Reactants: 2-Bromo-6-methyl-pyridine (300 μ L, 2.72 mmol), aminoethanol (884 μ L, 10.9 mmol)

Reaction time: 18 h

Yield: Silica column chromatography (PE:EtOAc = 4:1 –0:1) gave **95b** as a colorless solid (226 mg, 1.36 mmol, 50%).

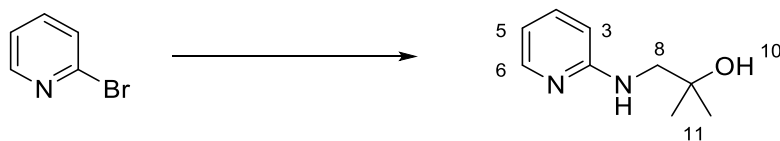
$^1\text{H-NMR}$ (400 MHz, CDCl_3): δ 7.30 (t, $J = 7.2$ Hz, 1H, 4-H), 6.43 (d, $J = 7.2$ Hz, 1H, 3-H), 6.26 (d, $J = 7.2$ Hz, 1H, 5-H), 5.39 (bs, 1H, O-H), 4.88 (bs, 2H, N-H), 3.98 (ddq, $J = 6.5, 2.1, 6.6$ Hz, 1H, 9-H), 3.46 (ddd, $J = 14.1, 6.2, 2.1$ Hz, 1H, 8- H_a), 3.27 (ddd, $J = 14.1, 6.5, 5.2$ Hz, 1H, 8- H_b), 2.36 (s, 3H, 12-H), 1.21 (d, $J = 6.6$ Hz, 3H, 11-H) ppm;

$^{13}\text{C-NMR}$ (100 MHz, CDCl_3): δ 158.6 (C-2), 156.1 (C-6), 138.3 (C-4), 112.5 (C-3), 105.4 (C-5), 68.7 (C-9), 51.0 (C-8), 23.9 (C-12), 21.2 (C-11) ppm;

HRMS (ESI) m/z calcd. for $[\text{M}+\text{Na}]^+$:189.1004; found 189.1000;

R_f (EtOAc): 0.31;

T_m : 45 °C.

2-Methyl-1-(pyridin-2-ylamino)propan-2-ol (96a)

Procedure: A, 140 °C

Reactants: 2-Bromopyridine (300 μ L, 3.15 mmol), 1-amino-2-methylpropan-2-ol (1.17 mL, 12.6 mmol)

Reaction time: 24 h

Yield: Silica column chromatography (PE:EtOAc = 1:0 - 6:1) gave **96a** as a colorless solid (426 mg, 2.57 mmol, 81%).

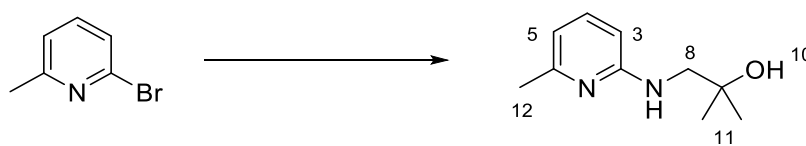
$^1\text{H-NMR}$ (400 MHz, CDCl_3): δ 8.00 (ddd, $J = 5.2, 1.80, 0.8$ Hz, 1H, 6-H), 7.38 (ddd, $J = 8.5, 7.0, 1.80$ Hz, 1H, 4-H), 6.56 (ddd, $J = 7.0, 5.2, 1.0$ Hz, 1H, 5-H), 6.40 (ddd, $J = 8.5, 1.0, 0.8$ Hz, 1H, 3-H), 4.80 (bs, 1H, 10-H), 3.35 (d, $J = 7.0$ Hz, 2H, 8-H), 1.25 (s, 6H, 11-H) ppm;

$^{13}\text{C-NMR}$ (100 MHz, CDCl_3): δ 159.1 (C-2), 146.0 (C-6), 137.6 (C-4), 113.1 (C-5), 108.7 (C-3), 71.1 (C-9), 54.0 (C-8), 27.6 (C-11) ppm;

HRMS (ESI) m/z calcd. for $[\text{M}+\text{Na}]^+$: 189.1004; found 189.1004;

R_f (PE:EtOAc = 1:1): 0.19;

T_m : 77 °C.

2-Methyl-1-(6-methylpyridin-2-ylamino)propan-2-ol (96b)

- Procedure:** A, 140 °C
- Reactants:** 2-Bromo-6-methyl-pyridine (300 μ L, 2.72 mmol), 1-amino-2-methyl-propan-2-ol (1.0 mL, 10.9 mmol)
- Reaction time:** 2 d
- Yield:** Silica column chromatography (PE:EtOAc = 1:0 - 6:1) gave **96b** as a colorless solid (462 mg, 2.57 mmol, 94%).

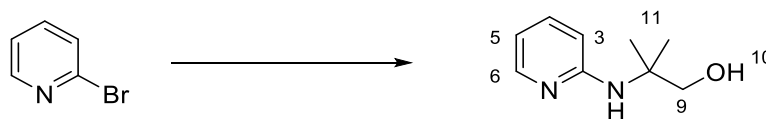
$^1\text{H-NMR}$ (400 MHz, CDCl_3): δ 7.31 (dd, $J = 8.2, 7.5$ Hz, 1H, 4-H), 6.44 (d, $J = 7.5$ Hz, 1H, 3-H), 6.30 (d, $J = 8.2$ Hz, 1H, 5-H), 4.94 (bs, 1H, 10-H), 3.33 (d, $J = 5.9$ Hz, 2H, 8-H), 2.37 (s, 3H, 12-H), 1.25 (s, 6H, 11-H) ppm;

$^{13}\text{C-NMR}$ (100 MHz, CDCl_3): δ 158.4 (C-2), 155.7 (C-6), 138.2 (C-4), 112.3 (C-3), 105.5 (C-5), 71.0 (C-9), 54.5 (C-8), 27.6 (C-11), 23.7 (C-12) ppm;

HRMS (ESI) m/z calcd. for $[\text{M}+\text{Na}]^+$: 203.1160; found 203.1163;

R_f (PE:EtOAc = 1:1): 0.29;

T_m : 84 - 85 °C.

2-Methyl-2-(pyridin-2-ylamino)propan-1-ol (97a)

Procedure: A, 140 °C

Reactants: 2-Bromopyridine (300 μ L, 3.15 mmol), 2-amino-2-methylpropan-1-ol (1.20 mL, 12.6 mmol)

Reaction time: 72 h

Yield: Silica column chromatography (PE:EtOAc = 1:0 - 6:1) gave **97a** as a colorless solid (240 mg, 1.45 mmol, 46%).

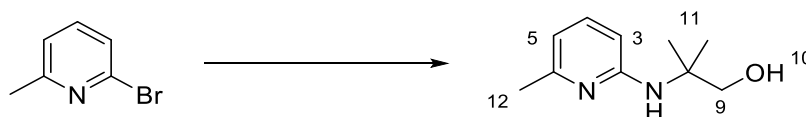
$^1\text{H-NMR}$ (400 MHz, CDCl_3): δ 7.95 (dd, $J = 5.6, 1.4$ Hz, 1H, 6-H), 7.35 (ddd, $J = 8.8, 7.4, 2.0$ Hz, 1H, 4-H), 6.54 (ddd, $J = 7.5, 5.4, 1.0$ Hz, 1H, 5-H), 6.40 (d, $J = 8.8$ Hz, 1H, 3-H), 4.46 (bs, 1H, 10-H), 3.60 (s, 2H, 9-H), 1.32 (s, 6H, 11-H) ppm;

$^{13}\text{C-NMR}$ (100 MHz, CDCl_3): δ 157.4 (C-2), 146.0 (C-6), 137.9 (C-4), 112.7 (C-5), 110.8 (C-3), 72.1 (C-9), 56.4 (C-8), 25.6 (C-11) ppm;

HRMS (ESI) m/z calcd. for $[\text{M}+\text{H}]^+$: 167.1184; found 167.1183;

R_f (PE:EtOAc = 1:1): 0.19;

T_m : 92 °C.

2-Methyl-2-((6-methylpyridin-2-yl)amino)propan-1-ol (97b)

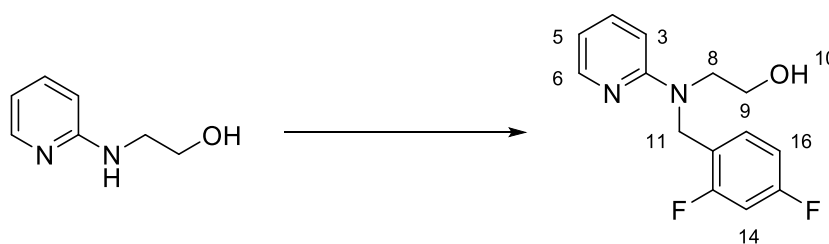
- Procedure:** A, 140 °C
- Reactants:** 2-Bromo-6-methyl-pyridine (300 μ L, 2.72 mmol), 2-amino-2-methyl-propan-2-ol (1.0 mL, 10.9 mmol)
- Reaction time:** 2 d
- Yield:** Silica column chromatography (PE:EtOAc = 1:0 - 6:1) gave **97b** as a colorless solid (164 mg, 0.91 mmol, 33%).

$^1\text{H-NMR}$ (400 MHz, CDCl_3): δ 8.17 (bs, 1H, *N*-H), 7.26 (dd, $J = 8.2, 7.5$ Hz, 1H, 4-H), 6.40 (d, $J = 7.5$ Hz, 1H, 3-H), 6.21 (d, $J = 8.2$ Hz, 1H, 5-H), 4.41(bs, 1H, 10-H), 3.60 (s, 2H, 9-H), 2.36 (s, 3H, 12-H), 1.32 (s, 6H, 11-H) ppm;

$^{13}\text{C-NMR}$ (100 MHz, CDCl_3): δ 156.7 (C-2), 154.6 (C-6), 138.1 (C-4), 111.8 (C-3 or C-5), 107.4 (C-3 or C-5), 72.2 (C-9), 56.2 (C-8), 25.4 (C-11), 23.4 (C-12) ppm;

HRMS (ESI) m/z calcd. for $[\text{M}+\text{Na}]^+$:203.1160; found 203.1158;

R_f (PE:EtOAc = 1:1): 0.22.

2-((2,4-Difluorobenzyl)(pyridin-2-yl)amino)ethan-1-ol (85a)

Procedure: B, 300 W, 66 °C

Reactants: 2-(Pyridin-2-ylamino)propan-1-ol (**94a**, 23.5 mg, 0.17 mmol), 2,4-difluorobenzylbromide **98** (0.05 mL, 0.35 mmol)

Reaction time: 4.5 h

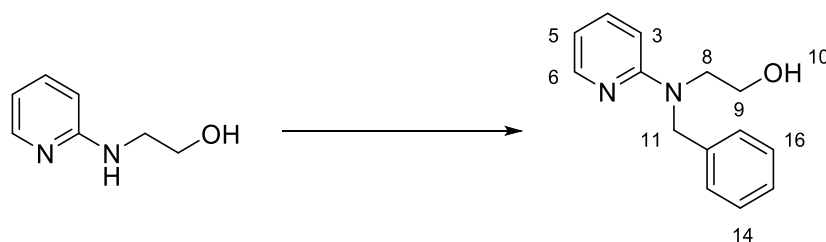
Yield: Silica column chromatography (PE:EtOAc = 1:1) gave **85a** as a colorless solid (10.0 mg, 0.04 mmol, 22%)

¹H-NMR (400 MHz, DMSO-*d*₆): δ 8.05 (dd, *J* = 4.8, 2.0 Hz, 1H, 6-H), 7.48 (ddd, *J* = 8.8, 6.8 Hz, 2.0 1H, 4-H), 7.23 (ddd, *J* = 10.3, 9.2, 2.4 Hz, 1H, 14-H), 7.15 (dt, *J* = 6.8, 8.8 Hz, 1H, 17-H), 6.98 (ddd, *J* = 9.0, 8.8, 2.4 Hz, 1H, 16-H), 6.65 (d, *J* = 8.6 Hz, 1H, 3-H), 6.57 (dd, *J* = 6.8, 4.8 Hz, 1H, 5-H), 4.79 (s, 2H, 11-H), 4.75 (bs, 1H, *O*-H), 3.60 – 3.53 (m, 4H, 8-H, 9-H) ppm;

¹³C-NMR (100 MHz, DMSO-*d*₆): δ 161.1 (dd, *J* = 246.3, 12.0 Hz, C-13 or C-15), 160.2 (dd, *J* = 246.3, 12.0 Hz, C-13 or C-15), 157.53 (s, C-2), 147.5 (s, C-6), 137.3 (s, C-4), 129.7 (dd, *J* = 9.9, 7.1 Hz, C-17), 122.2 (dd, *J* = 15.0, 3.6 Hz, 1C, C-12), 111.82 (s, C-5), 111.2 (dd, *J* = 21.2, 4.0 Hz, C16), 105.8 (s, C-3), 103.7 (t, *J* = 25.6 Hz, 1C, C-14), 58.6 (s, C-8), 50.5 (s, C-9), 45.3 (d, *J* = 3.0 Hz, C-11) ppm;

HRMS (ESI) *m/z* calcd. for [M+Na]⁺:287.0972; found 287.0971;

R_f (EtOAc, 0.1% Et₃N) = 0.60.

2-((Benzyl)(pyridin-2-yl)amino)ethan-1-ol (89)

Procedure: B, 66 °C

Reactants: 2-(Pyridin-2-ylamino)propan-1-ol (**94a**, 100 mg, 0.72 mmol), benzylbromide **99** (170 μ L, 1.4 mmol)

Reaction time: 18 h

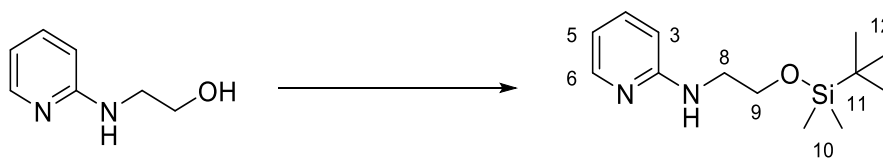
Yield: Silica column chromatography (PE:EtOAc = 2:1 0.1% Et₃N) gave **89** as a colorless oil (82 mg, 0.36 mmol, 50%).

¹H-NMR (400 MHz, CDCl₃): δ 8.08 (ddd, J = 5.4, 2.0, 1.1 Hz, 1H, 6-H), 7.38 (ddd, J = 8.5, 6.8 Hz, 2.0 1H, 4-H), 7.34 - 7.30 (m, 2H, 14,16-H), 7.28 - 7.24 (m, 1H, 15-H), 7.23 - 7.19 (m, 2H, 13,17-H), 6.60 (ddd, J = 6.8, 5.4 Hz, 0.8, 1H, 5-H), 6.47 (ddd, J = 8.5, 1.0, 0.8 Hz, 1H, 3-H), 5.82 (bs, 1H, *O*-H), 4.66 (s, 2H,11-H), 4.75 (bs, 1H, *O*-H), 3.90 - 3.84 (m, 2H, 8-H), 3.84 - 3.70 (m, 2H, 9-H) ppm;

¹³C-NMR (100 MHz, CDCl₃): δ 159.4 (C-2), 147.2 (C-6), 138.3 (C-4), 137.8 (C-12), 129.2 (C-14,16), 127.6 (C-15), 126.7(C-13,17), 113.1 (C-5), 107.5 (C-3), 63.7 (C-8), 54.1 (C-11), 53.3 (C-9) ppm;

HRMS (ESI) m/z calcd. for [M+Na]⁺: 251.1160; found 251.1160;

R_f(toluene:acetone = 5:1) = 0.38.

N-(2-((*tert*-Butyldimethylsilyl)oxy)ethyl)pyridin-2-amine (**100**)

Procedure: C, during workup the pH of the aq. phase was adjusted to 10 with aq. NaOH (1M)

Reactants: 2-(Pyridine-2-ylamino)ethan-1-ol (**94a**, 54.0 mg, 0.39 mmol), TBSCl (120 mg, 0.80 mmol), imidazole (147 mg, 2.16 mmol, 6 eq.)

Reaction time: 5 h

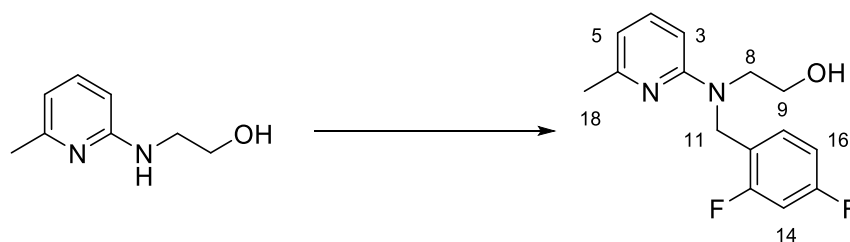
Yield: Silica column chromatography (PE:EtOAc = 6:1) gave **100** as a colorless oil (69.3 mg, 0.27 mmol, 70%)

¹H-NMR (400 MHz, CDCl₃): δ 8.08 (dd, *J* = 5.2, 2.0 Hz, 1H, 6-H), 7.40 (ddd, *J* = 8.4, 7.0, 2.0 Hz, 1H, 4-H), 6.56 (ddd, *J* = 7.0, 5.2, 0.8 Hz, 1H, 5-H), 6.40 (dd, *J* = 8.4, 0.8 Hz, 1H, 3-H), 4.28 (bs, 1H, 7-H), 3.80 (t, *J* = 5.3 Hz, 2H, 9-H), 3.41 (q, *J* = 5.3 Hz, 2H, 8-H), 0.90 (s, 9H, 12-H), 0.06 (s, 6H, 10-H) ppm;

¹³C-NMR (100 MHz, CDCl₃): δ 158.9 (C-2), 148.2 (C-6), 137.5 (C-4), 112.2 (C-5), 107.5 (C-3), 62.1 (C-9), 44.3 (C-8), 26.1 (C-12), 18.5 (C-11), -5.2 (C-10) ppm;

HRMS (ESI) *m/z* calcd. for [M+H]⁺: 253.1737; found 253.2736;

R_f(PE:EtOAc = 4:1): 0.30.

2-((2,4-Difluorobenzyl)(6-methylpyridin-2-yl)amino)ethan-1-ol (85b)

Procedure: B, 66 °C

Reactants: 2-(6-methylpyridin-2-ylamino)ethan-1-ol (**94b**, 202 mg, 1.33 mmol),
2,4-difluorobenzylbromide **98** (210 μ L, 2.65 mmol)

Reaction time: 24 h

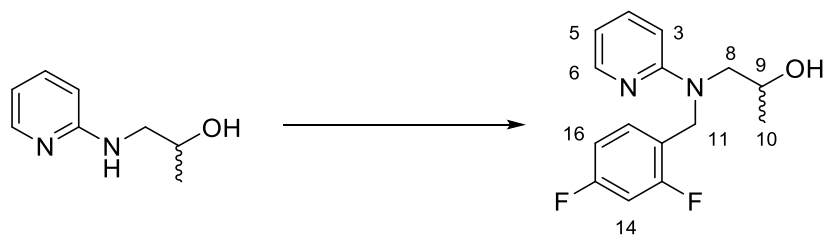
Yield: Silica column chromatography (PE:EtOAc = 1:0 – 6:1) gave **85b** as a colorless oil (218 mg, 0.78 mmol, 59%)

¹H-NMR (400 MHz, CDCl₃): δ 7.31 (t, J = 7.6 Hz, 1H, 4-H), 7.10 (dt, J = 6.5, 8.2 Hz, 1H, 17-H), 6.89-6.75 (m, 2H, 14-H, 16-H), 6.49 (d, J = 7.6 Hz, 1H, 3-H), 6.36 (bs, 1H, O-H), 6.24 (d, J = 7.6 Hz, 1H, 5-H), 4.63 (s, 2H, 11-H), 3.89 – 3.83 (m, 2H, 8-H), 3.82-3.74 (m, 2H, 9-H), 2.40 (s, 3H, 18-H) ppm;

¹³C-NMR (100 MHz, CDCl₃): δ 162.3 (dd, J = 247.2, 14.4 Hz, C-13 or C-15), 160.8 (dd, J = 247.2, 14.4 Hz, C-13 or C-15), 158.5 (s, 2-C), 156.2 (s, 6-C), 138.7 (s, 4-C), 128.9 (dd, J = 10.0, 6.2 Hz, 14-C), 120.6 (dd, J = 14.7, 3.4 Hz, 12-C), 112.7 (s, 3-C), 111.5 (dd, J = 20.9, 4.5 Hz, C-16), 104.2 (t, J = 24.9 Hz, C-14), 103.9 (s, 5-C), 63.9 (s, 9-C), 53.4 (s, 8-C), 47.9 (s, 11-C), 24.1 (s, 18-C) ppm;

HRMS (ESI) m/z calcd. for [M+H]⁺:279.1306; found 279.1309;

R_f(PE:EtOAc = 1:1): 0.50.

2-((2,4-Difluorobenzyl)(pyridin-2-yl)amino)propan-1-ol (86a)

- Procedure:** B, 300 W, 66 °C
- Reactants:** 2-(Pyridin-2-ylamino)propan-1-ol (**95a**, 222 mg, 1.61 mmol),
2,4-difluorobenzylbromide **98** (260 μ L, 3.2 mmol)
- Reaction time:** 3 h
- Yield:** Silica column chromatography (PE:EtOAc = 1:0 – 1:1 + 0.1% Et₃N) gave **86a** as a colorless oil (187 mg, 0.67 mmol, 42%).

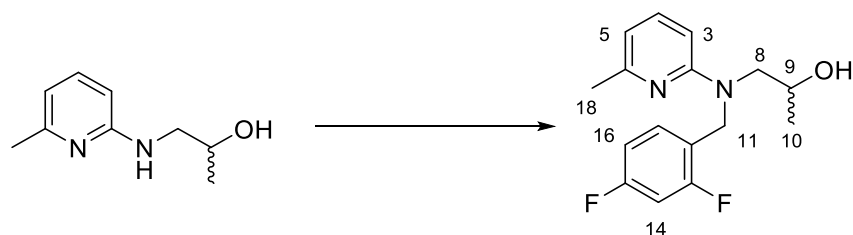
¹H-NMR (400 MHz, CDCl₃): δ 8.09 (dd, J = 5.2, 2.0 Hz, 1H, H-6), 7.41 (ddd, J = 9.0, 7.2, 2.0 Hz, 1H, H-4), 7.07 (dt, J = 7.0, 8.5 Hz, 1H, H-17), 6.85 (ddd, J = 10.6, 9.0, 2.4 Hz, 1H, H-14), 6.79 (ddd, J = 9.0, 8.5, 2.4 Hz, 1H, H-16), 6.62 (dd, J = 7.2, 5.2 Hz, 1H, H-5), 6.41 (d, J = 9.0 Hz, 1H, H-3), 6.03 (bs, 1H, *O*-H), 4.74 (d, J = 18.2 Hz, 1H, H-11_a), 4.61 (d, J = 18.2 Hz, 1H, H-11_b), 4.08 (ddq, J = 8.0, 2.0, 6.4 Hz, 1H, H-9), 3.86 (dd, J = 15.5, 8.0 Hz, 1H, H-8_a), 3.42 (dd, J = 15.5, 2.0 Hz, 1H, H-8_b), 1.21 (t, J = 6.4 Hz, 3H, H-10) ppm;

¹³C-NMR (100 MHz, DMSO-*d*₆): δ 162.7 (dd, J = 246.3, 12.0 Hz, C-13 or C-15), 160.1 (dd, J = 246.3, 12.0 Hz, C-13 or C-15), 158.8 (s, C-2), 147.1 (s, C-6), 138.1 (s, C-4), 128.6 (dd, J = 9.9, 7.1 Hz, 1C, C-17), 120.2 (dd, J = 15.0, 3.6 Hz, C-12), 113.1 (s, C-5), 111.3 (dd, J = 21.2, 4.0 Hz, 1C, C16), 106.7 (s, C-3), 104.1 (t, J = 25.6 Hz, 1C, C-14), 68.12 (s, C-9), 58.2 (s, C-8), 47.8 (s, C-11), 21.4 (C-10) ppm;

HRMS (ESI) m/z calcd. for [M+Na]⁺: 301.1128; found 301.1133;

R_f(EtOAc, 0.1% Et₃N): 0.64.

2-((2,4-Difluorobenzyl)(6-methylpyridin-2-yl)amino)propan-1-ol (86b)



Procedure: B, 66 °C

Reactants: 2-(6-Methylpyridin-2-ylamino)propan-1-ol (**95b**, 220 mg, 1.33 mmol),
2,4-difluorobenzylbromide **98** (210 μ L, 2.65 mmol)

Reaction time: 18 h

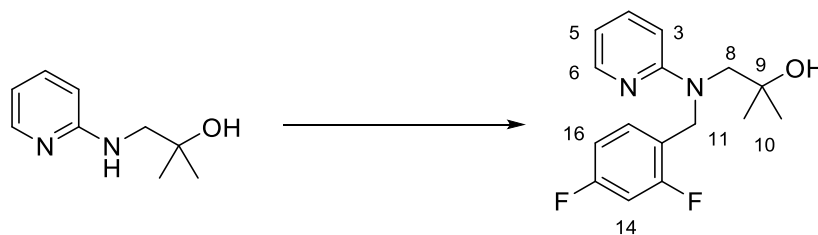
Yield: Silica column chromatography (PE:EtOAc = 1:0 – 6:1) gave **86b** as a colorless oil (216 mg, 0.74 mmol, 56%)

¹H-NMR (400 MHz, CDCl₃): δ 7.30 (t, J = 7.5 Hz, 1H, 4-H), 7.07 (dt, J = 7.0, 8.5 Hz, 1H, 17-H), 6.90 (bs, 1H, O-H), 6.84 (ddd, J = 10.6, 9.0, 2.4 Hz, 1H, 14-H), 6.79 (ddd, J = 9.0, 8.5, 2.4 Hz, 1H, 16-H), 6.49 (d, J = 7.5 Hz, 1H, 3-H or 5-H), 6.21 (d, J = 7.5 Hz, 1H, 3-H or 5-H), 4.69 (d, J = 17.9 Hz, 1H, 11_a-H), 4.61 (d, J = 17.9 Hz, 1H, 11_b-H), 4.08 (ddq, J = 7.6, 2.0, 6.4 Hz, 1H, 9-H), 3.86 (dd, J = 14.1, 7.6 Hz, 1H, 8_a-H), 3.42 (dd, J = 14.1, 2.0 Hz, 1H, 8_b-H), 2.40 (s, 3H, 18-H), 1.21 (d, J = 6.4 Hz, 3H, H-10) ppm;

¹³C-NMR (100 MHz, CDCl₃): δ 162.1 (dd, J = 248, 12 Hz, C-13 o. 15), 160.7 (dd, J = 248, 12 Hz, C-13 o. 15), 158.3 (s, C-2), 156.0 (s, C-6), 138.5 (s, C-4), 128.6 (dd, J = 10, 6 Hz, C-17), 120.2 (d, J = 15 Hz, C-12), 112.5 (s, C-5 o. C-3), 111.3 (dd, J = 20, 4 Hz, C-16), 104.0 (t, J = 25 Hz, C-14), 103.6 (s, C-5 o. C-3), 68.5 (s, C-9), 58.5 (s, C-8), 48.2 (d, J = 5 Hz, C-11), 23.8 (s, C-18), 21.4 (s, C-10) ppm;

HRMS (ESI) m/z calcd. for [M+H]⁺: 293.1470; found 293.1465;

R_f(PE:EtOAc = 1:1): 0.55.

1-((2,4-Difluorobenzyl)(pyridin-2-yl)amino)-2-methylpropan-2-ol (87a)

Procedure: B, 66 °C

Reactants: 2-Methyl-1-(pyridin-2-ylamino)propan-2-ol (**96a**, 220 mg, 1.33 mmol), 2,4-difluorobenzylbromide **98** (210 μ L, 2.65 mmol)

Reaction time: 24 h

Yield: Silica column chromatography (PE:EtOAc = 1:0 – 6:1) gave **87a** as a colorless solid (153 mg, 0.53 mmol, 40%)

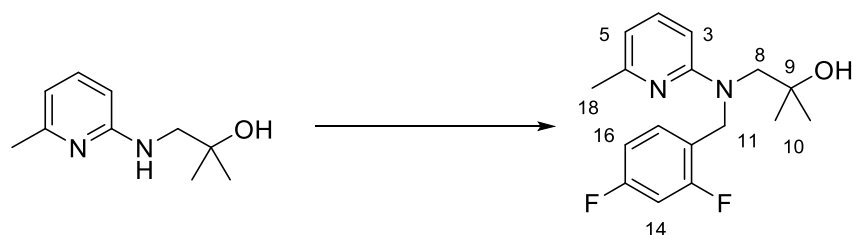
¹H-NMR (400 MHz, CDCl₃): δ 8.08 (ddd, J = 5.1, 2.0, 0.9 Hz, 1H, 6-H), 7.39 (ddd, J = 8.5, 7.0, 2.0 Hz, 1H, 4-H), 7.14 (bs, 1H, *O*-H), 6.96 (dt, J = 6.4, 8.8 Hz, 1H, 17-H), 6.85 (ddd, J = 9.6, 8.7, 2.5 Hz, 1H, 14-H), 6.78 (dddd, J = 8.9, 8.2, 2.5, 0.8 Hz, 1H, 16-H), 6.62 (ddd, J = 7.0, 5.1, 0.9 Hz, 1H, 5-H), 6.37 (dd, J = 8.5, 0.9 Hz, 1H, 3-H), 4.68 (s, 2H, 11-H), 3.65 (s, 2H, 8-H), 1.27 (s, 6H, 10-H) ppm;

¹³C-NMR (100 MHz, CDCl₃): δ 162.3 (dd, J = 248, 12 Hz, C-13 o. 15), 160.8 (dd, J = 248, 12 Hz, C-13 o. 15), 158.8 (s, C-2), 147.0 (s, C-6), 138.3 (s, C-4), 128.4 (dd, J = 10, 6 Hz, C-17), 119.9 (dd, J = 15, 4 Hz, C-12), 113.3 (s, C-5), 111.3 (dd, J = 21, 4 Hz, C-16), 106.9 (s, C-5), 104.3 (t, J = 25 Hz, C-14), 103.6 (s, C-3), 71.7 (s, C-9), 62.3 (s, C-8), 49.0 (d, J = 5.0 Hz, C-11), 28.0 (s, C-10) ppm;

HRMS (ESI) m/z calcd. for [M+H]⁺: 293.1466; found 293.1465;

R_f (PE:EtOAc = 1:1): 0.54;

T_m = 91 °C.

1-((2,4-Difluorobenzyl)(6-methylpyridin-2-yl)amino)-2-methylpropan-2-ol (87b)

Procedure: B, 66 °C

Reactants: 2-Methyl-1-(6-methylpyridin-2-ylamino)propan-2-ol (**96b**, 239 mg, 1.33 mmol), 2,4-difluorobenzyl bromide **98** (210 μ L, 2.65 mmol)

Reaction time: 42 h

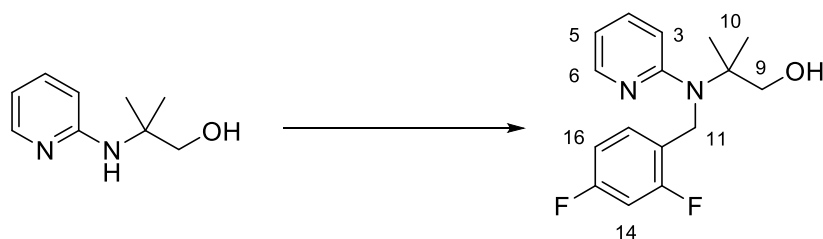
Yield: Silica column chromatography (PE:EtOAc = 1:0 – 6:1) gave **87b** as a yellow oil (190 mg, 0.67 mmol, 51%)

$^1\text{H-NMR}$ (400 MHz, CDCl_3): δ 7.78 (bs, 1H, O-H), 7.30 (dd, $J = 8.5, 7.7$ Hz, 1H, 4-H), 6.97 (dt, $J = 6.4, 8.5$ Hz, 1H, 17-H), 6.85 (ddd, $J = 9.6, 8.7, 2.5$ Hz, 1H, 14-H), 6.78 (dddd, $J = 8.9, 8.5, 2.5, 1.0$ Hz, 1H, 16-H), 6.49 (d, $J = 7.7$ Hz, 1H, 3-H or 5-H), 6.18 (d, $J = 8.5$ Hz, 1H, 3-H or 5-H), 4.65 (s, 2H, 11-H), 3.63 (s, 2H, 8-H), 2.40 (s, 6H, 10-H) ppm;

$^{13}\text{C-NMR}$ (100 MHz, CDCl_3): δ 162.3 (dd, $J = 248, 12$ Hz, C-13 o. 15), 160.9 (dd, $J = 248, 12$ Hz, C-13 o. 15), 158.3 (s, C-2), 156.1 (s, C-6), 138.7 (s, C-4), 128.5 (dd, $J = 10, 6$ Hz, C-17), 120.0 (dd, $J = 15, 4$ Hz, C-12), 112.7 (s, C-5 o. C-3), 111.4 (dd, $J = 21, 4$ Hz, C-16), 104.3 (t, $J = 25$ Hz, C-14), 103.8 (s, C-5 o. C-3), 71.6 (s, C-9), 62.7 (s, C-8), 49.2 (d, $J = 5.0$ Hz, C-11), 28.0 (s, C-18), 23.9 (s, C-10) ppm;

HRMS (ESI) m/z calcd. for $[\text{M}+\text{Na}]^+$: 307.1622; found 307.1623;

R_f (PE:EtOAc = 1:1): 0.55.

2-((2,4-Difluorobenzyl)(pyridin-2-yl)amino)-2-methylpropan-1-ol (88a)

Procedure: B, 66 °C

Reactants: 2-Methyl-2-(pyridin-2-ylamino)propan-1-ol (**97a**, 220 mg, 1.33 mmol), 2,4-difluorobenzylbromide **98** (210 μ L, 2.65 mmol)

Reaction time: 48 h

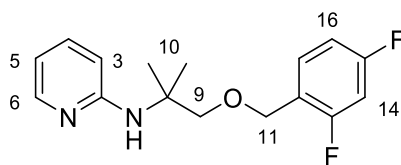
Yield: Silica column chromatography (PE:EtOAc = 1:0 – 6:1) gave **88a** as an inseparable mixture with an unknown compound present of a colorless oil (42 mg) and **102a** as a side product (30 mg, 10.6 mmol, 8%)

¹H-NMR (400 MHz, CDCl₃): δ 7.96 (dd, J = 6.0, 2.2 Hz, 1H, 6-H), 7.48 (dt, J = 7.9, 7.9 Hz, 1H, 17-H), 7.30 (ddd, J = 9.0, 7.5, 2.2 Hz, 1H, 4-H), 6.60-6.50 (m, 2H, 16-H, 17-H), 6.40 (d, J = 9.0 Hz, 1H, 3-H), 6.15 (dd, J = 7.5, 6.0 Hz, 1H, 5-H), 5.10 (s, 2H, 11-H), 4.49 (bs, 1H, O-H), 3.60 (s, 2H, 9-H), 1.32 (s, 6H, 10-H) ppm;

¹³C-NMR (100 MHz, CDCl₃): δ 162.7 (dd, J = 250, 11 Hz, C-13 o. 15), 161.0 (dd, J = 250, 11 Hz, C-13 o. 15), 157.2 (s, C-2), 145.6 (s, C-6), 139.6 (s, C-4), 132.6 (dd, J = 10, 5 Hz, C-17), 119.3 (dd, J = 15, 4 Hz, C-12), 111.8 (dd, J = 21, 4 Hz, C-16), 110.7 (s, C-3), 106.3 (s, C-5), 103.8 (t, J = 25 Hz, C-14), 72.0 (s, C-9), 56.3 (s, C-8), 45.9 (d, J = 5.0 Hz, C-11), 25.4 (s, C-10) ppm;

HRMS (ESI) m/z calcd. for [M+Na]⁺:315.1285; found 315.1292;

R_f(PE:EtOAc = 1:1): 0.36.

***N*-(1-((2,4-Difluorobenzyl)oxy)-2-methylpropan-2-yl)pyridin-2-amine (102a)**

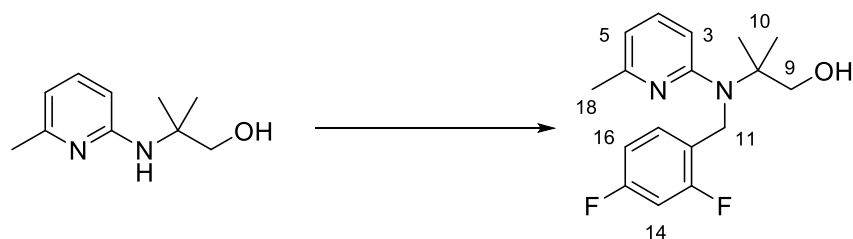
¹H-NMR (400 MHz, CDCl₃): δ 8.02 (dd, *J* = 5.2, 2.0 Hz, 1H, 6-H), 7.46 -7.23 (m, 2H, 4-H, 17-H), 6.87 – 6.72 (m, 2H, 16-H, 14-H), 6.52 (ddd, *J* = 7.0, 5.4, 0.5 Hz, 1H, 5-H), 6.40 (dd, *J* = 8.5, 0.5 Hz, 1H, 3-H), 4.67 (bs, 1H, *O*-H), 4.54 (s, 2H, 11-H), 3.59 (s, 2H, 9-H), 1.43 (s, 6H, 10-H) ppm;

¹³C-NMR (100 MHz, DMSO-*d*₆): δ 162.5 (dd, *J* = 248, 13 Hz, C-13 or C-15), 160.7 (dd, *J* = 248, 13 Hz, C-13 or C-15), 158.5 (s, C-2), 147.6 (s, C-6), 136.7 (s, C-4), 128.6 (dd, *J* = 9, 5 Hz, 1C, C-17), 121.4 (dd, *J* = 15, 4 Hz, C-12), 112.5 (s, C-5), 111.2 (dd, *J* = 20, 3 Hz, 1C, C-16), 109.6 (s, C-3), 103.6 (t, *J* = 26 Hz, 1C, C-14), 76.8 (s, C-9), 66.2 (d, *J* = 4 Hz, C-11), 53.7 (s, C-8), 24.7 (C-10) ppm;

HRMS (ESI) *m/z* calcd. for [M+Na]⁺:315.1285; found 315.1287;

R_f(PE:EtOAc = 1:1): 0.61.

2-((2,4-Difluorobenzyl)(6-methylpyridin-2-yl)amino)-2-methylpropan-1-ol (88b)



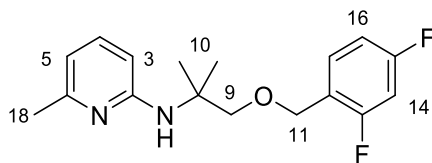
Procedure: B, 66 °C
Reactants: 2-Methyl-2-((6-methylpyridin-2-yl)amino)propan-1-ol (**97b**, 103 mg, 0.57 mmol), 2,4-difluorobenzylbromide **98** (90 μL, 1.14 mmol)
Reaction time: 48 h
Yield: Silica column chromatography (PE:EtOAc = 1:0 – 6:1) gave **88b** as a colorless oil (8.0 mg, 0.05 mmol, 8%) and **102b** as side product (7.8 mg, 0.05 mmol, 8%)

¹H-NMR (400 MHz, CDCl₃): δ 8.09 (bs, 1H, *O*-H), 7.30 (t, *J* = 8.0 Hz, 1H, 4-H), 7.25 -7.17 (m, 1H, 17-H), 6.85 – 6.78 (m, 2H, 14-H, 16-H), 6.57 (d, *J* = 8.0 Hz, 1H, 3-H), 6.27 (d, *J* = 8.0 Hz, 1H, 5-H), 4.54 (s, 2H, 11-H), 3.71 (s, 2H, 9-H), 2.44 (bs, 3H, 18-H), 1.38 (s, 6H, 10-H) ppm;

¹³C-NMR (100 MHz, CDCl₃): δ 162.0 (dd, *J* = 248, 12 Hz, C-13 or C-15), 159.8 (dd, *J* = 248, 12 Hz, C-13 or C-15), 159.4 (s, C-2), 154.6 (s, C-6), 138.6 (s, C-4), 129.2 (dd, *J* = 9, 6 Hz, 1C, C-17), 123.3 (dd, *J* = 15, 4 Hz, C-12), 114.1 (s, C-3), 111.3 (dd, *J* = 20, 3 Hz, 1C, C-16), 109.8 (s, C-5), 103.8 (t, *J* = 25 Hz, 1C, C-14), 71.3 (s, C-9), 61.9 (s, C-8), 46.6 (d, *J* = 4 Hz, C-11), 25.1 (s, C-10), 23.6 (s, C-18) ppm;

HRMS (ESI) *m/z* calcd. for [M+Na]⁺:329.1441; found 329.1439;

R_f(PE:EtOAc = 1:1): 0.42.

***N*-((2,4-Difluorobenzyl)oxy)-2-methylpropan-2-yl)-6-methylpyridin-2-amine (102b)**

¹H-NMR (400 MHz, CDCl₃): δ 7.37 -7.24 (m, 2H, 4-H, 17-H), 6.82 (ddd, $J = 2.0, 8.2, 9.3$ Hz, 1H, 14-H or 16-H), 6.77 (ddd, $J = 2.7, 9.3, 10.5$ Hz, 1H, 14-H or 16-H), 6.40 (d, $J = 7.2$ Hz, 1H, 3-H), 6.34 (bs, 1H, 5-H), 4.67 (bs, 1H, O-H), 4.55 (s, 2H, 11-H), 3.57 (s, 2H, 9-H), 2.36 (bs, 3H, 18-H), 1.42 (s, 6H, 10-H) ppm;

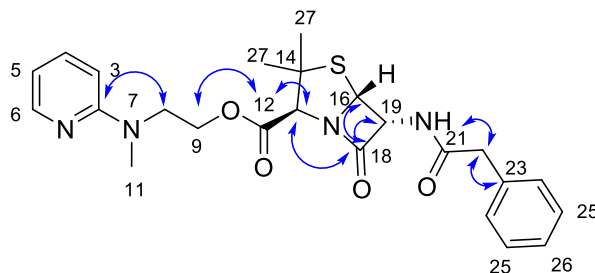
¹³C-NMR (100 MHz, CDCl₃): δ 162.4 (dd, $J = 248, 12$ Hz, C-13 or C-15), 160.7 (dd, $J = 248, 12$ Hz, C-13 or C-15), 157.2 (bs, C-2), 156.2 (s, C-6), 137.6 (bs, C-4), 131.0 (s, C-17), 121.3 (d, $J = 16$ Hz, C-12), 111.5 (bs, C-3 or C-5), 111.1 (dd, $J = 20, 3$ Hz, 1C, C-16), 106.3 (bs, C-3 or C-5), 103.6 (t, $J = 26$ Hz, 1C, C-14), 77.1 (s, C-9), 66.2 (d, $J = 4$ Hz, C-11), 53.9 (bs, C-8), 24.7 (s, C-10) ppm;*

HRMS (ESI) m/z calcd. for [M+Na]⁺:329.1441; found 329.1438;

R_f(PE:EtOAc = 1:1): 0.61.

*C-18 could not be detected in the ¹³C-NMR spectrum.

2-(Methyl(pyridin-2-yl)amino)ethyl (2S,5R,6R)-3,3-dimethyl-7-oxo-6-(2-phenylacetamido)-4-thia-1-azabicyclo[3.2.0]heptane-2-carboxylate (105)



Penicillin G sodium salt (**104**) (43.5 mg, 0.12 mmol, 1.0 eq.) was dissolved in CH_2Cl_2 (4.4 mL) and cooled to 0 °C. DMAP (**103**, 4.30 mg, 0.037 mmol, 0.3 eq.) and EDC·HCl (46.45 g, 0.242 mmol, 2.0 eq.) and the alcohol **84a** (22.3 mg, 0.15 mmol, 1.2 eq.) were added and the mixture was stirred for 18 h while allowing it to warm up to rt. The reaction was terminated by addition of H_2O (1 mL) and the aq. phase was extracted with CH_2Cl_2 (3 x 5 mL). The combined organic phases were dried over Na_2SO_4 , filtered and the solvent was removed *in vacuo*. Silica column chromatography (PE:EtOAc = 1:1) gave the ester **105** (20.2 mg, 0.04 mmol, 36%) as a pale yellow oil along with *O*-acyl derivative **106** as byproduct.

$^1\text{H-NMR}$ (400 MHz, CDCl_3): δ 8.12 (dd, $J = 5.0, 2.0$ Hz, 1H, 6-H), 7.46 (ddd, $J = 8.5, 7.0, 2.0$ Hz, 1H, 4-H), 7.38 – 7.24 (m, 5H, 24-H - 26-H), 6.56 (ddd, $J = 7.0, 5.0, 0.8$ Hz, 1H, 5-H), 6.52 (dd, $J = 8.5, 0.8$ Hz, 1H, 3-H), 6.05(d, $J = 9.2$ Hz, 1H, 20-H), 5.61 (dd, $J = 9.2, 4.3$ Hz, 1H, 19-H), 5.41 (d, $J = 4.3$ Hz, 1H, 16-H), 4.36 (ddd, $J = 6.5, 5.8, 2.8$ Hz, 2H, 9-H), 4.31 (s, 1H, 13-H), 3.96-3.82 (m, 2H, 8-H), 3.63 (s, 2H, 22-H), 3.04 (s, 3H, 11-H), 1.38 (s, 6H, 27-H) ppm;

$^{13}\text{C-NMR}$ (100 MHz, CDCl_3): δ 173.5 (C-18), 170.4 (C-21), 167.7 (C-12), 158.4 (C-2), 148.0 (C-6), 137.5 (C-4), 133.9 (C-23), 129.7 (C-24 o. C-25), 129.3(C-24 o. C-25), 127.8 (C-26), 112.4 (C-5), 105.8 (C-3), 70.5 (C-13), 68.1 (C-16), 64.6 (C-14), 63.5 (C-9), 58.8 (C-19), 48.3 (C-8), 43.5 (C-22), 37.2 (C-11), 32.0 (C-27), 26.8 (C-27) ppm;

Blue arrows indicate selected HMBC correlations.

HRMS (ESI) m/z calcd. for $[\text{M}+\text{H}]^+$: 469.1910; found 469.1910;

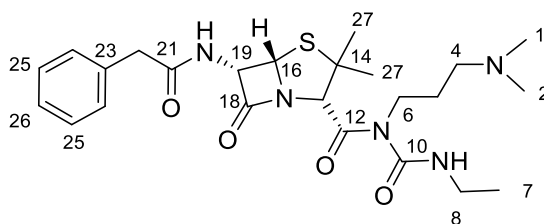
R_f (EtOAc): 0.91.

Additional NMR Data (from Release Study at 25 °C in D₂O:DMSO-d₆ = 4:6 on day 0):

¹H-NMR (400 MHz, DMSO-d₆:D₂O = 6:4): δ 7.95 (dd, J = 5.0, 2.0 Hz, 1H, 6-H), 7.45 (ddd, J = 8.5, 7.0, 2.0 Hz, 1H, 4-H), 7.26 – 7.23 (m, 2H, 24-H), 7.21 – 7.17 (m, 3H, 25-H, 26-H), 6.56 (dd, J = 8.5, 0.8 Hz, 1H, 3-H), 6.53 (dd, J = 7.0, 5.0 Hz, 1H, 5-H), 5.33 (d, J = 4.2 Hz, 1H, 16-H), 5.27 (d, J = 4.2 Hz, 1H, 19-H), 4.25 (ddd, J = 5.7, 5.2, 1.7 Hz, 2H, 9-H), 4.22 (s, 1H, 13-H), 3.81 (dt, J = 15.3, 5.7 Hz, 1H, 8-H_a), 3.73 (dt, J = 15.3, 5.2 Hz, 1H, 8-H_b), 3.50 (d, J = 14.3 Hz, 1H, 22-H_a), 3.45 (d, J = 14.3 Hz, 1H, 22-H_b), 2.91 (s, 3H, 11-H), 1.42 (s, 3H, 27a-H), 1.22 (s, 3H, 27b-H) ppm;

¹³C-NMR (100 MHz, DMSO-d₆:D₂O = 13:8): δ 174.5 (C-18), 172.5 (C-21), 168.8 (C-12), 159.0 (C-2), 148.1 (C-6), 138.8 (C-4), 136.1 (C-23), 130.0 (C-25), 129.4(C-24), 127.8 (C-26), 112.9 (C-5), 107.2 (C-3), 71.0 (C-13), 68.1 (C-19), 65.1 (C-14), 64.1 (C-9), 59.4 (C-16), 48.4 (C-8), 42.3 (C-22), 37.3 (C-11), 31.1 (C-27), 27.1 (C-27) ppm;

(2*S*,5*S*,6*S*)-*N*-(3-(Dimethylamino)propyl)-*N*-(ethylcarbamoyl)-3,3-dimethyl-7-oxo-6-(2-phenylacetamido)-4-thia-1-azabicyclo[3.2.0]heptane-2-carboxamide (106)



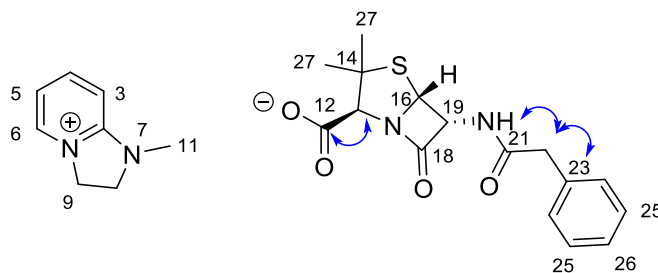
¹H-NMR (400 MHz, CDCl₃): δ 9.67 (bs, 1H, 11-H), 7.4– 7.24 (m, 5H, 24-H - 26-H), 6.17 (d, J = 9.9 Hz, 2H, 20-H), 5.58 (d, J = 4.6 Hz, 1H, 16-H), 5.55 (dd, J = 9.9, 4.6 Hz, 1H, 19-H), 4.00 – 3.90 (m, 1H, 6-H_a), 3.67 (s, 2H, 22-H), 3.40 – 3.30 (m, 2H, 6-H_b), 3.30 – 3.11 (m, 2H, 8-H), 2.50-2.40 (m, 1H, 4-H_a), 2.25 (s, 6H, 1-H, 2-H), 2.21-2.10 (m, 1H, 4-H_b), 1.50 (s, 3H, 27a-H), 1.38 (s, 3H, 27b-H), 1.25 (m, 2H, 5-H), 1.16 (t, J = 7.6 Hz, 3H, 7-H) ppm;*

¹³C-NMR (100 MHz, CDCl₃): δ 173.0 (C-12, C-18), 170.4 (C-21), 134.0 (C-23), 129.8 (C-24), 129.3 (C-25), 127.7 (C-26), 68.9 (C-16), 66.5 (C-14), 59.3 (C-19), 54.1 (C-4), 44.2 (C-1, C-2), 43.7 (C-22), 35.9 (C-8), 34.1 (C_b-27), 32.0, 29.8 (C-5), 29.8, 29.5, 26.3 (C_a-27), 22.8, 14.7 (C-7) ppm;*

HRMS (ESI) m/z calcd. for [M+H]⁺: 490.2388; found 490.2490.

*13-H and 13-C were not identified in ¹H and ¹³C-NMR, respectively.

1-Methyl-2,3-dihydro-1H-imidazo[1,2-a]pyridin-4-ium and (2S,5R,6R)-3,3-dimethyl-7-oxo-6-(2-phenylacetamido)-4-thia-1-azabicyclo[3.2.0]heptane-2-carboxylate (104 and 107)

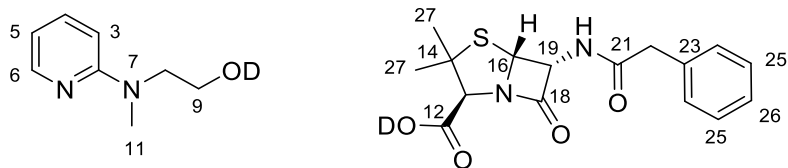


¹H-NMR (400 MHz, CDCl₃): δ 8.47* (dd, $J = 6.6, 1.3$ Hz, 1H, 6-H), 7.79* (ddd, $J = 9.0, 7.4, 1.3$ Hz, 1H, 4-H), 7.38– 7.24 (m, 5H, 24-H - 26-H), 6.82* (ddd, $J = 7.4, 6.6, 0.8$ Hz, 1H, 5-H), 6.73* (dd, $J = 9.0, 0.8$ Hz, 1H, 3-H), 6.19 (d, $J = 9.2$ Hz, 1H, 20-H), 5.51-5.48 (m, 2H, 19-H, 16-H), 4.95* (t, $J = 9.9$ Hz, 2H, 9-H), 4.13 (s, 1H, 13-H), 4.02* (t, $J = 9.9$ Hz, 2H, 8-H), 3.60 (s, 2H, 22-H), 3.08* (s, 3H, 11-H), 1.56 (s, 3H, 27a-H), 1.46 (s, 3H, 27b-H) ppm;

¹³C-NMR (100 MHz, CDCl₃): δ 174.0 (C-18), 171.6 (C-12), 170.5 (C-21), 154.7* (C-2), 144.7* (C-4), 139.2* (C-6), 134.1 (C-23), 129.7 (C-24 o. C-25), 129.2 (C-24 o. C-25), 127.6 (C-26), 113.5* (C-5), 106.9* (C-3), 74.2 (C-13), 67.2 (C-16), 64.9 (C-14), 57.8 (C-19), 50.5* (C-9), 40.2* (C-8), 43.6 (C-22), 32.8* (C-11), 32.1 (C-27b), 27.5 (C-27a) ppm;

HRMS (ESI) m/z calcd. for [M]⁻: 333.0900; found 333.0910 and calcd. for [M]⁺: 135.0922; found 135.0922.

(2*S*,5*R*,6*R*)-3,3-dimethyl-7-oxo-6-(2-phenylacetamido)-4-thia-1-azabicyclo[3.2.0]heptane-2-carboxylic acid-*d* (79` and 84a`)

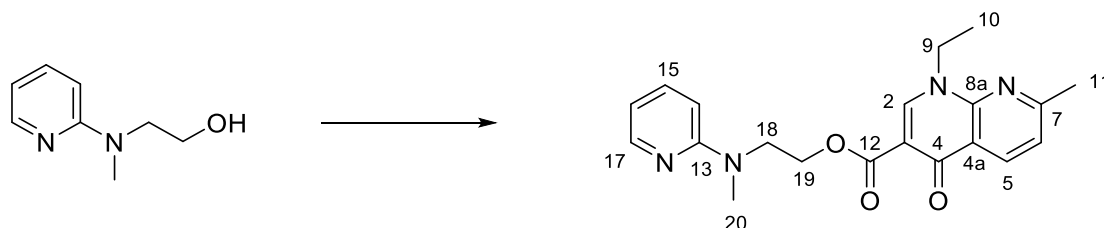


Penicillin ester **105** (37 mg, 0.08 mmol, 1 eq.) was dissolved in D₂O:DMSO-*d*₆ = 4:6 (1.0 mL) and left for 20 d at 25 °C. The solution contained deuterated penicillin **79'** and deuterated alcohol **84a'** along with ¹H-NMR signals of a third, unidentified compound.

¹H-NMR (400 MHz, DMSO-*d*₆:D₂O = 6:4): δ 7.96 (dd, *J* = 6.8, 1.3 Hz, 1H, 6-H), 7.87 (ddd, *J* = 9.0, 7.0, 1.3 Hz, 1H, 4-H), 7.28–7.23 (m, 2H, 24-H), 7.22–7.17 (m, 3H, 25-H), 6.98 (dd, *J* = 9.0, 0.8 Hz, 1H, 3-H), 6.80 (ddd, *J* = 7.0, 6.8, 0.8 Hz, 1H, 5-H), 5.31 (d, *J* = 4.0 Hz, 1H, 16-H), 5.27 (d, *J* = 4.0 Hz, 1H, 19-H), 4.53 (t, *J* = 10.0, 9-H), 3.94 (s, 1H, 13-H), 3.84 (t, *J* = 10.0 Hz, 2H, 8-H), 3.10 (d, *J* = 14.3 Hz, 1H, 22-H_a), 3.45 (d, *J* = 14.3 Hz, 1H, 22-H_b), 2.98 (s, 3H, 11-H), 1.50 (s, 3H, 27a-H), 1.38 (s, 3H, 27b-H) ppm;

¹³C-NMR (100 MHz, DMSO-*d*₆:D₂O = 6:4): δ 174.2 (C-18), 172.5 (C-21), 172.1 (C-12), 155.4 (C-2), 145.5 (C-6), 138.2 (C-4), 136.2 (C-23), 130.0 (C-25), 129.4(C-24), 127.8 (C-26), 113.5 (C-5), 108.4 (C-3), 74.2 (C-13), 67.6 (C-19), 65.5 (C-14), 58.5 (C-16), 50.5 (C-9), 50.1 (C-9), 42.4 (C-22), 32.9 (C-11), 31.8 (C-27), 28.2 (C-27) ppm;

2-(Methyl(pyridin-2-yl)amino)ethyl 1-ethyl-7-methyl-4-oxo-1,4-dihydro-1,8-naphthyridine-3-carboxylate (108a)



- Procedure:** D, a
- Reactants:** Nalidixic acid (**81**) (16.8 mg, 0.07 mmol, 1.0 eq.), COMU® (**109**, 46.4 mg, 0.11 mmol, 1.5 eq.), DBU (11.0 μ L, 0.07 mmol, 1.0 eq.), alcohol **84a** (11.0 mg, 0.07 mmol, 1.0 eq.)
- Reaction time:** 18 h
- Yield:** Silica column chromatography (1. EtOAc, 2. CH₂Cl₂ 1% - 2% MeOH) gave **108a** (9.0 mg, 0.02 mmol, 34%) as a colorless solid.

¹H-NMR (400 MHz, CDCl₃): δ 8.64 (d, J = 8.3 Hz, 1H, 5-H), 8.48 (s, 1H, 2-H), 8.15 (dd, J = 5.2, 1.7 Hz, 1H, 17-H), 7.44 (ddd, J = 8.8, 6.8, 1.7 Hz, 1H, 15-H), 7.24 (d, J = 8.3 Hz, 1H, 6-H), 6.60 (d, J = 8.8 Hz, 1H, 14-H), 6.53 (dd, J = 6.8, 5.2 Hz, 1H, 14-H), 4.53 (t, J = 5.7 Hz, 2H, 19-H), 4.40 (q, J = 7.2 Hz, 2H, 9-H), 4.00 (t, J = 5.7 Hz, 2H, 18-H), 3.18 (s, 3H, 20-H), 2.65 (s, 3H, 10-H), 1.45 (t, J = 7.2 Hz, 2H, 10-H) ppm;

¹³C-NMR (100 MHz, CDCl₃): δ 174.8 (C-4), 165.2 (C-12), 162.8 (C-7), 158.6 (C-13), 148.9 (C-2), 148.7 (C-8a), 147.9 (C-17), 137.4 (C-15), 137.0 (C-5), 121.6 (C-3), 121.2 (C-6), 111.8 (C-16), 111.7 (C-4a), 105.9 (C-14), 62.6 (C-19), 48.7 (C-18), 46.7 (C-9), 37.2 (C-20), 25.2 (C-11), 15.3 (C-10) ppm;*

HRMS (ESI) m/z calcd. for [M+Na]⁺: 389.1590; found 389.1588;

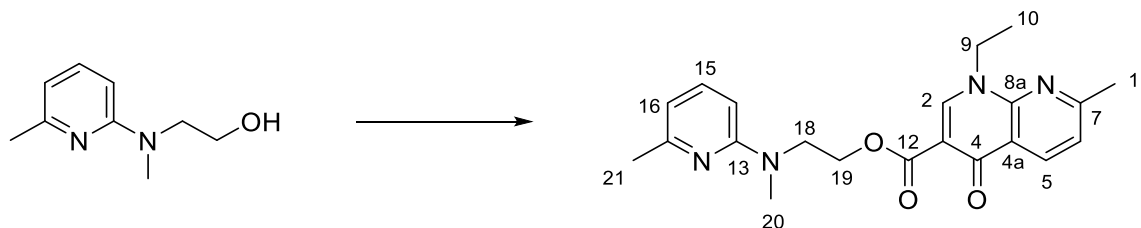
R_f(EtOAc, 1% Et₃N): 0,18;

T_m (decomp) 131 °C;

HPLC-UV (ACN : H₂O + 0.1% FA = 15% - 25% for 3 min; 25% - 100% for 2.3 min; 100% for 0.7 min, 100% - 15% for 0.3 min): t_R (**108a**) = 0.87 min, t_R (**81**) = 2.45 min, λ = 256 nm.

*C-1 could not be detected in the ¹³C-NMR spectrum.

2-(Methyl(6-methylpyridin-2-yl)amino)ethyl 1-ethyl-7-methyl-4-oxo-1,4-dihydro-1,8-naphthyridine-3-carboxylate (108b)



Procedure: D, a

Reactants: Nalidixic acid (**81**) (100.0 mg, 0.42 mmol, 1.0 eq.), COMU® (**109**, 276 mg, 0.65 mmol, 1.5 eq.), DBU (64.0 μ L, 0.43 mmol, 1.0 eq.), alcohol **84b** (85.8 mg, 0.52 mmol, 1.2 eq.)

Reaction time: 18 h

Yield: Silica column chromatography (toluene, 5% - 20% acetone) was followed by preparative TLC (toluene, 40% acetone) which gave **108b** (21 mg, 0.05 mmol, 12%) as a colorless solid.

¹H-NMR (600 MHz, DMSO-*d*₆): δ 8.65 (s, 1H, 2-H), 8.44 (d, J = 8.0 Hz, 1H, 5-H), 7.41 (d, J = 8.0 Hz, 1H, 6-H), 7.37 (dd, J = 8.3, 7.2 Hz, 1H, 15-H), 6.46 (d, J = 8.0 Hz, 1H, 14 o. 16-H), 6.40 (d, J = 7.2 Hz, 1H, 14 o. 16-H), 4.41 (q, J = 7.0 Hz, 1H, 9-H), 4.35 (t, J = 5.8 Hz, 2H, 19-H), 3.87 (t, J = 5.8 Hz, 1H, 18-H), 3.06 (s, 3H, 20-H), 2.62 (s, 3H, 11-H), 2.25 (s, 3H, 21-H), 1.33 (t, J = 7.0 Hz, 1H, 10-H), ppm;*

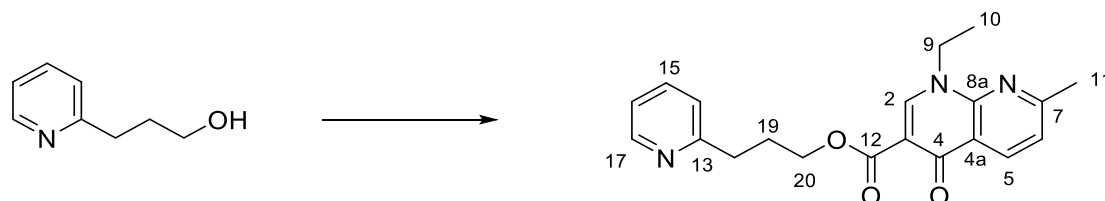
¹³C-NMR (150 MHz, DMSO-*d*₆): δ 173.2 (C-4), 164.1 (C-12), 162.5 (C-7), 157.7 (C-13), 155.6 (C-17), 149.3 (C-2), 148.2 (C-8a), 137.6 (C-15), 136.1 (C-5), 121.2 (C-3 o. C-6), 120.6 (C-3 or C-6), 110.8 (C-4a o. C-16), 110.5 (C-4a o. C-16), 102.5 (C-14), 61.7 (C-19), 47.8 (C-18), 45.7 (C-9), 36.5 (C-20), 24.7 (C-11), 24.4 (C-21), 14.9 (C-10) ppm;

HRMS (ESI) m/z calcd. for [M+Na]⁺: 403.1746; found 403.1740;

HPLC-UV (ACN : H₂O + 0.1% FA = 15% - 35% for 3 min; 35% - 100% for 0.2 min; 100% for 1.2 min, 100% - 15% for 0.6 min): t_R (**108b**) = 1.16 min, t_R (**81**) = 2.30 min, λ = 256 nm.

*C-1 could not be detected in the ¹³C-NMR spectrum.

3-(Pyridin-2-yl)propyl 1-ethyl-7-methyl-4-oxo-1,4-dihydro-1,8-naphthyridine-3-carboxylate (118)



- Procedure:** D, a
- Reactants:** Nalidixic acid (**81**) (50.0 mg, 0.21 mmol, 1.0 eq.), COMU® (**109**, 138 mg, 0.32 mmol, 1.5 eq.), DBU (32.0 μ L, 0.21 mmol, 1.0 eq.), alcohol **83a** (35.0 mg, 0.21 mmol, 1.0 eq.)
- Reaction time:** 18 h
- Yield:** Silica column chromatography (PE:EtOAc = 2:1 – 0:1) was followed by preparative HPLC (C18, H₂O:MeOH 20% - 100% over 30 min, then 100% for 10 min) gave **118** (19 mg, 0.05 mmol, 25%) as a colorless solid.

¹H-NMR (400 MHz, CDCl₃): δ 8.65 (d, J = 8.2 Hz, 1H, 5-H), 8.59 (s, 1H, 2-H), 8.53 (dd, J = 5.2, 2.0 Hz, 1H, 17-H), 7.60 (ddd, J = 9.0, 7.5, 2.0 Hz, 1H, 15-H), 7.26 (dd, J = 7.4, 1.0 Hz, 1H, 14-H), 7.24 (d, J = 8.2 Hz, 1H, 6-H), 7.11 (ddd, J = 7.5, 5.2, 1.0 Hz, 1H, 16-H), 4.48 (q, J = 7.2 Hz, 2H, 9-H), 4.38 (t, J = 6.6 Hz, 2H, 20-H), 3.02 (dd, J = 8.2, 7.6 Hz, 2H, 14-H), 2.66 (s, 3H, 11-H), 2.25 (ddt, J = 8.2, 7.4, 6.6 Hz, 2H, 19-H), 1.50 (t, J = 7.2 Hz, 3H, 10-H) ppm;*

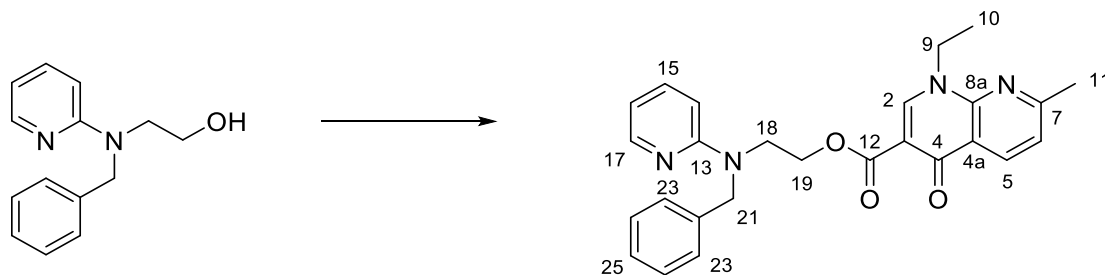
¹³C-NMR (100 MHz, CDCl₃): δ 174.8 (C-4), 165.7 (C-12), 162.8 (C-7), 161.1 (C-13), 149.1 (C-17), 148.8 (C-2), 148.7 (C-8a), 137.0 (C-5), 136.7 (C-15), 123.4 (C-14), 121.6 (C-4a), 121.3 (C-16), 121.2 (C-6), 112.1 (C-3), 64.3 (C-20), 46.7 (C-9), 34.6 (C-18), 28.7 (C-19), 25.2 (C-11), 15.3 (C-10) ppm;

HRMS (ESI) m/z calcd. for [M+Na]⁺: 374.1481; found 374.1482;

HPLC-UV (ACN : H₂O + 0.1% FA = 10% - 65% for 3 min; 65% - 100% for 0.5 min; 100% - 10% for 0.5 min): t_R (**118**) = 1.68 min, t_R (**81**) = 2.25 min, λ = 256 nm.

*C-1 could not be detected in the ¹³C-NMR spectrum.

2-(Benzyl(pyridin-2-yl)amino)ethyl 1-ethyl-7-methyl-4-oxo-1,4-dihydro-1,8-naphthyridine-3-carboxylate (119)



- Procedure:** D, a
- Reactants:** Nalidixic acid (**81**) (85.0 mg, 0.37 mmol, 1.0 eq.), COMU[®] (**109**, 235 mg, 0.549 mmol, 1.5 eq.), DBU (55.0 μ L, 0.37 mmol, 1.0 eq.), alcohol **89** (100 mg, 0.44 mmol, 1.2 eq.)
- Reaction time:** 18 h
- Yield:** Silica column chromatography (toluene, 5-20 % acetone) was followed by crystallization from CH₂Cl₂ with MeOH and gave **119** (64.7 mg, 0.15 mmol, 40%) as a colorless solid.

¹H-NMR (400 MHz, DMSO-*d*₆): δ 8.72 (s, 1H, 2-H), 8.47 (d, *J* = 8.3 Hz, 1H, 5-H), 8.10 (dd, *J* = 5.2, 2.0 Hz, 1H, 17-H), 7.46 (ddd, *J* = 9.0, 7.5, 2.0 Hz, 1H, 15-H), 7.42 (d, *J* = 8.3 Hz, 1H, 6-H), 7.32-7.24 (m, 2H, 24-H), 7.24-7.14 (m, 3H, 23-H, 25-H), 6.68 (d, *J* 9.0 Hz, 1H, 14-H), 6.58 (dd, *J* 7.5, 5.2 Hz, 1H, 16-H), 4.89 (s, 2H, 21-H), 4.43 (q, *J* = 7.0 Hz, 2H, 9-H), 4.38 (t, *J* = 5.7 Hz, 2H, 19-H), 3.92 (t, *J* = 5.7 Hz, 2H, 18-H), 2.64 (s, 3H, 11-H), 1.35 (t, *J* = 7.0 Hz, 3H, 10-H) ppm;

¹³C-NMR (100 MHz, DMSO-*d*₆): δ 173.2 (C-4), 164.1 (C-12), 162.5 (C-7), 157.7 (C-13), 149.2 (C-2), 148.2 (C-8a), 147.6 (C-17), 139.0 (C-22), 137.4 (C-15), 136.1 (C-5), 128.4 (C-24), 126.6 (C-23, C-25), 121.2 (C-6), 120.7 (C-4a), 111.9 (C-16), 110.7 (C-3), 106.0 (C-14), 61.9 (C-19), 51.4 (C-21), 46.8 (C-18), 45.7 (C-9), 24.7 (C-11), 14.9 (C-10) ppm; *

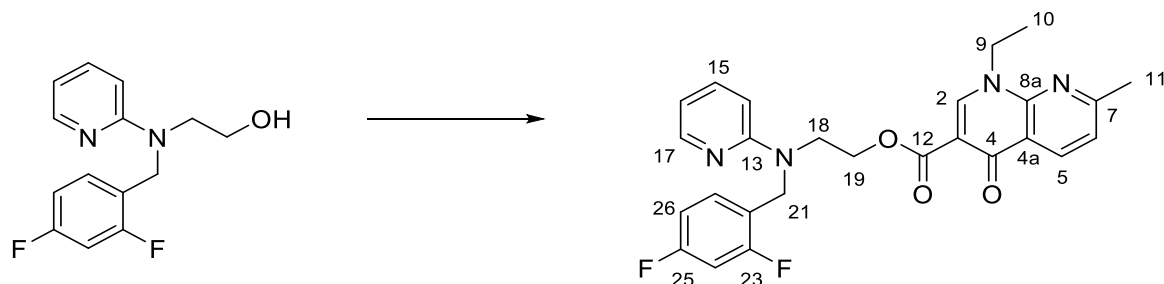
HRMS (ESI) *m/z* calcd. for [M+Na]⁺: 443.2074; found 443.2083;

R_f(toluene:acetone = 5:1): 0.2;

HPLC-UV (ACN : H₂O + 0.1% FA = 15% - 35% for 3 min; 35% - 100% for 0.2 min; 100% for 1.2 min, 100% - 15% for 0.6 min): *t_R* (**119**) = 2.92 min, *t_R* (**81**) = 2.39 min, λ = 256 nm.

*C-1 could not be detected in the ¹³C-NMR spectrum.

2-((2,4-Difluorobenzyl)(pyridin-2-yl)amino)ethyl 1-ethyl-7-methyl-4-oxo-1,4-dihydro-1,8-naphthyridine-3-carboxylate (120)



Procedure: D, a

Reactants: Nalidixic acid (**81**) (75 mg, 0.32 mmol, 1.0 eq.), COMU[®] (**109**, 207 mg, 0.39 mmol, 1.5 eq.), DBU (48 μ L, 0.32 mmol, 1.0 eq.), alcohol **85a** (102 mg, 0.39 mmol, 1.2 eq.)

Reaction time: 18 h

Yield: Silica column chromatography (toluene, 5% - 20% acetone) was followed by crystallization from a CHCl₃ with EtOH followed by semipreparative HPLC (C18, H₂O:MeOH = 20% - 100% over 30 min, then 100% for 10 min) and gave **120** (4.7 mg, 0.01 mmol, 3%) as a colorless solid.

¹H-NMR (400 MHz, DMSO-d₆): δ 8.72 (s, 1H, 2-H), 8.46 (d, J = 8.3 Hz, 1H, 5-H), 8.09 (dd, J = 5.2, 2.0 Hz, 1H, 17-H), 7.50 (ddd, J = 9.0, 7.5, 2.0 Hz, 1H, 15-H), 7.43 (d, J = 8.3 Hz, 1H, 6-H), 7.21-7.13 (m, 2H, 24-H, 27-H), 6.95 (ddd, J = 10.0, 8.5, 2.0 Hz, 1H, 26-H), 6.74 (d, J = 8.3 Hz, 1H, 14-H), 6.1 (dd, J = 7.5, 5.2 Hz, 1H, 16-H), 4.89 (s, 2H, 21-H), 4.43 (q, J = 7.0 Hz, 2H, 9-H), 4.39 (t, J = 5.9 Hz, 2H, 19-H), 3.93 (t, J = 5.9 Hz, 2H, 18-H), 2.65 (s, 3H, 11-H), 1.35 (t, J = 7.0 Hz, 3H, 10-H) ppm;*

¹³C-NMR (100 MHz, DMSO-d₆): δ 173.1 (C-4), 164.1 (C-12), 162.5 (C-7), 161.2 (dd, J = 244, 11 Hz, C-23 or C-25), 162.2 (dd, J = 246, 12 Hz, C-23 or C-25), 157.3 (C-13), 149.3 (C-2), 148.2 (C-8a), 147.6 (C-17), 137.5 (C-15), 136.1 (C-5), 129.6 (dd, J = 11, 6 Hz, C-27), 122.0 (dd, J = 15, 4 Hz, C-22), 121.2 (C-6), 120.6 (C-4a), 112.2 (C-16), 111.1 (dd, J = 21, 4 Hz, C-26), 110.6 (C-3), 106.0 (C-14), 103.7 (t, J = 27 Hz, C-24), 61.9 (C-19), 46.9 (C-18), 45.7 (C-9), 45.6 (d, J = 5 Hz, C-21), 24.7 (C-11), 14.8 (C-10) ppm;

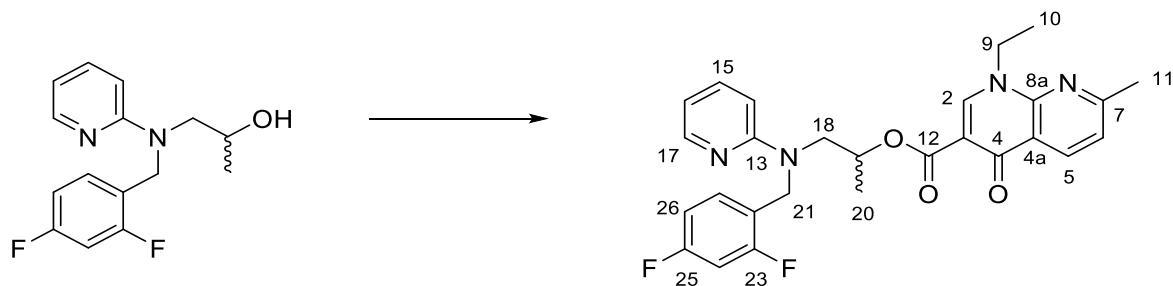
HRMS (ESI) m/z calcd. for [M+Na]⁺: 501.1714; found 501.1703;

R_f (toluene:acetone = 5:1): 0.17;

HPLC-UV (ACN : H₂O + 0.1% FA = 10% - 65% for 3 min; 65% - 100% for 0.5 min; 100% - 10% for 0.5 min): t_R (**120**) = 2.58 min, t_R (**81**) = 2.25 min, λ = 256 nm.

*C-1 could not be detected in the ¹³C-NMR spectrum.

1-((2,4-Difluorobenzyl)(pyridin-2-yl)amino)propan-2-yl 1-ethyl-7-methyl-4-oxo-1,4-dihydro-1,8-naphthyridine-3-carboxylate (121a)



- Procedure:** D, a
- Reactants:** Nalidixic acid (**81**) (50.0 mg, 0.22 mmol, 1.0 eq.), COMU[®] (**109**, 138 mg, 0.32 mmol, 1.5 eq.), DBU (32 μ L, 0.22 mmol, 1.0 eq.), alcohol **86a** (7 mg, 0.26 mmol, 1.2 eq.)
- Reaction time:** 18 h
- Yield:** Preparative HPLC chromatography (C18, H₂O : MeOH = 20% - 100% over 30 min then 100% for 10 min) gave conjugate **121a** (90 mg, 0.19 mmol, 85%) as a colorless solid.

¹H-NMR (500 MHz, MeOD): δ 8.92 (s, 1H, 2-H), 8.72 (d, J = 8.5 Hz, 1H, 5-H), 8.04 (dd, J = 5.2, 2.0 Hz, 1H, 17-H), 7.55 (d, J = 8.5 Hz, 1H, 6-H), 7.48 (ddd, J = 9.0, 7.1, 2.0 Hz, 1H, 15-H), 7.03 (dt, J = 6.7, 8.6 Hz, 1H, 27-H), 6.81 (ddd, J = 10.8, 9.5, 2.2 Hz, 1H, 24-H), 6.73 (ddd, J = 9.4, 8.6, 2.2 Hz, 1H, 26-H), 6.66 (d, J = 9.0 Hz, 1H, 14-H), 6.58 (dd, J = 7.1, 5.2 Hz, 1H, 16-H), 5.70-5.62 (m, 1H, 19-H), 4.95 (d, J = 17.2 Hz, 1H, 21-H_a), 4.79 (d, J = 17.2 Hz, 1H, 21-H_b), 4.70 – 4.54 (m, 2H, 9-H), 4.00 (dd, J = 15.5, 4.0 Hz, 1H, 18-H_a), 3.96 (dd, J = 15.5, 9.0 Hz, 1H, 18-H_b), 2.73 (s, 3H, 11-H), 1.48 (t, J = 7.5 Hz, 3H, 10-H), 1.47 (d, J = 6.8 Hz, 3H, 20-H) ppm;

¹³C-NMR (125 MHz, MeOD): δ 178.1 (C-4), 166.8 (C-7), 163.2 (dd, J = 246, 14 Hz, C-23 or C-25), 162.2 (dd, J = 246, 12 Hz, C-23 or C-25), 159.2 (C-13), 151.9 (C-2), 149.6 (C-8a), 148.4 (C-17), 139.1 (C-15), 137.7 (C-5), 130.5 (dd, J = 11, 6 Hz, C-27), 124.1 (C-6), 122.7 (dd, J = 15, 4 Hz, C-22), 121.3 (C-4a), 114.0 (C-16), 112.1 (dd, J = 21, 3 Hz, C-26), 108.3 (C-14), 104.5 (t, J = 27 Hz, C-24), 73.9 (C-19), 54.5 (C-18), 49.0 (C-9), 47.9 (d, J = 4 Hz, C-21), 25.3 (C-11), 17.8 (C-20), 15.5 (C-10) ppm; *

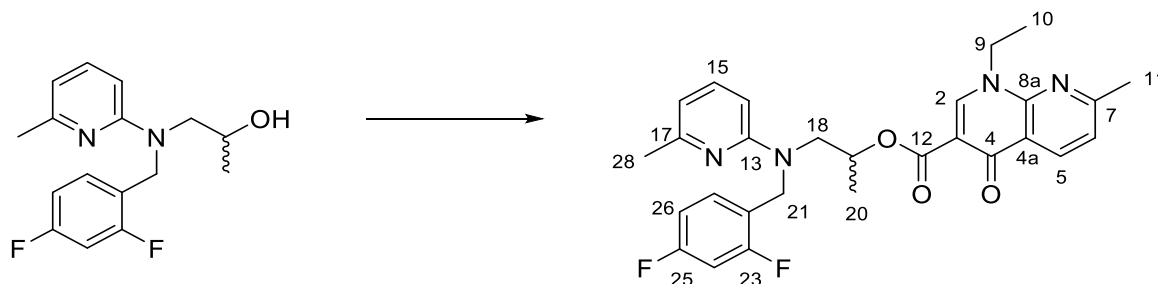
HRMS (ESI) m/z calcd. for [M+Na]⁺: 515.1871; found 515.1865;

T_m (decomp): 192 °C;

HPLC-UV (ACN : H₂O + 0.1% FA = 10% - 65% for 3 min; 65% - 100% for 0.5 min; 100% - 10% for 0.5 min): t_R (**121a**) = 2.63 min, t_R (**81**) = 2.27 min, λ = 256 nm.

*C-1, C-3 and C-12 could not be detected in the ¹³C-NMR spectrum.

1-((2,4-Difluorobenzyl)(6-methylpyridin-2-yl)amino)propan-2-yl 1-ethyl-7-methyl-4-oxo-1,4-dihydro-1,8-naphthyridine-3-carboxylate (121b)



- Procedure:** D, a
- Reactants:** Nalidixic acid (**81**) (50.0 mg, 0.22 mmol, 1.0 eq.), COMU® (**109**, 138 mg, 0.32 mmol, 1.5 eq.), DBU (32 μ L, 0.22 mmol, 1.0 eq.), alcohol **86b** (75 mg, 0.26 mmol, 1.2 eq.)
- Reaction time:** 18 h
- Yield:** Silica column chromatography (1. toluene, 5-20 % acetone, 2. PE:EtOAc = 1:1) gave **121b** (41 mg, 0.08 mmol, 38%) as a colorless oil.

¹H-NMR (600 MHz, MeOD): δ 8.60 (s, 1H, 2-H), 8.55 (d, J = 8.1 Hz, 1H, 5-H), 7.40 (d, J = 8.1 Hz, 1H, 6-H), 7.32 (dd, J = 8.4, 7.4 Hz, 1H, 15-H), 7.05 (dt, J = 6.7, 8.6 Hz, 1H, 27-H), 6.72 - 6.67 (m, 2H, 24-H, 26-H), 6.44 (d, J = 7.4 Hz, 1H, 14-H or 16-H), 6.58 (d, J = 8.4 Hz, 1H, 14-H or 16-H), 5.50 - 5.44 (m, 1H, 19-H), 4.94 (d, J = 17.0 Hz, 1H, 21-H_a), 4.78 (d, J = 17.0 Hz, 1H, 21-H_b), 4.53 - 4.43 (m, 2H, 9-H), 4.02 (dd, J = 15.0, 4.0 Hz, 1H, 18-H_a), 3.81 (dd, J = 15.0, 8.7 Hz, 1H, 18-H_b), 2.69 (s, 3H, 11-H), 2.31 (s, 3H, 28-H), 1.43 (t, J = 6.9 Hz, 3H, 10-H), 1.39 (d, J = 6.6 Hz, 3H, 20-H) ppm;

¹³C-NMR (150 MHz, MeOD): δ 176.7 (C-4), 165.2 (C-7), 164.9 (C-12), 163.0 (dd, J = 247, 13 Hz, C-23 or C-25), 161.9 (dd, J = 247, 11 Hz, C-23 or C-25), 158.8 (C-13), 157.6 (C-17), 150.5 (C-2), 149.7 (C-8a), 138.8 (C-15), 137.3 (C-5), 130.8 (dd, J = 10, 6 Hz, C-27), 123.3 (dd, J = 15, 4 Hz, C-22), 122.6 (C-6), 122.0 (C-4a), 112.6 (C-14 or C-16), 112.0 (C-3), 111.8 (dd, J = 21, 4 Hz, C-26), 104.3 (C-14 or C-16), 104.0 (t, J = 26.0 Hz, C-24), 71.5 (C-19), 54.6 (C-18), 47.8 (C-9), 47.6 (d, J = 4.0 Hz, C-21), 25.0 (C-11), 24.4 (C-28), 17.9 (C-20), 15.3 (C-10) ppm; *

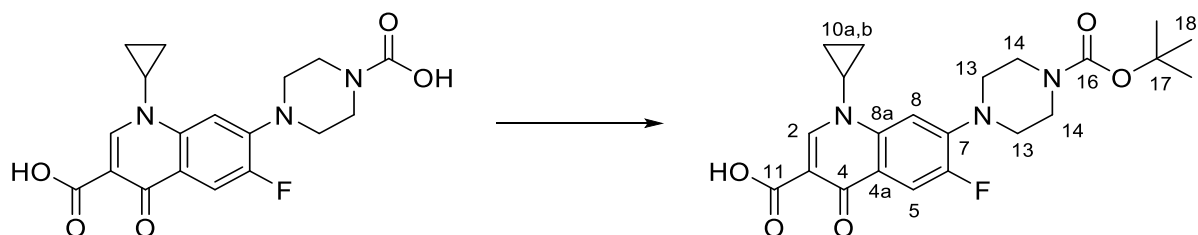
HRMS (ESI) m/z calcd. for $[M+Na]^+$: 507.2208; found 507.2209;

R_f (Toluene, 30% acetone): 0.48;

HPLC-UV (ACN : H₂O + 0.1% FA = 10% - 65% for 3 min; 65% - 100% for 0.5 min; 100% - 10% for 0.5 min): t_R (**121b**) = 2.76 min, t_R (**81**) = 2.25 min, λ = 256 nm.

*C-1 could not be detected in the ¹³C-NMR spectrum.

7-(4-(tert-Butoxycarbonyl)piperazin-1-yl)-1-cyclopropyl-6-fluoro-4-oxo-1,4-dihydroquinoline-3-carboxylic acid (123)

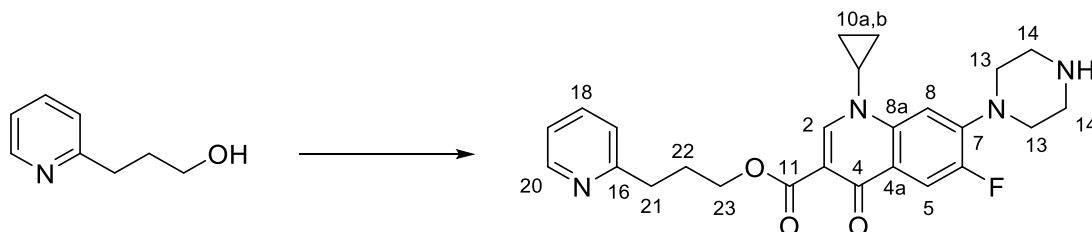


Ciprofloxacin (**82**, 1.2 g, 3.60 mmol, 1.0 eq.) was dissolved in H₂O:dioxane (1:1, 20 mL) and NaOH (1 M in H₂O, 5.4 mL, 1.5 eq.). Di-*tert*-butyldicarbonate (1.18 g, 5.4 mmol, 1.5 eq.) was added. After stirring for 18 h at rt, about three quarters of the solvent were removed *in vacuo* and acetone (10 mL) was added. The solid was filtered, washed with acetone and dried under vacuum. The product **123** (1.55 g, 3.58 mmol, 99.4%) was obtained as a colorless solid.

¹H-NMR (400 MHz, CDCl₃): δ 8.79 (s, 1H, 2-H), 8.07 (d, $J = 12.3$ Hz, 1H, 5-H), 7.37 (d, $J = 7.8$ Hz, 1H, 8-H), 3.67 (dd, $J = 4.4, 3.4$ Hz, 4H, 13-H), 3.57-3.50 (m, 1H, 9-H), 3.29 (dd, $J = 4.4, 3.4$ Hz, 4H, 14-H), 1.50 (s, 9H, 18-H), 1.43 – 1.37 (m, 2H, 10a-H), 1.24 - 1.18 (m, 2H, 10b) ppm;

The analytical data are in accordance with those reported in the literature.^[146]

4-(1-Cyclopropyl-6-fluoro-4-oxo-3-((3-(pyridin-2-yl)propoxy)carbonyl)-1,4-dihydroquinolin-7-yl)piperazine-1-carboxylic acid (124**)**



Procedure: D, b

Reactants: Boc-ciprofloxacin **123** (100 mg, 0.23 mmol, 1.0 eq.), COMU® (**109**, 49 mg, 0.35 mmol, 1.5 eq.), DBU (36 μ L, 0.23 mmol, 1.0 eq.), alcohol **83a** (38 mg, 0.28 mmol, 1.2 eq.)

Reaction time: 18 h

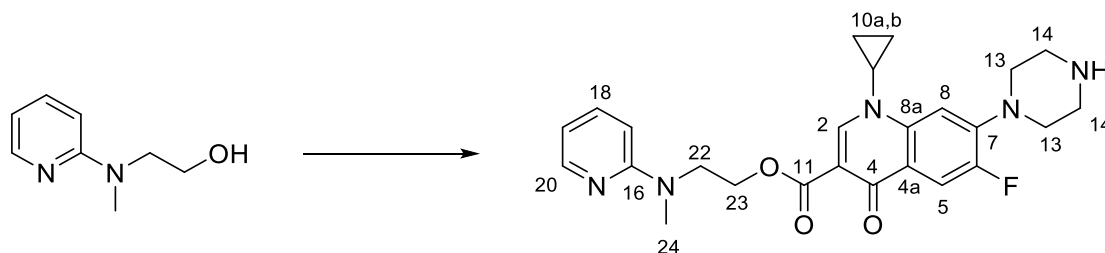
Yield: The residue was crystallized from CHCl_3 to yield the product **124** (3.5 mg, 0.78 μ mol, 3%).

$^1\text{H-NMR}$ (500 MHz, MeOD): δ 8.67 (s, 1H, 2-H), 8.46 (d, $J = 5.1$ Hz, 20-H), 7.98 (d, $J = 13.0$ Hz, 1H, 5-H), 7.77 (ddd, $J = 9.5, 7.5, 1.5$ Hz, 1H, 18-H), 7.61 (d, $J = 7.3$ Hz, 1H, 8-H), 7.41 (d, $J = 7.5$ Hz, 1H, 17-H), 7.26 (dd, $J = 7.0, 5.3$ Hz, 1H, 19-H), 4.34 (t, $J = 6.0$ Hz, 2H, 21-H), 3.70 (tt, $J = 7.0, 3.1$ Hz, 1H, 9-H), 3.59-3.56 (m, 4H, 13-H), 3.48-3.44 (m, 4H, 14-H), 2.98 (t, $J = 7.7$ Hz, 2H, 23-H), 2.20 (tt, $J = 7.7, 6.0$ Hz, 2H, 22-H) 1.43-1.37 (m, 2H, 10_a), 1.22-1.16 (m, 2H, 10_b) ppm;

$^{13}\text{C-NMR}$ (125 MHz, MeOD): δ 175.5 (C-4), 166.0 (C-11), 162.4 (C-16), 154.8 (d, $J = 246$ Hz, C-6), 150.2 (C-2), 149.6 (C-20), 145.1 (d, $J = 11$ Hz, C-7), 139.9 (d, $J = 2$ Hz, C-8a), 138.9 (C-18), 124.8 (C-17), 124.4 (d, $J = 7$ Hz, C-4a), 122.9 (C-19), 113.5 (d, $J = 28$ Hz, C-5), 110.6 (C-3), 107.9 (d, $J = 3$ Hz, C-8), 65.0 (C-23), 48.4 (C-13), 44.9 (C-14), 36.3 (C-9), 35.3 (C-21), 30.0 (C-22), 8.6 (C-10) ppm;

HRMS (ESI) m/z calcd. for $[\text{M}+\text{Na}]^+$: 473.1965; found 473.1964.

4-(1-Cyclopropyl-6-fluoro-3-((2-(methyl(pyridin-2-yl)amino)ethoxy)carbonyl)-4-oxo-1,4-dihydroquinolin-7-yl)piperazine-1-carboxylic acid (125)



Procedure: D, a

Reactants: Boc-ciprofloxacin **123** (200 mg, 0.46 mmol, 1.0 eq.), COMU[®] (**109**, 298.0 mg, 0.70 mmol, 1.5 eq.), DBU (70 μ L, 0.23 mmol, 1.0 eq.), alcohol **84a** (85 mg, 0.56 mmol, 1.2 eq.)

Reaction time: 18 h

Yield: Silica column chromatography (PE:EtOAc = 1:1) was performed to remove major impurities. The residue was dissolved in CH₂Cl₂ (2 mL) and TFA (0.5 mL) and stirred for 1 h at rt. The reaction was terminated by addition of a sat. aq. Na₂CO₃ solution, extracted with CH₂Cl₂ (3 x 2 mL), washed with a sat. aq. NaCl solution, dried over Na₂SO₂, filtered and the solvent was removed *in vacuo*.

The residue was crystallized from CHCl₃ to yield the product **125** (4.5 mg, 0.97 μ mol, 2.1%).

¹H-NMR (400 MHz, DMSO-d₆): δ 8.35 (s, 1H, 2-H), 8.06 (dd, J = 5.0, 2.0 Hz, 1H, 20-H), 7.78 (d, J = 13.0 Hz, 1H, 5-H), 7.49 (ddd, J = 8.7, 7.0, 2.0 Hz, 1H, 18-H), 7.45 (d, J = 7.3 Hz, 1H, 8-H), 6.67 (d, J = 8.7 Hz, 1H, 17-H), 6.54 (dd, J = 7.0, 5.0 Hz, 1H, 19-H), 4.43 (t, J = 6.0 Hz, 2H, 23-H), 3.88 (t, J = 6.0 Hz, 2H, 22-H), 3.66-3.60 (m, 1H, 9-H), 3.43-3.37 (m, 4H, 13 or 14-H), 3.31-3.21 (m, 4H, 13 or 14-H), 3.08 (s, 3H, 24-H), 1.27-1.17 (m, 2H, 10a-H), 1.11-1.03 (m, 2H, 10b-H) ppm;

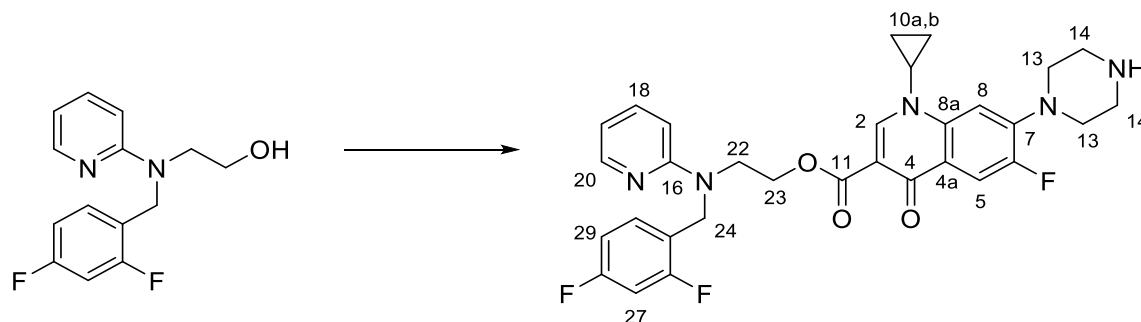
¹³C-NMR (100 MHz, DMSO-d₆): 171.6 (C-4), 164.1 (C-11), 158.1 (C-16), 152.5 (d, J = 246 Hz, C-6), 148.5 (C-2), 147.5 (C-20), 142.9 (d, J = 11 Hz, C-7), 138.0 (d, J = 2 Hz, C-8a), 137.3 (C-18), 122.5 (d, J = 7 Hz, C-4a), 111.8 (d, J = 23 Hz, C-5), 111.5 (C-19), 108.9 (C-3), 106.7 (d, J = 3 Hz, C-8), 105.7 (C-17), 61.7 (C-23), 47.9 (C-22), 47.2 (C-13 o. C-14), 43.1 (C-13 or C-14), 36.7 (C-24), 34.8 (C-9), 7.6 (C-10) ppm;

HRMS (ESI) m/z calcd. for [M+H]⁺:466.2254; found 466.2250;

R_f(CH₂Cl₂, 10% MeOH, 1% Et₃N): 0.22;

HPLC-UV (ACN : H₂O + 0.1% FA = 5% - 35% for 3 min; 35% - 100% for 0.5 min; 100%, 100% - 15% for 0.5 min): t_R (**125**) = 1.63 min, t_R (**82**) = 2.00 min, $\lambda = 277$ nm.

4-(1-Cyclopropyl-3-((2-((2,4-difluorobenzyl)(pyridin-2-yl)amino)ethoxy)carbonyl)-6-fluoro-4-oxo-1,4-dihydroquinolin-7-yl)piperazine-1-carboxylic acid (126)



Procedure: D, b

Reactants: Boc-ciprofloxacin **123** (100 mg, 0.23 mmol, 1.0 eq.), COMU® (**109**, 149 mg, 0.35 mmol, 1.5 eq.), DBU (36 μ L, 0.23 mmol, 1.0 eq.), alcohol **85a** (74 mg, 0.28 mmol, 1.2 eq.)

Reaction time: 18 h

Yield: The residue was crystallized from CHCl_3 to yield the product **126** (40.0 mg, 0.07 mmol, 30%).

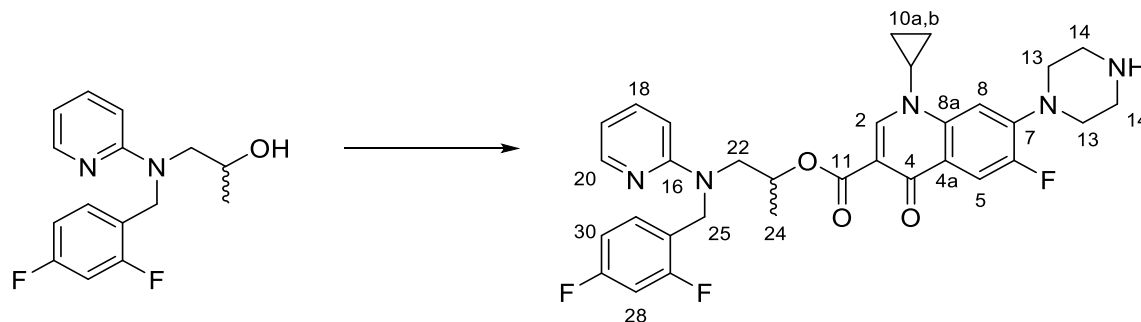
$^1\text{H-NMR}$ (400 MHz, DMSO-d_6): δ 8.36 (s, 1H, 2-H), 8.09 (dd, $J = 5.3, 2.0$ Hz, 2H, 20-H), 7.80 (d, $J = 13.2$ Hz, 1H, 5-H), 7.50 (ddd, $J = 8.7, 7.3, 2.0$ Hz, 1H, 18-H), 7.45 (d, $J = 7.3$ Hz, 1H, 8-H), 7.23-7.13 (m, 2H, 27-H and 30-H), 6.96 (ddd, $J = 8.8, 8.3, 2.7$ Hz, 1H, 29-H), 6.73 (d, $J = 8.5$ Hz, 1H, 17-H), 6.60 (dd, $J = 7.0, 5.3$ Hz, 1H, 19-H), 4.88 (s, 2H, 24-H), 4.37 (t, $J = 5.6$ Hz, 2H, 23-H), 3.92 (t, $J = 5.6$ Hz, 2H, 22-H), 3.68-3.61 (m, 1H, 9-H), 3.37-3.27 (m, 4H, 13-H or 14-H), 3.22-3.15 (m, 4H, 13-H or 14-H), 1.28-1.21 (m, 2H, 10a-H), 1.07-1.00 (m, 2H, 10b-H) ppm;

$^{13}\text{C-NMR}$ (100 MHz, DMSO-d_6): 171.3 (C-4), 163.9 (C-11), 157.1 (C-16), 152.41 (d, $J = 244$ Hz, C-6), 148.0 (C-2), 147.4 (C-20), 143.2 (d, $J = 11$ Hz, C-7), 137.8 (C-8a), 137.3 (C-18), 129.5 (dd, $J = 8, 8$ Hz, C-30), 122.0 (d, $J = 8$ Hz, C-4a), 121.8 (dd, $J = 15, 5$ Hz, C-25), 112.1 (C-19), 111.5 (d, $J = 22$ Hz, C-5), 111.0 (d, $J = 18$ Hz, C-29), 108.5, 106.3 (C-8), 105.8 (C-17), 103.6 (d, $J = 16$ Hz, C-27) 61.7 (C-23), 48.0 (bs, C-13 or C-14), 46.8 (C-22), 45.3 (bs, C-24), 43.5 (C-13 or C-14), 34.5 (C-9), 7.3 (C-10) ppm; *

HRMS (ESI) m/z calcd. for $[\text{M}+\text{Na}]^+$: 600.2198; found 600.2197;

*C-1, C-26, C-28 could not be detected in the $^{13}\text{C-NMR}$ spectrum.

1-((2,4-Difluorobenzyl)(pyridin-2-yl)amino)propan-2-yl 1-cyclopropyl-6-fluoro-4-oxo-7-(piperazin-1-yl)-1,4-dihydroquinoline-3-carboxylate (127)



Procedure: D, b

Reactants: Boc-ciprofloxacin **123** (100 mg, 0.23 mmol, 1.0 eq.), COMU® (**109**, 149 mg, 0.35 mmol, 1.5 eq.), DBU (36 μ L, 0.23 mmol, 1.0 eq.), alcohol **86a** (77 mg, 0.28 mmol, 1.2 eq.)

Reaction time: 18 h

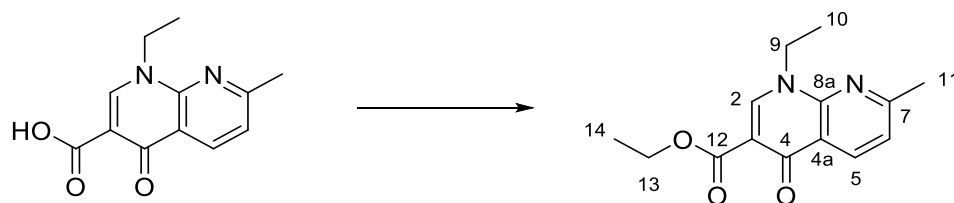
Yield: MPLC chromatography (NP, DCM:MeOH = 0% for 5 min, 0% - 6% over 20 min, 6% for 5 min; fractions from 26 - 30 min were collected) yielded conjugate **127** (14.9 mg, 0.25 mmol, 11%) as a colorless solid.

¹H-NMR (400 MHz, MeOD): δ 8.41 (s, 1H, 2-H), 8.05 (ddd, J = 5.3, 2.0, 1.0 Hz, 2H, 20-H), 7.86 (d, J = 13.7 Hz, 1H, 5-H), 7.47 (d, J = 7.2 Hz, 1H, 8-H), 7.43 (ddd, J = 8.5, 7.2, 2.0 Hz, 1H, 18-H), 6.96 (dt, J = 6.7, 8.4 Hz, 1H, 31-H), 6.75 – 6.65 (m, 2H, 28-H, 30-H), 6.61 (dd, J = 8.5, 1.0 Hz, 1H, 17-H), 6.57 (ddd, J = 7.2, 5.3, 1.0 Hz, 1H, 19-H), 5.5 – 5.4 (m, 1H, 23-H), 4.93 (d, J = 17.4 Hz, 1H, 23-H_a), 4.78 (d, J = 17.4 Hz, 1H, 23-H_b), 4.00 (dd, J = 14.5, 2.8 Hz, 1H, 22-H_a), 3.82 (dd, J = 14.5, 9.8 Hz, 1H, 22-H_b), 3.63-3.54 (m, 1H, 9-H), 3.33-3.30 (m, 4H, 13-H), 3.09-3.05 (m, 4H, 14-H), 1.38 (d, J = 6.4 Hz, 3H, 24-H), 1.35-1.31 (m, 2H, 10a-H), 1.15-1.00 (m, 2H, 10b-H) ppm;

¹³C-NMR (100 MHz, MeOD): δ 175.3 (C-4), 165.7 (C-11), 165.7 (dd, J = 246, 13 Hz, C-27 or C-29), 162.0 (dd, J = 247, 12 Hz, C-27 or C-29), 159.3 (C-16), 154.9 (d, J = 250 Hz, C-6), 149.6 (C-2), 148.6 (C-20), 146.6 (d, J = 10 Hz, C-7), 139.7 (C-8a), 138.9 (C-18), 130.5 (dd, J = 10, 7 Hz, C-31), 123.4 (d, J = 7 Hz, C-4a), 123.0 (dd, J = 14, 3 Hz, C-26), 113.7 (C-19), 113.2 (d, J = 23 Hz, C-5), 111.8 (d, J = 22, 4 Hz, C-30), 108.0 (C-17), 107.0 (d, J = 3 Hz, C-8), 104.2 (t, J = 25 Hz, C-28), 71.4 (C-23), 54.9 (C-22), 51.41 (d, J = 4 Hz, C-13), 46.3 (C-14), 36.1 (C-24), 17.9 (C-10) ppm;

HRMS (ESI) m/z calcd. for $[M+Na]^+$: 614.2355; found 614.2360;

HPLC-UV (ACN : H₂O + 0.1% FA = 5% - 65% for 3 min; 65% - 100% for 0.5 min; 100% - 5% for 0.5 min): t_R (**127**) = 2.04 min, t_R (**82**) = 1.67 min, $\lambda = 277$ nm

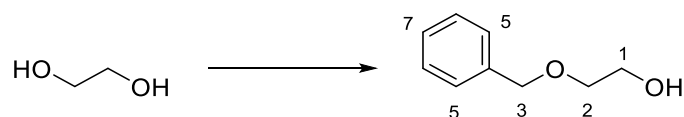
Ethyl 1-ethyl-7-methyl-4-oxo-1,4-dihydro-1,8-naphthyridine-3-carboxylate (128)

Nalidixic acid (**81**) (42 mg, 0.18 mmol, 1.0 eq.) was dissolved in EtOH (2 mL). H₂SO₄ (98%, 10 μ L, 1.0 eq.) was added and the reaction was stirred for 4 d at 90 °C. The reaction was terminated by addition of a sat. aq. Na₂CO₃ solution until gas evolution terminated and extracted with EtOAc (3 x 3 mL). The combined organic phases were washed with a sat. aq. NaCl solution, dried over Na₂SO₄, filtered and the solvent was removed *in vacuo* giving ester **128** (24.5 mg, 0.09 mmol, 52%) as a colorless solid.

¹H-NMR (400 MHz, CDCl₃): δ 8.66 (d, $J = 9.1$ Hz, 1H, 5-H), 7.25 (d, $J = 9.1$ Hz, 1H, 6-H), 4.50 (q, $J = 7.2$ Hz, 2H, 9-H or 13-H), 4.42 (q, $J = 7.2$ Hz, 2H, 9-H or 13-H), 2.67 (s, 3H, 11-H), 1.51 (t, $J = 7.2$ Hz, 3H, 10-H or 14-H), 1.43 (t, $J = 7.2$ Hz, 3H, 10-H or 14-H) ppm.

HPLC-UV (ACN : H₂O + 0.1% FA = 15% - 25% for 5 min; 25% - 100% for 0.3 min; 100% - 15% for 0.7 min): t_R (**128**) = 3.47 min, t_R (**81**) = 2.71 min, $\lambda = 256$ nm.

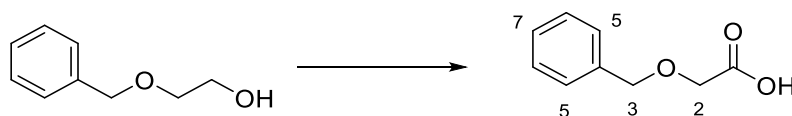
The analytical data are in accordance with those reported in the literature.^[130]

2-(Benzyloxy)ethan-1-ol (131)

NaH (52.85 mg, 1.98 mmol, 1.1 eq.) was dissolved in THF (3.5 mL) and cooled to 0 °C. Ethyleneglycol (590 μ L, 10.5 mmol, 6 eq.) was added and the reaction mixture was stirred at rt for 1 h before benzylbromide (214 μ L, 1.80 mmol, 1.0 eq.) was added. The reaction mixture was stirred at 66 °C for 12 h. After cooling to rt the reaction was terminated by addition of a sat. aq. NH₄Cl solution (3 mL). The aq. phase was extracted with EtOAc (3 x 3 mL). The combined organic phases were washed with a sat. aq. NaCl solution (3 mL), dried over Mg₂SO₄, filtered and the solvent was removed *in vacuo*. Silica column chromatography (PE:EtOAc = 3:1) gave the product **131** (220 mg, 1.48 mmol, 82% based on benzylbromide) as a colorless oil.

¹H-NMR (400 MHz, CDCl₃): δ 7.40-7.28 (m, 5H, 3-H –5-H), 4.57 (s, 2H, 3-H), 3.76 (dd, J = 4.7, 4.6 Hz, 2H, 2-H), 3.60 (dd, J = 4.7, 4.6 Hz, 2H, 1-H), 2.07 (bs, 1H, O-H) ppm.

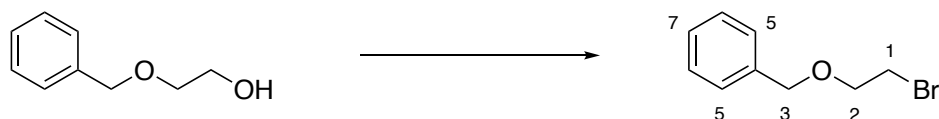
The analytical data are in accordance with those reported in the literature.^[144]

2-(Benzyloxy)acetic acid (134)

The alcohol **131** (20 mg, 0.13 mmol, 1.0 eq.) was dissolved in CH_2Cl_2 (0.5 mL), DESS-MARTIN periodinane (84 mg, 0.20 mmol, 1.5 eq.) was added and the reaction mixture was stirred for 1 h. The reaction was terminated by addition of H_2O (0.5 mL) and the aq. phase was acidified with 1 M HCl to pH 2 and extracted with CH_2Cl_2 (3 x 0.5 mL). The combined organic phases were dried over Na_2SO_4 , filtered and the solvent was removed *in vacuo*. A solution of sodium chlorite (67.8 mg, 0.75 mL, 5.0 eq.), KH_2PO_4 (106 mg, 0.78 mmol, 5.2 eq.) in 2-methyl-2-butene (2.4 mL) and H_2O (0.5 mL) was added to a solution of the crude aldehyde dissolved in THF (5 mL). The reaction mixture was stirred at rt for 40 min under argon atmosphere before it was terminated by addition of H_2O . The aq. phase was basified by addition of a sat. aq. Na_2CO_3 solution and extracted with EtOAc (3 x 5 mL). The combined organic phases were dried over Na_2SO_4 , filtered and the solvent was removed *in vacuo*. The acid **134** (25 mg, 0.3 mmol, >99%) was obtained as a colorless solid.

$^1\text{H-NMR}$ (400 MHz, CDCl_3): δ 7.40-7.28 (m, 5H, 3-H - 5-H), 4.64 (s, 2H, 3-H), 4.10 (s, 2H, 2-H) ppm.

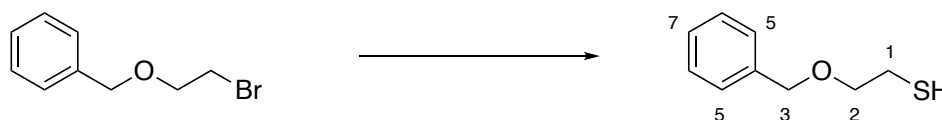
The analytical data are in accordance with those reported in the literature.^[147]

((2-Bromoethoxy)methyl)benzene (S2)

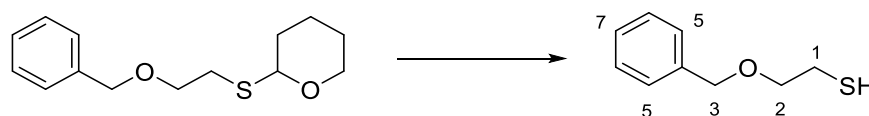
The alcohol **131** (65 mg, 0.43 mmol, 1.0 eq.) was dissolved in CH₂Cl₂ (4.0 mL). Triphenylphosphine (123 mg, 0.47 mmol, 1.1 eq.) and tetrabromomethane (155 mg, 0.47 mmol, 1.1 eq.) were added and the reaction mixture was stirred at rt for 45 min before it was terminated by addition of a sat. aq. NaHCO₃ solution (4 mL). The aq. phase was separated and extracted with CH₂Cl₂ (2 x 4 mL). The combined organic phases were dried over MgSO₄, filtered and the solvent was removed *in vacuo*. Silica column chromatography (PE:EtOAc = 20:1) gave the title product (68 mg, 0.32 mmol, 74%) as a colorless oil.

¹H-NMR (400 MHz, CDCl₃): δ 7.40-7.28 (m, 5H, 3-H -5-H), 4.57 (s, 2H, 3-H), 3.76 (t, *J* = 6.0 Hz, 2H, 2-H), 3.47 (t, *J* = 6.0 Hz, 2H, 1-H) ppm.

The analytical data are in accordance with those reported in the literature.^[148]

2-(Benzyloxy)ethan-1-thiol (132)

To a solution of bromide (60.8 mg, 0.28 mmol, 1.0 eq.) in dry EtOH (0.5 mL) was added thiourea (21.5 mg, 0.28 mmol, 1.0 eq.). The mixture was stirred at 75 °C für 3 h before 10% aq. NaOH (0.1 mL) was added and stirring was continued at the same temperature for 3 h. After cooling to rt EtO₂ (1 mL) was added and the organic phase was separated. The aq. phase was acidified to pH 2 and extracted with CH₂Cl₂ (1 mL). The combined organic phases were dried over Mg₂SO₄, filtered and the solvent was removed *in vacuo* to yield the product **132** (6.0 mg, 0.12 mmol, 44%) as a yellow oil with a strong smell.



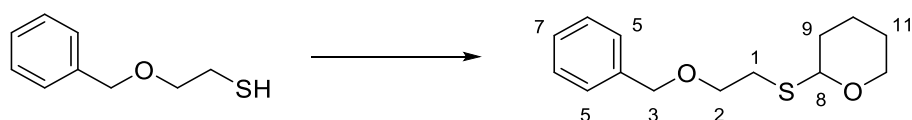
The protected thiol (6.0 mg, 0.24 mmol, 1.0 eq.) was dissolved in CH₂Cl₂:TFA = 1:1 (200 μL). The mixture was stirred for 2 h at rt before it was terminated by slow addition of NaHCO₃ until gas evolution ceased. The mixture was extracted with CH₂Cl₂ (3 x 100 μL). The combined organic phases were dried over Mg₂SO₄, filtered and the solvent was removed *in vacuo* to yield the product **132** (4.5 mg, 0.24 mmol, quant.) as a yellow oil with a strong smell.

¹H-NMR (400 MHz, CDCl₃): δ 7.40-7.28 (m, 5H, (3-5)-H), 4.55 (s, 2H, 3-H), 3.63 (t, *J* = 6.0 Hz, 2H, 2-H), 2.73 (dt, *J* = 6.0 Hz, 2H, 1-H) 1.60 (t, *J* = 8.3 Hz, 2H, S-H) ppm.

¹³C-NMR (100 MHz, CDCl₃): δ 138 (C-4), 128.6 (C-6), 127.9 (C-5, C-7), 73.1 (C-3), 72.0 (C-2), 24.6 (C-1) ppm;

HRMS (ESI) *m/z* calcd. for [M+Na]⁺: 191.0507; found 191.0502;

R_f(PE:EtOAc = 4:1): 0.58.

2-((2-(Benzyloxy)ethyl)thio)tetrahydro-2H-pyran (133)

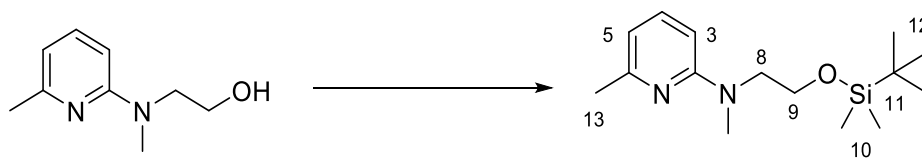
To a solution of thiol **132** (9.0 mg, 54 μmol , 1.0 eq.) in CH_2Cl_2 (4.0 mL) was added dihydropyran (5 μL , 54 μmol , 1.0 eq.) and $\text{MgBr}_2 \cdot \text{Et}_2\text{O}$ (0.41 mg, 1.6 μmol , 0.3 eq.). The reaction mixture was stirred at rt for 2 h. The solvent was removed *in vacuo*, the residue was dissolved in H_2O (1 mL) and extracted with EtOAc (3 x 1 mL). The combined organic phases were dried over Mg_2SO_4 , filtered and the solvent was removed *in vacuo*. Silica column chromatography (PE:EtOAc = 8:1) gave the product **133** (6.0 mg, 24 μmol , 44%) as a colorless oil.

$^1\text{H-NMR}$ (400 MHz, CDCl_3): δ 7.40-7.28 (m, 5H, 3-H – 5-H), 4.89 (dd, $J = 5.9, 3.2$ Hz, 1H, 8-H), 4.55 (s, 2H, 3-H), 4.11-4.02 (m, 1H, 12- H_a), 3.76-3.58 (m, 2H, 2-H) 3.52-3.44 (m, 1H, 12- H_b), 2.87-2.87 (m, 1H, 1- H_a), 2.82-2.73 (m, 1H, 1- H_b), 1.97-1.51 (m, 6H, 9-H – 11-H) ppm.

$^{13}\text{C-NMR}$ (100 MHz, CDCl_3): δ 138 (C-4), 128.5 (C-6), 127.8 (C-5), 127.7 (C-7), 82.7 (C-8), 73.1 (C-3), 72.0 (C-2), 64.7 (C-12), 31.5 (C-9), 30.0 (C-1), 25.7 (C-10), 21.8 (C-11) ppm;

R_f (PE:EtOAc = 4:1): 0.58.

HRMS could not be recorded.

N-(2-((*tert*-Butyldimethylsilyl)oxy)ethyl)-*N*,6-dimethylpyridin-2-amine (**135**)

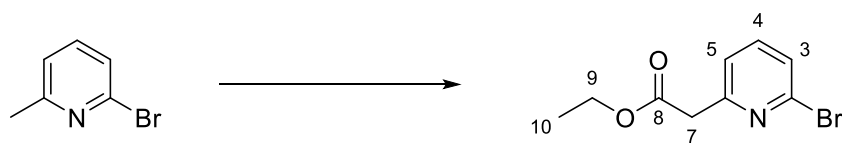
- Procedure:** C, the organic phase was washed with a sat. aq. NaHCO₃ solution
- Reactants:** Alcohol **84b** (89.6 mg, 0.54 mmol), TBSCl (195 mg, 1.29 mmol, 2.4 eq.), imidazole (220 mg, 3.23 mmol, 6.0 eq.)
- Reaction time:** 48 h
- Yield:** The impurities were by addition of PE. The filtrate was removed *in vacuo* to yield **135** as a colorless solid (136.4 mg, 0.49 mmol, 90%)

¹H-NMR (400 MHz, CDCl₃): δ 7.31 (dd, *J* = 8.3, 7.2 Hz, 1H, 4-H), 6.38 (d, *J* = 7.2 Hz, 1H, 3-H), 6.28 (d, *J* = 8.3, 1H, 5-H), 3.79 (t, *J* = 6.3 Hz, 2H, 9-H), 3.68 (q, *J* = 6.3 Hz, 2H, 8-H), 3.07 (s, 3H, 7-H), 2.37 (s, 3H, 13-H), 0.89 (s, 9H, 12-H), 0.04 (s, 6H, 10-H) ppm;

¹³C-NMR (100 MHz, CDCl₃): δ 158.3 (C-2), 156.7 (C-6), 137.5 (C-4), 110.6 (C-3), 102.3 (C-5), 61.0 (C-9), 52.3 (C-8), 37.5 (C-14), 26.0 (C-12), 24.8 (C-13), 18.4 (C-11), -5.2 (C-10) ppm;

HRMS (ESI) *m/z* calcd. for [M+Na]⁺: 303.1869; found 303.1870;

R_f(PE:EtOAc = 1:1): 0.83.

Ethyl 2-(6-bromopyridin-2-yl)acetate (139)

N-BuLi (2.5 M, 7.2 mL, 18.1 mmol, 4 eq.) was added dropwise at 0 °C to a solution of *N,N*-diisopropylamine (2.5 mL, 18.1 mmol, 4 eq.) in THF (45 mL) and stirred for 30 min. The solution was cooled to -78 °C, 2-bromo-6-methylpyridine **93b** (1.00 mL, 9.06 mmol, 2 eq.) was added dropwise and the mixture was stirred for 30 min at this temperature. Ethylchloroformate (0.43 mL, 4.35 mmol, 1.0 eq.) was added dropwise and after stirring for further 30 min the mixture was slowly warmed up to rt. After 1 h the reaction was terminated by addition of a sat. aq. NH₄Cl solution (10 mL) and extracted with EtOAc (3 × 50 mL) and washed with brine (10 mL). The combined organic phases were washed with a sat. aq. NaCl solution, dried over Na₂SO₄, filtered, and concentrated *in vacuo*. Silica column chromatography (PE:EtOAc = 7:1 - 1:1) yielded the the product **139** (785 mg, 3.09 mmol, 71%) as a yellow oil.

¹H-NMR (400 MHz, CDCl₃): δ 7.52 (t, *J* = 8.0 Hz, 1H, 4-H), 7.39 (d, *J* = 8.0 Hz, 1H, 5-H), 7.28 (d, *J* = 8.0 Hz, 1H, 3-H), 4.18 (q, *J* = 6.8 Hz, 2H, 9-H), 3.82 (s, 2H, 7-H), 1.26 (t, *J* = 6.8 Hz, 3H, 10-H) ppm;

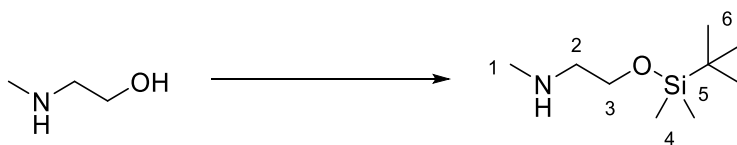
The analytical data are in accordance with those reported in the literature.^[134]

2-(6-Bromopyridin-2-yl)ethan-1-ol (137)

The ester **139** (785 mg, 3.2 mmol, 1.0 eq.) was dissolved in dry THF (13 mL) and the mixture was cooled to 0 °C. DIBAL-H (1M in THF, 8.00 mL, 2.5 eq.) was added dropwise. The reaction mixture was warmed up to rt and stirred for 4 h before it was terminated by addition of a sat. aq. sodium tartrate solution (20 mL) and extracted with EtOAc (3 x 10 mL). The combined organic phases were washed with a sat. aq. NaCl solution, dried over Na₂SO₄, filtered and evaporated *in vacuo*. Silica column chromatography (PE:EtOAc = 2:1 – 1:1) yielded the product **137** (645 mg, 3.17 mmol, 99%) as a colorless liquid.

¹H-NMR (400 MHz, CDCl₃): δ 7.46 (t, *J* = 8.0 Hz, 1H, 4-H), 7.35 (d, *J* = 8.0 Hz, 1H, 5-H), 7.14 (d, *J* = 8.0 Hz, 1H, 3-H), 4.00 (t, *J* = 5.7 Hz, 2H, 8-H), 3.08 (bs, 1H, *O*-H), 3.00 (t, *J* = 5.7 Hz, 2H, 7-H) ppm;

The analytical data are in accordance with those reported in the literature.^[134]

2-((tert-Butyldimethylsilyl)oxy)-N-methylethan-1-amine (146)

Procedure: C

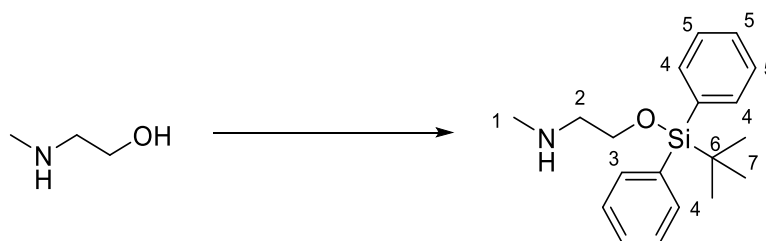
Reactants: Methylaminoethanol (100.0 mg, 1.33 mmol), TBSCl (221 mg, 1.47 mmol), imidazole (182 mg, 2.67 mmol)

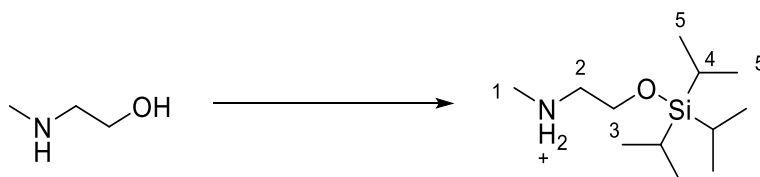
Reaction time: 2 h

Yield: The product **146** (181 mg, 0.96 mmol, 72%) was used without further purification.

¹H-NMR (400 MHz, CDCl₃): δ 3.72 (t, *J* = 5.2 Hz, 1H, 3-H), 2.68 (t, *J* = 5.2 Hz, 1H, 2-H), 2.45 (s, 3H, 1-H), 2.44 (bs, 1H, *N*-H), 0.89 (s, 9H, 6-H), 0.59 (s, 6H, 4-H) ppm;

The analytical data are in accordance with those reported in the literature.^[149]

2-((tert-Butyldiphenylsilyl)oxy)-N-methylethan-1-amine (147)**Procedure:** C**Reactants:** Methylaminoethanol (47.0 mg, 0.63 mmol, 1.0 eq.), TBDPSCl (176,16 μ L, 0.69 mmol, 1.1 eq.), imidazole (69.27mg, 1.25 mmol, 2.0 eq.)**Reaction time:** 20 h**Yield:** The crude product **147** was use without further purification.**¹H-NMR** (400 MHz, CDCl₃): δ 7.70 – 7.65 (m, 4H, 4-H), 7.44 – 7.35 (m, 6H, 5-H), 3.78 (t, J = 5.2 Hz, 1H, 3-H), 2.74 (t, J = 5.2 Hz, 1H, 2-H), 2.45 (s, 3H, 1-H), 1.06 (s, 9H, 7-H) ppm;**¹³C-NMR** (100 MHz, CDCl₃): δ 135.7 (C-4), 133.81 (C-8), 129.8 (C-5), 127.8 (C-5), 63.0 (C-3), 53.7 (C-2), 36.4 (C-1), 27.0 (C-7), 19.3 (C-6) ppm;**HRMS** (ESI) m/z calcd. for [M+Na]⁺: 336.1760; found 336.1747.

***N*-Methyl-2-((triisopropylsilyl)oxy)ethan-1-amine (148)**

Procedure: C, addition of silylchloride at 0 °C

Reactants: Methylaminoethanol (100.0 mg, 1.33 mmol, 1.0 eq.), TIPSCl (314 μ L, 1.47 mmol, 1.1 eq.), imidazole (182 mg, 2.67 mmol, 2.0 eq.)

Reaction time: 20 h

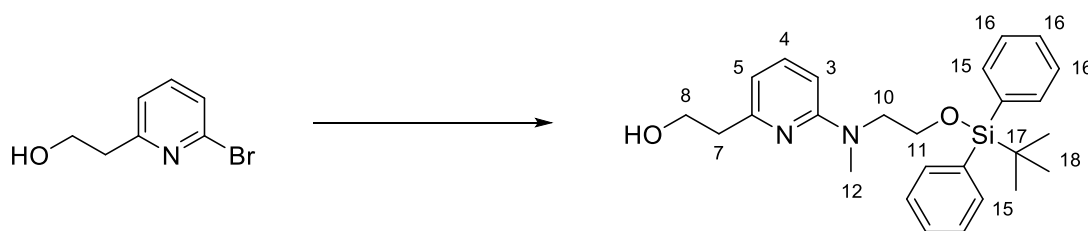
Yield: Silica column chromatography (CH₂Cl₂, MeOH 10%-20%, 1% Et₃N) gave the product **148** (212 mg, 0.92 mmol, 69%) as a yellow oil.

¹H-NMR (400 MHz, CDCl₃): δ 6.96 (bs, 1H, *N*-H), 3.87 (t, J = 5.2 Hz, 1H, 3-H), 2.85 (t, J = 5.2 Hz, 1H, 2-H), 2.56 (s, 3H, 1-H), 1.98 (s, 2H, *N*-H), 1.15-1.00 (m, 21H, 4-H, 5-H) ppm;

¹³C-NMR (100 MHz, CDCl₃): δ 60.8 (C-3), 52.3 (C-2), 34.5 (C-1), 18.1 (18C, C-5), 12.0 (3C, C-4) ppm;

HRMS (ESI) m/z calcd. for [M+H]⁺: 232.2097; found 232.2097.

2-(6-((2-((tert-Butyldiphenylsilyl)oxy)ethyl)(methyl)amino)pyridin-2-yl)ethan-1-ol (151)



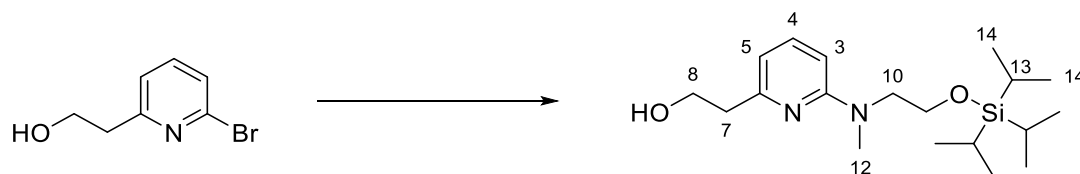
$\text{Pd}_2(\text{dba})_3$ (2.3 mg, 2.5 μmol , 0.1 eq.), BINAP (1.7 mg, 2.7 μmol , 0.1 eq.) and Cs_2CO_3 (21.0 mg, 61.9 μmol , 2.5 eq.) were mixed in THF (350 μL). The bromide **137** (5 mg, 24.7 μmol , 1.0 eq.) and the amine **147** (9.3 mg, 29.7 μmol , 1.2 eq.) were added and argon was bubbled through the mixture for 5 min. The mixture was stirred at 85 °C for 18 h before the reaction was terminated by addition of H_2O (1 mL) and extracted with EtOAc (3 x 1 mL). The combined organic phases were washed with a sat. aq. NaCl solution, dried over Na_2SO_4 , filtered and the solvent was removed *in vacuo*. Silica column chromatography (PE:EtOAc = 5:1) gave the product **151** as a colorless yellow oil (3.8 mg, 8.65 μmol , 35%).

$^1\text{H-NMR}$ (400 MHz, CDCl_3): δ 7.64-7.58 (m, 4H, 15-H), 7.45 – 7.26 (m, 7H, 4-H, 16-H), 6.34 (d, J = 7.6 Hz, 1H, 5-H), 6.27 (d, J = 8.5 Hz, 1H, 3-H), 3.92 (dd, J = 5.0, 4.5 Hz, 2H, 8-H), 3.83 (t, J = 5.8 Hz, 2H, 11-H), 3.63 (t, J = 5.8 Hz, 2H, 10-H), 3.05 (s, 3H, 12-H), 2.81 (dd, J = 5.0, 4.5 Hz, 2H, 7-H), 1.01 (s, 9H, 18-H) ppm;

$^{13}\text{C-NMR}$ (100 MHz, C_6D_6): δ 159.6 (C-2), 157.9 (C-6), 137.9 (C-4), 135.8 (C-15), 133.5 (C-14), 129.8 (C-16), 127.8 (C-16), 110.5 (C-5), 103.9 (C-3), 62.2 (C-10), 61.7 (C-11), 52.56 (C-8), 38.2 (C-7), 37.9 (C-12), 27.0 (C-18), 19.2 (C-17) ppm;

R_f (PE:EtOAc = 2:1): 0.20.

2-(6-(Methyl(2-((triisopropylsilyl)oxy)ethyl)amino)pyridin-2-yl)ethan-1-ol (152)



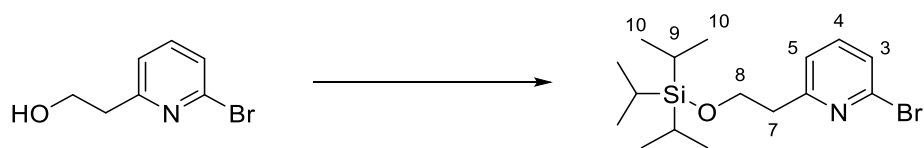
$\text{Pd}_2(\text{dba})_3$ (2.3 mg, 2.5 μmol , 0.1 eq.), BINAP (1.7 mg, 2.7 μmol , 0.1 eq.) and Cs_2CO_3 (21.0 mg, 61.9 μmol , 2.5 eq.) were mixed in THF (350 μL). The bromide **137** (5 mg, 24.7 μmol , 1.0 eq.) and the amine **148** (6.8 mg, 29.7 μmol , 1.2 eq.) were added and argon was bubbled through the mixture for 5 min. The mixture was stirred at 85 $^\circ\text{C}$ for 18 h before it was terminated by addition of H_2O (1 mL) and extracted with EtOAc (3 x 1 mL). The combined organic phases were washed with a sat. aq. NaCl solution, dried over Na_2SO_4 , filtered and the solvent was removed *in vacuo*. Silica column chromatography (PE:EtOAc = 5:1) gave the product **152** as a colorless yellow oil (3.0 mg, 8.40 μmol , 34%).

$^1\text{H-NMR}$ (400 MHz, C_6D_6): δ 7.06 (dd, $J = 8.0, 7.0$ Hz, 1H, 4-H), 6.15 (d, $J = 7.0$ Hz, 1H, 5-H), 6.11 (d, $J = 8.0$ Hz, 1H, 3-H), 4.0 (dd, $J = 5.0, 4.5$ Hz, 2H, 8-H), 3.75 (t, $J = 5.8$ Hz, 2H, 10-H), 3.47 (t, $J = 5.8$ Hz, 2H, 11-H), 2.81 (s, 3H, 12-H), 2.74 (dd, $J = 5.0, 4.5$ Hz, 2H, 7-H), 1.09 - 0.09 (m, 21H, 13-H, 14-H) ppm;

$^{13}\text{C-NMR}$ (100 MHz, C_6D_6): δ 159.4 (C-2), 158.0 (C-6), 138.1 (C-4), 110.8 (C-5), 103.9 (C-3), 62.4 (C-10), 61.9 (C-11), 53.16 (C-8), 39.3 (C-7), 38.0 (C-12), 18.2 (C-13), 12.2 (C-14) ppm;

HRMS (ESI) m/z calcd. for $[\text{M}+\text{H}]^+$: 353.2624; found 353.2634;

R_f (PE:EtOAc = 5:1): 0.25.

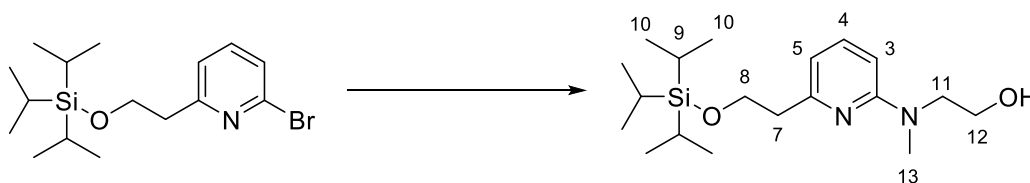
2-Bromo-6-(2-((triisopropylsilyl)oxy)ethyl)pyridine (153)

- Procedure:** C, addition of silyltriflate at 0 °C
- Reactants:** Alcohol **137** (105 mg, 0.52 mmol, 1.0 eq.), TIPSCl (110 mg, 0.57 mmol, 1.1 eq.), imidazol (71.0 mg, 1.0 mmol, 2 eq.)
- Reaction time:** 20 h
- Yield:** Silica column chromatography (PE:EtOAc = 100:1) gave the product **153** (119 mg, 0.51 mmol, 99%) as a colorless oil.

¹H-NMR (400 MHz, CDCl₃): δ 7.43 (t, *J* = 7.8 Hz, 1H, 4-H), 7.31 (d, *J* = 7.8 Hz, 1H, 5-H), 7.19 (d, *J* = 7.8 Hz, 1H, 3-H), 4.03 (t, *J* = 6.2 Hz, 2H, 8-H), 3.08 (bs, 1H, O-H), 2.97 (t, *J* = 6.2 Hz, 2H, 7-H), 1.08 – 0.92 (m, 21H, 9-H, 10-H) ppm;

The analytical data are in accordance with those reported in the literature.^[133]

2-(Methyl(6-(2-((triisopropylsilyl)oxy)ethyl)pyridin-2-yl)amino)ethan-1-ol (154)



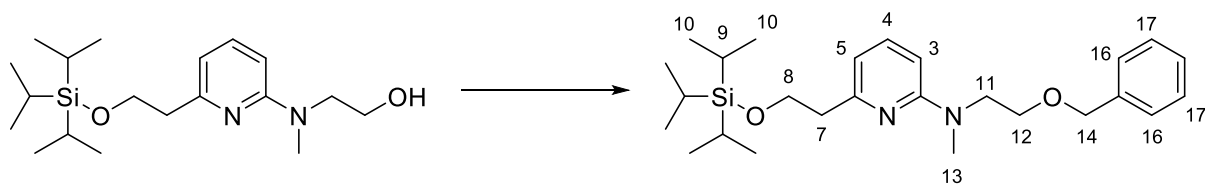
$\text{Pd}_2(\text{dba})_3$ (25.0 mg, 0.03 mmol, 0.1 eq.), BINAP (19.1 mg, 0.03 mmol, 0.1 eq.) and Cs_2CO_3 (230 mg, 0.70 mmol, 2.5 eq.) were mixed in toluene (1.4 mL). The bromide **153** (100 mg, 0.28 mmol, 1.0 eq.) and the amine (27 μL , 0.33 mmol, 1.2 eq.) were added and argon was bubbled through the mixture for 5 min. The mixture was stirred at 85 °C for 18 h before it was terminated by addition of H_2O (2 mL) and extracted with EtOAc (3 x 2 mL). The combined organic phases were washed with a sat. aq. NaCl solution, dried over Na_2SO_4 , filtered and the solvent was removed *in vacuo*. Silica column chromatography (PE:EtOAc = 4:1) gave the product **154** as a colorless yellow oil (75 mg, 0.21 mmol, 76%).

$^1\text{H-NMR}$ (400 MHz, CDCl_3): δ 7.39 (dd, $J = 8.2, 7.3$ Hz, 1H, 4-H), 6.53 (d, $J = 7.3$ Hz, 1H, 5-H), 6.37 (d, $J = 8.2$ Hz, 1H, 3-H), 3.99 (t, $J = 6.9$ Hz, 2H, 8-H), 3.84 (dd, $J = 5.4, 4.0$ Hz, 2H, 12-H), 3.70 (dd, $J = 5.4, 4.0$ Hz, 2H, 11-H), 3.04 (s, 3H, 13-H), 2.86 (t, $J = 6.9$ Hz, 2H, 7-H), 1.10 – 0.92 (m, 21H, 9-H, 10-H) ppm;

$^{13}\text{C-NMR}$ (100 MHz, CDCl_3): δ 159.1 (C-2), 157.0 (C-6), 138.2 (C-4), 112.7 (C-5), 104.1 (C-3), 63.5 (C-8), 63.3 (C-12), 54.7 (C-11), 41.7 (C-7), 38.2 (C-13), 18.1 (C-10), 12.1 (C-12) ppm;

HRMS (ESI) m/z calcd. for $[\text{M}+\text{Na}]^+$: 375.2451; found 375.2444;

R_f (PE:EtOAc = 4:1): 0.16.

***N*-(2-(Benzyloxy)ethyl)-*N*-methyl-6-(2-((triisopropylsilyl)oxy)ethyl)pyridin-2-amine (155)**

To a solution of alcohol **154** (323 mg, 0.82 mmol, 1.0 eq.) in THF (2 mL) was added NaH (90% in mineral oil, 26.2 mg, 0.98 mmol, 1.2 eq.) at 0 °C. The mixture was warmed up to rt and stirred for 1 h before benzylbromide (126 μ L, 1.06 mmol, 1.3 eq.) and TBAI (30 mg, 0.08 mmol, 10 mol%) were added. After 18 h at rt the reaction was terminated by addition of a sat. aq. NH_4Cl solution (2 mL), basified with a sat. aq. NaHCO_3 solution and extracted with EtOAc (3 x 4 mL). The combined organic phases were washed with a sat. aq. NaCl solution, dried over Na_2SO_4 , filtered and the solvent was removed *in vacuo*. Silica column chromatography (PE:EtOAc = 40:1 – 20:1) gave the product **155** (259.6 mg, 0.59 mmol, 72%) as a colorless oil.

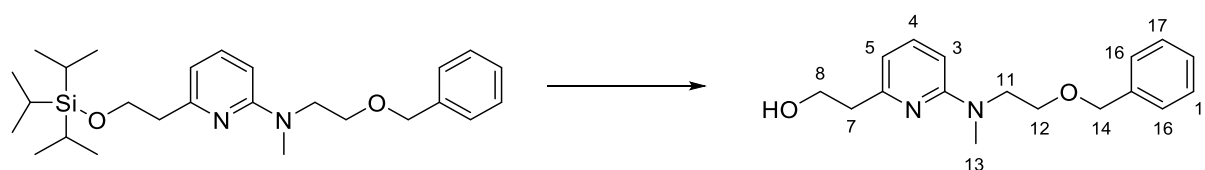
$^1\text{H-NMR}$ (400 MHz, CDCl_3): δ 7.38-7.23 (m, 6H, 4-H, 16-H, 17-H, 18-H), 6.43 (d, J = 7.6 Hz, 1H, 5-H), 6.37 (d, J = 8.2 Hz, 1H, 3-H), 4.52 (s, 2H, 14-H), 4.01 (t, J = 7.0 Hz, 2H, 8-H), 3.80 (t, J = 6.0 Hz, 2H, 12-H), 3.68 (t, J = 6.0 Hz, 2H, 11-H), 3.08 (s, 3H, 13-H), 2.86 (t, J = 67.0 Hz, 2H, 7-H), 1.10 – 0.92 (m, 21H, 9-H, 10-H) ppm;

$^{13}\text{C-NMR}$ (100 MHz, CDCl_3): δ 158.2 (C-2), 157.3 (C-6), 138.6 (C-15), 137.4 (C-4), 128.4 (C-17), 127.6 (C-16), 111.3 (C-5), 103.0 (C-3), 73.2 (C-14), 68.7 (C-11), 63.7 (C-8), 49.8 (C-12), 42.2 (C-7), 37.4 (C-13), 18.1 (C-10), 12.1 (C-9) ppm;

HRMS (ESI) m/z calcd. for $[\text{M}+\text{H}]^+$: 443.3094; found 443.3097;

R_f (PE:EtOAc = 10:1): 0.31.

2-(6-((2-(Benzyloxy)ethyl)(methyl)amino)pyridin-2-yl)ethan-1-ol (156)



The TIPS ether **155** (224 mg, 0.51 mmol, 1.0 eq.) was dissolved in dry THF (2.50 mL) and cooled to 0 °C. TBAF (1M in THF, 1.26 mL, 2.5 eq.) was added and the mixture was slowly warmed up to rt. After stirring at rt for 1 h the reaction was terminated by addition of a sat. aq. NH₄Cl solution and the aq. phase was extracted with EtOAc (3 x 2 mL). The combined organic phases were dried over MgSO₄, filtered and the solvent was removed *in vacuo*. Silica column chromatography (PE:EtOAc = 1:1) gave the product **156** (130 mg, 0.46 mmol, 90%) as a colorless oil.

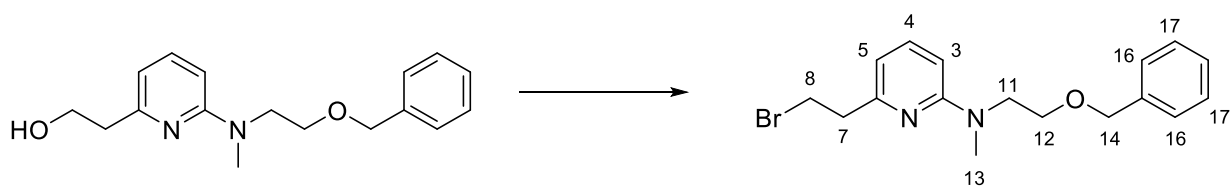
¹H-NMR (400 MHz, CDCl₃): δ 7.37 (t, *J* = 8.8 Hz, 1H, 4-H) 7.33-7.23 (m, 6H, 4-H, 16-H, 17-H, 18-H), 6.38 (t, *J* = 8.8 Hz, 2H, 3-H, 5-H), 4.51 (s, 2H, 14-H), 3.98 (t, *J* = 6.0 Hz, 2H, 8-H), 3.76 – 3.70 (m, 2H, 11-H), 3.70-3.66 (m, 2H, 12-H), 3.08 (s, 3H, 13-H), 2.85 (bs, 2H, 7-H), 1.10 – 0.92 (m, 21H, 9-H, 10-H) ppm;

¹³C-NMR (100 MHz, CDCl₃): δ 158.2 (C-6), 157.6 (C-2), 138.5 (C-4 o. C-15), 138.0 (C-4 o. C-15), 128.5 (C-17), 127.6 (C-16), 110.7(C-5), 103.9 (C-3), 73.3 (C-14), 68.4 (C-12), 62.2 (C-8), 50.4 (C-11), 38.1 (C-7), 37.7 (C-13) ppm; *

HRMS (ESI) *m/z* calcd. for [M+Na]⁺: 309.1579; found 309.1576;

R_f(PE:EtOAc = 2:1): 0.16.

*C-18 could not be detected in the ¹³C-NMR spectrum.

***N*-(2-(Benzyloxy)ethyl)-6-(2-bromoethyl)-*N*-methylpyridin-2-amine (157)**

Under light exclusion, the alcohol **156** (100 mg, 0.35 mmol, 1.0 eq.) was dissolved in dry CH₂Cl₂ (3.50 mL). Triphenylphosphine (100 mg, 0.38 mmol, 1.1 eq.) and carbon tetrabromide (127 mg, 0.38 mmol, 1.1 eq.) were added and the mixture was stirred at rt for 2 h. The reaction was terminated by addition of H₂O, the pH was adjusted to 9 by addition of a sat. aq. NaHCO₃ solution and the aq. phase was extracted with CH₂Cl₂ (3 x). The combined organic phases were dried over Na₂SO₄, filtered and the solvent was removed *in vacuo*. Silica column chromatography (PE:EtOAc = 40:1 – 20:1) gave the product **157** (105 mg, 0.30 mmol, 92%) as a colorless oil.

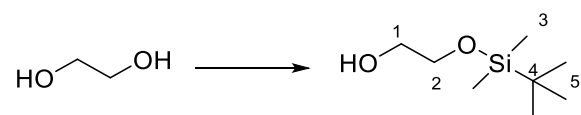
¹H-NMR (400 MHz, CDCl₃): δ 7.37-7.27 (m, 6H, 4-H, 16-H, 17-H, 18-H), 6.40 (d, *J* = 8.0 Hz, 1H, 3 o. 5-H), 6.37 (d, *J* = 8.5 Hz, 1H, 3 o. 5-H), 4.97 (s, 2H, 14-H), 3.81 (t, *J* = 6.0 Hz, 2H, 11-H), 3.75 (t, *J* = 8.0 Hz, 1H, 7-H), 3.70 (t, *J* = 6.0 Hz, 1H, 12-H), 3.15 (t, *J* = 8.0 Hz, 1H, 8-H), 3.08 (s, 3H, 13-H) ppm;

¹³C-NMR (100 MHz, CDCl₃): δ 158.3 (C-6), 156.4 (C-2), 138.6 (C15), 137.7 (C-4), 128.5 (C-17), 127.6 (C-16), 110.8 (C-5), 103.8 (C-3), 73.3 (C-14), 68.5 (C-12), 48.9 (C-11), 41.4 (C-8), 37.5 (C-13), 32.2 (C-7) ppm; *

HRMS (ESI) *m/z* calcd. for [M+Na]⁺: 349.0915; found 349.0913;

R_f(PE:EtOAc = 10:1): 0.5.

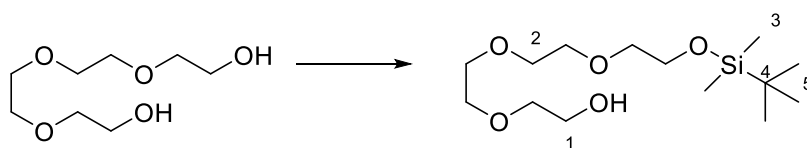
*C-18 could not be detected in the ¹³C-NMR spectrum.

2-((tert-Butyldimethylsilyl)oxy)ethan-1-ol (159a)

Ethylene glycol **130** (148 μL , 2.65 mmol, 0.8 eq.), imidazole (678 mg, 9.95 mmol, 3 eq.), and DMAP (**103**, 81.0 mg, 0.66 mmol, 0.2 eq.) were dissolved in CH_2Cl_2 (15.0 mL) and DMF (660 μL) was added. The suspension was cooled to 0 $^\circ\text{C}$ and a solution of TBSCl (500 mg, 3.32 mmol, 1.0 eq.) in CH_2Cl_2 (10 mL) was added over a period of 1 h. The reaction mixture was warmed up to rt and stirred for 18 h over night before it was terminated by addition of H_2O . The phases were separated, and the aq. phase was extracted with EtOAc (3 x 10 mL). The combined organic phases were dried over MgSO_4 , filtered and the solvent was removed *in vacuo*. Silica column chromatography (PE:EtOAc = 3:1) gave the monoprotected ethylene glycol **159a** (110 mg, 0.80 mmol, 24%) as a colorless oil.

$^1\text{H-NMR}$ (400 MHz, CDCl_3): δ 3.70-3.60 (m, 4H, 1-H, 2-H), 0.94 (s, 9H, 5-H), 0.11 (s, 6H, 3-H) ppm.

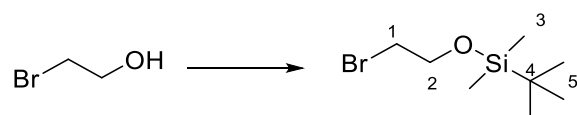
The analytical data are in accordance with those reported in the literature.^[150]

2,2,3,3-Tetramethyl-4,7,11-trioxa-3-silatridecan-13-ol (159b)

Tetraethylene glycol **158** (460 μL , 2.65 mmol, 0.8 eq.), imidazole (678 mg, 9.95 mmol, 3 eq.), and DMAP (**103**, 81.0 mg, 0.66 mmol, 0.2 eq.) were dissolved in CH_2Cl_2 (15.0 mL) and DMF (660 μL) was added. The suspension was cooled to 0 $^\circ\text{C}$ and a solution of TBSCl (500 mg, 3.32 mmol, 1.0 eq.) in CH_2Cl_2 (10 mL) was added over 1 h. The reaction mixture was warmed up to rt and stirred for 18 h over night before it was terminated by addition of H_2O . The phases were separated, and the aq. phase was extracted with EtOAc (3 x 10 mL). The combined organic phases were dried over MgSO_4 , filtered and the solvent was removed *in vacuo*. Silica column chromatography (PE:EtOAc = 2:1) gave the monoprotected ethylene glycol **159b** (254 mg, 1.02 mmol, 31%) as a colorless oil.

$^1\text{H-NMR}$ (400 MHz, CDCl_3): δ 3.84-3.45 (m, 16H, 1-H, 2-H), 2.51 (bs, 1H, O-H), 0.90 (s, 9H, 5-H), 0.07 (s, 6H, 3-H) ppm.

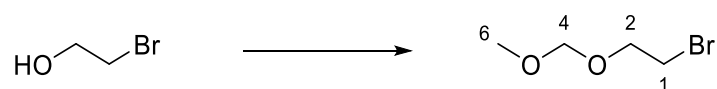
The analytical data are in accordance with those reported in the literature.^[151]

(2-Bromoethoxy)(tert-butyl)dimethylsilane (163a)

To a solution of 2-bromoethanol (**162**, 290 μL , 4.00 mmol, 1.0 eq.) in CH_2Cl_2 (4.0 mL) was added TBSCl (720 mg, 4.80 mmol, 1.2 eq.). The reaction mixture was cooled to 0 $^\circ\text{C}$ and diisopropylethylamine (1.00 mL, 6.00 mmol, 1.5 eq.) was added dropwise before it was warmed up to rt and stirred for 18 h. The reaction was terminated by addition of H_2O (5 mL), the aq. phase was separated and extracted with EtOAc (2 x 5 mL). The combined organic phases were dried over MgSO_4 , filtered and the solvent was removed *in vacuo*. Silica column chromatography (PE:EtOAc = 10:1) gave the product **163a** (900 mg, 0.38 mmol, 95%) as a colorless oil.

$^1\text{H-NMR}$ (400 MHz, CDCl_3): δ 3.89 (t, $J = 7.2$ Hz, 2H, 2-H), 3.39 (t, $J = 7.2$ Hz, 2H, 1-H), 0.91 (s, 9H, 5-H), 0.09 (s, 6H, 3-H) ppm.

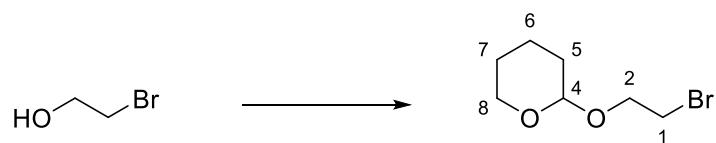
The analytical data are in accordance with those reported in the literature.^[152]

1-Bromo-2-(methoxymethoxy)ethane (163b)

2-Bromoethanol (**162**, 114 μ L, 1.6 mmol, 1.0 eq.) was dissolved under argon in dimethoxymethane (850 μ L, 9.6 mmol, 6 eq.) and cooled to 0 °C. P₂O₅ (227 mg, 0.8 mmol, 0.5 eq.) was added. The reaction mixture was stirred at 0 °C for 30 min before it was warmed up to rt over a period of 18 h. The reaction was terminated by addition of water (1 mL) and the aq. phase was extracted with Et₂O (1 mL). The combined organic phases were washed with water, then with a sat. aq. Na₂CO₃ solution and dried over Mg₂SO₄, filtered and the solvent was removed *in vacuo*. The crude product **163b** was directly used for the next reaction step.

¹H-NMR (400 MHz, CDCl₃): δ 4.68 (s, 2H, 4-H), 3.87 (t, J = 6.3 Hz, 2H, 2-H), 3.51 (t, J = 6.3 Hz, 2H, 1-H), 3.40 (s, 3H, 6-H) ppm.

The analytical data are in accordance with those reported in the literature.^[153]

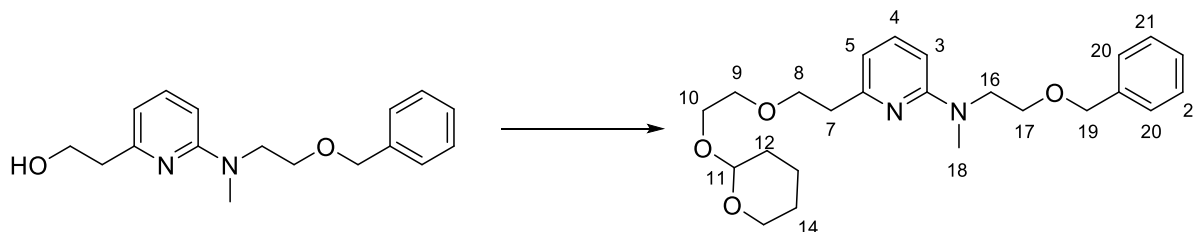
2-(2-Bromoethoxy)tetrahydro-2H-pyran (163c)

To a solution of 2-bromoethanol (**162**, 215 μL , 1.60 mmol, 1.0 eq.) in CH_2Cl_2 (1.6 mL) was added 3,4-dihydro-2H-pyran (DHP) (220 μL , 2.40 mmol, 1.5 eq.) and pyridinium tosylate monohydrate (25.0 μL , 0.16 mmol, 0.1 eq.). The reaction mixture was stirred for 18 h at rt. Et_2O (3 mL) was added and the organic phase was washed with a semi sat. aq. NaCl solution (3 mL), dried over MgSO_4 , filtered and the solvent was removed *in vacuo*. Silica column chromatography (PE:EtOAc = 20:1) gave the product **163c** (211 mg, 1.01 mmol, 63%) as a colorless solid.

$^1\text{H-NMR}$ (400 MHz, CDCl_3): δ 4.67 (t, $J = 3.0$ Hz, 1H, 4-H), 4.00 (dt, $J = 11.0, 6.6$ Hz, 1H, 2- H_a), 3.90 – 3.84 (m, 1H, 8- H_a) 3.77 (dt, $J = 11.0, 6.6$ Hz, 1H, 2- H_b) 3.57 – 3.46 (m, 3H, 1-H, 8- H_b) 1.90 – 1.50 (m, 6H, 5-H – 7-H) ppm.

The analytical data are in accordance with those reported in the literature.^[154]

***N*-(2-(Benzyloxy)ethyl)-*N*-methyl-6-(2-(2-((tetrahydro-2*H*-pyran-2-yl)oxy)ethoxy)ethyl)pyridin-2-amine (164b)**



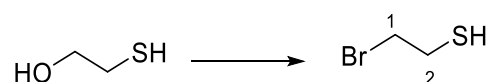
The alcohol **156** (11.0 mg, 3.84 μmol , 1.0 eq.) was dissolved in dry THF (190 μL). NaH (90%, 1.2 mg, 1.2 eq.) was added at 0 $^{\circ}\text{C}$ and the reaction mixture was stirred for 1 h at rt before bromide **163c** (10.2 mg, 5.00 μmol , 1.5 eq.) was added. The reaction mixture was heated under refluxing conditions and stirred for 36 h. The reaction was terminated by addition of a sat. aq. NH_3Cl solution (1 mL) and EtOAc (1 mL). The organic phase was separated and the aq. phase was extracted with EtOAc (2 x 1 mL). The combined organic phases were dried over Na_2SO_4 , filtered and the solvent was removed *in vacuo*. Silica column chromatography (PE:EtOAc = 2:1) gave the product **164b** (4.0 mg, 0.97 μmol , 25%) as a colorless solid.

$^1\text{H-NMR}$ (400MHz, CDCl_3): 7.39 – 7.21 (m, 6H, 4-H, (20-22)-H), 6.44 (d, $J = 7.3$ Hz, 1H, 3-H o. 5-H), 6.31 (d, $J = 8.2$ Hz, 1H, 3-H o. 5-H), 4.61 (t, $J = 3.3$ Hz, 1H, 11-H), 4.53 (s, 2H, 19-H), 3.91-3.76 (m, 6H, 8-H, 10- H_a , 15- H_a , C16), 3.73-3.55 (m, 6H, 9-H, 10- H_b , 15- H_b , 17-H), 3.54-3.42 (m, 1H, 15- H_b), 3.01 (s, 3H, 18-H), 2.90 (t, $J = 7.3$ Hz, 2H, 7-H), 1.91-1.44 (m, 6H, (12-14)-H)

$^{13}\text{C-NMR}$ (100 MHz, CDCl_3): δ 158.2 (C-6), 157.1 (C-2), 138.6 (C-4 or C-15), 137.5 (C-4 or C-15), 128.4 (C-21), 127.6 (C-20, C-22), 111.0 (C-5), 103.9 (C-3), 99.0 (C-11), 73.2 (C-19), 70.9 (C-8), 70.2 (C-9), 68.6 (C-17), 66.7 (C-10), 62.3 (C-15), 49.7 (C-16), 38.7 (C-7), 37.7 (C-18), 30.7 (C-12), 25.6 (C-13), 19.6 (C-14) ppm;

HRMS (ESI) m/z calcd. for $[\text{M}+\text{Na}]^+$: 437.2416; found 437.2412;

R_f (PE:EtOAc = 2:1): 0.32.

2-Bromoethan-1-thiol (166)

At 0 °C PBr₃ (730 μL, 7.7 mmol, 0.3 eq.) was added dropwise to mercaptoethanol (**165**, 1.8 mL, 25.6 mmol, 1.0 eq.). The reaction mixture was stirred for 3 h at rt before it was washed with H₂O (2 x 2 mL). The organic phase was dried over Na₂SO₄ and filtered. Distillation gave the product **165** (278 mg, 2.05 mmol, 8%) as a colorless oil with strong odor.

¹H-NMR (400 MHz, CDCl₃): δ 3.51 (t, *J* = 9.8 Hz, 2H, 1-H), 2.92 (t, *J* = 9.8 Hz, 2H, 2-H), 1.73 (t, *J* = 9.8 Hz, 2H, S-H), ppm;

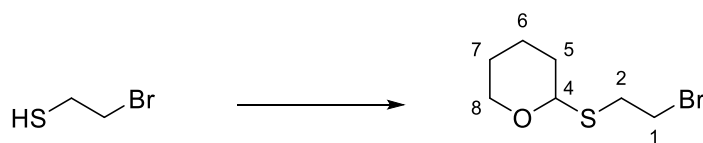
¹³C-NMR (100 MHz, CDCl₃): δ 34.0 (C-2), 26.9 (C-1) ppm;

HRMS (ESI) *m/z* calcd. for [M+H]⁺: 139.9396; found 139.9395;

R_f(PE:EtOAc = 10:1): 0.5;

T_b = 50 °C, 30 mbar.

The analytical data are in accordance with those reported in the literature.^[155]

2-((2-Bromoethyl)thio)tetrahydro-2H-pyran (167)

To a solution of thiol **166** (143 mg, 1.01 mmol, 1.0 eq.) in CH_2Cl_2 (2.0 mL) was added dihydropyran (92 μL , 1.01 mol, 1.0 eq.) and $\text{MgBr}_2 \cdot \text{Et}_2\text{O}$ (8.0 mg, 0.03 mmol, 0.3 eq.). The reaction mixture was stirred at rt for 2 h. The solvent was removed *in vacuo*, the residue was dissolved in distilled water (1 mL) and extracted with EtOAc (3 x 1 mL). The combined organic phases were dried over Mg_2SO_4 , filtered and the solvent was removed *in vacuo*. Silica column chromatography (PE:EtOAc = 50:1) gave the product (200 mg, 0.89 mmol, 88%) as a colorless oil.

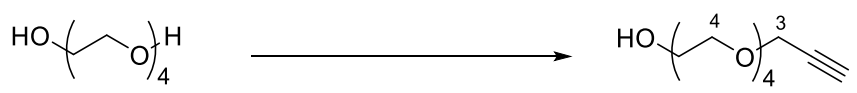
$^1\text{H-NMR}$ (400 MHz, CDCl_3): δ 4.90 (dd, $J = 6.0, 3.5$ Hz, 1H, 4-H), 4.10-4.02 (m, 1H, 8- H_a) 3.62 – 3.45 (m, 3H, 2-H, 8- H_b) 3.09 (ddd, $J = 13.5, 11.0, 5.7$ Hz, 1H, 1- H_a), 2.97 (ddd, $J = 13.5, 11.0, 5.7$ Hz, 1H, 1- H_b), 1.97 – 1.50 (m, 6H, 5-H – 7-H) ppm.

$^{13}\text{C-NMR}$ (100 MHz, CDCl_3): δ 83.0 (C-4), 64.6 (C-8), 33.1 (C-1), 31.3 (C-5), 31.3 (C-2), 25.5 (C-6), 21.6 (C-7) ppm;

138 (C-4), 128.5 (C-6), 127.8 (C-5), 127.7 (C-7), 82.7 (C-8), 73.1 (C-3), 72.0 (C-2), 64.7 (C-12), 31.5 (C-9), 30.0 (C-1), 25.7(C-10), 21.8 (C-11) ppm;

R_f (PE:EtOAc = 10:1): 0.6;

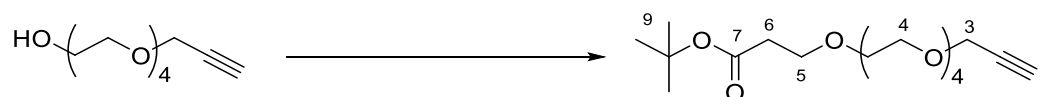
HRMS could not be recorded.

3,6,9,12-Tetraoxapentadec-14-yn-1-ol (174)

Tetraethylenglycol (**158**, 8.9 mL, 51.4 mmol, 2.9 eq.) was dissolved in dry THF (90 mL) under argon atmosphere. NaH (1.0 g, 41.2 mmol, 2.3 eq.) was added at 0 °C portionwise. The mixture was warmed up to rt and stirred for 20 min before propargyl bromide (80% in toluene, 18.0 mmol, 2.0 mL, 1.0 eq.) was added over 15 min. After 48 h at rt the reaction was terminated by addition of EtOH. The solvent was removed under reduced pressure and the crude oil was purified by silica column chromatography (PE:EtOAc = 5:1-1.1). The alkyne **174** (3.73 g, 45.7 mmol, 89%) was isolated as a colorless oil.

¹H-NMR (400 MHz, CDCl₃): δ 4.12 (d, *J* = 2.3 Hz, 2H, 3-H), 3.73 – 3.64 (m, 14 H, 4-H), 3.62 – 3.58 (m, 2H, 4-H), 2.63 (bs, 1H, *O*-H), 2.42 (t, *J* = 2.3 Hz, 1H, 1-H) ppm;

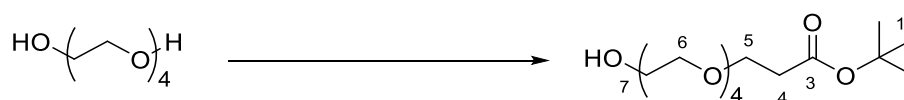
The analytical data are in accordance with those reported in the literature.^[156]

***tert*-Butyl 4,7,10,13,16-pentaoxanonadec-18-ynoate (175)**

The alkyne **174** (3.7 g, 16.1 mmol, 1.0 eq.) was dissolved in dry THF (23 mL) under argon. NaOMe (25% in MeOH, 35.0 μ L, 0.01 eq.) and *t*-butyl acrylate (**170**, 3.5 mL, 24.1 mmol, 1.5 eq.) were added. The reaction mixture was stirred for 48 h at rt before it was terminated by addition of H₂O (20 mL). The aq. phase was extracted with EtOAc (3 x 20 mL). The combined organic phases were washed with a sat. aq. NaCl solution (20 mL), dried over Na₂SO₄, filtered, and the solvent was removed *in vacuo*. Silica column chromatography (PE:EtOAc = 3:1 – 1:1) gave the product **175** (4.56 g, 12.7 mmol, 79%) as a colorless oil.

¹H-NMR (400 MHz, CDCl₃): δ 4.20 (d, J = 2.3 Hz, 2H, 3-H), 3.73 – 3.58 (m, 18H, 4-H), 2.49 (t, J = 6.7 Hz, 1H, 3-H), 2.43 (t, J = 2.3 Hz, 1H, 1-H), 1.44 (s, 9H, 9-H) ppm;

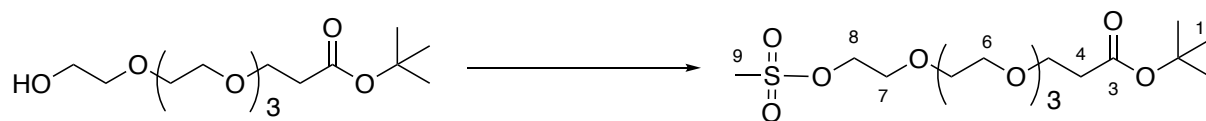
The analytical data are in accordance with those reported in the literature.^[157]

***tert*-Butyl 3-(2-hydroxyethoxy)propanoate (176)**

Tetraethylene glycol (**158**, 3.1 g, 16.1 mmol, 1.0 eq.) was dissolved in dry THF (23 mL) under argon. NaOMe (25% in MeOH, 35.0 μ L, 0.01 eq.) and *t*-butyl acrylate (**170**, 3.5 mL, 24.1 mmol, 1.5 eq.) were added. The reaction mixture was stirred for 48 h at rt before it was terminated by addition of H₂O (20 mL). The aq. phase was extracted with EtOAc (3 x 20 mL). The combined organic phases were washed with a sat. aq. NaCl solution (20 mL), dried over Na₂SO₄, filtered and the solvent was removed *in vacuo*. Silica column chromatography (PE:EtOAc = 1:1) gave the product **176** (2.60 g, 8.05 mmol, 50%) as a colorless oil.

¹H-NMR (400 MHz, CDCl₃): δ 3.73 – 3.58 (m, 18H, 5-H – 6-H), 2.51 (t, J = 6.7 Hz, 1H, 4-H) 1.44 (s, 9H, 1-H) ppm;

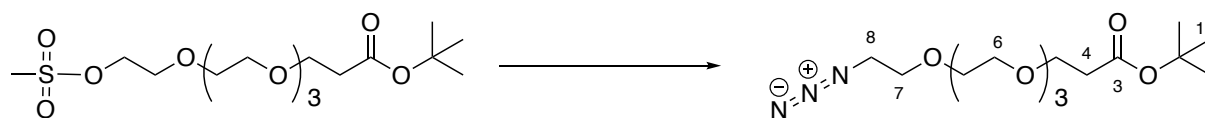
The analytical data are in accordance with those reported in the literature.^[158]

tert-Butyl 3-(2-((methylsulfonyl)oxy)ethoxy)propanoate (S3)

The alcohol **176** (200 mg, 0.62 mmol, 1.0 eq.) and Et₃N (130 μL, 0.93 mmol, 1.5 eq.) were dissolved in CH₂Cl₂ (3.0 mL) and the solution was cooled to 0 °C. Methanesulfonylchloride (60 μL, 0.75 mmol, 1.2 eq.) was added dropwise. The reaction mixture was warmed up to rt and stirred for 18 h before it was terminated by addition of citric acid (0.5 M, 4 mL). EtOAc (10 mL) was added and the aq. phase was separated. The organic phase was washed with a sat. aq. NaHCO₃ solution (10 mL), a sat. aq. NaCl solution (10 mL) and dried over Na₂SO₄. The mixture was filtered, and the solvent was removed *in vacuo*. Silica column chromatography (PE: EtOAc = 2:1) gave the title compound (147 mg, 0.37 mmol, 59%) as a yellow oil.

¹H-NMR (400 MHz, CDCl₃): δ 4.38 (dd, *J* = 5.5, 4.0 Hz, 2H, 8-H), 3.76 (dd, *J* = 5.5, 4.0 Hz, 2H, 7-H), 3.73 – 3.58 (m, 12H, 5-H, 6-H), 3.01 (s, 3H, 9-H), 2.50 (t, *J* = 6.7 Hz, 1H, 4-H) 1.44 (s, 9H, 1-H) ppm;

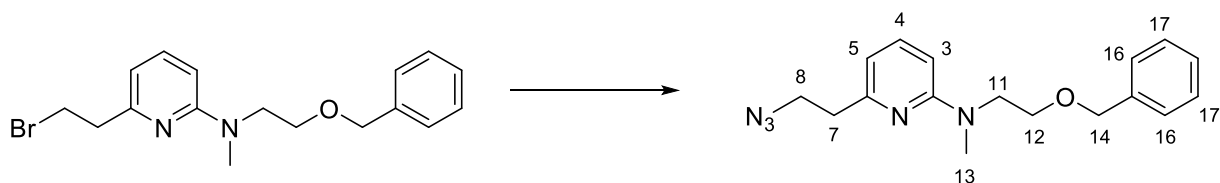
The analytical data are in accordance with those reported in the literature.^[159]

tert-Butyl 3-(2-azidoethoxy)propanoate (177)

The mesylate (146 mg, 0.36 mmol, 1.0 eq.) collected from the previous experiment was dissolved in DMF (1.8 mL) and NaN₃ (35 mg, 0.55 mmol, 1.5 eq.) was added. The reaction mixture was stirred at 60 °C for 18 h. DMF was concentrated *in vacuo* at 60 °C and 7 mbar and taken up in EtOAc (5 mL). The solution was washed with a sat. aq. NH₄Cl solution (3 x 2 mL), dried over Na₂SO₄, filtered and the solvent was removed *in vacuo*. Silica column chromatography (PE:EtOAc = 4:1) gave the azide **177** (100 mg, 0.28 mmol, 79%) as a pale yellow oil.

¹H-NMR (400 MHz, CDCl₃): δ 3.73 – 3.58 (m, 14H, 5-H - 7-H), 3.38 (d, *J* = 5.2 Hz, 2H, 8-H), 2.50 (t, *J* = 6.7 Hz, 1H, 4-H) 1.44 (s, 9H, 1-H) ppm;

The analytical data are in accordance with those reported in the literature.^[158]

6-(2-Azidoethyl)-N-(2-(benzyloxy)ethyl)-N-methylpyridin-2-amine (178)

Under light exclusion and argon, the bromide **157** (200 mg, 0.57 mmol, 1.0 eq.) was dissolved in DMF (2.0 mL) and NaN₃ (55 mg, 0.86 mmol, 1.5 eq.) was added. The mixture was stirred at rt for 18 h. The reaction was terminated by addition of a sat. aq. NH₄Cl solution and the aq. phase was extracted with CH₂Cl₂ (3 x 3 mL). The combined organic phases were dried over Na₂SO₄, filtered and the solvent was removed *in vacuo*. Silica column chromatography PE:EtOAc = 20:1 gave the azide **177** (157 mg, 0.50 mmol, 88%) as a colorless oil.

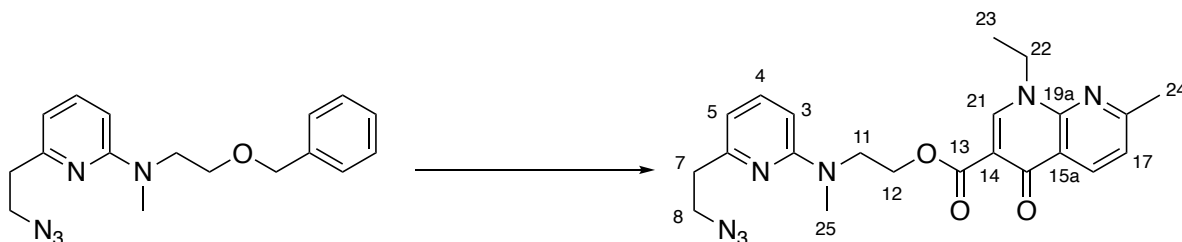
¹H-NMR (400 MHz, CDCl₃): δ 7.36 (t, *J* = 8.0 Hz, 1H, 4-H), 7.35-7.27 (m, 5H, 16-H, 17-H, 18-H), 6.40 (d, *J* = 8.0 Hz, 1H, 3 o. 5-H), 6.36 (d, *J* = 8.5 Hz, 1H, 3 o. 5-H), 4.53 (s, 2H, 14-H), 3.81 (t, *J* = 6.0 Hz, 2H, 11-H), 3.81 (t, *J* = 6.0 Hz, 1H, 11-H), 3.68 (t, *J* = 6.0 Hz, 1H, 12-H), 3.65 (t, *J* = 7.0 Hz, 1H, 8-H), 3.09 (s, 3H, 13-H) 2.87 (t, *J* = 7.0 Hz, 1H, 7-H), ppm;

¹³C-NMR (100 MHz, CDCl₃): δ 158.3 (C-6), 155.9 (C-2), 138.6 (C-15), 137.8 (C-4), 128.5 (C-17), 127.6 (C-16, C-18), 110.9 (C-5), 103.7 (C-3), 73.3 (C-14), 68.5 (C-12), 50.7 (C-8), 48.9 (C-11), 37.5 (C-7 or C-13), 37.4 (C-7 or C-13) ppm;

HRMS (ESI) *m/z* calcd. for [M+Na]⁺: 334.1644; found 334.1650;

R_f(PE:EtOAc = 10:1): 0.45.

2-((6-(2-Azidoethyl)pyridin-2-yl)(methyl)amino)ethyl 1-ethyl-7-methyl-4-oxo-1,4-dihydro-1,8-naphthyridine-3-carboxylate (179)



To a solution of azide **178** (344 mg, 1.11 mmol, 1.2 eq.) in CH_2Cl_2 (150 mL) at $-78\text{ }^\circ\text{C}$ was added BCl_3 (1.0 M in hexane, 11.0 mL, 12.0 eq.) over a period of 15 min. The solution was stirred for 30 min at the same temperature before it was terminated by slow addition of an excess of a sat. aq. NaHCO_3 solution (50 mL) at $0\text{ }^\circ\text{C}$ and followed by warming up to rt. The aq. phase was separated and extracted with CH_2Cl_2 (3 x 100 mL). The combined organic phases were dried over Na_2SO_4 , filtered and the solvent was removed *in vacuo* to yield a yellow residue containing **172** which was directly used for the next step.

Nalidixic acid (**81**, 214 mg, 0.92 mmol, 1.0 eq.) was dissolved in dry CH_2Cl_2 (11 mL). COMU[®] (**109**, 592 mg, 1.4 mmol, 1.5 eq.) and DBU (138 μL , 0.92 mmol, 1.0 eq.) were added and the reaction mixture was stirred for 5 min at rt. The crude residue from the previous step was dissolved in CH_2Cl_2 (3 mL) and added dropwise and the mixture was stirred for 18 h at rt. The reaction was terminated by addition of a sat. aq. Na_2CO_3 solution (10 mL) and extracted with CH_2Cl_2 (3 x 10 mL), washed with a sat. aq. NaCl solution, dried over Na_2SO_2 , filtered and the solvent was removed *in vacuo*. Size exclusion chromatography (Sephadex LH-20 in CH_2Cl_2 , H:30 cm W:2.5 cm) was used to remove the urea derivative **110** followed by silica column chromatography (CH_2Cl_2 :acetone = 100:1 – 10:1; silica loaded with Et_3N). The product **179** (120 mg, 0.28 mmol, 30%) was obtained as a colorless solid.

¹H-NMR (400MHz, CDCl₃): δ 8.64 (d, J = 8.0 Hz, 1H, 16-H), 8.52 (s, 1H, 21-H), 7.37 (t, J = 8.0 Hz, 1H, 4-H), 7.24 (d, J = 8.0 Hz, 1H, 17-H), 6.42 (d, J = 8.0 Hz, 2H, 3-H, 5-H), 4.52 (t, J = 5.8 Hz, 2H, 12-H), 4.43 (q, J = 7.0 Hz, 2H, 22-H), 4.00 (t, J = 5.8 Hz, 2H, 11-H), 3.69 (t, J = 6.6 Hz, 2H, 8-H), 3.17 (s, 3H, 25-H), 2.87 (t, J = 6.6 Hz, 2H, 7-H), 2.65 (s, 3H, 24-H), 1.43 (t, J = 7.0 Hz, 1H, 23-H), ppm;

¹³C-NMR (100 MHz, CDCl₃): δ 174.8 (C-15), 165.6 (C-13), 162.8 (C-19a), 158.3 (C-2), 156.0 (C-6), 149.0 (C-18), 148.8 (C-21), 137.8 (C-4), 137.0 (C-16), 121.7 (C-15a), 121.4 (C-17), 111.2 (C-5 o. C-3), 103.9 (C5 o. C3), 62.9 (C-12), 50.8 (C-8), 48.7 (C-11), 46.8 (C-22), 37.3 (C-7), 37.2 (C-25), 25.3 (C-24), 15.4 (C-23) ppm; *

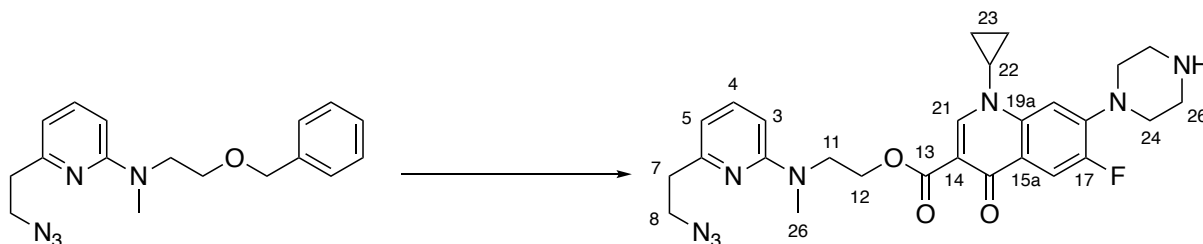
HRMS (ESI) m/z calcd. for [M+Na]⁺: 458.1917; found 458.1912;

R_f (EtOAc:acetone = 10:1): 0.5;

T_m (decomp): 83 °C.

*C-14 could not be detected in the ¹³C-NMR spectrum.

2-((6-(2-Azidoethyl)pyridin-2-yl)(methyl)amino)ethyl 1-cyclopropyl-6-fluoro-4-oxo-7-(piperazin-1-yl)-1,4-dihydroquinoline-3-carboxylate (180)



To a solution of azide **178** (156 mg, 0.50 mmol, 1.2 eq.) in CH_2Cl_2 (50 mL) at $-78\text{ }^\circ\text{C}$ was added BCl_3 (1.0 M in hexane, 5.0 mL, 12 eq.) over a period of 15 min. The solution was stirred for 30 min at the same temperature before it was terminated by slow addition of an excess of a sat. aq. NaHCO_3 solution at $0\text{ }^\circ\text{C}$ followed by warming up to rt. The aq. phase was separated and extracted with CH_2Cl_2 (3 x 30 mL). The combined organic phases were dried over Na_2SO_4 , filtered and the solvent was removed *in vacuo* to yield a yellow residue containing **172** which was directly used for the next step.

Boc-protected ciprofloxacin **123** (178 mg, 0.41 mmol, 1.0 eq.) was dissolved in dry CH_2Cl_2 (4.0 mL). $\text{COMU}^{\text{®}}$ (**109**, 265 mg, 0.62 mmol, 1.5 eq.) and DBU (62.0 μL , 0.41 mmol, 1.0 eq.) were added and the reaction mixture was stirred for 5 min at rt. The crude residue from the previous step was dissolved in CH_2Cl_2 (1.0 mL) and added dropwise. The mixture was stirred for 18 h at rt before the reaction was terminated by addition of a sat. aq. Na_2CO_3 solution (3 mL). The aq. phase was extracted with CH_2Cl_2 (2 x 3 mL). The combined organic phases were washed with a sat. aq. NaCl solution, dried over Na_2SO_2 , filtered and the solvent was removed *in vacuo*. Silica column chromatography (CH_2Cl_2 :acetone = 100:1 – 1:1) was employed to remove major impurities.

The residue was dissolved in CH_2Cl_2 (6 mL) and TFA (0.5 mL) was added at $0\text{ }^\circ\text{C}$. The mixture was stirred for 1 h during which it was allowed to warm to rt. The reaction was terminated by addition of a sat. aq. NaHCO_3 solution until gas evolution terminated. The aq. phase was extracted with CH_2Cl_2 (2 x 3 mL). The combined organic phases were washed with a sat. aq. NaCl solution, dried over Na_2SO_2 , filtered and the solvent was removed *in vacuo*. Silica column chromatography (CH_2Cl_2 :MeOH = 100:1 – 5:1) gave the product **180** (20 mg, 0.04 mmol, 9%) as a colorless solid.

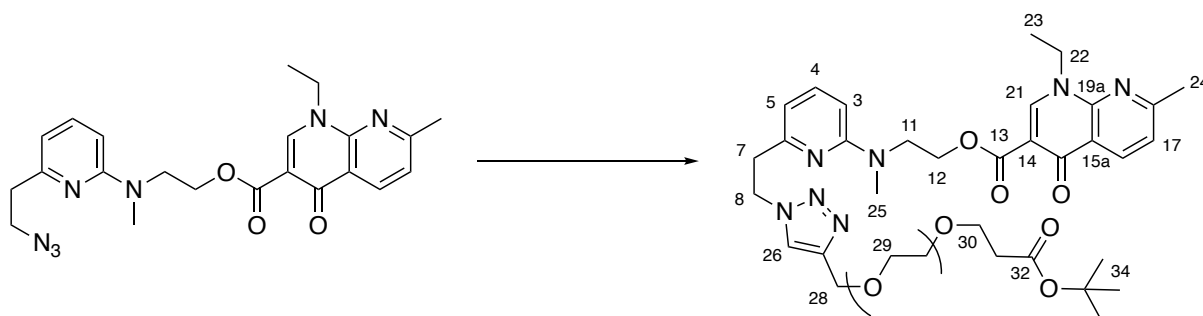
¹H-NMR (600 MHz, DMSO-d₆): δ 8.33 (s, 1H, 21-H), 7.81 (d, $J = 13.0$ Hz, 1H, 16-H), 7.45 (d, $J = 7.2$ Hz, 1H, 18-H), 7.44 (dd, $J = 8.6, 7.2$ Hz, 1H, 4-H), 6.53 (d, $J = 8.6$ Hz, 1H, 3-H), 6.48 (d, $J = 7.2$ Hz, 1H, 5-H), 4.35 (t, $J = 5.5$ Hz, 2H, 12-H), 3.89 (t, $J = 5.5$ Hz, 2H, 11-H), 3.65 (t, $J = 6.7$ Hz, 2H, 8-H), 3.70 - 3.60 (m, 1H, 22-H), 3.42 - 3.38 (m, 4H, 24-H), 3.28 - 3.23 (m, 4H, 25-H), 3.09 (s, 3H, 26-H), 2.79 (t, $J = 6.7$ Hz, 2H, 7-H), 1.27 - 1.19 (m, 2H, 23a-H), 1.02 - 0.98 (m, 2H, 23b-H) ppm;

¹³C-NMR (125 MHz, DMSO-d₆): 172.1 (C-15), 164.6 (C-13), 158.2 (C-2), 156.1 (C-6), 152.9 (d, $J = 246$ Hz, C-17), 148.8 (C-21), 143.5 (d, $J = 11$ Hz, C-18), 138.4 (C-19a), 138.3 (C-4), 122.5 (d, $J = 7$ Hz, C-15a), 112.3 (d, $J = 23$ Hz, C-16), 111.3 (C-5), 107.1 (d, $J = 3$ Hz, C-19), 104.0 (C-3), 62.3 (C-12), 50.1 (C-8), 48.4 (C-11), 47.7 (C-24), 43.6 (C-25), 37.1 (C-26), 36.9 (C-7), 35.2 (C-22), 8.0 (C-23) ppm;*

HRMS (ESI) m/z calcd. for [M+Na]⁺: 557.2401; found 557.2399.

*C-14 could not be detected in the ¹³C-NMR spectrum.

2-((6-(2-(4-(19,19-Dimethyl-17-oxo-2,5,8,11,14,18-hexaoxaicosyl)-1H-1,2,3-triazol-1-yl)ethyl)pyridin-2-yl)(methyl)amino)ethyl 1-ethyl-7-methyl-4-oxo-1,4-dihydro-1,8-naphthyridine-3-carboxylate (181)



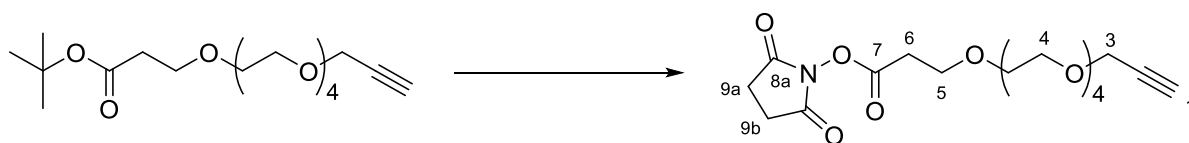
The azide **179** (22 mg, 0.05 mmol, 1.0 eq.) and the alkyne **175** (18 mg, 0.05 mmol, 1.0 eq.) were dissolved in THF (1.0 mL) at 0 °C. H₂O (1.0 mL), sodium ascorbate (3.0 mg, 0.02 mmol, 0.3 eq.) and copper sulfate (2.5 mg, 0.01 mmol, 0.2 eq.) were added. The reaction was stirred for 1 h at 0 °C before it was terminated by addition of a sat. aq. NaHCO₃ solution (1 mL). The mixture was extracted with EtOAc (3 x 1 mL) and the combined organic phases were washed with a sat. aq. NaCl solution (1 mL), dried over Na₂SO₄, filtered and the solvent was removed *in vacuo*. Silica column chromatography (CH₂Cl₂: acetone 1:0 – 3:2; silica loaded with Et₃N) gave the product **181** (22.7 mg, 0.03 mmol, 57%).

¹H-NMR (400MHz, DMSO-d₆): δ 8.69 (s, 1H, 21-H), 8.45 (d, *J* = 8.0 Hz, 1H, 16-H), 8.01 (s, 1H, 26-H), 7.41 (d, *J* = 8.0 Hz, 1H, 17-H), 7.39 (dd, *J* = 8.4, 7.3 Hz, 1H, 4-H), 6.52 (d, *J* = 8.4 Hz, 1H, 3-H), 6.39 (d, *J* = 7.3 Hz, 1H, 5-H), 4.71 (t, *J* = 7.6 Hz, 2H, 8-H), 4.46 (s, 2H, 28-H), 4.41 (q, *J* = 7.0 Hz, 1H, 22-H), 4.37 (t, *J* = 5.8 Hz, 2H, 12-H), 3.89 (t, *J* = 5.8 Hz, 2H, 11-H), 3.56 (t, *J* = 7.6 Hz, 2H, 30-H), 3.48 (m, 16H, 29-H), 3.12 (t, *J* = 7.0 Hz, 2H, 7-H), 3.09 (s, 3H, 25-H), 2.63 (s, 3H, 24-H), 2.39 (t, *J* = 7.0 Hz, 2H, 31-H), 1.37 (s, 9H, 34-H), 1.34 (t, *J* = 7.0 Hz, 1H, 23-H) ppm;

¹³C-NMR (100 MHz, DMSO-d₆): δ 173.1 (C-15), 170.4 (C-32), 164.2 (C-13), 162.5 (C-18), 157.7 (C-2), 155.0 (C-6), 149.3 (C-21), 148.2 (C-19a), 143.6 (C-27), 137.8 (C-4), 136.1 (C-16), 123.8 (C-26), 121.2 (C-17), 120.6 (C-15a), 110.8, 110.6 (C-5), 103.6 (C-3), 79.7, 69.7, 69.4, 69.6, 68.8, 66.2, 63.4, 61.8 (C-12), 48.4 (C-8), 47.9 (C-11), 45.7 (C-13 or C-22), 45.7 (C-13 or C-22), 37.4, 36.6 (C-25), 35.8 (C-7), 27.7 (C-33), 24.7 (C-24), 14.8 (C-23) ppm;

HRMS (ESI) *m/z* calcd. for [M+Na]⁺: 818.4065; found 818.4052;

HPLC-UV (ACN : H₂O + 0.1% FA = 15% - 40% for 4 min; 40% - 100% for 0.2 min; 100% for 1.1 min, 100% - 15% for 0.7 min): *t_R* (**181**) = 3.99 min, *t_R* (**81**) = 2.30 min, λ = 256 nm.

2,5-dioxopyrrolidin-1-yl 3-(2-(prop-2-yn-1-yloxy)ethoxy)propanoate (182)

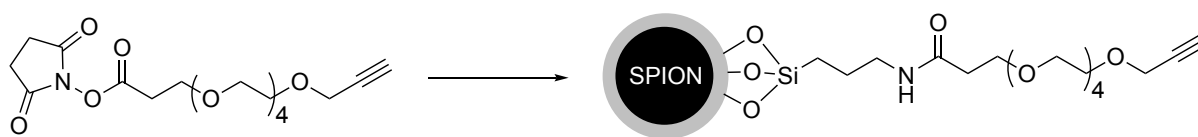
The *tert*-butyl ester **175** (4.55 g, 12.6 mmol, 1.0 eq.) was dissolved in MeOH (30 mL) and NaOH (3 M in H₂O, 30 mL). The reaction mixture was warmed to 40 °C and stirred for 1 h at this temperature. MeOH was removed under reduced pressure and the aq. phase was acidified to pH = 2 with HCl (2 M in H₂O). A sat. aq. NaCl solution (50 mL) was added and the mixture was extracted with EtOAc (3 x 50 mL). The combined organic phases were dried over Na₂SO₄, filtered and the solvent was removed *in vacuo*. The residue was dissolved in CH₂Cl₂ (50 mL). *N*-hydroxysuccinimide (1.62 g, 14.1 mmol, 1.12 eq.) and EDC·HCl (2.80 g, 14.6 mmol, 1.15 eq.) were added and the mixture was stirred at rt for 6 h. The reaction was terminated by addition of H₂O (30 mL). The organic phase was separated, and the aq. phase was extracted with CH₂Cl₂ (2 x 30 mL). The combined organic phases were dried over Na₂SO₄, filtered and the solvent was removed under reduced pressure. The NHS-ester **182** (5.0 g, 12.4 mmol, 99% o2s) was obtained as a pale yellow oil.

¹H-NMR (400 MHz, CDCl₃): δ 4.19 (d, *J* = 2.3 Hz, 2H, 3-H), 3.83 (t, *J* = 6.6 Hz, 2H, 5-H), 3.70 – 3.62 (m, 16H, 4-H), 2.89 (t, *J* = 6.6 Hz, 2H, 6-H), 2.83 (bs, 4H, 9-H), 2.43 (t, *J* = 2.3 Hz, 1H, 1-H) ppm;

¹³C-NMR (100 MHz, CDCl₃): δ 169.1 (2C, C-8), 166.8 (C-7), 79.8 (C-2), 74.6 (C-1), 70.8 (2C, C-4), 70.7 (3C, C-4) 70.6 (2C, C-4), 69.2 (C-4), 65.8 (C-5), 58.5 (C-3), 32.3 (C-6), 25.7 (C-9) ppm;

R_f(EtOAc:acetone= 4:1): 0.6;

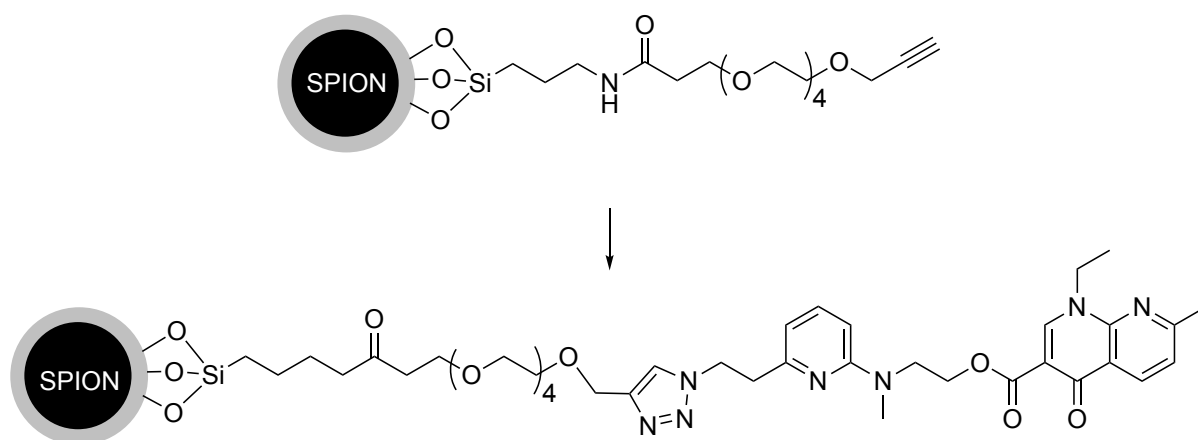
HRMS (ESI) *m/z* calcd. for [M+Na]⁺: 424.1584; found 424.1581.

SPION@alkyne (186b)

The NHS ester **182** (1.55 g, 3.87 mmol, 1.2 eq.) was dissolved in dry THF (8 mL). APTES (**46**, 0.8 mL, 3.2 mmol, 1.0 eq.) was added and the mixture was stirred at rt for 1 h. The solvent was removed *in vacuo*. Silica column chromatography (EtOAc:acetone =1:0 - 4:1) was performed to remove residual APTES **46**.

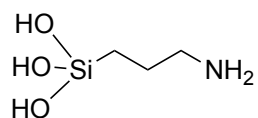
MagSilica[®] SPIONs were heated to 150 °C for 3 h *in vacuo*. 25 mg of this preheated SPIONs were mixed with toluene (2 mL) containing Et₃N (20 μL) and heated under magnetic stirring without a magnetic stirrbar for 72 h at 65 °C. The SPIONs@alkyne were fixed with a magnet, washed with toluene (3 x 2 mL) and MeOH (3 x 2 mL) and dried *in vacuo* for 18 h.

FTIR: $\lambda = 3281, 2864$ (alkane, C-H stretching), 1637 (amide, C=O stretching), 1550 (amide, N-H bending), 1443, 1348 (C-N, stretching), 1196, 1080 (C-O-C, stretching), 1028, 546, 432 cm^{-1} .

SPION@nalidixic acid (187b)

Under an argon atmosphere SPION@alkyne **186b** (20 mg) was mixed with THF (1 mL) in an EPPENDORF Tube[®] and cooled to 0 °C. H₂O (200 μL), sodium ascorbate (3.0 mg, 0.14 mmol) and CuSO₄ (2.0 mg, 0.09 mmol) were added, and the mixture was shaken with an IKA VXR Vibrax[®] shaker equipped with an IKA VX5 at 300 rpm for 18 h at rt. The SPIONs@nalidixic acid were fixed with a magnet, washed with MeOH (5 x 2 mL) and dried *in vacuo* for 18 h.

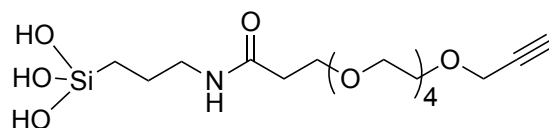
FTIR: $\lambda = 3294, 2870$ (alkane, C-H stretching), 1720 (C=O stretching), 1618 (amide, C=O stretching), 1591, 1560, 1545 (amide, N-H bending), 1491, 1441 (aromatic, C=C, stretching), 1364 (C-N, stretching), 1203, 1086 (C-O-C, stretching), 800, 548, 441 cm⁻¹.

(3-Aminopropyl)silanetriol (190)

SPION@amine **185** (2.0 mg) was mixed with H₂O:DMSO = 10:1 (0.5 mL) in an EPPENDORF tube[®] and heated to 95 °C for 24 h. The SPIONs were fixed with a magnet and the solution was analyzed by LCMS.

HRMS (ESI) m/z calcd. for [M+ H]⁺: 138.0586; found 138.0584;

HPLC-MS (ACN : H₂O + 0.1% FA = 15% - 40% for 4 min; 40% - 100% for 0.2 min; 100% for 1.1 min, 100% - 15% for 0.2 min): $t_R = t_0$.

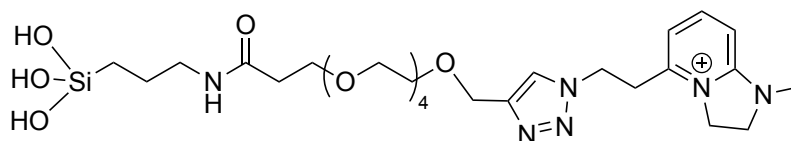
3-(2-(Prop-2-yn-1-yloxy)ethoxy)-N-(3-(trihydroxysilyl)propyl)propenamide (191)

SPION@lakyne **187a** (2.0 mg) was mixed with H₂O:DMSO = 10:1 (0.5 mL) in an EPPENDORF tube[®] and heated to 95 °C for 24 h. The SPIONs were fixed with a magnet and the solution was analyzed by LCMS.

HPLC-MS (ACN : H₂O + 0.1% FA = 15% - 40% for 4 min; 40% - 100% for 0.2 min; 100% for 1.1 min, 100% - 15% for 0.2 min): $t_R = 2.10$ min.

MSMS {446.03 [M+Na]⁺}: 428.1, 406.1, 255.1, 215.1, 196.0.

1-Methyl-5-(2-(4-((2-((3-oxo-7-(trihydroxysilyl)heptyl)oxy)ethoxy)methyl)-1H-1,2,3-triazol-1-yl)ethyl)-2,3-dihydro-1H-imidazo[1,2-a]pyridin-4-ium (192)



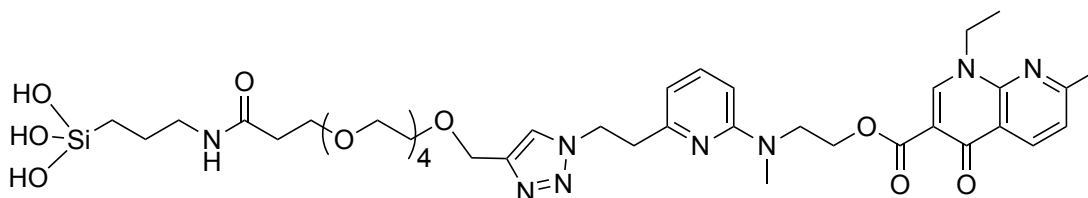
SPION@nalidixic acid **187b** (0.6 mg) was mixed with H₂O:DMSO = 10:1 (0.5 mL) in an EPPENDORF tube[®] and heated to 95 °C for 24 h. The SPIONs were fixed with a magnet and the solution was analyzed by LCMS.

HRMS (ESI) m/z calcd. for [M]⁺: 627.3174; found 627.3174;

HPLC-MS (ACN : H₂O + 0.1% FA = 15% - 40% for 4 min; 40% - 100% for 0.2 min; 100% for 1.1 min, 100% - 15% for 0.2 min): t_R = 1.64 min.

MSMS {627.05[M]⁺}: 599.3, 408.2,, 214.1, 174.1, 161.1, 148.1, 147.1.

2-(Methyl(6-(2-(4-((2-((3-oxo-7-(trihydroxysilyl)heptyl)oxy)ethoxy)methyl)-1H-1,2,3-triazol-1-yl)ethyl)pyridin-2-yl)amino)ethyl 1-ethyl-7-methyl-4-oxo-1,4-dihydro-1,8-naphthyridine-3-carboxylate (193)



SPION@nalidixic acid **187b** (0.6 mg) was mixed with H₂O:DMSO = 10:1 (0.5 mL) in an EPPENDORF tube[®] and heated to 95 °C for 30 min. The SPIONs were fixed with a magnet and the solution was analyzed by LCMS.

HRMS (ESI) m/z calcd. for [M+Na]⁺: 818.4065; found 818.4052;

HPLC-MS (ACN : H₂O + 0.1% FA = 15% - 40% for 4 min; 40% - 100% for 0.2 min; 100% for 1.1 min, 100% - 15% for 0.2 min): t_R = 3.19 min.

10 Literature

- [1] D. J. Newman, G. M. Cragg, *J. Nat. Prod.* **2020**, *83*, 770–803.
- [2] L. Katz, R. H. Baltz, *J. Ind. Microbiol. Biotechnol.* **2016**, *43*, 155–176.
- [3] A. E. Yñíguez-Gutierrez, B. O. Bachmann, *J. Med. Chem.* **2019**, *62*, 8412–8428.
- [4] P. M. Wright, I. B. Seiple, A. G. Myers, *Angew. Chem. Int. Ed.* **2014**, *53*, 8840–8869.
- [5] J. E. Sears, D. L. Boger, *Acc. Chem. Res.* **2015**, *48*, 653–662.
- [6] R. J. Melander, A. K. Basak, C. Melander, *Nat. Prod. Rep.* **2020**, *37*, 1454–1477.
- [7] A. Kirschning, F. Taft, T. Knobloch, *Org. Biomol. Chem.* **2007**, *5*, 3245.
- [8] J. Kennedy, *Nat. Prod. Rep.* **2008**, *25*, 25–34.
- [9] K. L. Rinehart, *Pure Appl. Chem.* **1977**, *49*, 1361–1384.
- [10] E. Higashide, M. Asai, K. Ootsu, S. Tanida, Y. Kozai, T. Hasegawa, T. Kishi, Y. Sugino, M. Yoneda, *Nature* **1977**, *270*, 721–722.
- [11] S. M. Kupchan, Y. Komoda, W. A. Court, G. J. Thomas, R. M. Smith, A. Karim, C. J. Gilmore, R. C. Haltiwanger, R. F. Bryan, *J. Am. Chem. Soc.* **1972**, *94*, 1354–1356.
- [12] M. C. Wani, H. L. Taylor, M. E. Wall, *J. Chem. Soc., Chem. Commun.* **1973**, 390.
- [13] R. G. Powell, D. Weisleder, C. R. Smith, *J. Org. Chem.* **1981**, *46*, 4398–4403.
- [14] K. Sakai, T. Ichikawa, K. Yamada, M. Yamashita, M. Tanimoto, A. Hikita, Y. Ijuin, K. Kondo, *J. Nat. Prod.* **1988**, *51*, 845–850.
- [15] K. Suwanborirux, C.-J. Chang, R. W. Spjut, J. M. Cassady, *Experientia* **1990**, *46*, 117–120.
- [16] S. Kusari, M. Lamshöft, P. Kusari, S. Gottfried, S. Zühlke, K. Louven, U. Hentschel, O. Kayser, M. Spittler, *J. Nat. Prod.* **2014**, *77*, 2577–2584.
- [17] J. M. Cassady, K. K. Chan, H. G. Floss, E. Leistner, *Chem. Pharm. Bull.* **2004**, *52*, 1–26.
- [18] K. L. Rinehart, L. S. Shield, in *Fortschritte Der Chemie Organischer Naturstoffe / Progress in the Chemistry of Organic Natural Products* (Eds.: W. Herz, H. Grisebach, G.W. Kirby), Springer Vienna, Vienna, **1976**, pp. 231–307.

- [19] A. E. Prota, K. Bargsten, J. F. Diaz, M. Marsh, C. Cuevas, M. Liniger, C. Neuhaus, J. M. Andreu, K.-H. Altmann, M. O. Steinmetz, *Proc. Nat. Acad. Sci.* **2014**, *111*, 13817–13821.
- [20] M. J. R. Ravry, G. A. Omura, R. Birch, *Am. J. Clin. Oncol.* **1985**, *8*, 148–150.
- [21] B. Boyraz, M. A. N. Sendur, S. Aksoy, T. Babacan, E. C. Roach, M. C. Kizilarlanoglu, I. Petekkaya, K. Altundag, *Curr. Med. Res. Opin.* **2013**, *29*, 405–414.
- [22] K. Seidel, A. Balakrishnan, C. Alexiou, C. Janko, R.-M. Komoll, L.-L. Wang, A. Kirschning, M. Ott, *Chem. Eur. J.* **2017**, *23*, 12326–12337.
- [23] S. Ullah, K. Seidel, S. Türkkan, D. P. Warwas, T. Dubich, M. Rohde, H. Hauser, P. Behrens, A. Kirschning, M. Köster, D. Wirth, *J. Control. Release* **2019**, *294*, 327–336.
- [24] S. M. Kupchan, Y. Komoda, A. R. Branfman, R. G. Dailey, V. A. Zimmerly, *J. Am. Chem. Soc.* **1974**, *96*, 3706–3708.
- [25] S. M. Kupchan, A. T. Sneden, A. R. Branfman, G. A. Howie, L. I. Rebhun, W. E. McIvor, R. W. Wang, T. C. Schnaitman, *J. Med. Chem.* **1978**, *21*, 31–37.
- [26] A. Kawai, H. Akimoto, N. Hashimoto, H. Nomura, *Chem. Pharm. Bull.* **1984**, *32*, 2194–2199.
- [27] S. Eichner, T. Knobloch, H. G. Floss, J. Fohrer, K. Harmrolfs, J. Hermene, A. Schulz, F. Sasse, P. Spitteller, F. Taft, A. Kirschning, *Angew. Chem. Int. Ed.* **2012**, *51*, 752–757.
- [28] F. Taft, M. Brünjes, H. G. Floss, N. Czempinski, S. Grond, F. Sasse, A. Kirschning, *ChemBioChem* **2008**, *9*, 1057–1060.
- [29] T. Knobloch, K. Harmrolfs, F. Taft, B. Thomaszewski, F. Sasse, A. Kirschning, *ChemBioChem* **2011**, *12*, 540–547.
- [30] A. T. Sneden, G. L. Beemsterboer, *J. Nat. Prod.* **1980**, *43*, 637–640.
- [31] F. Mandelbaum-Shavit, M. K. Wolpert-DeFilippes, D. G. Johns, *Biochem. Biophys. Res. Commun.* **1976**, *72*, 47–54.
- [32] H. G. Floss, T.-W. Yu, K. Arakawa, *J. Antibiot.* **2011**, *64*, 35–44.
- [33] C. G. Kim, A. Kirschning, P. Bergon, Y. Ahn, J. J. Wang, M. Shibuya, H. G. Floss, *J. Am. Chem. Soc.* **1992**, *114*, 4941–4943.
- [34] C.-G. Kim, A. Kirschning, P. Bergon, P. Zhou, E. Su, B. Sauerbrei, S. Ning, Y. Ahn,

- M. Breuer, E. Leistner, H. G. Floss, *J. Am. Chem. Soc.* **1996**, *118*, 7486–7491.
- [35] T.-W. Yu, L. Bai, D. Clade, D. Hoffmann, S. Toelzer, K. Q. Trinh, J. Xu, S. J. Moss, E. Leistner, H. G. Floss, *Proc. Natl. Acad. Sci.* **2002**, *99*, 7968–7973.
- [36] S. J. Admiraal, C. T. Walsh, C. Khosla, *Biochemistry* **2001**, *40*, 6116–6123.
- [37] B. J. Carroll, S. J. Moss, L. Bai, Y. Kato, S. Toelzer, T.-W. Yu, H. G. Floss, *J. Am. Chem. Soc.* **2002**, *124*, 4176–4177.
- [38] F. Taft, M. Brünjes, T. Knobloch, H. G. Floss, A. Kirschning, *J. Am. Chem. Soc.* **2009**, *131*, 3812–3813.
- [39] P. Spiteller, L. Bai, G. Shang, B. J. Carroll, T.-W. Yu, H. G. Floss, *J. Am. Chem. Soc.* **2003**, *125*, 14236–14237.
- [40] C.-G. Kim, T.-W. Yu, C. B. Fryhle, S. Handa, H. G. Floss, *J. Biol. Chem.* **1998**, *273*, 6030–6040.
- [41] S. Eichner, T. Eichner, H. G. Floss, J. Fohrer, E. Hofer, F. Sasse, C. Zeilinger, A. Kirschning, *J. Am. Chem. Soc.* **2012**, *134*, 1673–1679.
- [42] K. Harmrolfs, L. Mancuso, B. Drung, F. Sasse, A. Kirschning, *Beilstein J. Org. Chem.* **2014**, *10*, 535–543.
- [43] S. Eichner, H. G. Floss, F. Sasse, A. Kirschning, *Chem. Eur. J. of Chem. Bio.* **2009**, *10*, 1801–1805.
- [44] I. Bułyszko, G. Dräger, A. Klenge, A. Kirschning, *Chem. Eur. J.* **2015**, *21*, 19231–19242.
- [45] F. Wesemann, A. Heutling, P. Wienecke, A. Kirschning, *ChemBioChem* **2020**, *21*, 2927–2930.
- [46] N. Li, S. Chen, Z. Yan, J. Han, Y. Ta, T. Pu, Y. Wang, *Front. Microbiol.* **2021**, *12*, 703093.
- [47] J. Hermane, Synthetische Und Mutasynthetische Zugänge Zu Neuen Hsp90 Inhibitoren, Dissertation, University of Hanover, **2013**
- [48] T. J. Maimone, S. L. Buchwald, *J. Am. Chem. Soc.* **2010**, *132*, 9990–9991.
- [49] S. W. Wright, D. L. Hageman, A. S. Wright, L. D. McClure, *Tetrahedron Lett.* **1997**,

38, 7345–7348.

- [50] K. Munk, P. Dersch, B. Eikmanns, M. Eikmanns, R. Fischer, D. Jahn, M. Jahn, R. Nethe-Jaenchen, N. Requena, B. Schultze, Eds. , *Mikrobiologie: 43 Tabellen*, Georg Thieme Verlag, Stuttgart New York, **2018**.
- [51] K. Hatano, E. Higashide, S. Akiyama, M. Yoneda, *Agric. Biol. Chem.* **1984**, *48*, 1721–1729.
- [52] T. Knobloch, Studien Zur Flexibilität Der Ansamitocin-Biosynthese in *Actinosynnema Pretiosum*, Dissertation, University of Hanover, **2010**.
- [53] J. Lin, L. Bai, Z. Deng, J.-J. Zhong, *Bioresour. Technol.* **2011**, *102*, 1863–1868.
- [54] J. Lin, J.-J. Zhong, *Bioprocess. Biosyst. Eng.* **2017**, *40*, 1133–1139.
- [55] Z. Du, J. Zhong, *Biotechnol. Bioeng.* **2018**, *115*, 2456–2466.
- [56] Z.-Q. Du, Y. Zhang, Z.-G. Qian, H. Xiao, J.-J. Zhong, *Biotechnol. Bioeng.* **2017**, *114*, 2794–2806.
- [57] R. Eibl, S. Werner, D. Eibl, in *Disposable Bioreactors* (Eds.: R. Eibl, D. Eibl), Springer Berlin Heidelberg, Berlin, Heidelberg, **2009**, pp. 55–87.
- [58] M. I. Hutchings, A. W. Truman, B. Wilkinson, *Curr. Opin. Microbiol.* **2019**, *51*, 72–80.
- [59] S. E. Rossiter, M. H. Fletcher, W. M. Wuest, *Chem. Rev.* **2017**, *117*, 12415–12474.
- [60] M. J. Hajipour, K. M. Fromm, A. Akbar Ashkarran, D. Jimenez de Aberasturi, I. R. de Larramendi, T. Rojo, V. Serpooshan, W. J. Parak, M. Mahmoudi, *Trends Biotechnol.* **2012**, *30*, 499–511.
- [61] P. Jelinkova, A. Mazumdar, V. P. Sur, S. Kociova, K. Dolezelikova, A. M. J. Jimenez, Z. Koudelkova, P. K. Mishra, K. Smerkova, Z. Heger, M. Vaculovicova, A. Moulick, V. Adam, *J. Control. Release* **2019**, *307*, 166–185.
- [62] O. I. Parisi, L. Scrivano, M. S. Sinicropi, F. Puoci, *Curr. Opin. Pharmacol.* **2017**, *36*, 72–77.
- [63] K. Divya, S. Vijayan, T. K. George, M. S. Jisha, *Fibers Polym.* **2017**, *18*, 221–230.
- [64] J. P. Ruparelia, A. K. Chatterjee, S. P. Duttgupta, S. Mukherji, *Acta Biomater.* **2008**,

4, 707–716.

- [65] A. N. Brown, K. Smith, T. A. Samuels, J. Lu, S. O. Obare, M. E. Scott, *Appl. Environ. Microbiol.* **2012**, *78*, 2768–2774.
- [66] M. Vert, Y. Doi, K.-H. Hellwich, M. Hess, P. Hodge, P. Kubisa, M. Rinaudo, F. Schué, *Pure Appl. Chem.* **2012**, *84*, 377–410.
- [67] K. Ohno, M. Tanaka, J. Takeda, Y. Kawazoe, *Nano- and Micromaterials*, Springer, Berlin, **2008**.
- [68] J. Kreuter, *J. Microencapsul.* **1988**, *5*, 115–127.
- [69] H. M. E. Azzazy, M. M. H. Mansour, *Clin. Chim. Acta* **2009**, *403*, 1–8.
- [70] V. C. Pierre, M. J. Allen, Eds. , *Contrast Agents for MRI: Experimental Methods*, Royal Society Of Chemistry, Cambridge, **2017**.
- [71] V. I. Shubayev, T. R. Pisanic, S. Jin, *Adv. Drug Deliv. Rev.* **2009**, *61*, 467–477.
- [72] S. M. Dadfar, K. Roemhild, N. I. Drude, S. von Stillfried, R. Knüchel, F. Kiessling, T. Lammers, *Adv. Drug Deliv. Rev.* **2019**, *138*, 302–325.
- [73] G. Chen, I. Roy, C. Yang, P. N. Prasad, *Chem. Rev.* **2016**, *116*, 2826–2885.
- [74] A. Puri, K. Loomis, B. Smith, J.-H. Lee, A. Yavlovich, E. Heldman, R. Blumenthal, *Crit. Rev. Ther. Drug Carrier Syst.* **2009**, *26*, 523–580.
- [75] B. L. Banik, P. Fattahi, J. L. Brown, *WIREs Nanomed. Nanobiotechnol.* **2016**, *8*, 271–299.
- [76] Y. Wang, Q. Zhao, N. Han, L. Bai, J. Li, J. Liu, E. Che, L. Hu, Q. Zhang, T. Jiang, S. Wang, *Nanomed.: Nanotechnol. Biol. Med.* **2015**, *11*, 313–327.
- [77] W. Yang, H. Liang, S. Ma, D. Wang, J. Huang, *SM&T* **2019**, *22*, e00109.
- [78] K. S. Park, X. Sun, M. E. Aikins, J. J. Moon, *Adv. Drug Deliv. Rev.* **2021**, *169*, 137–151.
- [79] M. D. Norris, K. Seidel, A. Kirschning, *Adv. Therap.* **2019**, *2*, 1800092.
- [80] A. E. Deatsch, B. A. Evans, *J. Magn. Magn. Mater.* **2014**, *354*, 163–172.
- [81] S. Laurent, D. Forge, M. Port, A. Roch, C. Robic, L. Vander Elst, R. N. Muller, *Chem.*

Rev. **2008**, *108*, 2064–2110.

[82] S. P. Pujari, L. Scheres, A. T. M. Marcelis, H. Zuilhof, *Angew. Chem. Int. Ed.* **2014**, *53*, 6322–6356.

[83] G. E. Fryxell, S. V. Mattigod, Y. Lin, H. Wu, S. Fiskum, K. Parker, F. Zheng, W. Yantasee, T. S. Zemanian, R. S. Addleman, J. Liu, K. Kemner, S. Kelly, X. Feng, *J. Mater. Chem.* **2007**, *17*, 2863.

[84] B. D. Cullity, C. D. Graham, *Introduction to Magnetic Materials*, John Wiley & Sons, Inc., Hoboken, NJ, USA, **2008**.

[85] A. Riedinger, P. Guardia, A. Curcio, M. A. Garcia, R. Cingolani, L. Manna, T. Pellegrino, *Nano Lett.* **2013**, *13*, 2399–2406.

[86] M. Arakha, S. Pal, D. Samantarrai, T. K. Panigrahi, B. C. Mallick, K. Pramanik, B. Mallick, S. Jha, *Sci Rep* **2015**, *5*, 14813.

[87] G. Subbiahdoss, S. Sharifi, D. W. Grijpma, S. Laurent, H. C. van der Mei, M. Mahmoudi, H. J. Busscher, *Acta Biomaterialia* **2012**, *8*, 2047–2055.

[88] L. M. Armijo, S. J. Wawrzyniec, M. Kopciuch, Y. I. Brandt, A. C. Rivera, N. J. Withers, N. C. Cook, D. L. Huber, T. C. Monson, H. D. C. Smyth, M. Osiński, *J. Nanobiotechnol.* **2020**, *18*, 35.

[89] H. Park, H.-J. Park, J. A. Kim, S. H. Lee, J. H. Kim, J. Yoon, T. H. Park, *J. Microbiol. Methods* **2011**, *84*, 41–45.

[90] T.-K. Nguyen, H. T. T. Duong, R. Selvanayagam, C. Boyer, N. Barraud, *Sci. Rep.* **2015**, *5*, 18385.

[91] M. Z. Hussein, S. Al Ali, B. Geilich, M. El Zowalaty, T. Webster, *Int. J. Nanomedicine* **2014**, 3801.

[92] P. Bhattacharya, S. Neogi, *Mater. Res. Express* **2017**, *4*, 095005.

[93] W. Zhang, X. Shi, J. Huang, Y. Zhang, Z. Wu, Y. Xian, *ChemPhysChem* **2012**, *13*, 3388–3396.

[94] H. Gu, P. L. Ho, E. Tong, L. Wang, B. Xu, *Nano Lett.* **2003**, *3*, 1261–1263.

[95] S. Hajdu, J. Holinka, S. Reichmann, A. M. Hirschl, W. Graninger, E. Presterl,

Antimicrob. Agents Chemother. **2010**, *54*, 4078–4084.

- [96] H. C. Kolb, M. G. Finn, K. B. Sharpless, *Angew. Chem. Int. Ed.* **2001**, *40*, 2004–2021.
- [97] H. C. Kolb, K. B. Sharpless, *Drug Discov. Today* **2003**, *8*, 1128–1137.
- [98] S. Bräse, C. Gil, K. Knepper, V. Zimmermann, *Angew. Chem.* **2005**, *117*, 5320–5374.
- [99] R. Huisgen, *Angew. Chem. Int. Ed. Engl.* **1963**, *2*, 565–598.
- [100] V. V. Rostovtsev, L. G. Green, V. V. Fokin, K. B. Sharpless, *Angew. Chem. Int. Ed.* **2002**, *41*, 2596–2599.
- [101] C. W. Tornøe, C. Christensen, M. Meldal, *J. Org. Chem.* **2002**, *67*, 3057–3064.
- [102] F. Himo, T. Lovell, R. Hilgraf, V. V. Rostovtsev, L. Noodleman, K. B. Sharpless, V. V. Fokin, *J. Am. Chem. Soc.* **2005**, *127*, 210–216.
- [103] R. J. Pounder, M. J. Stanford, P. Brooks, S. P. Richards, A. P. Dove, *Chem. Commun.* **2008**, 5158.
- [104] B. H. Northrop, S. H. Frayne, U. Choudhary, *Polym. Chem.* **2015**, *6*, 3415–3430.
- [105] S. Xie, Y. Tao, Y. Pan, W. Qu, G. Cheng, L. Huang, D. Chen, X. Wang, Z. Liu, Z. Yuan, *J. Control. Release* **2014**, *187*, 101–117.
- [106] D. Yoo, H. Jeong, S.-H. Noh, J.-H. Lee, J. Cheon, *Angew. Chem. Int. Ed.* **2013**, *52*, 13047–13051.
- [107] Z. Wang, Z. Chen, Z. Liu, P. Shi, K. Dong, E. Ju, J. Ren, X. Qu, *Biomaterials* **2014**, *35*, 9678–9688.
- [108] J.-P. Fortin, C. Wilhelm, J. Servais, C. Ménager, J.-C. Bacri, F. Gazeau, *J. Am. Chem. Soc.* **2007**, *129*, 2628–2635.
- [109] D.-H. Kim, E. A. Vitol, J. Liu, S. Balasubramanian, D. J. Gosztola, E. E. Cohen, V. Novosad, E. A. Rozhkova, *Langmuir* **2013**, *29*, 7425–7432.
- [110] T. T. T. N’Guyen, H. T. T. Duong, J. Basuki, V. Montembault, S. Pascual, C. Guibert, J. Fresnais, C. Boyer, M. R. Whittaker, T. P. Davis, L. Fontaine, *Angew. Chem. Int. Ed.* **2013**, *52*, 14152–14156.
- [111] R. J. Knipp, R. Estrada, P. Sethu, M. H. Nantz, *Tetrahedron* **2014**, *70*, 3422–3429.

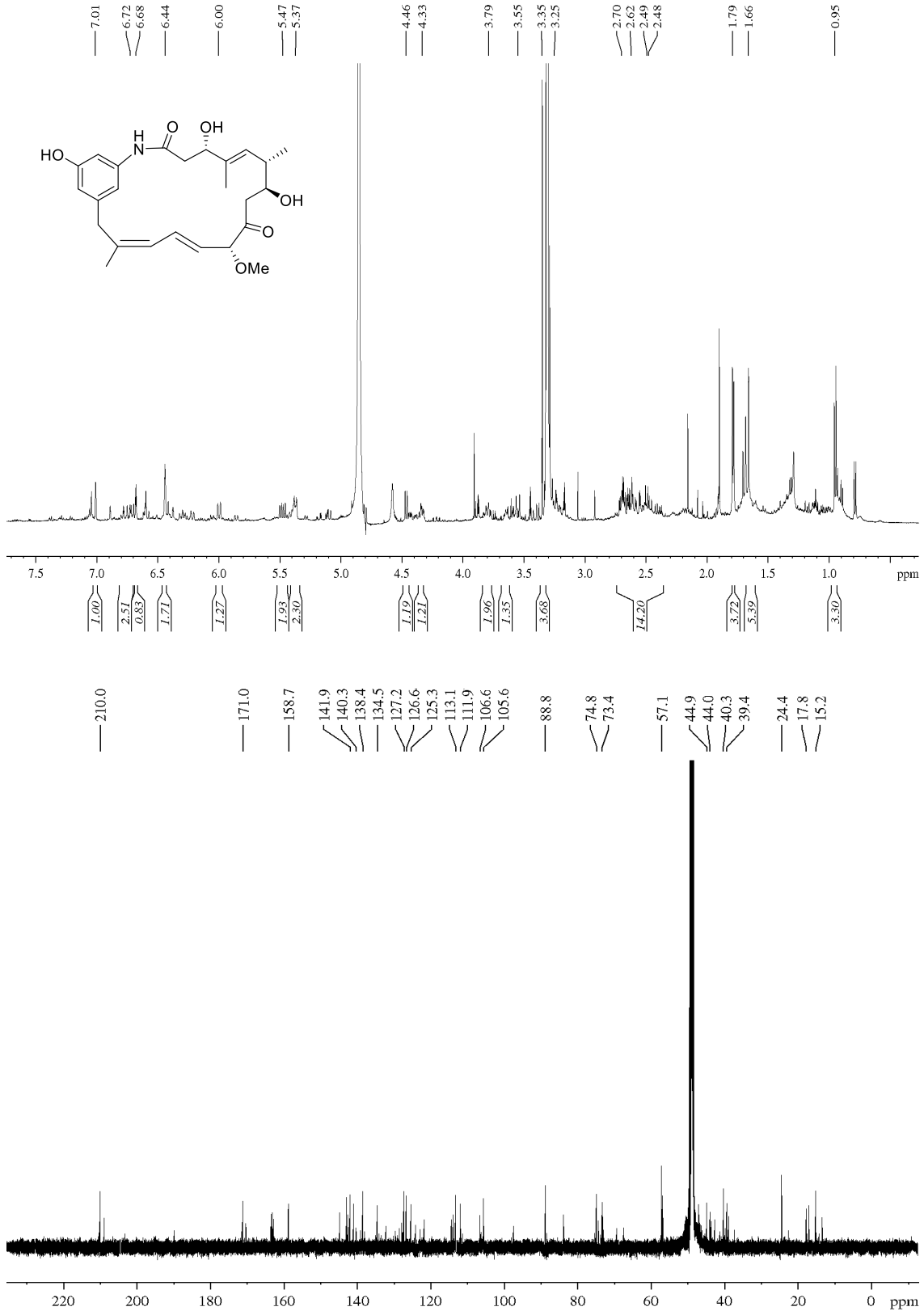
- [112] R. B. Greenwald, Y. H. Choe, C. D. Conover, K. Shum, D. Wu, M. Royzen, *J. Med. Chem.* **2000**, *43*, 475–487.
- [113] S. Türkkan, Novel Smart Drug Delivery Systems for Antitumor Therapy That Combines Chemotherapy with Hyperthermia, Hannover Medical School, **2020**.
- [114] J. Cieślak, S. L. Beaucage, *J. Org. Chem.* **2003**, *68*, 10123–10129.
- [115] M. K. Chmielewski, V. Marchán, J. Cieślak, A. Grajkowski, V. Livengood, U. Münch, A. Wilk, S. L. Beaucage, *J. Org. Chem.* **2003**, *68*, 10003–10012.
- [116] M. K. Chmielewski, E. Tykarska, W. T. Markiewicz, W. Rypniewski, *New J. Chem.* **2012**, *36*, 603–612.
- [117] O. Bremer, *Justus Liebigs Ann. Chem.* **1936**, *521*, 286–297.
- [118] M. K. Chmielewski, *Tetrahedron Lett.* **2012**, *53*, 666–669.
- [119] J. Brzezinska, A. Witkowska, S. Bałabańska, M. K. Chmielewski, *Org. Lett.* **2016**, *18*, 3230–3233.
- [120] C. K. Ingold, *J. Chem. Soc., Trans.* **1921**, *119*, 305–329.
- [121] D. Konrádová, H. Kozubíková, K. Doležal, J. Pospíšil, *Eur. J. Org. Chem.* **2017**, *2017*, 5204–5213.
- [122] B. Neises, W. Steglich, *Angew. Chem. Int. Ed. Engl.* **1978**, *17*, 522–524.
- [123] F. Zetsche, A. Fredrich, *Ber. dtsch. Chem. Ges. A/B* **1939**, *72*, 1735–1740.
- [124] E. Vowinkel, *Chem. Ber.* **1967**, *100*, 16–22.
- [125] A. D. Deshpande, K. G. Baheti, N. R. Chatterjee, *Curr. Sci.* **2004**, *87*, 1684–1695.
- [126] C. Boersch, E. Merkul, T. J. J. Müller, *Angew. Chem. Int. Ed.* **2011**, *50*, 10448–10452.
- [127] G. Grover, S. G. Kini, *Eur. J. Med. Chem.* **2006**, *41*, 256–262.
- [128] J. K. Twibanire, T. B. Grindley, *Org. Lett.* **2011**, *13*, 2988–2991.
- [129] H. Chen, X. Xu, L. L. Liu, G. Tang, Y. Zhao, *RSC Adv.* **2013**, *3*, 16247–16250.
- [130] R. Peraman, R. V. Varma, Y. P. Reddy, *Bioorganic Med. Chem. Lett.* **2015**, *25*, 4314–4319.

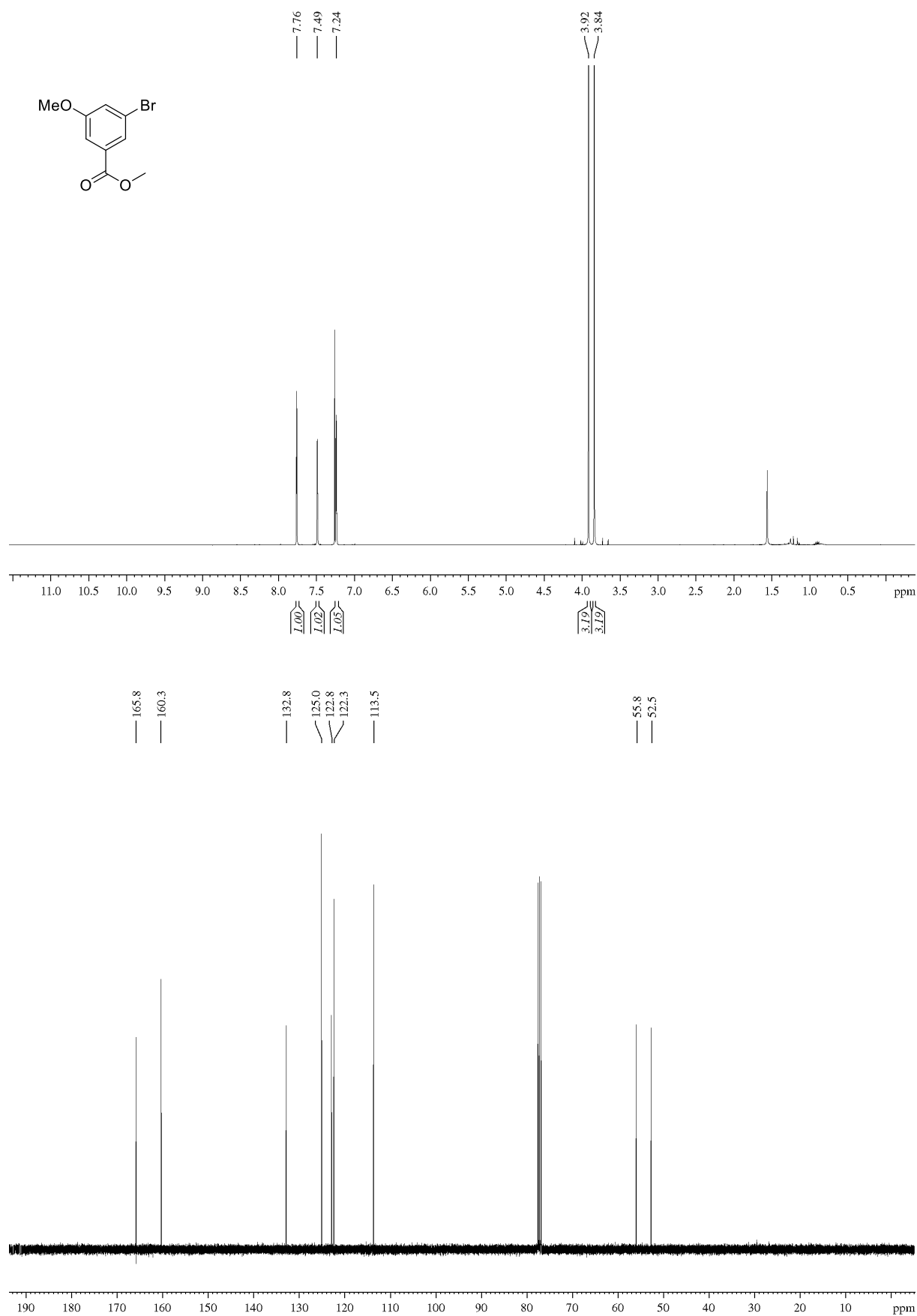
- [131] C. Belżeczki, R. Urbański, Z. Urbańczyk-Lipkowska, M. Chmielewski, *Tetrahedron* **1997**, *53*, 14153–14168.
- [132] A. Ries, R. Kumar, C. Lou, T. Kosbar, E. Vengut-Climent, P. T. Jørgensen, J. C. Morales, J. Wengel, *J. Org. Chem.* **2016**, *81*, 10845–10856.
- [133] H. Kroth, N. Sreenivasachary, A. Hamel, P. Benderitter, Y. Varisco, V. Giriens, P. Paganetti, W. Froestl, A. Pfeifer, A. Muhs, *Bioorganic Med. Chem. Lett.* **2016**, *26*, 3330–3335.
- [134] A. Lawer, J. A. Rossi-Ashton, T. C. Stephens, B. J. Challis, R. G. Epton, J. M. Lynam, W. P. Unsworth, *Angew. Chem. Int. Ed.* **2019**, *58*, 13942–13947.
- [135] D. W. Old, J. P. Wolfe, S. L. Buchwald, *J. Am. Chem. Soc.* **1998**, *120*, 9722–9723.
- [136] D. Maiti, B. P. Fors, J. L. Henderson, Y. Nakamura, S. L. Buchwald, *Chem. Sci.* **2011**, *2*, 57–68.
- [137] R. Huisgen, *ChemInform* **1985**, *16*, 1–176.
- [138] V. V. Rostovtsev, L. G. Green, V. V. Fokin, K. B. Sharpless, *Angew. Chem.* **2002**, *114*, 2708–2711.
- [139] P. M. Cromm, K. T. G. Samarasinghe, J. Hines, C. M. Crews, *J. Am. Chem. Soc.* **2018**, *140*, 17019–17026.
- [140] N. Aissaoui, L. Bergaoui, J. Landoulsi, J.-F. Lambert, S. Boujday, *Langmuir* **2012**, *28*, 656–665.
- [141] T. T. Luong, S. Knoppe, M. Bloemen, W. Brullot, R. Strobbe, J.-P. Locquet, T. Verbiest, *J. Magn. Magn. Mater.* **2016**, *416*, 194–199.
- [142] H. T. Clarke, *Chemistry of Penicillin*, Princeton University Press, Princeton, **2016**.
- [143] E. Pozo-Torres, C. Caro, A. Avasthi, J. M. Páez-Muñoz, M. L. García-Martín, I. Fernández, M. Pernia Leal, *Soft Matter* **2020**, *16*, 3257–3266.
- [144] A. P. Krinochkin, D. S. Kopchuk, N. V. Chepchugov, I. S. Kovalev, G. V. Zyryanov, V. L. Rusinov, O. N. Chupakhin, *Russ. J. Org. Chem.* **2017**, *53*, 963–970.
- [145] G. Meng, M. Zheng, M. Dong, Y. Gao, A. Zheng, Z. Li, R. Hu, *Res. Chem. Intermed.* **2016**, *42*, 2023–2033.

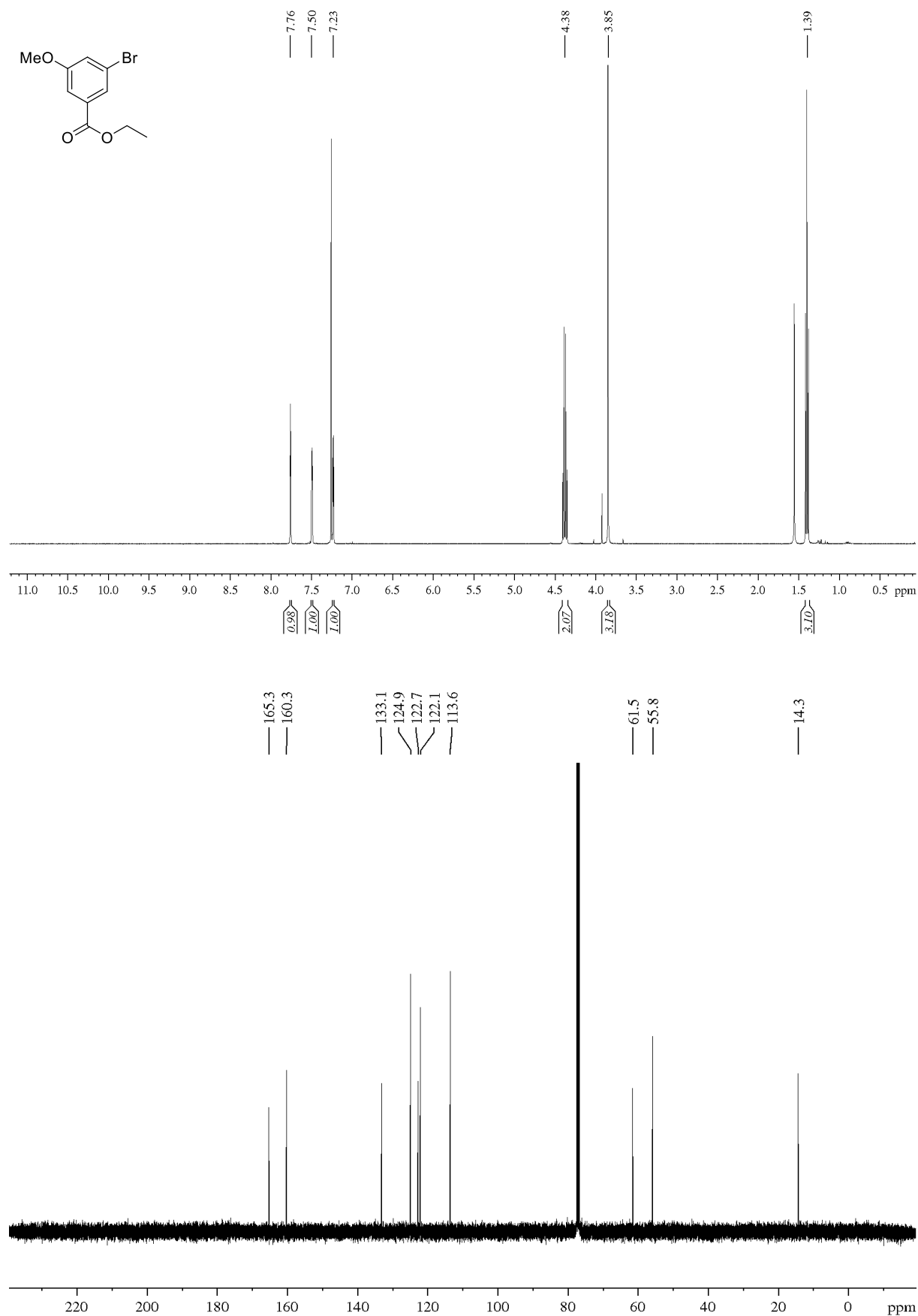
- [146] U. Tehler, J. H. Fagerberg, R. Svensson, M. Larhed, P. Artursson, C. A. S. Bergström, *J. Med. Chem.* **2013**, *56*, 2690–2694.
- [147] H. Yu, C. E. Ballard, P. D. Boyle, B. Wang, *Tetrahedron* **2002**, *58*, 7663–7679.
- [148] U. K. Bandarage, M. E. Kuehne, S. D. Glick, *Tetrahedron* **1999**, *55*, 9405–9424.
- [149] I. Kaviani, L. Kunalingam, P. W. R. Harris, G. Cook M., M. A. Brimble, *Org. Lett.* **2016**, *18*, 3878–3881.
- [150] P. G. McDougal, J. G. Rico, Y. I. Oh, B. D. Condon, *J. Org. Chem.* **1986**, *51*, 3388–3390.
- [151] Y. A. Lin, J. M. Chalker, B. G. Davis, *J. Am. Chem. Soc.* **2010**, *132*, 16805–16811.
- [152] C. Jin, S. Wen, Q. Zhang, Q. Zhu, J. Yu, W. Lu, *ACS Med. Chem. Lett.* **2017**, *8*, 762–765.
- [153] K. Tamao, Y. Nakagawa, Y. Ito, *Org. Synth.* **1996**, *73*, 94.
- [154] A. Krüger, J. Pyplo-Schnieders, H. Redlich, P. Winkelmann, *Collect. Czech. Chem. Commun.* **2004**, *69*, 1843–1876.
- [155] J. Hu, J. Shi, S. Li, Y. Qin, Z.-X. Guo, Y. Song, D. Zhu, *Chem. Phys. Lett.* **2005**, *401*, 352–356.
- [156] K. Pal, A. Sharma, A. L. Koner, *Org. Lett.* **2018**, *20*, 6425–6429.
- [157] H. Zhang, D. Laaf, L. Elling, R. J. Pieters, *Bioconjug. Chem.* **2018**, *29*, 1266–1275.
- [158] H. Herzner, H. Kunz, *Carbohydr. Res.* **2007**, *342*, 541–557.
- [159] X. Wu, X. Zong, M. Ji, *J. Chem. Res.* **2016**, *40*, 368–370.

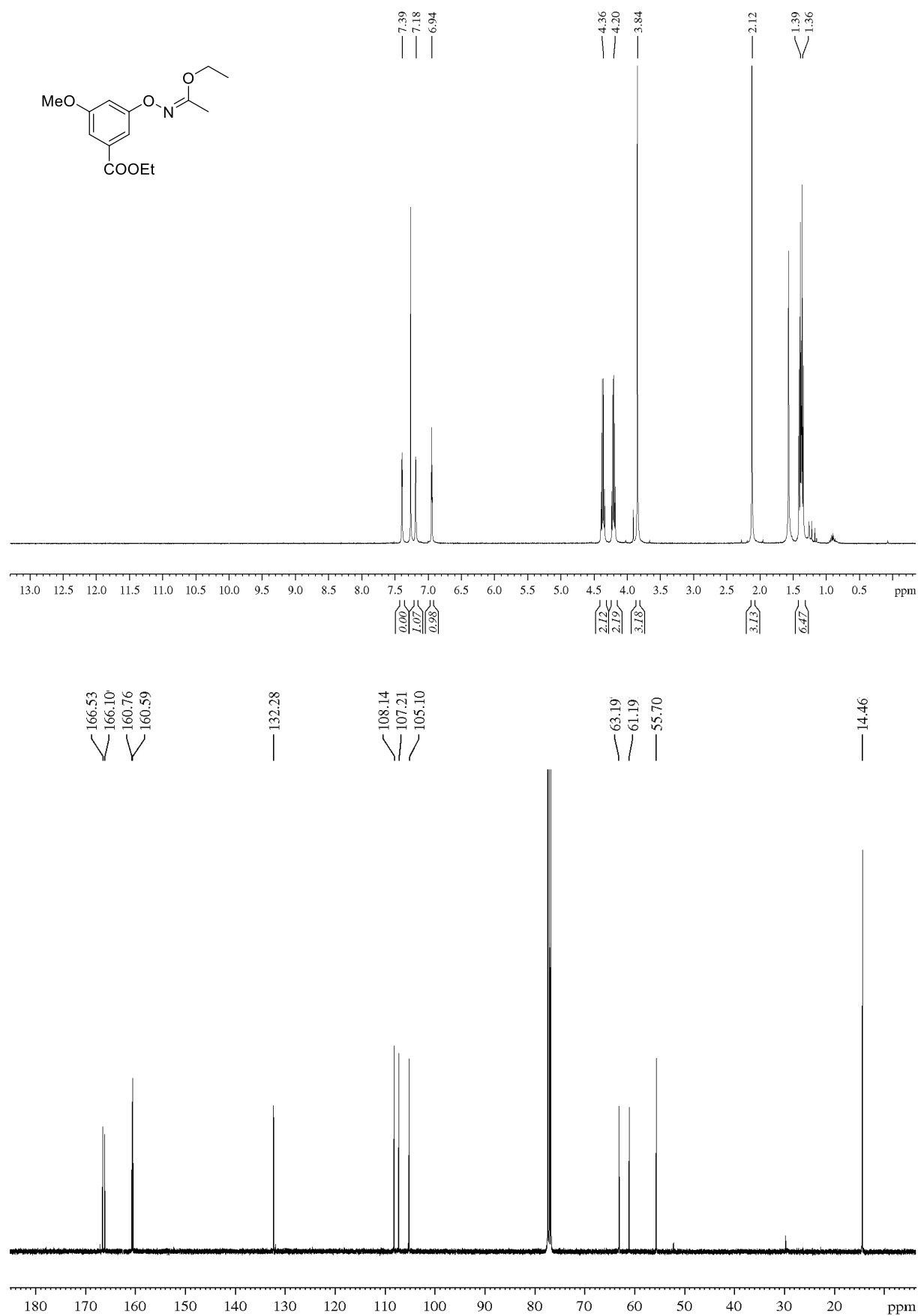
11 NMR Data

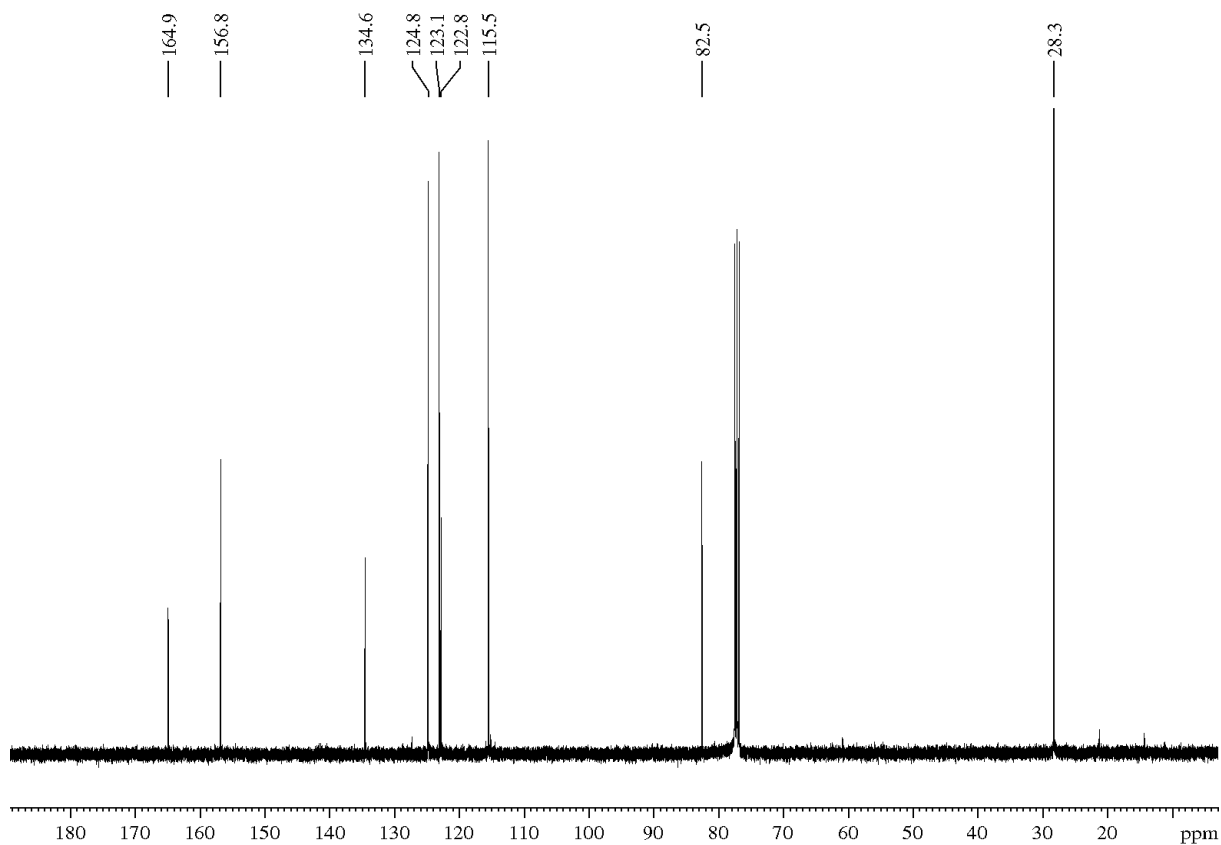
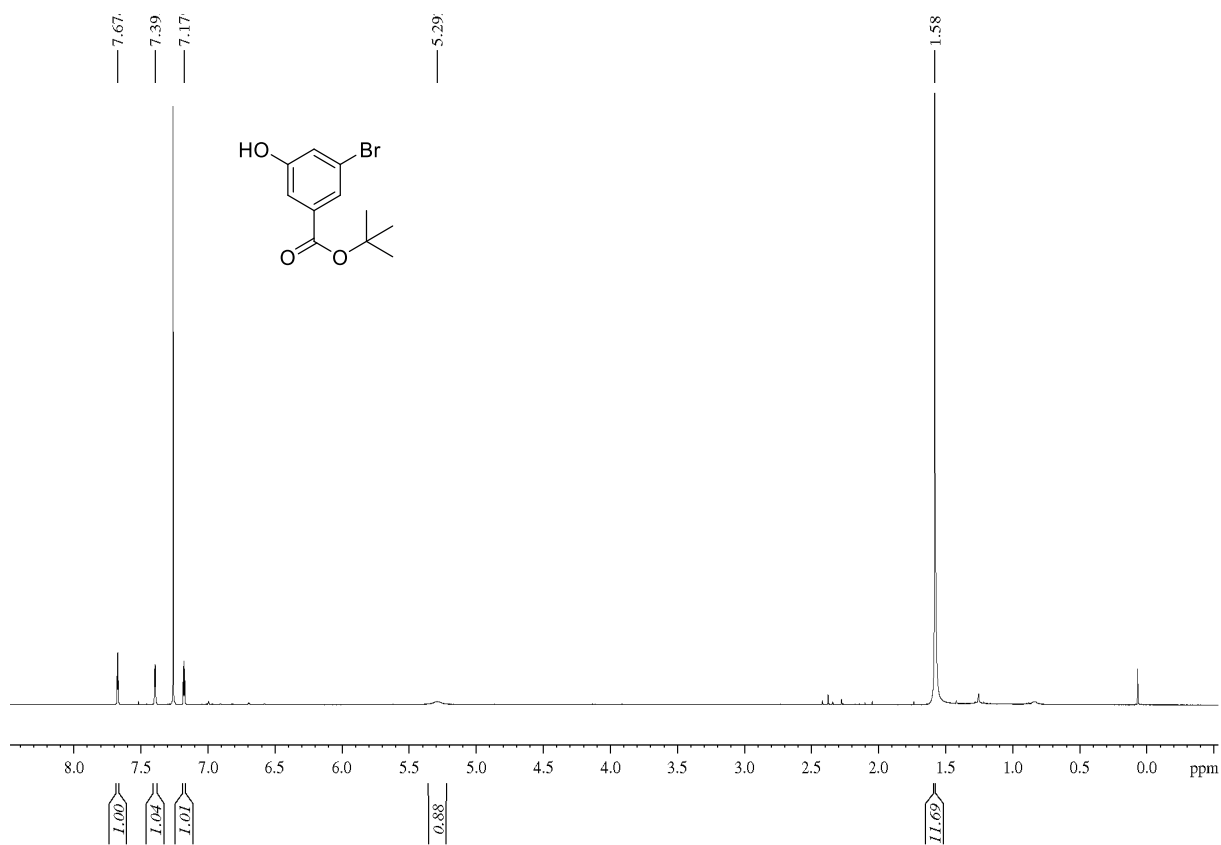
11.1 NMR Data Part I

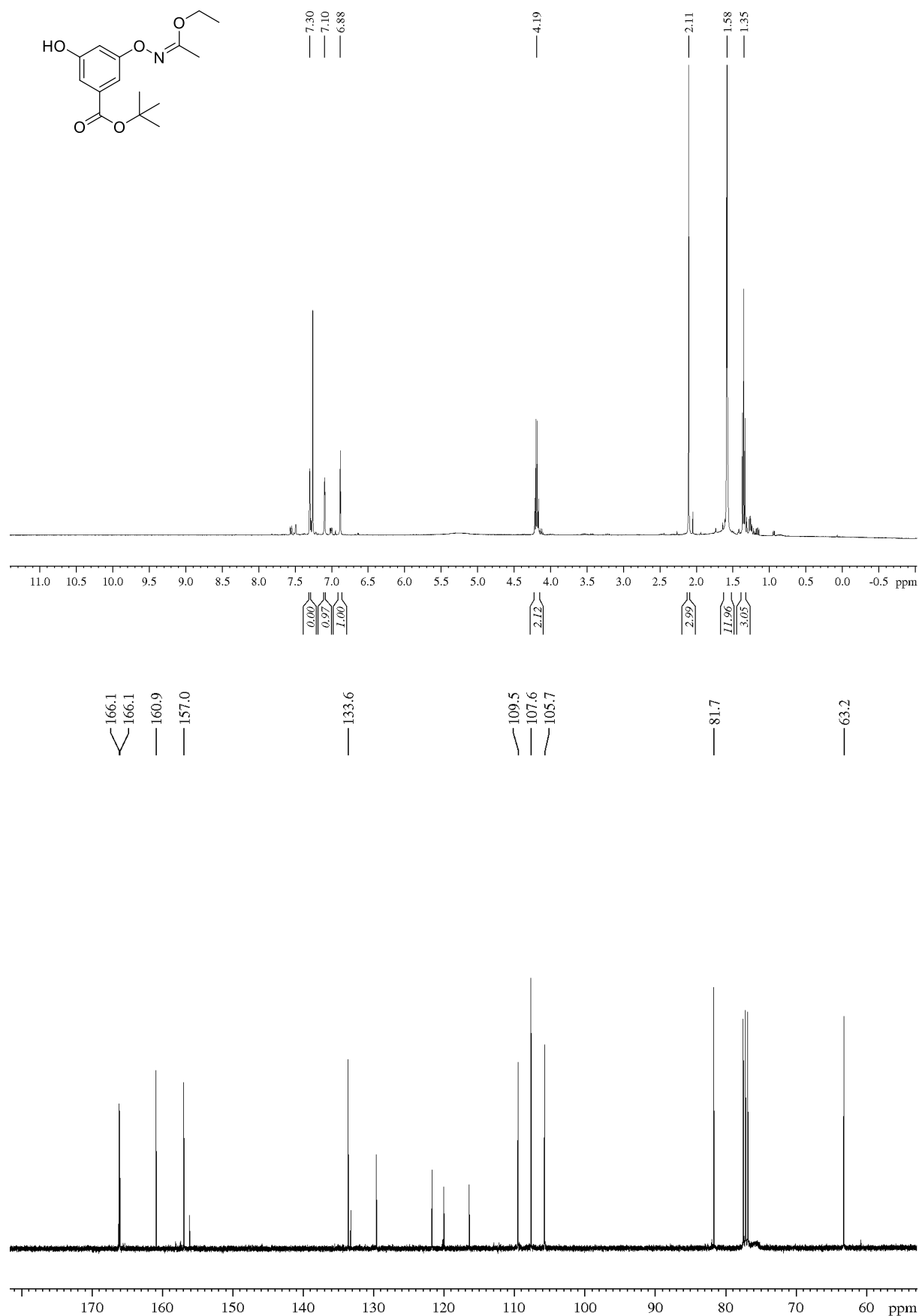
13,14-Z-proansamitocin (28)

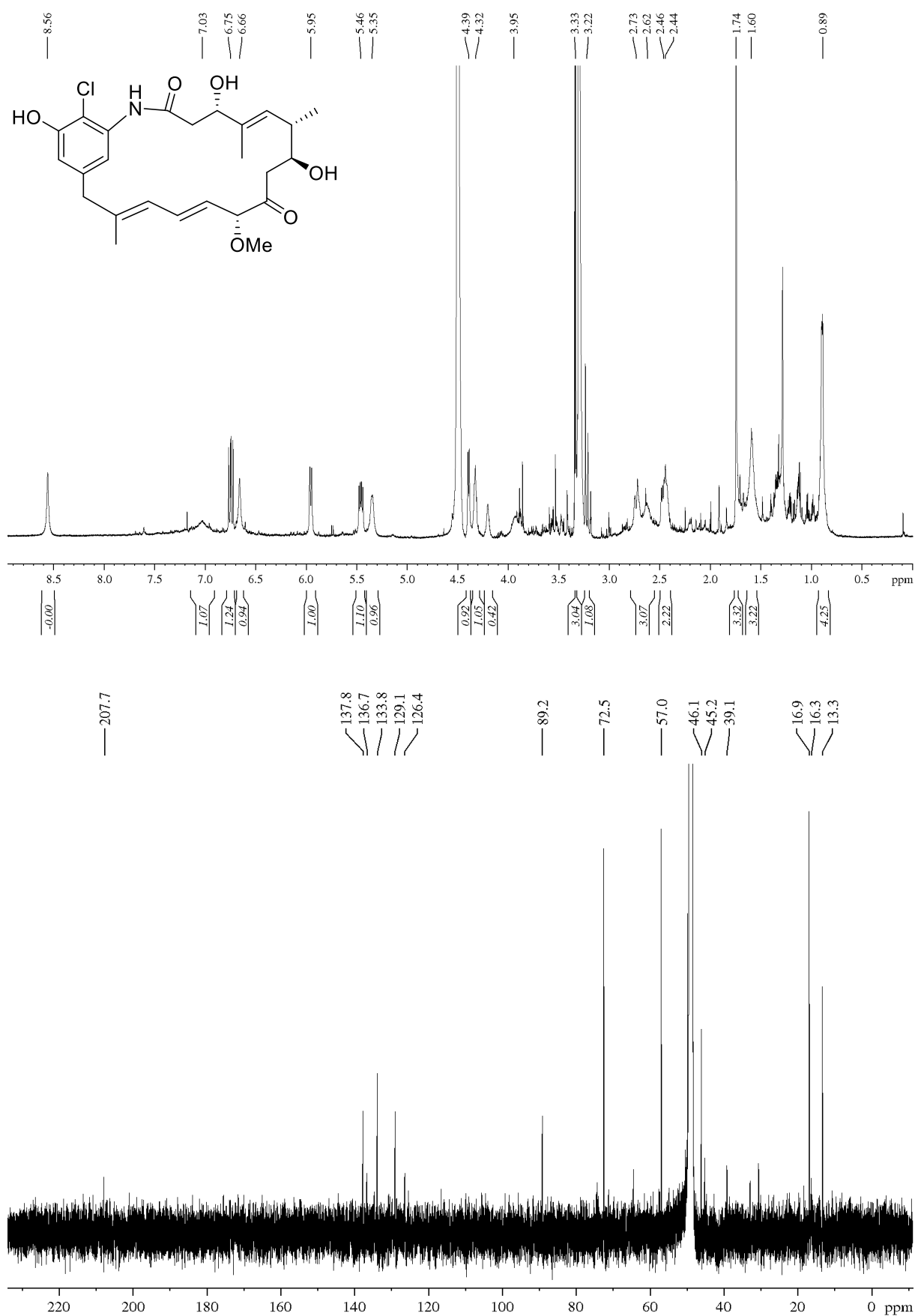
Methyl-3-bromo-5-methoxybenzoate (36a)

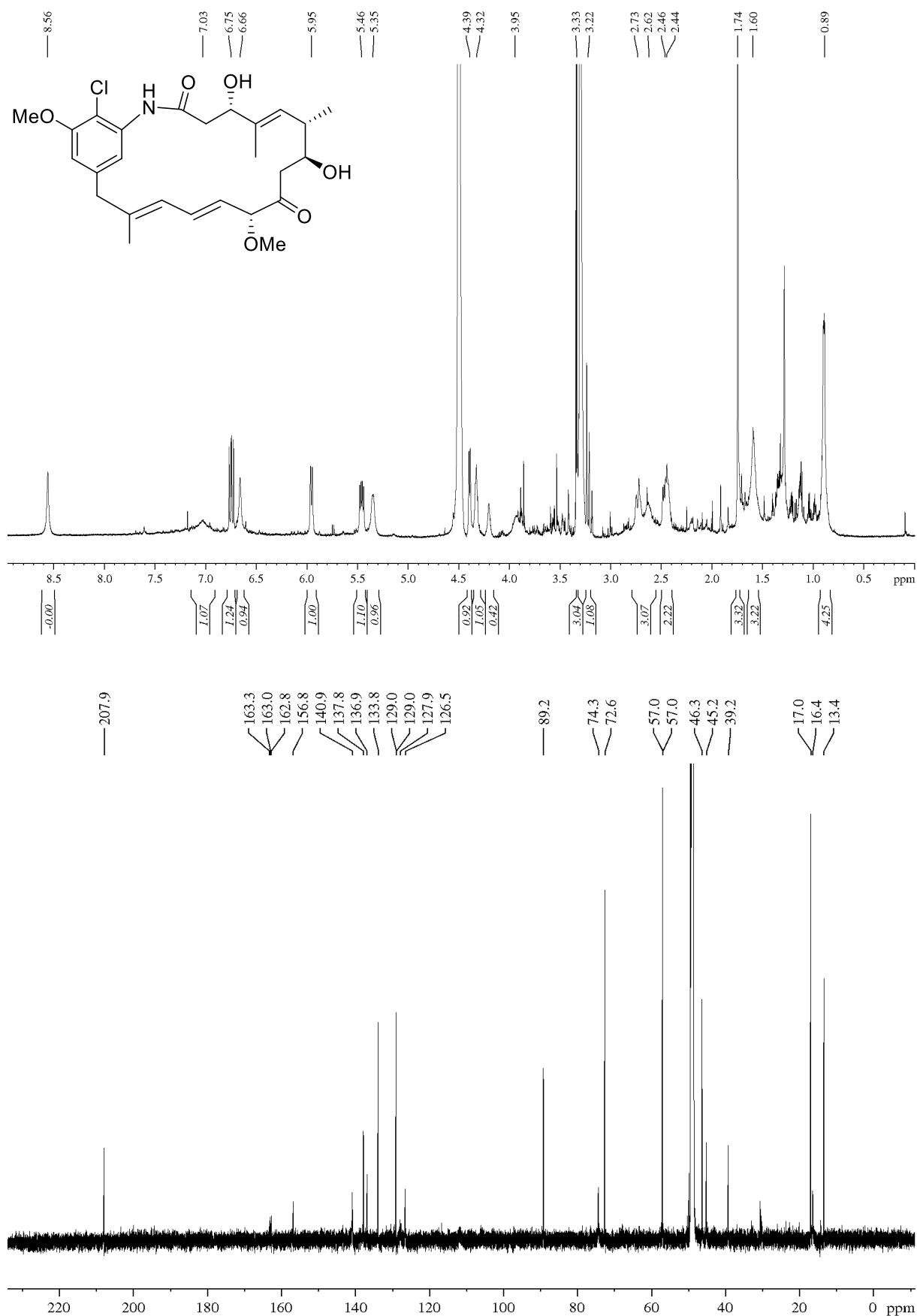
Ethyl-3-bromo-5-methoxybenzoate (36a)

Ethyl (Z)-3-(((1-ethoxyethylidene)amino)oxy)-5-methoxybenzoate (37b)

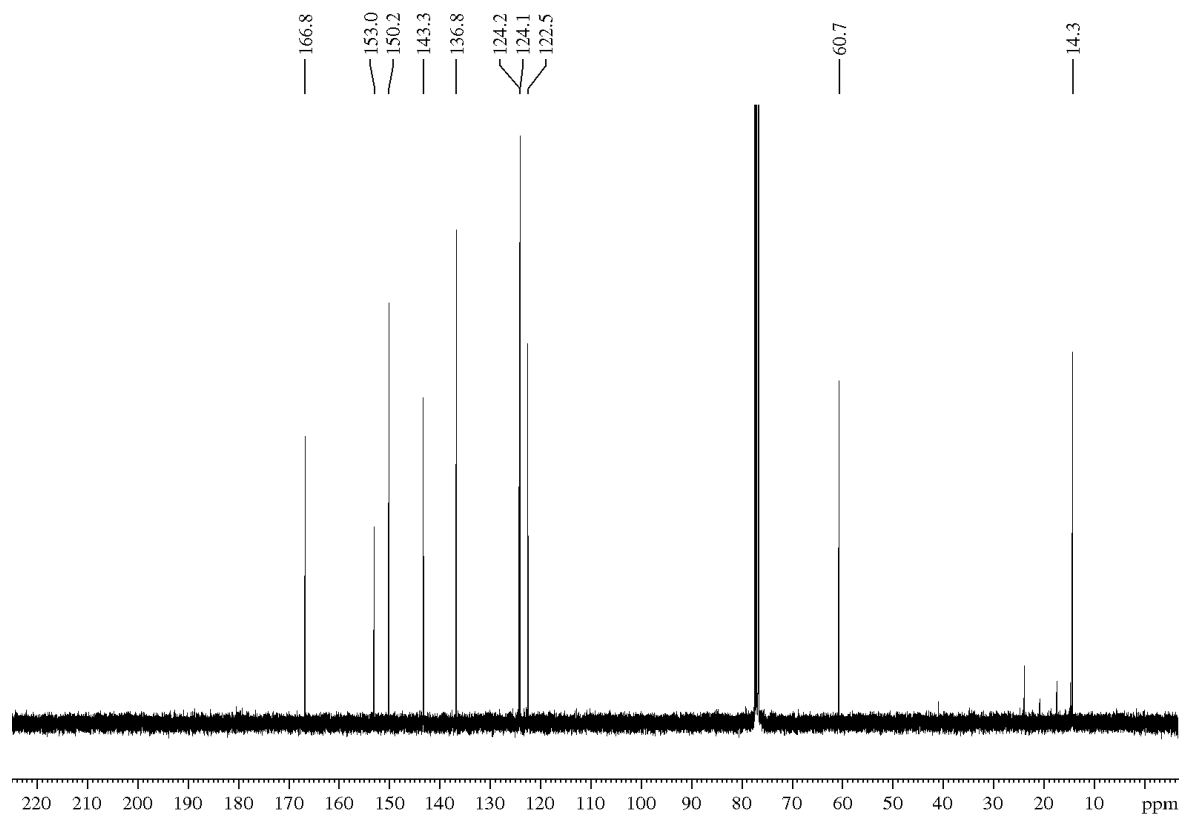
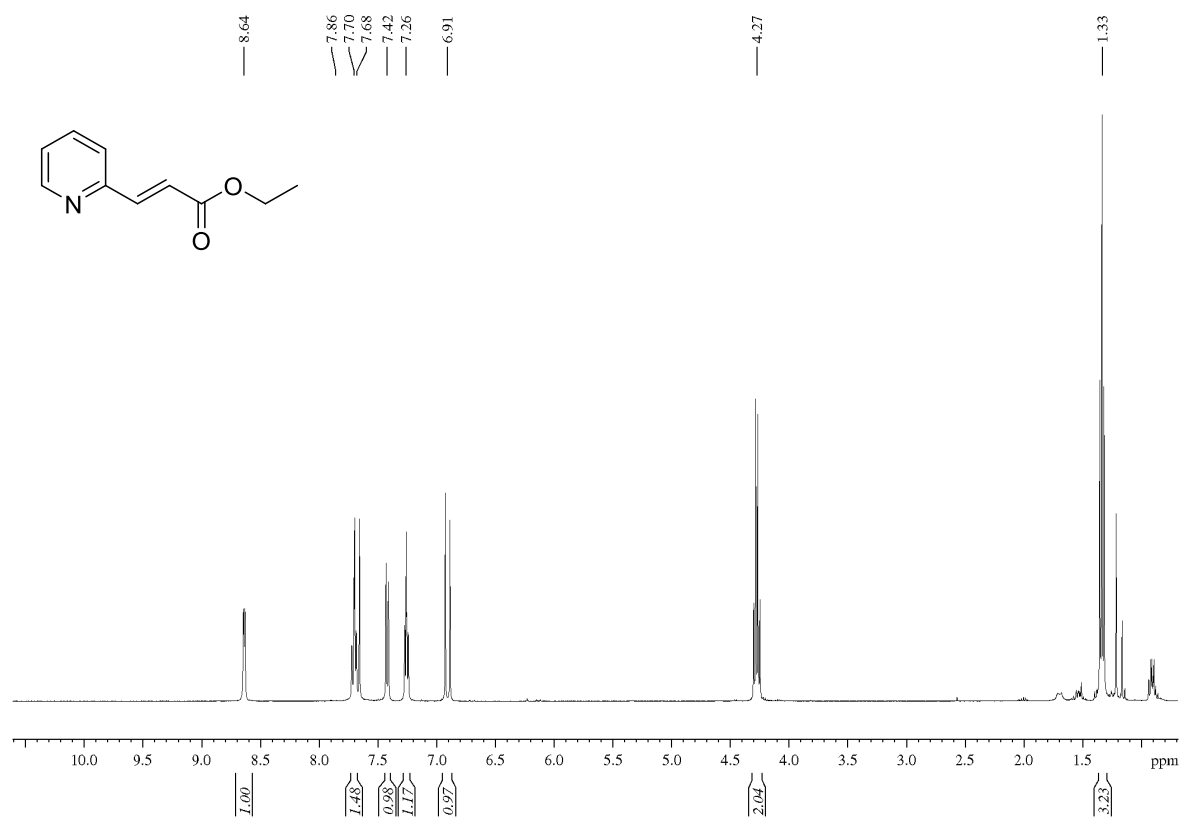
Tert-butyl 3-bromo-5-hydroxybenzoate (38)

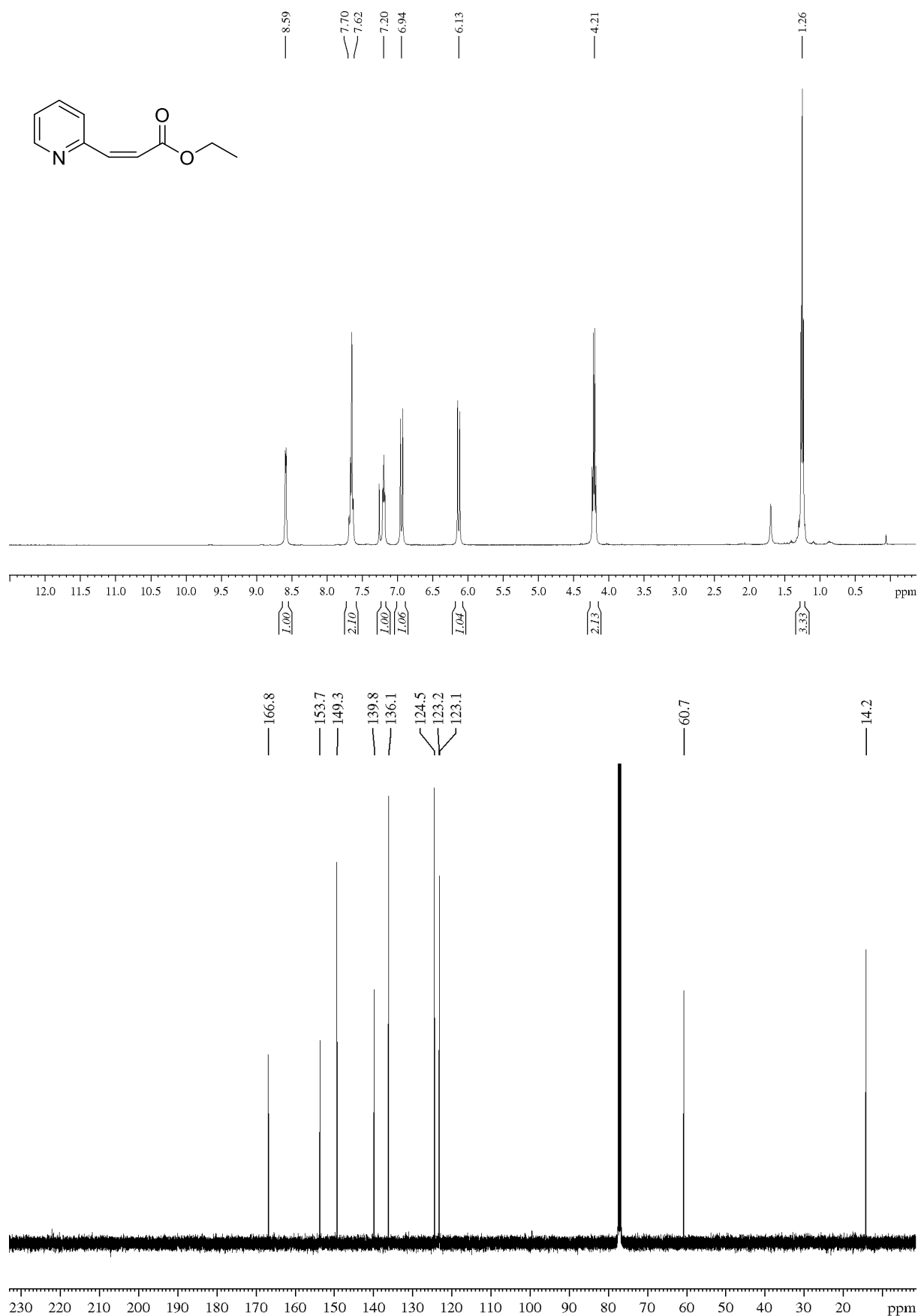
Tert-butyl (Z)-3-(((1-ethoxyethylidene)amino)oxy)-5-methoxybenzoate (39)

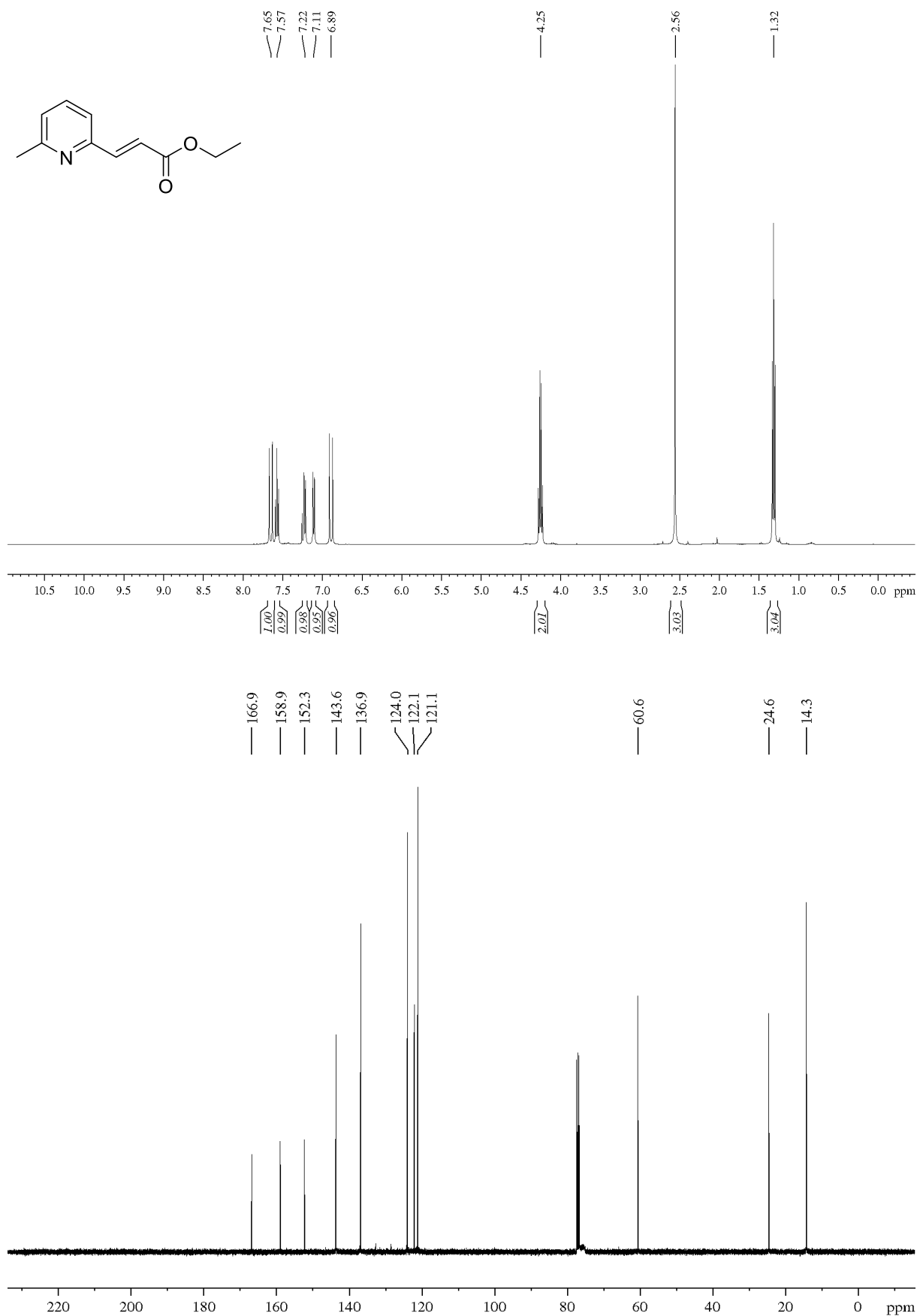
19-Chloroproansamitocin (42)

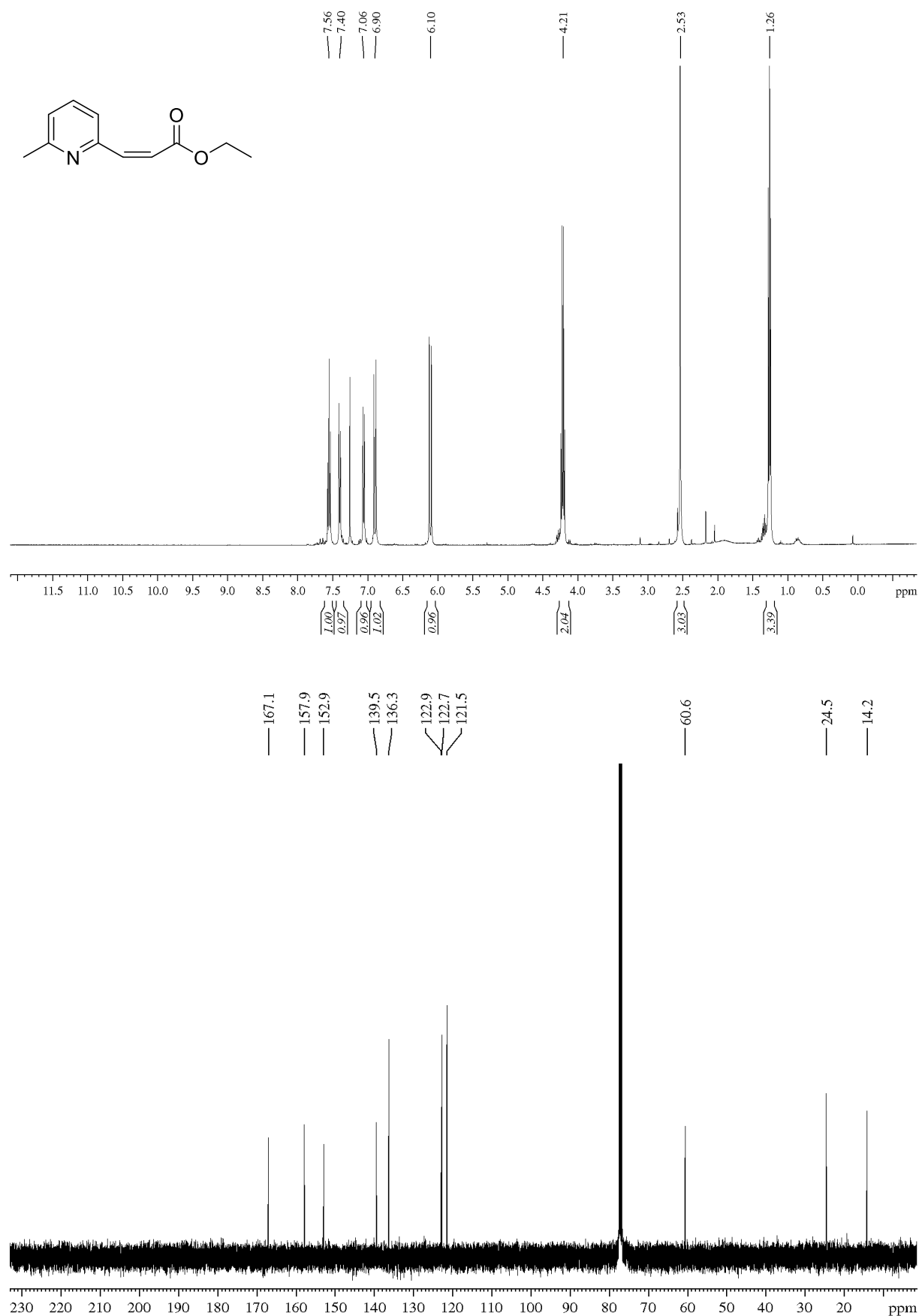
19-Chloroproansamitocin (43)

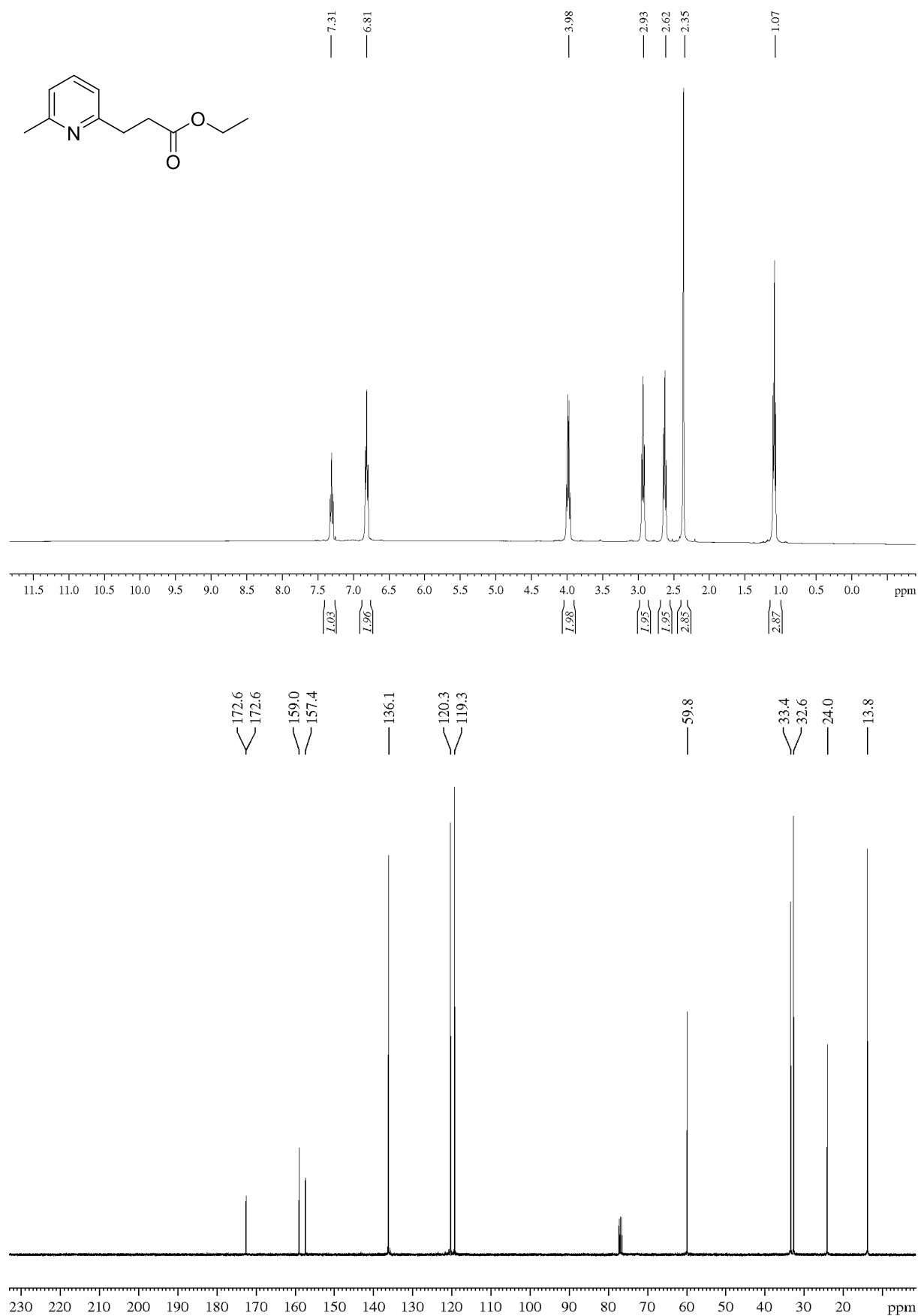
11.2 NMR Data Part II

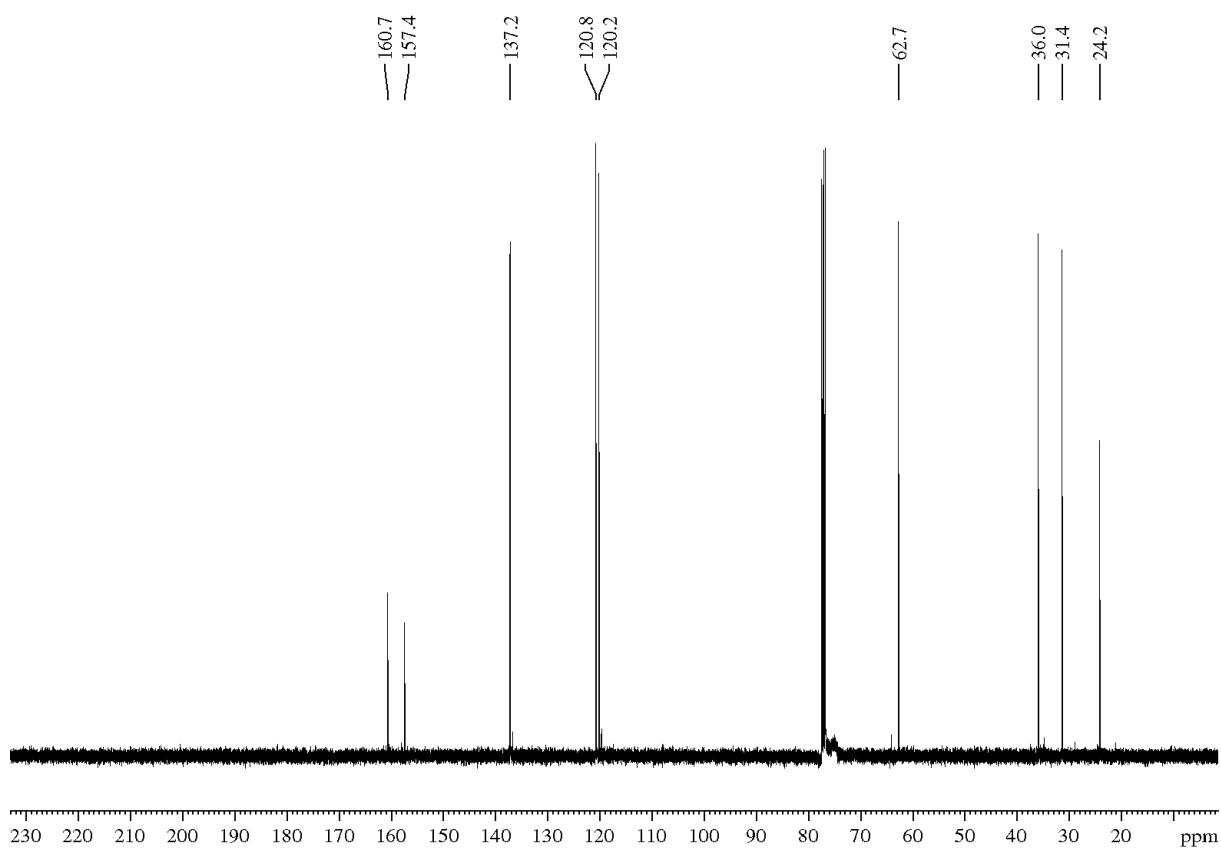
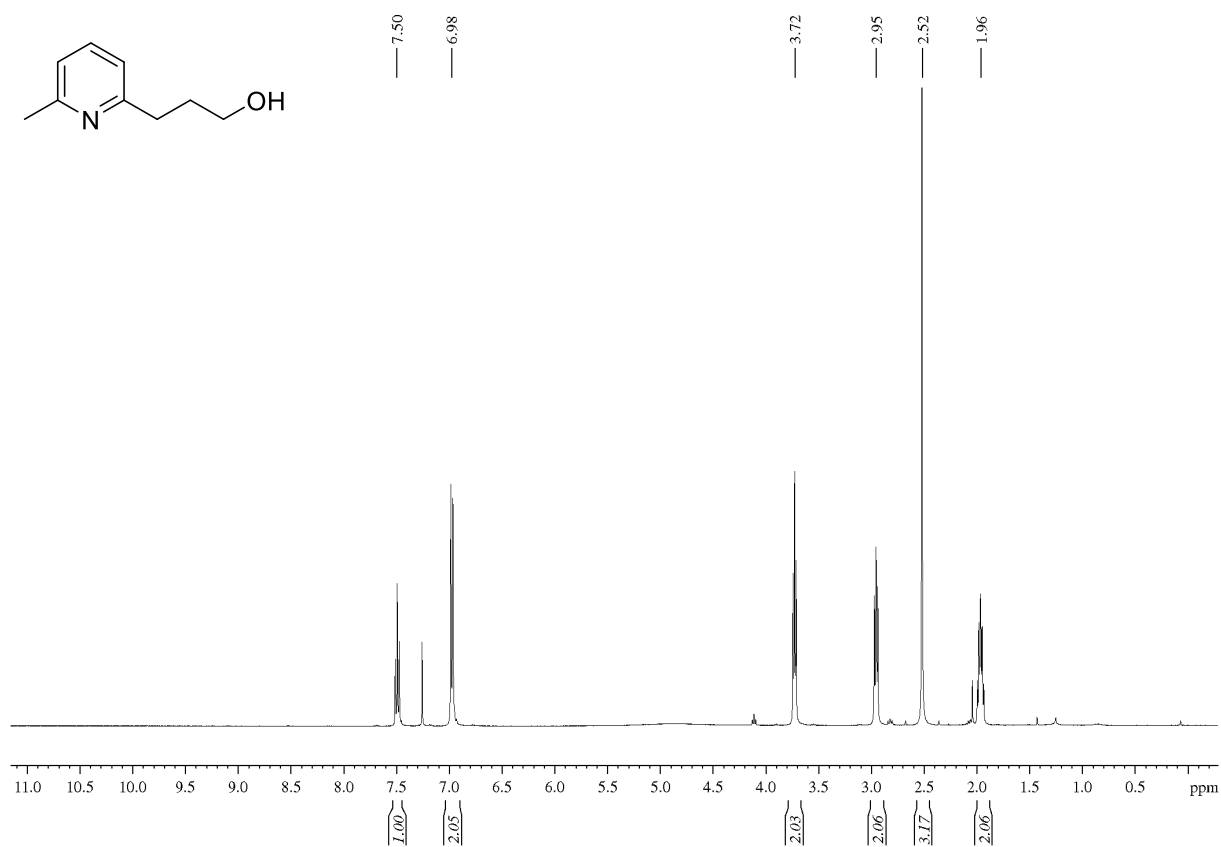
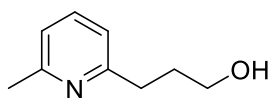
Ethyl (E)-3-(pyridin-2-yl)acrylate (90a)

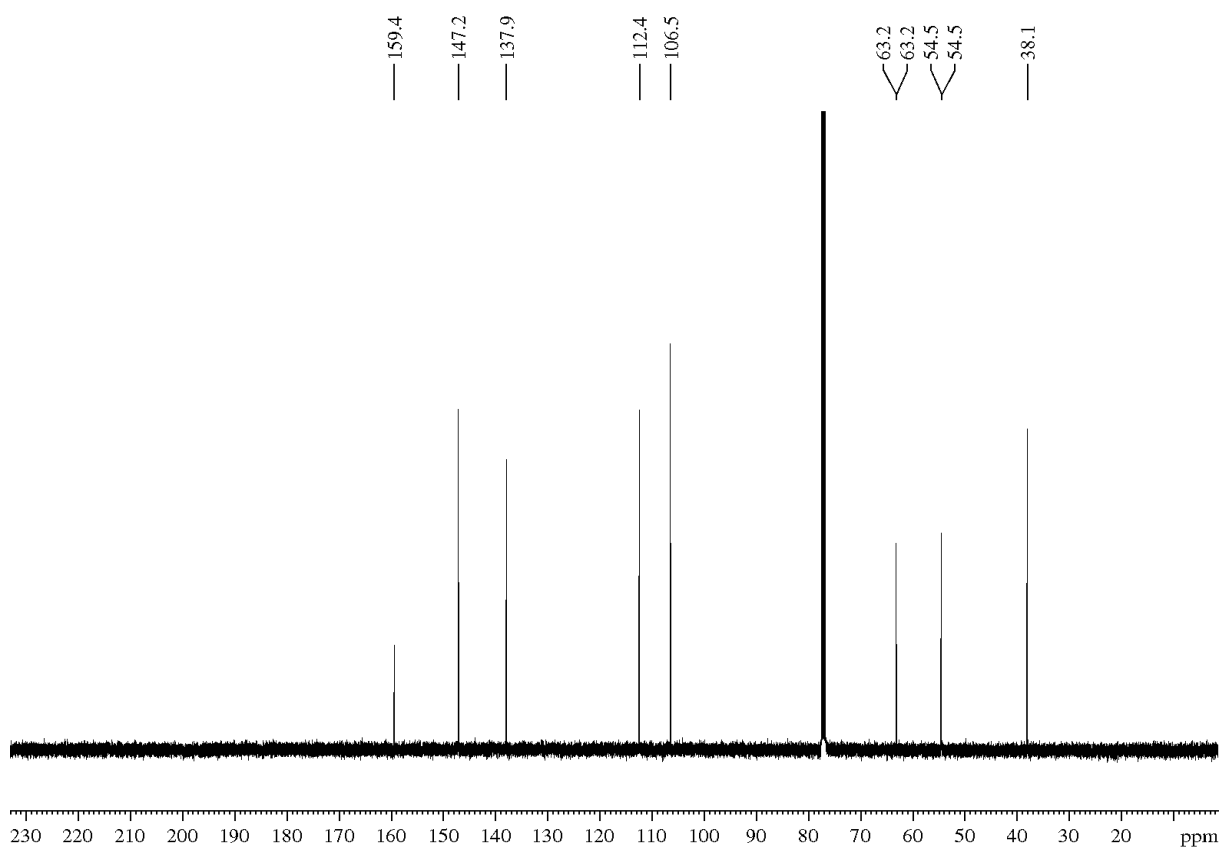
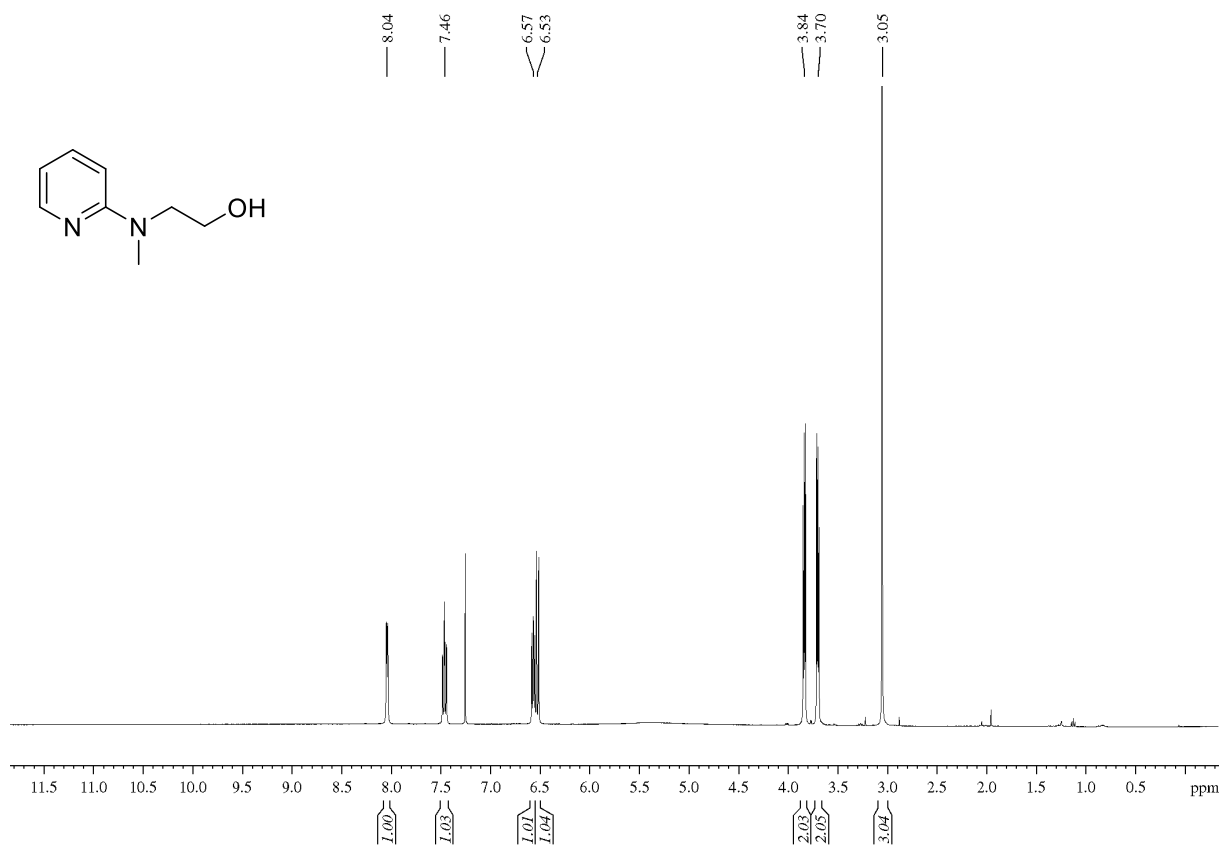
Ethyl (Z)-3-(pyridin-2-yl)acrylate (90a)

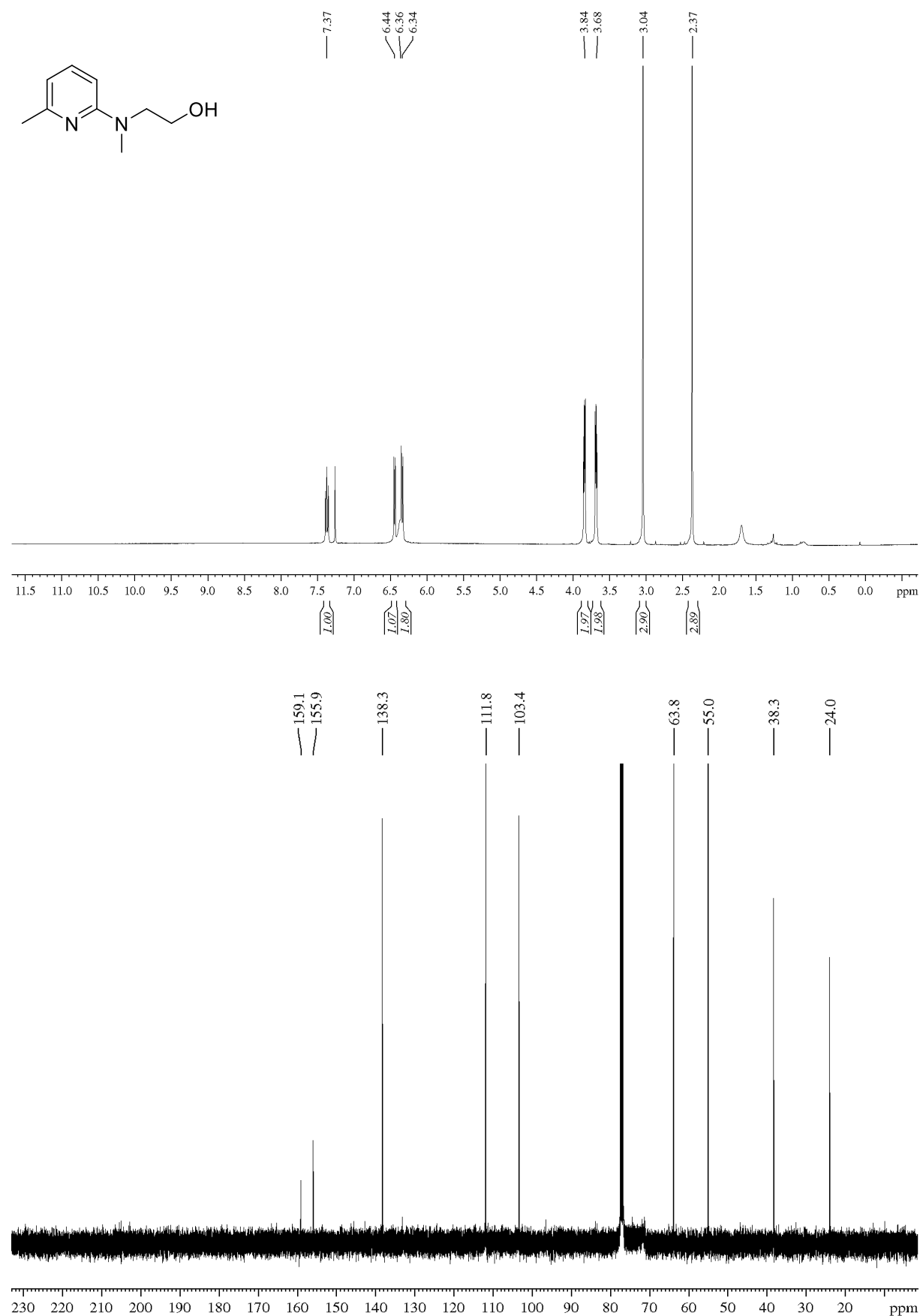
Ethyl (E)-3-(6-methylpyridin-2-yl)acrylate (91b)

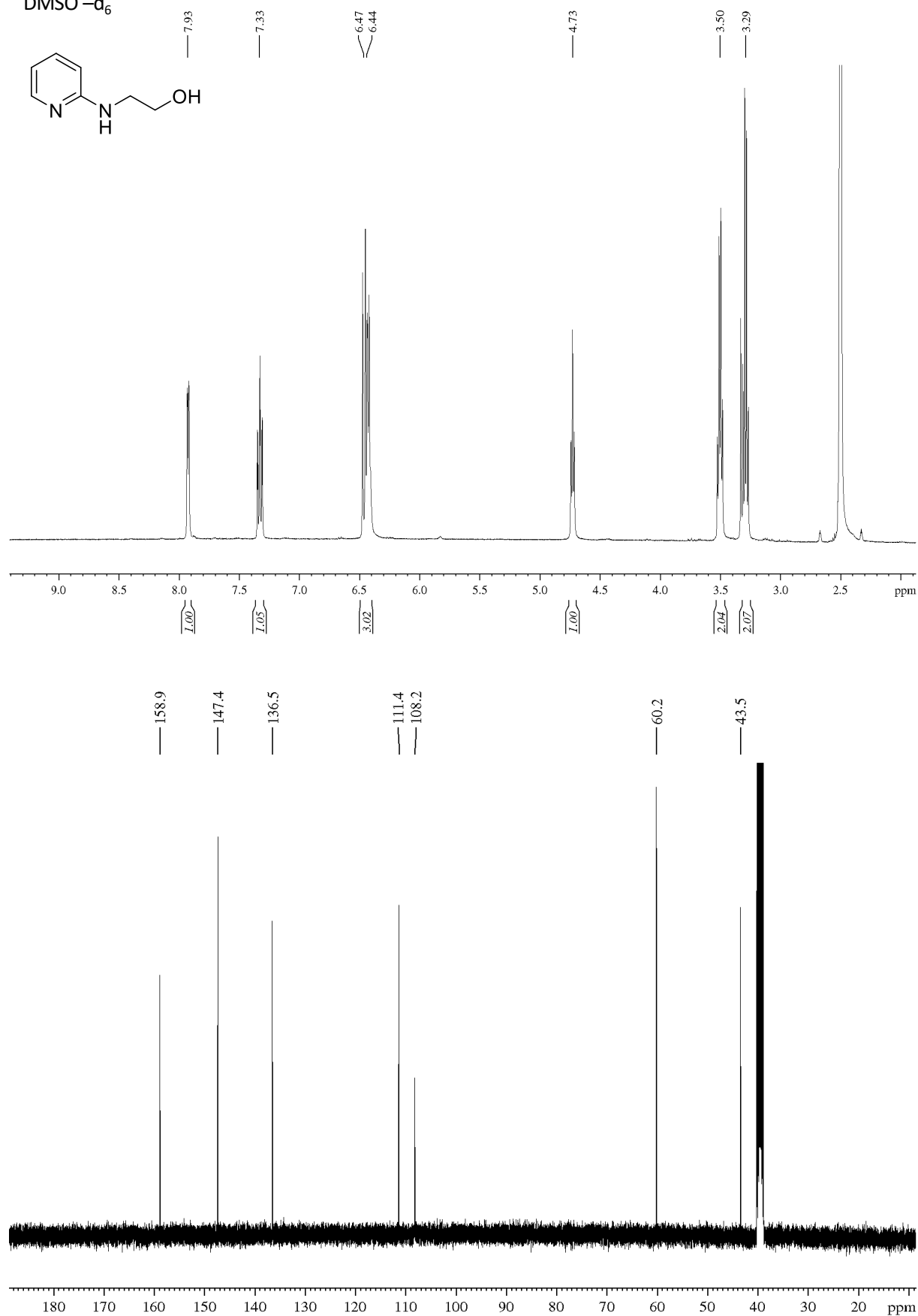
Ethyl (Z)-3-(6-methylpyridin-2-yl)acrylate (91b)

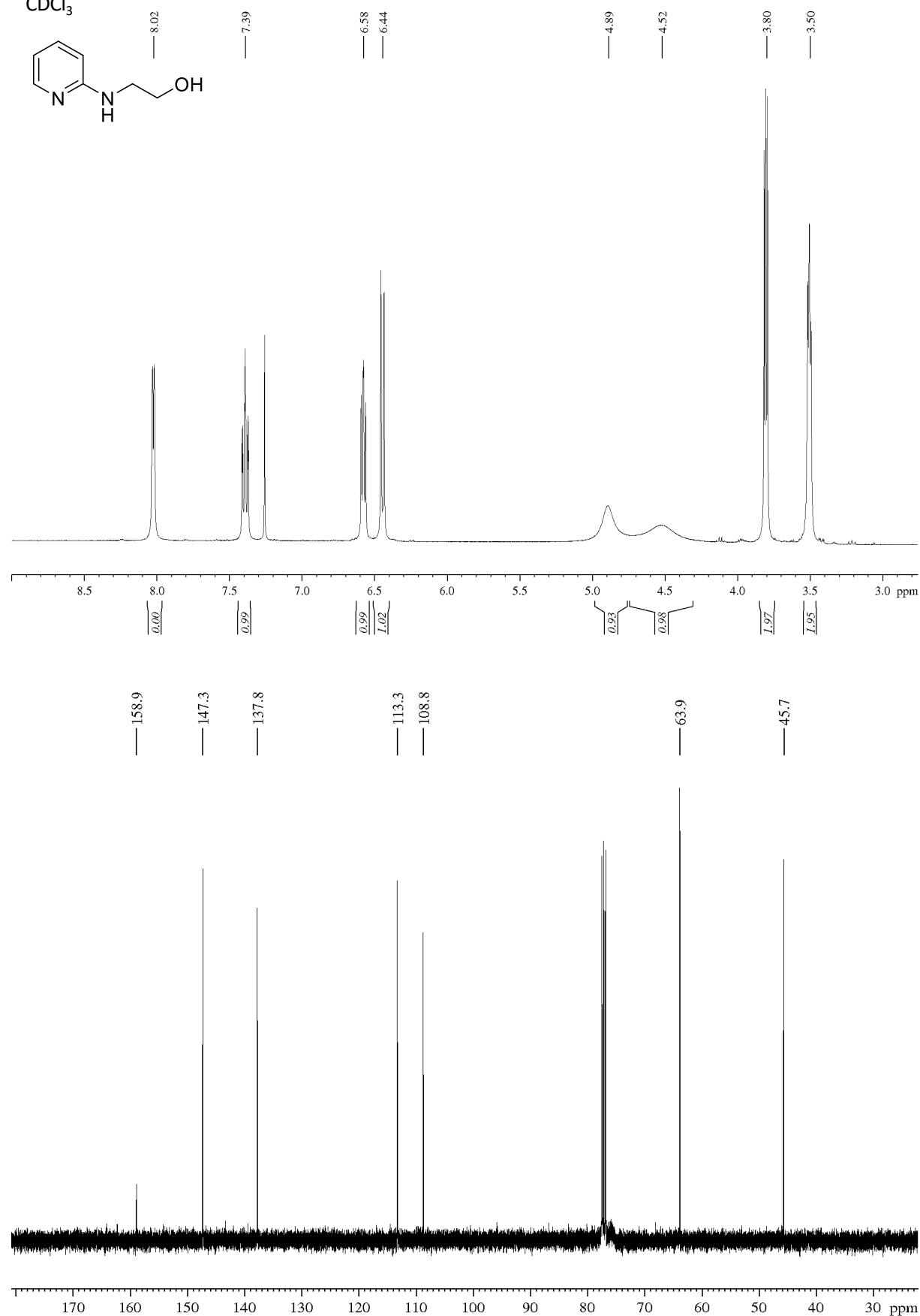
Ethyl 3-(6-methylpyridin-2-yl)propanoate (S1b)

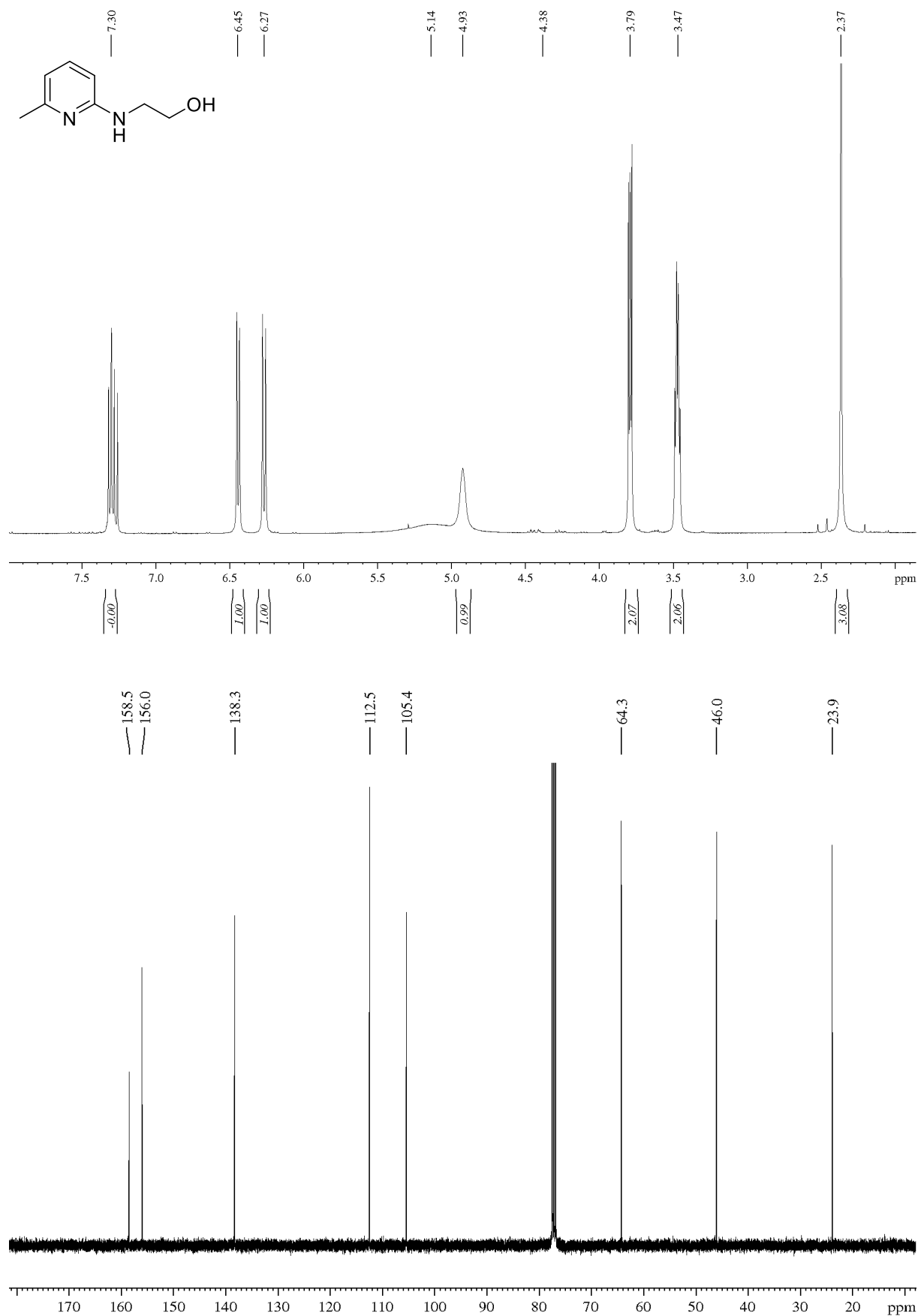
3-(6-Methylpyridin-2-yl)propan-1-ol (83b)

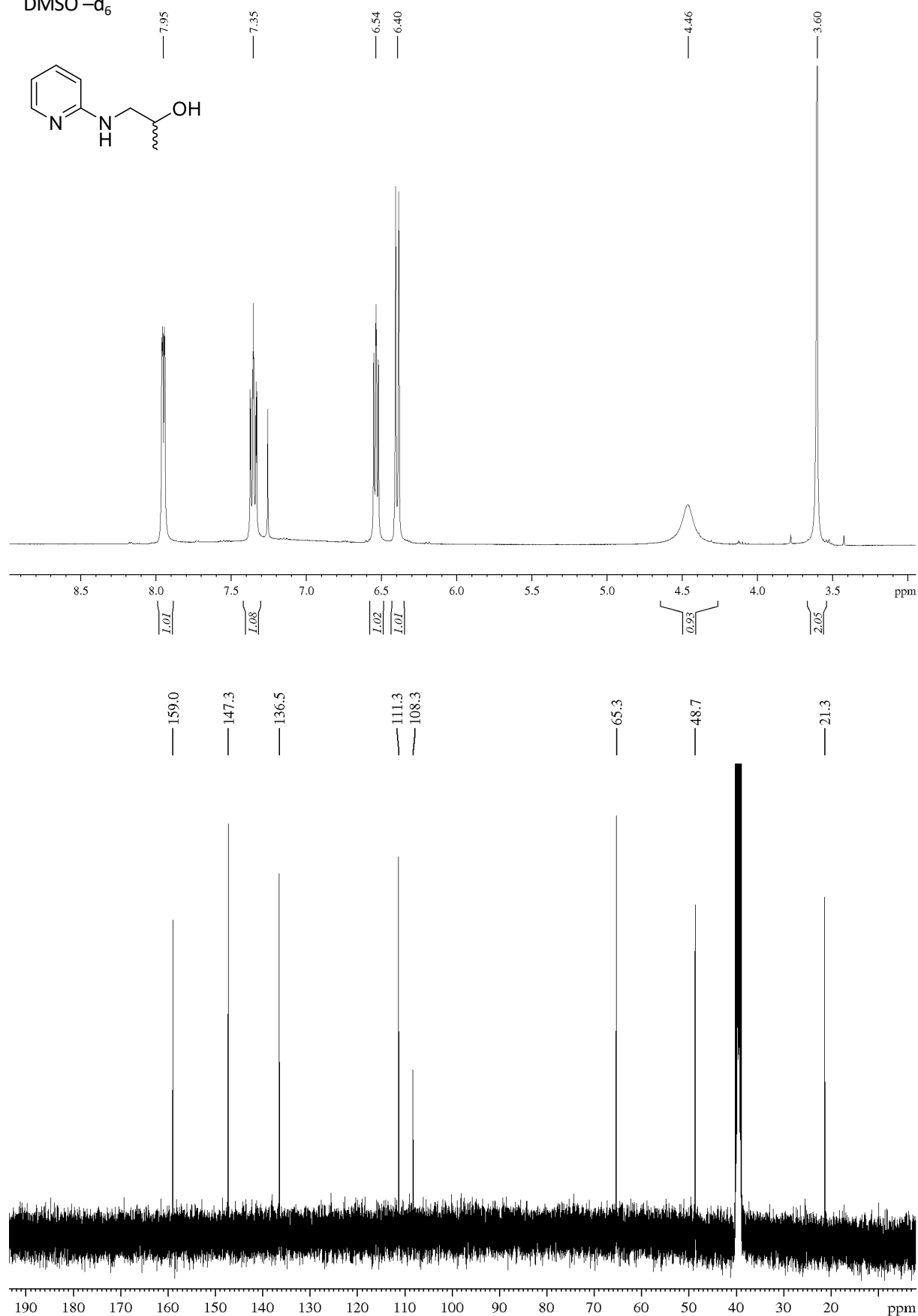
2-(Methyl(pyridin-2-yl)amino)ethan-1-ol (84a)

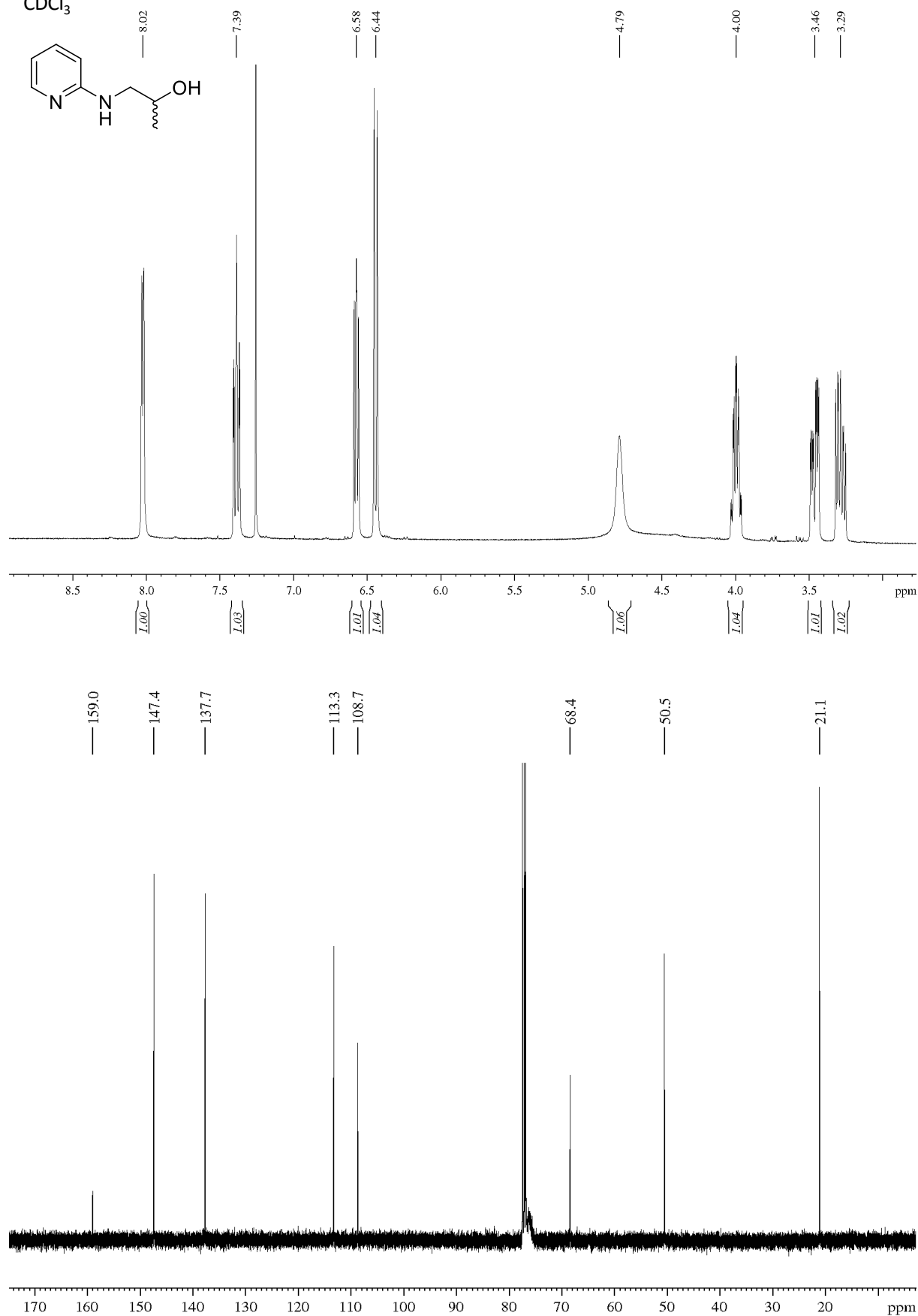
2-(Methyl(6-methylpyridin-2-yl)amino)ethan-1-ol (84b)

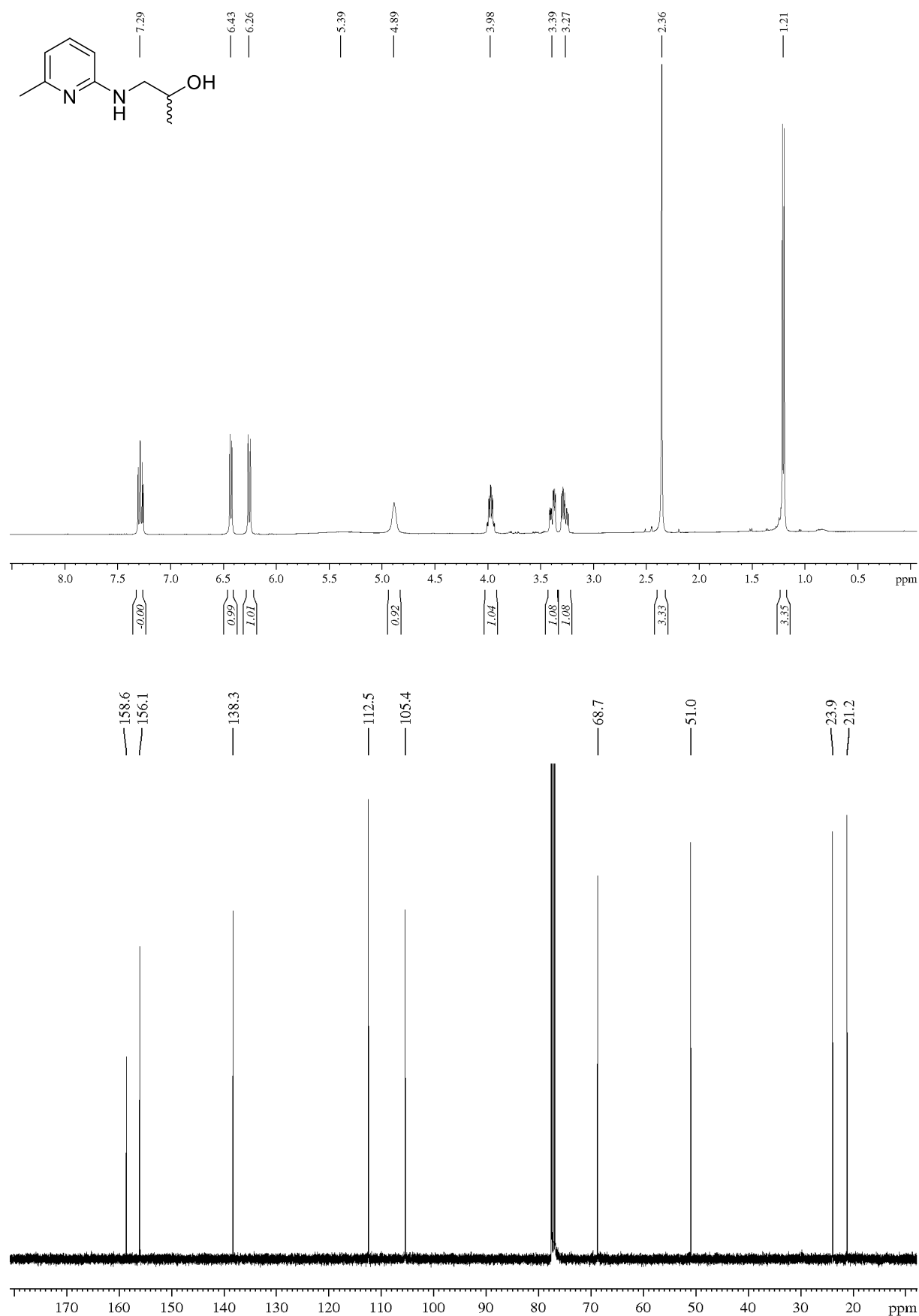
2-(pyridin-2-ylamino)ethan-1-ol (94a)DMSO-d₆

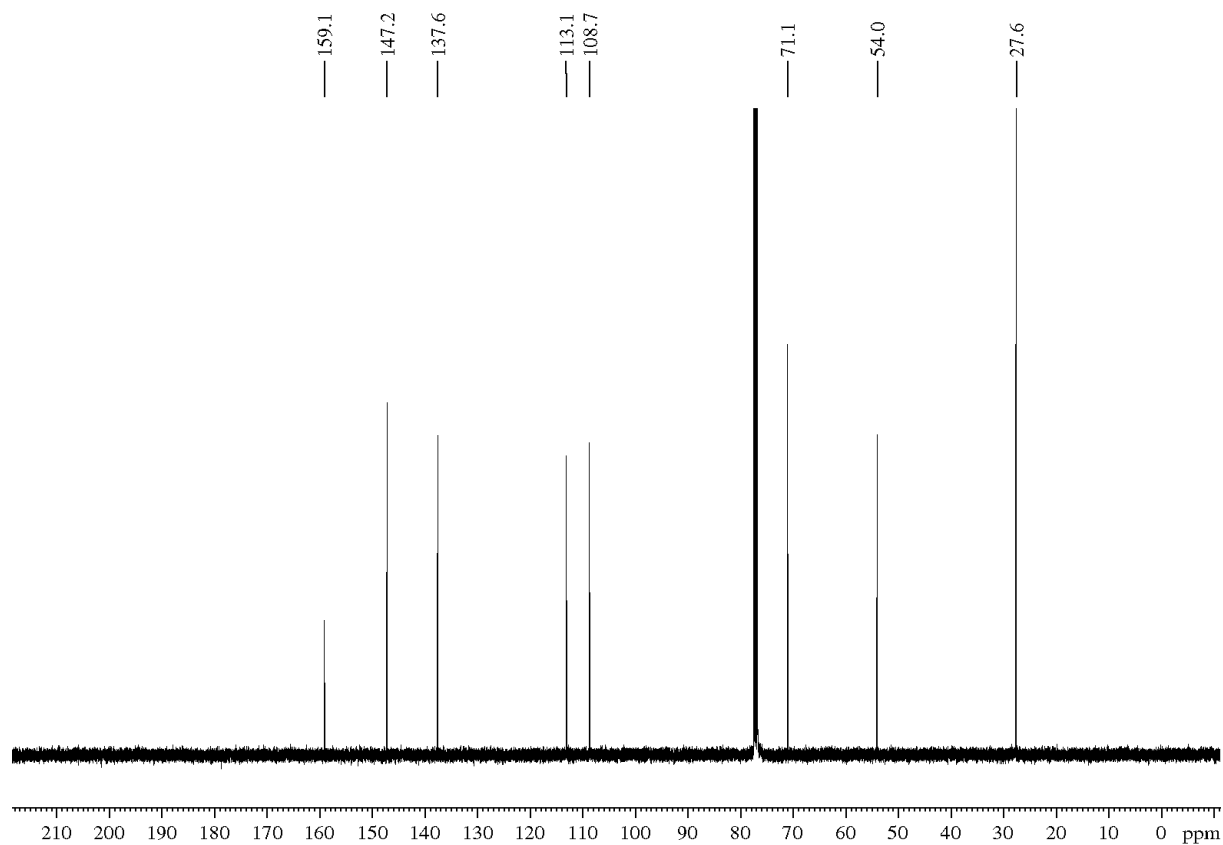
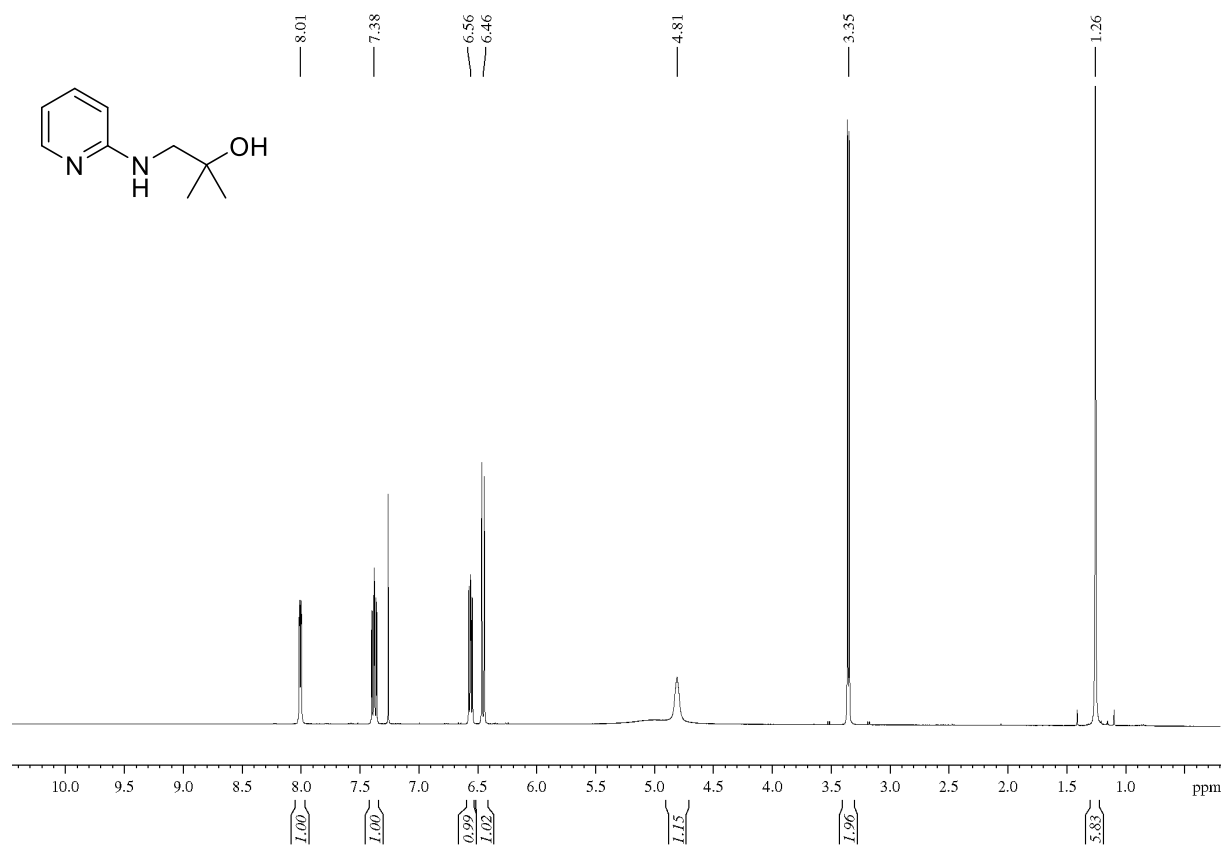
2-(pyridin-2-ylamino)ethan-1-ol (94a)CDCl₃

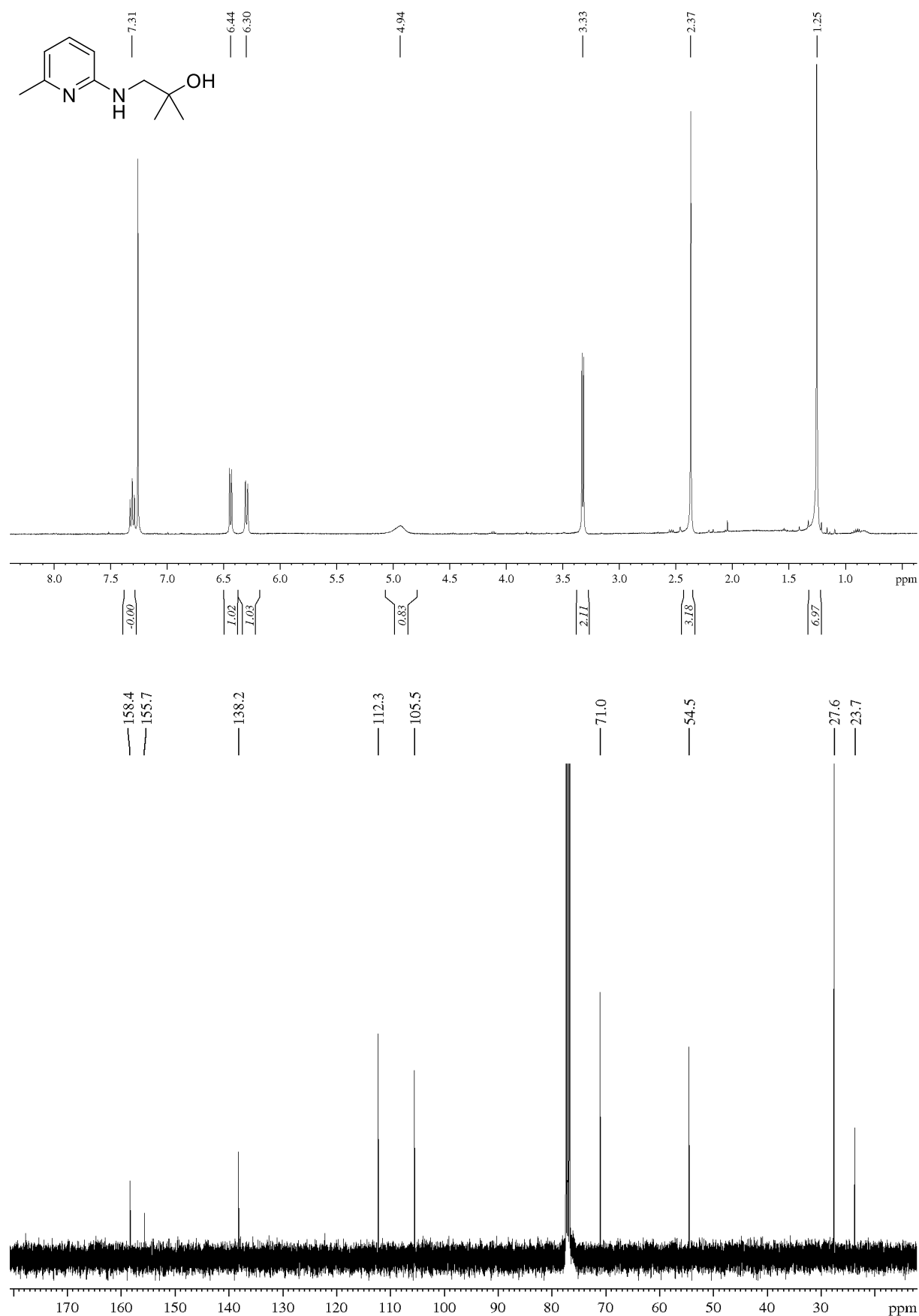
2-(6-methylpyridin-2-ylamino)ethan-1-ol (94b)

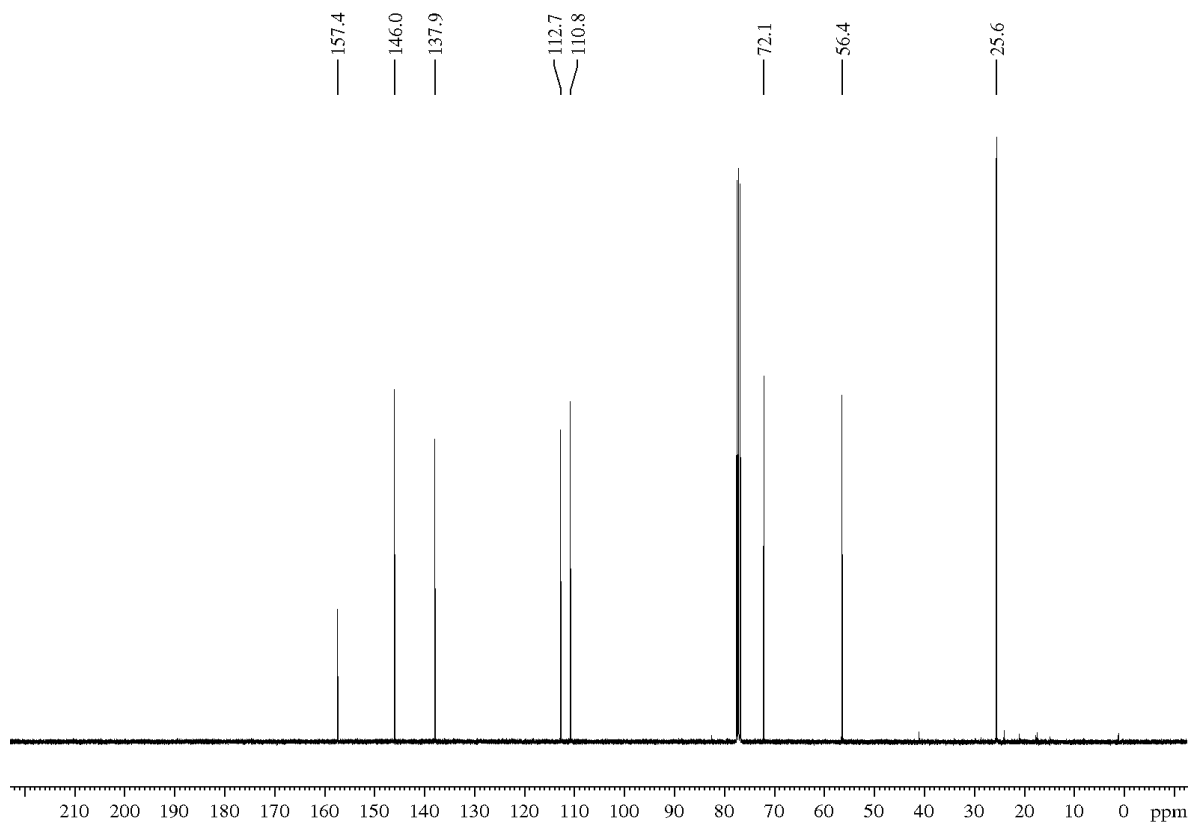
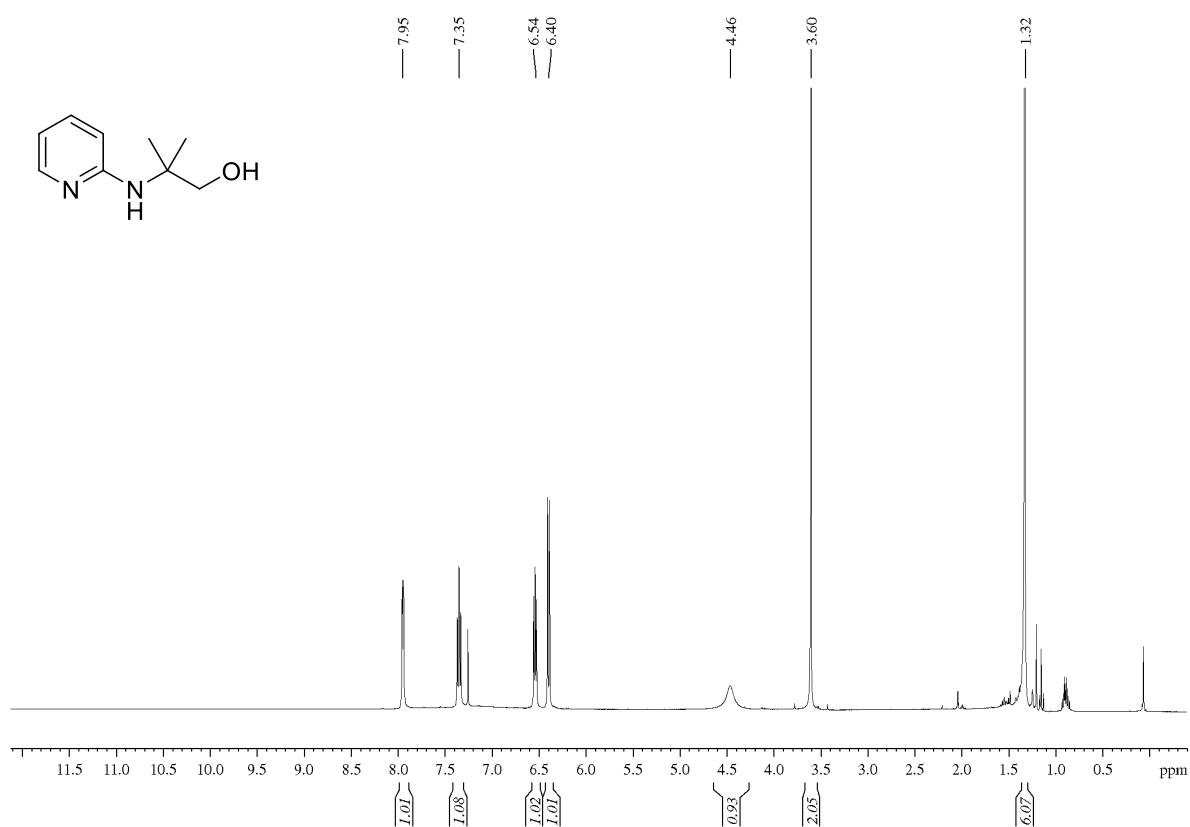
2-(pyridin-1-ylamino)propan-2-ol (95a)DMSO-d₆

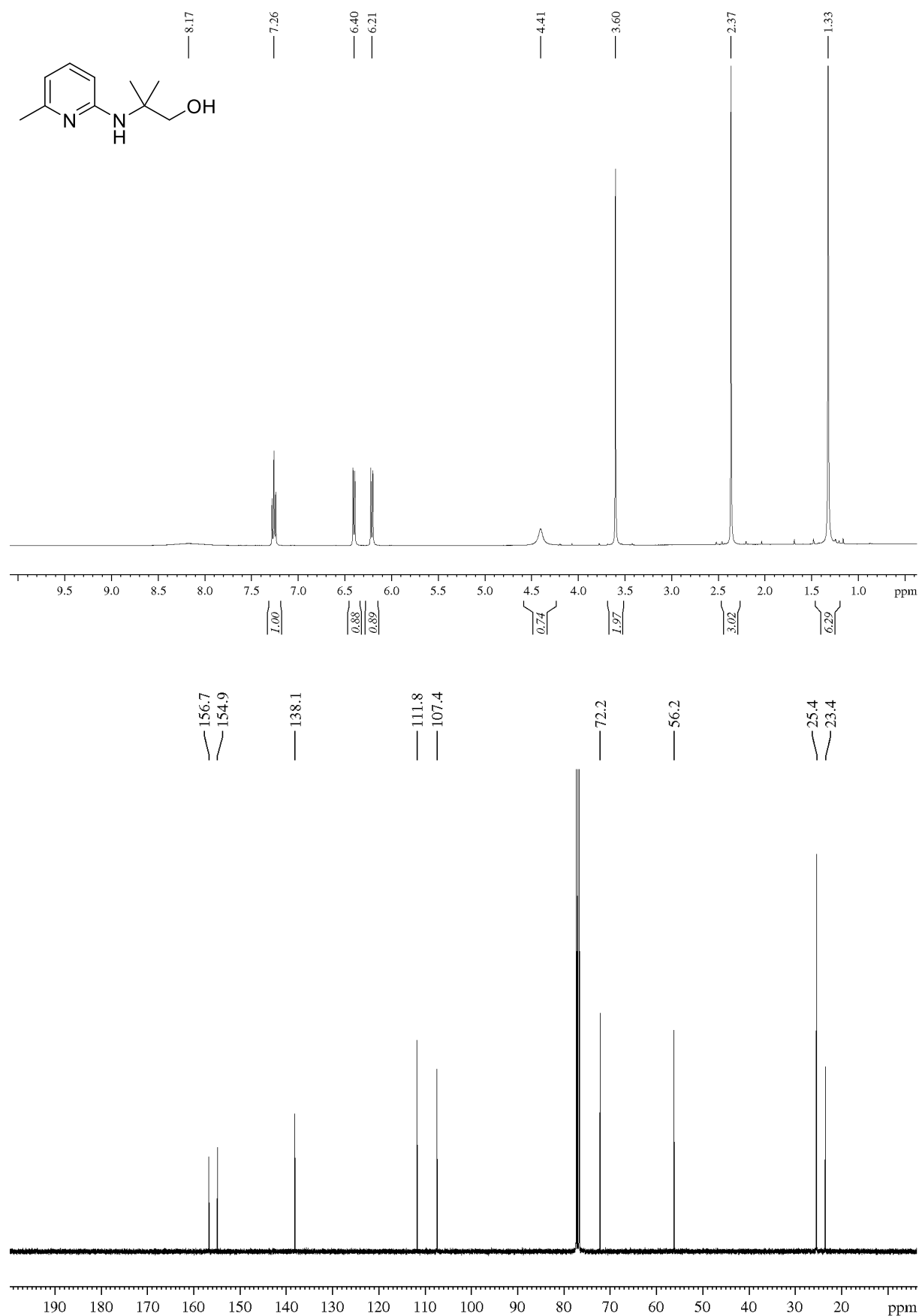
2-(pyridin-1-ylamino)propan-2-ol (95a)CDCl₃

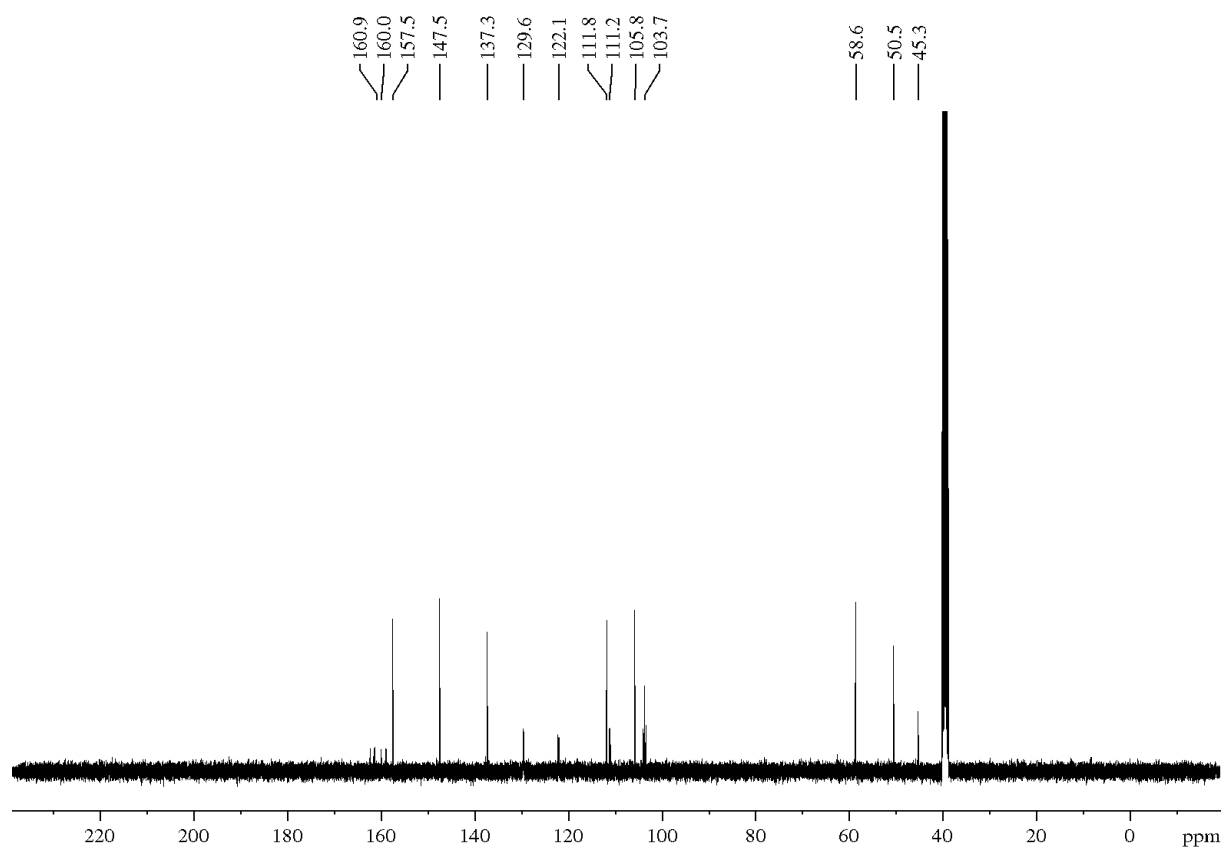
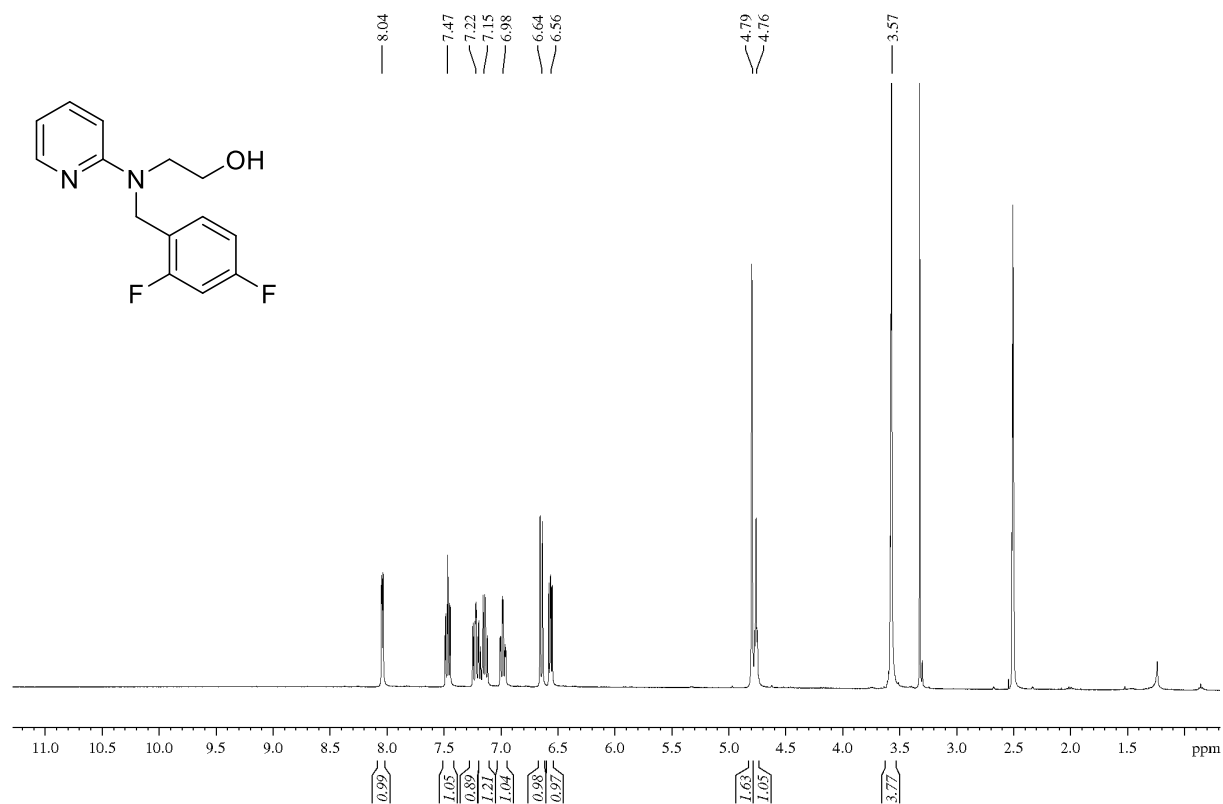
2-(6-methylpyridin-1-ylamino)propan-2-ol (95b)

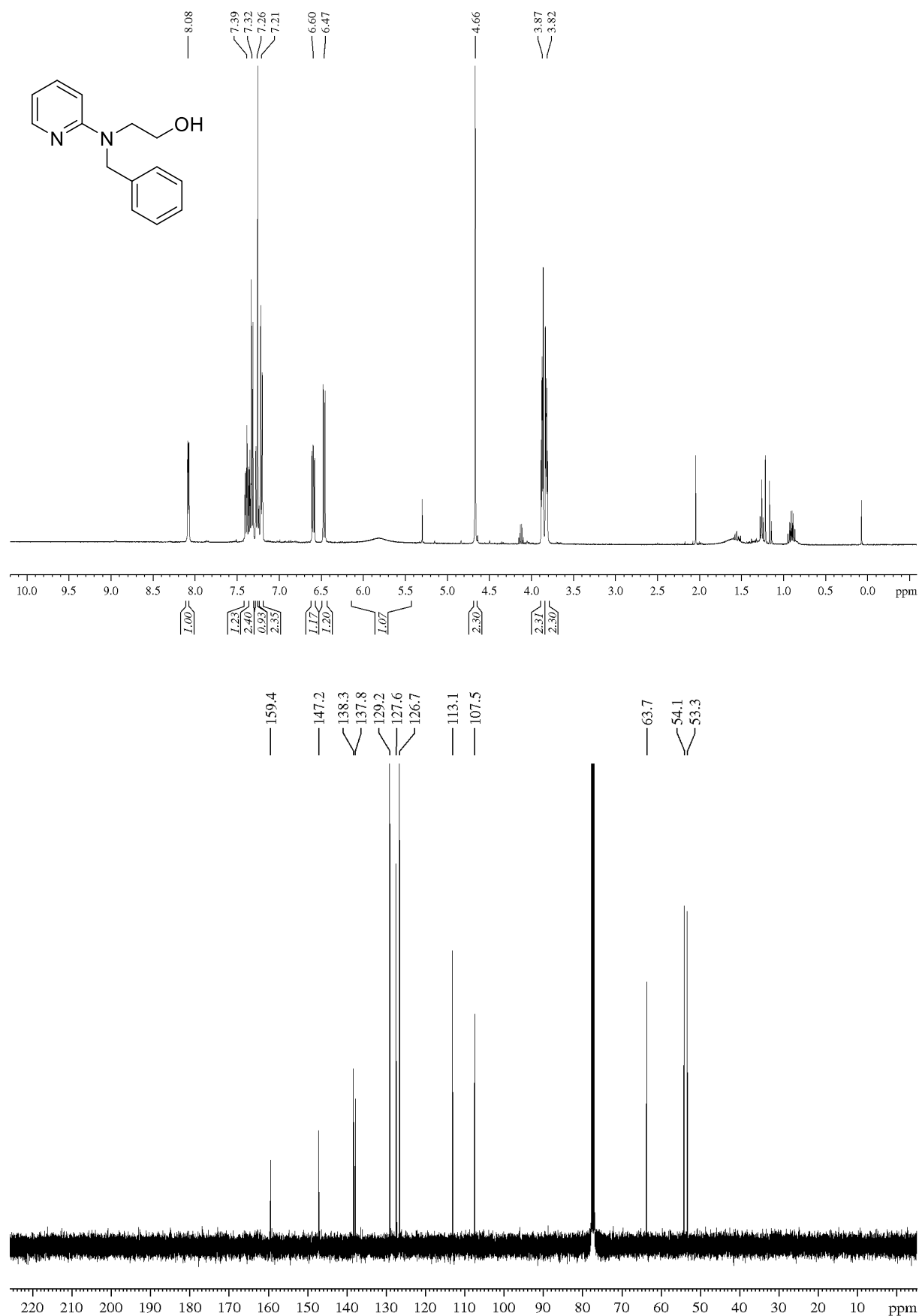
2-methyl-1-(pyridin-2-ylamino)propan-2-ol (96a)

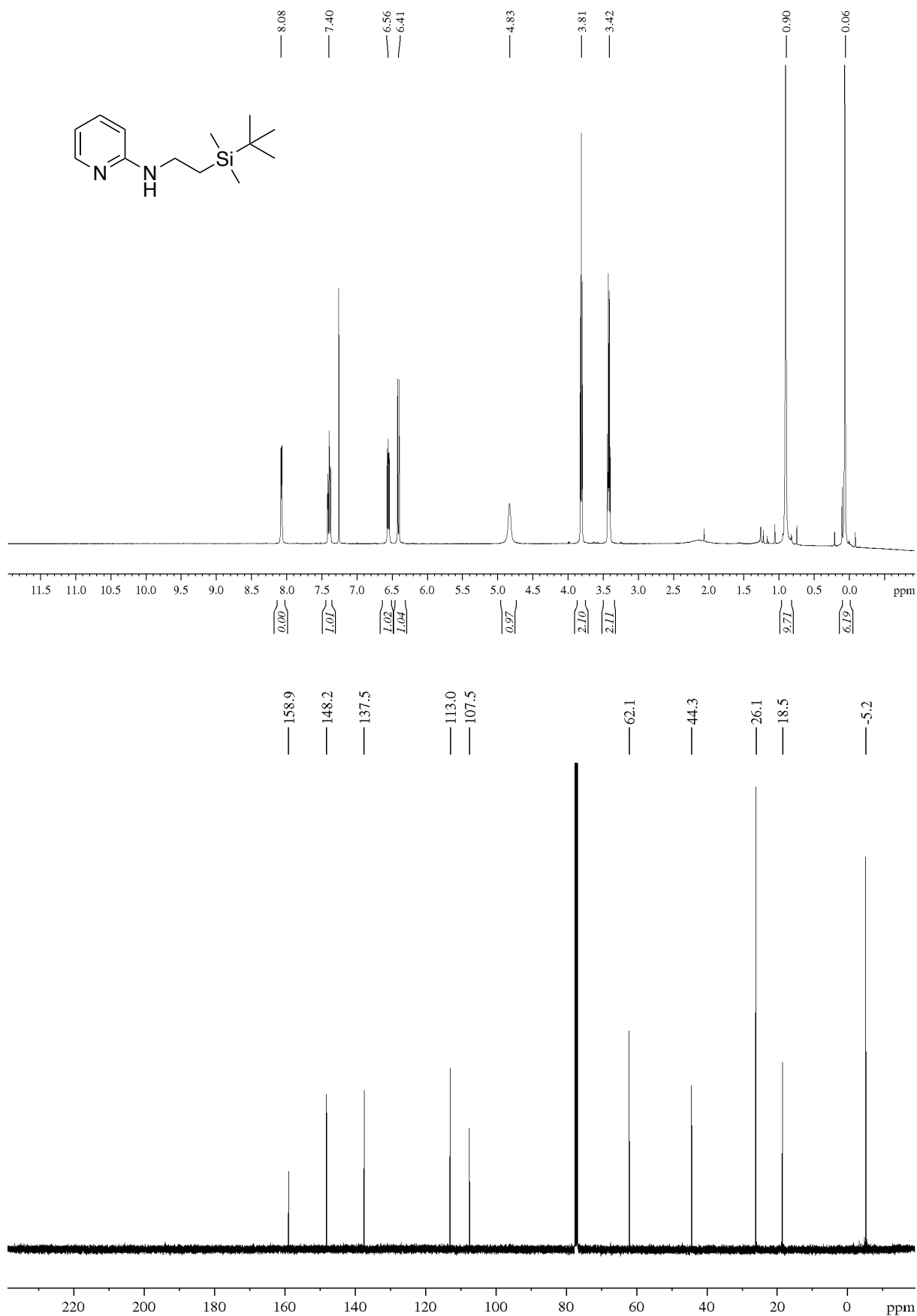
2-Methyl-1-(6-methylpyridin-2-ylamino)propan-2-ol (96b)

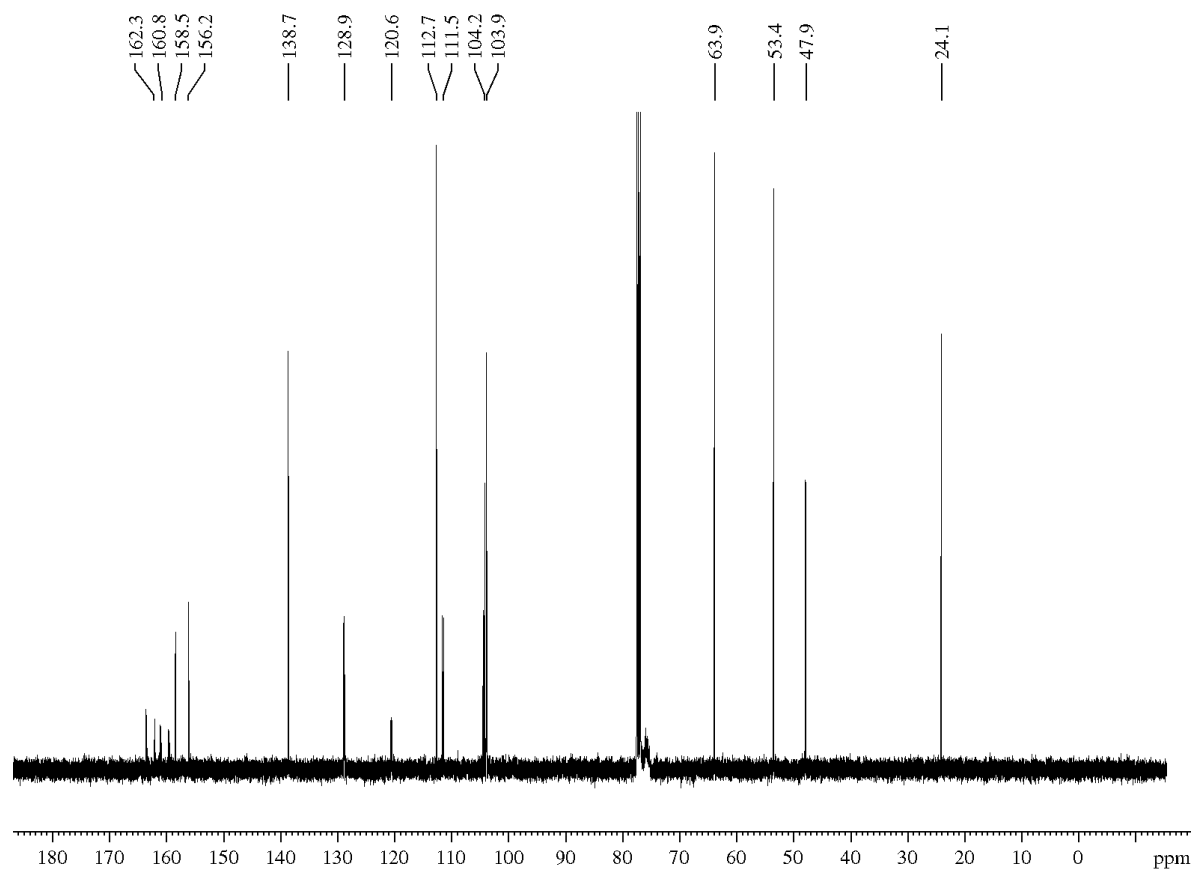
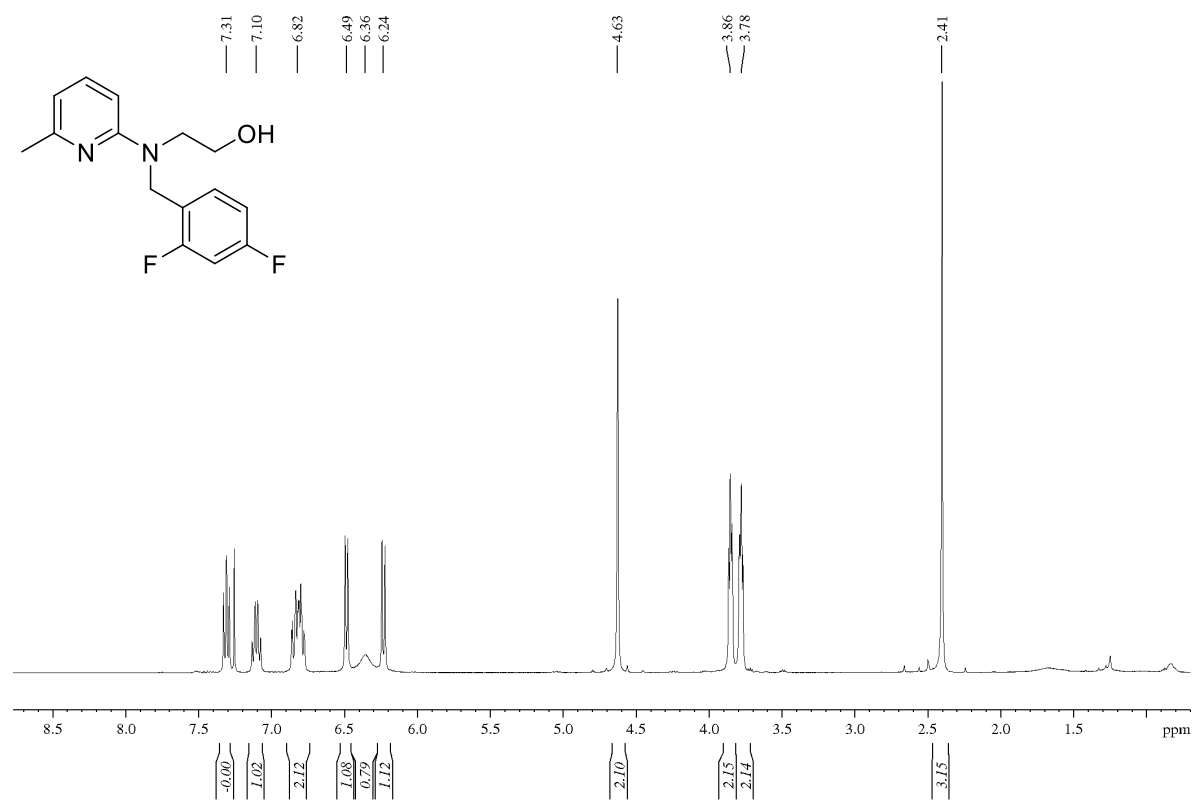
2-methyl-2-(pyridin-2-ylamino)propan-1-ol (97a)

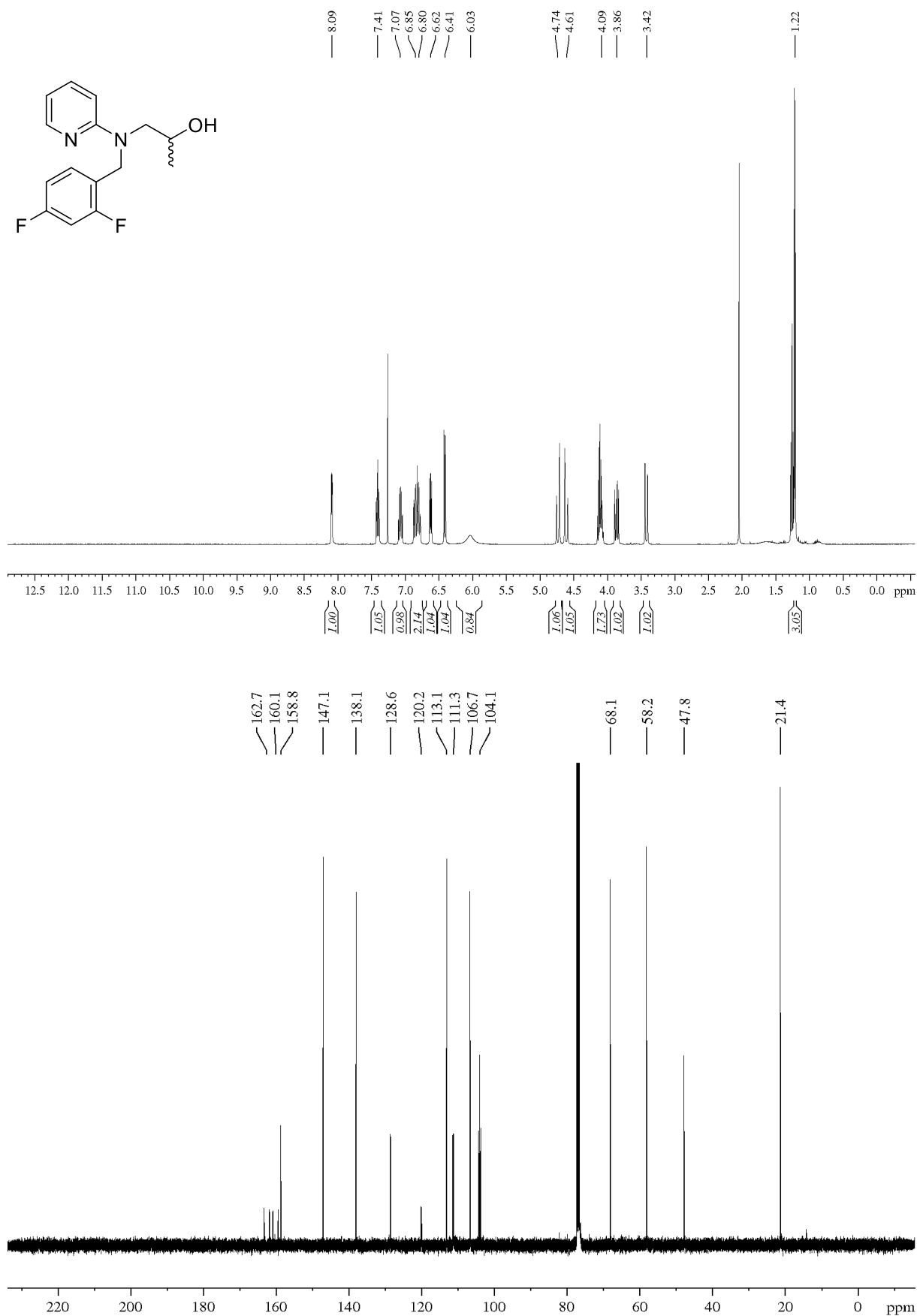
2-methyl-2-((6-methylpyridin-2-yl)amino)propan-1-ol (97b)

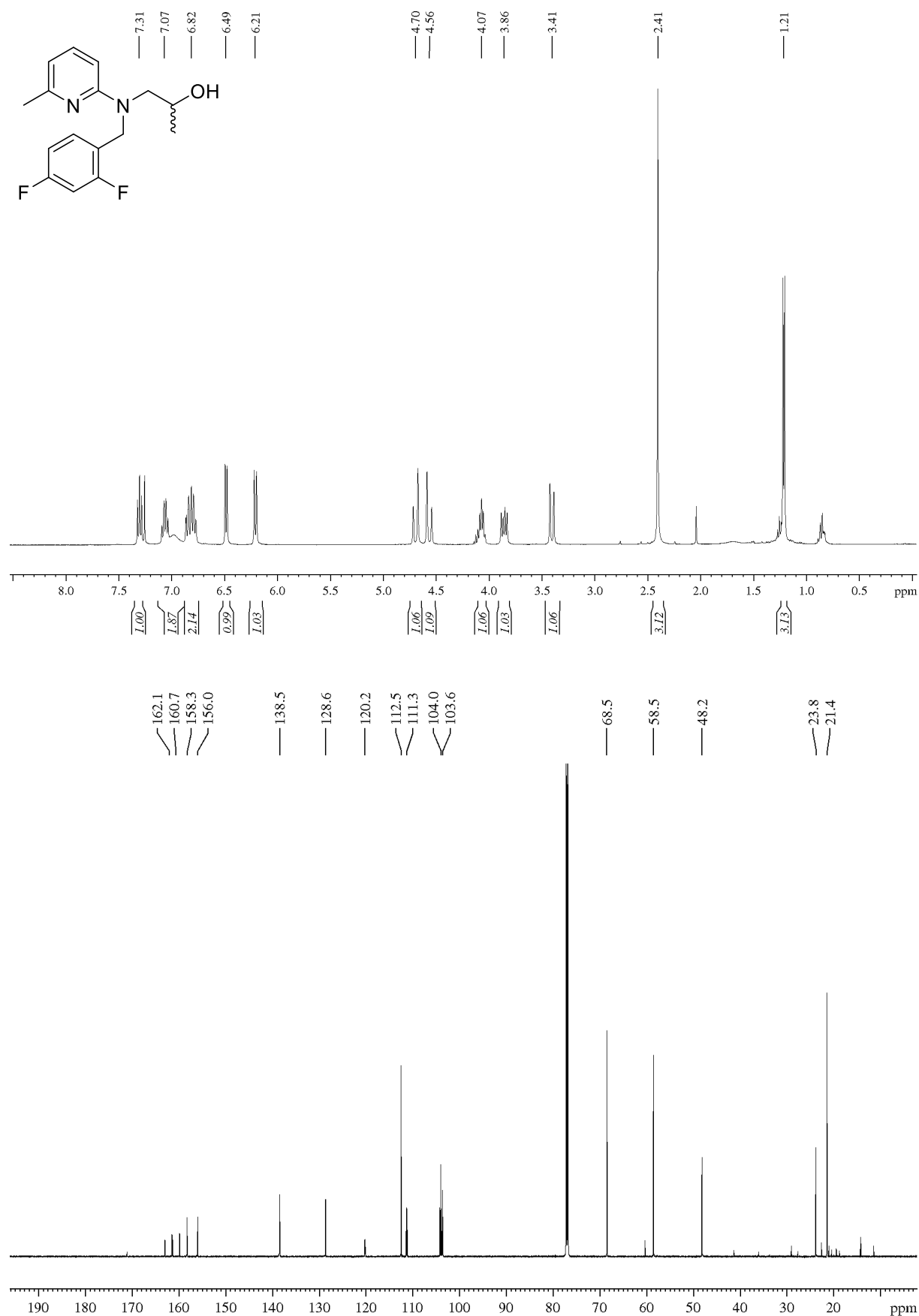
2-((2,4-difluorobenzyl)(pyridin-2-yl)amino)ethan-1-ol (85a)

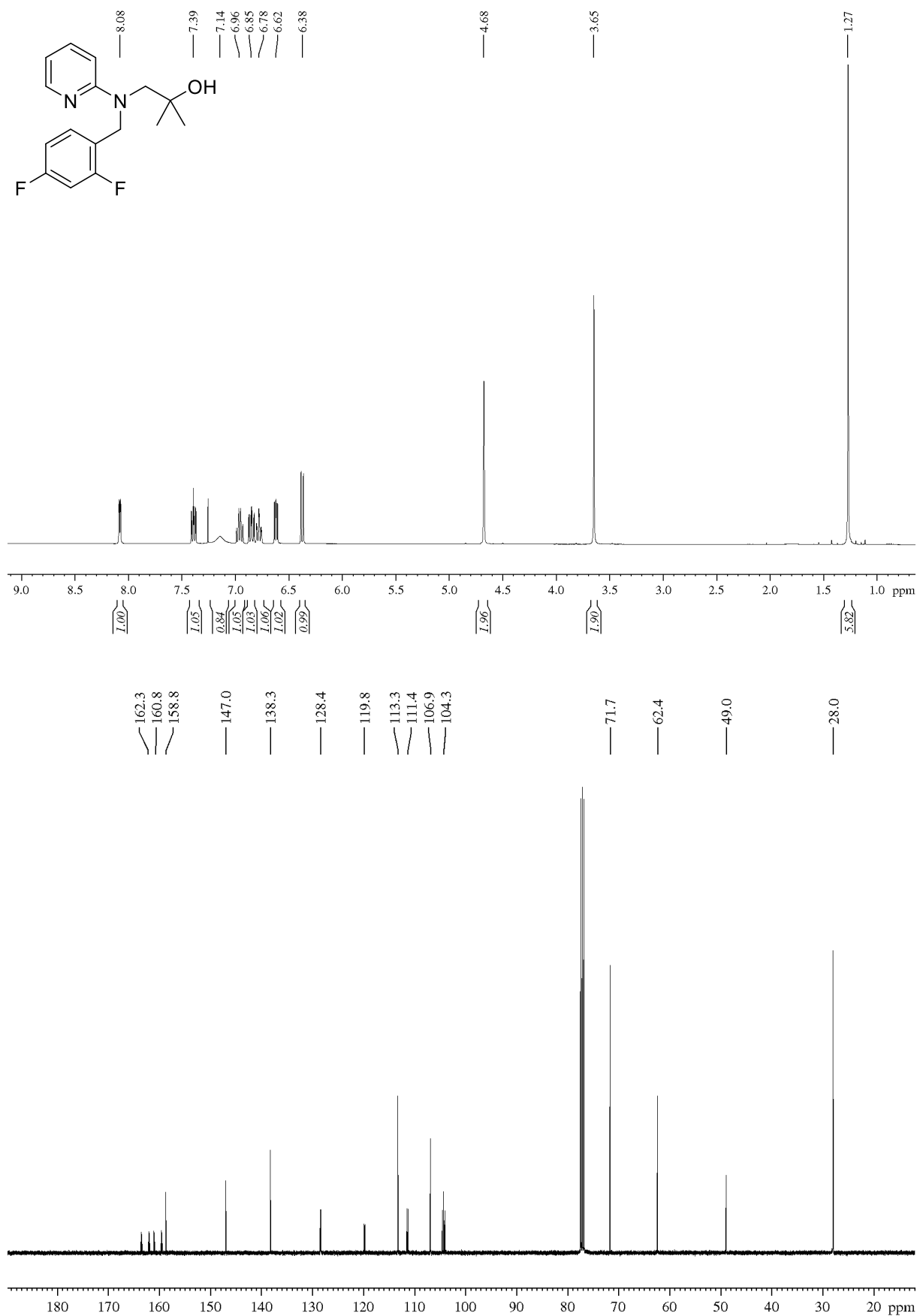
2-((benzyl)(pyridin-2-yl)amino)ethan-1-ol (89)

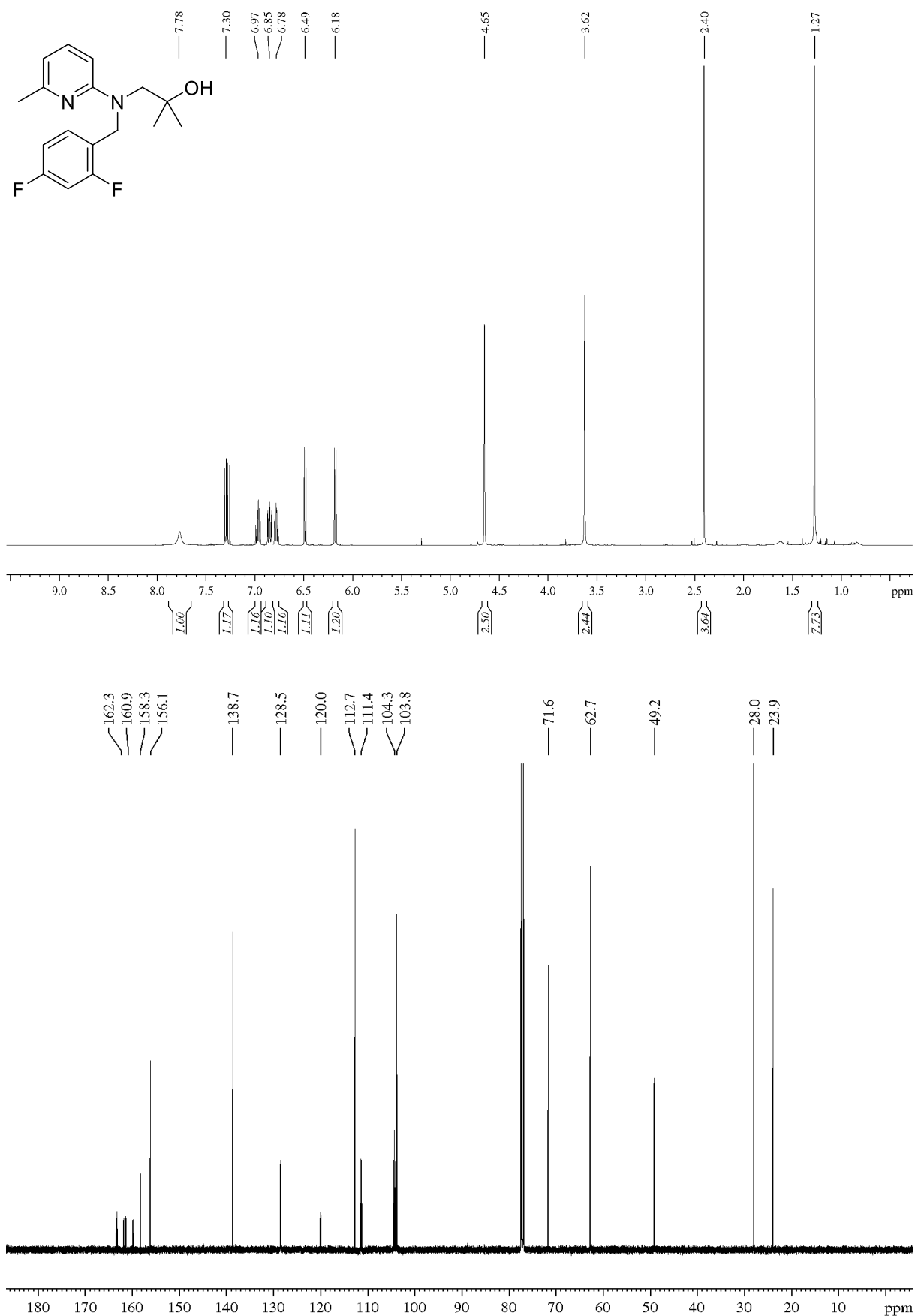
N-(2-((*tert*-butyldimethylsilyl)oxy)ethyl)pyridin-2-amine (100)

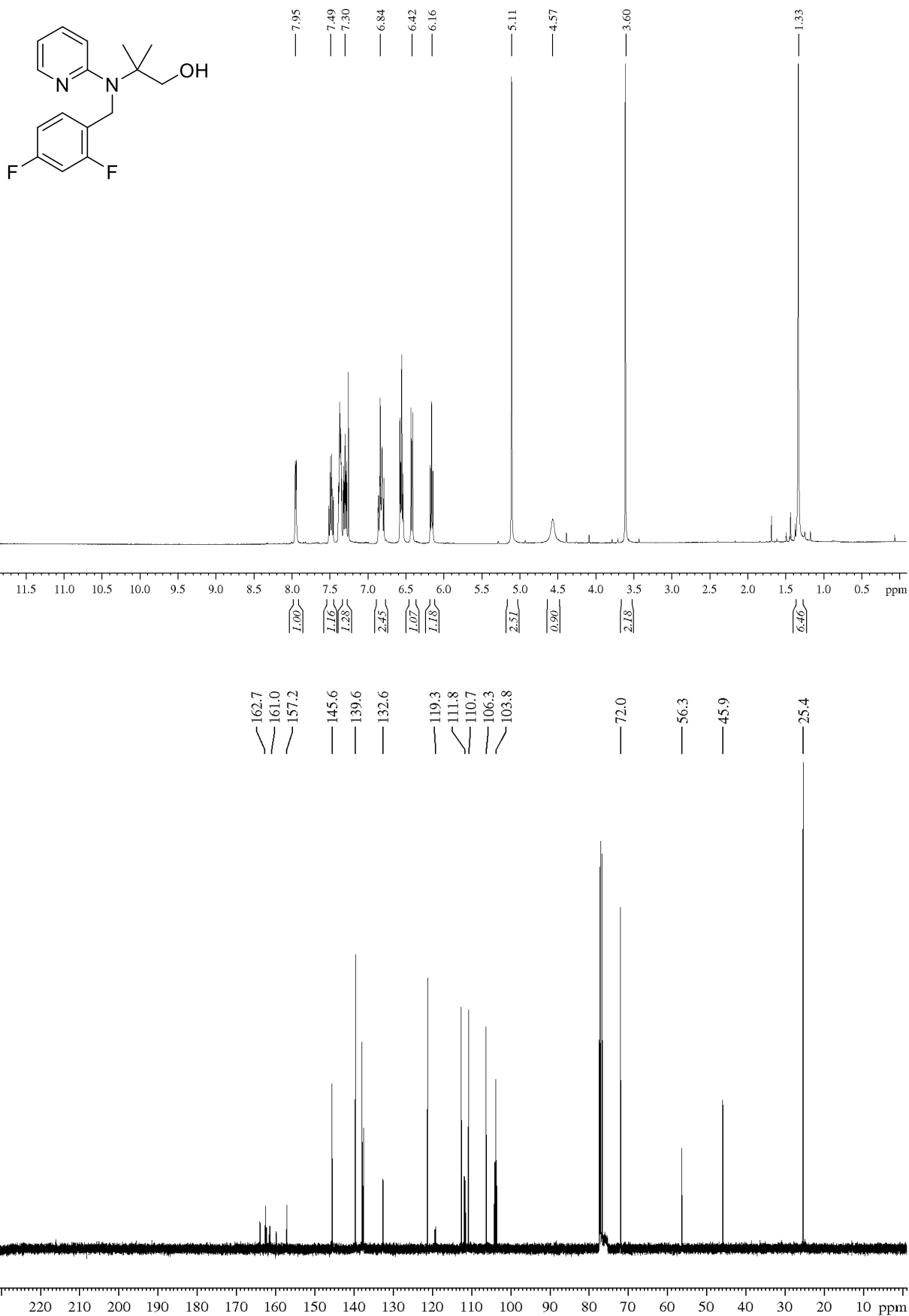
2-((2,4-difluorobenzyl)(6-methylpyridin-2-yl)amino)ethan-1-ol (85)

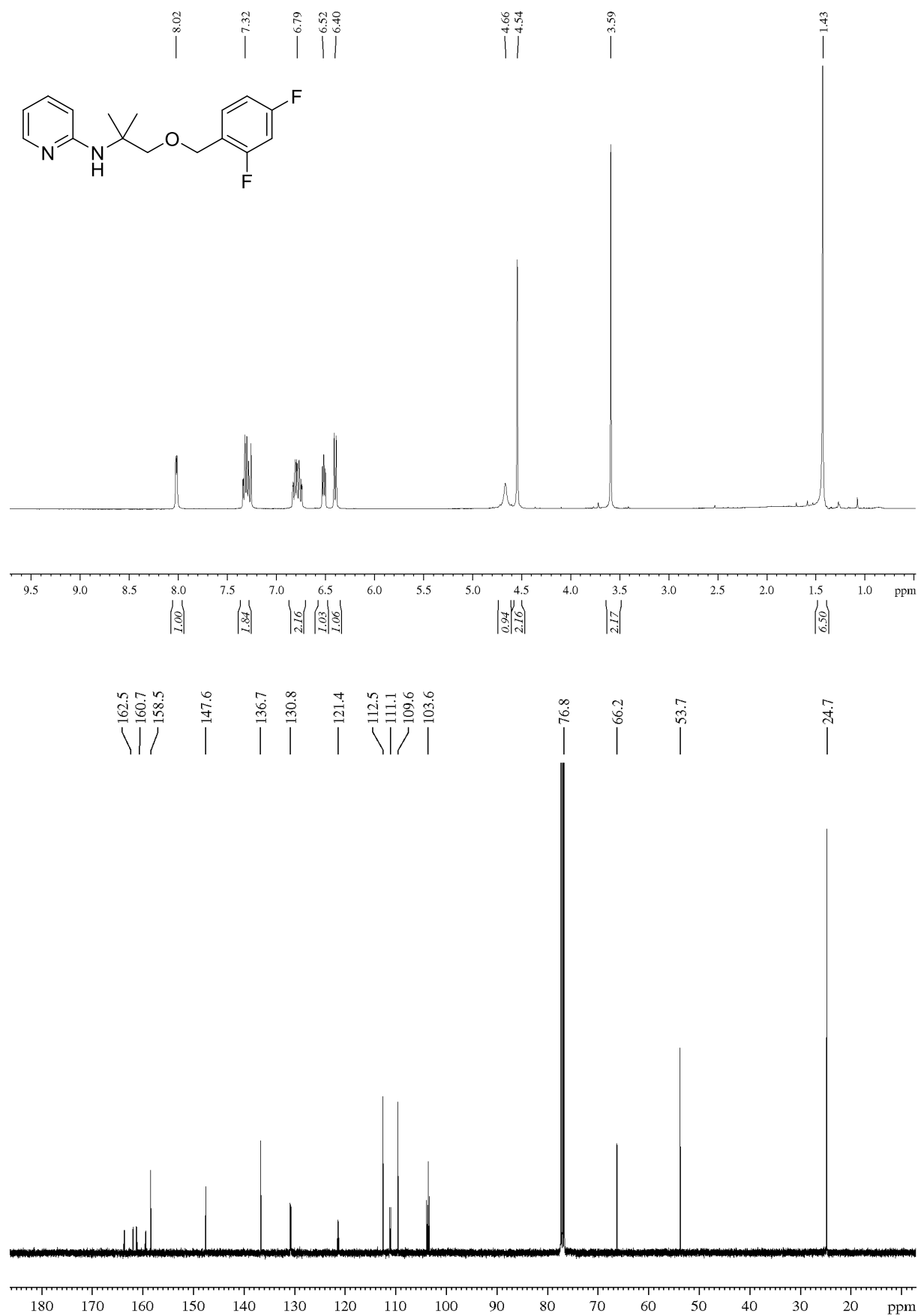
2-((2,4-difluorobenzyl)(pyridin-2-yl)amino)propan-1-ol (86)

2-((2,4-difluorobenzyl)(6-methylpyridin-2-yl)amino)propan-1-ol (86b)

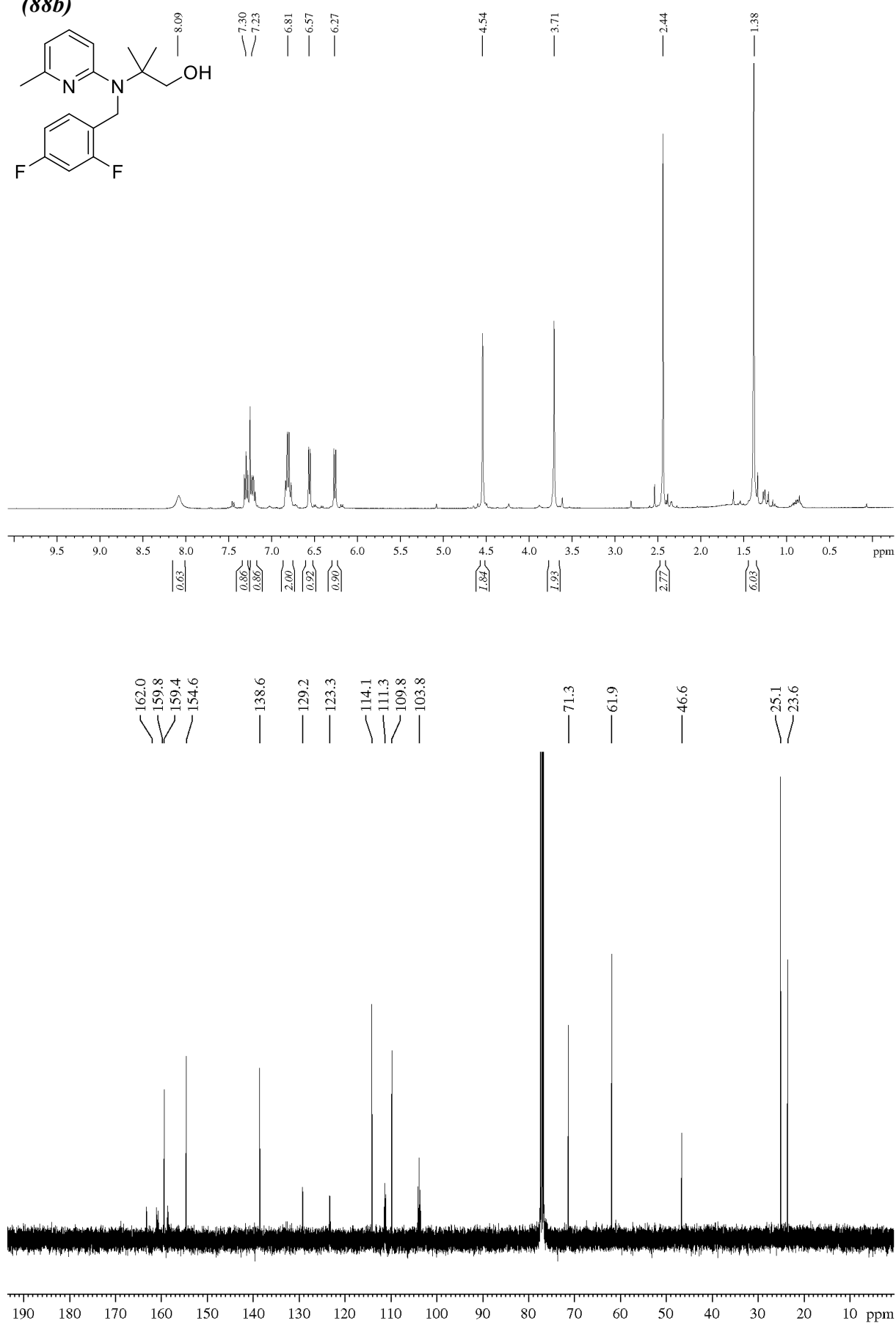
1-((2,4-difluorobenzyl)(pyridin-2-yl)amino)-2-methylpropan-2-ol (87a)

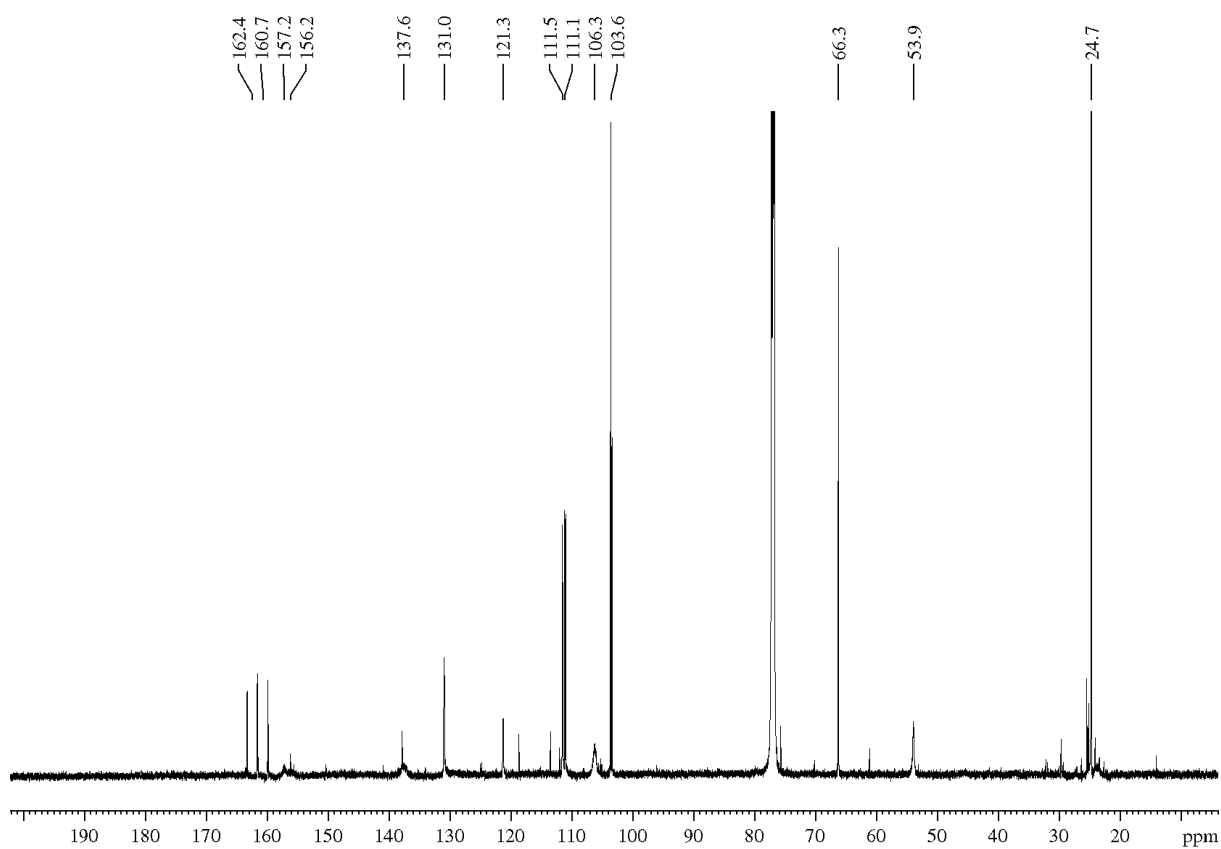
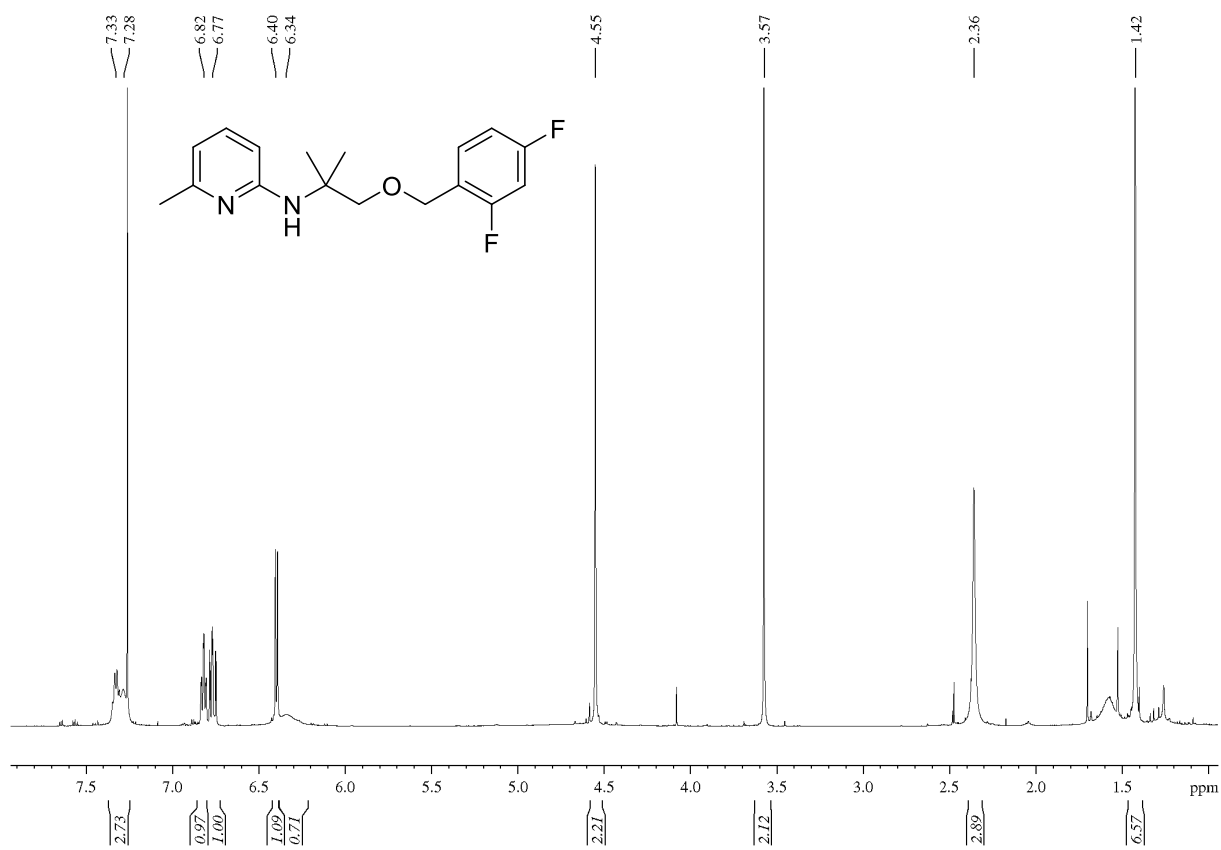
1-((2,4-difluorobenzyl)(6-methylpyridin-2-yl)amino)-2-methylpropan-2-ol (87b)

2-((2,4-difluorobenzyl)(pyridin-2-yl)amino)-2-methylpropan-1-ol (88a)

N-(1-((2,4-difluorobenzyl)oxy)-2-methylpropan-2-yl)pyridin-2-amine (102)

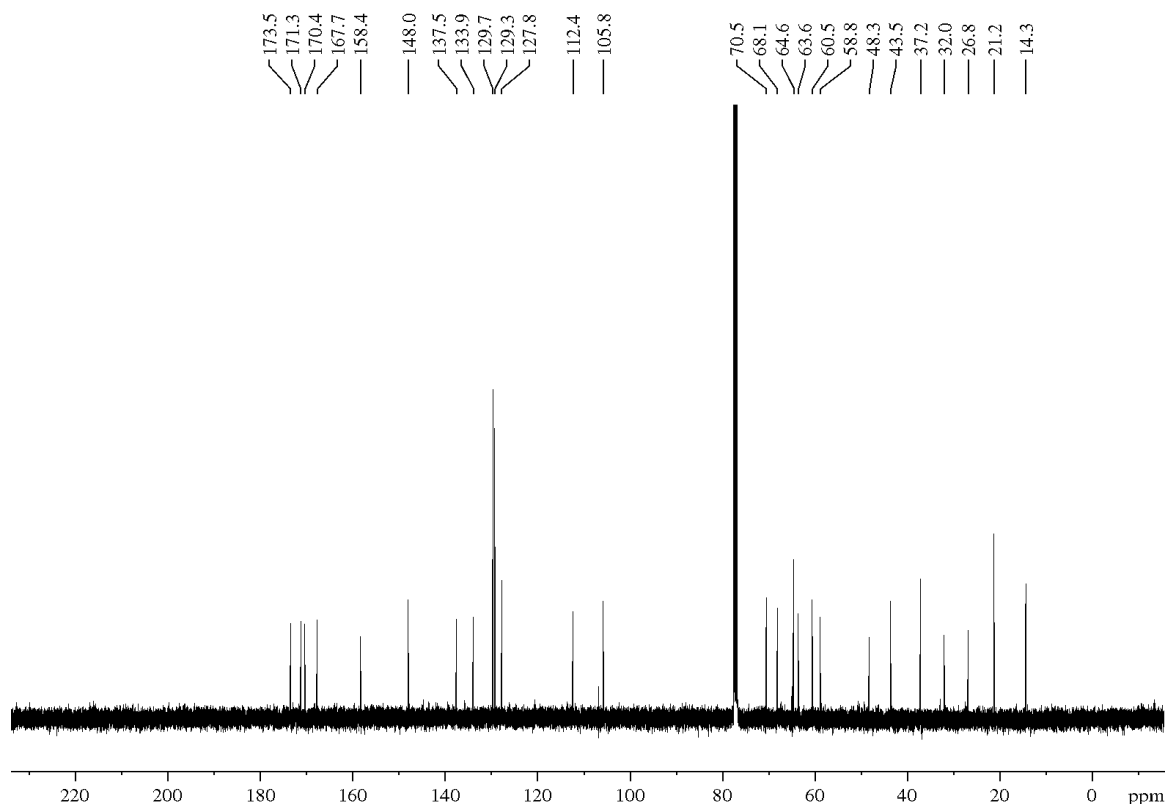
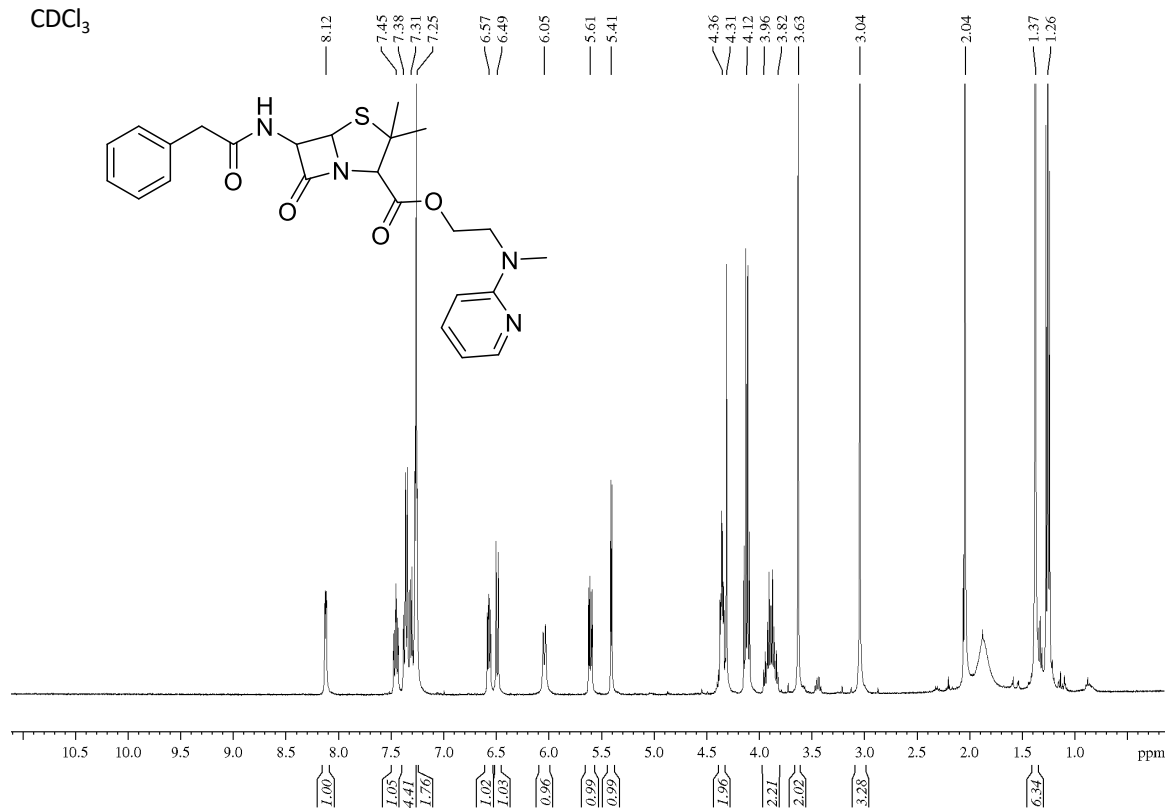
2-((2,4-difluorobenzyl)(6-methylpyridin-2-yl)amino)-2-methylpropan-1-ol
(88b)



N-(1-((2,4-difluorobenzyl)oxy)-2-methylpropan-2-yl)-6-methylpyridin-2-amine (102b)

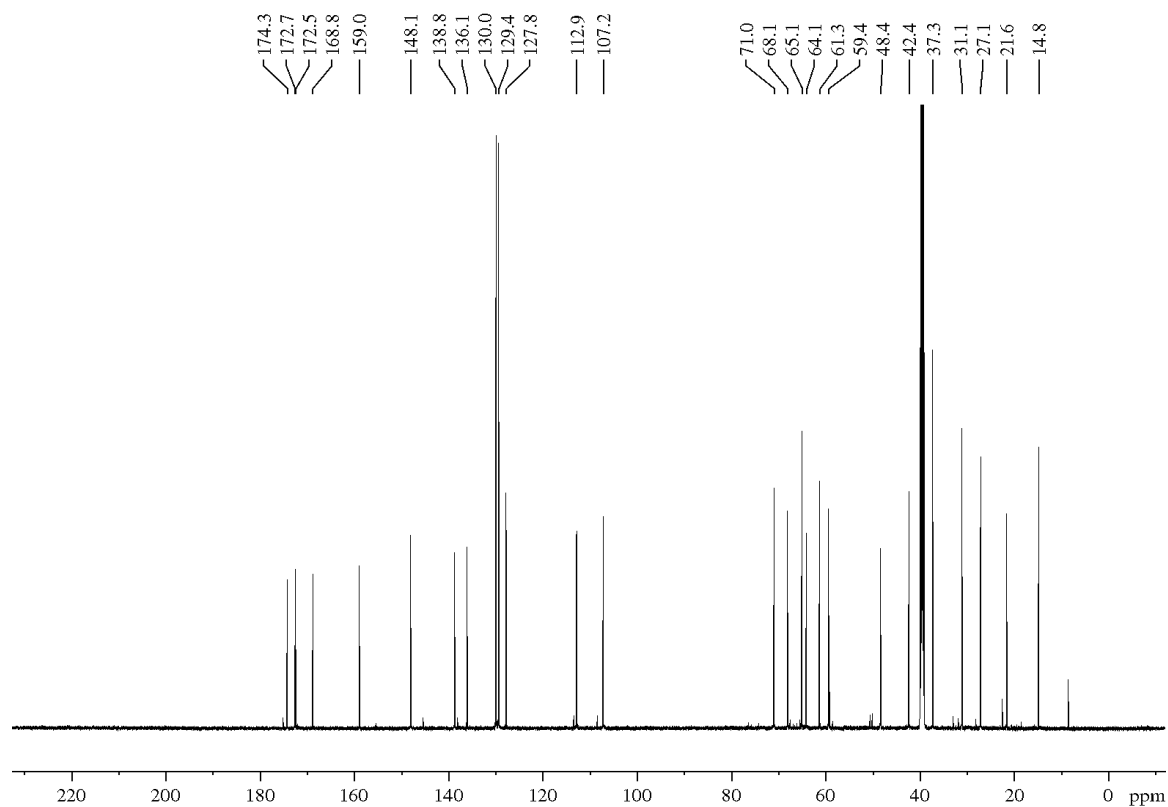
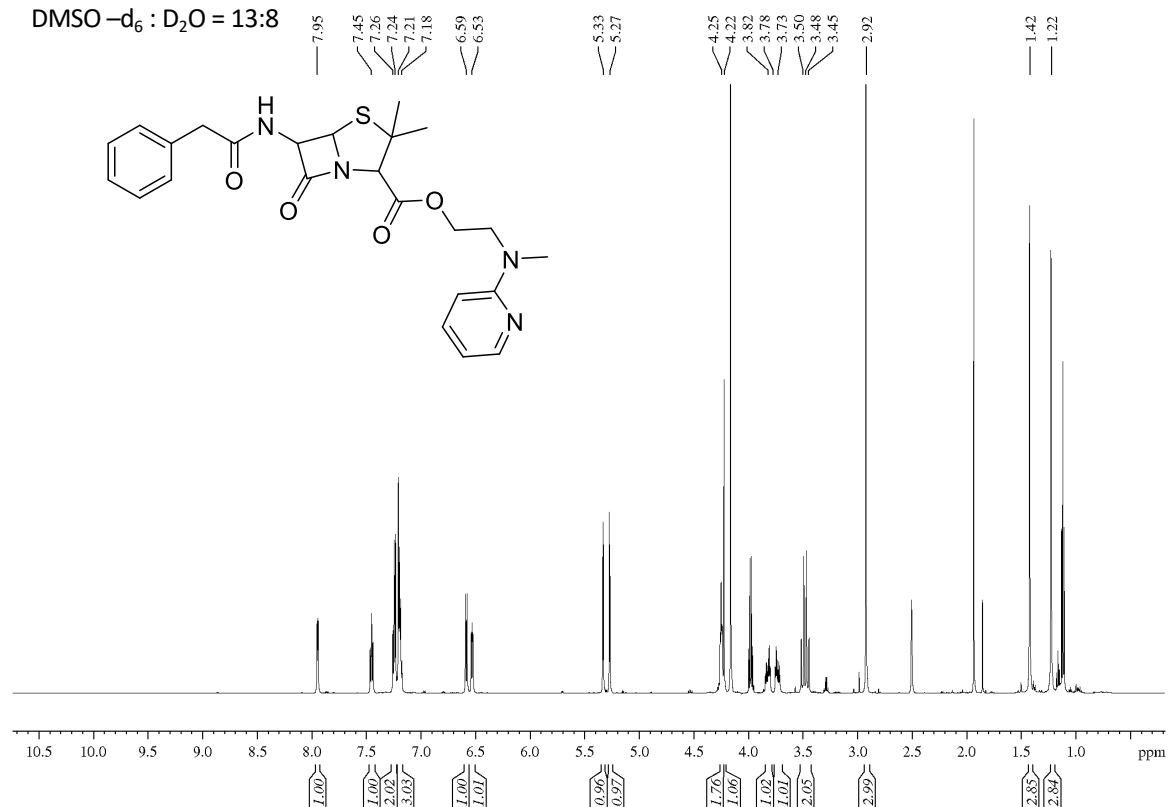
2-(methyl(pyridin-2-yl)amino)ethyl (2S,5R,6R)-3,3-dimethyl-7-oxo-6-(2-phenylacetamido)-4-thia-1-azabicyclo[3.2.0]heptane-2-carboxylate (105)

CDCl₃

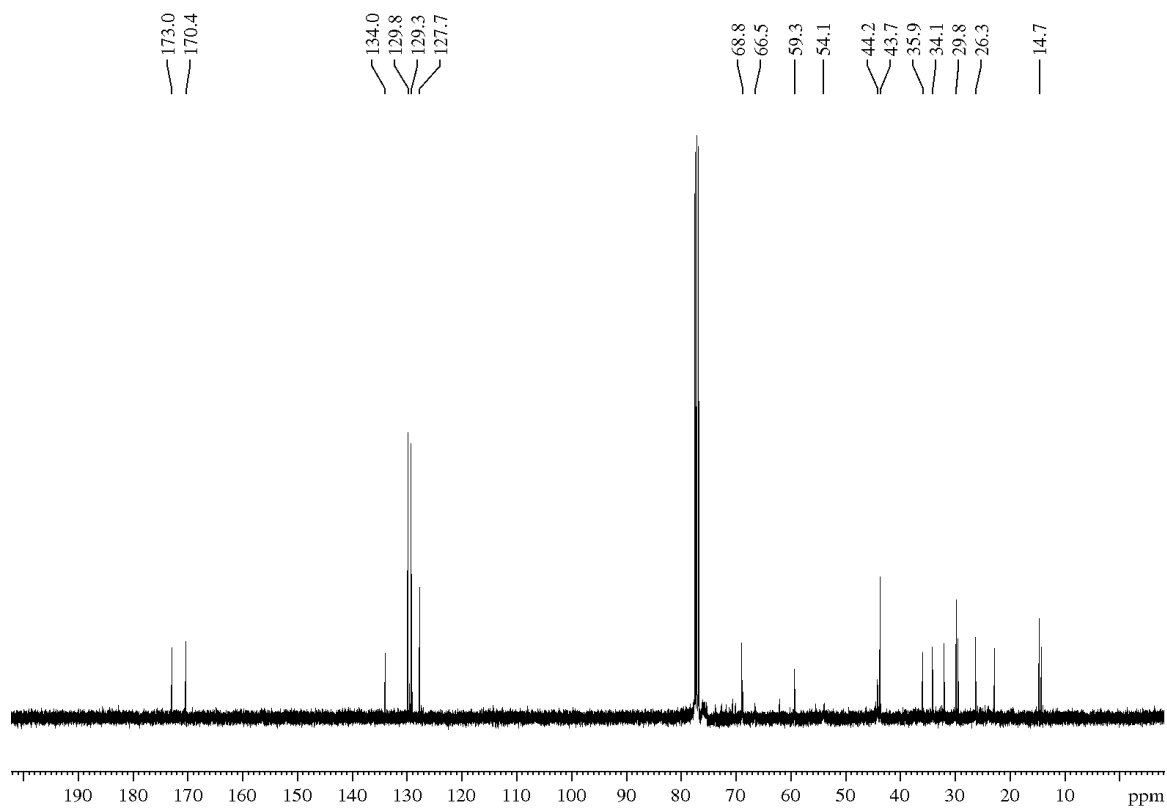
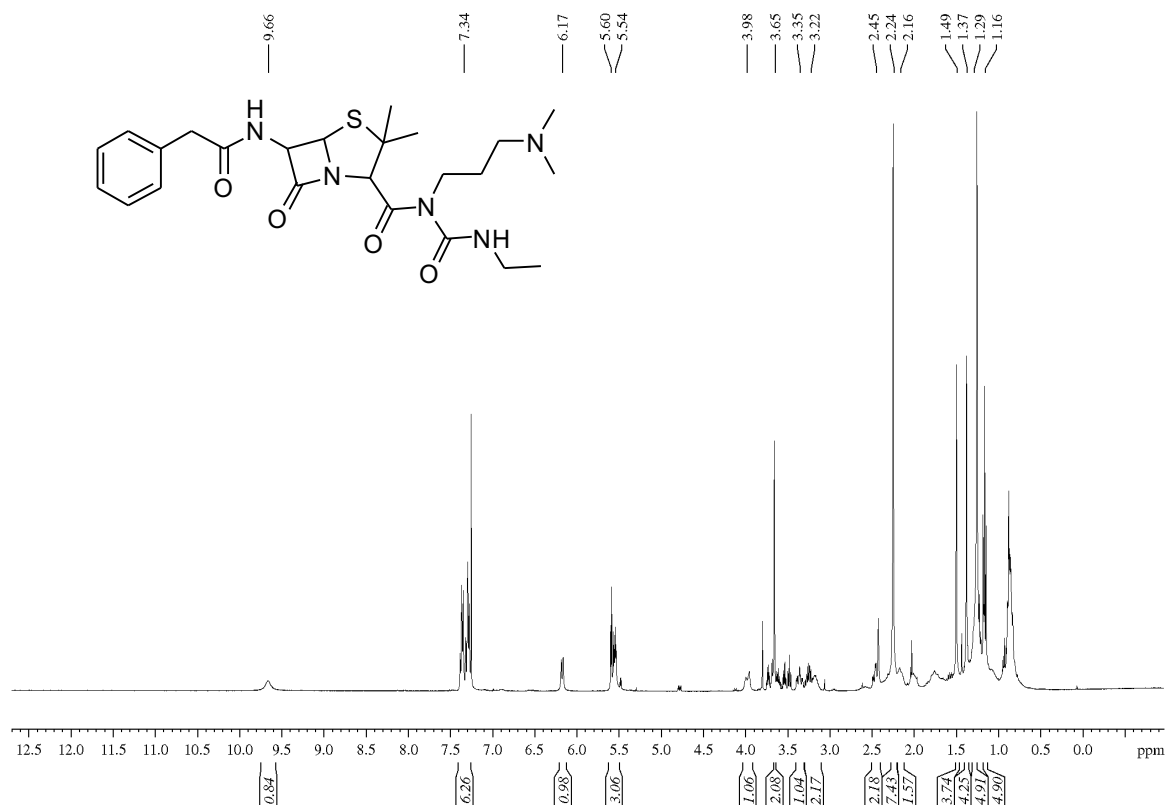


2-(methyl(pyridin-2-yl)amino)ethyl (2S,5R,6R)-3,3-dimethyl-7-oxo-6-(2-phenylacetamido)-4-thia-1-azabicyclo[3.2.0]heptane-2-carboxylate (105)

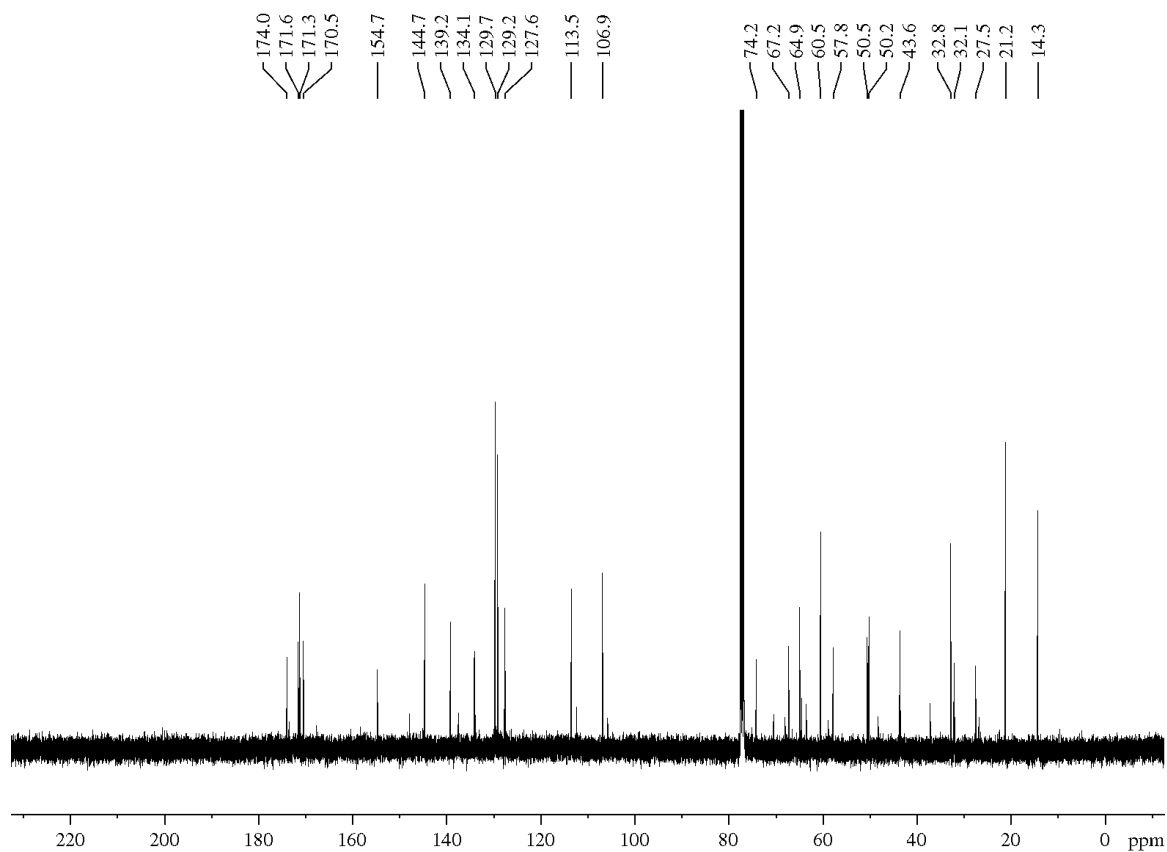
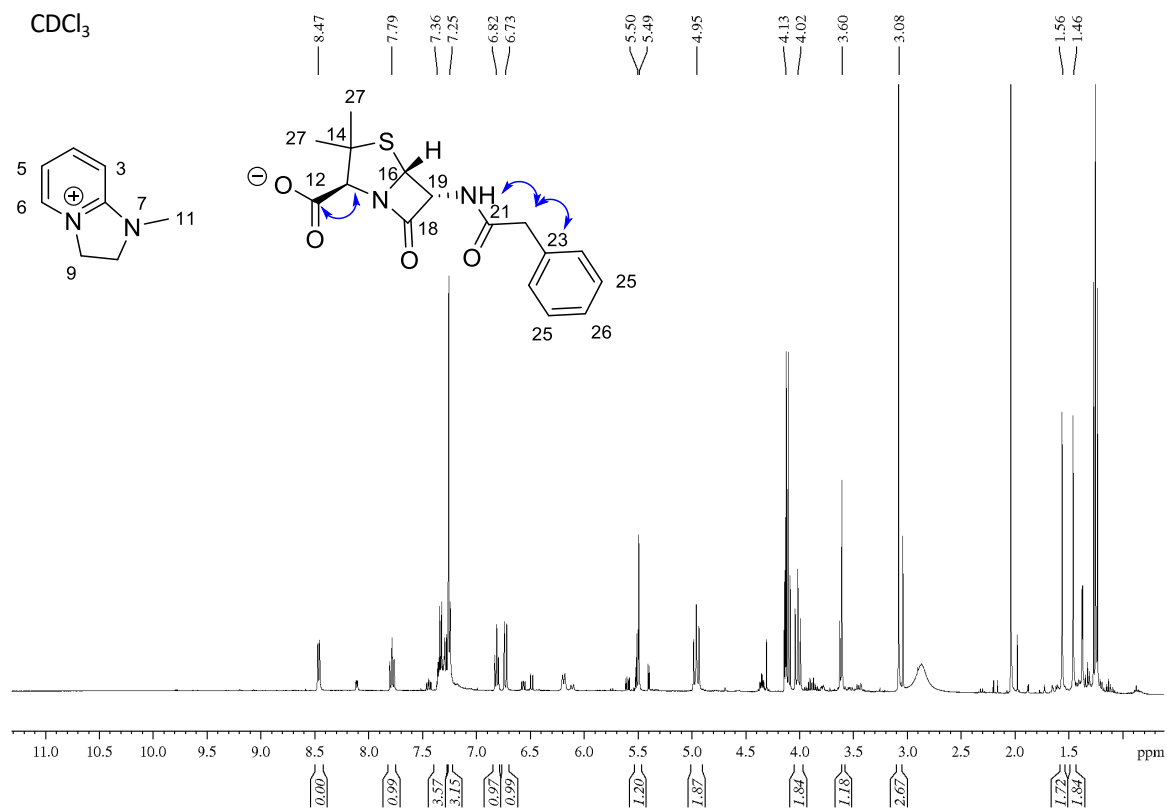
DMSO-d₆ : D₂O = 13:8



(2*S*,5*S*,6*S*)-*N*-(3-(dimethylamino)propyl)-*N*-(ethylcarbamoyl)-3,3-dimethyl-7-oxo-6-(2-phenylacetamido)-4-thia-1-azabicyclo[3.2.0]heptane-2-carboxamide (106)

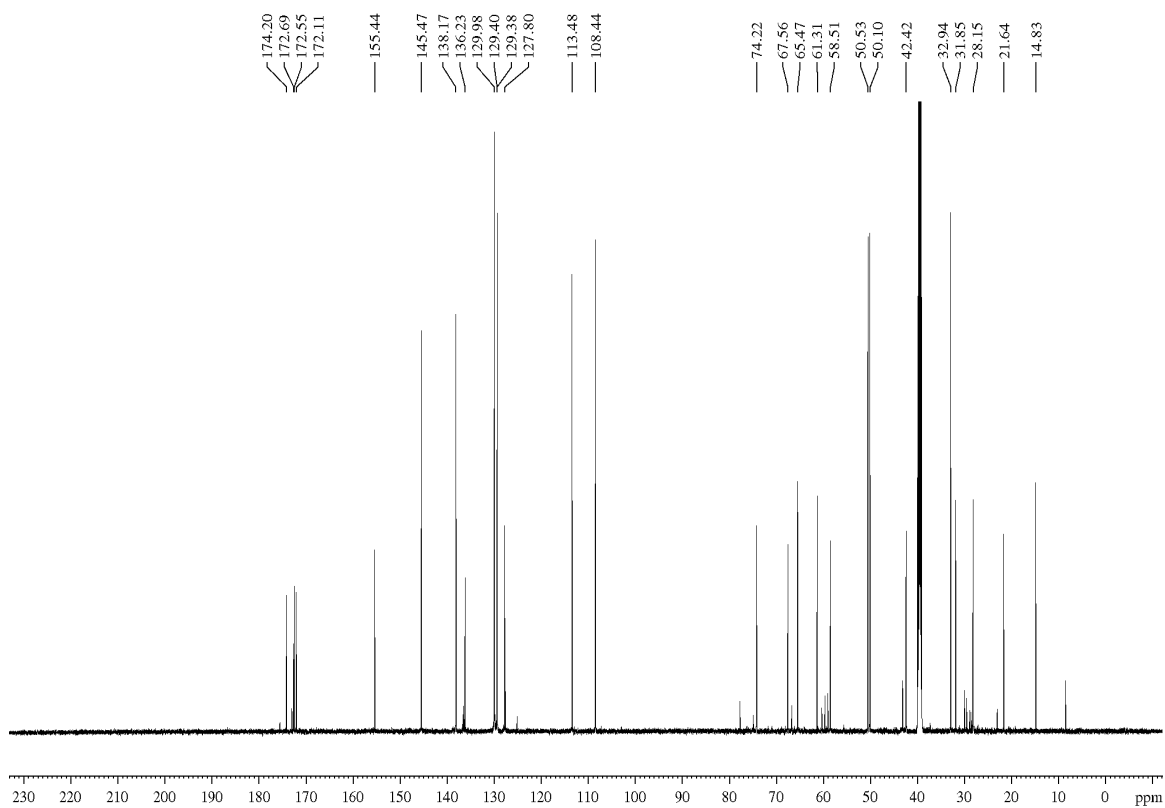
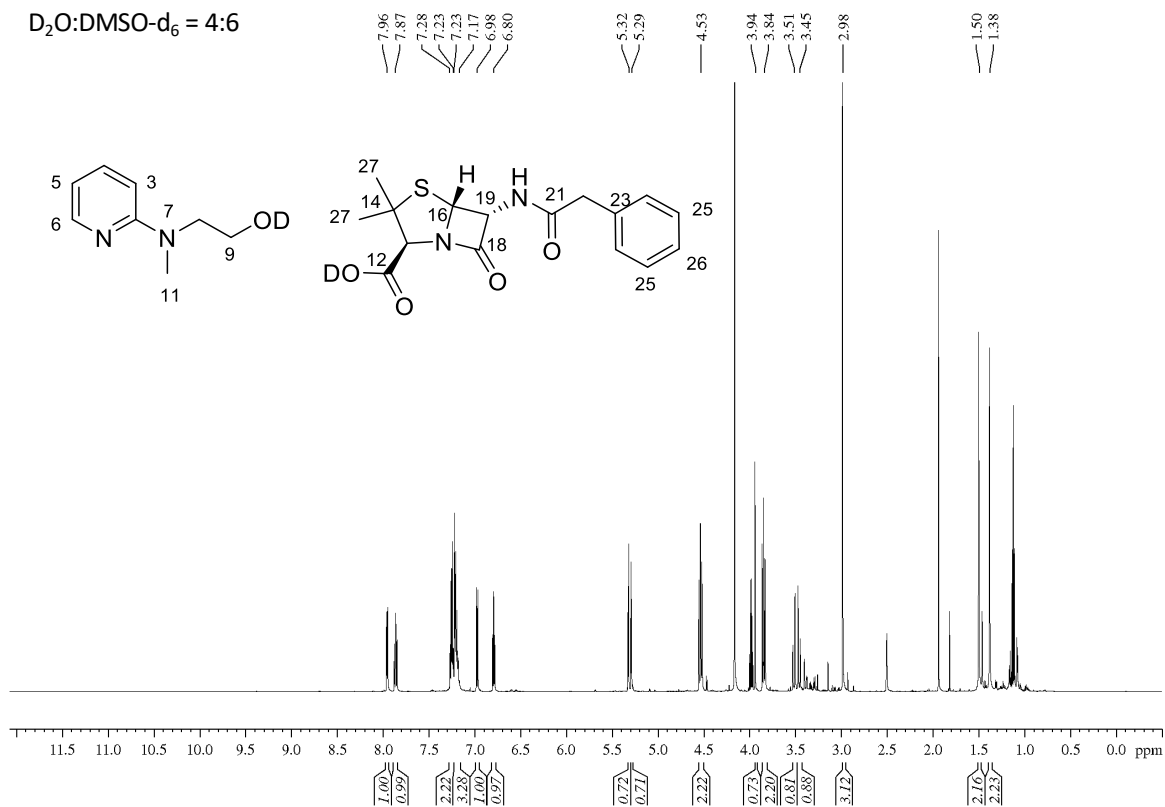


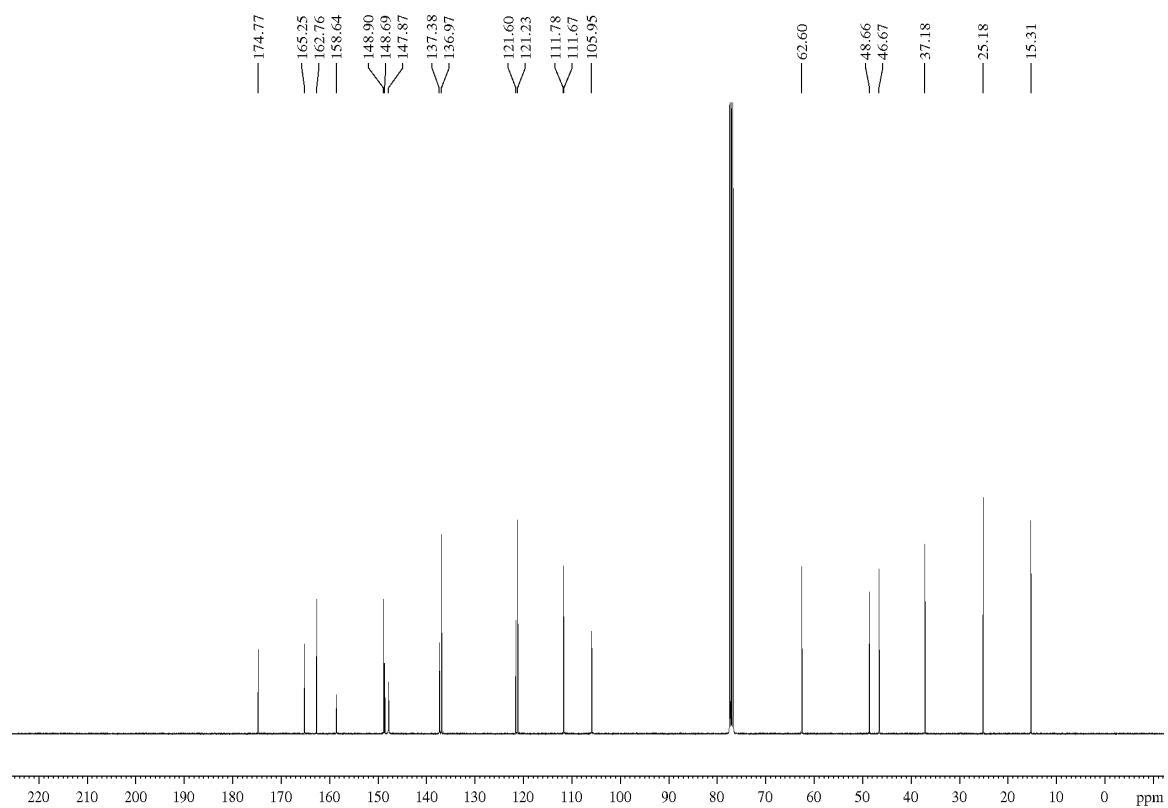
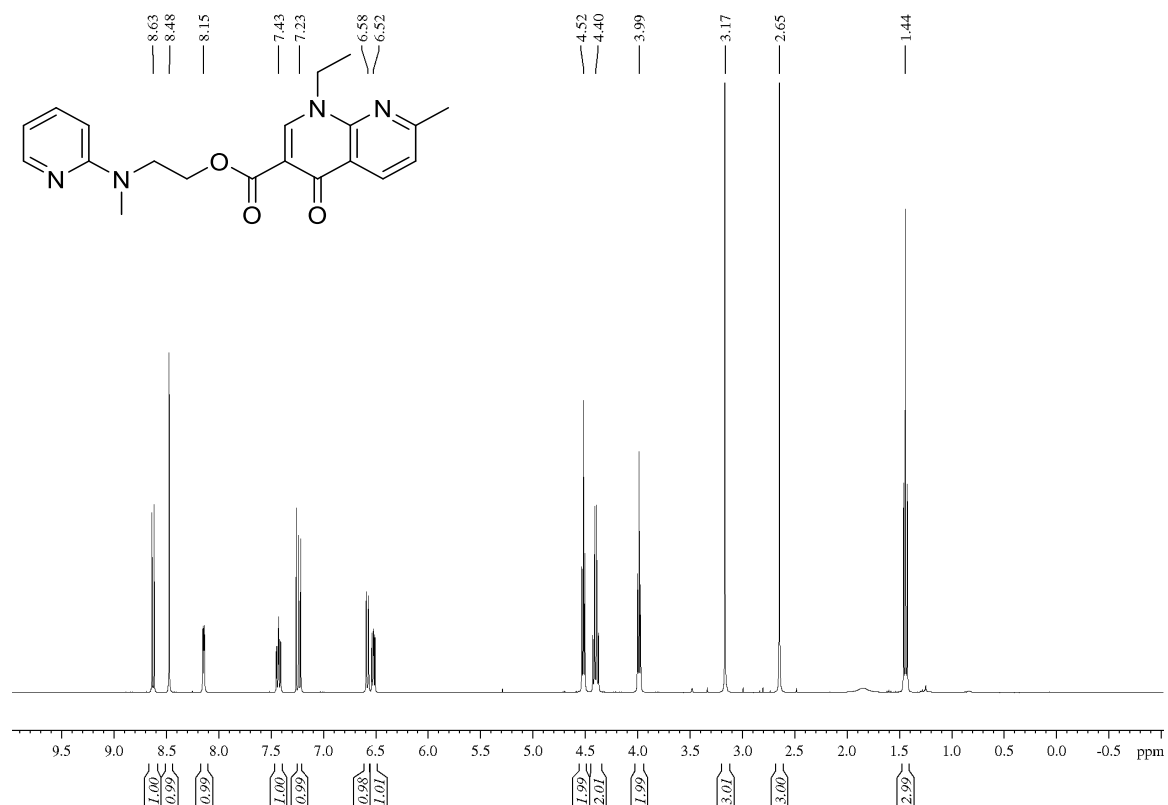
1-methyl-2,3-dihydro-1H-imidazo[1,2-a]pyridin-4-ium and (2S,5R,6R)-3,3-dimethyl-7-oxo-6-(2-phenylacetamido)-4-thia-1-azabicyclo[3.2.0]heptane-2-carboxylate (104 and 107)

CDCl₃

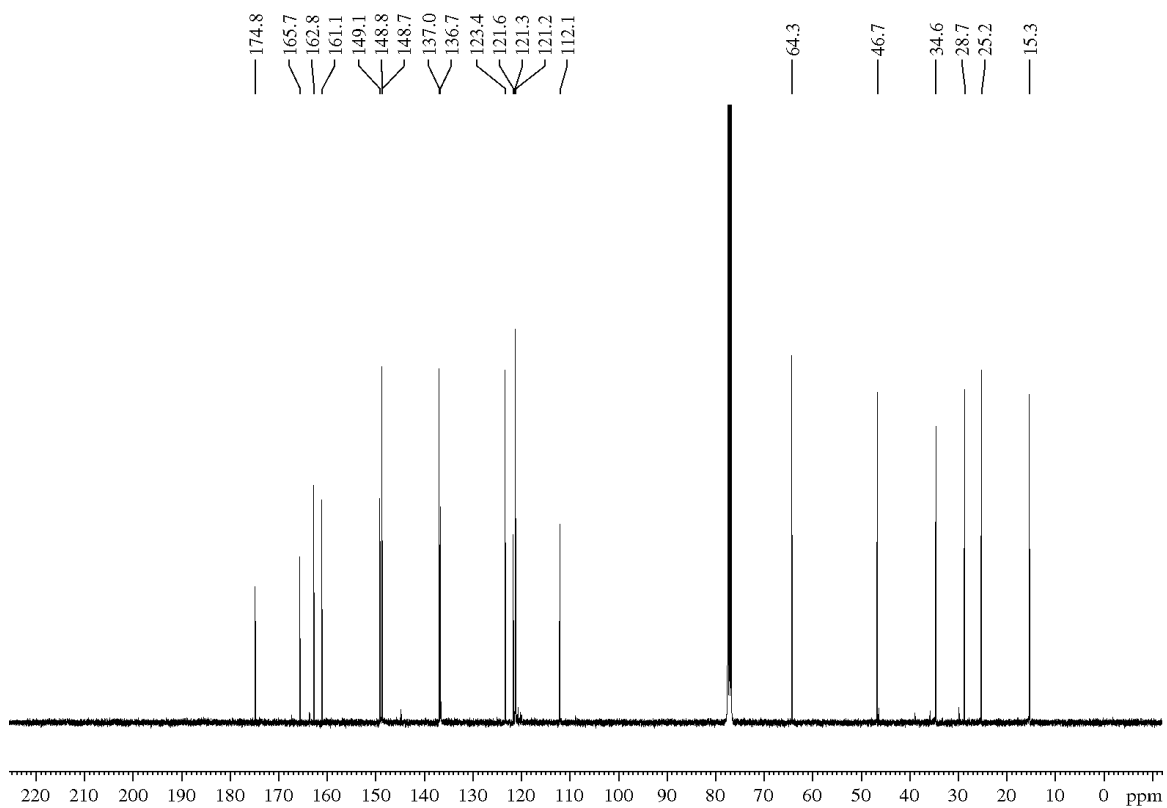
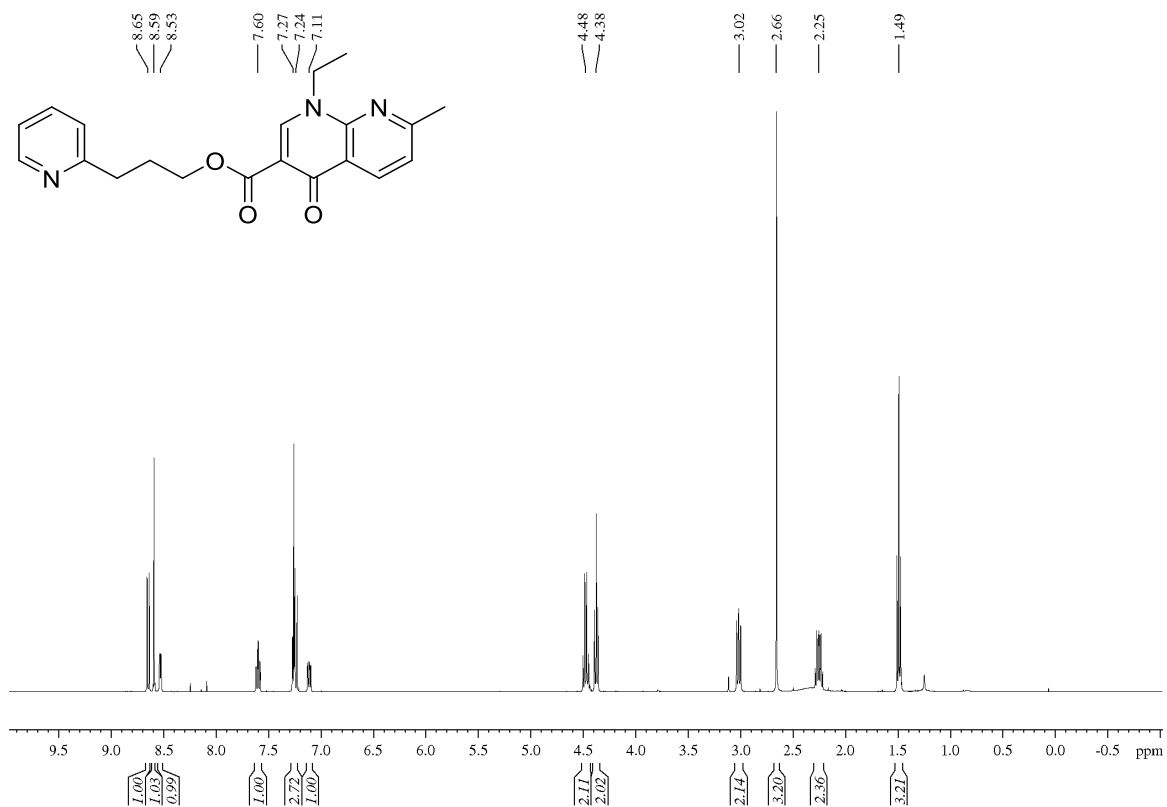
(2*S*,5*R*,6*R*)-3,3-dimethyl-7-oxo-6-(2-phenylacetamido)-4-thia-1-azabicyclo[3.2.0]heptane-2-carboxylic acid-d (79`and 84a`)

D₂O:DMSO-d₆ = 4:6

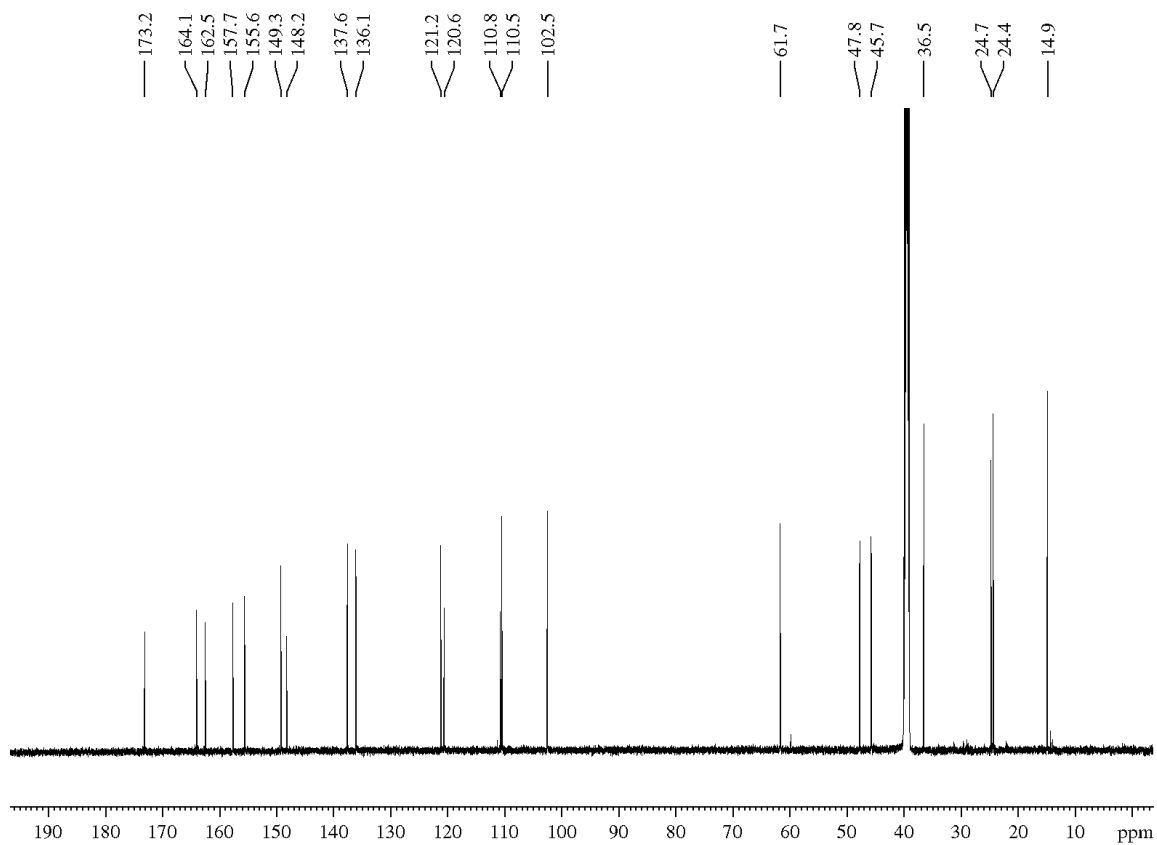
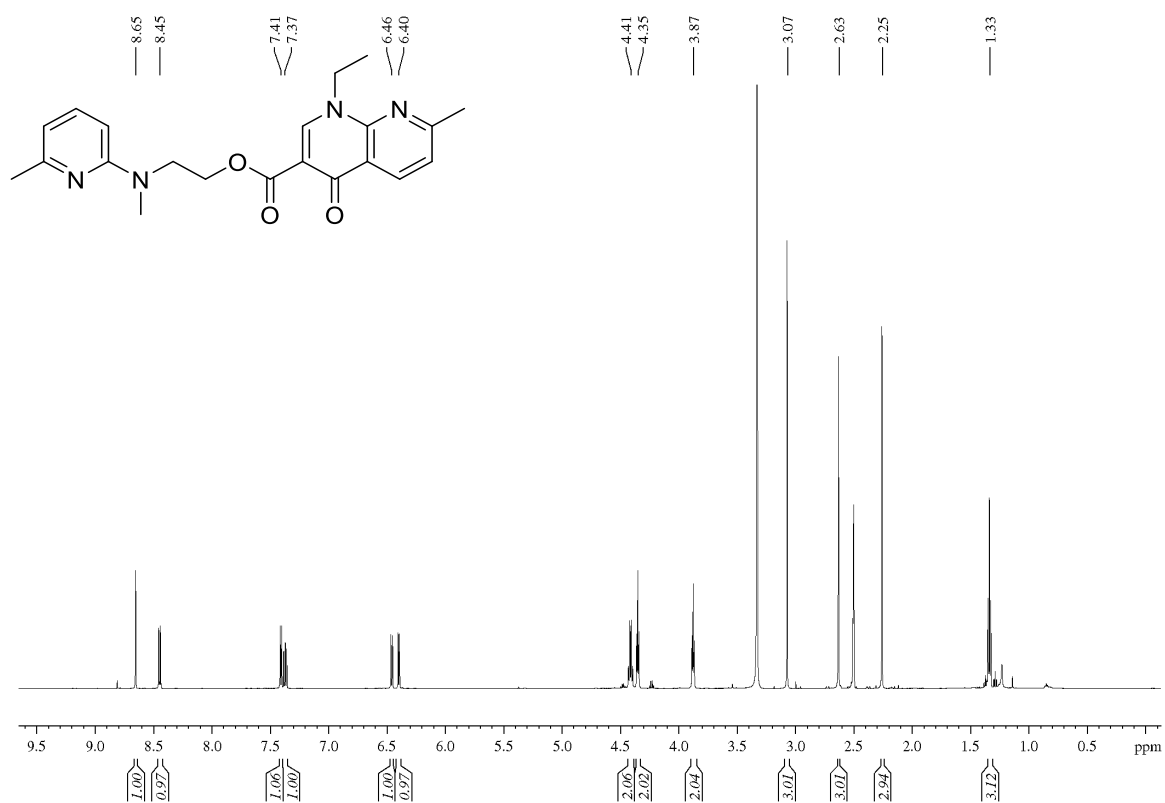


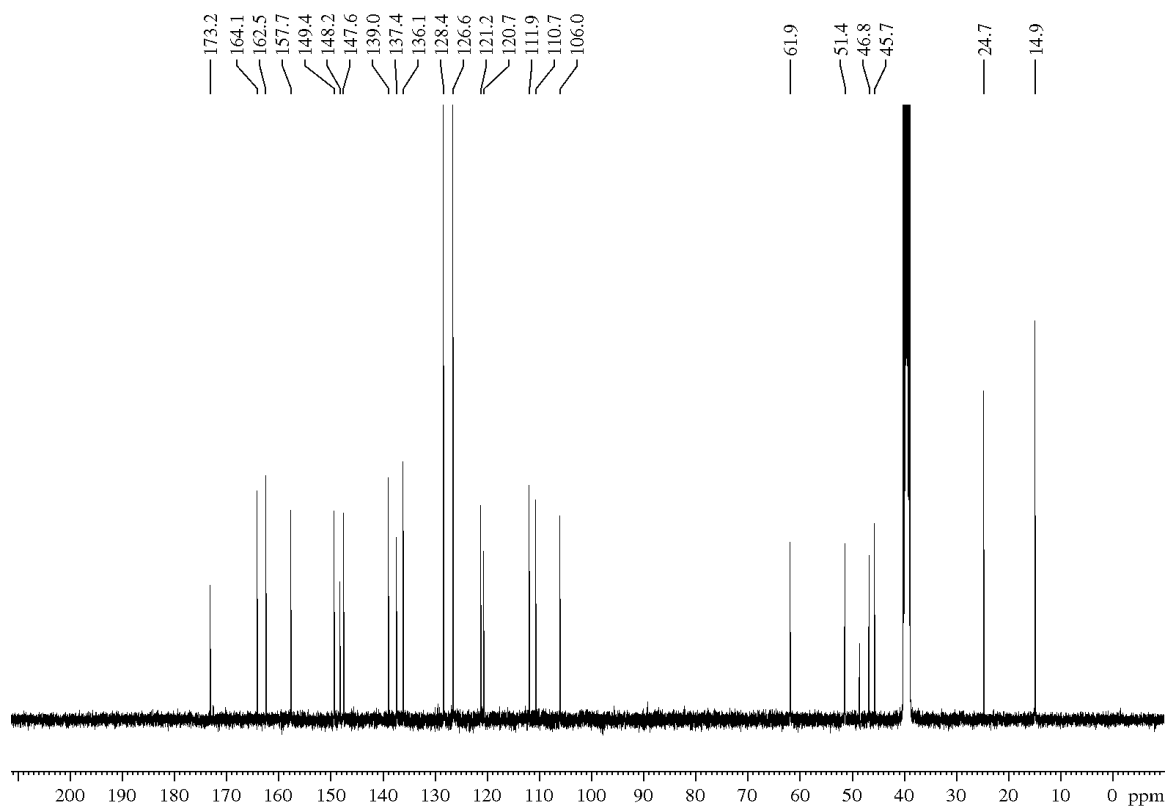
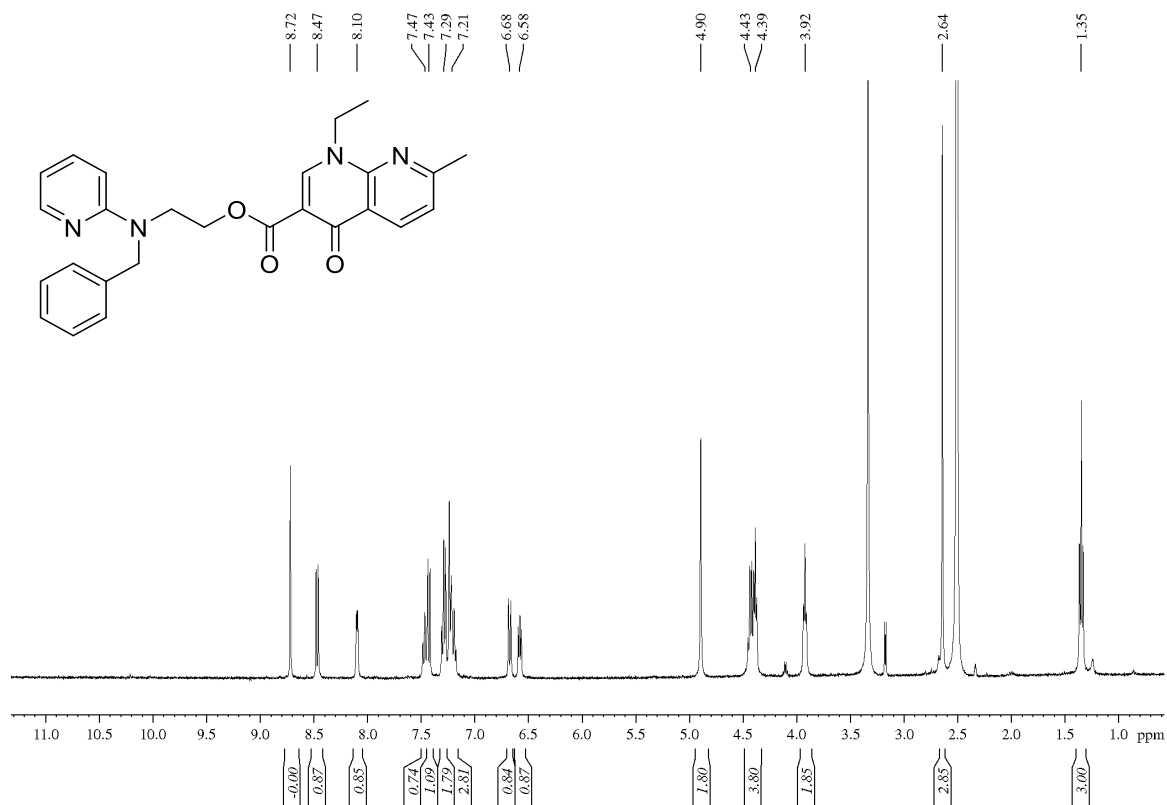
2-(Methyl(pyridin-2-yl)amino)ethyl 1-ethyl-7-methyl-4-oxo-1,4-dihydro-1,8-naphthyridine-3-carboxylate (108a)

3-(Pyridin-2-yl)propyl 1-ethyl-7-methyl-4-oxo-1,4-dihydro-1,8-naphthyridine-3-carboxylate (118)

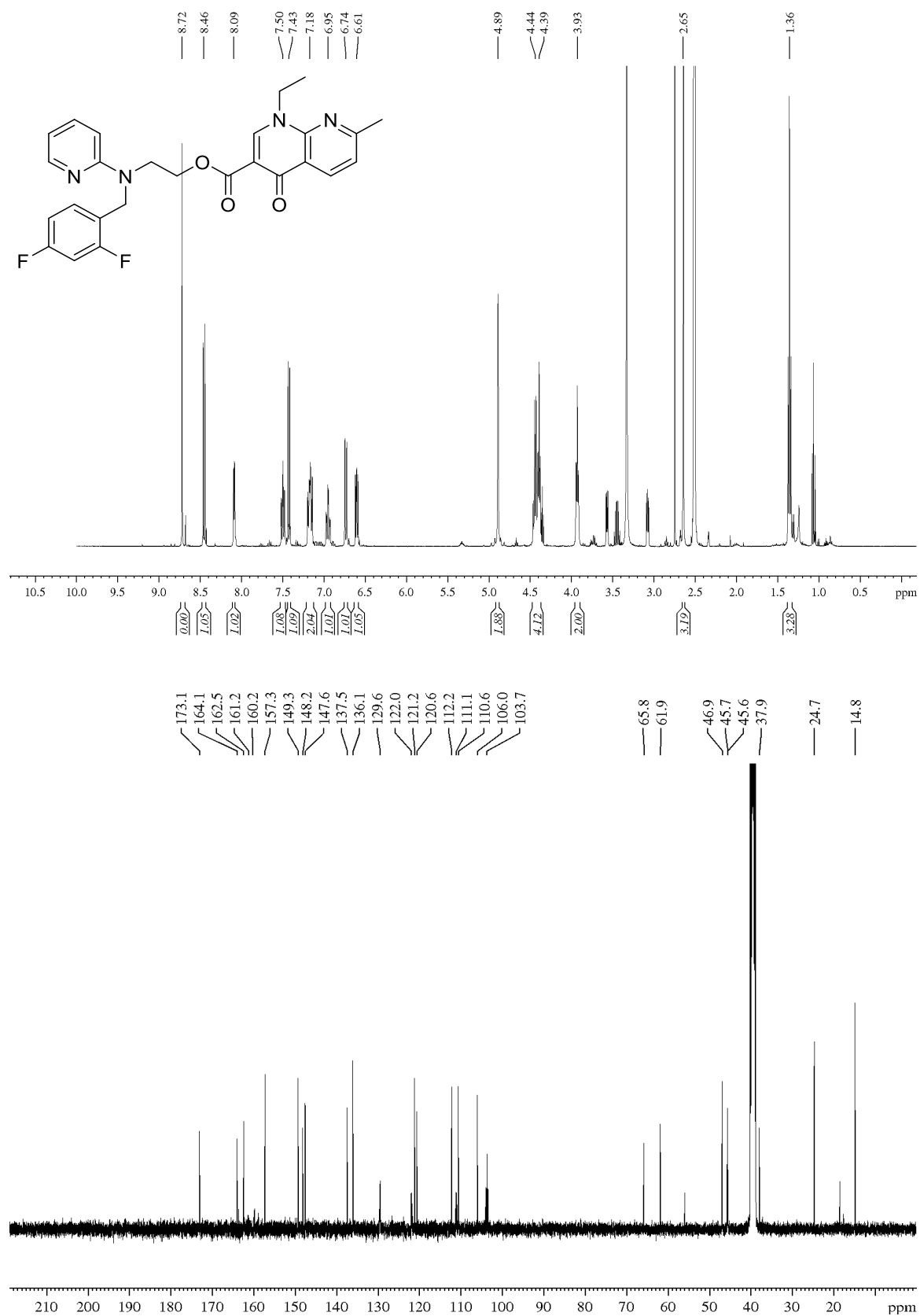


2-(Methyl(6-methylpyridin-2-yl)amino)ethyl 1-ethyl-7-methyl-4-oxo-1,4-dihydro-1,8-naphthyridine-3-carboxylate (108b)

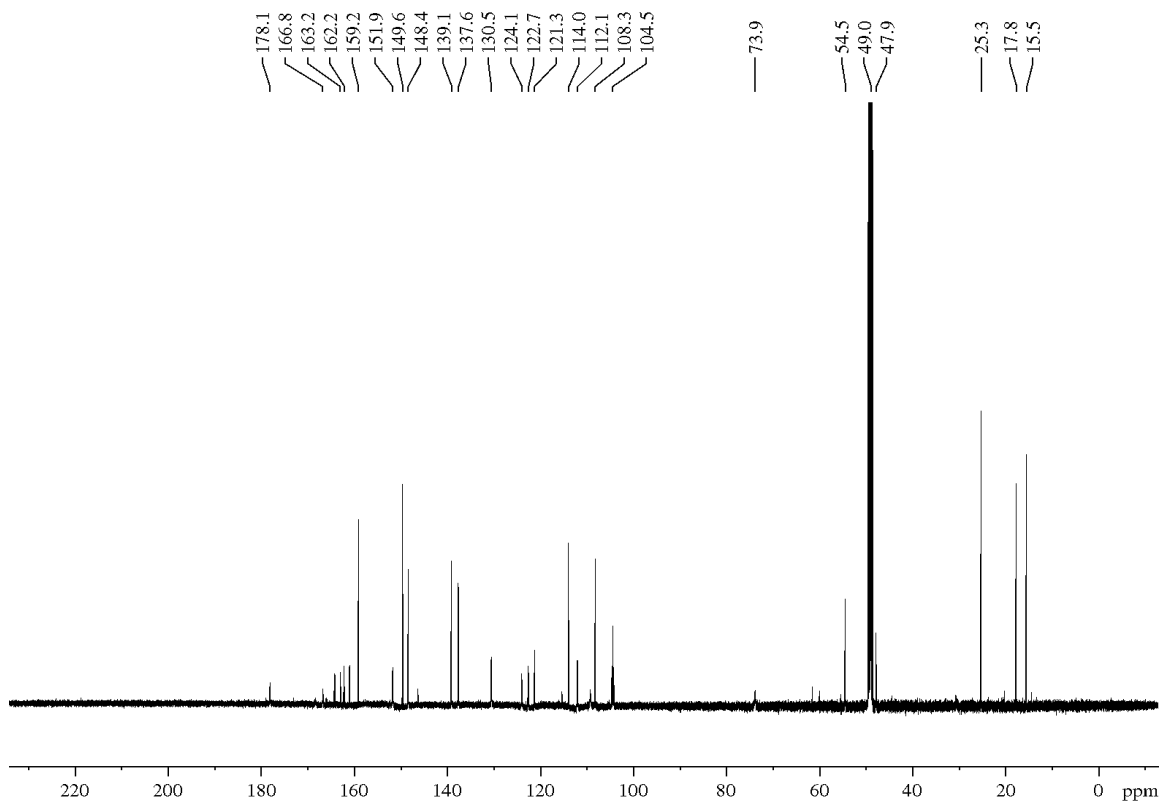
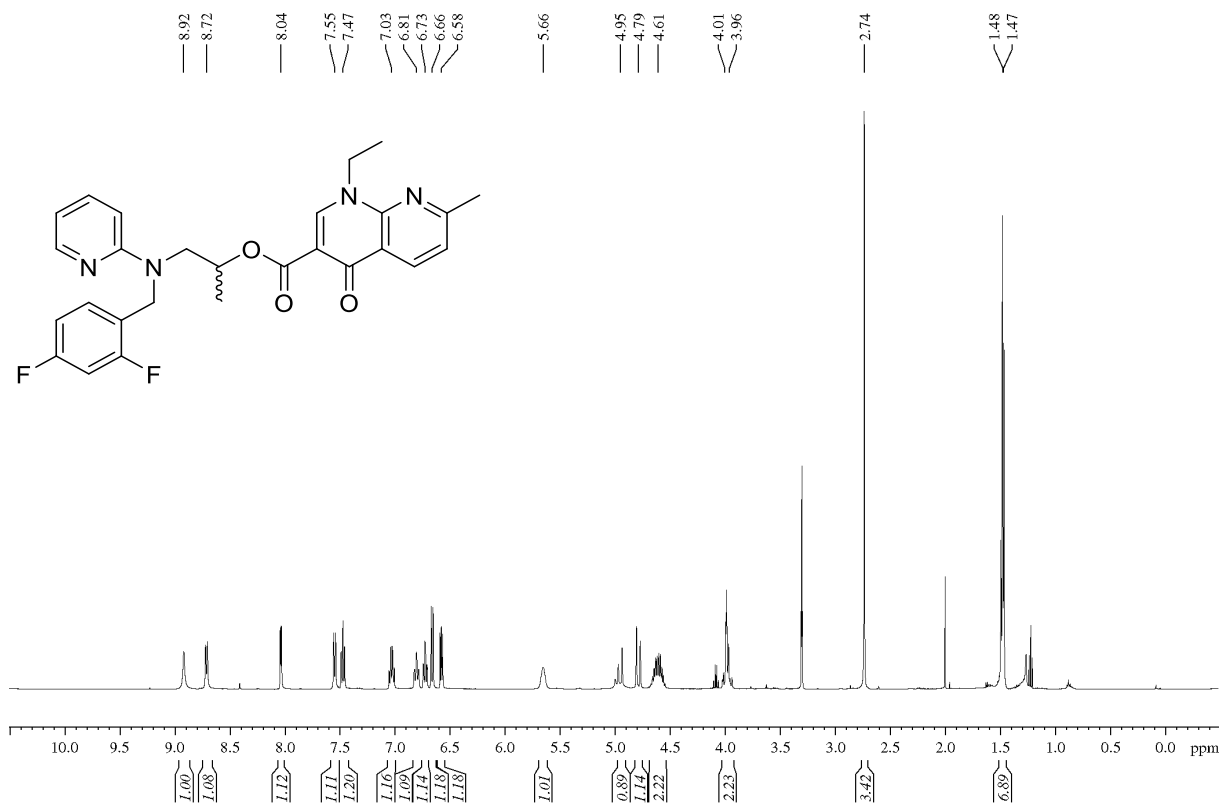


2-(Benzyl(pyridin-2-yl)amino)ethyl 1-ethyl-7-methyl-4-oxo-1,4-dihydro-1,8-naphthyridine-3-carboxylate (119)

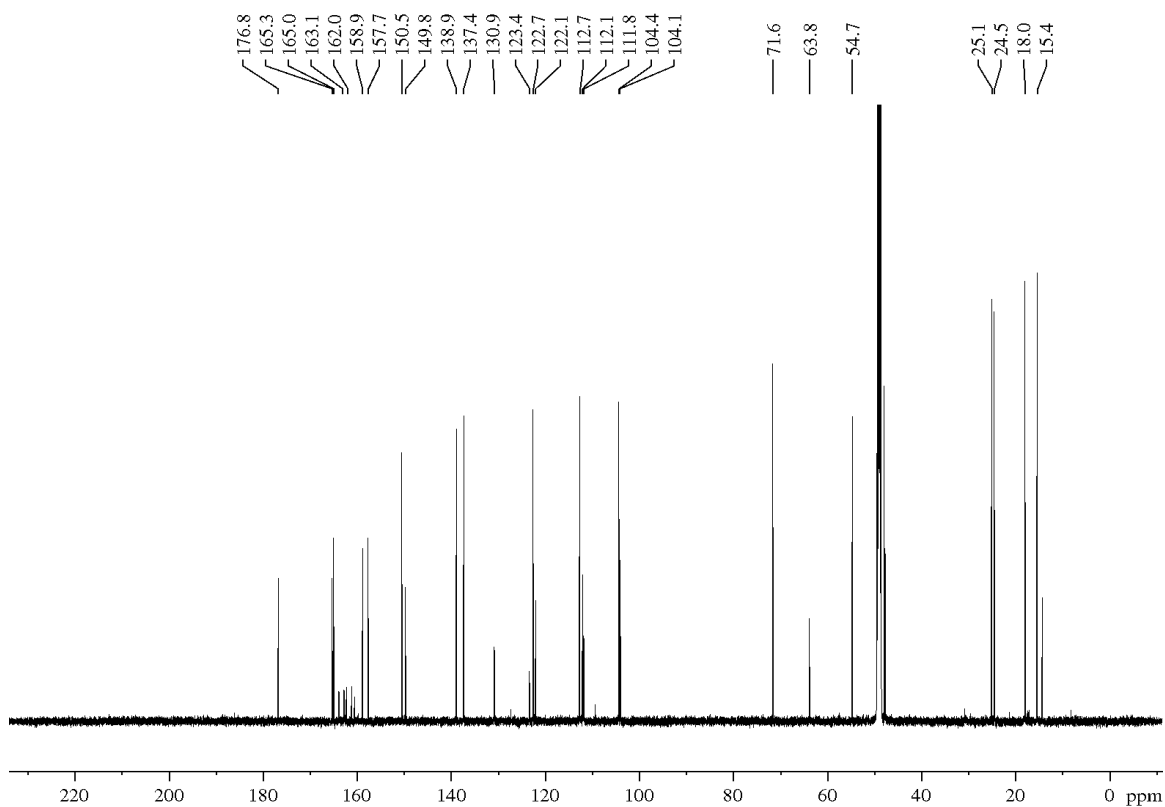
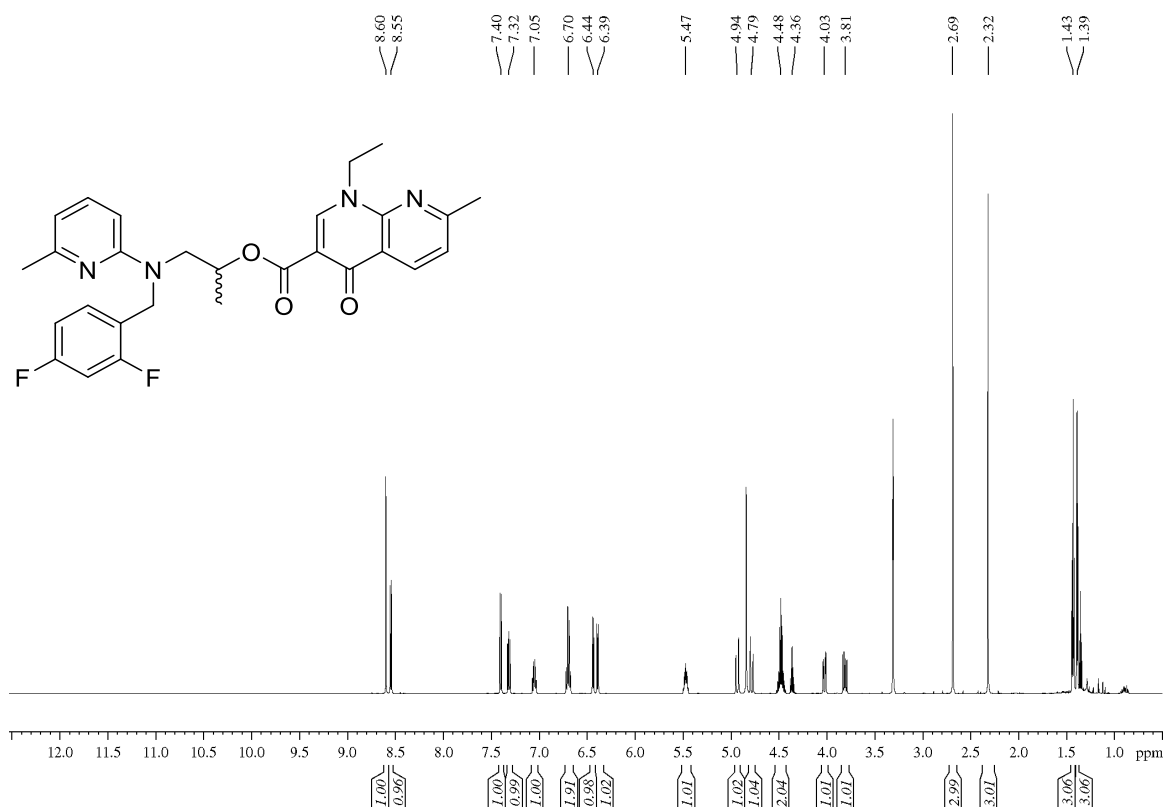
2-((2,4-Difluorobenzyl)(pyridin-2-yl)amino)ethyl 1-ethyl-7-methyl-4-oxo-1,4-dihydro-1,8-naphthyridine-3-carboxylate (120)



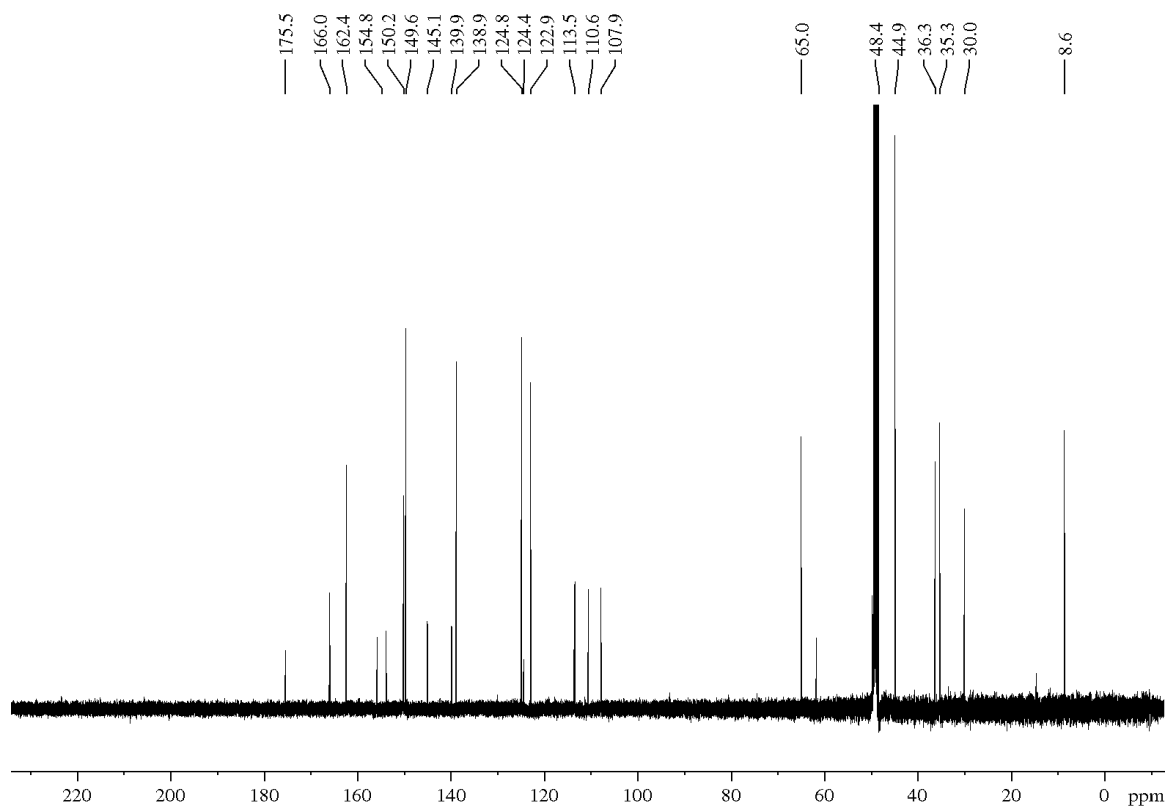
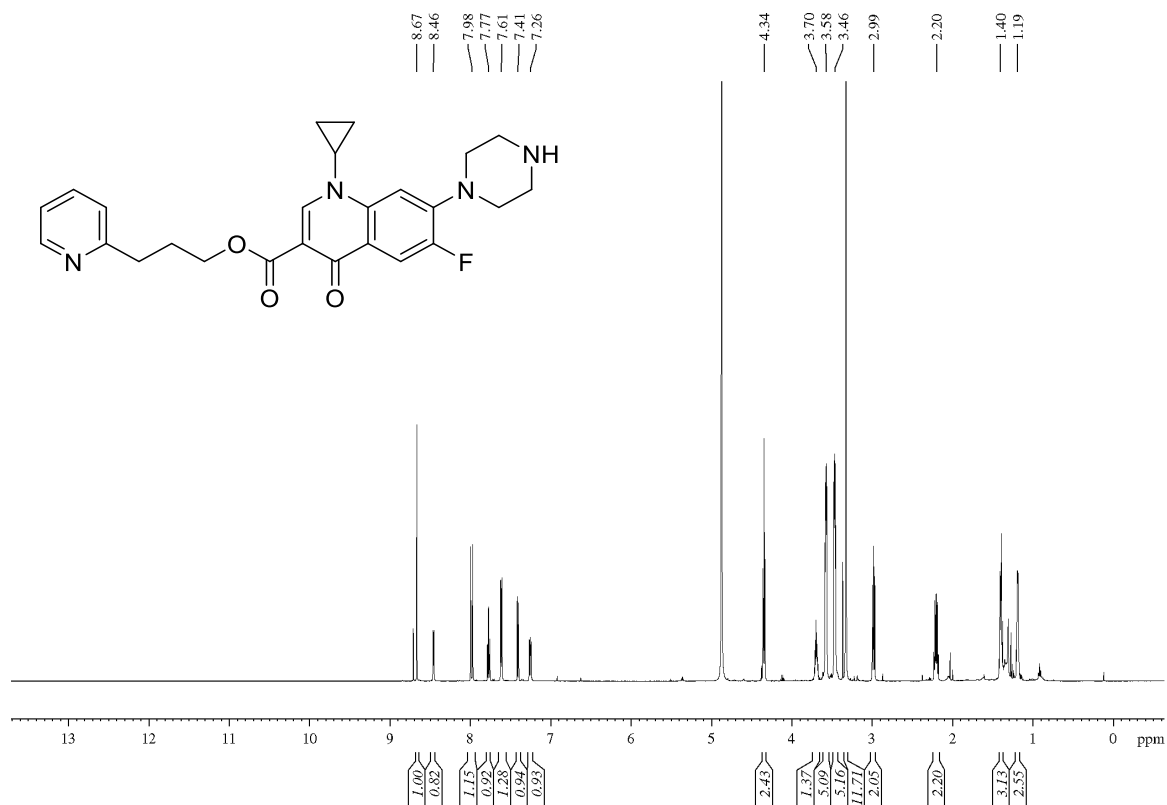
1-((2,4-Difluorobenzyl)(pyridin-2-yl)amino)propan-2-yl 1-ethyl-7-methyl-4-oxo-1,4-dihydro-1,8-naphthyridine-3-carboxylate (121a)



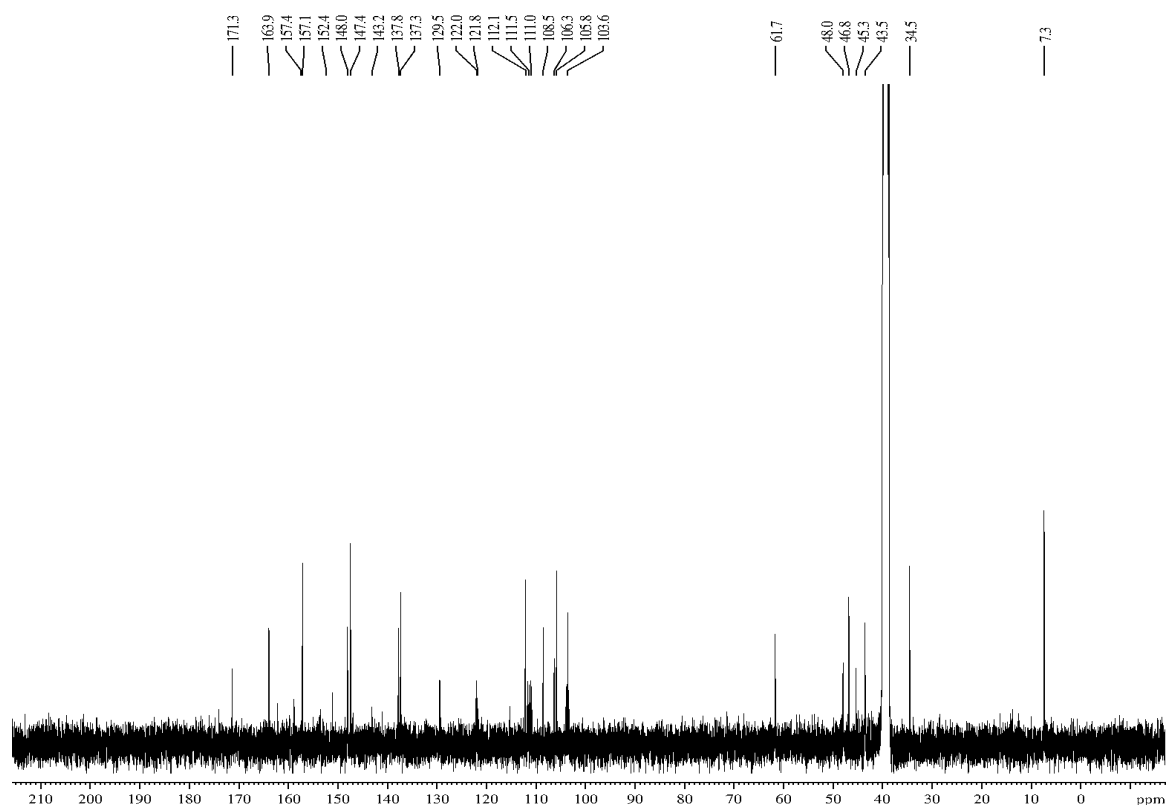
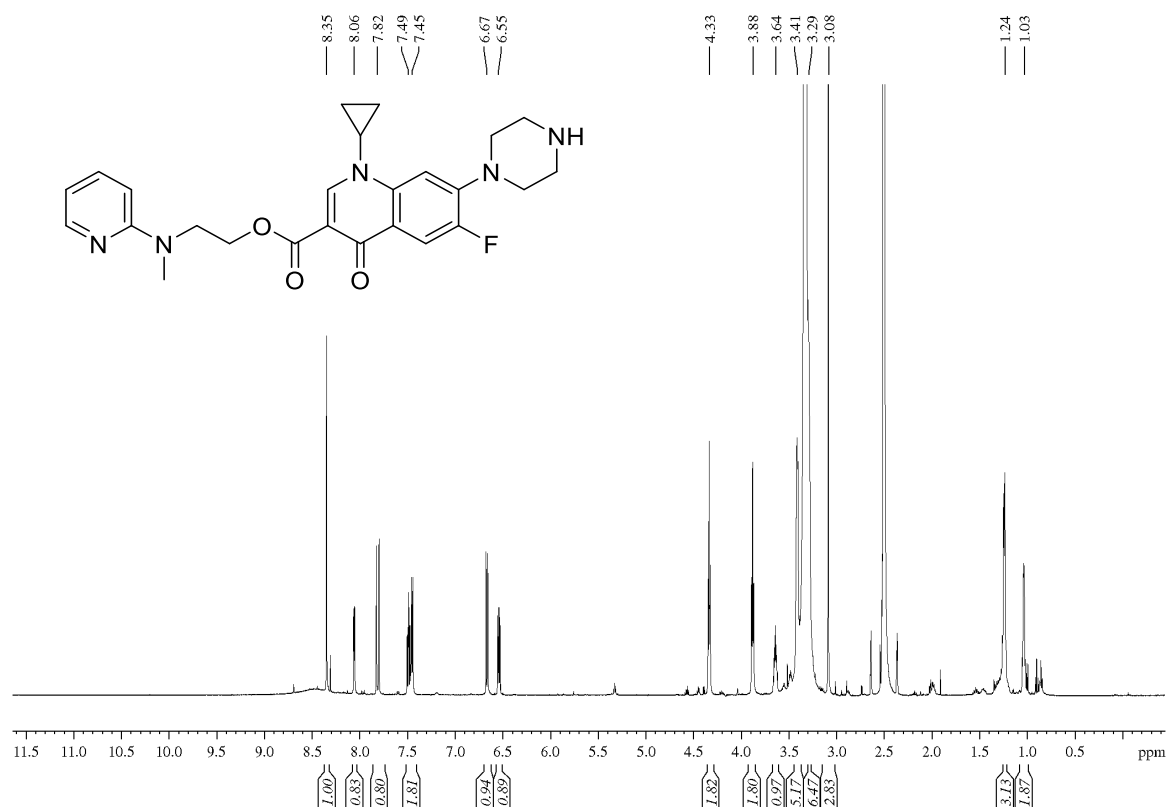
1-((2,4-Difluorobenzyl)(6-methylpyridin-2-yl)amino)propan-2-yl 1-ethyl-7-methyl-4-oxo-1,4-dihydro-1,8-naphthyridine-3-carboxylate (121b)



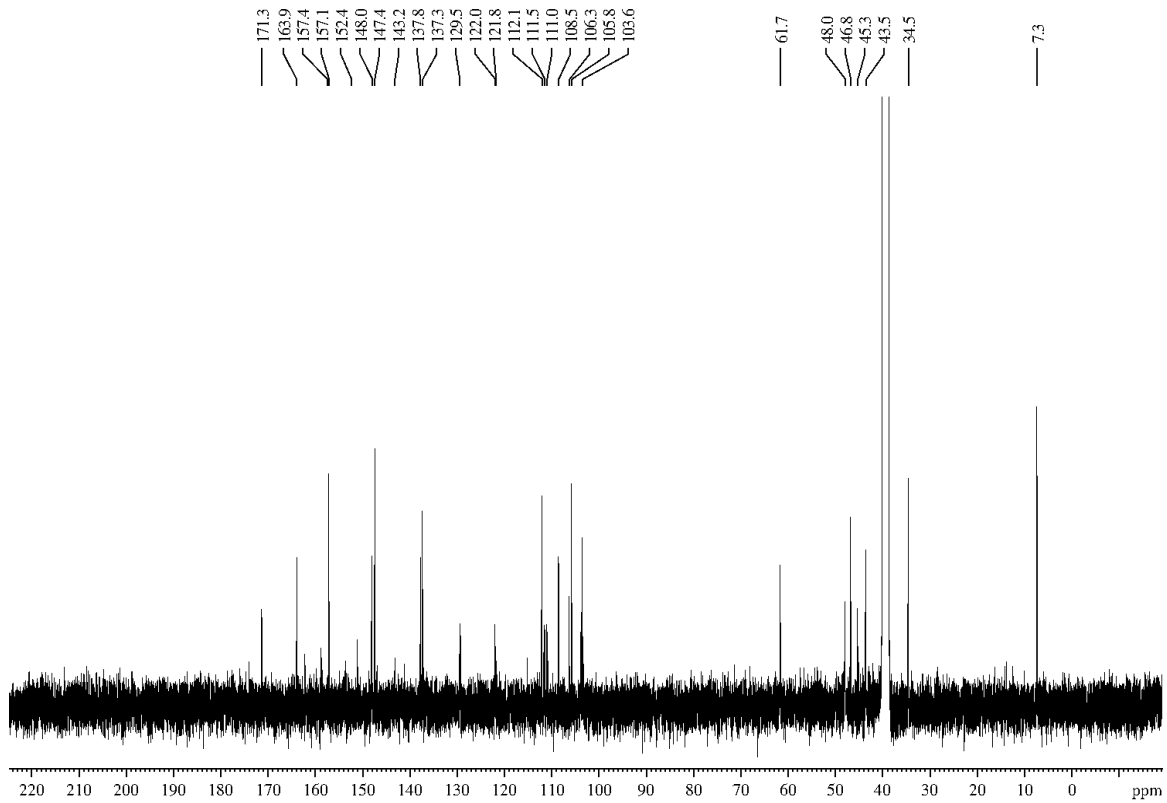
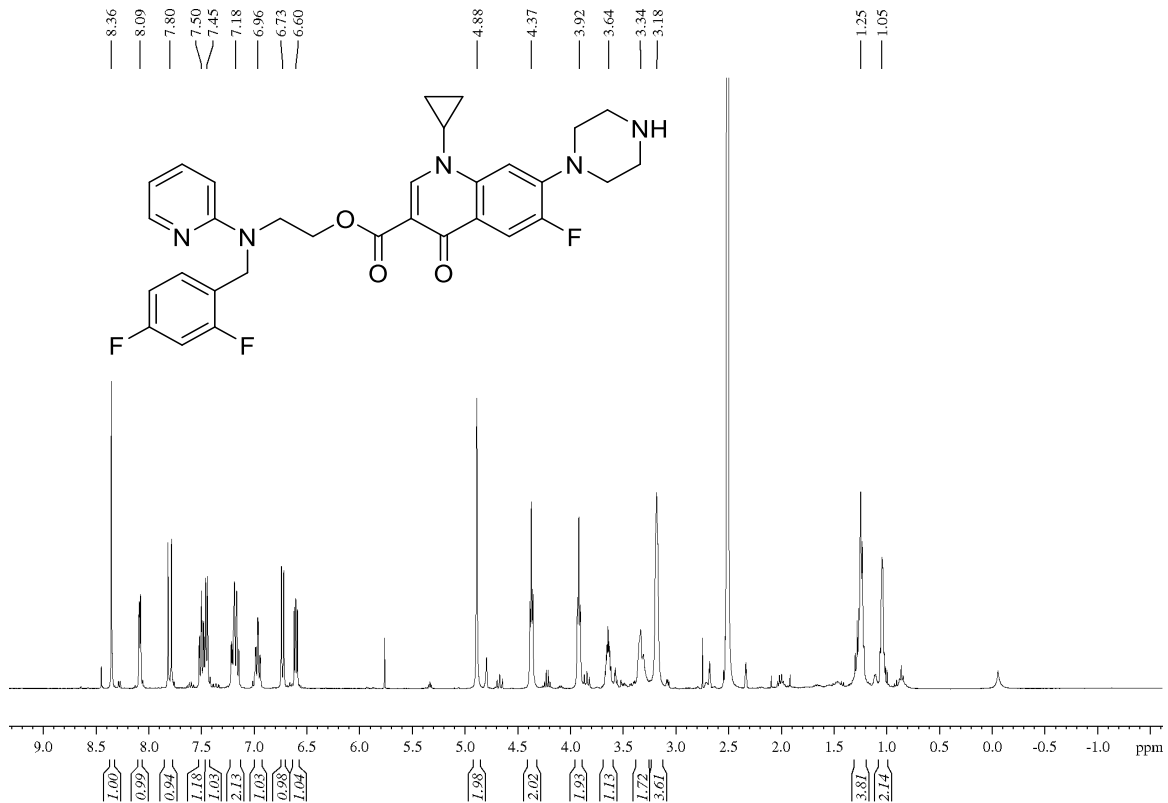
4-(1-Cyclopropyl-6-fluoro-4-oxo-3-((3-(pyridin-2-yl)propoxy)carbonyl)-1,4-dihydroquinolin-7-yl)piperazine-1-carboxylic acid (124)



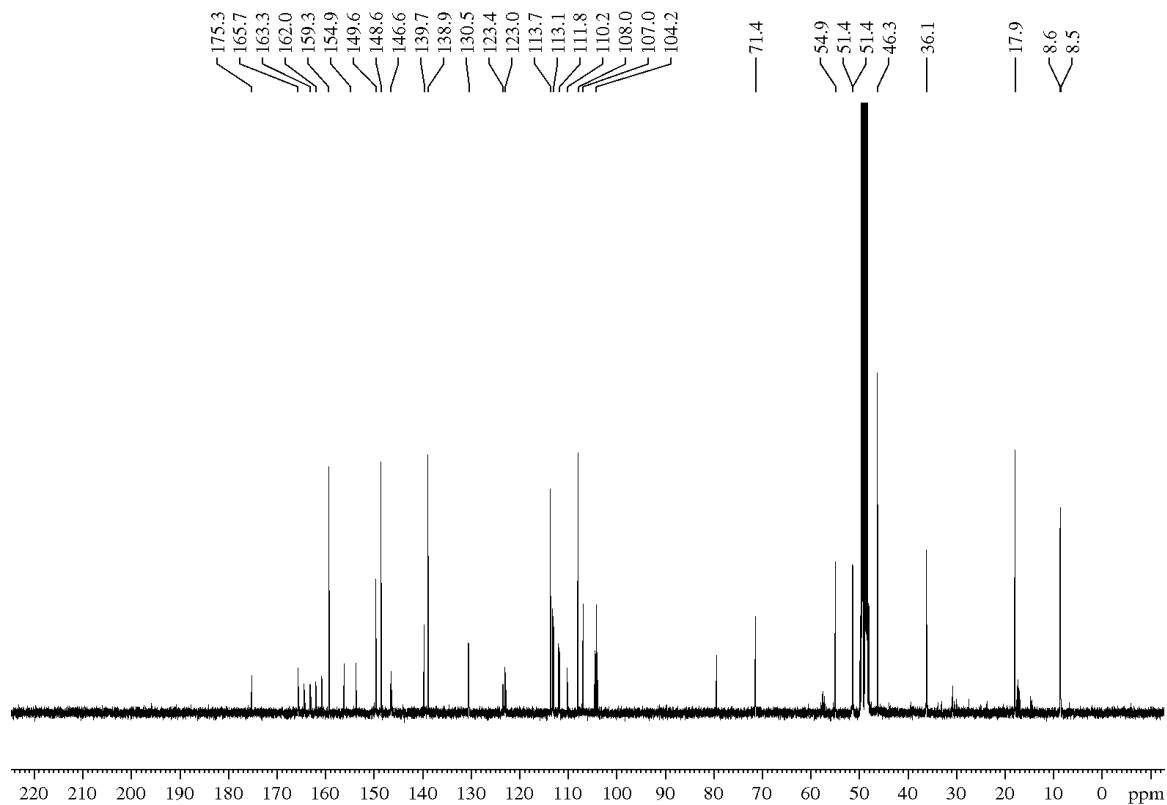
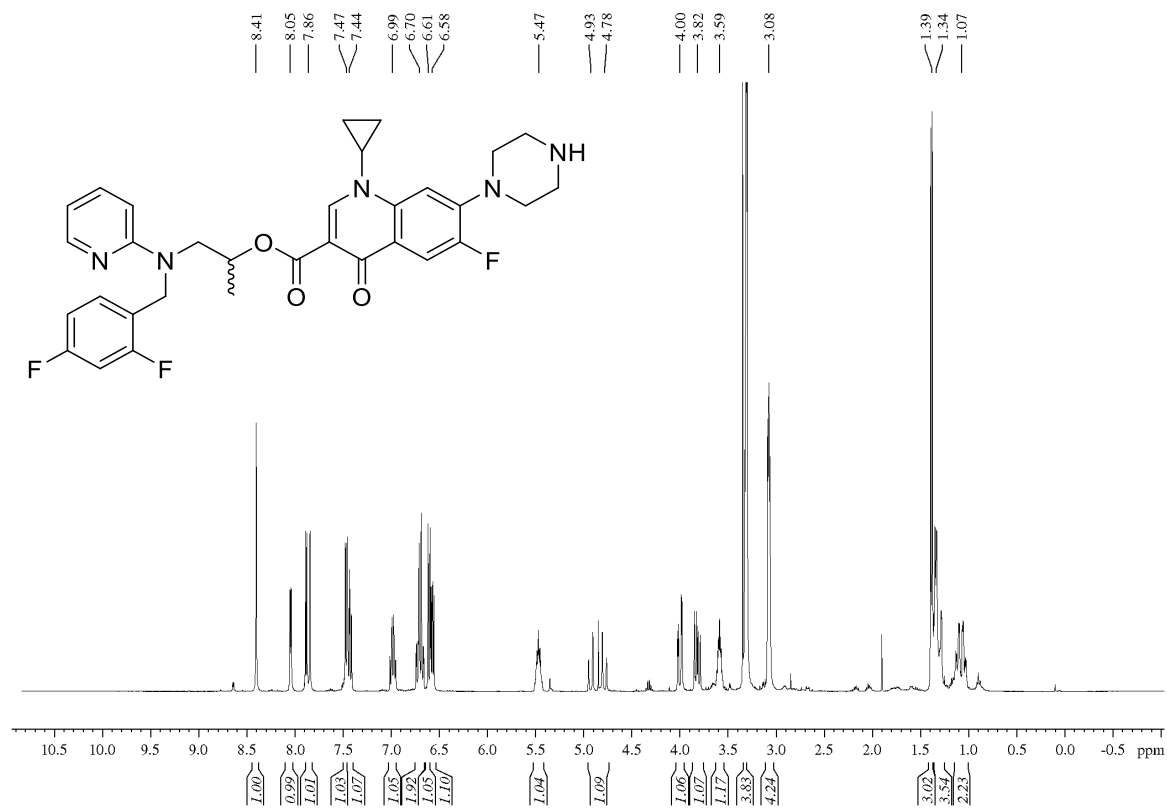
4-(1-Cyclopropyl-6-fluoro-3-((2-(methyl(pyridin-2-yl)amino)ethoxy)carbonyl)-4-oxo-1,4-dihydroquinolin-7-yl)piperazine-1-carboxylic acid (125)

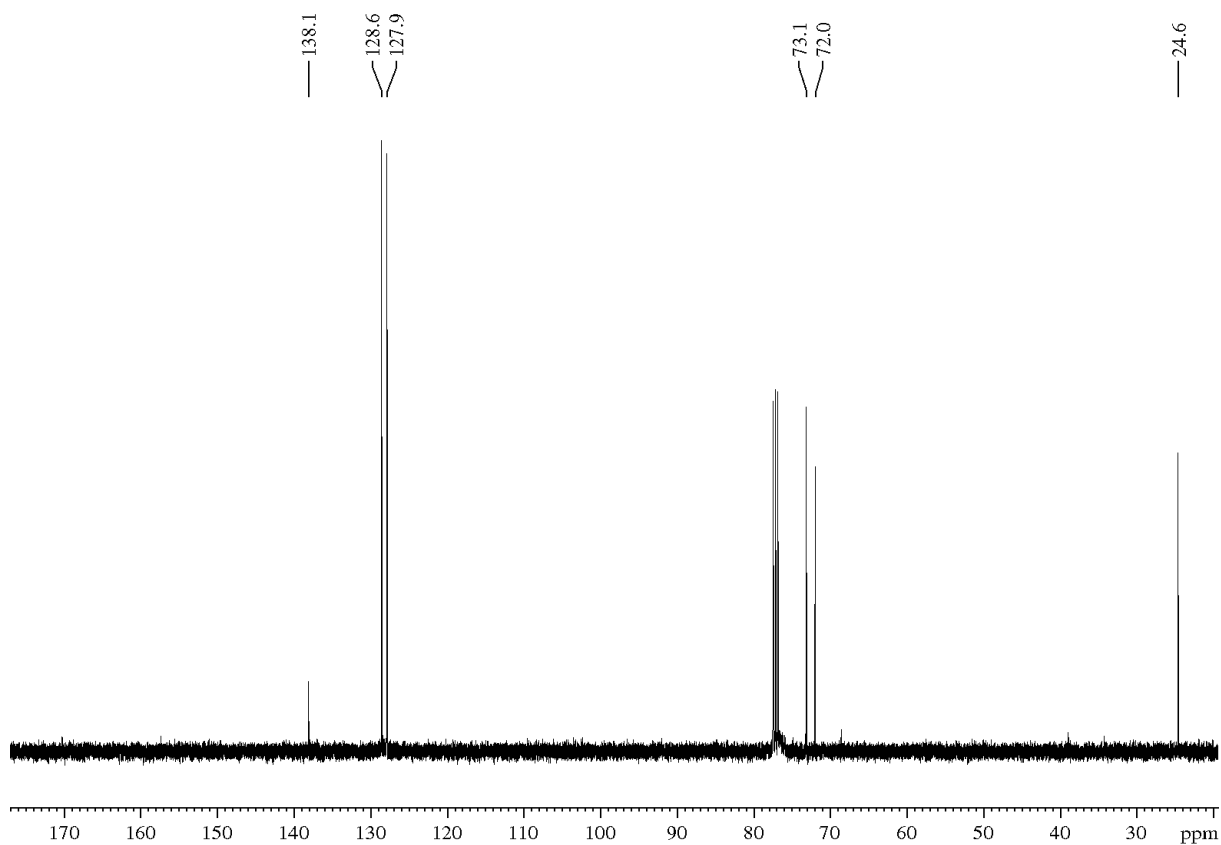
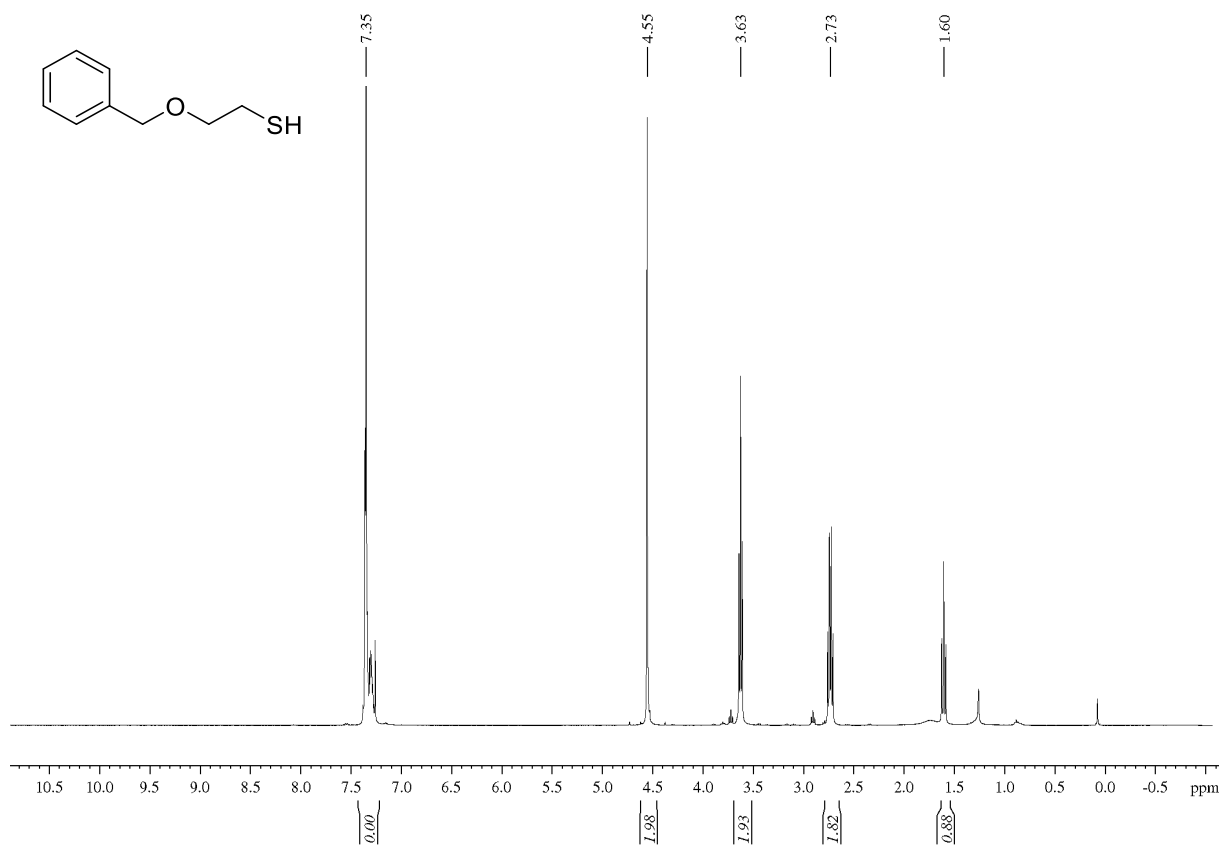
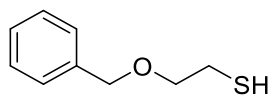


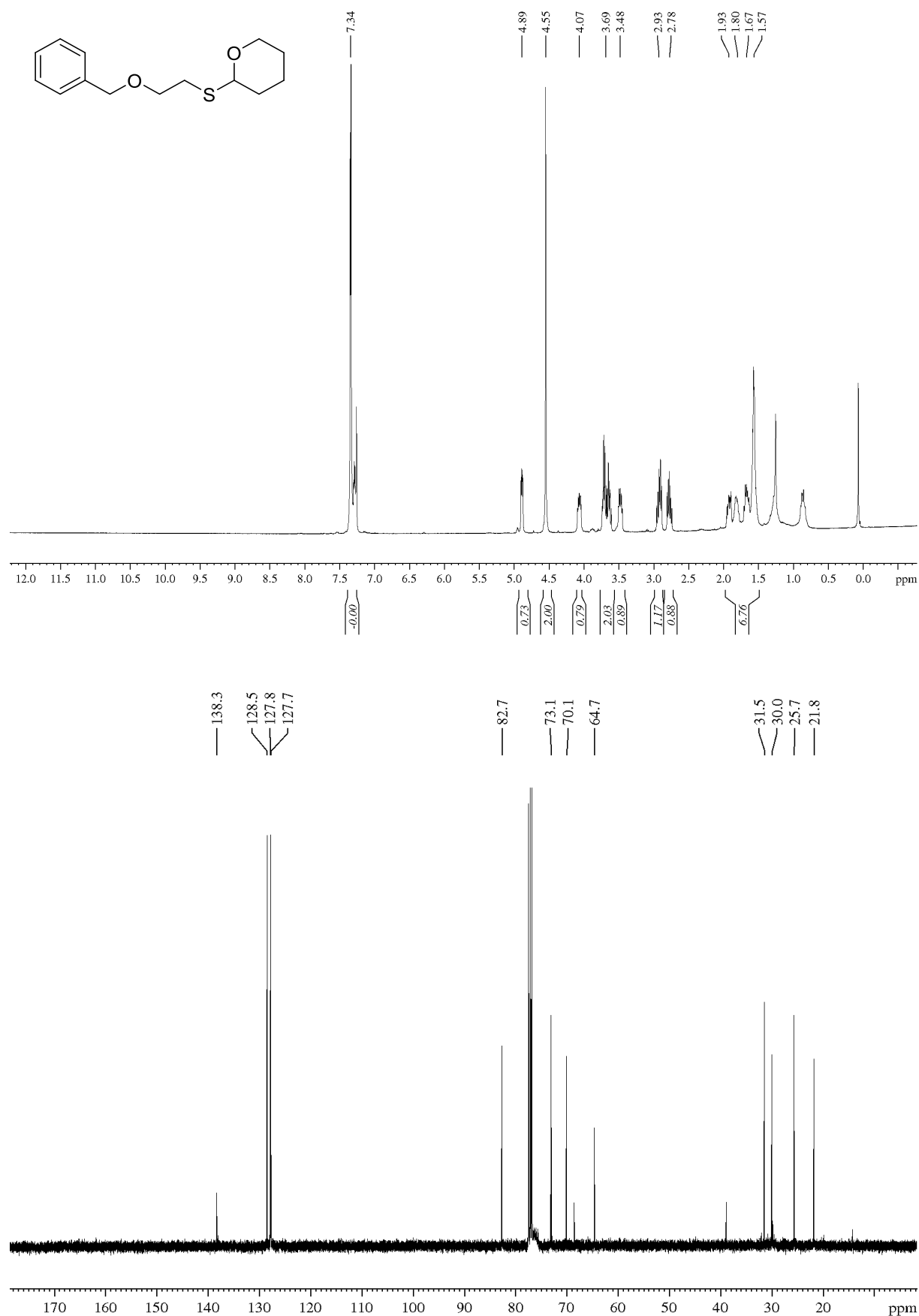
4-(1-Cyclopropyl-3-((2-((2,4-difluorobenzyl)(pyridin-2-yl)amino)ethoxy)carbonyl)-6-fluoro-4-oxo-1,4-dihydroquinolin-7-yl)piperazine-1-carboxylic acid (126)

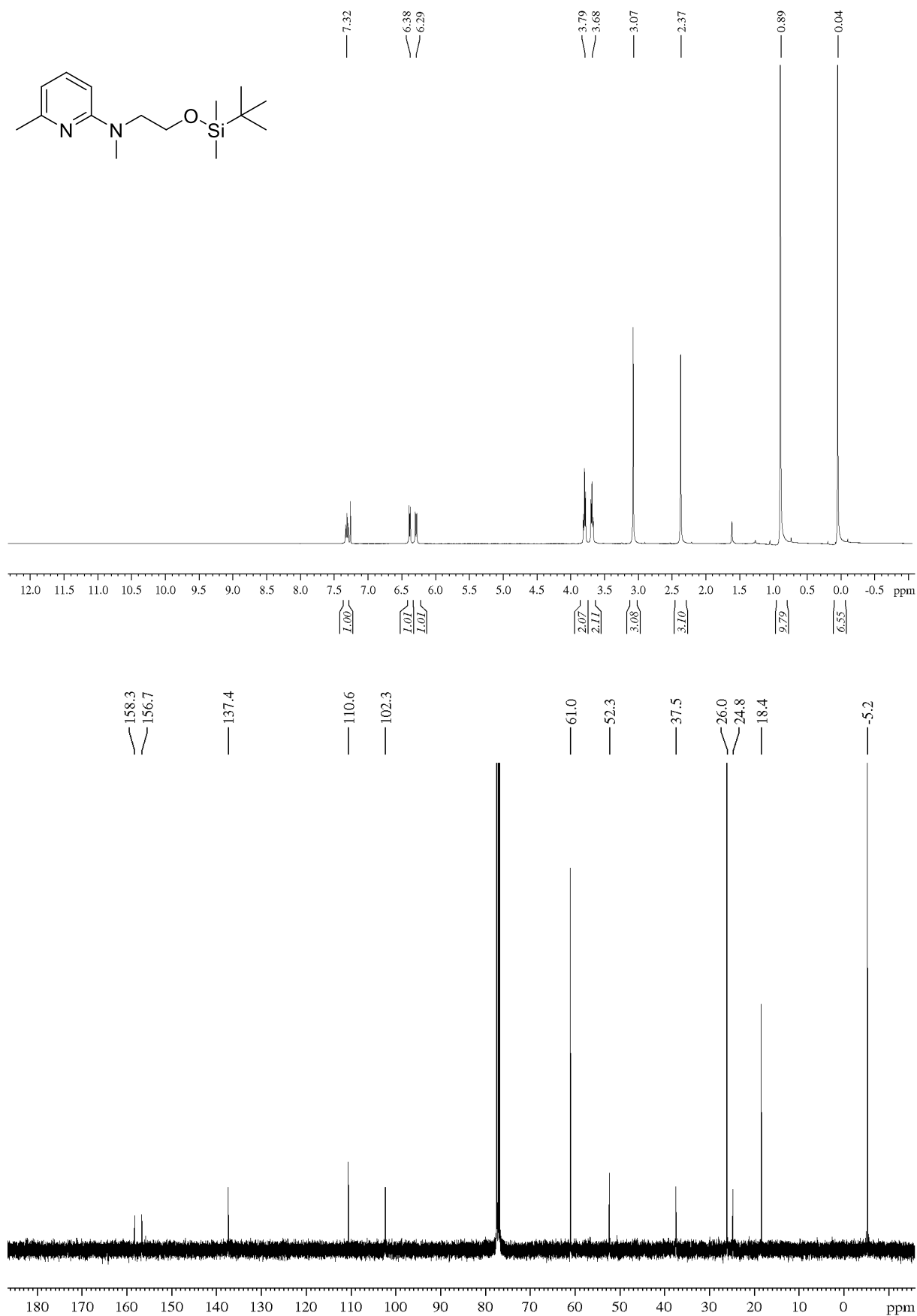


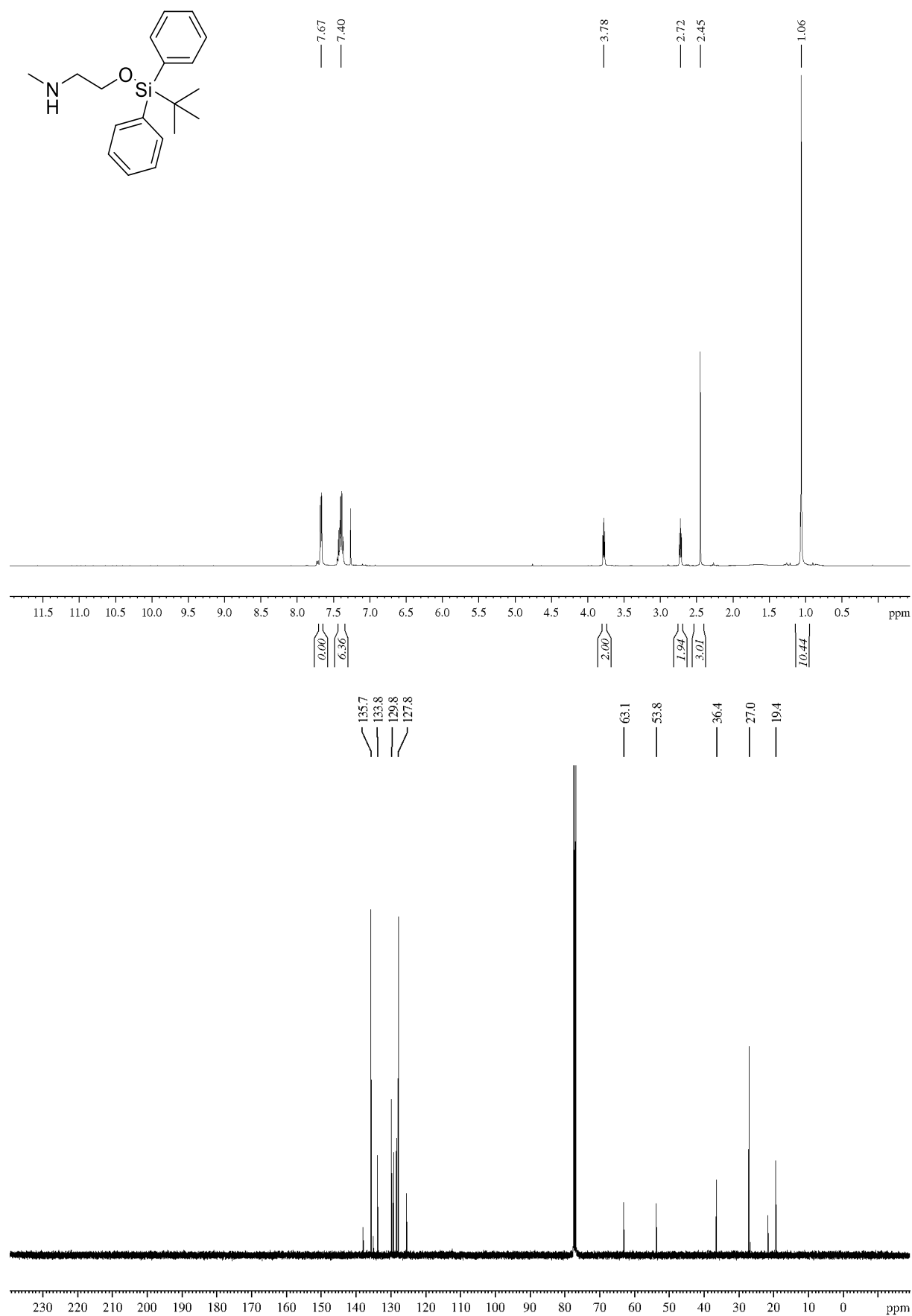
1-((2,4-Ddifluorobenzyl)(pyridin-2-yl)amino)propan-2-yl 1-cyclopropyl-6-fluoro-4-oxo-7-(piperazin-1-yl)-1,4-dihydroquinoline-3-carboxylate (127)

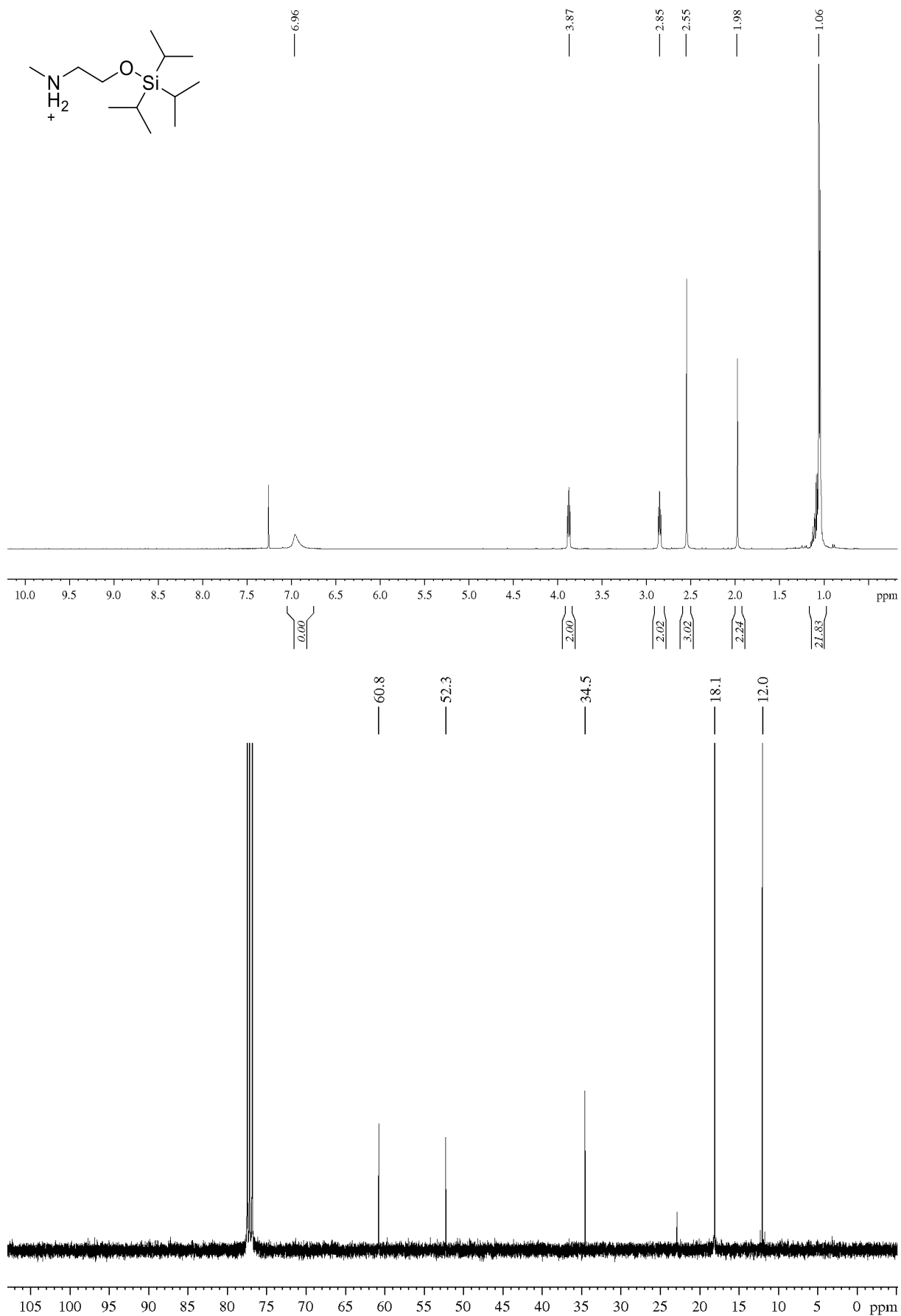


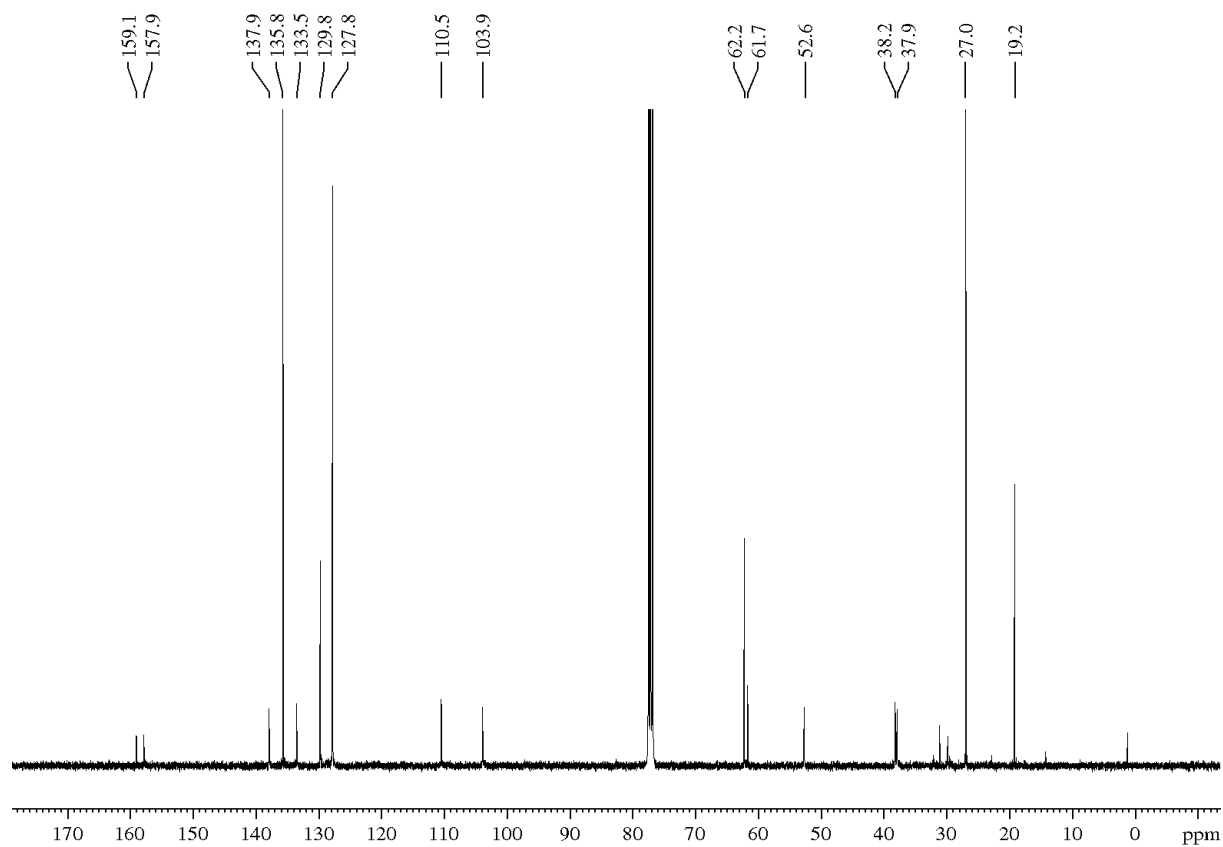
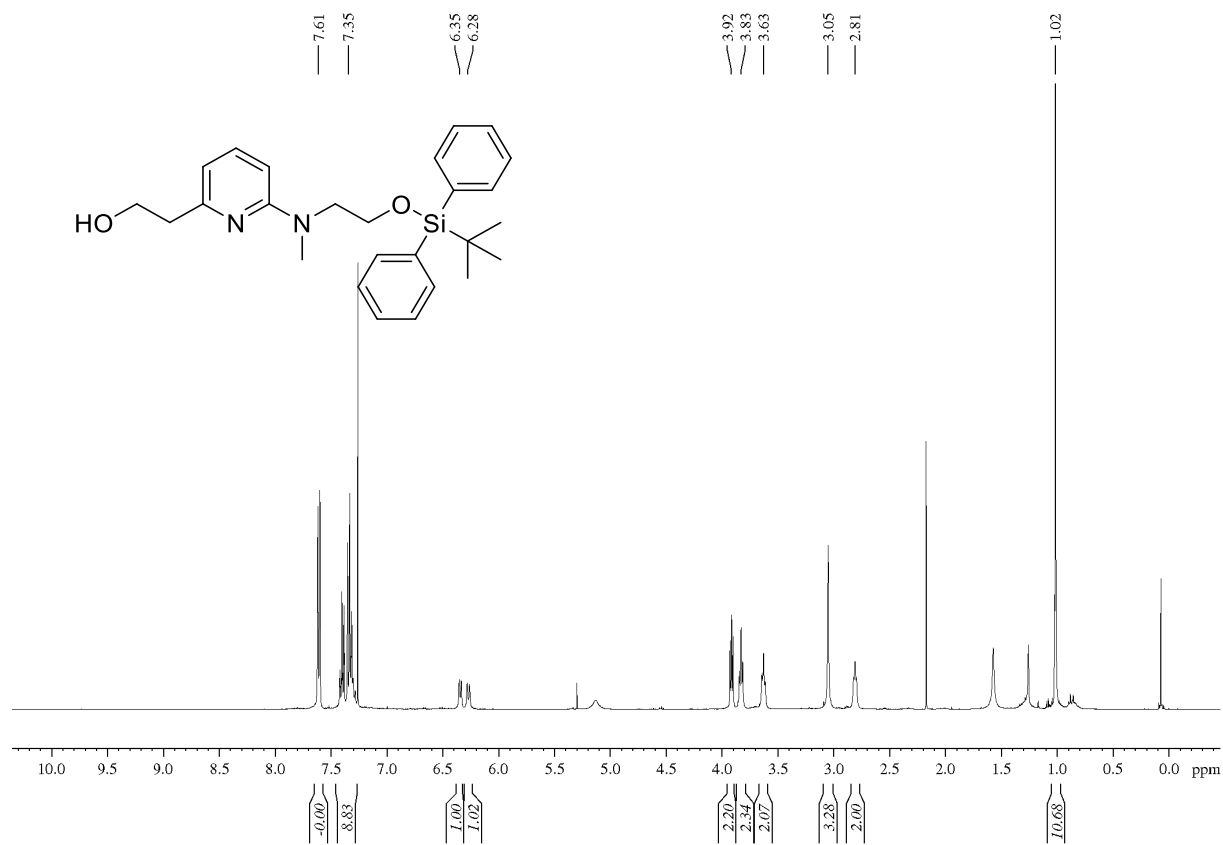
2-(Benzyloxy)methan-1-thiol (132)

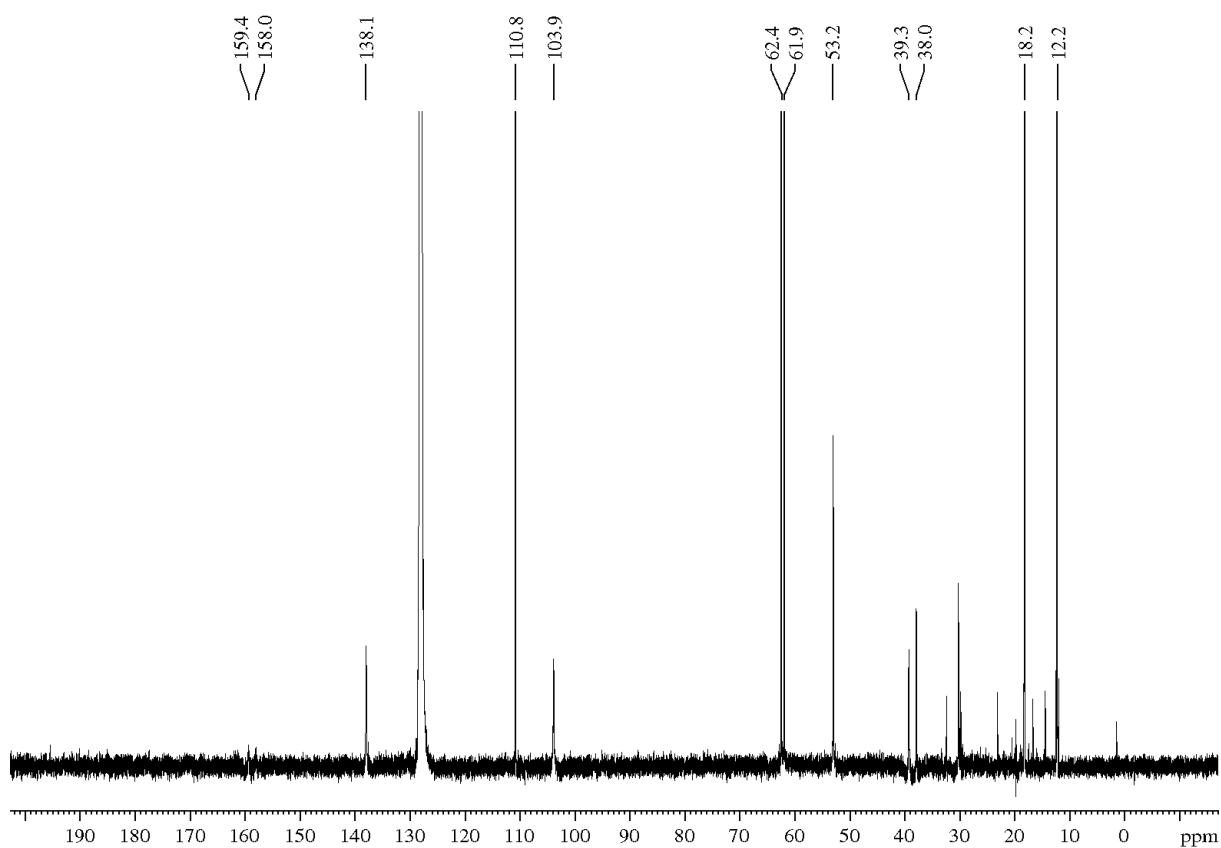
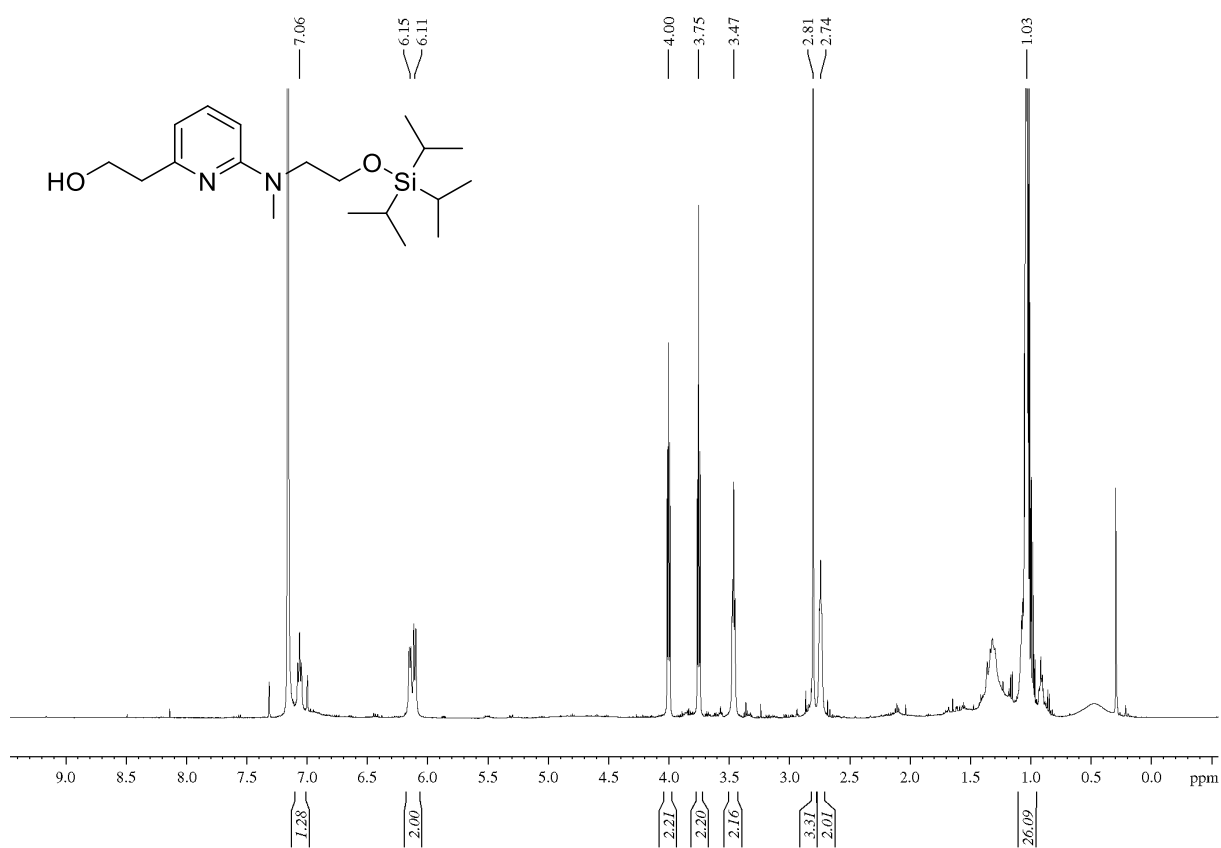
2-((2-(Benzyloxy)ethyl)thio)tetrahydro-2H-pyran (133)

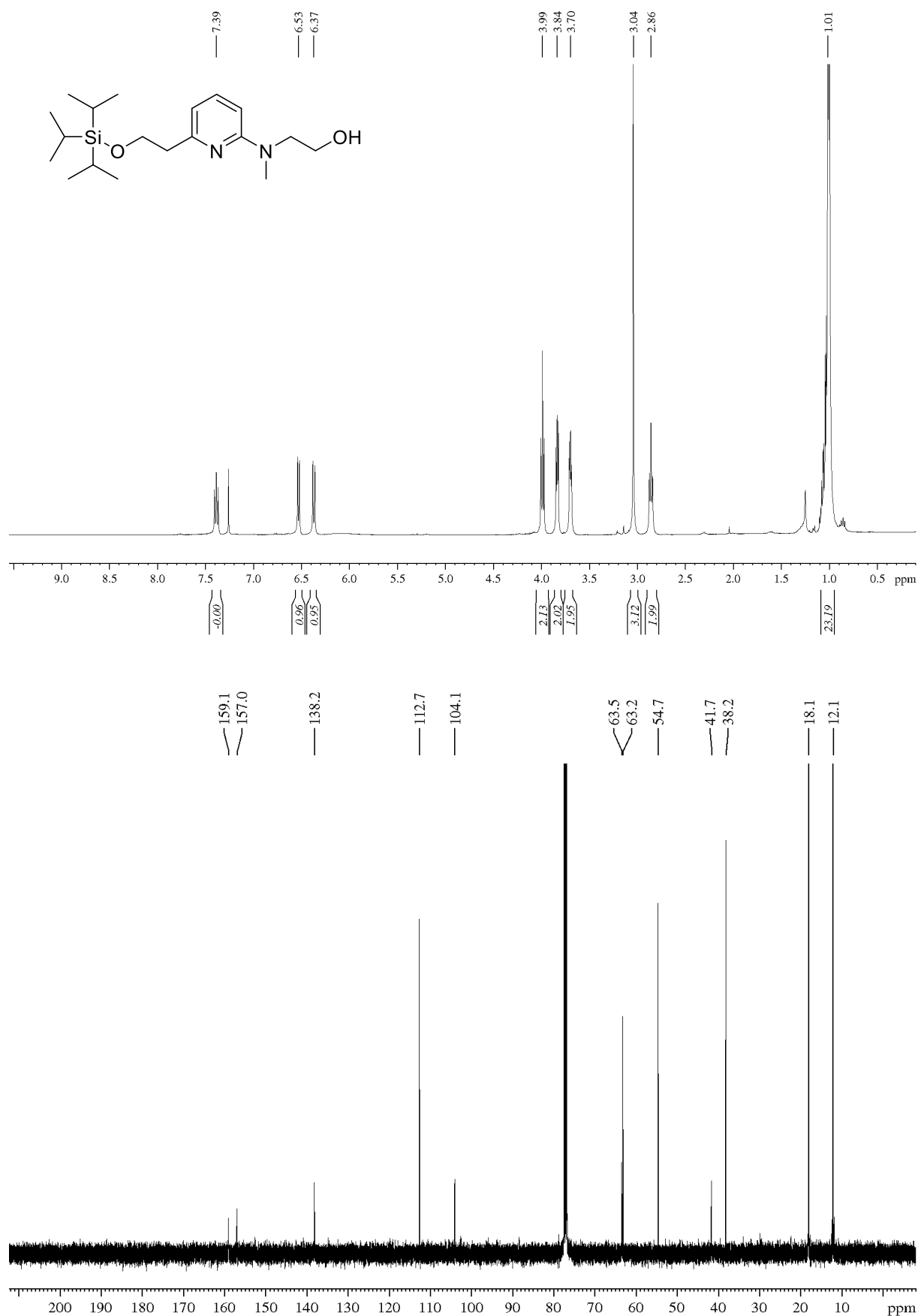
N-(2-((*tert*-Butyldimethylsilyl)oxy)ethyl)-*N*,6-dimethylpyridin-2-amine (135)

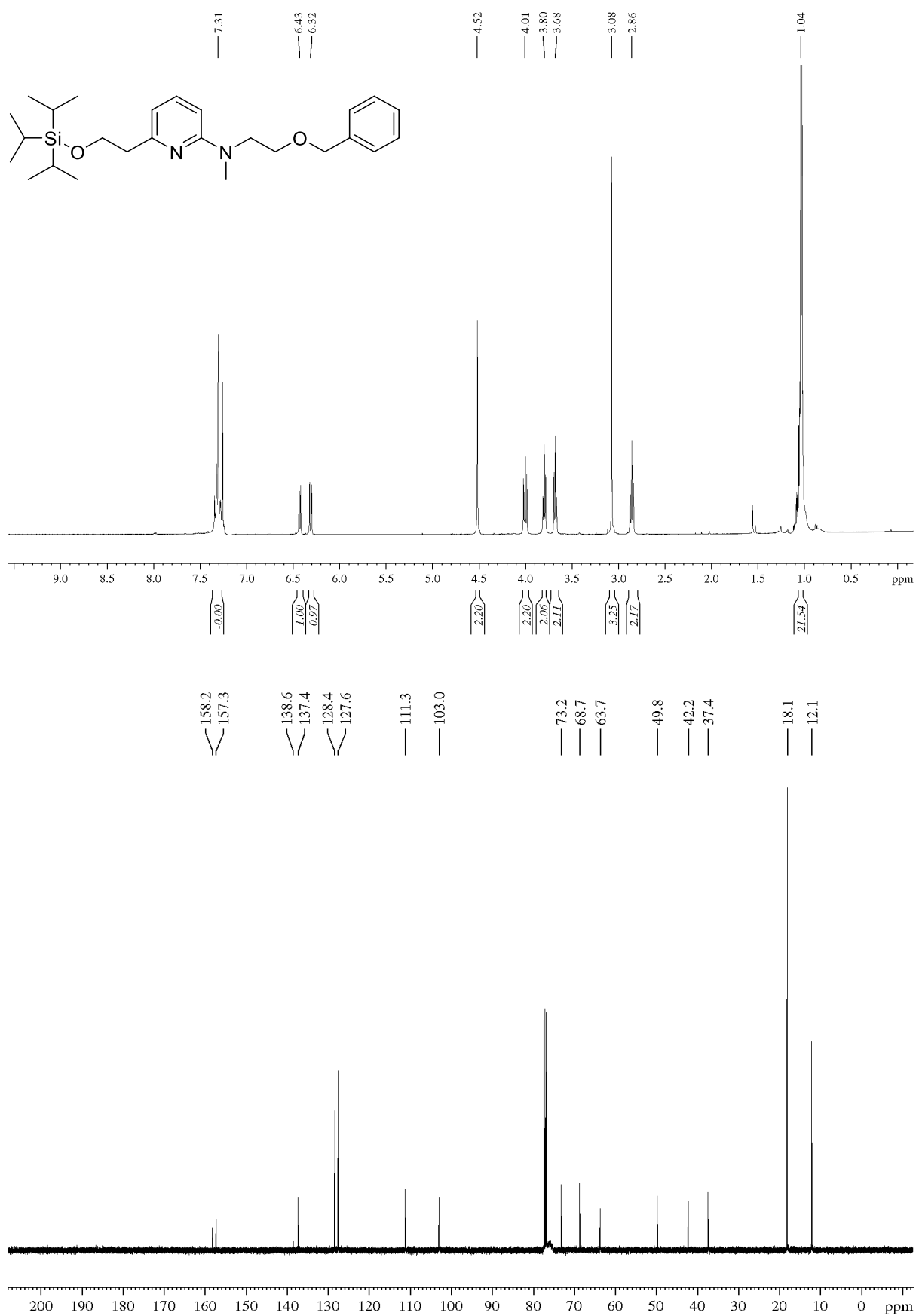
2-((tert-Butyldiphenylsilyl)oxy)-N-methylethan-1-amine (147)

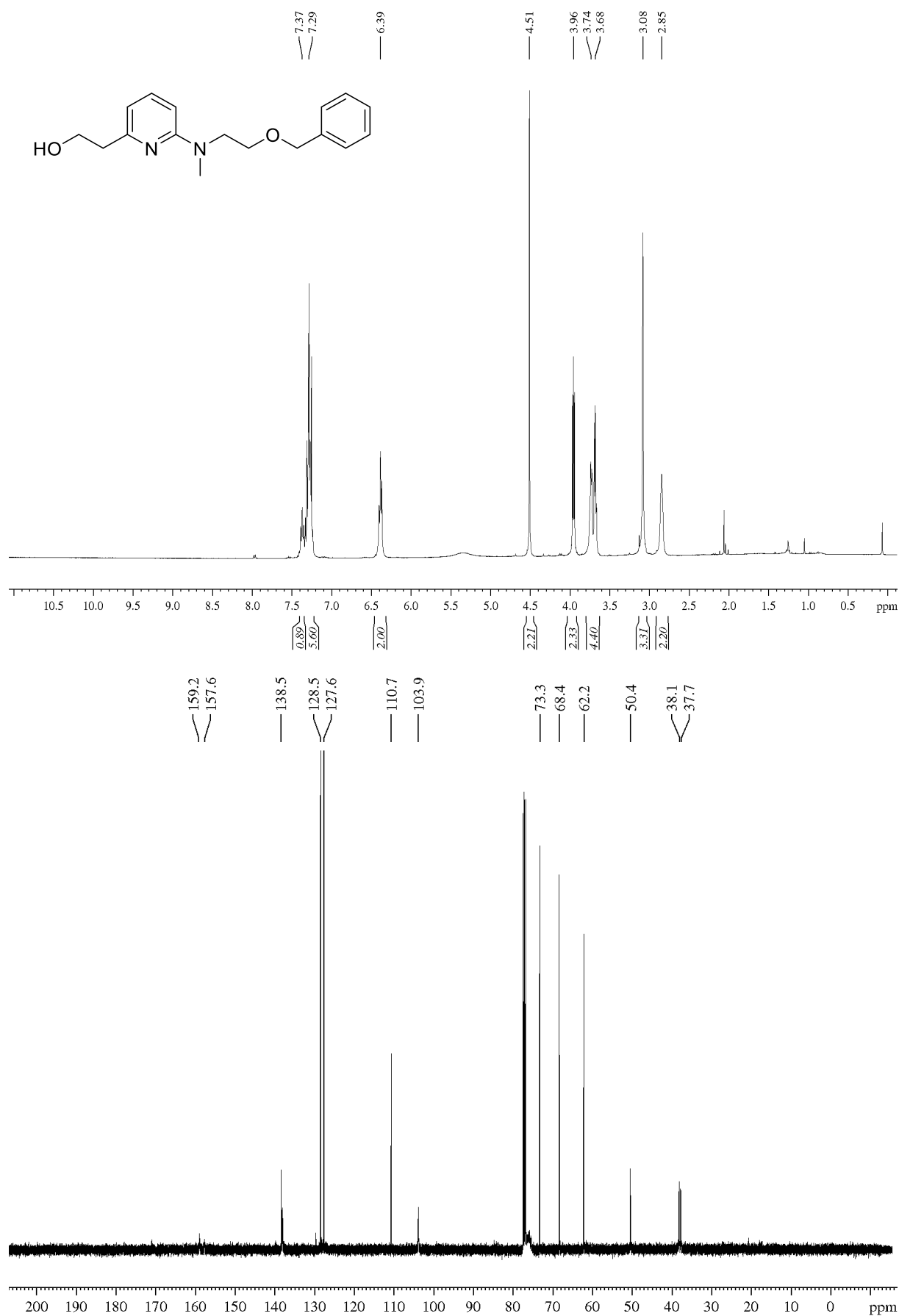
N-Methyl-2-((triisopropylsilyl)oxy)ethan-1-amine (148)

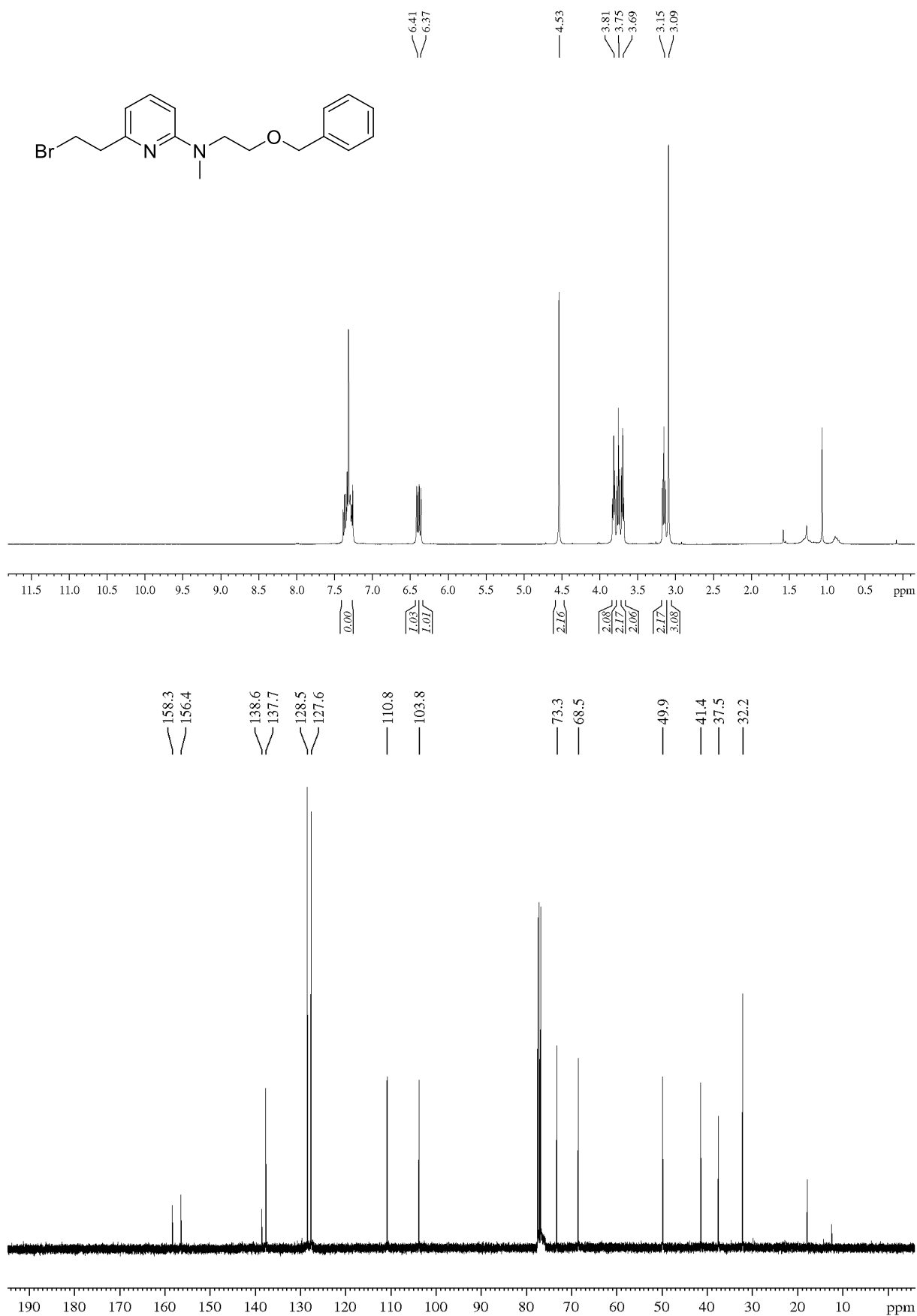
2-(6-((2-((*tert*-Butyldiphenylsilyl)oxy)ethyl)(methyl)amino)pyridin-2-yl)ethan-1-ol (151)

2-(6-(Methyl(2-((triisopropylsilyl)oxy)ethyl)amino)pyridin-2-yl)ethan-1-ol (152)

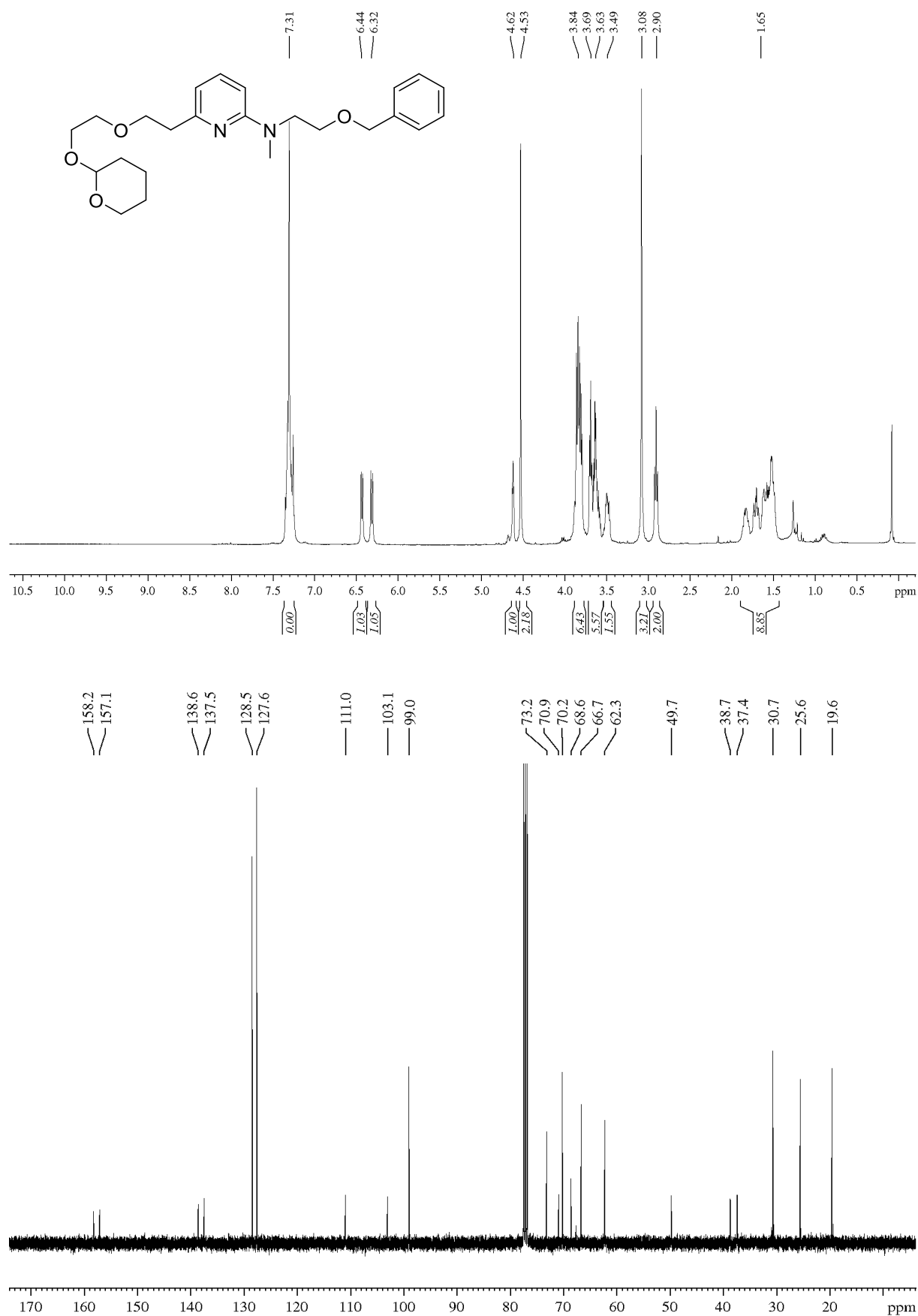
2-(Methyl(6-(2-((triisopropylsilyl)oxy)ethyl)pyridin-2-yl)amino)ethan-1-ol (154)

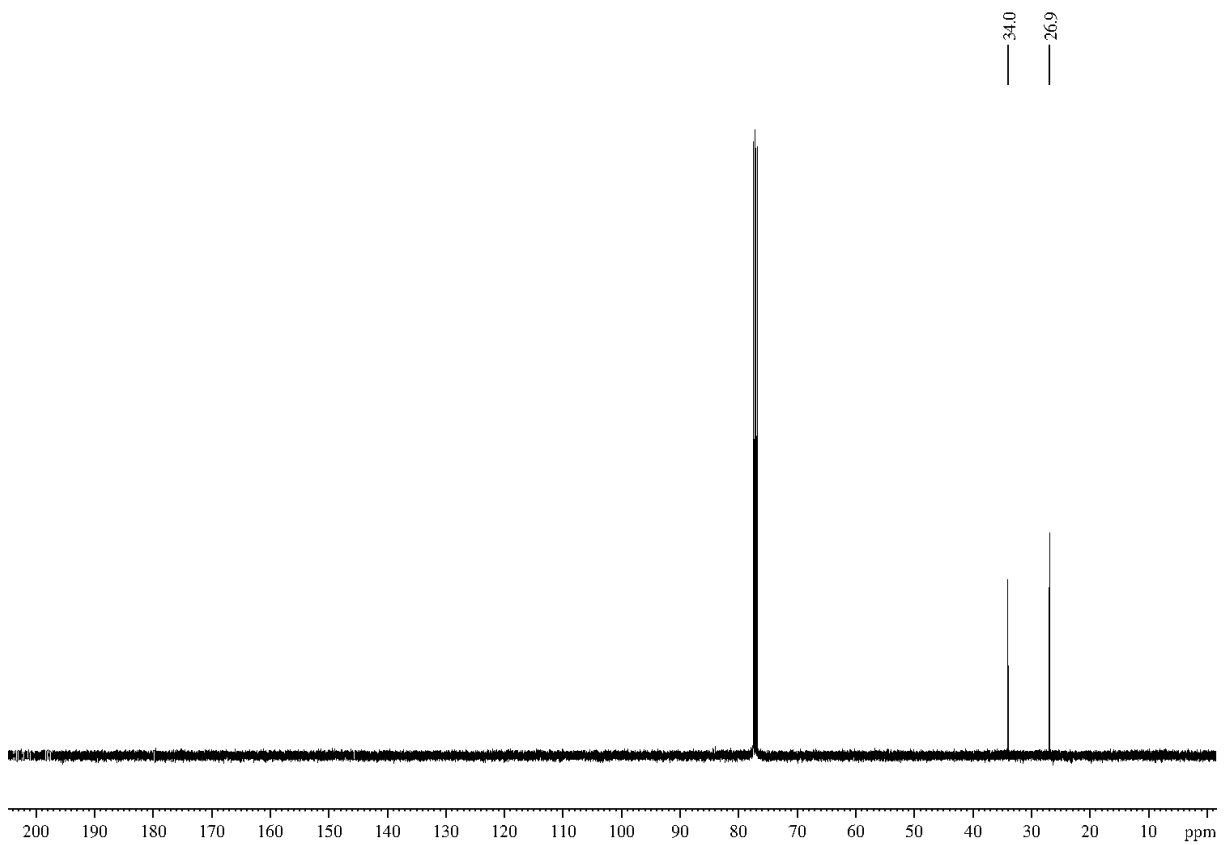
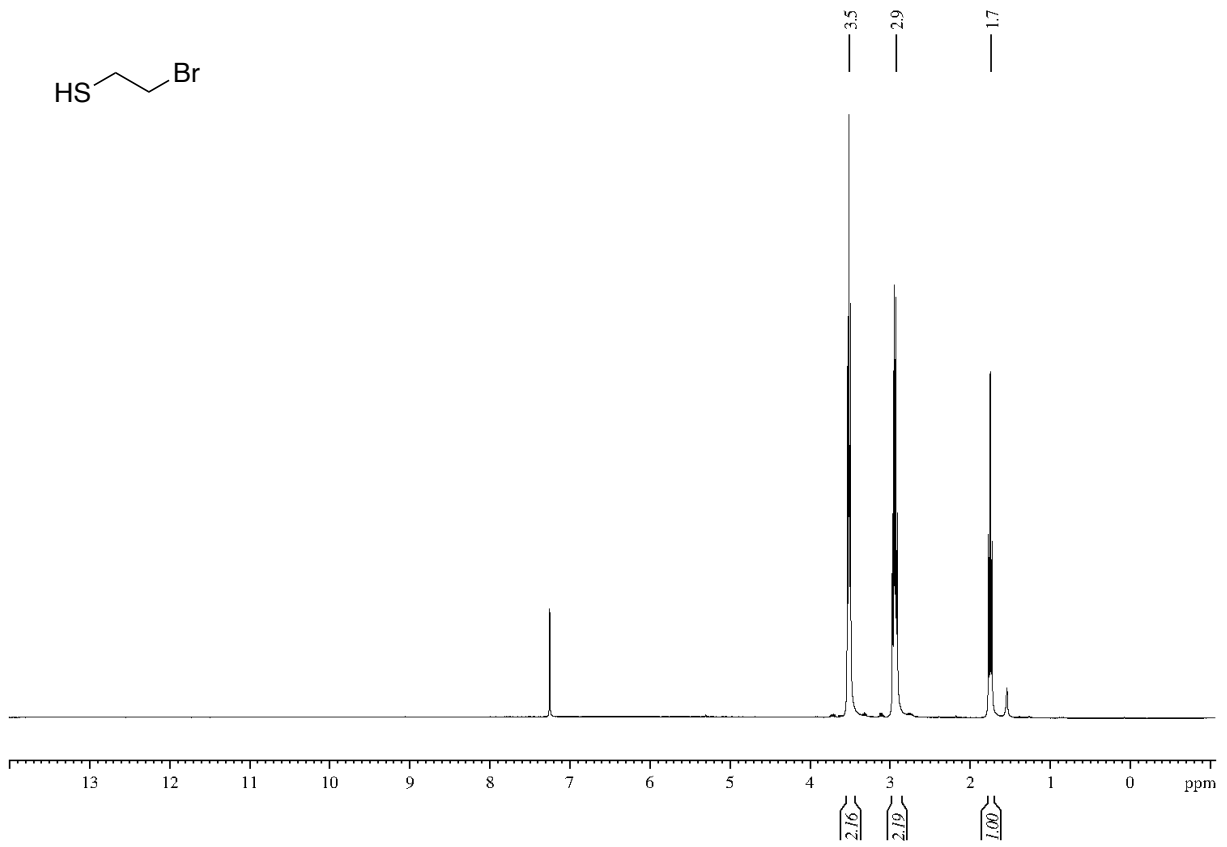
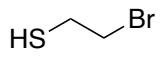
N-(2-(Benzyloxy)ethyl)-*N*-methyl-6-(2-((triisopropylsilyl)oxy)ethyl)pyridin-2-amine (155)

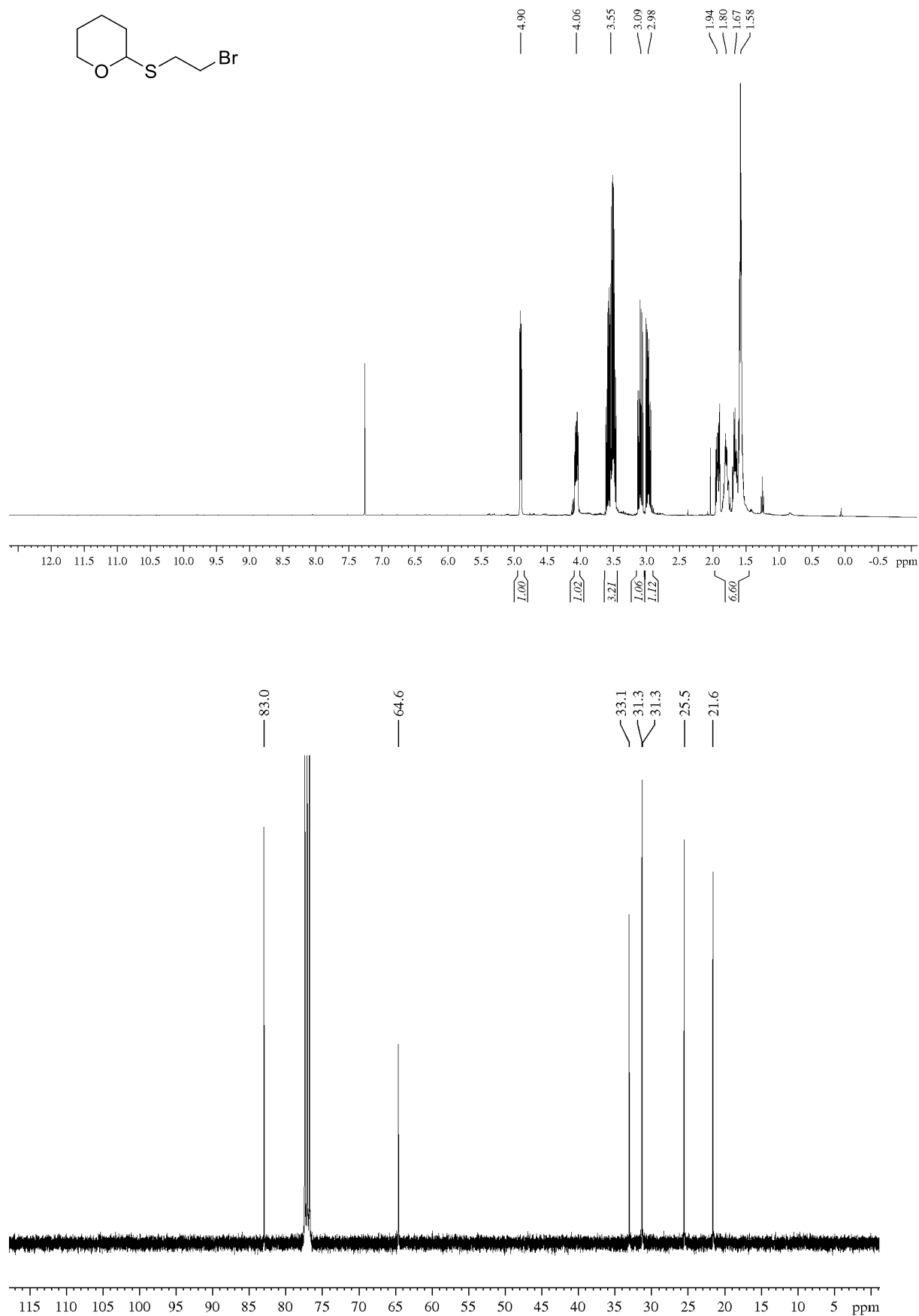
2-(6-((2-(Benzyloxy)ethyl)(methyl)amino)pyridin-2-yl)ethan-1-ol (156)

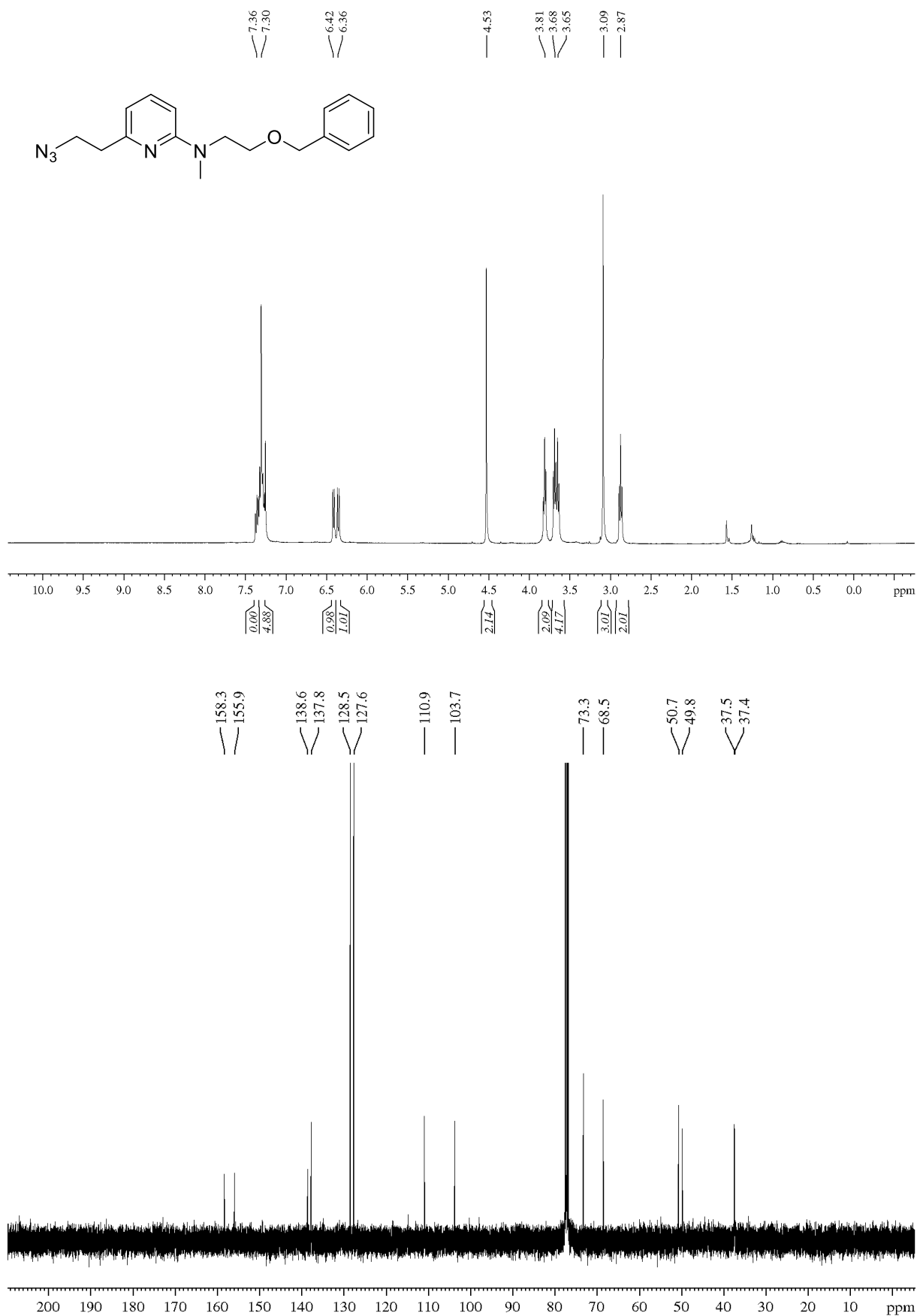
N-(2-(Benzyloxy)ethyl)-6-(2-bromoethyl)-*N*-methylpyridin-2-amine (157)

N-(2-(Benzyloxy)ethyl)-*N*-methyl-6-(2-(2-((tetrahydro-2H-pyran-2-yl)oxy)ethoxy)ethyl)pyridin-2-amine (164b)

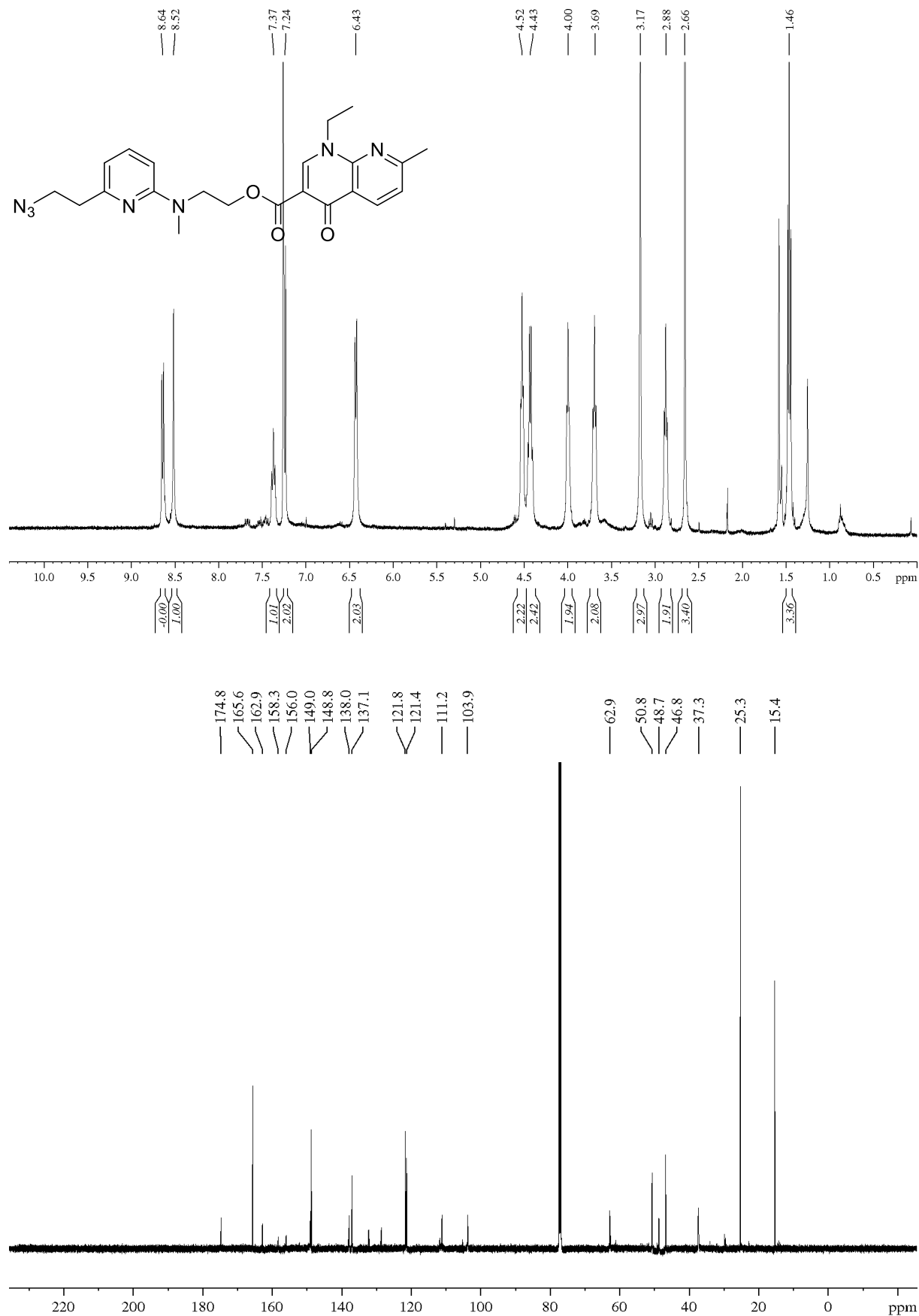


2-Bromoethan-1-thiol (166)

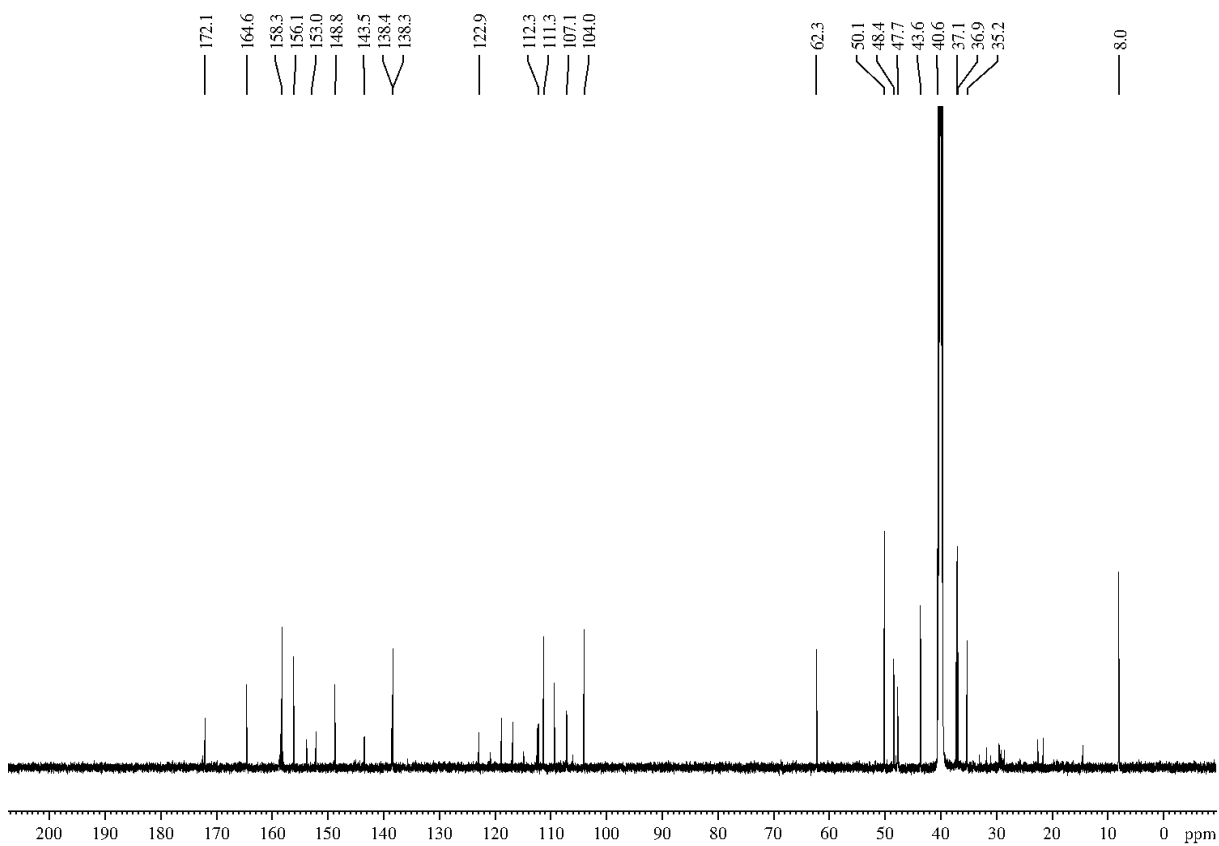
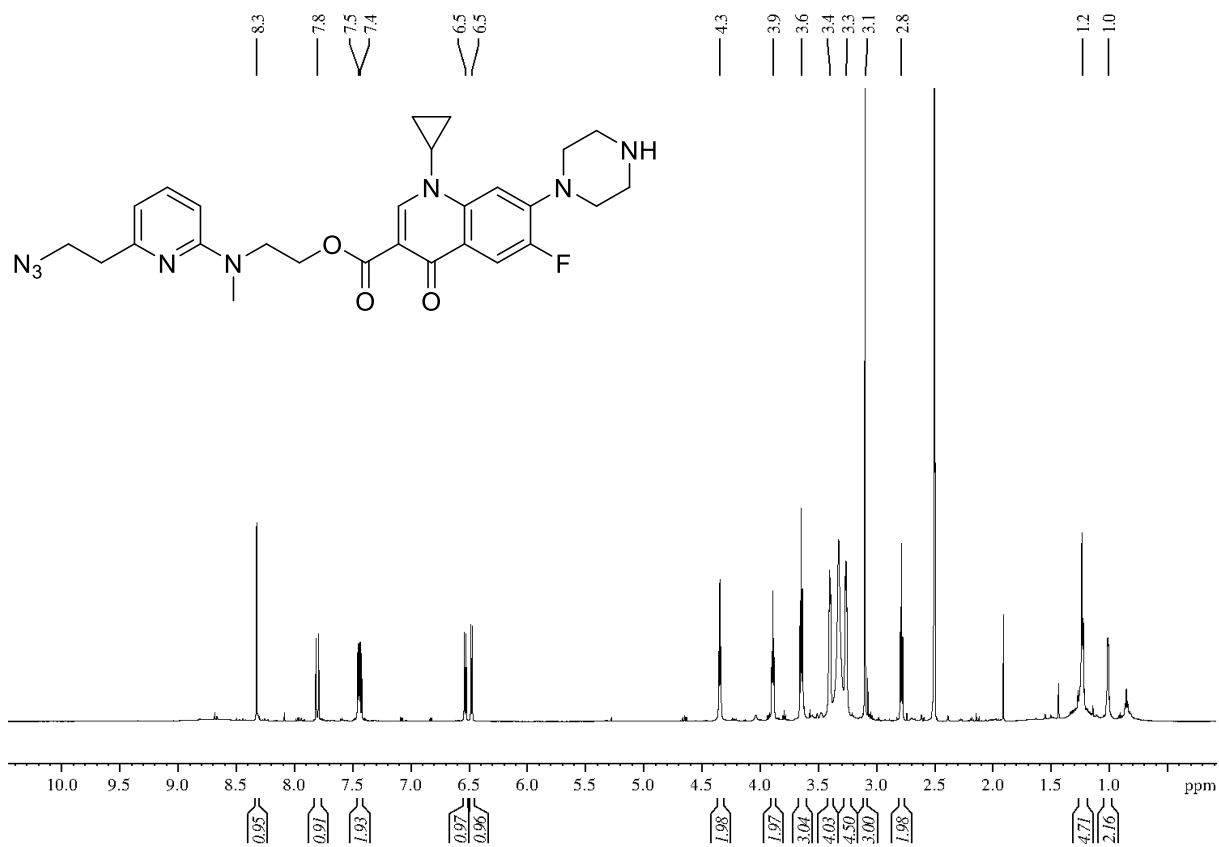
2-((2-Bromoethyl)thio)tetrahydro-2H-pyran (167)

6-(2-Azidoethyl)-N-(2-(benzyloxy)ethyl)-N-methylpyridin-2-amine (178)

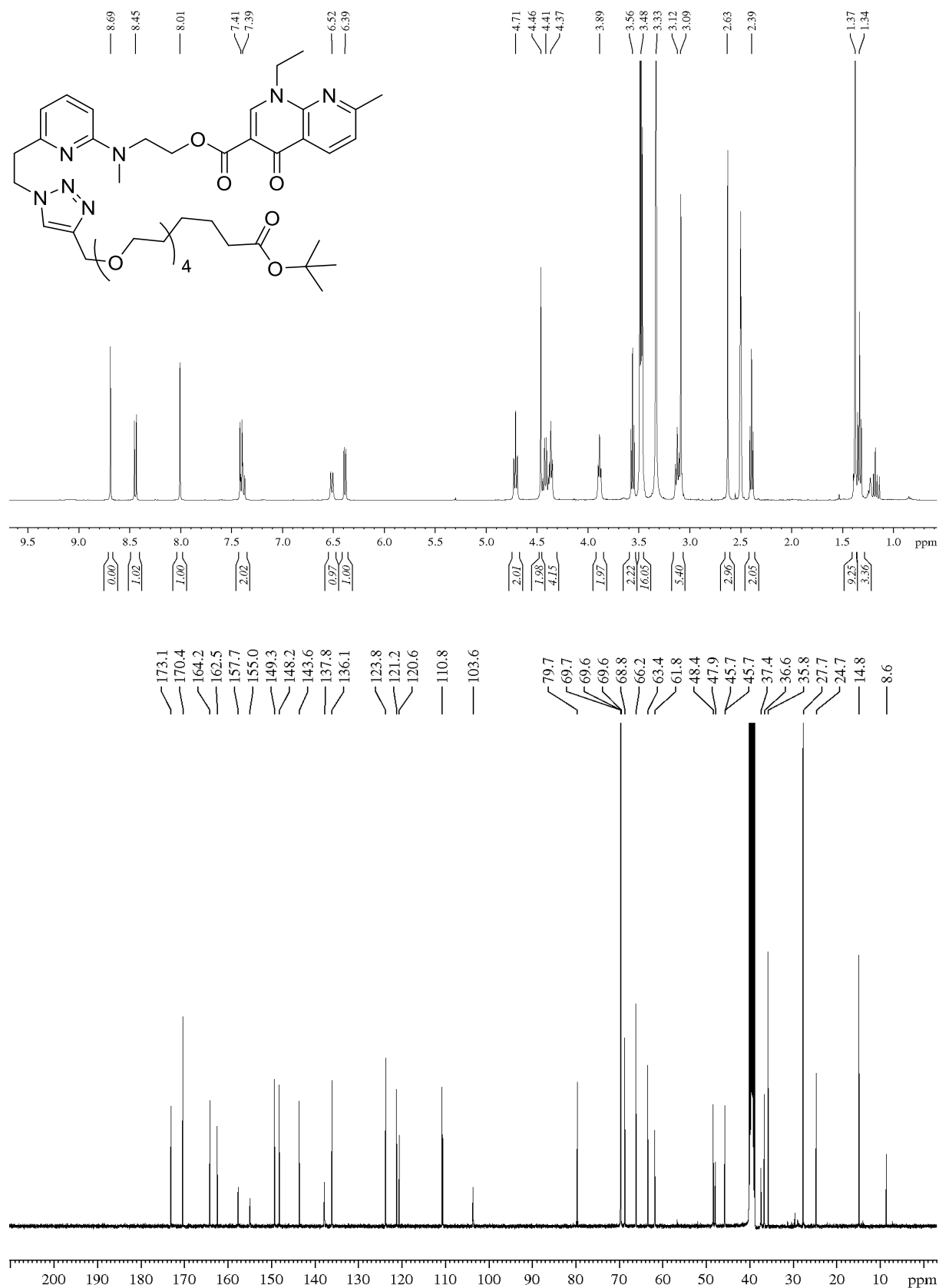
2-((6-(2-Azidoethyl)pyridin-2-yl)(methylamino)ethyl 1-ethyl-7-methyl-4-oxo-1,4-dihydro-1,8-naphthyridine-3-carboxylate (179)

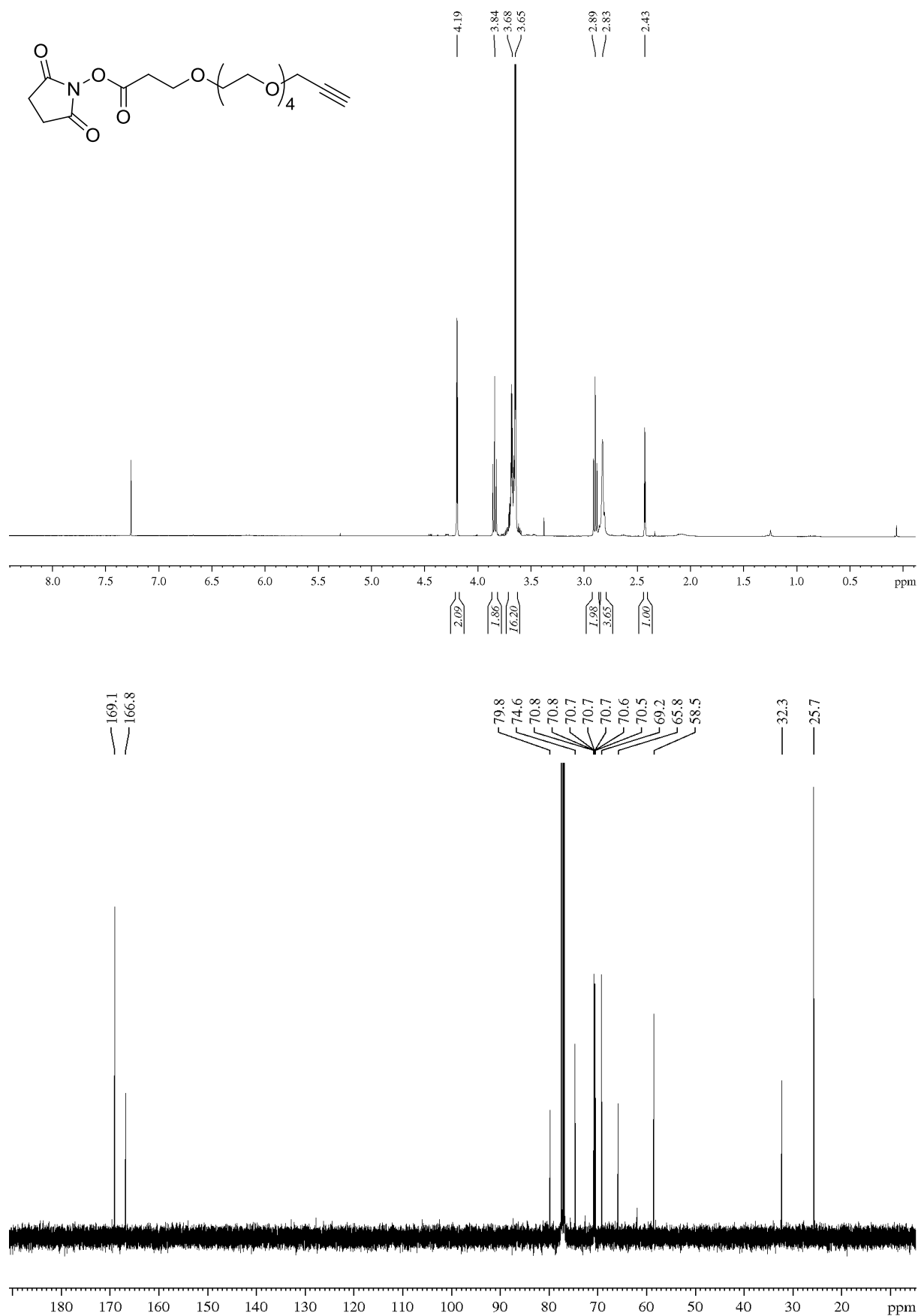


2-((6-(2-Azidoethyl)pyridin-2-yl)(methylamino)ethyl 1-cyclopropyl-6-fluoro-4-oxo-7-(piperazin-1-yl)-1,4-dihydroquinoline-3-carboxylate (180)



2-((6-(2-(4-(19,19-dimethyl-17-oxo-2,5,8,11,14,18-hexaoxaicosyl)-1H-1,2,3-triazol-1-yl)ethyl)pyridin-2-yl)(methylamino)ethyl 1-ethyl-7-methyl-4-oxo-1,4-dihydro-1,8-naphthyridine-3-carboxylate (181)



2,5-dioxopyrrolidin-1-yl 3-(2-(prop-2-yn-1-yloxy)ethoxy)propanoate (182)

Danksagung

An erster Stelle möchte ich mich bei meinem Doktorvater Prof. Dr. Andreas Kirsching bedanken. Er gab mir 2015 die einzigartige Möglichkeit nach meinem Biotechnologie Bachelor den chemisch orientierten Master Wirk- und Naturstoffchemie anzutreten. Seine unkonventionelle Art, seine Kreativität, sein Glaube an interdisziplinäre Forschung und sein Vertrauen in die Studenten haben mir diese Doktorarbeit erst ermöglicht. Als Betreuer meiner Doktorarbeit gab er mir die Chance eigenverantwortlich zu arbeiten und selber Ideen zu entwickeln, was nicht nur diese Doktorarbeit, sondern auch meine persönliche Entwicklung gefördert hat. Es war auch Prof. Dr. Kirschning, der es mir ermöglicht hat, neben der Doktorarbeit ein Studium auf Lehramt anzufangen, und soweit abzuschließen, dass ich nun meinen weiteren Weg gehen kann.

Zusätzlich möchte ich mich bei Prof. Dr. Oliver Plettenburg und Prof. Dr. Sascha Beutel für die Übernahme der Zweit- und Drittprüfung dieser Arbeit bedanken.

Mein Ausdrücklicher Dank geht auch an Dr. Gerald Dräger, dafür, dass er sich immer die Zeit genommen mögliche Analytik und Ergebnisse zu diskutieren. Dieser Austausch und sein immer offenes Ohr hat diese Arbeit in jeglicher Art positiv beeinflusst. Den gemeinsamen Besuch von Kooperationspartnern in Indien werde ich immer in schöner Erinnerung behalten.

Des Weiteren, möchte ich mich bei der analytischen Abteilung des OCI, Dr. Jörg Fohrer, Dr. Linn Müggenburg, Monika Rettstadt, Dagmar Körtje, Sabine Ohlrogge und Anne Schulz für die zuverlässige und sehr nette Zusammenarbeit bedanken. Außerdem danke ich sämtlichen technischen Assistenten des BMWZ's insbesondere Katja Körner, für die Bereitstellung von Medien, Materialien und sonstige Unterstützung bei den mikrobiologischen Arbeiten. Für die Möglichkeit der Großfermentation der Mutasynthese möchte ich erneut Dr. Sascha Beutel und seinen Mitarbeitern danken, die mir ihre Räumlichkeiten, Apparaturen und ihr Wissen zur Verfügung gestellt haben.

Bei Ines Britta Roloff, Monika Griese, Christine Bartetzko und Linda Hermanns bedanke ich mich herzlich für die unkomplizierte und persönliche Unterstützung in bürokratischen Angelegenheiten jeglicher Art Bedanken.

Ein großer Dank geht auch an Dr. Egor Geist, dafür dass er mich, nahezu ohne Kenntnisse im organisch chemischen Arbeiten, am Anfang des Masters Praktikantin betreut hat. Egor hat mich alle grundlegenden Kenntnisse der praktischen Arbeit gelehrt und mich darin bestärkt diese Richtung weiterhin einzuschlagen, was zu dieser Doktorarbeit geführt hat.

Meinen Kollegen möchte ich danken, insbesondere meinen Laborkollegen Dr. Clara Oberhauser, Dr. Peijun Li, Duc Tran und Catherine Victoria. Sie alle, und alle anderen Mitarbeiter des AK Kirschning, haben mir diese Zeit nicht nur zu einem unvergesslichen Erlebnis gemacht, sondern standen mir auch mit Rat und Tat beiseite. Die gemeinsamen Ausflüge, Bierabenden und Flunkyballturniere werde ich mein Leben lang in Erinnerung behalten.

Bei meinen Freunden und meiner Familie möchte ich mich für ihr Verständnis und ihre emotionale Unterstützung während dieser Zeit bedanken. Insbesondere bedanke ich mich bei meinen Eltern, die mich darin bestärkt haben, meine Träume zu verfolgen und mir in jeglicher Hinsicht den Weg bereitet haben, der erst zu dieser Arbeit führte.

Zuletzt bedanke ich mich bei meinem Ehemann Christian, der in jeder Situation immer an meiner Seite steht, für mich da ist und mir den ein oder anderen nicht chemischen Rat gegeben hat.

Lebenslauf und Publikationsliste

Persönliche Daten

Name Friederike Wesemann geb. Schäkel
Geburtsdatum/Ort 23.07.1991, Bochum, Deutschland
Staatsangehörigkeit Deutsch

Akademischer Werdegang

- 01/2018-01/2022 **Promotionsstudium**
Gottfried Wilhelm Leibniz Universität Hannover
Thema: *“Mutasyntetic Production of Proansamitocin Derivatives - Development of Nanoparticle-Antibiotic Conjugates for Selective Drug Release upon Inductive Heating“*
Institut für Organische Chemie
Prof. Dr. Andreas Kirschning
- 04/2015-01/2018 **M. Sc. Wirk- und Naturstoffchemie**
Gottfried Wilhelm Leibniz Universität Hannover
Thema: *“Mutasyntetic Production of Proansamitocin Derivatives Using an Δ AHBA, asm12/21 A. pretiosum Mutant Strain“*
Institut für Organische Chemie
Prof. Dr. Andreas Kirschning
- 09/2016 – 03/2017 **Forschungsaufenthalt**, Frankreich
Universität Paris Süd
Thema: *“Studies Towards the Total Synthesis of (\pm)-Clivonine Leading to an Unexpected N-O Bond Cleavage“*
Institut de Chimie Moléculaire et des Matériaux d’Orsay
Prof. Dr. Cyrille Kouklovsky, Dr. Valérie Alezra
- 10/2014 – 03/2015 **Forschungsaufenthalt**, Thailand
National Institute of Genetic Engineering and Biotechnology,
Thema: *“Application of CRISPR/Cas9 system as a tool for editing gene of interest in Plasmodium falciparum“*
Protein-Ligand Engineering and Molecular Biology
Dr. Chairat. Uthaiyibull
- 08/2014 – 09/2014 **Forschungspraktikum**, Deutschland
Universitätsklinik Tübingen, Deutschland
Institut für Medizinische Mikrobiologie und Hygiene
Prof. Dr. Julia Frick

- 10/2011 – 02/2015 **B. Sc. Biotechnologie**
Technische Universität Braunschweig
Thema: „Immunologische Charakterisierung der FLT3^{wmfl/wmf} Maus vor und nach Influenza A Infektion“
Helmholtz-Zentrum für Infektionsforschung
Prof. Dr. Klaus Schughart
- 08/2004 – 06/2011 **Abitur**, Marion-Dönhof-Gymnasium, Nienburg/Weser

Publikationen

- F. Wesemann, A. Heutling, P. Wienecke, A. Kirschning. First Ring-Expanded Maytansin Lactone Accessed by a New Mutasynthetic Variant. *ChemBioChem* **2020**, *21*, 2927–2930
- R. Campagne, F. Schäkel, R. Guillot, V. Alezra, C. Kouklovsky. Base-Mediated Fragmentation of Bicyclic Dihydro-3,6-oxazine: Transformation of Nitroso Diels-Alder Cycloadducts. *Org Lett.* **2018**, *20*, 1884-1887

Präsentationen

- The Chemistry and Biology of Natural Products Symposium XIII, Warwick, **2019**

Poster

- 4th Multistep Enzyme Catalyzed Processes Congress, Trondheim, **2018**
- 24th Young Researcher Fellow's Meeting of the French Medicinal Chemistry Society, Paris, **2017**